Preparative Chromatography

Preparative Chromatography

Edited by

Henner Schmidt-Traub
Michael Schulte
Andreas Seidel-Morgenstern

Third Edition

WILEY-VCH

Editors

Prof. (em.) Dr.-Ing. Henner Schmidt-Traub
TU Dortmund
Fakultüt für Bio- und
Chemieingenieurwesen Lehrstuhl für
Anlagen- und
Prozesstechnik Emil-Figge-Str. 70
44227 Dortmund
Germany

Dr. Michael Schulte
Merck KGaA
Life Science - Bioprocessing
Purification R&D Frankfurter Str. 250
64293 Darmstadt
Germany

Prof. Dr.-Ing. Andreas Seidel-Morgenstern
Otto-von-Guericke-Universität
Institut für
Verfahrenstechnik
Lehrstuhl für Chemische
Verfahrenstechnik and
Max-Planck-Institut für Dynamik
komplexer technischer
SystemeSandtorstraße 1
Universitätsplatz 239106
Magdeburg Germany

Cover
The cover image of a multicolumn
continuous plant is reproduced by
courtesy of Novasep, France.
The cover image of a column head is
reproduced by courtesy of Merck,
Germany.

Contents

Preface

In the 7 years after publishing the second edition of this book, both practical application as well as theoretical research on preparative chromatography have progressed significantly. This motivated us to this revision.

   New materials for stationary phases emerged especially for the separation of large biomolecules and widened the potentials for method developments. Although the fundamentals of chromatography are still the same as in the time of the second edition recent research expanded in order to better quantify multi-component equilibria, for instance by application of the ideal adsorbed solution theory (IAS theory). The inspiring concept of simulated moving bed chromatography was further extended. Now a variety of new multicolumn processes are available that connect a certain number of individual columns almost in an arbitrary manner. The main driving force for these developments was biotechnology, where increasing product titers, the need to replace batch separations as a bottleneck in downstream processing, and the high costs related to some specialized stationary phase materials fostered the development of new and more efficient continuous chromatographic processes. Recent achievements summarized in the book are improved rules and procedures for design and operation of chromatographic equipment. Further, through collaboration of process engineers and mathematicians, faster and more efficient algorithms for simulating and especially optimizing chromatographic processes have been developed and can be applied to a broad variety of concepts. Advanced process control systems are available to run chromatographic processes optimally. However, open literature gives the impression that up to now these procedures are not very common in practice. Therefore, we hope that this chapter will motivate practitioners to have a closer look at these promising methods.

   With this book, we address preparative and process chromatographic issues from both the chemist's and the process engineer's viewpoints in order to improve the mutual understanding and to transfer knowledge between both disciplines. In addition, we want to reach colleagues from industries as well as academia interested in chromatographic separation with preparative purpose. Students and other newcomers looking for detailed information about design and operation of preparative chromatography are hopefully other users of this book. Our message to all of them is that chromatography is nowadays rather well understood and not that difficult and expensive as it is often claimed and perceived. On the other

hand, chromatography is a challenging technique and of course not the solution for all separation problems.

Reinhard Ditz, Sebastian Engell, Andreas Jupke, Malte Kaspereit, and Arthur Susanto are former authors who joined our team again. New authors are Andreas Biselli, Achim Kienle, and Martin Leipnitz. All of them we thank for their contributions. We are aware that they have done the writing in addition to their daily work and apologize for sometimes getting on their nerves by pressing them to meet time limits. We also want to acknowledge the assistance of Matthias Etmanski, who produced new drawings, eliminated misprints, and was patient enough to handle all our revisions. The support by the editing team of Wiley was very helpful, they identified (hopefully all) misprints and created an excellent layout of the book. Last but not least, we thank our families and friends for their patience and support that was essential to bring out this book.

November 2019

Henner Schmidt-Traub
Michael Schulte
Andreas Seidel-Morgenstern

About the Editors

Henner Schmidt-Traub was professor of Plant and Process Design at the Department of Biochemical and Chemical Engineering, TU Dortmund University, Germany, until his retirement in 2005. He is still active in the research community, and his main areas of research focus on preparative chromatography, downstream processing, and plant design. Prior to his academic appointment, Prof. Schmidt-Traub gained 15 years of industrial experience in plant engineering.

Michael Schulte is head of Purification R&D at Merck KGaA Life Sciences, Darmstadt, Germany. In his PhD thesis at the University of Münster, Germany, he developed new chiral stationary phases for chromatographic enantioseparations. In 1995 he joined Merck, and since then he has been responsible for research and development in the area of preparative chromatography, including the development of new stationary phases, new separation processes, and the implementation of simulated moving bed technology at Merck. In his current position, he is responsible for the development of novel stationary phases for preparative chromatography.

Andreas Seidel-Morgenstern is director at the Max Planck Institute for Dynamics of Complex Technical Systems, Magdeburg, Germany, and holds the chair in Chemical Process Engineering at the Otto von Guericke University, Magdeburg, Germany. He received his PhD in 1987 at the Institute of Physical Chemistry of the Academy of Sciences in Berlin. In 1991 and 1992 he worked as a postdoctoral fellow at the University of Tennessee, Knoxville, TN. In 1994 he finished his habilitation at the Technical University in Berlin. His current research is focused on developing chromatographic and crystallization based separation and new reactor concepts.

List of Abbreviations

ACD	at-column dilution
AAV	adeno-associated virus
ADI	active pharmaceutical ingredient
AIEX	anion exchanger
ARX	autoregressive exogenous
ATEX	explosion proof (French: ATmospheres EXplosibles)
BET	Brunauer–Emmett–Teller
BJH	Barrett–Joyner–Halenda
BR	chromatographic batch reactor
BV	bed volume
CACR	continuous annular chromatographic reactor
CD	circular dichroism (detectors)
CEC	capillary electrochromatography
CFD	computational fluid dynamics
cGMP	current good manufacturing practice
CIEX	cation exchanger
CIP	cleaning in place
CLP	column liquid chromatography
CLRC	closed-loop recycling chromatography
COGS	cost of goods sold
CPG	controlled pore glass
CSEP®	chromatographic separator
CSF	circle suspension flow
CSP	chiral stationary phase
CST	continuous stirred tank
CTA	cellulose triacetate
CTB	cellulose tribenzoate
CV	column volume
DAC	dynamic axial compression
DAD	diode array detector
DMF	dimethylformamide
DMSO	dimethyl sulfoxide
DSC	distributed control system
DTA	differential thermal analysis
DVB	divinylbenzene
EC	elution consumption

ECP	elution by characteristic points
EDM	equilibrium dispersive model
EMG	exponential modified Gauss (function)
FACP	frontal analysis by characteristic points
FAT	factory acceptance test
FDA	food and drug administration
FDM	finite difference methods
FF-SMB	fractionation and feedback SMB
FFT	forward flow test
FT	flow through
GC	gas chromatography
GMP	good manufacturing practice
GRM	general rate model
HCP	healthcare provider
HETP	height of an equivalent theoretical plate
HFCS	high-fructose corn syrup
HIC	hydrophobic interaction chromatography
H-NMR	hydrogen nuclear magnetic resonance (spectroscopy)
HPLC	high-performance liquid chromatography
HPW	highly purified water
IAST	ideal adsorbed solution theory
ICH	International Guidelines for Harmonization
IEX	ion exchange
IMAC	immobilized metal affinity chromatography
IR	infrared
ISEC®	inverse size-exclusion chromatography
ISEP®	ion-exchange separation
iSMB	improved/intermittent simulated moving bed
LC	liquid chromatography
LGE	linear gradient elution
LHS	liquid-handling station
LOD	limit of detection
LOQ	limit of quantification
LPLC	low-pressure liquid chromatography
LSB	large-scale biotech project
mAb	monoclonal antibody
MCC	multicolumn capture chromatography
MCSGP	multicolumn countercurrent solvent gradient purification
MD	molecular dynamics
MPC	model predictive control
MS	mass spectroscopy
MW	molecular weight
NMPC	nonlinear model predictive control
NMR	nuclear magnetic resonance (spectroscopy)
NN	neural network
NP	normal phase
NPLC	normal phase liquid chromatography
NSGA	nondominating sorting generic algorithm

OC	orthogonal collocation
OCFE	orthogonal collocation on finite elements
ODE	ordinary differential equation
PAT	process analytical technology
PCC	periodic countercurrent chromatography
PDE	partial differential equation
PDT	pressure decay test
PEEK	poly(etheretherketone)
PES	poly-ether sulfone
PLC	programmable logic controller
PMP	polymethylpentene
PSD	particle size distribution
QC	quality control
R&D	research and development
RI	refractive index
RMPC	repetitive model predictive control
RP	reversed phase
SAT	site acceptance test
S/N	signal-to-noise ratio
SEC	size-exclusion chromatography
SEM	scanning electron microscopy
SFC	supercritical fluid chromatography
SIP	sanitization in place
SIP	steaming in place
SMCC	sequential multicolumn chromatography
SMB	simulated moving bed
SMBR	simulated moving bed reactor
SOP	standard operation procedure
SQP	sequential quadratic programming
SSRC	steady-state recycling chromatography
St-DVB	styrene-divinylbenzene
TDM	transport dispersive model
TEM	transmission electron microscopy
TEOS	tetraethoxysilane
TFA	trifluoroacetic acid
TG/DTA	thermogravimetric/differential thermal analysis
THF	tetrahydrofuran
TLC	thin-layer chromatography
TMB	true moving bed process
TMBR	true moving bed reactor
TPX™	transparent polymethylpentene
UPLC	ultrahigh-performance liquid chromatography
URS	user Requirements Specification
USP	United States Pharmacopeia
UV	ultraviolet
VSP	volume-specific productivity
WFI	water for injection
WIT	water intrusion test

Notation

Symbols

Symbol	Description	Units
a	Coefficient of the Langmuir isotherm	$cm^3\,g^{-1}$
a_s	Specific surface area	$cm^2\,g^{-1}$
A	Area	cm^2
A_c	Cross section of the column	cm^2
A	Coefficient in the van Deemter equation	cm
A_s	Surface area of the adsorbent	cm^2
ASP	Cross section-specific productivity	$g\,cm^{-2}\,s^{-1}$
b	Coefficient of the Langmuir isotherm	$cm^3\,g^{-1}$
B	Column permeability	m^2
B	Coefficient in the van Deemter equation	$cm^2\,s^{-1}$
c	Concentration in the mobile phase	$g\,cm^{-3}$
c_p	Concentration of the solute inside the particle pores	$g\,cm^{-3}$
C	Annual costs	€
C	Coefficient in the van Deemter equation	s
C_{DL}	Dimensionless concentration in the liquid phase	—
$C_{p,DL}$	Dimensionless concentration of the solute inside the particle pores	—
C_{spec}	Specific costs	$€\,g^{-1}$
D_c	Diameter of the column	cm
d_p	Average diameter of the particle	cm
d_{pore}	Average diameter of the pores	cm
D_{an}	Angular dispersion coefficient	$cm^2\,s^{-1}$
D_{app}	Apparent dispersion coefficient	$cm^2\,s^{-1}$
$D_{app,pore}$	Apparent dispersion coefficient inside the pores	$cm^2\,s^{-1}$
D_{ax}	Axial dispersion coefficient	$cm^2\,s^{-1}$
D_m	Molecular diffusion coefficient	$cm^2\,s^{-1}$
D_{pore}	Diffusion coefficient inside the pores	$cm^2\,s^{-1}$
D_{solid}	Diffusion coefficient on the particle surface	$cm^2\,s^{-1}$
EC	Eluent consumption	$cm^2\,s^{-1}$
fi	Specific prices	$€\,l^{-1},\,€\,g^{-1}$
f	Fugacity	—
h	Reduced plate height	—
R_f	Retardation factor	—
Δh_{vap}	Heat of vaporization	$kJ\,mol^{-1}$
H	Henry coefficient	—
H_p	Prediction horizon	—
H_r	Control horizon	—

Symbol	Description	Units
HETP	Height of an equivalent theoretical plate	cm
k_{ads}	Adsorption rate constant	$cm^3\,g^{-1}\,s^{-1}$
k_{des}	Desorption rate constant	$cm^3\,g^{-1}\,s^{-1}$
k_{eff}	Effective mass transfer coefficient	$cm^2\,s^{-1}$
K_{eq}	Equilibrium constant	Miscellaneous
K_{EQ}	Dimensionless equilibrium coefficient	—
k_{film}	Boundary or film mass transfer coefficient	$cm\,s^{-1}$
k'	Retention factor	—
$k\tilde{r}$	Modified retention factor	—
k_0	Pressure drop coefficient	—
k_{reac}	Rate constant	Miscellaneous
LF	Loading factor	—
L_c	Length of the column	cm
$\dot{m}$	Mass flow	$g\,s^{-1}$
m	Mass	g
m_j	Dimensionless mass flow rate in section j	—
m_s	Total mass	g
n_T	Pore connectivity	—
N	Column efficiency, number of plates	—
N_{col}	Number of columns	—
N_{comp}	Number of components	—
N_p	Number of particles per volume element	—
Δp	Pressure drop	Pa
Pe	Péclet number	—
Pr	Productivity	$g\,cm^{-3}\,h^{-1}$
P_s	Selectivity point	—
Pu	Purity	%
q	Solid phase loading	$g\,cm^{-3}$
q^*	Total loading	$g\,cm^{-3}$
$\overline{q}_i^*$	Averaged particle loading	$g\,cm^{-3}$
q_{sat}	Saturation capacity of the stationary phase	$g\,cm^{-3}$
Q_{DL}	Dimensionless concentration in the stationary phase	—
r	Radial coordinate	cm
r	Reaction rate	Miscellaneous
r_p	Particle radius	cm
R_f	Retardation factor	—
R_s	Resolution	—
Re	Reynolds number	—

Symbol	Description	Units
S_{BET}	Specific surface area	$m^2\,g^{-1}$
Sc	Schmidt number	—
Sh	Sherwood number	—
St	Stanton number	—
t	Time	s
t_0	Dead time of the column	s
$t_{0,e}$	Retention time of a non-retained component (related to external porosity)	s
$t_{0,t}$	Retention time of a non-retained component (related to total porosity)	s
t_{cycle}	Cycle time	s
t_g	Gradient time	s
t_{inj}	Injection time	s
t_{life}	Lifetime of adsorbent	h
t_{plant}	Extra-column dead time of the plant	s
t_R	Retention time	s
$t_{R,net}$	Net retention time	s
t_{shift}	Switching time of the SMB plant	s
t_{tank}	Dead time of tanks	s
t_{pipe}	Dead time of pipes	s
t_{Rmax}	Maximum of retention time	s
t_{Rmean}	Mean retention time, first statistical moment	s
t_{Rshock}	Retention time of a shock front	s
T	Temperature	K
T	Degree of peak asymmetry	—
u_0	Velocity in the empty column	$cm\,s^{-1}$
$u_{int,e}$	Interstitial velocity in the external fluid volume of the packed column	$cm\,s^{-1}$
$u_{int,t}^{hypo}$	Hypothetical effective velocity	$cm\,s^{-1}$
u_m	Effective velocity (total mobile phase)	$cm\,s^{-1}$
v_{sp}	Specific pore volume	$cm^3\,g^{-1}$
V	Volume	cm^3
$\dot{V}$	Volume flow	$cm^3\,s^{-1}$
V_{ads}	Volume of the stationary phase within a column	cm^3
V_c	Total volume of a packed column	cm^3
V_i	Molar volume	$cm^3\,mol^{-1}$
V_{int}	Interstitial volume	cm^3
V_m	Overall fluid volume	cm^3
V_{pore}	Volume of the pore system	cm^3

Symbol	Description	Units
V_{solid}	Volume of the solid material	cm^3
VSP	Volume-specific productivity	$\text{g}\,\text{cm}^{-3}\,\text{s}^{-1}$
w_i	Velocity of propagation	$\text{cm}\,\text{s}^{-1}$
x	Coordinate	cm
x	State of the plant	—
x	Fraction	—
X	Conversion	%
X_{cat}	Fraction of catalyst of the fixed bed	—
Y	Yield	%
Z	Dimensionless distance	—

Greek Symbols

Symbol	Description	Units
α	Selectivity	—
α_{exp}	Ligand density	$\mu\text{mol}\,\text{m}^{-2}$
β	Modified dimensionless mass flow rate	—
γ	Obstruction factor for diffusion or external tortuosity	—
Γ	Objective function	—
ε	Void fraction	—
ε^0	Solvent strength parameter	—
ε_{e}	External (interstitial) porosity	—
ε_{P}	Porosity of the solid phase	—
ε_{t}	Total column porosity	—
η	Dynamic viscosity	mPa s
Θ	Angle of rotation	°
Λ	Total ion-exchange capacity	mM
λ	Irregularity in the packing	—
μ	Chemical potential	$\text{J}\,\text{mol}^{-1}$
μ_{k}	k^{th} moment	—
ν	Kinematic viscosity	$\text{cm}^2\,\text{s}^{-1}$
ν	Stoichiometric coefficient	—
π	Spreading pressure	Pa
ϱ	Density	$\text{g}\,\text{cm}^{-3}$
σ_{t}	Standard deviation	—
σ	Steric shielding parameter	—
τ	Dimensionless time	—
ϕ	Running variable	—

Symbol	Description	Units
φ	Bed voidage	
ψ	Friction number	—
$\psi_{\text{reac/des}}$	Rate of the adsorption and desorption steps	$\text{g cm}^{-3}\,\text{s}^{-1}$
ω_j	Characteristic coefficient in equilibrium theory	—
ω	Rotation velocity	$°\text{s}^{-1}$
Θ_{cyc}	Cycle time	s

Subscripts

Symbol	Description
1, 2	Component 1/component 2
I, II, III, IV	Section of the SMB or TMB process
acc	Accumulation
ads	Adsorbent
c	Column
cat	Catalyst
conv	Convection
crude	Crude loss
des	Desorbent
diff	Diffusion
disp	Dispersion
DL	Dimensionless
eff	Effective
el	Eluent
exp	Experimental
ext	Extract
feed	Feed
het	Heterogeneous
hom	Homogeneous
i	Component i
in	Inlet
inj	Injection
j	Section j of the TMB or SMB process
l	Liquid
lin	Linear
max	Maximum
min	Minimum
mob	Mobile phase

Symbol	Description
mt	Mass transfer
opt	Optimal
out	Outlet
p	Particle
pore	Pore
pipe	Pipe within HPLC plant
plant	Plant without column
prod	Product
raf	Raffinate
reac	Reaction
rec	Recycles
s	solid
sat	Saturation
sec	Section
shock	Shock front
SMB	Simulated moving bed process
solid	Solid adsorbent
spec	Specific
stat	Stationary phase
tank	Tank within HPLC plant
theo	Theoretical
TMB	True moving bed process

Definition of Dimensionless Parameters

Péclet number	$Pe = \dfrac{u_{int}L_c}{D_{ax}}$	Convection to dispersion (column)
Péclet number of the particle	$Pe_p = \dfrac{u_{int}d_p}{D_{ax}}$	Convection to dispersion (particle)
Péclet number of the plant	$Pe_p = \dfrac{u_{plant}L_{plant}}{D_{ax,plant}}$	Convection to dispersion (plant without column)
Reynolds number	$Re = \dfrac{u_{unit}d_p\rho_l}{\eta_l}$	Inertial force to viscous force
Schmidt number	$Sc = \dfrac{\eta_l}{\rho_l D_m}$	Kinetic viscosity to diffusivity
Sherwood number	$Sh = \dfrac{k_{film}d_p}{D_m}$	Mass diffusivity to molecular diffusivity
Stanton number (modified)	$St_{eff,i} = k_{eff,i} \cdot \dfrac{6}{d_p} \cdot \dfrac{L_c}{u_{int}}$	Mass transfer to convection

1

Introduction

Henner Schmidt-Traub[1] and Reinhard Ditz[2]

[1]*TU Dortmund Fakultät für Bio- und Chemieingenieurwesen, Lehrstuhl für Anlagen- und Prozesstechnik, Emil-Figge-Str. 70, 44227 Dortmund, Germany*
[2]*Bristenstrasse 16, CH 8048 Zürich, Switzerland*

1.1 Chromatography, Development, and Future Trends

Ink dripping on a blotting paper thrills children when they realize the rainbow of colors spreading out. It is chromatography, an effect first coined by Tswett (1906) in 1903 for the isolation of chlorophyll constituents. Now, more than a hundred years later, children still enjoy chromatographic effects. Chromatography has developed into an important method for chemical analysis and production of high purity product in micro- and macroscale, and today pharmaceuticals are unthinkable without chromatography.

Liquid chromatography (LC) was first applied as a purification tool and has therefore been used as a preparative method. It is the only technique that enables to separate and identify both femtomoles of compounds out of complex matrices in life sciences and allows the purification and isolation of synthetic industrial products in the ton range. Figure 1.1 characterizes the development of chromatography and its future trends.

In the 1960s, analytical high-performance liquid chromatography (HPLC) emerged when stationary phases of high selectivity became available. At the same time, an essential technology push for preparative chromatography was created by the search of engineers for more effective purification technologies. The principle to enhance mass transfer by countercurrent flow in combination with high selectivity of HPLC significantly increased the performance of preparative chromatography in terms of productivity, eluent consumption, yield, and concentration. The first process of this kind was the simulated moving bed (SMB) chromatography for large-scale separation in the petrochemical area and in food processing (Broughton and Gerhold 1961).

These improvements were closely coupled to the development of adsorbents of high selectivity. In the 1980s, highly selective adsorbents were developed for the resolution of racemates into their enantiomers. The availability of enantioselective packing in bulk quantities enabled the production of pure enantiomers
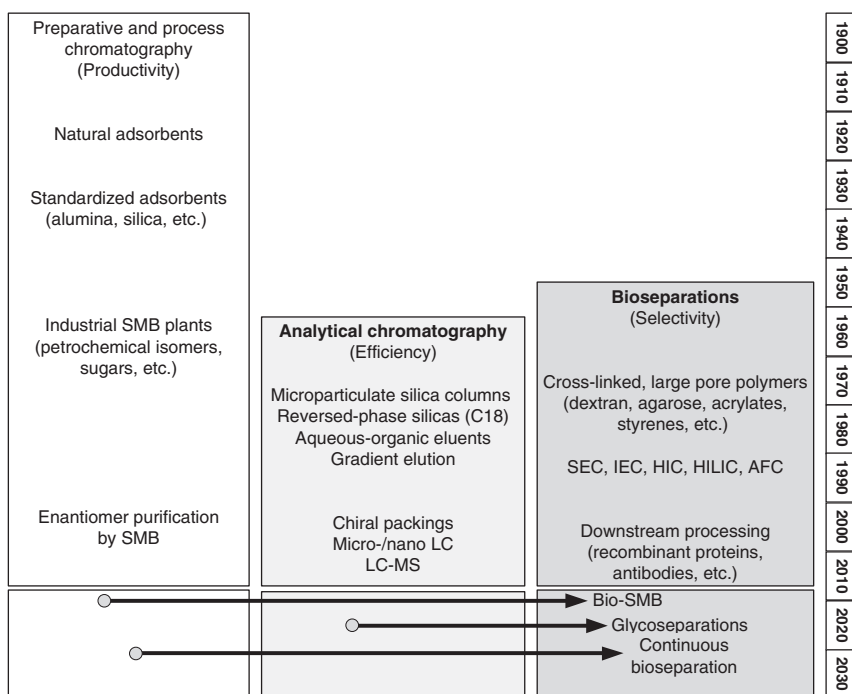
Figure 1.1 Development of chromatography. Source: Unger et al. (2010). Reproduced and modified with permission of John Wiley and Sons.

by the SMB technology in the multi-ton range. Productivities larger than 10 kg of pure product per kilogram of packing per day were achieved in the following years.

In the 1990s, the SMB process concept was adapted and downsized for the production of pharmaceuticals. The development of new processes was necessarily accompanied by theoretical modeling and process simulation, which are a prerequisite for better understanding of transport phenomena and process optimization.

While preparative as well as analytical LC were heavily relying on equipment and engineering and on the physical aspects of their tools for advancement in their fields, the bioseparation domain was built around a different key aspect, namely, selective materials that allowed the processing of biopolymers, for example, recombinant proteins under nondegrading conditions, thus maintaining bioactivity. Much less focus in this area was on process engineering aspects, leading to the interesting phenomenon, that large-scale production concepts for proteins were designed around the mechanical instability of soft gels (Janson and Jönsson 2010).

The separation of proteins and other biopolymers has some distinctly different features compared with the separation of low molecular weight (MW) molecules from synthetic routes or from natural sources. Biopolymers have an MW ranging from several thousand to several million. They are charged and characterized

by their isoelectric point. More importantly, they have a dynamic tertiary structure that can undergo conformational changes. These changes can influence or even destroy the bioactivity in the case of a protein denaturation. Biopolymers are separated in aqueous buffered eluents under conditions that maintain their bioactivity. Moreover, these large molecules exhibit approximately 100 times lower diffusion coefficients and consequently slower mass transfer than small molecules (Unger et al. 2010). Due to these conditions, processes for biochromatography differ substantially from the separation of low molecular weight molecules. For instance, process pressure, which is in many cases much lower for bioprocesses than for HPLC, requires a different plant design. Selectivity makes another difference; due to the very different retention times of biosolutes, an effective separation is only possible with solvent gradients.

Since the 1990s modeling and simulation tools for chromatographic separations of fine chemicals have developed considerably and are meanwhile well established, stimulating the efficiency of practical processes, while bioseparations were mainly based on empirical knowledge because of the complex nature of biomolecules. In the past regulation policies of FDA and other authorities focused on certified process schemes and process conditions as well as quality control by measuring the composition of intermediates and final products in order to guarantee drug safety. This resulted in overregulation and threatened to lead drug production into a dead end. Therefore, FDA started the process analysis technology (PAT) initiative in the 2000s and stated, "The goal of PAT is to enhance understanding and control of the manufacturing process, which is consistent with our current drug quality system: quality cannot be tested into products; it should be built-in or should be by design" (FDA 2004). PAT implies a paradigm change in pharmaceutical industries and created a momentum for better understanding of processes and products. Meanwhile it is extended by quality by design (QbD), which in summary aims at: "a systematic approach to development that begins with predefined objectives and emphasizes product and process understanding and control, based on sound science and quality risk management" (Yu et al. 2014).

In the recent past countercurrent SMB processes have been highlights of chromatographic separations. With a focus on increased productivity and to make chromatographic separations more economical especially for bioproducts, the SMB principles are becoming a source to create new and more flexible processes with a reduced number of columns. Here the extreme case is a proposal for a SMB-like process with only one column (Zobel et al. 2014). Process control is another example for improvements. Robust processes are essential for high-quality products. Prerequisites for all these developments are stable and highly selective stationary phases and reliable equipment and on the other side rigorous models and increased computer power, which enables fast and reliable process simulations.

Peeking into the future reveals a technology trend toward the use of continuous process operations and downstream processing for fine chemicals and especially biopharmaceuticals. Costs and production capacities will have to be addressed, asking for better integrated and efficient approaches. Adapting countercurrent

solvent gradient concepts for the isolation of antibodies from complex fermentation broths will allow for more cost-effective downstream processing of biopharmaceuticals within the next couple of years.

Preparative and large production chromatography in their current major fields of application and scale have reached a level of maturity, which turns it from a breakthrough technology into a commodity. Major future opportunities will be in the field of continuous operation in the form of new SMB variants and especially in combination with other unit operations like extraction, crystallization, precipitation, etc. Such combinations will provide new and viable opportunities in fields like natural and renewable plant-based products, for example, in healthcare applications and other regulated industries. Work in a variety of applications and combinations is in progress with a focus on regulated products. This, however, is outside and beyond the scope of this book.

1.2 Focus of the Book

The general objective of preparative chromatography is to isolate and purify products in high quality. During this process, the products have to be recovered in the same condition that they were in before undergoing the separation. As preparative chromatographic processes have to produce the target with a desired purity and as economical as possible, they are usually operated under overloaded (nonlinear) conditions.

In contrast to this, analytical chromatography, which is not in the core of this book, focuses on the qualitative and quantitative determination of a compound. Thus, the sample can be processed, handled, and modified in any way suitable to generate the required information, including degradation, labeling, or changing the nature of the compounds under investigation. Such processes operate generally under diluted (linear) conditions.

The book provides and develops access to chromatographic purification concepts through the eyes of both engineers and chemists. This includes on one side the fundamentals of natural science and the design of materials and functionalities. On the other side mathematical modeling, simulation, and plant design, as well as joint efforts in characterizing materials, designing processes, and operating plants, are exemplified. Such a joint approach is necessary at the earliest possible moment as interaction and cooperation between chemists and engineers is important to achieve time and cost-effective solutions and to develop consistent methods that can be scaled up to a process environment.

In comparison with the second edition published in 2012, this book is completely restructured, revised, and updated.

1.3 Suggestions on How to Read this Book

For most readers it is probably not necessary to read all chapters of this book in sequence. For some readers the book may be a reference to answer specific

questions depending on actual tasks; for others it may be a guide to acquire new fields of work in research or industrial applications. The book may not provide answers to all questions. In such situations, the reader can obtain further information from the cited literature.

The different chapters are complementary to each other. It is recommended to be familiar first with basic definitions explained in Chapter 2. This chapter presents the basic principles of chromatography and defines the most important parameters such as retention factor, selectivity, and resolution. It also explains the main model parameters as well as different kinds of isotherm equations including the IAS theory, the determination of pressure drop, and the effect of mass transfer. Other passages are devoted to plate numbers, height of an equivalent theoretical plate (HETP) values as well as their determination based on first and second moments and column overloading. The experienced reader may pass quickly through this chapter to recall the definitions used. For beginners this chapter is recommended in order to learn the general terminology and acquire a basic understanding. A further goal of this chapter is the harmonization of general chromatographic terms between engineers and chemists.

Chapter 3 gives a survey of packings and stationary phases. It explains the structure and specifies the properties of stationary phases such as generic and designed phases, reversed phase silicas, cross-linked organic polymers, and chiral phases and gives instructions for their maintenance and regeneration. This chapter may be used as reference for special questions and will help those looking for an overview of attributes of different stationary phases.

Chapter 4 deals with the selection of chromatographic systems, that is, the optimal combination of stationary phases and eluent or mobile phases for a given separation task. Criteria for choosing normal phase (NP), reversed phase (RP), and chiral stationary phase (CSP) systems are explained and are completed by practical recommendations. Other topics discussed are the processing of monoclonal antibodies and size exclusion. Finally, practical aspects of the overall optimization of chromatographic systems are discussed.

The selection of chromatographic systems is the most critical for process productivity and thus process economy. This step offers the biggest potential for optimization, but, on the other hand, it is also a potential source of severe errors in developing separation processes.

Chapter 5 gives an overview of process concepts available for preparative chromatography. Depending on the operating mode, several features distinguish chromatographic process concepts: batchwise or continuous feed introduction, operation in single- or multicolumn mode, elution under isocratic or gradient conditions, recycling of process streams, withdrawal of two or a multitude of fractions, integration of reaction, and separation in one process step. It finishes with guidelines for the choice of a process concept.

In Chapter 6, modeling and determination of model parameters are key aspects. "Virtual experiments" by numerical simulations can considerably reduce the time and amount of sample needed for process analysis and optimization. To reach this aim, accurate models and precise model parameters for chromatographic columns are needed. Validated models can be used predictively for optimal plant design. Other possible fields of application for

process simulation include process understanding for research purposes as well as training of personnel. This includes the discussion of different models for the column and plant peripherals.

Chapter 7 is devoted to the consistent determination of the model parameters, especially those for equilibrium isotherms. Methods of different complexity and experimental effort are presented, which allow a variation of the desired accuracy on the one hand and the time needed on the other hand. The chapter ends with a selection of different examples showing that an appropriate model combined with consistent parameters can simulate experimental data within high accuracy.

Chapter 8 focuses on process design and optimization and starts with basic principles and continues with single-column processes. Design and scaling procedures for batch as well as recycle processes are described, and a step-by-step optimization procedure is exemplified. In the case of isocratic and gradient SMB processes, rigorous process simulations combined with shortcut calculations based on the true moving bed process (TMB) model are useful tools for process optimization, which is illustrated by different examples. Further sections discuss the improvements of SMB chromatography by variable operating conditions as given by Varicol, PowerFeed, or Modicon processes and gradient operation. Comments on multicolumn systems for bioseparation are completing this chapter.

Chapter 9 starts with an introduction to standard process control and presents scientific results on theoretical online optimization of batch chromatography and model-based advanced control of SMB processes, which are compared with experimental results. Further aspects are adaptive parameter estimation and cycle control as well as control of coupled SMB processes.

Chapter 10 focuses on practical aspects concerning equipment and operation of chromatographic plants for the production and purification of fine chemicals and small pharmaceutical molecules as well as proteins and comparable biomolecules. It starts with chromatographic columns followed by chromatography systems, that is, all equipment required for production. This includes high-performance as well as low-pressure batch systems as well as continuous SMB systems, supplemented by remarks on auxiliary equipment. Further topics are detailed procedures for different methods of column packing. The section on troubleshooting might be an interesting source for practitioners. Especially for the manufacturing of biotherapeutics, special disposable technologies such as prepacked columns and single-use membrane chromatography are exemplified.

References

Broughton, D.B. and Gerhold, C.G. (1961) Continous sorption process employing fixed bed of sorbent and moving inlets and outlets, *US Patent* No. 2.985.589

FDA (2004). Guidance for industry PAT-A framework for innovative pharmaceutical development, manufacturing and quality assessment, http://www .fda.gov (accessed 03 October 2019).

Janson, J.C. and Jönsson, J.-A. (2010). *Protein Purification* (ed. J.C. Janson). Weinheim: VCH.

Tswett, M.S. (1906). Physical chemical studies on chlorophyll adsorption. *Berichte der Deutschen botanischen Gesellschaft*, 24, 316–323 (as translated and excerpted in H.M. Leicester, Source Book in Chemistry 1900–1950). Cambridge, MA: Harvard, 1968.

Unger, K., Ditz, R., Machtejevas, E., and Skudas, R. (2010). Liquid chromatography – its development and key role in life sciences applications. *Angew. Chem.* 49: 2300–2312.

Yu, L.X., Amidon, G., Khan, M.A. et al. (2014). Understanding pharmaceutical quality by design. *AAPS J.* 16 (4): 771–778.

Zobel, S., Helling, C., Ditz, R., and Strube, J. (2014). Design and operation of continuous countercurrent chromatography in biotechnological production. *Ind. Eng. Chem. Res.* 53: 9169–9185.

2

Fundamentals and General Terminology*

Andreas Seidel-Morgenstern

Otto-von-Guericke-Universität, Lehrstuhl für Chemische Verfahrenstechnik, Universitätsplatz 2, 39106 Magdeburg, Germany
Max-Planck-Institut für Dynamik komplexer technischer Systeme, Sandtorstraße 1, 39106 Magdeburg, Germany

This chapter introduces fundamental aspects and basic equations for the characterization and quantitative description of chromatographic separations. Evaluating conventional analytical separations of different compounds in a chromatographic column, the influences of void volumes, fluid dynamics, mass transfer resistances, and, in particular, distribution equilibria are explained. Important characteristics of preparative (overloaded) chromatography are highlighted, especially the concentration dependent migration behavior of substances in the nonlinear range of the adsorption isotherms. Essential differences compared to chromatography for analytical purposes (Fanali et al. 2017) are explained.

A goal of this chapter is also to contribute to the harmonization of chromatography related terms partly used differently by engineers and chemists.

2.1 Principles and Features of Chromatography

Chromatography belongs to the thermal separation processes used to separate homogeneous molecular mixtures. Performing such separations typically requires three steps (Sattler 1995):

(1) In addition to the initially homogeneous mixture phase, a second phase is generated by introduction of energy (e.g. during distillation) or an additive (e.g. during extraction or adsorption).
(2) An exchange of mass and energy occurs between the single phases. The driving force for these transport processes is a deviation from thermodynamic equilibrium.
(3) After completion of the exchange procedures, the two phases are characterized by different compositions and can be separated. Result of this phase separation is a partial separation of the initially homogeneous mixture.

*Michael Schulte and Achim Epping have contributed to the first and/or second edition.

Regarding chromatographic separation, the homogeneous mixture phase is a fluid. The additional second phase is a solid or a second immiscible fluid. The driving force for transport between the phases is the deviation of the specific compositions from the equilibrium state. A feed mixture introduced is separated by selective relative movements of the components between the two phases. Usually, the solid phase is fixed and designated accordingly as stationary phase. The fluid phase moves and is therefore called mobile phase. The chromatographic behavior is determined by the specific interactions of all single components present in the system with the mobile and stationary phases. The mixture of substances to be separated, the carrier (solvent) (which is used for dissolution and transport), and the adsorbent (stationary phase) are summarized as the chromatographic system (Figure 2.1). In laboratory practice a chromatographic system suitable to solve a given separation problem is selected by a process typically called "method development."

According to the state of aggregation of the fluid phase, chromatographic systems can be divided into several categories. If the fluid phase is gaseous, the process is called gas chromatography (GC). If the fluid phase is a liquid, the process is called liquid chromatography (LC). For a liquid kept at temperature and pressure conditions above its critical point, the process is called supercritical fluid chromatography (SFC). Thus, depending on the kind of interface between mobile and stationary phases, the following types of chromatographic systems can be distinguished:

- Gaseous mobile phases/solid stationary phases;
- Liquid mobile phases/solid stationary phases;
- Gaseous mobile phases/liquid stationary phases;
- Liquid mobile phases/liquid stationary phases;
- Supercritical mobile phases/solid stationary phases.
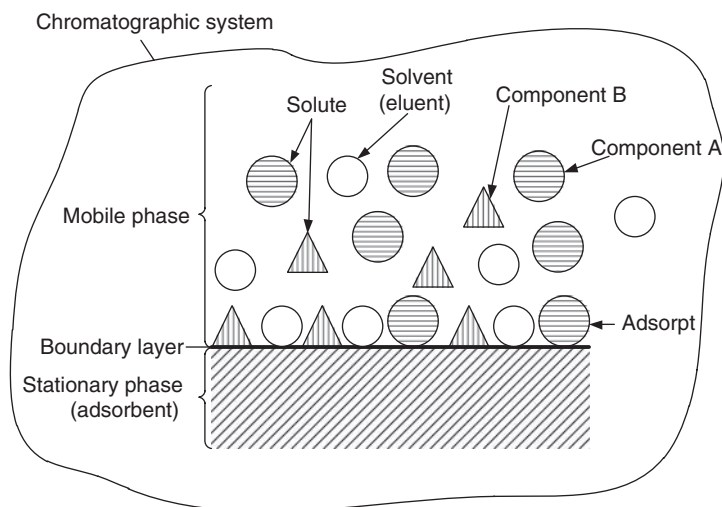
Figure 2.1 Definitions of a chromatographic system.

Examples of industrial relevance for the first two phase combinations are the adsorption of pollutants from waste air or water onto activated carbon. Combinations three and four are relevant, for example, related to foam formation and stabilization in the presence of surfactants on water/air interfaces or at the interface of two immiscible liquids (e.g. oil and water). Currently there is a renaissance of SFC in various applications with supercritical CO_2 as the mobile phase (Rossé 2019).

LC can be further divided according to the geometrical orientation of the phases. A widely used process for analytical purposes as well as rapid method development and, in some cases, even a preparative separation process is thin-layer chromatography (TLC). The adsorbent is fixed onto a support (glass, plastic, or aluminum foil) in a thin layer. The solute is placed onto the adsorbent in small circles or lines. In a closed chamber one end of the thin-layer plate is dipped into the mobile phase, which then progresses along the plate due to capillary forces. Individual substances can be visualized either by fluorescence quenching or after chemical reaction with detection reagents. Advantages of TLC are the visualization of all substances, even those sticking heavily to the adsorbent, as well as the easiness of parallel development.

In GC and LC the particles of the stationary phase are fixed into a cylinder (column chromatography) that is usually made of glass, polymer, or stainless steel. In the column the stationary phase (the adsorbent) is present as a porous or nonporous randomly arranged packing or as a monolithic block. If the columns are well packed with small particles and liquid mobile phases are used, a very successful and widely applied technique, designated as high-performance liquid chromatography (HPLC), is frequently applied.

This book deals mainly with the case most typical for preparative chromatographic separations, that is, the exploitation of solid surfaces, liquid mobile phases, and dissolved feed mixtures. Key information required for quantifying the chromatographic process is knowledge regarding equilibrium distributions of analytes between the two additional phases introduced to perform separations. Although these phase equilibria are specific for each separation mechanism, there is the possibility to describe them mathematically in a similar manner. Since most chromatographic processes exploit the principle of adsorption, i.e. specific depositions and accumulations of molecules on the surfaces of the solid stationary phases, and since there is a well-established theory of single component and multicomponent adsorption thermodynamics, the terminology and notation of adsorption is suitable to characterize and quantify preparative chromatography.

The following definitions are expedient and used below: the solid onto which adsorption occurs is defined as the adsorbent. The adsorbed molecule is defined in its free state as the adsorptive and in its adsorbed state as the adsorpt. There are typically different solutes, which are often called components (for example, A and B; Figure 2.1).

On a molecular level the adsorption process is the formation of binding forces between the surface of the adsorbent and the molecules of the fluid phase.

The binding forces can be different in nature and strength. Basically two different types of binding can be distinguished (Atkins 1990; IUPAC 1972):

(1) Physisorption or physical adsorption is a weak binding based essentially on van der Waals forces, for example, dipole, dispersion, or induction forces. These forces are weaker than the intramolecular binding forces of molecular species. Therefore, physisorbed molecules maintain their chemical identity.
(2) The stronger binding type is chemisorption or chemical adsorption. It is caused by valence forces, equivalent to chemical, mainly covalent, bindings.

Table 2.1 gives estimated values for adsorption enthalpies. In gaseous systems these enthalpies are proportional to the accessible values of the heat of vaporization h_{vap}.

As periodic chromatographic processes require complete reversibility of the adsorption step, only adsorption processes based on physisorption can be exploited. The related energies are sufficient to increase the temperature of gases due to their low volumetric heat capacities (Ruthven 1984). Fluids, however, are characterized by volumetric heat capacities $10^2–10^3$ times higher. Thus, the energies connected to adsorption processes have not much influence on the local temperatures. All of the following processes can, therefore, be considered to be approximately isothermal.

In a LC process the mobile phase is forced through a column, packed with a multitude of fixed particles of the stationary phase. Figure 2.2 illustrates the injection of a homogeneous binary mixture (components A and B represented by triangles and circles) into the system at the column inlet. Hereby the triangles represent the component B with the higher affinity to the stationary phase. Therefore, the mean adsorption time of this component on the stationary phase surface is higher than that of component A with the lower affinity (circles).

Table 2.1 Ranges of adsorption enthalpies.

Fluid phase	Physisorption	Chemisorption	Reference
Liquid phase	$<50\,kJ\,mol^{-1}$	$\geq60–450\,kJ\,mol^{-1}$	Kümmel and Worch (1990)
Gas phase	$1.5\,\Delta h_{vap}$	$2–3\,\Delta h_{vap}$	Ruthven (1984)
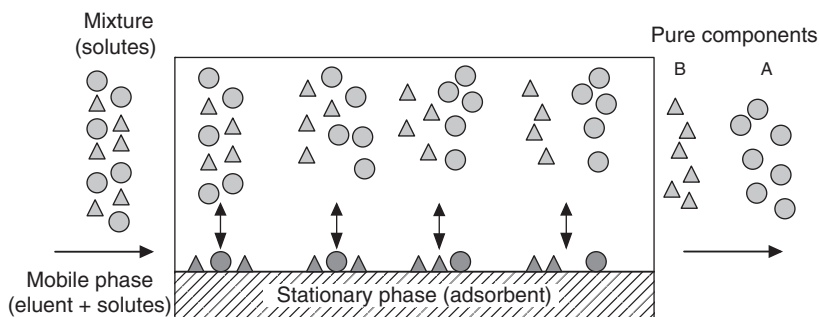
Figure 2.2 Principle of adsorption chromatography.

The difference in affinities, and thus adsorption time, results in a reduced migration speed through the column of the more adsorbed component B. This delays its arrival at the column outlet compared with the less adsorbed component A. If the process conditions are chosen well, the two substances can be completely separated and collected as pure components at the column outlet.

2.2 Analysis and Description of Chromatograms

2.2.1 Voidage and Porosity

Important information required to describe and simulate chromatograms concerns the column and particle porosities (Guiochon et al. 2006; Nicoud 2015). As illustrated in Figure 2.3, the total volume of a packed column (V_c) can be divided into two main subvolumes: the interstitial volume of the fluid phase (V_{int}) and the volume of the stationary adsorbent phase (V_{ads}) (Eq. (2.1)):

$$V_c = \pi \frac{d_c^2}{4} L_c = V_{ads} + V_{int} \tag{2.1}$$

The volume V_{ads} consists of the volume of the solid material (V_{solid}) and the volume of the pore system, V_{pore} (Eq. (2.2)):

$$V_{ads} = V_{solid} + V_{pore} \tag{2.2}$$

From these volumes, three different porosities can be calculated (Eqs. (2.3)–(2.5)):

$$\text{External (interstitial) porosity (void fraction of the column)} : \varepsilon_e = \frac{V_{int}}{V_c} \tag{2.3}$$

$$\text{Porosity of the porous solid phase (internal porosity)} : \varepsilon_p = \frac{V_{pore}}{V_{ads}} \tag{2.4}$$

$$\text{Total porosity} : \varepsilon_t = \frac{V_{int} + V_{pore}}{V_c} = \varepsilon_e + (1 - \varepsilon_e)\varepsilon_p \tag{2.5}$$

The experimental determination of these porosities is not trivial. The most common method for determining the total porosity ε_t is the injection of nonretained, pore-penetrating tracer substances (gray and small
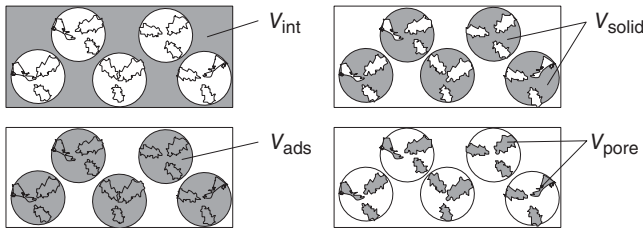
Figure 2.3 Different volumes in beds packed with porous particles.
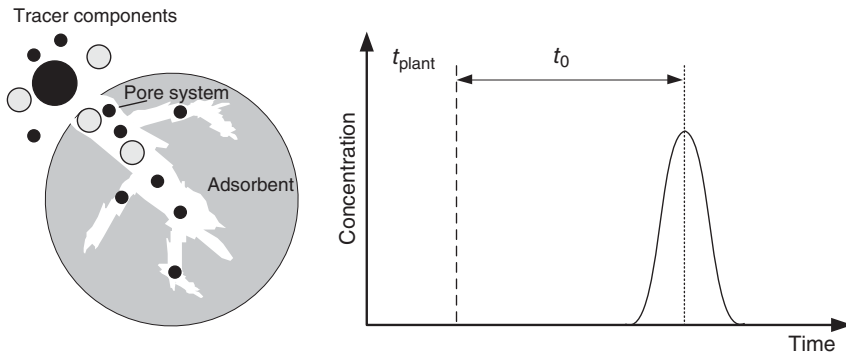
Figure 2.4 Illustration of chromatography with tracer components and the relevant retention times.

black circles in Figure 2.4). In normal phase chromatography, toluene or 1,3,5-tri-*tert*-butylbenzene is often used, while in reversed phase chromatography uracil is typically selected as the tracer component of choice.

The total retention time of a nonretained substance depends on the holdup time within the column itself, t_0, as well as on the additional holdup time in the system or plant, t_{plant}, which is, for instance, influenced by pipe lengths and diameters and pump head volumes (if the sample is introduced via a pump). The extra-column dead time of the plant has to be determined without the column to get the correct dead time of the column. From the column dead time, $t_{0,t}$, and the value of the volumetric flow rate delivered by the pump, the total porosity can be calculated according to Eq. (2.6):

$$\varepsilon_t = \frac{t_{0,t} \cdot \dot{V}}{V_c} \tag{2.6}$$

A corresponding hypothetical interstitial velocity of the mobile phase based on ε_t can be calculated with the volumetric flow rate and a hypothetically column cross section (Eq. (2.7)):

$$u_{int,hypo} = \frac{\dot{V}}{\varepsilon_t \cdot \pi \cdot (d_c^2/4)} \tag{2.7}$$

With Eqs. (2.1) and (2.6) holds

$$u_{int,hypo} = \frac{L_c}{t_{0,t}} \tag{2.8}$$

To confirm the fact that no binding occurred, tracer experiments carried out at different temperature should provide the same retention times $t_{0,t}$.

To obtain the external (interstitial) porosity of a column, ε_e, the same methodology can be used based on injecting a high molecular weight substance that is unable to penetrate into the pores (large black circles in Figure 2.4). For a non-retained and nonpenetrating molecule from the measurable dead time, $t_{0,e}$, the

external porosity and a (real) interstitial velocity u_{int} can be calculated according to Eq. (2.9):

$$\varepsilon_e = \frac{t_{0,e} \dot{V}}{V_c} \quad \text{and} \quad u_{int,e} = \frac{L_c}{t_{0,e}} \tag{2.9}$$

There are often experimental problems during the injection of high molecular weight substances. Ideal tracers should be globular and exhibit no adsorption or penetration into any pore but should still be highly mobile. Unfortunately, there is no ideal high molecular weight volume marker. Therefore, alternative methods for determining the void fraction are of interest.

If certain adsorbent parameters can be determined with high accuracy from physical measurements, porosities can also be calculated from the mass of the adsorbent m_{solid}, its density ϱ_{solid}, and the specific pore volume v_{sp} (determined, for example, by nitrogen adsorption or mercury porosimetry). The volume of the solid material follows Eq. (2.10):

$$V_{solid} = \frac{m_{solid}}{\varrho_{solid}} \tag{2.10}$$

The absolute pore volume can be obtained from Eq. (2.11):

$$V_{pore} = v_{sp} \cdot m_{solid} \tag{2.11}$$

The sum of solid volume and pore volume gives the volume of the stationary phase, which, subtracted from the column volume, leads to the interstitial volume (Eq. (2.12))

$$V_{int} = V_c - (V_{solid} + V_{pore}) \tag{2.12}$$

The void fraction can then be determined using Eq. (2.3). Subsequently, the other porosities can be obtained by Eqs. (2.4) and (2.5).

An alternative method for reliable determination of total porosities can be used for small-scale columns. As long as a column can be weighed exactly, the mass difference of the same column filled with two solvents of different densities can be used to determine the porosity. The column is first completely flushed with one solvent and then weighed; afterward, the first solvent is completely displaced by a second solvent of different density. For normal phase systems, methanol and dichloromethane can be used; for reversed phase systems, water and methanol are quite commonly employed. The volume of the solvent, representing the sum of the interstitial volume and the pore volume, is determined by Eq. (2.13):

$$V_{int} + V_{pore} = \frac{m_{s,1} - m_{s,2}}{\varrho_{s,1} - \varrho_{s,2}} \tag{2.13}$$

The total porosity can be then calculated using Eq. (2.5).

High-efficiency adsorbent particles are very often spherical and monodisperse in order to reduce pressure drops. In this case void fractions for spherical particles lie theoretically in the range $0.26 < \varepsilon_e < 0.48$, and mean values of ε_e of approximately 0.37 can be roughly applied (Brauer 1971). Particle porosities lie in the

range $0.50 < \varepsilon_p < 0.90$, meaning that 50–10% of the solid is impermeable skeleton. Total porosities are often in the range $0.65 < \varepsilon_t < 0.80$. With monolithic columns these total porosities can lie in the range $0.80 < \varepsilon_t < 0.90$. In case of large porosities, sufficient stability of the bed has to be ensured.

2.2.2 Retention Times and Capacity Factors

A chromatogram generated by injecting small (analytical) amounts of three different components into a column is illustrated in Figure 2.5. The interaction strength of each of a component i with the stationary phase is proportional to its retention time $t_{R,i}$. Instead of evaluating the retention time, it is also useful to consider the retention volume, which is obtained by multiplying $t_{R,i}$ with the corresponding volumetric flow. The first peak, which elutes at $t_{plant} + t_0$, corresponds to a nonretained component and is a source of determining the column porosity (see Section 2.2.1).

For well-packed columns symmetrical peaks should be achieved as long as the amounts injected into the column are small, restricting the concentrations to the linear range of the adsorption isotherms. In the case of symmetrical peak shapes, the retention times can be easily determined from the positions of the peak maxima. If increased amounts of substances are injected, that is, in the nonlinear range of the adsorption isotherms, the peaks are distorted and asymmetrical. In that case, a mean retention time can be calculated from the point of gravity of the peaks applying the method of moments (see Section 2.2.3)

The overall retention time $t_{R,i}$ of a retained component i is the sum of the dead time t_0 and the net retention time $t_{R,i,net}$. The net retention time represents the time during which molecules of a substance are adsorbed onto the surface of the adsorbent.

Because the retention time of a substance depends on the column geometry, the porosity, and the mobile phase flow rate, a normalization is expedient. For
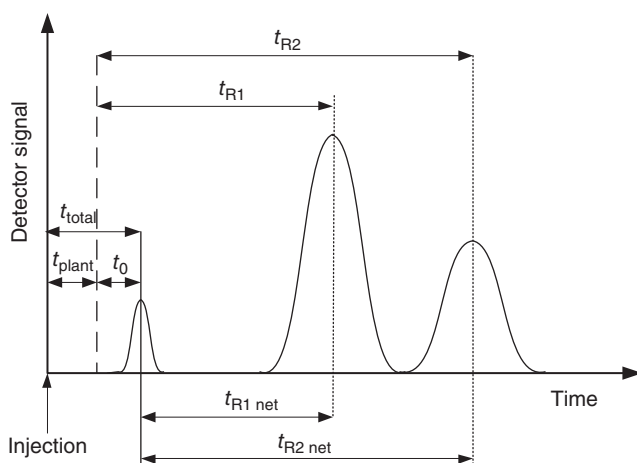
Figure 2.5 Chromatogram of one unretained and two retained components.

this the capacity factor k'_i, which is also called the retention factor, is applied. This factor is defined according to Eq. (2.14):

$$k'_i = \frac{t_{R,i} - t_0}{t_0} \tag{2.14}$$

Both the capacity factor and the net retention time depend on the nature of the tracer substance, which is used to determine t_0. Therefore, for different components only k'_i values that are based on experiments with the same tracer substance should be directly compared.

Chromatographic processes aim to separate dissolved components. Therefore, the distance between the peak maxima of two neighboring is of large importance. A selectivity α of a separation of two components i and j can be used to quantify based on the two capacity factors

$$\alpha = \frac{k'_j}{k'_i} = \frac{t_{R,j} - t_0}{t_{R,i} - t_0} \tag{2.15}$$

Hereby, by convention, the capacity factor of the more retained component is placed in the numerator. Thus, the selectivity of two separated components is always >1. The selectivity is also called separation factor.

The retention times and the capacity factors contain thermodynamic information regarding the distribution equilibria of the solutes between the mobile and stationary phases. These equilibria are typically described by adsorption isotherms, which quantify the correlations between the loadings of the solute on the adsorbent, q_i, as a function of the corresponding fluid-phase concentrations, c_i, at a given constant temperature. Single-component and competitive adsorption isotherms are discussed in more detail in Section 2.4.

2.2.3 Efficiency of Chromatographic Separations

The positions and shapes of chromatograms are influenced, besides the thermodynamics of the distribution of the components between the two phases, by several other factors, in particular by the fluid dynamics inside the packed bed and the rate of the mass transfer in and around the particles. The incorporation of these phenomena can be performed using discrete equilibrium stage models or continuous models as explained in Chapter 6.

One instructive key parameter indicating the performance of a chromatographic separation is widely used in analytical chromatography. This is the number of equilibrium stages (or plates), N, which is an indicator for the column efficiency. Due to the fact that knowledge regarding the specific plate number of a column captures deviations from ideal behavior and provides several important parameters of mathematical models, it is also an important quantity in preparative chromatography. The plate number N is directly equivalent to a corresponding height of a theoretical plate (*HETP*) considering the column length (Eq. (2.16)):

$$HETP = \frac{L_c}{N} \tag{2.16}$$

The plate numbers N and *HETP* values contain various contributions due to fluid dynamics, mass transfer resistances, and rates of adsorption and desorption steps, which all cause undesired band broadening. The larger the plate number or the smaller the plate height, that is, the higher the efficiency, the narrower the peaks. Narrow peaks are attractive since they result in a good peak resolution, small elution volumes, and thus higher outlet concentrations, all favorable conditions for preparative applications of chromatography. However, due to limited rates of mass transfer and nonidealities of fluid dynamics, real columns are characterized by limited efficiencies.

An estimation of the column efficiency can be easily performed by determining from a peak recorded at the column outlet the corresponding first normalized initial moment, μ'_1, and the second normalized central moments, μ_2. For such estimations small amounts of retained test components are injected. The two moments, which indicate the mean residence time, $t_{R,\,mean}$, and the variance of the peak, σ^2, can be calculated with Eqs. (2.17) and (2.18):

$$\mu'_1 = \frac{\int_0^\infty t^1 \cdot c(t) \cdot \mathrm{d}t}{\int_0^\infty c(t) \cdot \mathrm{d}t} = t_{R,\mathrm{mean}} \tag{2.17}$$

$$\mu_2 = \frac{\int_0^\infty (t - \mu'_1)^2 \cdot c(t) \cdot \mathrm{d}t}{\int_0^\infty c(t) \cdot \mathrm{d}t} = \sigma^2 \tag{2.18}$$

The number of plates is related to these two moments according to Eq. (2.19):

$$N = \frac{(\mu'_1)^2}{\mu_2} = \frac{t_{R,\mathrm{mean}}^{\,2}}{\sigma^2} \tag{2.19}$$

For highly efficient columns rather symmetrical peaks are detected. Then the mean retention time of the chromatogram can be easily estimated from the retention time corresponding to the peak maximum, $t_{R,\,max}$. Furthermore, assuming that the peak can be described by a Gaussian distribution, there are several options for an easy estimation of the variance. Figure 2.6 illustrates the possibilities to evaluate the temporal peak width at various peak heights. The most widely used simple option is to determine the width at half height of the measured peak, $w_{1/2}$, which corresponds to $2.354\,\sigma$. This results in the widely used approximation (Eq. (2.20)):

$$N \approx 5.54 \left(\frac{t_{R,\mathrm{max}}}{w_{1/2}} \right)^2 \tag{2.20}$$

In a similar manner holds Eq. (2.38) if the variance is taken from an analysis of the two inflection points (ip$_1$ and ip$_2$ in Figure 2.6):

$$N \approx 16 \left(\frac{t_{R,\mathrm{max}}}{w} \right)^2 \tag{2.21}$$

An aspect limiting the applicability of the plate numbers to predict chromatograms is the fact that the results are typically different for different components.

A characterization of asymmetrical peaks requires more parameters connected to the third- and higher-order moments (Bidlingmeyer and Waren 1984).
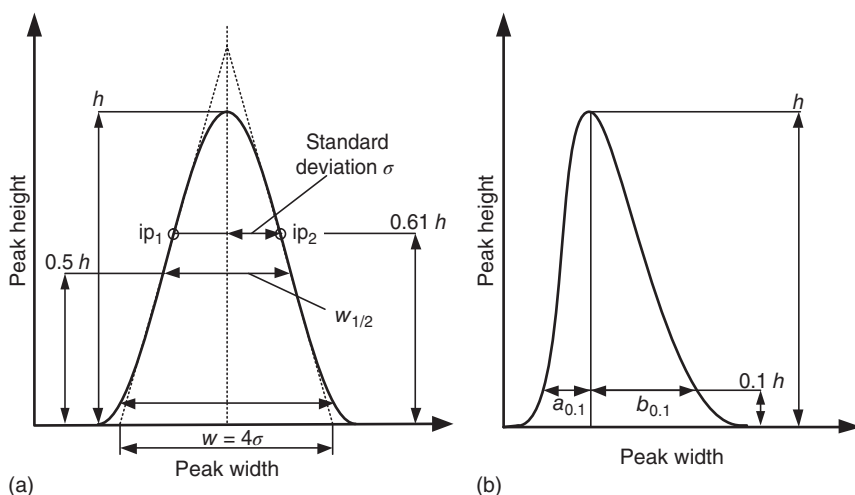
Figure 2.6 Determination of variance for Gaussian peaks (a) and estimation of asymmetry (b).

A simple empirically derived equation has been introduced to quantify the degree of peak asymmetry T by evaluating the difference between the two peak halves at 1/10th of the peak height (Figure 2.6, Eq. (2.22)):

$$T = \frac{b_{0.1}}{a_{0.1}} \tag{2.22}$$

Another calculation method to evaluate peak asymmetry can be found in the different pharmacopoeias, for example, United States Pharmacopeia (USP) or Pharmacopoeia Europaea (PhEUR). These pharmacopoeias calculate peak tailing from an analysis at 5% of the peak height (Eq. (2.23)):

$$T_{USP} = \frac{a_{0.05} + b_{0.05}}{2 \cdot a_{0.05}} \tag{2.23}$$

Since the efficiency is a central characteristic quantity of a chromatographic system, there have been numerous attempts to describe it in more detail in order to find options for enhancing it. Of particular interest is to quantify the influence of the mobile phase velocity, which determines the time needed for the separation, on different band broadening parameters and, thus, on the overall efficiency. An important contribution in this area is the derivation of the van Deemter equation (Van Deemter, Zuiderweg, and Klinkenberg 1956) (Eq. (2.24))

$$HETP = A + \frac{B}{u_{int}} + Cu_{int} \tag{2.24}$$

The three terms of Eq. (2.24) describe different effects that have to be taken into account when selecting a combination of stationary and mobile phases in preparative chromatography and the operating conditions (Figure 2.7).

The A term, which is almost constant over the whole velocity range, is mainly governed by eddy diffusion. It results from packing imperfections as well as adsorbents with very broad particle size distributions. The absolute value of the A term is proportional to the mean particle diameter. The plate height can therefore be decreased by using smaller particles.
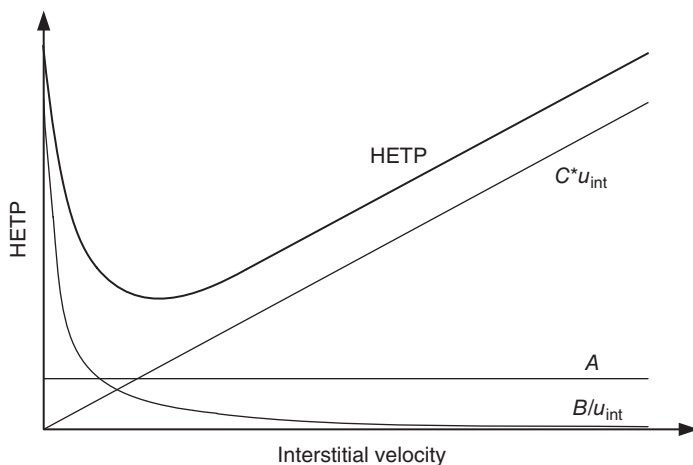
Figure 2.7 Dependence of *HETP* on interstitial phase velocity.

The hyperbolic *B* term expresses the influence of backmixing due to axial diffusion of the solute molecules in the fluid phase. In preparative chromatography, it is typically only relevant for large adsorbent particles operated at low flow rates. In most cases of preparative chromatography, it can be neglected, as the velocities of the mobile phase are sufficiently large. As the longitudinal diffusion depends on the diffusion coefficient of the solute, it can be influenced by changing the mobile phase composition. To achieve higher diffusion coefficients, low viscosity solvents should be preferred, which will, in addition, result in also desired lower column pressure drops.

The linear increase of the plate height at higher velocities is captured by the *C* term. It is caused by the increasing influence of increasingly relevant mass transfer resistances. Mass transfer resistances inside the pores cannot be reduced by increasing the fluid velocity. Their relative contribution to overall band broadening increases linearly with an increase of the flow velocity. The slope of the *C* term depends on the nature of the packing material. The more optimized an adsorbent is in terms of pore accessibility and minimal diffusion path lengths, the lower the contribution of the *C* term and the higher the column efficiency at high mobile phase velocities.

It should be mentioned that in addition to Eq. (2.24), several more sophisticated plate height equations have been suggested, for instance, by Knox (2002).

2.2.4 Resolution

In analytical chromatography, it is possible to deconvolute overlapping peaks and to obtain even quantitative information from nonresolved peaks. Preparative chromatography often requires complete peak resolution if the components of interest are to be isolated with 100% purity and yield.

Chromatographic resolution R_S is a simple measure of how well two adjacent peaks of similar area are separated. It is mostly defined as (Eq. (2.25))

$$R_S = \frac{2 \cdot (t_{R,j} - t_{R,i})}{w_i + w_j} \tag{2.25}$$

where $t_{R,j}$ and $t_{R,i}$ are the retention times of the two neighboring components j and i, of which component i elutes first ($t_{R,j} > t_{R,i}$), and w_j and w_i are the peak widths for components j and i ($w = 4\sigma$; see Figure 2.6). A resolution of 1.5 corresponds to a baseline separation at touching band situation. At a resolution of 1.0, there is still an overlap of 3% of the peaks.

The assumption of equivalent peaks, where the peak width is the same for both components, leads to the following connection with the capacity factors k', the separation factor α, and the plate number N:

$$R_S = \left(\frac{\alpha - 1}{\alpha} \right) \left(\frac{k'_j}{k'_j + 1} \right) \frac{\sqrt{N_j}}{4} \tag{2.26}$$

Note that the index j belongs to the component with the longer retention time. The equivalent expression for resolution based on the less retained component i is

$$R_S = (\alpha - 1) \left(\frac{k'_i}{k'_i + 1} \right) \frac{\sqrt{N_i}}{4} \tag{2.27}$$

In theory, the above equations offer three possibilities for increasing the resolution. Increasing the capacity factor k' is only of limited use because it is linked to a higher retention time and, thus, to an increase of the cycle time that reduces the productivity. This leads not only to lower throughput but also to more band broadening and reduced column efficiency.

The two more attractive options for resolution optimization are illustrated in Figure 2.8. Figure 2.8a shows a separation of two peaks corresponding to a resolution factor of $R_S = 0.9$. The column efficiency is given by a "length related plate number," $N_L = N/L_c$, of 1000 m^{-1}, while the selectivity α is equal to 1.5. The first approach optimizes the column fluid dynamics, for example, by improving the column packing quality, reducing the particle diameter of the adsorbent, or optimizing the mobile phase flow rate. The resulting chromatogram is shown in Figure 2.8b. The resolution has been increased to $R_S = 1.5$ essentially due to the higher plate number of 2000 N m^{-1}. Applying the same adsorbent and mobile phase, the selectivity remains at 1.5. Conversely, the system thermodynamics can be changed by optimizing the temperature or altering the chromatographic system by changing the mobile phase and/or the adsorbent. Figure 2.8c shows the effect of this "thermodynamic" approach. The length related plate number is still 1000 m^{-1}, but the selectivity has increased to 2.0, resulting in an increased resolution of also 1.5.

The above two optimization approaches have different effects on the cost of preparative chromatography. Efficiency is increased by decreasing the particle diameter of the stationary phase. However, then the costs of the phases rapidly increase, along with the costs of the equipment, which needs to provide higher pressures for operation with smaller particle diameters. Therefore, it is advantageous looking for systems with optimized selectivities (Chapter 4).

With Eqs. (2.26) and (2.27), it is also possible to calculate the plate number necessary for a given resolution (Eq. (2.28)):

$$N = 16 \cdot R_S^2 \left(\frac{\alpha}{\alpha - 1} \right)^2 \left(\frac{1 + k'_j}{k'_j} \right)^2 \tag{2.28}$$
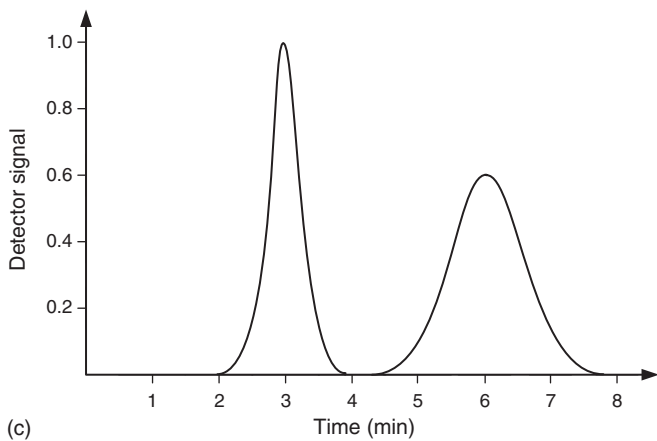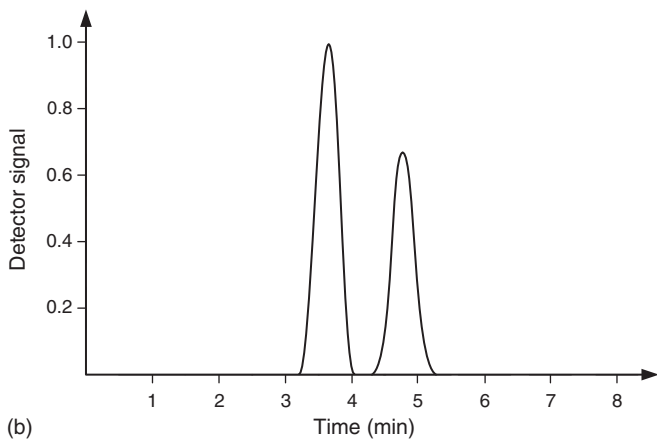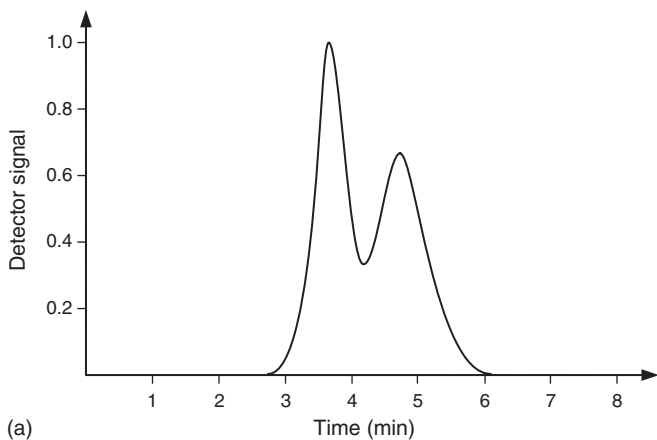
Figure 2.8 Optimization of peak resolution. (a) Base case. (b) Improved efficiency due to smaller particles. (c) More selective chromatographic system.
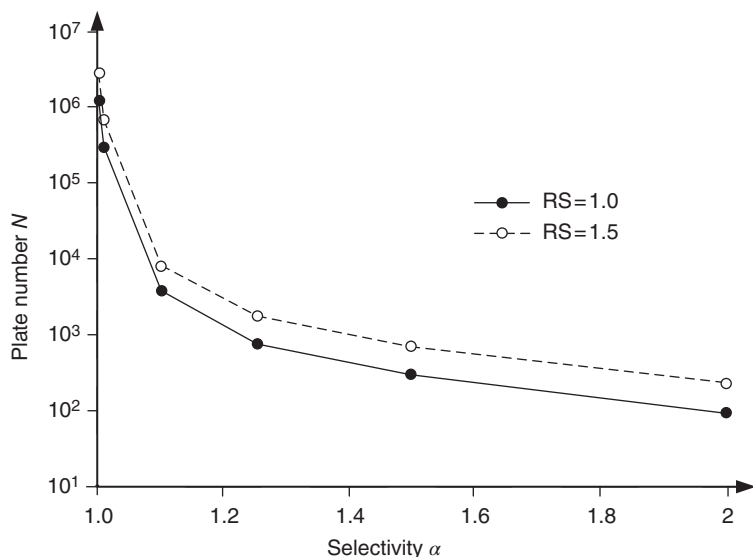
Figure 2.9 Influence of selectivity on efficiency for two different resolutions R_s (Eq. (2.28)).

Figure 2.9 shows the necessary plate numbers for two values of the resolution (1.5 and 1.0) versus the selectivity. For separation systems with selectivities <1.2, the necessary plate numbers are very high. As higher plate numbers are linked to high pressure systems with small particles, these separations obviously cause higher costs compared with separations that can exploit higher selectivities. This emphasizes that rigorous screening for the most selective separation system is necessary.

Another important parameter in preparative chromatography is the pressure drop, which should be minimized to allow applying larger flowrate.

2.2.5 Pressure Drop

In chemical engineering the Ergun equation (Eq. (2.29)) is well known for the estimation of friction numbers and corresponding pressure drops for fixed beds with granular particles. It covers a broad range from fine particles to coarse materials (Brauer 1971):

$$\psi = \frac{150}{Re} + 1.75 \tag{2.29}$$

For chromatographic columns, small more or less spherical particles are used. Therefore, the Reynolds numbers are very small and inertial forces can be neglected. The right-hand side of Eq. (2.29) then reduces to its first term, capturing the pressure drop due to viscous forces only. The friction number is connected with the pressure drop as expressed by (Eq. (2.30))

$$\psi = \frac{\varepsilon_e^3}{(1 - \varepsilon_e)^2} \frac{\Delta p}{\varrho u_0^2} \frac{d_p}{L_c} \tag{2.30}$$

where u_0 is the velocity in the empty column (superficial velocity) (Eq. (2.31)):

$$u_0 = \frac{\dot{V}}{A_c} = \frac{\dot{V}}{\pi d_c^2/4} = \varepsilon_e \cdot u_{int} \tag{2.31}$$

Substituting Eq. (2.30) in Eq. (2.29) leads to Eq. (2.32):

$$\Delta p = 150 \frac{(1 - \varepsilon_e)^2}{\varepsilon_e^3} \frac{\eta u_0 L_c}{d_p^2} \tag{2.32}$$

This equation corresponds to the well-known Darcy law (Eq. (2.33)) (Guiochon, Golshan-Shirazi, and Katti 1994):

$$\Delta p = \frac{1}{k_0} \frac{\eta u_0 L_c}{d_p^2} \tag{2.33}$$

The key coefficient k_0 captures the specific situation in the column:

$$k_0 = \frac{\varepsilon_e^3}{150 \cdot (1 - \varepsilon_e)^2} \tag{2.34}$$

This coefficient typically lies between 0.5×10^{-3} and 2×10^{-3}. For example, when the external void fraction is 0.4, it results in a corresponding value of 1.2×10^{-3}. If more precise values are required, k_0 has to be measured for a given packing.

Another parameter derived from Darcy's equation, which is often used to characterize a column, is the column permeability B (Eq. (2.35)):

$$B = \frac{\eta u_0 L_c}{\Delta p} \tag{2.35}$$

Comparing Eqs. (2.33) and (2.35), the permeability is related to k_0 by

$$B = k_0 \cdot d_p^2 \tag{2.36}$$

Pressure drop measurements are used to check the stability of a column bed as a function of eluent flow rate. Deviations from linearity at ascending and descending flow rates serve as a strong indication of irreversible changes in the column bed. It is also important to notice the linear dependency between pressure drop and viscosity. The pressure drop for high-performance columns may exceed 100 bar. Therefore, the viscosity is also an important criterion in selecting the eluent. To pack column beds properly, a liquid with low viscosity has to be chosen. If ethanol, for instance, is the eluent, methanol may be used for the packing procedure as its viscosity is 1.9 times lower. It has to be considered that alcohol/water mixtures do not exhibit a linear composition/viscosity relationship. Details can be found in Figure 4.7 for methanol, ethanol, *n*-propanol, and acetonitrile. Equation (2.32) indicates the influence of the void fraction on the pressure drop. For particles with varying diameters, the void fraction of the column can decrease tremendously. Therefore, the span of the particle size distribution for chromatographic adsorbents should be chosen in the narrow range between 1.7 and 2.5 for analytical columns (Section 3.6.3). For preparative columns, packed frequently with 10–20 µm particles, the distribution can be much broader or even bimodal.

2.3 Mass Transfer and Fluid Dynamics

Preparative and production-scale chromatographic separations should typically provide target components as highly concentrated as possible. A hypothetical ideal case would be a rectangular outlet profile with the same width as the pulse injected into the column. This behavior cannot be achieved in reality. In every chromatographic system, nonidealities of fluid distribution occur, resulting in broadenings of the residence time distributions of the solutes (increased variances σ^2). Hydrodynamic effects that contribute to the total band broadening are frequently captured in an axial dispersion term. Figure 2.10 illustrates the effect of the axial dispersion. Further band broadening can result from finite rates of adsorption and desorption and mass transfer resistances.

Figure 2.10 illustrates how rectangular pulse introduced at the column inlet ($x = 0$) is symmetrically broadened as it travels along the column. As a consequence of this broadening, the maximum concentration of the solute decreases. This causes an unfavorable dilution of the target component fraction.

Main factors that influence axial dispersion are discussed below.

2.3.1 Principles of Mass Transfer

Most chromatographic production systems use particulate adsorbents with specific pore structures that provide higher loadabilities compared with nonporous adsorbents. Adsorption of the target molecules on the inner surface of a particle has a significant influence on the efficiency of a preparative separation. Regarding mass transfer, several factors that contribute to band broadening can be distinguished Figure 2.11), namely:

- Convective and diffusive transport toward the particles;
- Film diffusion in the laminar boundary layer around the particles;
- Pore (a) and surface (b) diffusion in the particles;
- Kinetics of the actual adsorption and desorption steps.

Individual adsorbent particles within a packed bed are surrounded by a boundary layer, which is looked upon as a stagnant liquid film of the fluid phase. The thickness of the film depends on the fluid distribution in the bulk phase of the packed bed. Molecular transport toward the boundary layer of the particle by convection or diffusion is the first step (1) of the separation process.

Figure 2.10 Band broadening in a column due to axial dispersion.
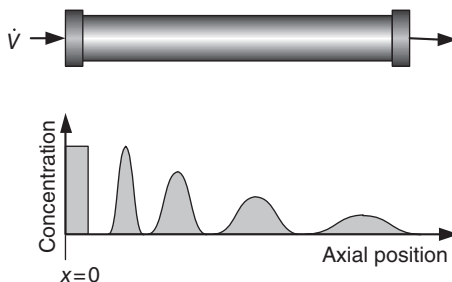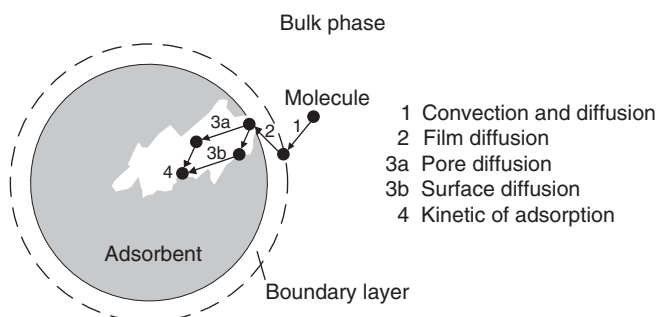
Figure 2.11 Mass transfer phenomena during the adsorption of a molecule.

The second relevant step is diffusive transport of the solute molecule through the film layer, which is called film diffusion (2). Transport of the solute molecules toward the adsorption centers inside the pore system of the adsorbent particles is the third step of the adsorption process. This step can follow two different transport mechanisms, which can occur separately or parallel to each other: pore diffusion (3a) and surface diffusion (3b).

If mass transport occurs by surface diffusion (3b), a solute molecule is adsorbed and transported deeper into the pore system by movement along the pore surface. During the whole transport process, molecules are within the attraction forces of the adsorbent surface. Notably, the attractive forces between the surface and adsorbed molecules are often so strong that, for many common adsorpt–adsorbent systems encountered in preparative chromatography, surface diffusion is not very relevant (Ruthven 1984).

Pore diffusion (3a) is driven by restricted Fickian diffusion of the solute molecules within the free pore volume. During the transport process, the solute molecules are outside the attraction forces of the adsorbent surface.

Once a solute molecule reaches a free adsorption site on the surface, actual adsorption takes place (4). If the adsorption processes (1–4) are slow compared with the convective fluid flow through the packed bed, the eluted peaks show a nonsymmetrical band broadening. Severe tailing can be observed, due to the slower movement of those solute molecules, which penetrate deeper into the pore system.

External mass transfer (1) and kinetics of adsorption (4) are normally comparatively fast in the fluid phase (Ruthven 1984; Guiochon et al. 2006). Rate-limiting processes are typically the film diffusion (2) and the transport inside the pore system (3a, 3b).

For particle diameters >5 μm, which are applied in most preparative chromatographic separations, transport resistances within the pore are the dominant contribution to the total mass transfer resistance (Ludemann-Hombourger, Bailly, and Nicoud 2000a,b).

The transport factors described above are influenced by the morphology of the adsorbent particles as well as by their surface chemistry. Pore sizes influence chromatographic properties in two main ways. The first effect is due to steric hindrance. Molecules can only penetrate into pores of sizes above a certain threshold. For bigger molecules the theoretically available surface area is only

partly accessible. The second factor is related to pore size distributions. Because transport within a mesoporous system is diffusive, band broadening increases dramatically when pores with large differences in sizes are present within an adsorbent backbone. This is due to the fact that molecules in the larger pores have a shorter residence time than molecules adsorbed in the smaller pores.

Within an ideal adsorbent all adsorption sites should be equal and accessible within short distances, thus keeping diffusion pathways short. This prerequisite favors that all pores should be of equal size, that no deep dead-end pores are present, and that the accessibility of the pores from the region of convective flow within a packed bed should be equal for all pores.

The abovementioned factors indicate that ideal chromatographic adsorbents would exhibit high surface areas but moderate pore volumes and pore sizes (which are large enough to ensure good accessibility for the adsorptive molecules), as these three physical parameters are interlinked. They cannot be independently adjusted. Their interdependence is summarized in the Wheeler equation, which assumes constant pore diameters within the particle. In Eq. (2.37), d_{pore} is the pore diameter (nm), V_{pore} the pore volume (ml g^{-1}), and S_{BET} the specific surface area (m^2 g^{-1}):

$$d_{\text{pore}} = 4000 \frac{V_{\text{pore}}}{S_{\text{BET}}} \tag{2.37}$$

The design of an adsorbent for preparative chromatography is always a compromise between a high surface area (with good loadability and limited mechanical strength) and a high mechanical strength (with reduced surface area). It should be noted that, due to the impact on intraparticle diffusivity, the sizes of the pores affect the efficiency via the C term of the van Deemter given above (Eq. (2.24)).

2.3.2 Fluid Distribution in the Column

Critical points for axial dispersion in column chromatography are the fluid distribution at the column head and the fluid collection at the column outlet (Section 10.3.2.2). Especially with large-diameter columns, these effects have to be carefully considered. Fluid distribution in the column head is widely driven by the pressure drop of the packed bed, which forces the sample to be radially distributed within the inlet frit. It is, therefore, important to use high-quality frits, which ensure an equal radial fluid distribution. In low-pressure chromatography with large dimensions, as well as with new types of adsorbents, such as monolithic packings, which exhibit much lower pressure drops, the fluid distribution is of even greater importance. Several approaches to optimize the distribution have been made by column manufacturers to overcome this problem of low-pressure flow distribution. The introduction of specially designed fluid distributors has greatly improved the situation (Section 10.3.2.2).

The reasons for nonidealities in fluid distribution can be divided into macroscopic, mesoscopic, and microscopic effects (Tsotsas 1987). The different effects are illustrated in Figure 2.12.

Microscopic fluid distribution nonideality is caused by fluid dynamic adhesion between the fluid and the adsorbent particle inside the microscopic channels of the packed bed. Adhesion results in a higher fluid velocity in the middle of
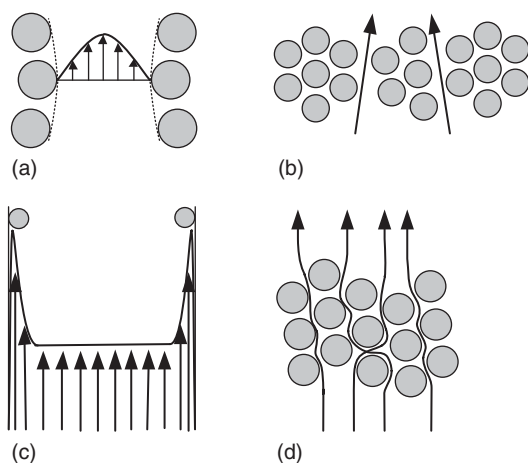
Figure 2.12 Fluid distribution nonidealities according to Tsotsas (1987). (a) Microscopic, (b) mesoscopic, (c) macroscopic, and (d) eddy diffusion. Source: Tsotsas (1987). Reproduced with permission of Elsevier.

the channel compared to regions close to the solid surface (Figure 2.12a). Solute molecules in the middle of the channel thus have a shorter retention time than those at the channel walls.

Local inhomogeneities of the voidage are a second source of broadening the mean residence time distribution. For small particles, the formation of particle agglomerates, which cannot be penetrated by the fluid, is another reason for axial dispersion. Figure 2.12b illustrates this mesoscopic fluid distribution nonideality. This effect results in local differences in fluid velocity and differences in path length of the solute molecules traveling straight through the particle agglomerates compared with those molecules moving around the particle aggregates. The second effect is also known as eddy diffusion (Figure 2.12d). Due to its similar origin, this statistical phenomenon is related to mesoscopic fluid dynamic nonidealities.

Macroscopic fluid distribution nonidealities are caused by local nonuniformities of the void space between the particles, which might occur especially in the wall region (Figure 2.12c).

All the abovementioned effects cause an increase of the peak width and contribute, besides mass transfer resistances discussed below, to total band broadening.

2.3.3 Packing Nonidealities

The packed bed of a chromatographic column will never attain optimum hexagonal dense packing due to the presence of imperfections. Those imperfections can be divided into effects due to the packing procedure and influences from the packing material. During the packing procedure several phenomena occur. The two most important are wall effects and particle bridges. Knox, Laird, and Raven (1976) determined a layer of about $30d_p$ thicknesses where wall effects influence the column efficiency. Therefore, attention has to be paid to this effect with small-diameter columns. The larger the column diameter, the less severe this effect. The second reason why imperfect packing may occur in columns is

inappropriate packing procedures. If the particles cannot arrange themselves optimally during the packing process, they will form bridges, which can only be destroyed by immense axial pressure, with the danger of damaging the particles. One way to reduce particle bridging is to pack the column by vacuum and, afterward, by axial compression of the settled bed. For more details, see Section 10.5.

Insufficient bed compression, which leads to void volumes at the column inlet, is another source of axial dispersion. Preparative columns therefore benefit from possibilities to compress the packed bed.

2.3.4 Extra-Column Effects

Every extra-column volume sitting in connecting pipes as well as any detector located between the point of solute injection and the point of fraction withdrawal contributes to the axial dispersion of the samples and thus decreases the analyte concentrations and separation efficiencies. Obviously, the length of connecting lines should be minimized. Critical are smooth connections of tubing and column, avoiding any dead space where fluid and, especially, sample can accumulate. The tubing diameter depends on the flow rate of the system and has to be chosen in accordance with the system pressure. The tubing should contribute as little as possible to the system pressure drop, without adding additional holdup volumes.

2.4 Equilibrium Thermodynamics

2.4.1 Definition of Isotherms

The most important difference between analytical and preparative chromatography is the extension of the working range into the nonlinear region of the adsorption isotherms. Therefore, the behavior of single components as well as their mixtures has to be known over a wide concentration range.

As with any other phase equilibrium, the adsorption equilibrium is defined by the equality of the chemical potentials of all interacting components in all phases. A more detailed description of the thermodynamic fundamentals can be found in the literature (Ruthven 1984; Guiochon et al. 2006).

Knowledge regarding the amount adsorbed on a solid surface is of key relevance to quantify chromatographic processes. The surface concentration can be defined as the quotient of the adsorbed amount of substance and the surface of the adsorbent in $mol\,m^{-2}$ or $g\,m^{-2}$. However, internal surface areas of adsorbent are difficult to specify because they depend on the nature and size of the solutes. It is therefore advisable to refer instead to the mass or the volume of the adsorbent. The loading is then expressed as $mol\,g^{-1}$ (or $g\,g^{-1}$) or $mol\,l^{-1}$ ($g\,l^{-1}$). As discussed above, the adsorbent volume can be in an equivalent way expressed as total adsorbent volume, V_{ads}, or as solid adsorbent volume, $V_{solid} = V_{ads} - V_{pore}$ (Eq. (2.2)). In Eq. (2.38) $c_{p,i}$ represents the concentration of component i within the fluid present in the pores. The total amount of a component i adsorbed can be expressed by a loading q_i^*. This loading can be divided respecting the internal porosity ε_P and into two storages with the

concentration of the fluid phase in the pores, $c_{p,i}$, and a corresponding solid phase loading related to the solid skeleton, q_i:

$$q_i^* = \varepsilon_p \cdot c_{P,i} + (1 - \varepsilon_p) \cdot q_i \tag{2.38}$$

The dependencies of equilibrium loadings q_i on the concentrations of the solute in the fluid phase surrounding the adsorbent particles at constant temperature are called the adsorption isotherms. In equilibrium the fluid-phase concentrations in the pores and in the fluid surrounding the adsorbent particles are identical, i.e. $c_i = c_{P,i}$.

In a broad literature (e.g. Brunauer, Emmett, and Teller 1938; Giles, Smith, and Huitson 1974; Kümmel and Worch 1990), different types of possible courses of adsorption isotherms are reported. In Figure 2.13 depicted are typical courses $q_i(c_i)$.

In contrast to well-developed thermodynamic methods for determining and correlating gas/liquid equilibria, the reliable theoretical prediction of adsorption isotherms is not yet state of the art. A few approaches for determining multicomponent isotherms from experimentally determined single-component
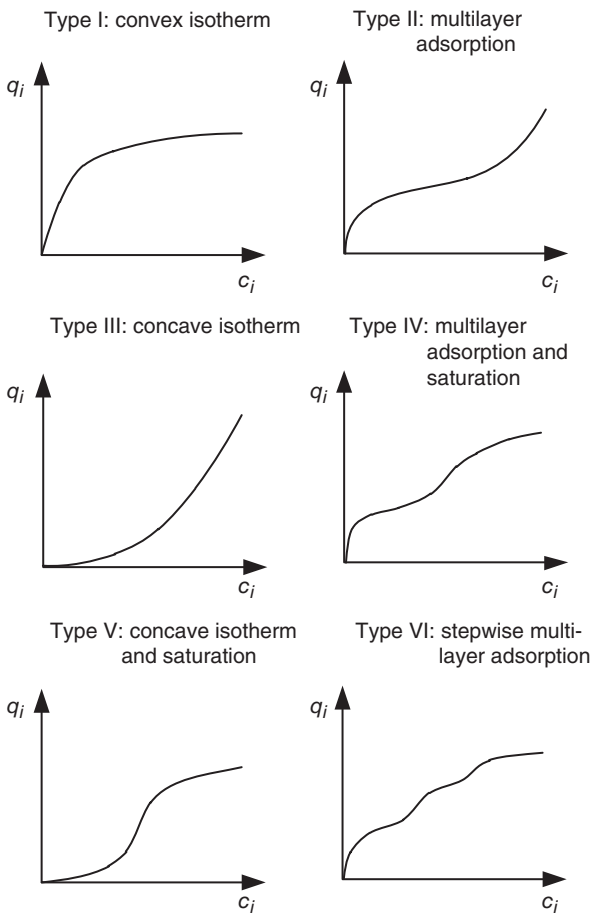
Figure 2.13 Different types of courses of adsorption isotherms.

isotherms are known (see Section 2.4.2.3). Careful experimental determination of the single-component adsorption isotherms is therefore necessary. Different approaches for isotherm determination are discussed in Section 7.5.

2.4.2 Models of Isotherms

For modeling and simulation of preparative chromatography, experimentally determined adsorption equilibrium data have to be represented by suitable mathematical equations. From the literature, a multitude of different isotherm equations is known. Many of these equations are derived from equations developed for gas-phase adsorption. Detailed literature can be found, for example, in the textbooks of Guiochon et al. (2006), Everett (1984), and Ruthven (1984) or articles of Bellot and Condoret (1993), Seidel-Morgenstern and Nicoud (1996), and Seidel-Morgenstern (2004).

Isotherm models have to be divided into single-component and multicomponent models. Because most of the multicomponent models are directly derived from single-component models, the latter will be presented first.

2.4.2.1 Single-Component Isotherms

Figure 2.14 illustrates the course of a single-component adsorption isotherm of the type described and quantified by Langmuir in 1918. This is the most common type, which describes many situations encountered in preparative chromatography. Increasing the concentration of the solute in the mobile phase above certain limits does not anymore cause an increase of the amount adsorbed onto the stationary phase. Only in the very first low mobile phase concentration region there is a linear relationship. This region is used for quantitative analysis in analytical chromatography, because only in this region it is ensured that no retention time shifts take place if different amounts are injected.

In the initially linear range of the adsorption isotherm, the relationship between the mobile and stationary phase concentrations c and q is expressed by Eq. (2.39):

$$q = H \cdot c \tag{2.39}$$

Figure 2.14 Single-component Langmuir isotherm.
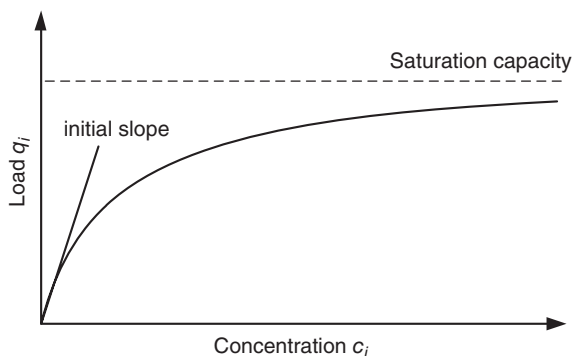
There is a direct link between the Henry coefficient H, the total porosity, and the corresponding capacity factor, which can be determined from the measured retention time of a substance and the column dead time (see Eq. (2.73)):

$$H = k' \frac{\varepsilon_t}{1 - \varepsilon_t} = \frac{t_R - t_{0,t}}{t_{0,t}} \frac{\varepsilon_t}{1 - \varepsilon_t} \tag{2.40}$$

The higher the Henry coefficient for a substance, the longer its retention time under analytical conditions. For two components to be separated, their Henry coefficients have to differ sufficiently. According to Eqs. (2.15) and (2.40), also the ratio of the Henry coefficients specifies the selectivity of a separation system:

$$\alpha = \frac{H_j}{H_i} \tag{2.41}$$

Figure 2.15 illustrates the isotherms of two different components and their Henry coefficients.

The Langmuir isotherm model is represented by Eq. (2.42). The following assumptions are the theoretical basis of Langmuir-type isotherms:

- All adsorption sites are considered energetically equal (homogeneous surface).
- Each adsorption site can only adsorb one solute molecule.
- Only a single layer of adsorbed solute molecules can be formed.
- There are no lateral interferences between the adsorbed molecules:

$$q = q_{sat} \cdot \frac{b \cdot c}{1 + b \cdot c} = \frac{H \cdot c}{1 + b \cdot c} \tag{2.42}$$

In the above q_{sat} is the saturation capacity of the monolayer, and the parameter b quantifies the adsorption energy:

$$b = \frac{H}{q_{sat}} \tag{2.43}$$

Experimental data can be often fitted more precisely to an adsorption isotherm model when an additional linear term is introduced that covers the nonspecific
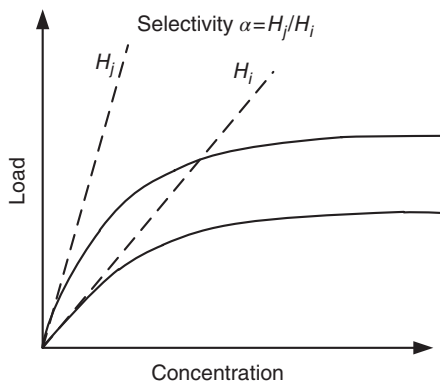
Figure 2.15 Initial slopes of the isotherms for two different components.

adsorption of the solute to the adsorbent. This modifies the single-component Langmuir isotherm (Eq. (2.44)) (Seidel-Morgenstern 2004)

$$q = \lambda \cdot c + q_{sat} \frac{b \cdot c}{1 + b \cdot c} = \lambda \cdot c + \frac{H \cdot c}{1 + b \cdot c} \tag{2.44}$$

An even more flexible equation is given by the bi-Langmuir isotherm (Graham 1953) (Eq. (2.45))

$$q = q_{sat,1} \frac{b_1 \cdot c}{1 + b_1 \cdot c} + q_{sat,2} \frac{b_2 \cdot c}{1 + b_2 \cdot c} = \frac{H_1 \cdot c}{1 + b_1 \cdot c} + \frac{H_2 \cdot c}{1 + b_2 \cdot c} \tag{2.45}$$

The second Langmuir term covers the adsorption of the solute molecules on a second, completely independent group of adsorption sites of the adsorbent. Those completely independent adsorption sites can occur on reversed phase adsorbents with remaining silanol groups or on chiral stationary phases with a chiral selector coated or bonded to a silica surface (Guiochon et al. 2006).

Limitations of the Langmuir model can also be overcome, adding a third model parameter, for example, by the Toth isotherm model (Toth 1971):

$$q = q_{sat} \cdot \frac{c}{((1/b) + c^e)^{1/e}} \tag{2.46}$$

The model shown in Eq. (2.46) has three independent fitting parameters, q_{sat}, e, and b, which allow independent control of slope and curvature. For $e = 1$ it approaches the Langmuir model.

Other flexible isotherm models extending the Langmuir model are based on the theory of heterogeneous surfaces (Jaroniec and Madey 1988) and on concepts provided by statistical thermodynamics (Hill 1960). The latter approach allows deriving the following second-order isotherm model that is capable to describe inflection points in the isotherm courses:

$$q = q_{sat} \frac{c(b_1 + 2 \cdot b_2 \cdot c)}{1 + b_1 \cdot c + b_2 \cdot c^2} \tag{2.47}$$

2.4.2.2 Multicomponent Isotherms Based on the Langmuir Model

If mixtures of solutes are injected into a chromatographic system, not only interferences between the amount of each component and the adsorbent but also interferences between the molecules of different solutes occur. The resulting competition and displacement effects cannot be described with independent single-component isotherms. Therefore, an extension of single-component isotherms that also takes into account the interference is necessary. The competition can be included in the denominator of the multicomponent Langmuir isotherm equation (Eq. (2.48)):

$$q_i = q_{sat} \frac{b_i c_i}{1 + \sum\limits_{j=1}^{n} b_j c_j} = \frac{H_i c_i}{1 + \sum\limits_{j=1}^{n} b_j c_j} \tag{2.48}$$

A prerequisite for Eq. (2.48) is the equality of the maximum loadability q_{sat} of all n solutes. In the case of different loadabilities for the different solutes

$q_{\mathrm{sat},i} \neq q_{\mathrm{sat},j}$, Eq. (2.48) no longer fulfills the Gibbs–Duhem equation and is thus thermodynamically inconsistent (Broughton 1948). This is, for example, the case if solutes with substantially different molecular masses are separated on sorbents where the pore accessibility is hindered for large molecules.

A multicomponent Langmuir isotherm based on Eq. (2.44) is shown in Eq. (2.49) (Charton and Nicoud 1995):

$$q_i = \lambda_i c_i + \frac{H_i c_i}{1 + \sum\limits_{j=1}^{n} b_j c_j} \tag{2.49}$$

The bi-Langmuir isotherm (Eq. (2.45)) can be extended in the same way to give the multicomponent bi-Langmuir isotherm (Eq. (2.50)) (Guiochon et al. 2006):

$$q_i = q_{\mathrm{sat},1} \frac{b_{1,i} c_i}{1 + \sum\limits_{j=1}^{n} b_{1,j} c_j} + q_{\mathrm{sat},2} \frac{b_{2,i} c_i}{1 + \sum\limits_{j=1}^{n} b_{2,j} c_j} = \frac{H_{1,i} c_i}{1 + \sum\limits_{j=1}^{n} b_{1,j} c_j} + \frac{H_{2,i} c_i}{1 + \sum\limits_{j=1}^{n} b_{2,j} c_j} \tag{2.50}$$

Modified multicomponent Langmuir and multicomponent bi-Langmuir isotherms offer a large flexibility for adjustment to measured data if all coefficients are chosen individually. To limit the number of free parameters that need to be specified, it is sometimes possible to use in Eqs. (2.49) and (2.50) constant adjustment terms ($\lambda_i = \lambda$) or equal saturation capacities ($q_{\mathrm{sat},1,i} = q_{\mathrm{sat},2,i} = q_{\mathrm{sat},i}$).

2.4.2.3 Competitive Isotherms Based on the Ideal Adsorbed Solution Theory

There are several methods available that allow the prediction of mixture isotherms based on general single-component information. An application can significantly reduce the necessary number of experiments. The most successful approach is the ideal adsorbed solution (IAS) theory initially developed by Myers and Prausnitz (1965) to describe competitive gas-phase adsorption. This theory was subsequently extended by Radke and Prausnitz (1972) to quantify adsorption from dilute (i.e. also ideal) solutions.

Adsorption occurs in a three-phase system consisting of the solid (stationary) phase (adsorbent), the fluid (mobile) phase, and the adsorbed phase (Figure 2.1). According to Gibbs' classical theory, the adsorbed phase is viewed as a two-dimensional boundary layer between the other two phases. This allows describing adsorption as a two-phase process based on interactions between the adsorbed and fluid phases. It is further assumed that the surface of the adsorbent, A, is identical for all components. Based on the fundamental property relation (Myers and Prausnitz 1965), the starting point for the derivation of the IAS theory is the following expression for the free Gibbs' energy of the adsorbed phase:

$$\mathrm{d}G_{\mathrm{ads}} = -S_{\mathrm{ads}} \mathrm{d}T + A \, d\pi + \sum_{i=1}^{n} \mu_{i,\mathrm{ads}} \mathrm{d}q_i, \quad i = 1, \dots, n \tag{2.51}$$

The two-dimensional spreading pressure π is an intensive property of the adsorbed phase. Considering the adsorption of just a single (superscript 0) component i and respecting the Gibbs–Duhem equation provides for constant

temperature and pressure and equilibrium conditions the well-known Gibbs' adsorption isotherm (Myers and Prausnitz 1965):

$$A \, d\pi_i = q_i^0 \mathrm{d}\mu_{i,\mathrm{ads}} \tag{2.52}$$

In order to apply this expression, the better accessible identical chemical potentials in the fluid phase, μ_i, can be used to substitute the corresponding adsorbed phase chemical potentials:

$$\mu_{i,\mathrm{ads}} = \mu_i = \mu_i^{\mathrm{ref}} + RT \ln \frac{c_i^0}{c_i^{\mathrm{ref}}} \quad \text{or} \quad \mathrm{d}\mu_{i,\mathrm{ads}} = RT \, d \ln c_i^0 \tag{2.53}$$

Integration of the *Gibbs' adsorption isotherm* over a running variable ξ leads to

$$\pi_i(c_i^0) = \frac{RT}{A} \int_0^{c_i^0} q_i^0(\xi) \mathrm{d} \ln \xi = \frac{RT}{A} \int_0^{c_i^0} \frac{q_i^0(\xi)}{\xi} \mathrm{d}\xi \tag{2.54}$$

The requirement of phase equilibrium in mixtures is established by stating that all the components in the adsorbed phase exert the same spreading pressure, that is:

$$\pi_j = \cdots = \pi_N, \quad j = 1, \dots, n \tag{2.55}$$

or

$$\int_0^{c_1^0} \frac{q_1^0(\xi)}{\xi} \mathrm{d}\xi = \int_0^{c_j^0} \frac{q_j^0(\xi)}{\xi} \mathrm{d}\xi, \quad j = 2, \dots, n \tag{2.56}$$

The single-component isotherm equations forming the input information for the IAS theory are the functions $q^0(=c^0)$. Under ideal conditions, the following analogy to Raoult's law exploiting the fractions of the components in the adsorbed phase x_i holds for each component in a mixture:

$$c_i = c_i^0 x_i, \quad i = 1, \dots, n \tag{2.57}$$

Equations (2.56) and (2.57) contain the c_i^0 and the x_i as $2n$ unknowns. An important drawback of the IAS theory is related to the fact that these unknowns can often not be determined analytically and the application of numerical methods is needed.

Once the c_i^0 are known, the remaining explicit equations allowing to calculate the loadings q_i as a function of given fluid-phase concentration c_i are

$$q_i = \left[\sum_{j=1}^{n} \frac{c_j}{c_j^0 \cdot q_j^0(c_j^0)} \right]^{-1} \frac{c_i}{c_i^0}, \quad i = 1, \dots, n \tag{2.58}$$

Only for a small number of relatively simple single-component adsorption isotherm models analytical solutions of the set of IAS theory equations can be derived. This is possible, for example, for the Langmuir model. If the saturation capacities of all components in the corresponding single-component isotherm equations (Eq. (2.42)) are identical, the IAS theory generates the same competitive isotherm model as given by Eq. (2.48).

Ilić, Flockerzi, and Seidel-Morgenstern (2010) derived a flexible explicit solution of the IAS theory equations for the calculation of adsorbed phase concentrations of binary systems whose individual component behavior can be represented

by flexible second-order (quadratic) adsorption isotherms (Eq. (2.47)). In this case Eq. (2.56) provides

$$\int_0^{c_1^0} \frac{b_{11} + 2 \cdot b_{12} \cdot \xi}{1 + b_{11} \cdot \xi + b_{12} \cdot \xi^2} d\xi = \int_0^{c_2^0} \frac{b_{21} + 2 \cdot b_{22} \cdot \xi}{1 + b_{21} \cdot \xi + b_{22} \cdot \xi^2} d\xi \tag{2.59}$$

Integration and exploitation of Eq. (2.57) results in

$$1 + b_{11} \cdot \frac{c_1}{x_1} + b_{12} \cdot \left[\frac{c_1}{x_1}\right]^2 = 1 + b_{21} \cdot \frac{c_2}{1 - x_1} + b_{22} \cdot \left[\frac{c_2}{1 - x_1}\right]^2 \tag{2.60}$$

This equation provides the following third-order polynomial in terms of the adsorbed phase fraction of the first component x_1:

$$a_1(c_1, c_2) \cdot x_1^3 + a_2(c_1, c_2) \cdot x_1^2 + a_3(c_1, c_2) \cdot x_1 + a_4 = 0 \tag{2.61}$$

with

$$a_1(c_1, c_2) = \alpha \cdot c_1 + c_2$$
$$a_2(c_1, c_2) = c_1 \cdot [\beta \cdot c_1 - 2 \cdot \alpha] - c_2 \cdot [1 + \gamma \cdot c_2]$$
$$a_3(c_1, c_2) = c_1 \cdot [\alpha - 2 \cdot \beta \cdot c_1]$$
$$a_4(c_1, c_2) = \beta \cdot c_1^2$$
$$\alpha = \frac{b_{11}}{b_{21}} > 0, \quad \beta = \frac{b_{12}}{b_{21}} \geq 0, \quad \gamma = \frac{b_{22}}{b_{21}} \geq 0$$

The only physically meaningful solution for x_1 in the interval $[0, 1]$ can be identified (Ilić, Flockerzi, and Seidel-Morgenstern 2010), and the IAS theory delivers the following flexible and widely applicable explicit isotherm model:

$$q_i(c_1, c_2) = \left[\frac{x_1}{q_1^0(c_1^0)} + \frac{x_2}{q_2^0(c_2^0)}\right]^{-1} \cdot x_i \tag{2.62}$$

with

$$x_2 = 1 - x_1, \quad c_i^0 = \frac{c_i}{x_i}, \quad i = 1, 2$$

Numerous further attempts were undertaken in order to facilitate the solution of the set of IAS equations. Typically, iterative Newton-type methods have been applied to solve the equations in their original form or after suitable transformations. Hereby, a crucial point is always the selection of initial estimates, leading to convergence of the iteration schemes applied. A new approach, based on reformulating the equations into a dynamic problem, avoids this drawback (Rubiera Landa et al. 2013). The following simple decoupled system of ordinary differential equations describes the orbit along a running variable φ building up the spreading pressure:

$$\frac{dc_1^0}{d\varphi} = 1$$
$$\frac{dc_i^0}{d\varphi} = \frac{q_1^0(\varphi)/c_1^0}{q_i^0(\varphi)/c_i^0}, \quad i = 2, \dots, n \tag{2.63}$$

The integration starts at well-defined initial values

$$c_i^0(\varphi = 0) = 0, \quad i = 1, \dots, n \tag{2.64}$$

and stops when the closure condition originating from Eq. (2.57) is fulfilled, that is, if the following holds:

$$\sum_i^n \frac{c_i}{c_i^0(\varphi^{\text{stop}})} = 1 \tag{2.65}$$

After specifying the c_i^0, it remains again just solving the explicit Eq. (2.58). The described algorithm can be efficiently applied to solve the set of IAS equations for arbitrary increasing single-component adsorption isotherm models and any component number n.

2.4.2.4 Steric Mass Action Isotherms

In order to illustrate for another separation mechanism an equilibrium model, we consider here just shortly ion-exchange chromatography, which is frequently used for the purification of charged or chargeable molecules, for example, proteins (Carta and Jungbauer 2010). The state of equilibrium is currently described by stoichiometric models where the solute, for example, a protein, displaces a stoichiometric number of salt ions bound on an ion-exchange resin. A basic concept is the stoichiometric displacement model developed by Kopaciewicz et al. (1983). For monovalent counterions the reaction is described as follows:

$$c_i + v_i q_S = q_i + v_i c_S \tag{2.66}$$

where q_S is the salt load of the adsorbent, q_i the solute load of the adsorbent, c_i the concentration of the solute, and c_S the salt concentration in the mobile phase. The characteristic charge representing the number of sites on the resin surface the solute interacts with is given by v_i. Due to the mass action law, the equilibrium constant is

$$K_{\text{M},i} = \frac{q_i}{c_i} \left(\frac{c_S}{q_S} \right)^{v_i} \tag{2.67}$$

Brooks and Cramer (1992) extended this model considering the steric shielding of ion-exchange groups by large solutes such as proteins as illustrated in Figure 2.16.

Figure 2.16 Protein adsorption on ion-exchange resin with steric shielding.
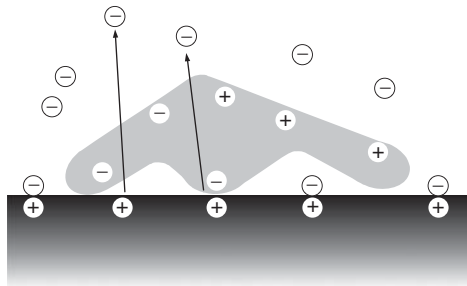
Because of the shielding, the equilibrium constant is given as

$$K_{M,i} = \frac{q_i}{c_i} \left(\frac{c_S}{\hat{q}_S} \right)^{\nu_i} \tag{2.68}$$

with the free accessible salt load $\hat{q}_S$. The total ion-exchange capacity, that is, the total number of binding sites on the resin surface, is

$$\Lambda = \hat{q}_S + \sum_{i=2}^{N_{comp}} (\nu_i + \sigma_i) q_i \tag{2.69}$$

where σ_i is the steric shielding parameter and ν_i the characteristic protein charge. The component index for the salt is $i = 1$. From Eqs. (2.68) and (2.69), it results in the implicit form of the steric mass action (SMA) isotherm that has the same concave curvature as Langmuir isotherms for high concentrations:

$$c_i = \frac{1}{K_{M,i}} \frac{q_i (c_S)^{\nu_i}}{\left(\Lambda - \sum_{i=2}^{N_{comp}} (\nu_i + \sigma_i) q_i \right)^{\nu_i}} \tag{2.70}$$

For dilute protein solutions or at high salt concentration, the protein load is very small so that the total ion-exchange capacity is

$$\Lambda \gg \sum_{i=2}^{N_{comp}} (\nu_i + \sigma_i) q_i \tag{2.71}$$

and, similarly to Langmuir isotherms, the SMA isotherm reduces for $c_i \to 0$ to a linear function:

$$q_i = K_{M,i} \left(\frac{\Lambda}{c_S} \right)^{\nu_i} c_i \tag{2.72}$$

Brooks and Cramer (1992) recommend experimental procedures such as using isocratic/gradient elution chromatography to determine the parameters $K_{M,i}$, ν_i, and σ_i. SMA isotherms do not take into account an influence of the pH value. Corresponding extensions have been developed by Gerstner, Bell, and Cramer (1994) and Bosma and Wesselingh (1998). Alternative more detailed concepts were summarized comprehensively by Carta and Jungbauer (2010).

The important aspect how to determine specific parameters of equilibrium functions will be addressed in a more general way in Chapter 7.

2.4.3 Relation Between Isotherms and Band Shapes

The elution profile of an ideal chromatogram developing in a column characterized by a plate number N of infinity depends only on the courses of the equilibrium functions. Depending on the shapes of these functions, specific band shapes develop.

This connection is illustrated in Figure 2.17. In an ideal analytical chromatogram, that is, in the linear range of the adsorption isotherms, the mean retention time of a component i is a function of the isotherm slope, quantified

Type of isotherm

(a) Linear

(b) Convex

(c) Concave

Ideal chromatogram

(d)

(e)

(f)

Real chromatogram

(g)

(h)

(i)
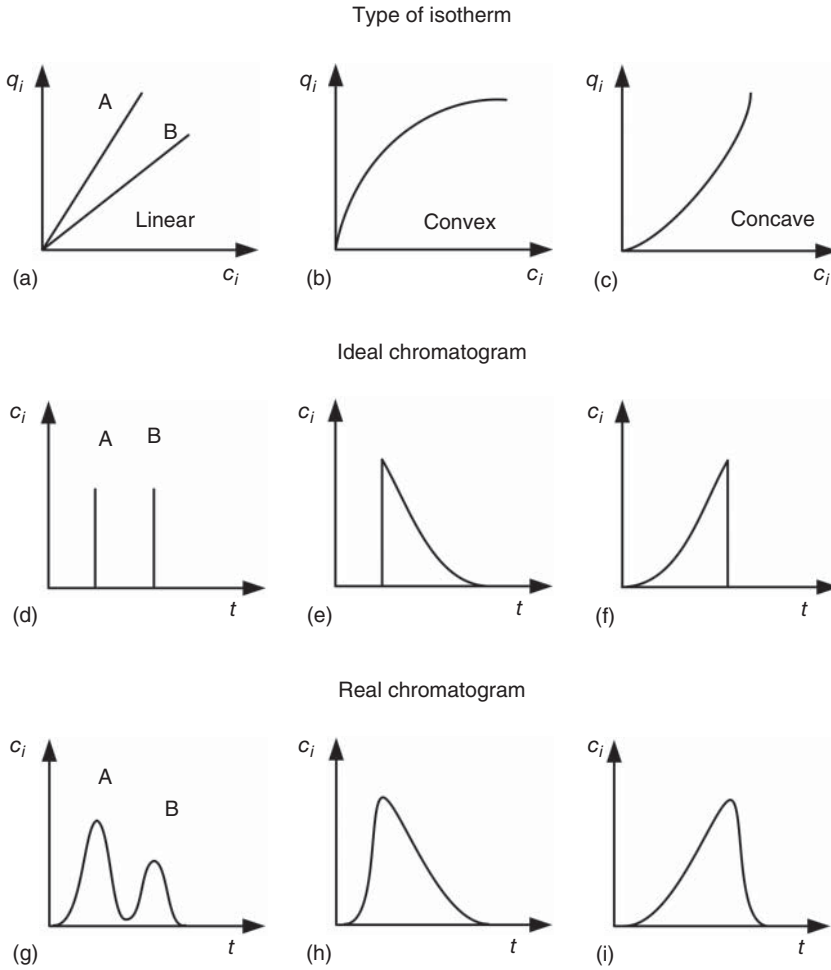
Figure 2.17 Influence of the course of the equilibrium isotherms on the shapes of chromatographic elution profiles, a) types of isotherm, b) ideal chromatograms, c) real chromatograms.

by the Henry constant H_i (Figure 2.17a), according to the basic equation of chromatography (Eq. (2.73)), which will be derived in Chapter 6 (Guiochon et al. 2006):

$$t_{R,i} = t_{0,t}\left(1 + \frac{1-\varepsilon_t}{\varepsilon_t}H_i\right) = t_{0,t}(1 + k_i') \tag{2.73}$$

Thus, for very efficient columns under linear (diluted) conditions, the retention time does not depend on the fluid-phase concentration (Figure 2.17d). In contrast, under nonlinear conditions peak deformations occur, and the retention times become functions of concentration. This leads, under thermodynamically controlled ideal conditions, to the formation of disperse waves and shock fronts (Figure 2.17e,f). The "retention times" of specific concentrations c_i^+ in waves are

then related to the local slopes of the specific adsorption isotherm as follows:

$$t_{R,i}(c_i^+) = t_{0,t} \left(1 + \frac{1 - \varepsilon_t}{\varepsilon_t} \frac{dq_i}{dc_i}\bigg|_{c_i^+} \right) \tag{2.74}$$

For convex isotherms (Figure 2.17b) the desorption fronts of the peak (the "tails") form waves (Figure 2.17e), whereas for concave isotherms (Figure 2.17c) the adsorption fronts form waves ("peak fronting"; Figure 2.17f).

The second type of wave propagation of overloaded ideal peaks is characterized by sharp shock fronts that can be described between the two limiting states of the shock front by Eq. (2.75):

$$t_{R,i}^{shock} = t_{0,t} \left(1 + \frac{1 - \varepsilon_t}{\varepsilon_t} \frac{q_{after} - q_{before}}{c_{after} - c_{before}}\bigg|_{shock} \right) \tag{2.75}$$

In many cases, the adsorption isotherms are of the Langmuir type with a linear slope at the initial part and a saturation value at higher amounts of adsorbed solute (Figure 2.17b). More complex band shapes develop in the case of inflection points in the courses of the equilibrium functions (Zhang et al. 2006). In real columns, the discussed additional mass transfer effects broaden the equilibrium controlled peak shapes as illustrated in Figure 2.17g–i. A more detailed discussion of the equilibrium theory of chromatography will be given in Chapter 6.

In the nonlinear isotherm range in the case of mixtures, there are additional effects occurring due to the competition of the solutes for the adsorption sites. This competition is illustrated in Figure 2.18 for the isotherms of two components. The single-component isotherm of component A (dashed line) is lower than the single-component isotherm of component B (solid line). In Figure 2.18a–c are shown in addition three pairs of corresponding competitive isotherms for three fixed compositions of mixtures (1 : 9, 1 : 1, and 9 : 1). The specific effects of competition can be clearly seen.

The two most important mixture effects caused by competition are the displacement effect and the tag-along effect (Guiochon et al. 2006). To explain these effects Figure 2.19 depicts elution profiles that have been theoretically calculated based on the transport dispersion model (Section 6.2.5.1). To generate the chromatograms the isotherms given in Figure 2.18 were used. The feed concentrations were in the three ranges 1 : 9, 1 : 1, and 9 : 1. In the first case a small amount of the earlier eluting component A (dashed line) is displaced by a large amount of the second eluting component B (Figure 2.19a). By reducing the retention time of this low-affinity component, the elution profile is sharpened and productivity increased. Characteristic for displacement is the strong reduction of the isotherm of the first eluting component in the mixture situation compared with the single-component behavior, while the isotherms of the late-eluting component B in the mixture and for the pure component are nearly the same (Figure 2.18a). To exploit the displacement effect, the chromatographic systems can also be operated by adding an additional displacer with well-defined adsorption characteristics.

If the two components are present in similar amounts in the feed, both equilibrium loadings are reduced to a similar extent compared to the corresponding
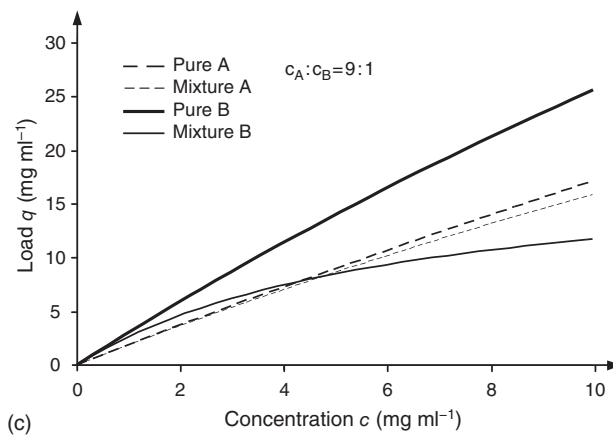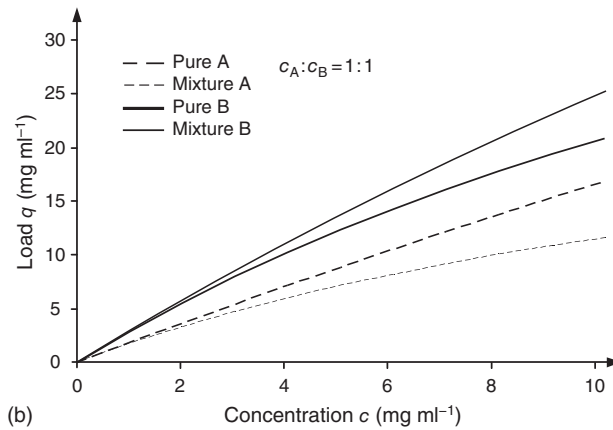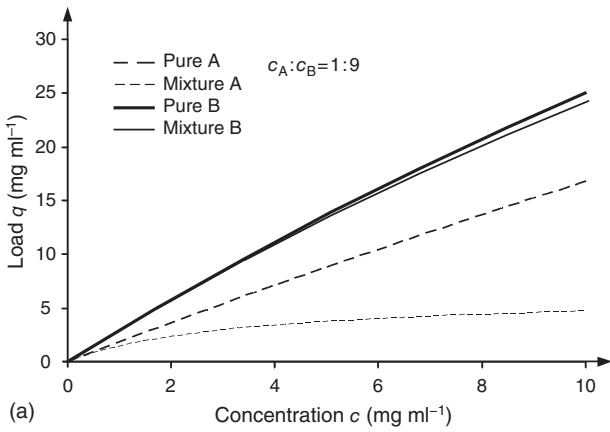
Figure 2.18 Single-component Langmuir isotherms and multicomponent Langmuir isotherm for different mixture compositions. a) 1 : 9, b) 1 : 1, c) 9 : 1.
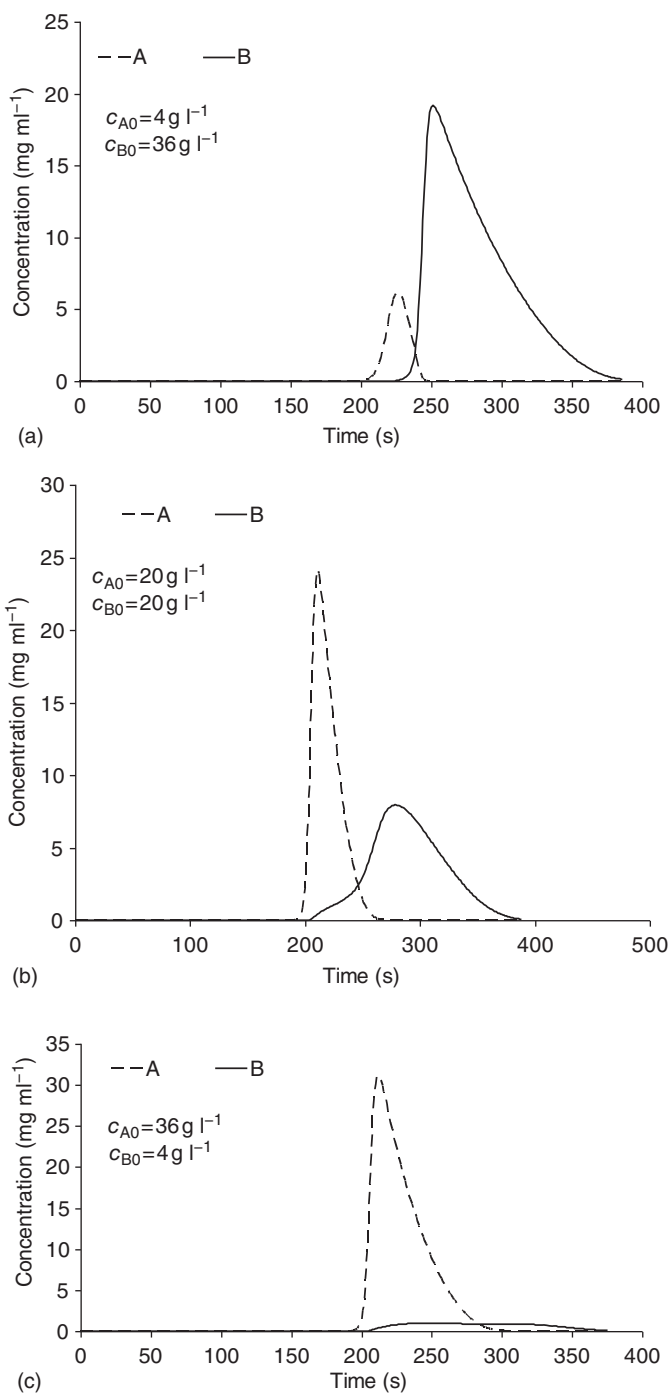
Figure 2.19 Elution profiles for different mass ratios of the feed mixtures. a) 1 : 9, b) 1 : 1, c) 9 : 1.

single-component isotherms. The corresponding elution profiles are deformed in a similar way and have an enhanced tendency to overlap (Figures 2.18b and 2.19b).

The second so-called tag-along effect can occur if the feed composition is dominated by the first eluting component. Under these conditions, the highly concentrated molecules of the first component A desorb the molecules of the second component, thus forcing them into the mobile phase and resulting in shorter retention times of the second component. Analogous to case (a) the isotherm for the late-eluting component B is strongly influenced by the presence of large amounts of A crossing the mixture isotherm of this component (Figure 2.18c). The tag-along effect causes a long and undesired plateau of the second component under the elution profile of the first eluting component (Figure 2.19c).

The two described effects origin from nonlinear thermodynamic interactions between the components. If in a concrete separation the peak resolution is not high enough, there is typically no way to overcome this problem by increasing column efficiency. If a tag-along effect occurs, the use of a smaller particle diameter has no effect, as long as the surface chemistry of the stationary phase and the mobile phase composition are kept constant. In such cases, only an improved chromatographic system can lead to a more productive separation process.
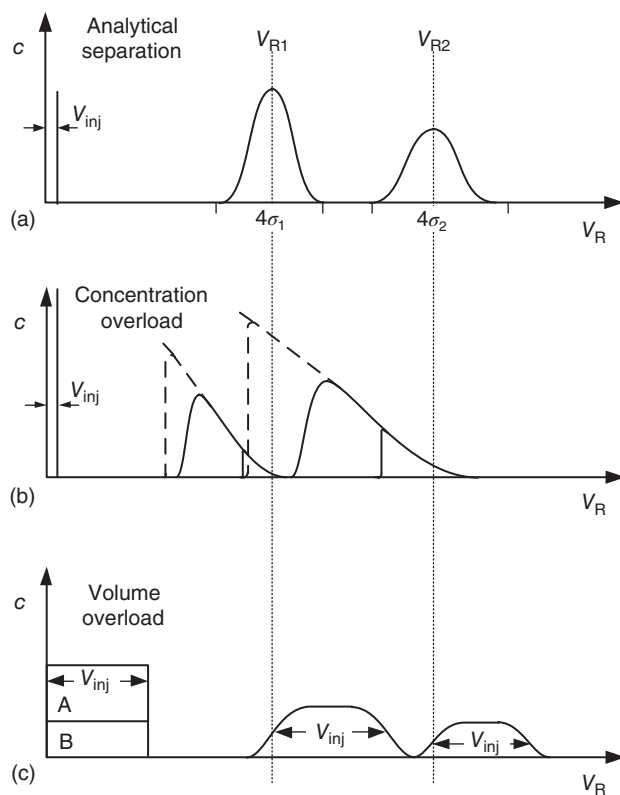
Figure 2.20 Illustration of different types of overloading chromatographic columns. a) analytical case, b) concentration overloading, c) volume overloading.

In analytical chromatography, typically very dilute samples are injected into the column. Therefore, one stays within the linear range of isotherm, and retention times are independent of the amount injected. The concentration profiles are symmetrical and Gaussian (Figure 2.20a).

2.5 Column Overloading and Operating Modes

2.5.1 Overloading Strategies

Analytical chromatography aims to achieve an adequate, not necessarily a maximum, resolution of solute bands to identify and to quantify the analytes based on their retention coefficient, peak height, and peak area. Information on the analytes is the target.

In preparative chromatography, the goal is to purify and to isolate compounds with high productive, purity, and yield. Productivity is often a major goal, being the mass of isolate (target compound) per unit mass of packing and per unit time. To increase productivity, samples are applied on the column with much higher injected amounts than in analytical chromatography.

In order to be productive the columns are overloaded. For this the term "overloading" has been introduced by analytical chemists. They avoid for analysis column overloading in order to achieve constant retention times for reproducible analytical detection of each component peak.

At higher column loadings the peak shapes change typically connected with reduced selectivities and efficiencies. From the engineering viewpoint, overloaded chromatographic systems are nonlinear because nonlinear isotherms connect the phases involved.

The injected sample mass for a certain component i, m_i, is given by Eq. (2.76):

$$m_{i,\text{inj}} = c_{i,\text{inj}} \, V_{\text{inj}} \tag{2.76}$$

where c_{inj} is the sample concentration and V_{inj} the sample volume. Typically, 10–100 µl of a sample mixture is injected into an analytical HPLC column. Injection concentrations of solutes are often around 1 mg ml−1.

When one increases the sample concentrations at constant sample volume, the peak profiles change as indicated in Figure 2.20b. A differently shaped profile is obtained when the sample volume is increased at constant sample concentration (Figure 2.20c). The first case is called concentration overload, and the second case is called volume overload. Due to the resulting smaller bandwidths, concentration overload is preferable. It is however limited by the solubilites of the components in the solvent used. This thermodynamic constraint provides another important parameter in optimizing preparative chromatography.

A column is sometimes called overloaded by analytical chemists when the injection causes a 10% decrease in the retention factor k' or a 50% decrease of the plate number N compared to analytical conditions. A more suitable measure of overloading is provided by the loading factor, which is the ratio of injected sample amount to the corresponding column saturation capacity (Guiochon et al. 2006).

It should be emphasized that the productivity optimum of preparative chromatography is typically found beyond the so-called touching band situation for which still 100% yields at 100% purity are possible. Often, a joint multiobjective optimization of productivity and yield is required as discussed in Section 8.2.2.

2.5.2 Beyond Isocratic Batch Elution

There are various options to modify for preparative purposes the batchwise operated isocratic single column elution discussed so far. Here an example will be shortly explained.

In classical isocratic elution, the composition of the eluent is kept constant throughout the operation. One powerful modification frequently applied in analytical chromatography is solvent gradient elution. In this mode, the eluent composition is changed during the separation. Typically, one starts with a weak solvent A and adds then into the mobile phase in a certain time regime a stronger solvent B. Frequently a linear gradient is applied. Alternatively, stepwise gradients or more complex gradient shapes can be used.

At isocratic elution, the peaks broaden and become flatter with increasing retention and might even disappear in the baseline noise. As a rule of thumb, the retention factor k' of strongly bound and thus later-eluting solutes should not be larger than 10. This corresponds to an elution volume of less than 10
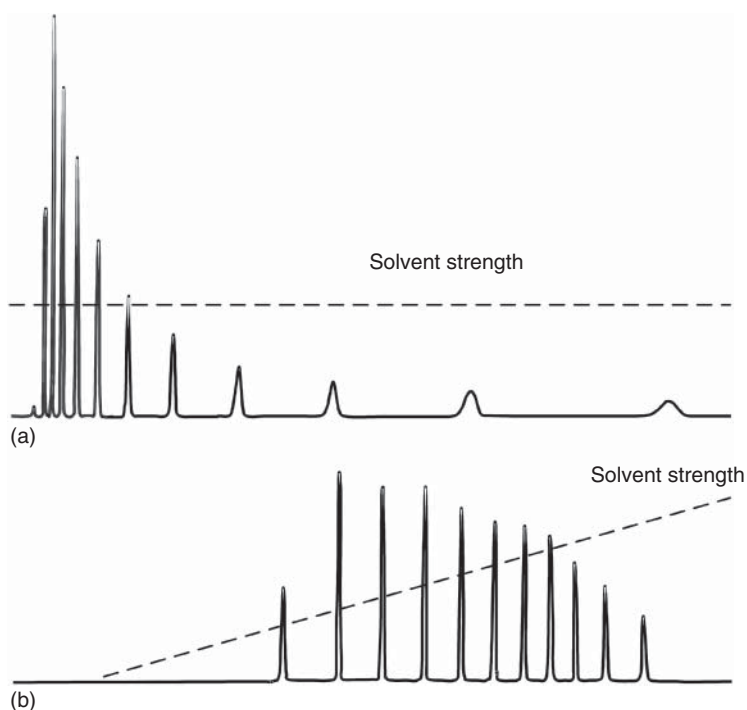
Figure 2.21 Chromatograms (signal over time) for (a) isocratic elution and (b) gradient elution using a linear solvent strength gradient.

column volumes. As a result of gradients, retention times and in particular the differences between first and last eluting peaks, i.e. cycle times, can be decreased. Connected with gradients the peaks become sharper and narrower. Gradient elution is frequently applied for screening of complex mixtures to obtain information on the number and polarity of the components.

A comparison between isocratic and gradient operation is given in Figure 2.21. Free parameters to adjust during gradient operation are the starting and final eluent composition and the gradient time and shape. Of course, after running a gradient before injecting, the next sample one has to go back to the initial conditions. This means that the column has to be washed and reconditioned. For this reason, gradient elution is less frequently used at preparative scale. This is also due to the fact that one deals with solvent mixtures, which makes distillation and reuse more difficult and expensive.

More advanced operating regimes and modes exploiting gradients will be explained in Section 5.1.2.

References

Atkins, P.W. (1990). *Physikalische Chemie.* Wiley-VCH Verlag GmbH: Weinheim.

Bellot, J.C. and Condoret, J.S. (1993). Modelling of liquid chromatography equilibria. *Process Biochem.* 28: 365–376.

Bidlingmeyer, B.A. and Waren, F.V. (1984). Column efficient measurement. *Anal. Chem.* 56: 1588–1595.

Bosma, J. and Wesselingh, J. (1998). pH dependence of ion-exchange equilibrium of proteins. *AIChE J.* 50: 848–853.

Brauer, H. (1971). *Grundlagen der Einphasen und Mehrphasenströmungen*. Aarau, Frankfurt am Main: Verlag Sauerländer.

Brooks, C. and Cramer, S. (1992). Steric-mass-action ion exchange: displacement profiles and induced salt gradients. *AIChE J.* 38: 1968–1978.

Broughton, D.B. (1948). Adsorption isotherms for binary gas mixtures. *Ind. Eng. Chem.* 40 (8): 1506–1508.

Brunauer, S., Emmett, P.H., and Teller, E. (1938). Adsorption of gases on multimolecular layers. *J. Am. Chem. Soc.* 60 (2): 309–319.

Carta, G. and Jungbauer, A. (2010). *Protein Chromatography: Process Development and Scale-Up*. Weinheim: Wiley-VCH.

Charton, F. and Nicoud, R.-M. (1995). Complete design of a simulated moving bed. *J. Chromatogr. A* 702: 97–112.

Everett, D.H. (1984). Thermodynamics of adsorption from solutions. In: *Fundamentals of Adsorption Processes* (eds. A.L. Meyers and G. Belfort). New York: Engineering Foundation.

Fanali, S., Haddad, P.R., Poole, C.F., and Riekkola, M.-L. (eds.) (2017). *Liquid Chromatography Fundamentals and Instrumentation*, Handbooks in Separation Science, vol. 1. Amsterdam: Elsevier.

Gerstner, J., Bell, J., and Cramer, S. (1994). Gibbs free energy of adsorption for bio molecules in ion exchange systems. *Biophys. Chem.* 52: 97–106.

Giles, C.H., Smith, D., and Huitson, A.J. (1974). General treatment and classification of the solute adsorption isotherm. I. Theoretical. *Colloid Interface Sci.* 47: 755–765.

Graham, D. (1953). The characterization of physical adsorption systems. I. The equilibrium function and standard free energy of adsorption. *J. Phys. Chem.* 57: 665–669.

Guiochon, G., Golshan-Shirazi, S., and Katti, A. (1994). *Fundamentals of Preparative and Nonlinear Chromatography*. Boston: Academic Press.

Guiochon, G., Felinger, A., Shirazi, D.G., and Katti, A.M. (2006). *Fundamentals of Preparative and Nonlinear Chromatography*. Amsterdam: Elsevier/Academic Press.

Hill, T.L. (1960). *An Introduction to Statistical Thermodynamics*. Reading, MA: Addison-Wesley.

Ilić, M., Flockerzi, D., and Seidel-Morgenstern, A. (2010). A thermodynamically consistent explicit competitive adsorption isotherm model based on second-order single component behaviour. *J. Chromatogr. A* 1217: 2132–2137.

IUPAC (1972). Manual of symbols and terminology, appendix 2, Pt. 1, colloid and surface chemistry. *Pure Appl. Chem.* 31: 578.

Jaroniec, M. and Madey, R. (1988). *Physical Adsorption on Heterogeneous Solids*. Amsterdam: Elsevier.

Knox, J.H. (2002). Band dispersion in chromatography – a universal expression for the contribution from the mobile zone. *J. Chromatogr. A* 960: 7–18.

Knox, J.H., Laird, G., and Raven, P. (1976). Interaction of radial and axial dispersion in liquid chromatography in relation to the "infinite diameter effect". *J. Chromatogr.* 122: 129–145.

Kopaciewicz, W., Rounds, M., Fausnaugh, J., and Regnier, F. (1983). Retention model for high performance ion-exchange chromatography. *J. Chromatogr.* 266: 3–21.

Kümmel, R. and Worch, E. (1990). *Adsorption aus Wäßrigen Lösungen*. Leipzig: VEB Deutscher Verlag für Grundstoffindustrie.

Ludemann-Hombourger, O., Bailly, M., and Nicoud, R.-M. (2000a). Design of a simulated moving bed: optimal size of the stationary phase. *Sep. Sci. Technol.* 35 (9): 1285–1305.

Ludemann-Hombourger, O., Bailly, M., and Nicoud, R.-M. (2000b). The VARICOL-process: a new multicolumn continuous chromatographic process. *Sep. Sci. Technol.* 35 (12): 1829.

Myers, A.L. and Prausnitz, J.M. (1965). Thermodynamics of mixed-gas adsorption. *AIChE J.* 11 (1): 121–127.

Nicoud, R.-M. (2015). *Chromatographic Processes: Modeling, Simulation, and Design*. Cambridge University Press.

Radke, C.J. and Prausnitz, J.M. (1972). Thermodynamics of multi-solute adsorption from liquid solutions. *AIChE J.* 18 (1): 761–768.

Rossé, G. (ed.) (2019). *Supercritical Fluid Chromatography*. Berlin/Boston: de Gruyter.

Rubiera Landa, H.O., Flockerzi, D., and Seidel-Morgenstern, A. (2013). A method for efficiently solving the IAST equations with an application to adsorber dynamics. *AIChE J.* 59 (4): 1263–1277.

Ruthven, D.M. (1984). *Principles of Adsorption and Adsorption Processes*. New York: Wiley.

Sattler, K. (1995). *Thermische Trennverfahren – Grundlagen, Auslegung, Apparate*. Weinheim: Wiley-VCH GmbH.

Seidel-Morgenstern, A. (2004). Experimental determination of single solute and competitive adsorption isotherms. *J. Chromatogr. A* 1037: 255–272.

Seidel-Morgenstern, A. and Nicoud, R.-M. (1996). Adsorption isotherms: experimental determination and application to preparative chromatography. *Isolation Purif.* 2: 165–200.

Toth, J. (1971). State equations of the solid–gas interface layers. *Acta Chim. Acad. Sci. Hung.* 69: 311.

Tsotsas, E. (1987). *Über die Wärme- und Stoffübertragung in durchströmten Festbetten, VDI Fortschrittsberichte*, 3rd Series, No. 223. Düsseldorf: VDI-Verlag.

Van Deemter, J.J., Zuiderweg, F.J., and Klinkenberg, A. (1956). Longitudinal diffusion and resistance to mass transfer as causes of nonideality in chromatography. *Chem. Eng. Sci.* 5: 271–289.

Zhang, W., Shan, Y., and Seidel-Morgenstern, A. (2006). Breakthrough curves and elution profiles of single solutes in case of adsorption isotherms with two inflection points. *J. Chromatogr. A* 1107: 216–225.

3

Stationary Phases*

Michael Schulte

Merck KGaA, Life Science – Bioprocessing, Purification R&D, Frankfurter Str. 250, 64293 Darmstadt, Germany

3.1 Survey of Packings and Stationary Phases

Adsorbents can be grouped according to the chemical composition of their base material and mode of interaction with the target molecules. In general, one distinguishes the base materials between inorganic types such as activated carbon, zeolites, porous glass, and porous oxides, for example, silica, alumina, titania, zirconia, and magnesia, and the families of cross-linked organic polymers. The former are classical adsorbents and possess a crystalline or amorphous bulk structure. They show hydrophobic as well as hydrophilic surface properties. The main criterion that distinguishes them from cross-linked polymers is their high bulk density and the porosity, which is permanent except under certain conditions, for example, very high pressures. The texture of inorganic adsorbents resembles a corpuscular structure rather than a cross-linked network more closely.

The mechanical strength of polymers is achieved through extensive cross-linking whereby a three-dimensional network of hydrocarbon chains is formed. Depending on the extent of cross-linking, soft gels, for example, agarose, and highly dense polymer gels are obtained. The bulk density is much lower than that of inorganic adsorbents. The hydrophilicity and hydrophobicity of cross-linked polymer gels are tuned by the chemical composition of the backbone polymer as well as by the surface chemistry. Organic chemistry provides enormous scope in designing the functionality of the surface of polymeric adsorbents. Even at a high degree of cross-linking, polymers still show a swelling porosity, that is, the porosity of a polymeric adsorbent depends on the type of solvent. For example, the volume of a soft gel can be 10 times higher when immersed in a solvent than in the dry state. For both types of adsorbents, the porosity and pore structure can be manipulated by additives such as templates, volume modifiers (so-called porogens), and other additives.

---

*The following authors Matthias Jöhnck, Romas Skudas, Klaus K. Unger, Cedric du Fresne von Hohenesche, Wolfgang Wewers, Jules Dingenen, and Joachim Kinkel have contributed to the first and/or second edition.

A note associated with hydrophobicity and hydrophilicity: these are frequently employed in characterizing adsorbents. Hydrophilicity/hydrophobicity is a qualitative measure of an adsorbent, characterizing its behavior toward water. The term lipophilicity/lipophobicity is applied to characterize the polarity of a compound. The overall parameter of hydrophobicity and hydrophilicity is a combination of different interaction principles between the sorbent surface and the adsorbed molecule. The most prominent interaction forces are hydrogen bonds, van der Waals forces, and ionic and $\pi-\pi$-interactions. For the characterization of solvents, Reichardt introduced a betaine dye as a solvatochromic indicator that has since been known as Reichardt's dye (Reichardt 2003). This principle has been extended to solid surfaces giving a value for the average surface functionality of the sorbent (Macquarrie et al. 1999). With hydroxyl functions dominating the interaction, the obtained value can be nevertheless used as a simple correlation to the composition of the sorbent surface. Figure 3.1 gives a summary of adsorbents used in preparative chromatography and their main interaction principles.

3.2   Inorganic Sorbents

The main advantage of inorganic sorbents is generally their high mechanical stability. The combination of stable $10-15\,\mu m$ $10\,nm$ silica particles with high-pressure stainless steel dynamic axial compression columns made it possible to obtain packed columns with $40\,000\,N\,m^{-1}$ in a diameter of over $1\,m$. These high-efficiency columns are widely used for the polishing step of peptide drugs, with insulin being the most prominent example. Besides their good physical properties, the versatility of surface modification reagents, usually silanes, is another advantage. Stability toward the full used pH range of $2-14$ on the other side is the weak point of some inorganic sorbents. Table 3.1 lists inorganic sorbents used in preparative chromatography.

3.2.1   Activated Carbons

Activated carbons are the most widely used adsorbents in gas and liquid-adsorption processes. They are manufactured from carbonaceous precursors by a chain of chemical and thermal-activation processes. The temperature for carbonization and activation reaches up to $1100\,°C$ in thermal processes. Activated carbons develop a large surface area, between 500 and $2000\,m^2\,g^{-1}$, and micropores with an average pore diameter $<2\,nm$. Mesoporosity and macroporosity are generated by secondary procedures such as agglomeration. The products are shaped as granules, powders, and pellets depending on their application. The bulk structure is predominantly amorphous and the surface is hydrophobic. During activation with polar oxygen functional groups such as hydroxyl, both carbonyl and carboxyl functions are formed, which act as acidic and basic surface sites.

As a result, hydrophilicity is introduced to the surface. The world production of activated carbons in 2002 was estimated to be about $750\,000$ metric tons. There
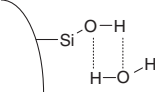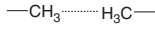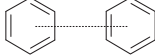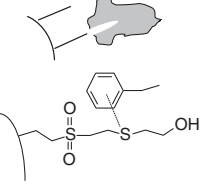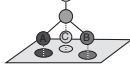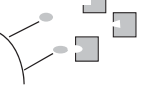
Type	Adsorbents	Interactions		Separation according to	Applications
Adsorption chromatography	Silica, aluminiumoxide	Surface binding, H-bridges, steric interactions, Bronsted and Lewis-acidity, cation-exchange		Molecular structure	Natural products, isomers
Reverse phase (RP)- chromatography	Alkyl- and aryl-silica, polymer	Hydrophobic interaction		Hydrophobicity	Peptides side components
Hydrophobic interaction chromatography (HIC)	Alkyl-polymer, hydroxyl apatite	Hydrophobic complexes, salting out		Hydrophobicity	Proteins, antibodies
Group-specific Chromatography	Sulfur-containing sorbents, Ag-dotted sorbents	Nucleophilic electrophilic, dipole, v.d.Waals-forces		Molecular structure	Antibodies, unsaturated fatty acids
Chiral chromatography	Cellulose/amylose on silica, chiral polymers and monomers on silica	Steric 3-point interaction		Spacial orientation	Racemates, isomers
Affinity-chromatography	Protein A, pseudo-affinity ligands (dyes, peptides)	"Biospecific adsorption" multipoint-interaction		Groupspecific molecular structure	Antibodies

The left margin brackets: "Adsorption" spanning the first four rows, and "Multipoint-adsorption" spanning the last two rows.

Figure 3.1 Types of chromatographic sorbents and their interaction principles.

Ionic interaction	Ion exchange-chromatography	SO_3+COOH/TMAE-DEAE-groups on silica and polymer	Ionic binding		Surface-charge	Sugars, proteins
Ionic interaction	Metal-chelate-chromatography	Ni, Co, Cu, boronate-complexes on silica and polymer	Coordination complexes		Complexing groups (SH)	Proteins
Size	Size exclusion-chromatography	Organic polymer with defined pore sizes	Steric exclusion		Molecular size and shape	Proteins (aggregates), DNA, viruses
Solubility	Partitioning-chromatography	Non-miscible fluids	Solvation, ionic interactions		Solubility	Proteins, natural products

H_3N+ —

COO
COO — Ni
COO

His
His

pore system
adsorbent

Figure 3.1 (*Continued*)

Table 3.1 Inorganic packings for chromatography and their characteristic properties.

Designation	Bulk composition and bulk structure	Surface characteristics
Activated carbons	Microcrystalline carbon	Hydrophobic; terminating polar groups such as hydroxyl, carboxyl, and so on
Zeolites	Crystalline aluminosilicates; three-dimensional network of silica and alumina with adjusted silica to alumina ratio	Hydrophobic or hydrophilic depending on the silica to alumina ratio, cation exchanger, and Brønsted and Lewis acidity
Porous silica	Amorphous, partially crystalline	Hydrophilic, cation exchanger, Brønsted acid sites, point of zero charge at pH 2–3, pK_a of Brønsted acid sites 7
Reversed phase silica	Porous silica modified with silanes	Hydrophobically modified; hydrophobicity based on alkyl chain length
Porous alumina	γ-Alumina	Brønsted and Lewis acid and basic sites, cationic and anionic exchange groups, point of zero charge at pH 7, pK_a of Brønsted acid sites 8.5
Porous titania	Anatase	Brønsted and Lewis acid and basic sites, cationic and anionic exchange groups, point of zero charge at pH 5, pK_a of Brønsted acid sites 0.2–0.5
Porous MgO	Crystalline; decomposition of magnesium carbonate	Hydrophilic, point of zero charge at pH 11–13
Porous zirconia	Crystalline, monoclinic	Brønsted and Lewis acid and basic sites, cationic and anionic exchange groups, point of zero charge at pH 10–13, pK_a of Brønsted acid sites 7
Porous glass	Silicates	Hydrophilic, cation exchanger, Brønsted acid sites

is discrimination between gas-and liquid-phase carbons. Typical liquid-phase applications are potable water treatment, groundwater remediation, and industrial and municipal wastewater treatment and sweetener decolorization. Gas-adsorption applications are solvent recovery, gasoline emission control, and protection against atmospheric contaminants.

Activated carbons in the pharmaceutical industry are widely used for the decolorization of product streams of, e.g. antibiotics, enzymes, or vitamins or the removal of certain impurities. Other applications include the removal of odor, e.g. from process water or the haze removal from vaccines and the removal of organic compounds from plasma feed streams. In simple batch processes, the activated carbon is suspended in the process liquid and filtered off afterward.

Due to distribution of a multitude of different active groups on the surface of activated carbon, these adsorption processes can reach astonishing high selectivities.

An alternative to the batch suspension procedure is the use of depth filters where the activated carbon is fixed within layers of cellulose fibers. By using the depth filter system, the handling of small particle carbon can be eliminated, resulting in a much cleaner process with even improved flow characteristics in the fixed filter format. Using a stackable pod format, a straight scale-up is possible from 23 cm^2 filter area for the smallest lab-scale device to 33 m^2 in full production scale. Millistak+$^®$ CR40 is a carbon depth filter with a nominal micron rating of 1–2 μm with a high adsorption capacity of 200+ g m^{-2}.

Standard activated carbon materials are made from charcoal of organic materials, mainly coconut shell. Besides the fact that these materials are cheap, they suffer from a series of drawbacks: being of natural origin the purity of the material has to be carefully checked. In addition the porosity control is limited and maybe most severe when the material typically contains a certain amount of fine particles, which are hard to be removed. Pyrolysis of carbon-containing organic precursors is an alternative way toward a more controlled adsorption media. By choosing an appropriate organic precursor, it is possible to tailor-made porous nanostructures and custom-designed specific functional groups on the surface (Xu et al. 2017).

3.2.2 Synthetic Zeolites

Zeolites represent a family of crystalline aluminosilicates with a three-dimensional structure. They possess regularly shaped cavities with 8-, 10-, and 12-membered silicon–oxygen rings. The pore openings range from 0.6 nm (10-ring) to 0.8 nm (12-ring). Zeolites are cation exchangers. The exchange capacity is controlled by the aluminum content. Silica-rich zeolites, for example, MFI type, possess a hydrophobic surface. Zeolites are made from water–glass solutions under alkaline conditions. An amorphous gel is first formed, which is subjected to hydrothermal treatment. The amorphous gel then converts into crystallites 0.1–5 μm in size. Silica-rich zeolites are manufactured in the presence of a structure-directing template, for example, tetraalkylammonium salts. Table 3.2 gives a survey of the type of zeolites and their applications (Ruthven 1997).

The most important applications are the Universal Oil Products (UOP) Sorbex processes (Ruthven 1997). These are automated continuous processes that separate hydrocarbon mixtures mainly in the liquid phase.

3.2.3 Porous Oxides: Silica, Activated Alumina, Titania, Zirconia, and Magnesia

Porous inorganic oxides are made through a sol–gel process. The sol is converted into a hydrogel that is subjected to dehydration to form a porous xerogel. Special techniques have been developed to combine the sol–gel transition with an aim to develop spherical-shaped particles (Figure 3.2).

Table 3.2 Survey of the type of synthetic zeolites and their applications.

Structure	Cation	Window Obstructed	Window Free	Effective channel diameter (nm)	Applications
4A	Na^+	8-Ring		0.38	Desiccant; CO_2 removal; air separation (N_2)
5A	Ca^{2+}		8-Ring	0.44	Linear paraffin separation; air separation (O_2)
3A	K^+	8-Ring		0.29	Drying of reactive gases
13X	Na^+		12-Ring	0.84	Air separation (O_2); removal of mercaptans
10X	Ca^{2+}	12-Ring		0.80	
Silicalite			10-Ring	0.60	Removal of organics in aqueous systems

Figure 3.2 Procedures employed to manufacture spherical silica particles.
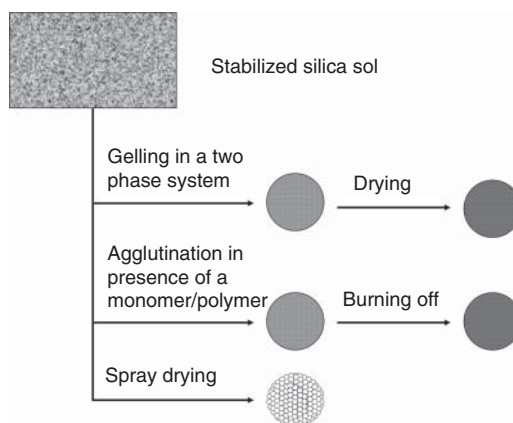
Porous oxides have in common that they form mechanically very stable particles. In terms of their chemical stability, they differ substantially. According to their isoelectric points, the adsorption properties toward charged molecules differs also from one oxide to another or in the case of amphoteric oxides, e.g. aluminum oxide, can be tuned.

Table 3.3 lists the isoelectric points of oxides, which are used as adsorbents.

3.2.4 Silica

Irregular-shaped silica particles are produced in multi-ton range per year for a variety of application areas from mild abrasive material for toothpastes to fillers for "green" car tires. Silica gel used in pharmaceutical production has to fulfill higher production standards with regard to the quality of raw materials,

Table 3.3 Isoelectric points of different oxides.

Oxide	Isoelectric point
SiO_2	1–2
ZrO_2	3.9
TiO_2	~6
Al_2O_3	7–9
MgO	12.1–12.7

Source: Data from Tian et al. (2013) and
Muhammad et al. (2012).

e.g. water, sulfuric acid, and sodium silicate, as well as the production process itself. The production process for materials used for pharmaceutical applications should include a closed production environment including milling, sieving, and downfilling. In addition, extended analytical control of the raw materials as well as the final product should be introduced.

The surface activity of silica gel can be widely tuned by applying different heat treatment steps. Silica in the wet state (the water content after production is typically between 2% and 10%) can be dried at ambient temperature under vacuum (Figure 3.3). During this procedure the physically adsorbed water is removed. If the silica is afterward operated with dried organic solvents, the low water state can be maintained for a quite high number of chromatographic runs. For the adjustment of an exact water content, the silica is dried at 200 °C, and afterward a defined amount of water is added to the dry silica. At higher temperatures around 400 °C, the chemically adsorbed water, i.e. the bonded silanols are as well opened, and the water is removed. At temperatures above 1200 °C, the silanol groups are completely removed, and siloxanes are build. This type of silica exhibits hydrophobic surface properties with substantially lower adsorption capacity.

Spherical Silica Particles: Different procedures have been developed to prepare silica beads, mainly starting from a stabilized silica sol (Figure 3.2). The silica sol can be prepared from the classical mixture of sodium silicate and sulfuric acids or by the partially hydrolysis of alkoxysilanes, e.g. tetraethoxysilane.

The alkoxysilane route is first producing a viscous liquid of polyalkoxysiloxane, which is forming an emulsion with a mixture of an organic solvent and water. The conversion to a silica hydrogel is initiated by a catalyst. If this reaction is done under rapid stirring, small droplets are formed with the stirrer speed influencing the final bead size. The formed hydrogel is filtered off and washed and undergoes a heating process to form the xerogel with a defined pore system (Unger and Schick-Kalb 1971).

An alternative process uses a spray-drying approach. The stabilized silica sol is introduced into the hot air stream of a spray-drying tower. The solvent evaporates during the procedure, the silica sol forms droplets due to the surface tension, and the beads are further dried and hardened by the hot air stream.

Physically adsorbed
("physisorbed") water

Monolayer of water
("chemisorbed")

25 °C (Vacuum)

"Dry surface"
(no adsorbed water)
(~8 µmol OH/m^2)

200 °C

Easily reversible

200 °C

Less reversible

No bonded silanols
(~4 µmol OH/m^2)

Siloxanes

OH

OH

OH

OH

Si–OH
(internal)

1200 °C

No silanols
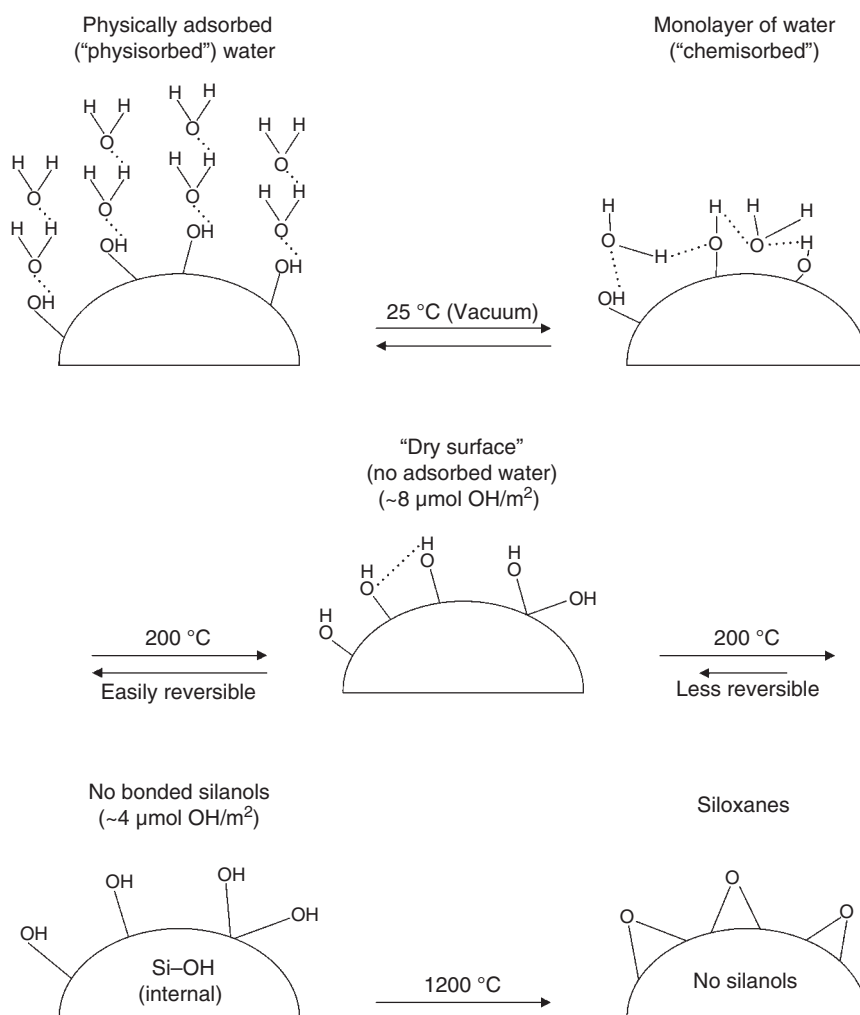
Figure 3.3 Dehydration and dihydroxylation of silica surfaces.

3.2.4.1 Surface Chemistry

In *normal phase* chromatography, the native, non-modified adsorbent is employed with organic solvent mixtures as eluents. Normal phase chromatography was the classical chromatography mode performed with native silica or alumina, that is, the adsorbent's surface is hydrophilic, and the interaction with the solutes takes place via the hydroxyl groups on the surface. As an example, the surface of silica consists of silanol groups of different types. One can distinguish between free (isolated, nonhydrogen bonded), terminal, vicinal (hydrogen bonded), germinal, and internal hydroxyl groups (Figure 3.4).

Knowledge of the materials surface chemistry is crucial. The required adsorbents are silicas with a chemically modified surface carrying bonded *n*-octadecyl or *n*-octyl groups. The long *n*-alkyl ligands invert the surface polarity from
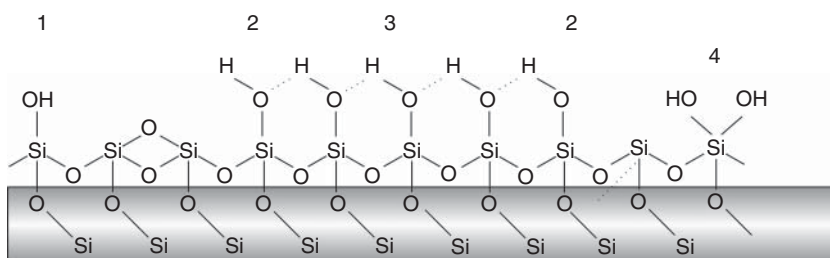
Figure 3.4 Types of silanol groups: isolated (1), terminal (2), vicinal (3), and germinal (4) species.

hydrophilic (native adsorbent) to hydrophobic. Silica-based reversed phase (RP) columns are operated with aqueous/organic eluents, and inversion of the elution order takes place (hydrophilic components elute first). More details are given in Table 3.4.

Table 3.4 Interrelationship between adsorbent characteristics and chromatographic properties.

Method	Parameter derived	Chromatographic properties affected
Light microscopy, scanning electron microscopy	Particle morphology, particle size distribution	Stability of packed bed, column performance
Light scattering Coulter counter	Particle size distribution, volume average particle diameter, number average particle diameter	Stability of packed bed, hydrodynamic column properties, column performance
Gas sorption (nitrogen at 77 K), mercury intrusion/extrusion (mercury porosimetry)	Specific surface area (Brunauer–Emmett–Teller [BET]), pore size distribution, average pore diameter, specific pore volume, particle porosity	Retention of solutes, mass loadability, column regeneration, column performance, pore and surface accessibility for solutes of given molecular weight, mechanical stability, column pressure drop, pore connectivity
Atomic absorption spectroscopy, neutron activation analysis, ICP optical emission spectroscopy	Inorganic bulk and surface impurities of packings	Chemical stability of packing, retention of solutes, peak tailing
Inverse size-exclusion chromatography (ISEC)	Accessibility of ligands in the porous network	Mass loadability, adsorption, and desorption kinetics
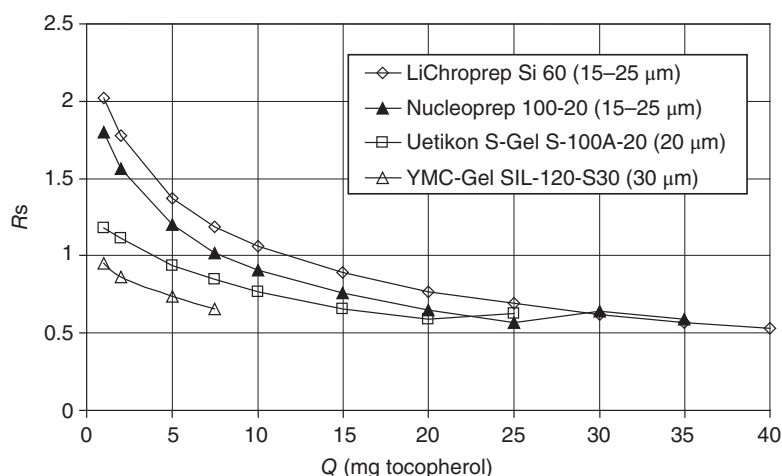
Figure 3.5 Determination of the resolution factor at different loads for four different silicas.

3.2.4.2 Mass Loadability

For lab-scale purifications as well as a quick adsorbent-screening method, the determination of the resolution as a function of the load is used. Increasing amounts of the feed mixture are injected onto the column, and the corresponding resolution of the compounds of interest is determined. With this methodology, the maximum load for 100% recovery and yield can be extrapolated from the graph at the point where the resolution of 1.5 (baseline resolution) cuts the curves for the single adsorbents at a given load. Even if no interactions between the substances in the nonlinear range of the isotherm are taken into account, this approach is useful for the near-linear range with resolution factors down to 1.0–0.8. Figure 3.5 shows the resolution versus load for different adsorbents. All adsorbents are normal phase silica with similar particle sizes. A mixture of two tocopherol isomers from a sunflower oil source was injected, and the resolution between the two main peaks calculated. The graph shows that the starting resolution is quite different for each adsorbent, which depends on the selectivity α and the efficiency of the column. As all resolution factors decline with increasing amounts of tocopherol loaded onto the column, the higher the load on the column, the smaller the differences between the columns. In that region, interactions between the compounds in the feed mixture have to be taken into account, and the complete isotherm should be determined. Nevertheless from Figure 3.5, a good solution for the isolation of amounts of the target compound in milligrams can be easily obtained.

3.2.5 Diatomaceous Earth

A naturally occurring silica material is diatomaceous earth, the fossilized remains of diatoms (single-celled algae). It can be found in different locations around the world. It was first explored in 1836 in the Lüneburg Heath and called kieselguhr. Wilhelm Berkefeld, a German engineer, first constructed the so-called Berke-feld filter using the adsorptive capacity of diatomaceous earth for the removal

of cholera toxins. His product was widely used during the 1892 cholera epidemic in Hamburg (Kirchner 1893). Diatomaceous earth consists of typically 80–90% silica, with 2–4% alumina and 0.5–2% iron oxide. As it is a natural material, other compounds of varying quantities are present as well. It has been widely used as filter aid or in-depth filters but is today more and more replaced by fully synthetic silica gel due to the better control of the properties for synthetic materials.

3.2.6 Reversed Phase Silicas

The term "reversed phase" stands for a hydrophobic packing. RP packings are operated with polar mobile phases, typically aqueous mobile phases containing organic solvents such as acetonitrile, alcohols (methanol, ethanol, *n-* or *iso*-propanol), or tetrahydrofuran (THF) as a second solvent. For hydrophobic solutes, the retention time increases with the hydrophobic character. The hydrophobic character of a solute is proportional to its carbon content, its number of methylene groups in the case of a homologue series, its number of methyl groups in the case of alkanes, or its number of aryl groups in the case of aromatic compounds.

The term RP packing is a synonym for a packing with a hydrophobic surface: the most common RP packings are silicas with surface-bonded long-chain *n*-alkyl groups, also termed RP silicas. The same term is used to describe silicas with hydrophobic polymer coatings. RP packings are also hydrophobic cross-linked organic polymers (cross-linked styrene-divinylbenzene [DVB] copolymers) and porous graphitized carbons. These RP packings differ in the degree of hydrophobicity in the relative sequence:

porous graphitized carbon > polymers made from cross-linked styrene-DVB > *n*-octadecyl (C18) bonded silicas > *n*-octyl bonded (C8) silicas > phenyl-bonded silicas > *n*-butyl (C4) bonded silicas > *n*-propylcyano-bonded silicas > diol-bonded silicas.

3.2.6.1 Silanization of the Silica Surface

Chemical surface modification of the silica serves to:

- Chemically bind desired functional groups (ligands) at the surface, mimicking the structure of solutes and thus achieving retention and selectivity (group-specific approach).
- Deactivate the original heterogeneous surface of the silica surface to avoid matrix effects. As silica has a weak acidic surface, basic solutes are strongly adsorbed, which should be minimized by surface modification.
- Enhance the chemical stability of silica, particularly at the pH range above pH 8.

3.2.6.2 Silanization

The silica surface bears $8–9\,\mu mol\,m^{-2}$ of weakly acidic hydroxyl groups (~5 silanol groups per nm^2) when silica is in its fully hydroxylated state. The hydroxyl groups react with halogen groups, OR groups, and other OH groups, leaving acids, alcohols, and water, respectively. The most suitable approach is the use of

organosilanes with reactive groups X. Thus, the surface reaction can be written as

$$\equiv SiOH + X - SiR_3 \rightarrow \equiv Si - O - SiR_3 + HX \tag{3.1}$$

As a result, a siloxane bond is formed, and the functional group R is introduced by the organosilane. Silanization can be performed in many ways, and thus the products differ in surface chemistry, which is reflected in the chromatographic behavior.

3.2.6.3 Starting Silanes

Silanes differ in the type of the reactive group X and in the type of the organic group R. At constant R and X, one can discriminate three types of silanes: mono-functional, bifunctional, and trifunctional. Monofunctional silanes undergo a monodentate reaction, that is, they react with one hydroxyl group, and bifunctional silanes may react with one or two X groups. Trifunctional silanes react with a maximum of two X groups per molecule in the case of anhydrous reaction conditions. When water is present in the reaction mixture, trifunctional silanes hydrolyze and form oligomers by intramolecular condensation. The starting compounds as well as the intermediate then perform a condensation with surface hydroxyl groups. The organic group R is an *n*-alkyl group with a chain length of 8 or 18. There are also silanes employed with terminal polar groups such as diol, cyano, and amino groups with a short *n*-alkyl spacer such as *n*-propyl. The latter are employed for consecutive reactions at the terminal polar group.

Depending on the surface modification, RP silicas can be grouped into (i) monomeric RP silicas chemically modified with monofunctional silanes and (ii) polymeric RP silicas with a polymeric layer made by surface reaction with trifunctional silanes.

3.2.6.4 Parent Porous Silica

The parent silica is usually subjected to activation prior to silanization, for example, treatment with diluted acids under reflux. In this way, the hetero-geneous surface becomes smoother with homogeneously distributed surface hydroxyl groups to ensure batch-to-batch reproducibility. Simultaneously, the treatment extracts traces of metals that would otherwise affect the chromato-graphic separation due to a secondary interaction mechanism, for example, ionic interaction of the solute with the adsorbent. Special care has to be devoted to the average pore diameter of the parent silica in relation to the size of the silanes and to the size of solute molecules to be resolved. For example, long-chain silanes drastically reduce the pore opening of the modified adsorbent, which leads to hindered diffusion of the components to be isolated. Peak broadening, reduced capacity, and low resolution are the resulting effects. Commonly, 10 nm pore diameter materials are recommended as starting silicas because a reduction of the specific surface area, a diminution of the specific pore volume, and a decrease of the average pore diameter occur by the silanization.

3.2.6.5 Reaction and Reaction Conditions

Silanization is a heterogeneous reaction. Silanes can be in the gas or liquid phase or in solution. The reaction is carried out at elevated temperatures, depending on the volatility of the silane and solvent, in a vessel under gentle stirring or in a fluidized bed reactor. To enhance the kinetics, catalysts are added. With chlorosilanes, organic bases are added as acid scavengers; acids are employed in the case of alkoxysilanes as reagents. By-products must be carefully removed by extraction with solvents.

3.2.6.6 Endcapping

The term endcapping originates from polymerization chemistry, when reactive groups are removed by a specific reaction after polymerization has occurred. After primary silanization, the maximum ligand density amounts to 3.5–4.5 $\mu mol\,m^{-2}$ for monofunctional silanes. As the initial hydroxyl group concentration is about 8 $\mu mol\,m^{-2}$, only half of the hydroxyl groups have reacted. The large size of the silanes makes it almost impossible to convert all hydroxyl groups due to steric reasons. The remaining are still present at the surface and provide the surface with a partially hydrophilic character. As a result, the chromatographic separation will show significant peak tailing due to the weak ion-exchange properties of the hydroxyl groups present. RP silicas, even those bonded with C_{18} groups, are operated with aqueous eluent up to approximately 70% v/v water/organic solvent, that is, the C_{18} bonded phases are not completely hydrophobic. To diminish the hydroxyl groups and the so-called silanophilic activity, the silanized materials are subjected to a second silanization with reactive short-chain silanes. Hexamethyldisilazane (HMDS) and others are the preferred reagent. Figure 3.6a represents the surface of a C_8-modified silica after endcapping.
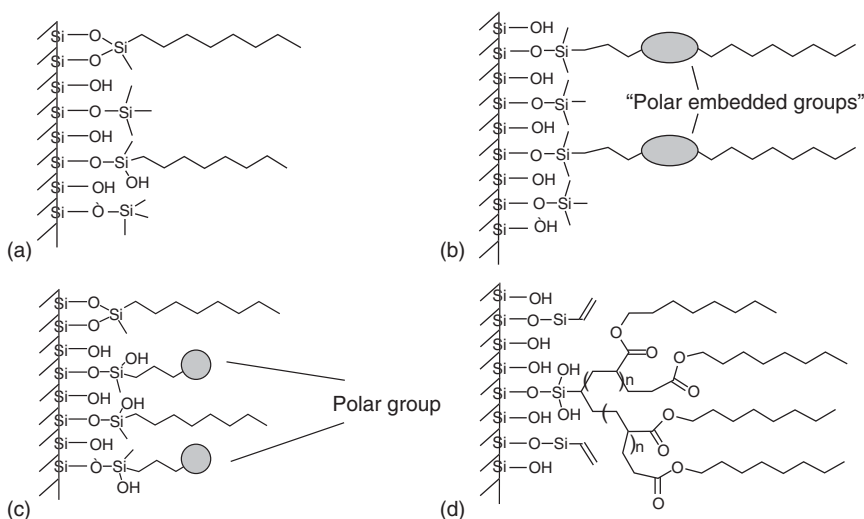
Figure 3.6 Types of RP columns. (a) "Brush" type; classical endcapping. (b) Shielded phases. (c) "Brush" type; "hydrophilic" endcapping. (d) PloyEncap-phase. Source: Engelhardt, Grüner, and Scherer (2001). Reprinted with permission of Springer Nature.

Endcapped RP silica packings exhibit a different selectivity toward polar solutes than nonendcapped materials. Unfortunately, these "base-deactivated" phases possess low polarity and therefore similar selectivity toward polar compounds. To overcome the lack of selectivity, a new type of base-deactivated stationary phase with polar groups, such as amides or carbamates, "embedded" in the bonded phase (Figure 3.6b) has been developed. These polar-embedded phases provide polar selectivity without the poor chromatographic performance associated with stationary phases that have high silanol activity. The use of polar or hydrophilic endcapping (Figure 3.6c) along with bonding of longer alkyl chains such as C_{18} is a successful approach for stationary phases that can retain polar analytes reproducibly under highly aqueous conditions. These polar or hydrophilic endcapping chemicals allow the silica surface to be wetted with water and allow the full interaction with the longer alkyl chains, that is, even 100% water can be applied as solvent.

Another option for RP silica packings is the introduction of a second brush-type modification, which exhibits an ionic-hydrophilic endgroup. This so-called doped reversed phase (DRP) has been developed by ZeoChem® especially for the separation of peptides and oligonucleotides. The best results are achieved in a separation mode, where the hydrophobic groups are used for attraction, while the ionic groups show repulsive characteristics.

Depending on the parent silica and the way the RP silica was modified with silanes, RP columns exhibit a distinct selectivity toward hydrophobic and polar solutes (Engelhardt, Grüner, and Scherer 2001).

3.2.6.7 Chromatographic Characterization of Reversed Phase Silicas

Surface-modified silica-based stationary phase packings in chromatography are mostly characterized under isocratic conditions. The employed tests help to assess chromatographic parameters and make it possible to compare different stationary phases. Robustness, reproducibility, and easy handling are the requirements for such tests. It is also important to separate extra-column effects in order to be able to evaluate the column itself rather than the whole high-performance liquid chromatography (HPLC) plant system. The following tests give information on hydrophobic properties (retention of nonpolar solutes), silanol activity (retention of base solutes), performance, purity, and shape selectivity toward selected solutes of modified materials in RP HPLC. It is impossible to find one single suitable test that covers the whole range of chromatographic properties. In addition, the following tests are performed under analytical chromatography conditions.

3.2.6.8 Chromatographic Performance

A general test procedure for RP phases should include the number of theoretical plates N as a function of column diameter and of loading. The number of theoretical plates N is a measure of the peak broadening of a solute during the separation process (for definitions see Chapter 2). The efficiency of a column can be given for any solute of a test mixture but is strongly dependent on the retention coefficient of the solute. It should be determined in columns of different diameter to make sure that the column packing process is reproducible over a certain range

Table 3.5 Performance of RP silica packed into columns with different i.d.

Packing material	*N* (reduced plate height) column i.d.			
	4.6 mm	**10 mm**	**25 mm**	**50 mm**
Kromasil® C8, 13 μm	36 000 (2.14 μm)	30 000 (2.56 μm)		28 000 (2.75 μm)
PharmPrep™ P 100 RP-18e, 10 μm	31 900 (3.13 μm)	32 900 (3.04 μm)	35 600 (2.81 μm)	39 200 (2.39 μm)

Kromasil®: acetophenone 500 μl or 1 : 300 diluted tracer, 70% acetonitrile, 30% water, all columns 250 mm long; data from Dave et al. (2008).
PharmPrep™ P 100: acetophenone, 75% acetonitrile, 25% water, column length 225 (5 cm i.d.); Merck internal data.

of column diameters. Table 3.5 gives results for two RP packings in columns with a diameter up to 50 mm.

In preparative chromatography it has to be taken into account that the concept of theoretical plate number is only valid in the linear range of the adsorption isotherm. As soon as the amount of sample is increased, the plate number decreases, so at high loads the column efficiency of 10 μm high-efficiency packings and packings of coarse 40–63 μm are no longer different in efficiency (Figure 3.7). Under these conditions the coarse, low-pressure packing should be preferred. On the other hand, if efficiency is needed for the separation of critical impurities, the load has to be kept at a certain maximum.
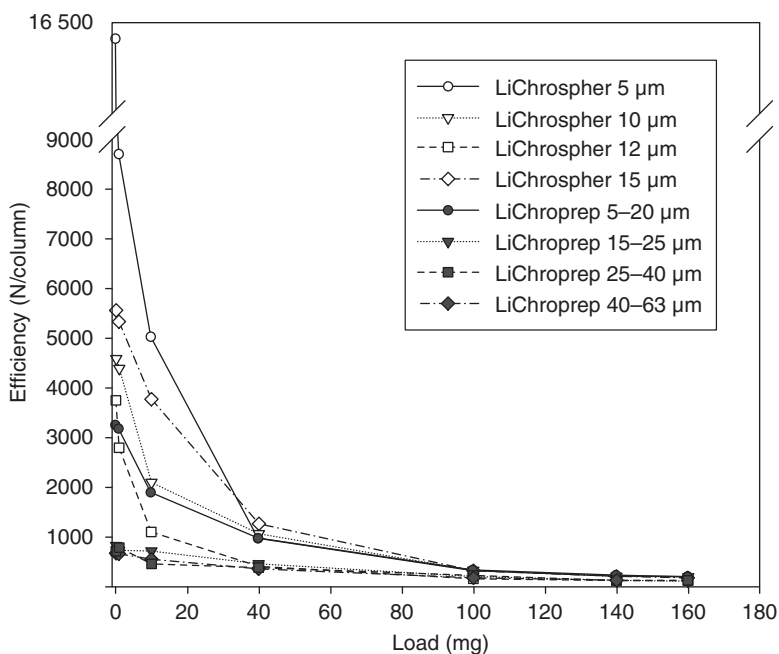
Figure 3.7 Column efficiency versus load for normal phase silica, LiChrosper® is a spherical silica material, while LiChroprep® is an irregular-shaped sorbent.
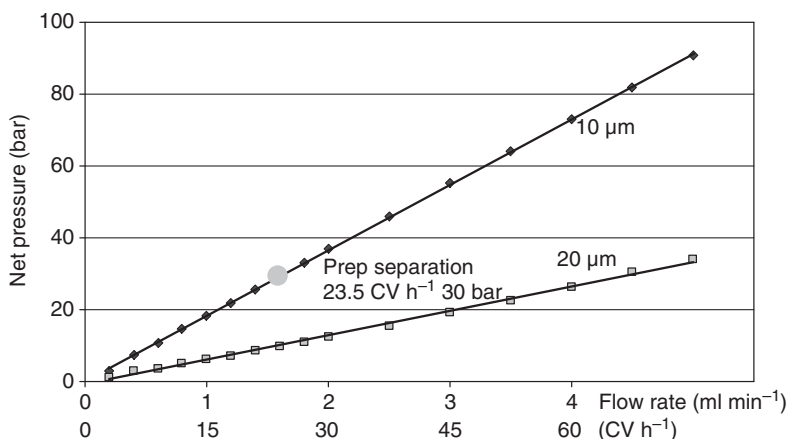
Figure 3.8 Pressure versus flow behavior of 10 and 20 μm PharmPrep® P 100 RP-18, analytical column size: 250 × 4.6 mm i. d., mobile phase: acetonitrile/water 75/25.

Another important general characterization parameter is the velocity versus pressure behavior. There should be a linear relationship between both over a long velocity range. As it can be seen from Figure 3.8, the slope of the pressure increase is different for 10 and 20 μm materials as expected. In addition, the single point for a column of 5 cm i.d. shows a good accordance with the measured parameter of the 4.6 mm i.d. test column.

3.2.6.9 Hydrophobic Properties Retention Factor (Amount of Organic Solvent for Elution), Selectivity

A dependency on the type of ligand, its density, the eluent used, and temperature is found when evaluating hydrophobicities of stationary phases. This property can be assessed by the retention factor of a hydrophobic solute or by the ratio of the retention factors of two nonpolar solutes. The latter is called selectivity; for example, when the components differ only in one methyl group, the term methylene selectivity coefficient is applied. Hence, hydrophobic properties describe the polarity of a column and its selectivity toward solutes with only small differences in polarity.

If the maximum retention is needed for a given solute, the RP column can be operated with 100% water as eluent. It has to be tested if the stationary phase is able to be operated under completely aqueous conditions. Especially for end-capped phases, there is a certain risk that the alkyl chains stick together and the retention factor drastically decreases. Figure 3.9 shows the retention of five test compounds on PharmPrep® P 100 RP-18e, 10 μm operated for seven days (>3.200 CV) with 1% acetic acid in 100% water as the eluent. It can be seen that the surface modification is not changing and even after seven days, the separation efficiency remains stable.

3.2.6.10 Shape Selectivity

Molecular recognition of the solute by the stationary phase with respect to its geometrical dimension is called shape selectivity. For this test, one
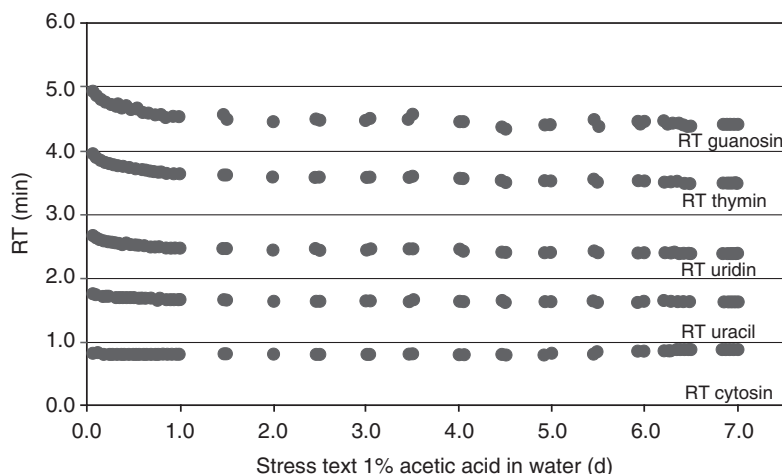
Figure 3.9 Evaluation of column stability under 100% water as the eluent. Stationary phase: PharmPrep® P 100 RP-18e, 10 µm, retention factor for five different test compounds (guanosine, thymin, uridine, uracil, and cytosine).

can employ aromatic components with identical hydrophobicity that differ only in their three-dimensional shape. The chromatographic selectivity of *o*-terphenyl/triphenylene or tetrabenzonaphthalene/benzo[*a*]pyrene are commonly used and show dependencies on several features of the phase, for example, pore structure, ligand type, and density. Figure 3.10 shows a chromatogram of a test mixture of uracil (t_0 marker), *n*-butylbenzene, and *n*-pentylbenzene (to assess hydrophobic properties and efficiency), and *o*-terphenyl and triphenylene
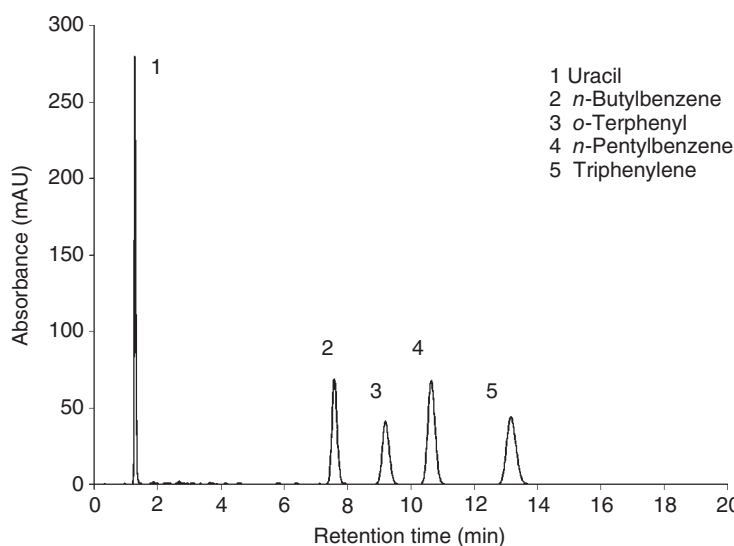
Figure 3.10 Chromatogram of a test mixture to assess hydrophobic properties, efficiency, and shape selectivity of an RP material (eluent: methanol/water, 75 : 25 v/v).

(to assess shape selectivity). The test mixture was chosen to provide a short analysis time and to facilitate calculation of parameters from baseline-separated peaks.

It has to be pointed out that RP sorbents are not the first choice for the separation of a special group of compounds with different shape selectivity, namely, stereoisomers. Stereoisomers or diastereomers differ only in the three-dimensional orientation of their chemical constituents. To separate them by chromatography, normal phase sorbents show a higher success rate as demonstrated by Eblinger and Weller (2013) for the separation of 258 stereoisomers tested in supercritical fluid chromatography (SFC) mode with different types of stationary phases. The highest number of separations for the individual stereoisomers could be achieved by normal phase silica and a 2-pyrenyl-ethyl-modified phase. This highlights the fact that for the separation of stereoisomers, the sorbent has to offer three-dimensionally orientated ligands, either in the presentation of silanol groups (for normal phase silica) or the three dimensional aromatic pyrenyl group.

3.2.6.11 Silanol Activity

As already mentioned, a certain amount of silanol groups remains unreacted on the surface after silanization. To suppress the resulting secondary interactions in HPLC, buffers can be applied. The selectivity of two basic compounds is a measure of silanol activity. Another way to gain information on this property is to assess the peak symmetry of a basic solute, which is defined as the tailing factor by the United States Pharmacopeia (USP) convention. Figure 3.11 shows a chromatogram of a test of uracil (t_0 marker), benzylamine, and phenol using a nonendcapped stationary phase. As can be seen, benzylamine shows peak tailing, indicating strong interaction with residual hydroxyl groups of the silica surface. Some novel adsorbents with hydrophilic endcapping have been developed, which
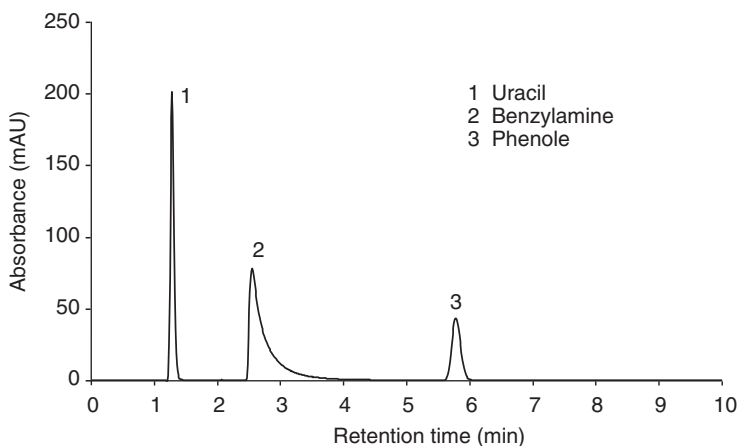
Figure 3.11 Chromatogram of a test mixture to assess the silanol activity of an RP material (eluent: methanol/buffer, 30 : 70 v/v, pH 7.0).

reduce peak tailing of base components while retaining high selectivity toward polar and nonpolar solutes.

Residual silanol groups on the other hand may contribute to the selectivity of a given stationary phase. It has been shown by Wenzel et al. (2010) that these additional groups are beneficial for the separation of constitutional and diastereomeric isomers.

3.2.6.12 Purity

Metals present at the surface of the phase increase the number of secondary interactions with basic substances. One of the proposed tests using 2,2′-bipyridine (complex-forming type) and 4,4′-bipyridine (inactive type) shows a good correlation between the metal content and the peak symmetry of the complexing base, starting at impurity levels around 100 ppm. However, the results change with increasing lifetime of the column as metal ions are accumulated during use.

3.2.6.13 Improved pH Stability Silica

One of the drawbacks of silica-based adsorbents is their limited stability toward alkaline conditions. Above a pH range of 11 silica is dissolved over a longer period of time. Addition of salts, e.g. buffers, is even accelerating this process during chromatographic operation. To overcome this instability, several adsorbents have been introduced, which are based on a mixture of silanol and organosilanol derivatives. As the Si—C bond is more pH stable compared with the Si—O bond, these materials give a higher total stability. On the other hand, as the number of reactive silanol groups is reduced, the derivatization with RP alkyl chains is more difficult. Table 3.6 shows the adsorbents that are available at least in 10 μm particle size for preparative purposes.

For classical inorganic silicas, Nawrocki summarized the conditions for silica dissolution in his extensive review in 1997 (Nawrocki 1997). It can be seen from Table 3.7 that the lifetime for the use of a silica stationary phase is heavily

Table 3.6 Reversed phase silica sorbents with extended alkaline stability.

Material	Particle size	Surface area	Pore size	pH stability	Modification	Chemistry
Kromasil® Eternity	1.8–10 μm	310 m^2 g^{-1}	10 nm	pH 1–12	C8, C18	Reinforced inorganic/organic silica
Waters XTerra®	2.5–10 μm		12 nm	pH 1–12	C8, C18	Hybrid inorganic/organic
Phenomenex® Gemini	3, 5, 10 μm	375 m^2 g^{-1}	11 nm	pH 1–12	C8, C18	
YMC, TriArt	10, 15, 20 μm	C18: 360 m^2 g^{-1} C8: 220 m^2 g^{-1}	C18: 12 nm C8: 20 nm	pH 2–10	C8, C18, phenyl, PFP, diol	Hybrid inorganic/organic

Table 3.7 Conditions influencing the stability of silica sorbents.

Higher stability	Lower stability
Monomeric C18 bonds	Bulky C18 substituents
Sol/gel silicas	Silicas from gelated soluble silicates
Acetonitrile	Methanol
Organic buffers	Inorganic buffers > carbonate, phosphate
Less concentrated buffers	Higher concentrated buffers
Low temperature	High temperature
Li > Na	K > NH_4

dependent on the chosen operating conditions. Thorough process development with a focus on milder conditions for the silica gel will result in better process economy related to the longer lifetime of the stationary phase.

Different methods have been established to test the alkaline stability of silica. Besides the simple monitoring of the shift in retention time or resolution, Kirkland, van Straten, and Claessens (1995) proposed a method where the amount of silica eluting from a packed column is determined with a colorimetric procedure by forming a yellow β-silicomolybdenic acid. Using these procedures, the total amount of cleaning-in-place (CIP) solution can be estimated. The productivity over lifetime of a stationary phase can then be roughly calculated using the simple Eq. (3.2):

$$\mathrm{Prod} = \frac{\mathrm{CV}}{V_{\mathrm{CIP}}} \times R_{\mathrm{in}} \times L \tag{3.2}$$

where

Prod (kg/kg) = amount of product injected per kg of silica
CV = column volumes of CIP solution
V_{CIP} = column volume of CIP solution per CIP run
R_{in} = number of injections between two CIP runs
L = load of product per amount of stationary phase (kg/kg)

Taking the polishing of insulin as one of the biggest processes, where RP silica chromatography is used, a value of 5 kg insulin injected per kg of stationary phase should be exceeded for an economic process.

3.2.7 Aluminum Oxide

Aluminum oxide was one of the first adsorbents introduced in the beginning of the twentieth century. The starting material for processing porous alumina is crystalline gibbsite, $Al(OH)_3$, which is subjected to a heat treatment, under controlled conditions, between 500 and 800 °C. During this process, water is released, leaving crystalline porous alumina (γ-alumina) (Unger 1990). Due to its chemical properties, aluminum oxide is the prototype of an amphoteric oxide. It

Table 3.8 Aluminum oxide with different surface properties.

Aluminum oxide type	pH
Basic	9.5 ± 0.3
Neutral	7.5 ± 0.5
Weakly acidic	6.0 ± 0.5
Acidic	4.5 ± 0.5

Table 3.9 Different Brockmann grades of aluminum oxide.

Brockmann grade	Amount of water to be added to Brockmann grade I (%)	Approximately water content (%, Karl Fischer method)
I	0	
II	3	4–4.5
III	6	7–7.5
IV	10	11–11.5
V	15	16–16.5

can act with acids and bases and is therefore obtained as neutral, acidic, and basic Al_2O_3. Through this variation, the adsorption properties can be widely tuned, making aluminum oxide a very versatile adsorbent, e.g. for the purification of alkaloids, amines, steroids, terpenes, and aromatic and aliphatic hydrocarbons. Different pH grades are commercially available. The apparent surface pH is measured as a 5% stirred aqueous suspension (Table 3.8).

It was as early as 1941 when Brockmann and Schodder described a system where the adsorption behavior of aluminum oxide is standardized via the addition of certain amounts of water (Brockmann and Schodder 1941). When aluminum oxide is heated up to 400–450 °C, water is completely removed, and aluminum oxide with an activity coefficient I according to the Brockmann scale is achieved. By addition of defined amounts of water, the higher Brockmann grades can be prepared (Table 3.9).

As the water is taking part in the separation process giving additional selectivity, the different Brockmann grades can be tested for their individual selectivities.

3.2.8 Titanium Dioxide

Another inorganic oxide with good stability properties is titanium dioxide. It has been produced by Sachtleben following a procedure described by Winkler and Marmé (2000).

One of the difficulties of porous titanium dioxide is its lower mechanical stability as well as its reduced activity compared with silica for the derivatization toward RP materials.

3.2.9   Other Oxides

Other types of oxides are used in preparative chromatography for special applications. Florisil® is a mixed sorbent of 15.5% magnesium oxide and 84.5% silicon dioxide. The material has a surface pH of around 8.5, a specific surface area of $300\,m^2\,g^{-1}$, and a high specific density of $2.51\,g\,ml^{-1}$. The activity is controlled via temperature, and a highly active form is achieved after heat treatment to 675 °C. Steroids and alkaloids are separated by Florisil.

The separation of hydrocarbons, cholesterol esters, triglycerides, free sterols, diglycerides, monoglycerides, and free fatty acids was one of the first examples reported for Florisil in comparison with silica gel. Ease of use, full sample recovery, and high reproducibility were some of the advantages. The order of elution was the same as that observed in silicic acid chromatography except that free fatty acids were eluted after monoglycerides. Phospholipids were not eluted under the conditions used for separating the above compounds and were eluted less readily from Florisil than from silicic acid with methanol (Carroll 1963). Glowniak (1991) evaluated the selectivity of silica and Florisil for the separation of naturally occurring pyranocoumarins. Florisil showed the higher selectivity for the isolation of visnadine, a vasodilating drug substance from *Ammi visnaga*.

3.2.9.1   Magnesium Oxide

More recently porous hierarchical magnesium oxide (MgO) has been prepared and evaluated according to its adsorption properties by Tian et al. (2013).

With a surface area of $148\,m^2\,g^{-1}$, the material has been able to adsorb up to $2.5\,g\,g^{-1}$ of the dye Congo red. MgO sorbents with similar surface areas have been previously described, but the high adsorption capacity seems to be attributed to the hierarchical ordered structure of the material.

3.2.9.2   Zirconium Dioxide

Zirconium dioxide exhibits a significant Lewis acid character showing high binding strength toward Lewis bases. The adsorption strength increases in the order chloride < formate < acetate < sulfate < citrate < fluoride < phosphate < hydroxide. Supel™ QuE Z-Sep sorbents are zirconia-coated silica particles, developed by Supelco for solid-phase extraction purposes, that show a very strong adsorption for different classes of phospholipids (Lu, Claus, and Bell 2013). For the purification of samples with a high amount of fat (>15%), a mixed-mode material has been developed (Supel QuE Z-Sep+) that exhibits both C18 alkyl chains and zirconia groups on a silica backbone.

A porous zirconia sorbent prepared by the oil emulsion method and the polymerization-induced colloid aggregation (PICA) method has been introduced by Rigney, Funkenbusch and Carr (1990).

Under the trade name ZirChrom™, zirconia-based sorbents have been introduced as 3 µm monodisperse particles with a pH stability from 1 to 14. If those materials should be transferred into RP packings, a coating with polybutadiene is typically added.

The selectivity of zirconia and magnesia-zirconia has been investigated by Wang et al. (2014) in hydrophilic interaction mode. For the separation of the

anti-vomiting drug ondansetron and five process-related impurities, a series of zirconia- and titania-based adsorbents were compared with standard RP silica materials by Zizkovsky, Kucera, and Klimes (2007). For the polybutadiene-coated zirconia, a good selectivity was observed with a mobile phase system based on acetonitrile and 25 mM ammonium phosphate.

3.2.10 Porous Glasses

Porous glass is a glass manufactured from silica (50–75%), sodium oxide (1–10%), and boric acid (to 100%) by special heat treatment and leaching processes where the porosity and pore size are adjusted and controlled (Janowski and Heyer 1982; Schnabel and Langer 1991). The pore size distribution of these controlled pore glasses (CPG) named sorbents is very homogeneous and can be varied from 7.5 to 400 nm. The particle shape due to the manufacturing process is irregular, but special treatments to obtain spherical materials are known. The high mechanical strength and defined chemical composition are the advantages of CPG. Modification chemistry is based on silane linkers comparable with those technologies described for modified silica gels. As silica gels, CPG does not remain alkali resistant above pH 8, but cleaning and sanitization procedures based on acidic solvents are well described and widely used in the biopharmaceutical industry.

The main application field of CPG is the use as solid-phase synthesis material for the synthesis of oligonucleotides. Different pore sizes (33, 50, or 100 nm) are applied according to the maximum length of the synthesized oligonucleotide. The typical particle size distribution is in the area of 100–180 µm with a total pore volume of $1.3 \, \text{ml} \, \text{g}^{-1}$. All CPG qualities are offered with the different starting nucleotides attached to the bead surface.

The second main application of CPG is its use as a support for larger affinity ligands, mainly protein A due to the large and very regular pore system. The even distribution of the pores results in short diffusion times for the large target molecules in the pore system of the adsorbent. Figure 3.12 shows a comparison of the remaining capacity for different protein A resins when they are operated at a fast speed (two minutes residence time) compared with the operation at maximum capacity (typically six or eight minutes residence time). It can be seen that the CPG-based ProSep® Ultra Plus and the polystyrene-based perfusion resin POROS™ maintain 90% of their starting capacity while all resins based on polyvinylether (Eshmuno® A), polymethacrylate (Amsphere™ A3), or cross-linked agarose (MabSelect™ SuRe™, PrismA, and LX) lose up to 50% of their initial capacity. High capacity at short residence times is a key benefit especially for intensified antibody capture processes using multicolumn setups.

To overcome the only drawback of CPG, its limited stability against caustic cleaning, several modifications have been recently tested. Hasanuzzaman, Rafferty, and Olabi (2014) substituted SiO_2 by $ZrSiO_4$ in the starting mixture of the borosilicate glass. They obtained a final product with similar porosity but a higher alkaline stability, resulting in a weight loss per total surface area of only $0.09 \, \text{mg} \, \text{dm}^{-1}$ versus $0.35 \, \text{mg} \, \text{dm}^{-1}$ for a standard product.
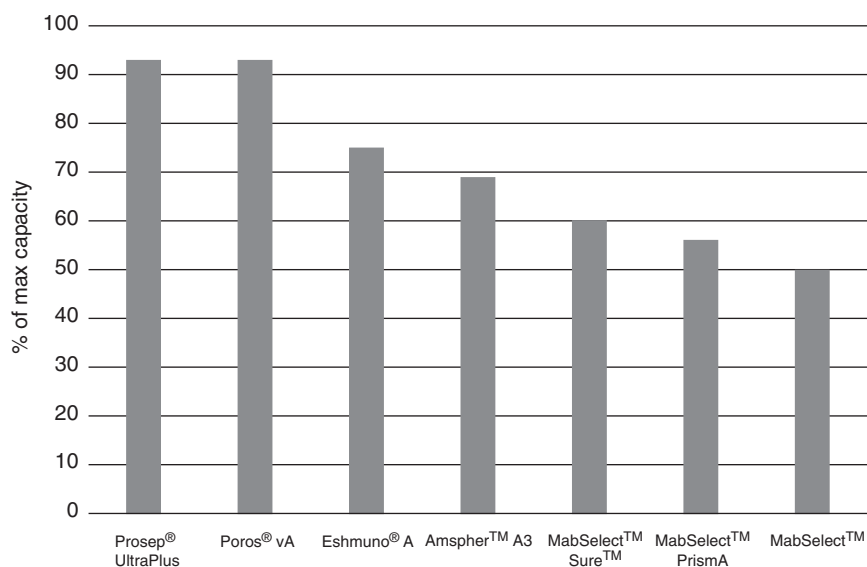
Figure 3.12 Comparison of the capacity at 2 min residence time versus the maximum capacity for different protein A resins. Source: Data from manufacturers technical data sheets and own experiments.

3.3 Cross-Linked Organic Polymers

Organic-based supports for use in liquid chromatography have appeared mostly through applications in biochromatography and in size-exclusion applications for organic polymers. Such applications also represent the two different basic "sources" of organic polymers for separation purposes: natural polymers, such as agaroses and dextrans with varying degrees of cross-linking, and synthetic organic polymers, such as hydrophobic styrene DVB copolymers as well as more hydrophilic materials such as poly(vinyl acetates), synthesized in the late 1960s by Heitz (1970) predominantly for use in size-exclusion chromatography (SEC). Between 1956 and 1962 three hydrophilic natural polymers had been introduced as chromatographic sorbents:

- Cellulose by Peterson and Sober (1956);
- Cross-linked dextran first introduced as size-exclusion material by Porath and Flodin (1959), later applied to ion-exchange (IEX) chromatography;
- Beaded agarose by Hjerten (1964).

These polymers show low unspecific binding to proteins due to their hydrophilic nature but are of limited stability when operated in large-scale columns. Due to the weight of the packing material, the packed bed is compressed, and the linear flow rate has to be drastically reduced. To overcome this drawback, some materials have been cross-linked to stabilize the particles. These classical-type materials have been widely reviewed elsewhere (Jungbauer 2005; Curling and Gottschalk 2007).

Synthetic organic porous polymers in chromatography suffered for a long time from structural problems. One was the diffusion hindrance in the porous structures – mostly traced back to a considerable amount of micropores generated during the synthesis. The other issue interfering with its more widespread use was the compressibility of the beads, limiting their use significantly, especially in high-pressure applications above around 5 MPa. Several approaches have helped to significantly overcome many of these drawbacks, allowing better utilization of their useful properties in loading, selectivity, and cleaning. One approach was the development of more selective synthesis procedures, generating better-defined pore structures with significantly reduced micropores together with the synthesis of macroporous material with much higher rigidity, making the use of porous polymers possible even in large-scale preparative chromatography environments. Another was the control of particle size during synthesis, leading to a much better particle size distribution and even to monodispersity, resulting in reduced backpressure during operation and longer maintenance of the initial system pressure due to lack of generation of fines during operation.

3.3.1 General Aspects

Synthetic cross-linked organic polymers were introduced as packings in column liquid chromatography one decade later than oxides. The first organic-based packings were synthetic ion exchangers made by condensation polymerization of phenol and formaldehyde (Adams and Holmers 1935). In the 1960s, procedures were developed by Moore (1964) to synthesize cross-linked polystyrenes with graduated pore sizes for SEC. The synthesis of cross-linked dextran (Porath and Flodin 1959; Janson 1987) and agarose (Hjerten 1964) was a milestone in the manufacture of polysaccharide-type packing. At the same time, polyacrylamide packings were synthesized from acrylamide and *N*,*N*-bismethylene acrylamide by Lea and Sehon (1962).

All the above products, except the first, served as packings in SEC. The major breakthrough in the synthesis of cross-linked organic polymers with tailor-made properties for column liquid chromatography occurred in the decade 1960–1970 (Seidl et al. 1967).

Textbooks often treat the structure of organic- and oxide-based materials according to different aspects (Epton 1978). On viewing a particle of an organic polymer and an oxide, its structure is best described by a coherent system either of three-dimensionally cross-linked chains or of a three-dimensional array of packed colloidal particles as limiting cases. Thus, previous classifications into xerogel, xerogel–aerogel hybrid, and aerogel appear to be inadequate. To provide a sufficient rigidity of particles, the chains or colloidal particles should be linked by chemical bonds rather than by physical attraction forces.

Some examples serve to illustrate the structure of organic-based packings. Figure 3.13 (Hjerten 1983) shows a scheme of the structure of a cross-linked polyacrylamide gel (Figure 3.13b) and a cross-linked agarose gel of an equivalent polymer concentration (Figure 3.13a). Both polymers possess a random coil structure. In the agarose, the double-helix-shaped chains are collected in bundles that generate quite an open structure (Arnott et al. 1974). The structure

(a)   (b)
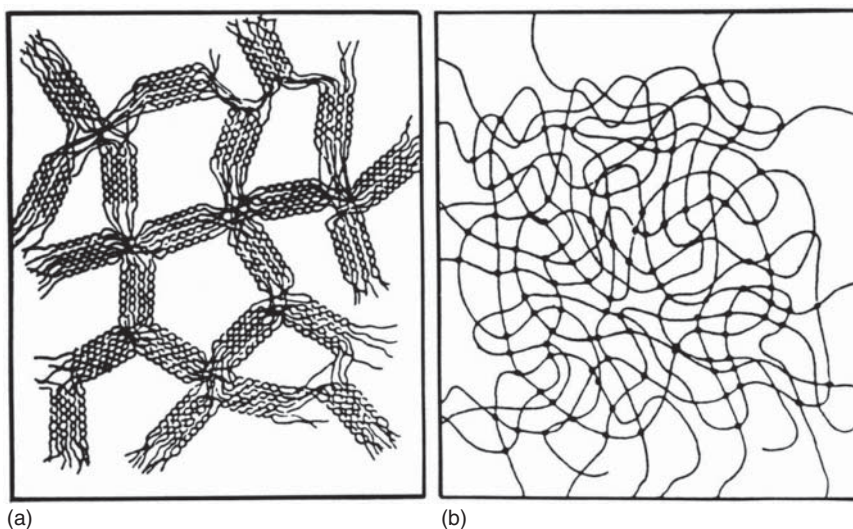
Figure 3.13 Scheme of the agarose gel network (a) compared with a network formed by random chains of Sephadex or Biogel P (b) at similar polymer concentrations. Source: Hjerten (1983). Reprinted with permission of Elsevier.

is stabilized by hydrogen bonds between the chains. When agarose is subjected to cross-linking, links are formed among the chains in these bundles (Porath, Laas, and Janson 1975).

Macroporous, macroreticular, or isoporous polymer packings exhibit another type of structure Figure 3.13. As the name implies, these polymers contain so-called macropores (>100 nm) and micropores (<2 nm), the latter being inaccessible to large solutes. In other words, macroporous polymer particles constitute an agglomerate made of secondary particles that themselves represent agglomerates of microspheres. This structure resembles that of porous silica particles, which are composed of agglomerates of spherical colloidal silica particles. With respect to the mechanical rigidity of the polymeric packings, cross-linking becomes an essential means in the synthesis. Other requirements that must be met are insolubility, resistance to oxidation and reduction, and a defined, controllable, and reproducible pore structure (Figure 3.14).

Polymerization is performed either by condensation or addition polymerization, depending on the type of starting monomer. For cross-linking, comonomers such as DVB (styrene), ethylene glycol dimethacrylate, epichlorohydrin, 2,3-dibromopropanol, and divinylsulfone (saccharides) are added (Ghethie and Schell 1967; Porath, Janson, and Laas 1971; Laas 1975). The cross-linking reagent can amount to as much as 70 wt%. Macroporous copolymers are synthesized in the presence of an inert solvent that functions as a volume modifier. Both the cross-linker and the inert solvent have a substantial impact on both the polymerization kinetics and the resulting properties of the copolymer. The decisive parameters relevant for the synthesis of macroporous copolymers have been reviewed by Mikeš et al. (1976). As in the synthesis of

(a)

(b)
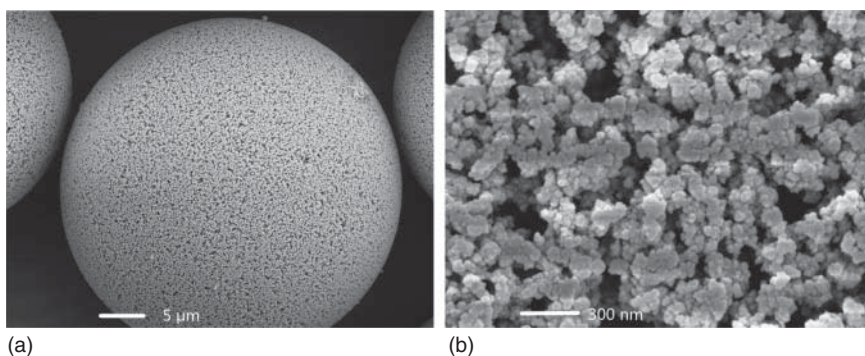
Figure 3.14 SEM picture of a macroporous polymer bead (Eshmuno®); magnification 2000×
(a) 50 000× (b).

silica packings, specific processes must be chosen in polymerization to manufacture polymeric packings with beads of controlled size (Bangs 1987). Emulsion polymerization starts with a solution of a detergent to which the monomers are added. As a result, micelles swollen with the monomer are formed. After a water-soluble initiator is added (for styrene as a monomer), polymerization leads to particles of exactly the same size as the swollen micelles. Emulsion polymerization processes generate particles of up to 0.5 μm in one step.

Suspension polymerization is usually designed to prepare larger beads, >5 μm mean particle diameter. The monomer or comonomer solution is vigorously agitated in water in the presence of a colloidal suspending agent. The colloidal agent coats the hydrophobic monomer droplets (in the case of, e.g. styrene or DVB). Coalescence of the droplets is prevented by their surface. Adding a lipophilic catalyst or initiator starts the polymerization in the droplets, and this continues until the beads are solidified in bulk. The size of the beads is thus controlled by the size of the droplets via the stirring speed.

A third variant in polymerization technology is the swollen emulsion polymerization pioneered by Ugelstad et al. (1980). The procedure is performed in two steps. First, the polymerization is started by adding a swelling agent, which causes the submicrometer polymer particles to swell by large volumes of the monomer. The increase in volume can reach a factor of 1000. Second, the monomer-swollen beads of defined size are polymerized in a consecutive step.

Having briefly examined the structure of organic packings and the various routes in their manufacture, the most important features may be summarized as follows:

- Hydrophilic as well as lipophilic organic packings are synthesized with a controlled pore and surface structure depending on the type of monomer/comonomer and the polymerization reaction. Surface structure can be altered by controlled consecutive surface reactions.
- In accordance with the bulk composition, polymer packings are stable across almost the entire pH range, particularly under strong alkaline conditions.
- Chemical stability is affected by oxidizing and reducing solutions.

- Although cross-linking reactions have been optimized in as much as rigid pressure stable particles can be manufactured, some remaining swelling property is often noted when changing the solvent composition of the chromatographic system.
- As in the manufacture of silica, porosity, pore size, and surface area of polymer packings can be adjusted over a wide range, and micro-, meso-, and macroporous as well as nonporous beads are synthesized reproducibly.

3.3.2 Hydrophobic Polymer Stationary Phases

The synthesis of cross-linked copolymers of styrene and DVB has been studied intensively and is well documented. The starting monomer is styrene, and DVB is used as cross-linker. The amount of DVB can reach up to 55 wt%. At 55% DVB, the copolymer shows practically no swelling and possesses a permanent porosity. Figure 3.15 illustrates the network structure of poly(styrene-divinylbenzene) (St-DVB).

Commercial products differ in bead size and pore size. There are even non-porous products on the market designed for the rapid separation of peptides and proteins by RP HPLC (Maa and Horvath 1988). St-DVB copolymers are stable in the pH range 0–14. They find increasing application in the separation of low molecular weight compounds, peptides, and proteins by means of RP chromatography (Tanaka, Hashizume, and Araki 1987; Tweeten and Tweeten 1986) and as parent materials for the synthesis of derivatized packings in inter-action chromatography of biopolymers (Unger, Janzen, and Jilge 1987; Regnier 1987). Numerous other organophilic polymer packings have been synthesized for size-exclusion and interactive HPLC after suitable derivatization. They are reviewed in depth by Mikes (1988).

The first styrene-divinylbenzene copolymers had been developed by Griesbach at Farbenfabrik Wolfen in 1937. These classical adsorbents are widely used in water deionization as well as in applications such as sugar separations and the separations of different ions, for example, in the nuclear industry and for the sep-aration of rare earth elements. Classical IEX resins are typically produced in the

Figure 3.15 Poly(styrene-divinylbenzene).
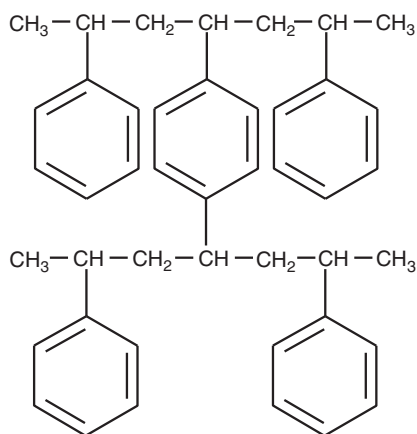
millimeter size and show a strong swelling behavior in different solvents. Due to their low-cross-linked polymer structure, they can only withstand a moderate pressure drop and are not intended for use in high-pressure liquid chromatography. They are directly modified mainly with sulfo groups (cation exchangers) and quaternary ammonium groups (anion exchangers). Today, the main products on the market are Lewatit® (Lanxess), Dowex® (Dow Chemicals), Amberlite® (Rohm and Haas), and Purolite® (Purolite).

Purolite has recently introduced a core–shell (or Shallow Shell™) technology resin with the Purolite SST product range. Taking into account that the volume of the inner core of a particle is very small and thus not contributing much to the overall capacity of the resin and on the other hand the diffusion path length toward this inner core is the longest, the idea of a core–shell particle is quite convincing. On a hard inner core, which increases the overall particle stability, a porous shell is constructed. Purolite claims that without significantly reducing the resins capacity, the regeneration costs for the resins can be reduced by 20–50% because of the lower amount of regeneration solvent that is needed.

The synthesis of high-pressure stable monodisperse polystyrene-based chromatographic resins is based on the previously described (Ugelstad 1984). The synthesis starts with a monodisperse, non-cross-linked submicron seed particle that is grown by a swelling process up to diameters typically ranging between 5 and 15 μm. The swelling monomer mixture typically consists of styrene and DVB monomers as well as the porogen solvent mixture determining the later pore structure. Resins of this type are, for example, Source™ (GE Healthcare), Amberchrom™ HPR10 (Rohm and Haas), Mitsubishi CHP 5C, and Varian PLRP-S. These resins are used mainly in the polishing step of small proteins and peptide-purification processes.

Another type of polystyrene resin has been introduced in 1990 by Perseptive Biosystems with the POROS® Perfusion Chromatography® resins. They are used as IEX and protein A resins for some biopharmaceutical downstream purification processes. It has to be pointed out that due to its hydrophobic nature, polystyrene is incompatible with protein purification. Any contact with the hydrophobic surface will lead to severe precipitation of the protein. Therefore, the surface has to be first hydrophilized by the application of a hydrophilic network polymer. Due to the particle diameter of around 45 μm, which is significantly smaller compared with other types of IEX resins, these resins show a steep breakthrough curve and high dynamic binding capacity compared with agarose-type resins. The overall performance is in accordance with that of other modern-type polymeric resin materials.

3.3.3 Hydrophilic Polymer Stationary Phases
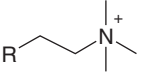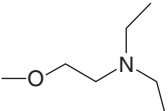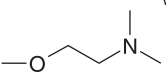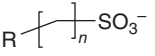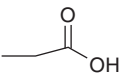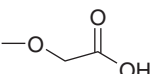
Hydrophilic polymer sorbents currently used in biochromatographic processes are based on natural polymers, e.g. agarose, polymethacrylate, and polyvinylether. These materials will be discussed in the form of their functionalized products. Nevertheless, some of the polymers are used in their native form as resins for SEC.

3.3.4 Ion Exchange (IEX)

Protein purification by IEX has been dominated in the past by soft gel matrices based on agarose, cross-linked cellulose, or dextran. These were the only hydrophilic base materials available that could be modified with ionic groups. Coarse and nonhydrophilized IEX materials based on polystyrene cannot be used for protein chromatography as the hydrophobic surface will denature the proteins and the pore sizes of PST-based materials are usually too small. Today, a huge variety of hydrophilic polymers based on methacrylate or vinylethers are available. These materials have a much higher rigidity and allow a faster operation even of large-diameter columns, opening a new dimension for the multi-ton production of modern therapeutic proteins as well as specialized enzymes.

IEX materials may be easily modified with anionic or cationic groups of different strength. Mixed interaction materials with more than one ionic interaction principle or an ionic active group in combination with, for example, hydrophobic groups are summarized under the group of mixed-mode resins and will be discussed in Section 3.3.5. The ionic groups can be divided into strong and weak ionic groups for both cation and anion exchangers. "Strong" ion exchangers exhibit their ionic nature over a broader pH range compared with "weak" ion exchangers. The binding strength toward a certain protein is not covered by this definition. The most common ionic groups together with their operating pH ranges are listed in Table 3.10. The two main groups for strong ion

Table 3.10 Ion-exchange ligands.

Functional group	Structure	Description	Operating range pH	pK_a value/ category
TMAE/Q		Trimethyl-ammoniumethyl	6–10	>13/strongly basic
DEAE		Diethyl-aminoethyl	6–8.5	11/weakly basic
DMAE		Dimethyl-aminoethyl	6–8.5	8–9/weakly basic
SO₃/SE/SP/S		Sulfoisobutyl/ sulfoethyl/ sulfopropyl/ sulfonate	4–8	<1/strongly acidic
COO		Carboxy	5–8	4.5/weakly acidic
CM		Carboxymethyl	5–8	4.5/weakly acidic
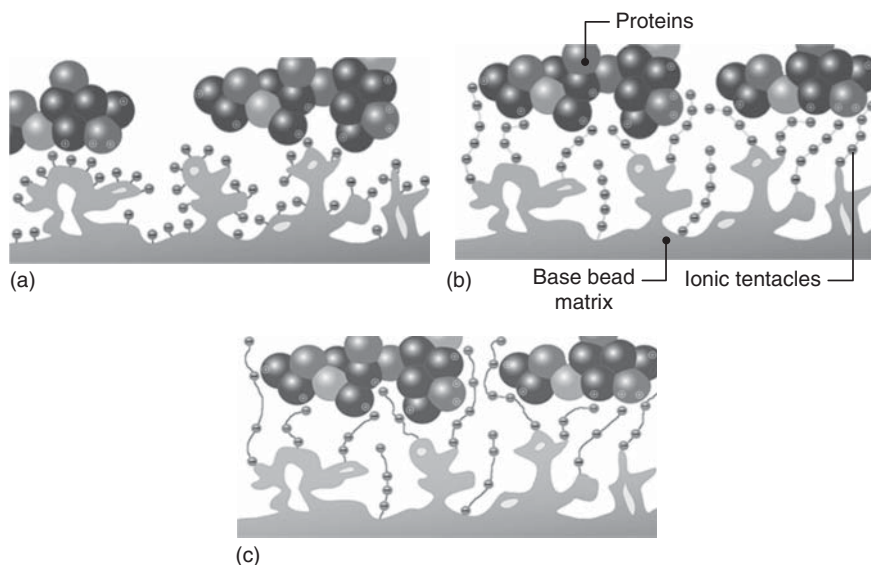
Figure 3.16 Presentation of ionic ligands on different ion-exchange type resins: (a) directly attached to the surface, (b) tentacle-type ion-exchange resin, and (c) enhanced flexibility tentacle resins.

exchangers are the Q-group (derived from the quaternary amino function of the trimethylammoniumethyl group) and the S-group from the sulfo group.

The type of attachment of the ion group on the surface of the base sorbent is of great importance, as the proteins to be separated have to come into close contact with the ionic group. If the ionic group is directly attached to the sorbent surface (Figure 3.16a), the pore has to be quite wide and open so that the ionic groups are presented on a plain surface able to bind the protein over its full footprint. Ionic groups hidden in small pores or on a rough sorbent surface will not take part in the adsorption of proteins and are therefore useless for the separation. To overcome this problem, sorbents have been developed where the ionic groups are presented on flexible polymer chains comparable to the tentacles of an octopus (Figure 3.16b). The advantage of this setup can be clearly seen with its flexibility toward the ionic groups of the protein, which can up to a certain extent be caught by the tentacles. Recent development optimized the ratio between charged and thus binding groups with nonbinding spacer groups enhancing the flexibility of the tentacle arms (Figure 3.16c).

The advantages of IEX chromatography are its straightforward adsorption principle that is based on the Coulomb interaction that can be adjusted according to the isoelectric point (pI) of the proteins to be separated. The binding mechanism can be tuned over a wide area of conditions by choosing different types of buffers at different pH and salt concentration for the feed, wash, and elution buffer. This high degree of freedom on the other hand leads to a high number of possible process conditions, which should be exploited in a consequential way. Robotic systems are more and more used to systematically screen for the best conditions of a given separation task.

IEX resins have additionally a relatively high protein binding capacity and a quite high resolving power, especially if linear gradients are applied. The ease of performance and good packing properties of modern ion exchangers allow to pack large-scale columns of up to 2 m diameter. Tables 3.11 and 3.12 list the properties of the most commonly used ion exchangers.

IEX sorbents are densely substituted with ionic groups, leading to a total ionic capacity of around 100–500 μmol ml^{-1} gel, corresponding to a concentration of ion exchanging groups of 0.1–0.5 M. The binding capacity for proteins is lower due to their size, and it strongly depends on the available surface area for the molecular weight and size of the protein as well as on the chemical nature (surface charge) of the protein.

3.3.4.1 Optimization of Ion-Exchange Resins

To optimize an IEX, sorbent several options have to be taken into account:

- The pores should be large enough so that the performance limiting pore diffusivity is maximized.
- On the other hand, the number of ionic groups that is in most cases proportional to the surface area should be as high as possible.
- To ensure that the sorbent can be packed in large-diameter columns without self-compression of the packed bed, the rigidity of the matrix, governed by the amount of stabilizing cross-linker, should be high.

Pore dimensions and their geometry play a vital role for the adsorption process in protein chromatography on ion exchangers. Different methods have been used to evaluate the pore network of a sorbent, which is always a random arrangement of holes in the matrix with different width and length (Chang and Lenhoff 1998; Kopaciewicz, Fulton, and Lee 1987). For all these analytical methods, it is of utmost importance to control the experimental conditions. The combination of confocal laser scanning microscopy (CLSM) with inverse size-exclusion chromatography (ISEC) is very well suited for the determination of intraparticle diffusion coefficients and thus the optimization of IEX sorbents.

Especially the tentacle-based ion exchangers make the analytical situation even more complex. The tentacles attached to the matrix surface have a three-dimensional structure stretching out into the free pore space. Even more, their structure depends on the salt concentration in the mobile phase. At high salt concentration, the ionic groups of the tentacles are neutralized, and the tentacles are able to pack much more densely. The difference in open pore space can be seen from Figure 3.17 where DePhillips and Lenhoff showed the influence of tentacles for two different IEX sorbents. In Figure 3.17 the open pore space is shown as a function of the IEX modification. All four IEX sorbents (TosoHaas SP-650M, TosoHaas CM-650M, Merck Fractogel SO$_3$ (M), and Fractogel COO (M)) are based on the matrix HW-65F. While the first two have an ordinary surface modification, the latter two exhibit the tentacle principle. The influence of the tentacle modification stretching out into the open pore space can be seen for the uncharged dextran molecules, which have been used as size markers. While the TosoHaas materials show the same pore accessibility for unmodified

Table 3.11 Properties of cation exchangers as provided by manufacturers.

Resin	Manufacturer	Base matrix/surface modification	Particle size (µm)	Pore size (nm)	Ionic capacity (µeq/ml gel)	Static protein binding capacity (mg protein/ml gel)	Operation range (cm h^{-1})
Fractogel® EMD SO$_3$	Merck Millipore	Polymethacrylate/tentacle	65	100	80–100	110–150	400 at 2 bar
Fractogel® EMD SE Hicap	Merck Millipore	Polymethacrylate/ tentacle	65	100	60–90	120–160	400 at 2 bar
Eshmuno® S	Merck Millipore	Polyvinyl derivative/tentacle optimized	75–95	80	50–100	115–165	1200 at 2 bar
Eshmuno® CPX	Merck Millipore	Polyvinyl derivative/tentacle optimized	50			120	500 at 3 bar 20 × 10 cm
SP Sepharose® FF	GE Healthare	Agarose/conventional	45–165	—	180–260	70	300–400 at 1 bar at 15 cm bed height
SP Sepharose® XL	GE Healthcare	Agarose/conventional	45–165	—	180–250	160	300–500
SP Sepharose® Big Beads	GE Healthcare	Agarose/conventional	100–300	—	180–250	70	1800 at 2 bar
SP Sepharose® HP	GE Healthcare	Agarose/conventional	34	—	150–200	55	—
Capto™ S	GE Healthcare	Agarose/three-dimensional network	90		110–140	120	700 at 3 bar (20 cm, water)

Capto™ SP ImpRes	GE Healthcare	"High-flow" agarose	36–44			95	220 at 3 bar 20 × 100 cm
MacroPrep® High S	Bio-Rad	Polymethacrylate/ conventional	50	100	120–200	55	400 at 2 bar, 14 × 17 cm
UNOsphere™ S	Bio-Rad	Polymethacrylate/ conventional	80		280	60	1200 at 2 bar, 1.1 × 20 cm
Nuvia™ cPrime	Bio-Rad	Polymethacrylate/ conventional	60–80		55–75	40	600 at 2 bar, 20 × 20 cm
Nuvia™ S	Bio-Rad	Polymethacrylate/ conventional	70–100		90–150	110	
Nuvia™ HR-S	Bio-Rad	Polymethacrylate/ conventional	40–60		100–180	70	
S F Ceramic HyperD®	BioSepra/Pall	Polyacrylamide gel in ceramic macrobead	50	—	>150	75	600 due to diffusion, maximum $\Delta P = 70$ bar
TOYOPEARL GigaCap® S	Tosoh	Polymethacrylate/ three-dimensional polymer network	50–100	—	100–200	150	1500 at 2.5 bar at 14 cm bed height
TOYOPEARL SP-650M	Tosoh	Polymethacrylate/ conventional	40–90	100	120–170	39[a] mAh 10% bt	400 cm at 2 bar
POROS 50 HS	Thermo Fisher Scientific	PST/DVB hydrophilized	44[a]	—	—	27[a], mAh 10% bt	—
POROS XS	Thermo Fisher Scientific	PST/DVB hydrophilized	50	—	—	102	
Praesto® SP45	Purolite	Highly cross linked agarose	45			80	200 at 3 bar 2.6 × 20 cm

a) **Staby et al.** (2004); **all other data is from the manufacturer's technical data sheets.**

Table 3.12 Properties of anion exchangers as provided by manufacturers.

Resin	Manufacturer	Base matrix/surface modification	Particle size (µm)	Pore size (nm)	Ionic capacity (µeq/ml gel)	Static protein binding capacity (mg protein ml^{-1} gel)	Operation range (cm h^{-1})
Fractogel® EMD TMAE (M)	Merck Millipore	Methacrylate/ tentacle	65	100	—	100 (static)	240 at 1.5 bar at 20 cm bed height
Fractogel® EMD TMAE Hicap (M)	Merck Millipore	Methacrylate/ tentacle	65	100	—	180 (static)	240 at 1.5 bar at 20 cm bed height
Fractogel® EMD DEAE (M)	Merck Millipore	Methacrylate/ tentacle	65	100	—	100 (static)	240 at 1.5 bar at 20 cm bed height
Fractogel® EMD DMAE (M)	Merck Millipore	Methacrylate/ tentacle	65	100	—	100 (static)	240 at 1.5 bar at 20 cm bed height
Eshmuno® Q	Merck Millipore	Polyvinyl derivative/ tentacle, optimized	85	80	90–190	>80	1000 at 2.5 bar 20 × 10 cm
TOYOPEARL SuperQ-650C, QAE-550C	Tosoh Bioscience	Methacrylate/ conventional	40–90	~50	200–300	105–155	—
Source™ 30Q	GE Healthcare	Methacrylate	50–150	~25	280–38	60–80	—
Q Sepharose® FF	GE Healthcare	Polystyrene/ divinylbenzene	30	Not given	—	>40[a]	—
Q Sepharose® XL	GE Healthcare	Agarose	45–165	Not given	180–250	120 HSA	—
Whatman® EXPRESS™-ION Q	GE Healthcare	Agarose with bound dextran	45–165	Not given	180–260	>130[b]	—

Capto™ Q	GE Healthcare	Agarose with bound dextran	90	—	—	—	700 at 3 bar, 20 × 100 cm
Capto™ DEAE	GE Healthcare	Agarose with bound dextran	90	—	—	—	700 at 3 bar, 20 × 100 cm
Capto™ Q ImpRes	GE Healthcare	"High-flow" agarose	36–44	—	—	55	220 at 3 bar, 20 × 100 cm
Capto™ adhere ImpRes	GE Healthcare	"High-flow" agarose	36–44	—	—	45–85	—
Capto™ adhere	GE Healthcare	Cross-linked agarose	75	—	—	—	600 at 3 bar 20 × 100 cm
Bioapplications Q Cellthru BigBead Plus	Sterogene	Microgranular cellulose/ conventional	60–130[c]	Not applicable	1 meq/dry g	55	—
POROS 50 HQ	Thermo Fisher Scientific	4% agarose/ conventional	300–500	Not given	Not given	65	—
POROS XQ	Thermo Fisher Scientific	PST/DVB hydrophilized	44	—	—	140 BSA	—
UNOsphere™ Q	Bio-Rad	Poly-methacrylate/ conventional	120	—	120	180 HSA at 150 cm h^{-1}	1200 at 2 bar 20 cm
Praesto® Q65	Purolite	Highly cross linked agarose	65	—	—	60 BSA at 6 min RT	400 at 3 bar 2.6 × 20 cm
Praesto® Q90	Purolite	Highly cross linked agarose	90	—	—	50 BSA at 6 min RT	800 at 3 bar 2.6 × 20 cm

a) 50% breakthrough.
b) 10% breakthrough.
c) Fiber length.
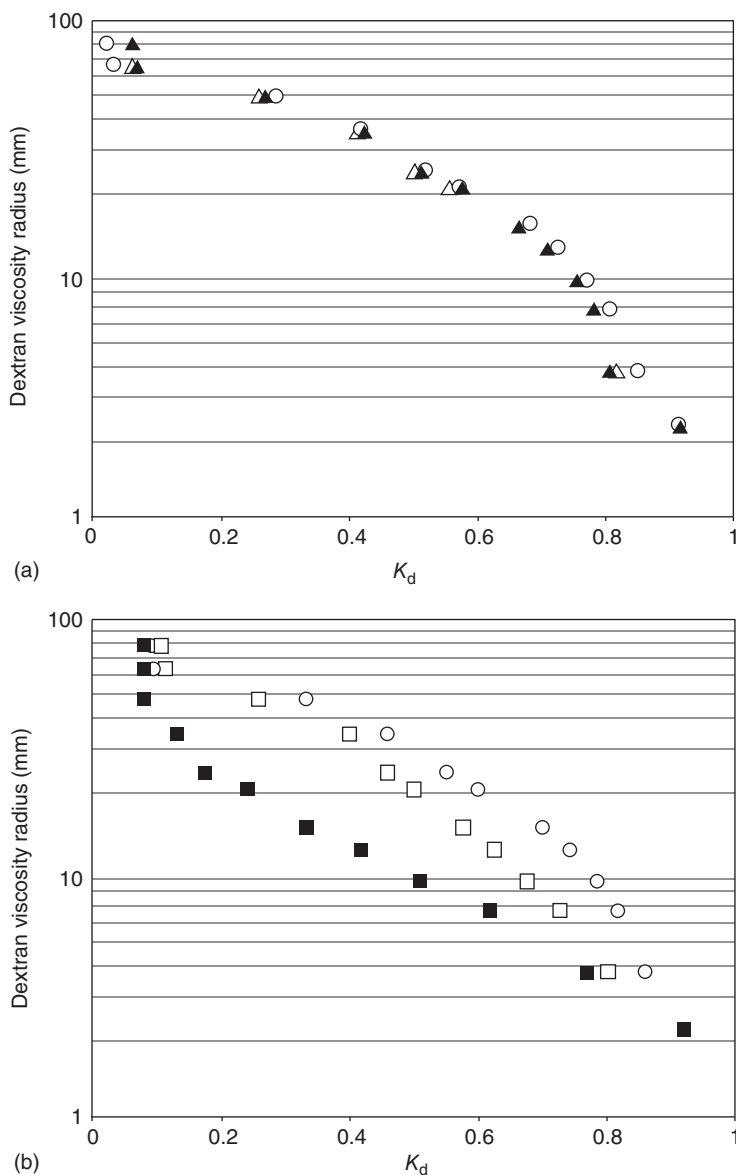
Figure 3.17 Inverse size exclusion data of different ion-exchange sorbents: (a) TosoHaas HW 65 F SEC (○) and TosoHaas SP 650 M cation exchanger (▲), TosoHaas CM 650 M (△), (b) TosoHaas HW 65 F SEC (○) and Merck Fractogel SO_3 (M) (■), Fractogel COO (M) (□). Source: DePhillips and Lenhoff (2000). Reproduced with permission of Elsevier.

and modified sorbents, the modified Fractogel tentacle materials have a smaller accessible pore volume.

K_d represents the extent of permeation into the pore volume, a totally excluded molecule would show a K_d equal to 0, and a molecule small enough to penetrate all pores shows a K_d of 1.

The accessibility of the pore volume is just one side of the medal: even with the lower accessible pore volume, the Fractogel tentacle ion exchangers show a very high protein binding capacity due to the fact that the tentacle network is very well able to bind charged molecules even if it excludes the noncharged marker molecules.

The pore diffusion coefficients in tentacle-based matrices are typically higher as the transport mechanism is not based on free diffusion but most probably on a faster film diffusion principle (Thomas et al. 2013; de Neuville, Thomas, and Morbidelli 2013).

The development in the imaging technologies, especially CLSM, enabled to investigate the pore diffusional mechanisms of such tentacle structures in detail (Stanislawski, Schmit, and Ohser 2010). Proteins marked by fluorophores can be followed in their uptake procedure inside the bead pore system, and the spatial distribution of the radial density can be reconstructed. Using this technology, it is possible to determine the influence of tentacle structure modifications on protein uptake clearly demonstrating that an optimum exists between charged groups and noncharged spacers forming the three-dimensional tentacle network inside the pore system. This optimization work led to the development of new sorbents with an optimized combination of protein loading and diffusivity allowing high linear flow rates without compromising protein dynamic binding capacity. Figure 3.18 shows the classical tentacle material Fractogel EMD SO_3 (M) in comparison with materials based on the same matrix but with an optimized ratio of ionic and spacer groups. The pictures taken at the identical residence time of four minutes clearly show that the diffusivity under binding conditions using a fluorophore-labeled antibody as the marker molecule is much faster for the optimized materials. Under column chromatographic conditions, it could be shown that dynamic binding capacities as high as $200 \, mg \, ml^{-1}$ can be achieved at a residence time of two minutes under experimental conditions (Urmann et al. 2010).

Besides microscopic technologies, the molecular dynamics (MD) simulation using coarse-grain models to speed up the simulations improved the understanding of the effects of tentacle surface modifications (Cavalloti 2008; Salvalaglio et al. 2015). The tentacular structure of IEX materials is characterized by a macroscopic reorganization caused by van der Waals interactions among the tentacle backbones and electrostatic interactions of charged groups with the solvent.

(a)   (b)   (c)
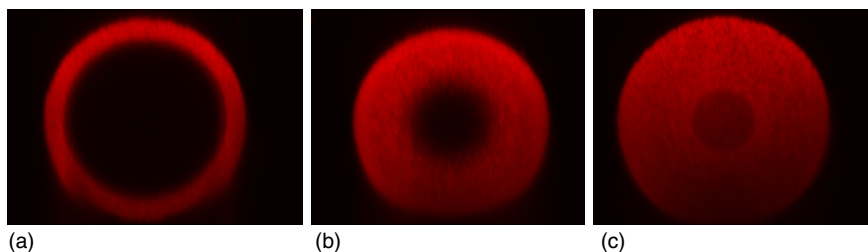
Figure 3.18 Adsorption of dye-labeled proteins on different ion-exchange sorbents: (a) Fractogel® EMD SO_3 (b, c) experimental Fractogel® EMD SO_3 modifications with advanced tentacle flexibility.

Thus, the density of tentacles and their structure in terms of tentacle length and number of charged groups per tentacle are important parameters for the material performance. Salt effects can be observed, which indicate that external parameters can trigger an important structural reorganization of the tentacular structure at a mesoscopic level.

The optimization of the tentacle structure still exhibits the possibility to optimize the mass transfer characteristics and thus develop improved resins for the purification of biopharmaceutical molecules of different shape, size, and ionic properties.

3.3.5 Mixed Mode

Over the last few years, new resins have been launched that exhibit more than one mode of interaction. The goal of the combination of hydrophobic interaction principles with ionic interactions is the generation of complementary selectivities for mixtures difficult to separate by just ionic or hydrophobic interactions (Johansson et al. 2003a,b). Especially, the separation of antibody aggregates from the corresponding monomeric form can be achieved with these resins. In addition, these resins allow to operate the chromatographic binding at a higher salt level compared to single-action IEX materials, which will result in lower dilution and better process economy.
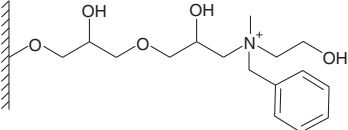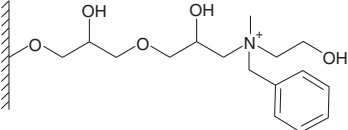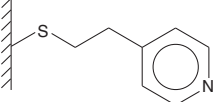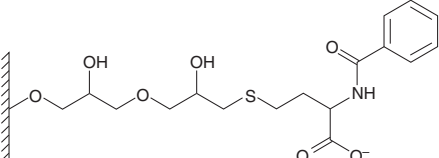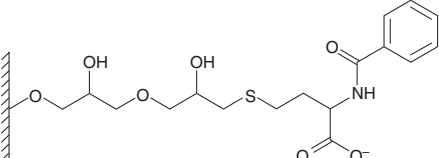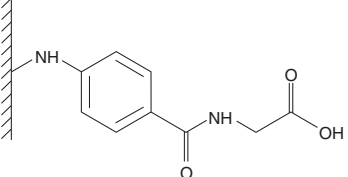
The most prominent materials of this interaction type use an aromatic moiety in combination with a quaternary amine function (Capto™ adhere) or a carboxy group (Capto MMC, Nuvia™ cPrime™, TOYOPEARL® MX-Trp). A unique ligand architecture is used in Eshmuno HCX, which is the only mixed-mode resin with the charged sulfo group and a benzyl group on two different side chains of a tentacle resin. A slightly different concept is the hydrophobic charge induction chromatography where the resin charge is generated by adjusting the pH accordingly (Pall MEP HyperCel™).

All resins exhibit quite remarkable selectivities but suffer from significantly higher efforts for the development of the operating conditions as two interaction principles have to be adjusted and controlled in parallel. Care has to be taken for the product recovery as the hydrophobic residue might cause some strong interaction with the protein of interest. Table 3.13 lists the commercially available mixed-mode resins.

3.3.6 Hydroxyapatite
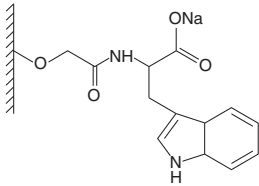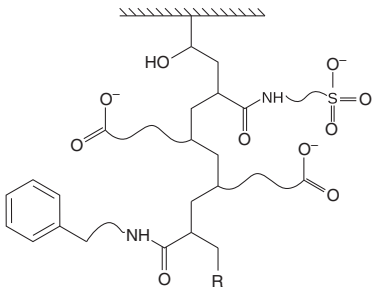
Hydroxyapatite, which has the formula of $Ca_{10}(PO_4)_6$ $(OH)_2$, is widely used as a sorbent for hydrophobic interaction chromatography. Hydroxyapatite is an underivatized matrix with a specific inherent surface functionality. In the 1980s, it had been introduced as ceramic-beaded material with good physical strength (Kato, Nakamura, and Hashimoto 1987). The interactions of the surface phosphate and calcium ions with the amino and carboxyl groups of proteins are complex and not fully understood. The elution of proteins is typically performed at a pH of 6.8. Even though it has been reported that lower pH is preferable with respect to separation, it has to be kept in mind that the crystalline character

Table 3.13 Properties of mixed-mode sorbents.

Adsorbent	Selector (base matrix)	Particle diameter d_p (µm)	Capacity	Working pH
Capto™ adhere (GE Healthcare)		75	50 mg ml⁻¹ Mab at 110 mM NaCl	3–12
Capto™ adhere ImpRes (GE Healthcare)		36–44		3–12
MEP HyperCel™ (Pall)		80–100	>20 mg ml⁻¹ hIgG	3–12
Capto™ MMC (GE Healthcare)		75	44 mg ml⁻¹ rHSA at 15 mS cm⁻¹	3–12
Capto™ MMC ImpRes (GE Healthcare)		36–44	60–90 mg ml⁻¹ MAb	3–12
Nuvia™ cPrime™ (Bio-Rad)		70	>40 mg ml⁻¹ hIgG	4–13

(Continued)

Table 3.13 (Continued)

Adsorbent	Selector (base matrix)	Particle diameter d_p (µm)	Capacity	Working pH
TOYOPEARL® MX-Trp-650M		50–100 µm	95 mg ml^{-1} pIgG at 12 mS cm^{-1}	
Eshmuno® HCX (Merck Millipore)		75–95 µm	>50 mg ml^{-1} IgG at 150 mM NaCl	2–12

of hydroxyapatite is rapidly destroyed at a pH below 5. As an alternative with a larger working pH range, CFT™ Ceramic Fluoroapatite (Bio-Rad) has been recently introduced. Fluoroapatite $(Ca_5(PO_4)_3 F)_2$ can be used under chromatographic conditions as low as pH 5. Two different types with 40 μm particle size have been introduced, which differ in the sintering temperature (Type I 400 °C, 33–36 m^2 ml^{-1} surface area and type II 700 °C 16–18 m^2 ml^{-1}) and the respective binding capacity for monoclonal antibodies (mAbs) (type I 14–17 mg ml^{-1}, type II 30–32 mg ml^{-1}).

3.3.7 Designed Adsorbents

In contrast to generic adsorbents, designed adsorbents have been developed for the isolation of specific groups of compounds with common physicochemical properties. They normally consist of a more or less generic sorbent base material with a surface modification of specific affinity toward the desired chemical function. Their adsorption principle might be based on a multitude of interactions as is the case for the specific proteins, for example, protein A, G, or L, or based on single complexing interaction, for example, as in the metal-chelating sorbents.

The use of designed adsorbents is widespread in the area of antibody-capture chromatography as antibodies are by far the largest homogeneous group of molecules of interest to the pharmaceutical industry. Therefore, a lot of approaches have been made to develop adsorbents, which can capture the antibodies from the fermentation broth based on a key–keylock (magic bullet) approach, binding to different recognition sites of the antibodies (Figure 3.19). The most successful of these approaches was the development of the protein A affinity sorbents.

3.3.7.1 Protein A Affinity Sorbents

Protein A affinity sorbents were first introduced in the analytical scale by Hjelm and Kronvall in the 1970s (Hjelm, Hjelm, and Sjoquist 1972; Kronvall 1973). Protein A is a highly selective and specific surface receptor protein originating from *Staphylococcus aureus*, which is capable of binding the Fc portion of
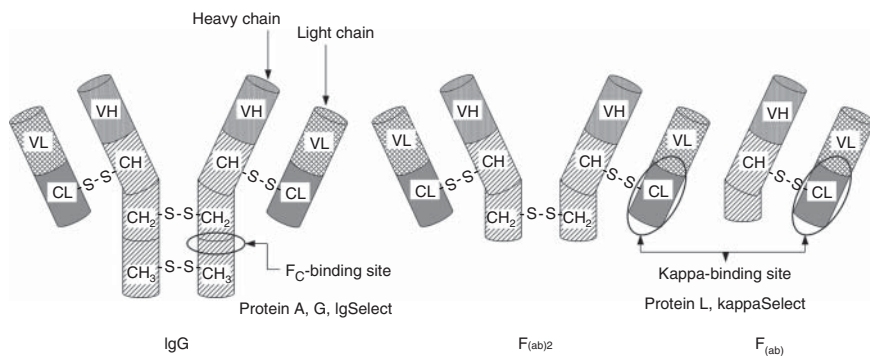
Figure 3.19 Binding sites of affinity selectors.

immunoglobulins, especially IgGs (IgG1, IgG2, and IgG4, but not IgG3), from a large number of species.

With the tremendous success of monoclonal antibodies in therapy, the development of protein A adsorbents that are robust enough for a preparative use has been started and has reached a certain level. Today, monoclonal antibodies are captured in the multi-ton range by the use of protein A affinity adsorbents.

The advantage of protein A affinity adsorbents is their ease of use. No feed adjustment is necessary; they are generic for all IgG antibodies, and only a limited method development is needed. In a single capture step, they offer a high binding capacity and a good purity of often >95%, and the separation of aggregates is possible by the application of linear gradients. Today, the use of protein A affinity adsorbents is well accepted by the regulative authorities so that they are a gold standard in the majority of current monoclonal antibody purification processes.

The drawbacks of protein A affinity chromatography are related to the labile chemical nature of protein A as an affinity selector: due to the necessary low elution pH, the target proteins might be denatured or fragmented. The formation of aggregates is a well-known problem, and a certain loss of biological activity might occur. Even though the stability of protein A affinity sorbents could be increased with the new generations of sorbents, the risk of a certain amount of leaching of the protein A selector is still present, making a subsequent IEX step that is able to capture the leached protein A necessary. The biggest challenge in protein A affinity chromatography is the cost of the sorbent itself and the need for replacement due to limited column lifetime. Table 3.14 lists the most commonly used protein A affinity sorbents, giving the chemical nature of their base material as well as the type of protein A selector.

In scientific publications and vendor product data sheets, 10% breakthrough values are typically given. Real processes are never run to such high breakthrough levels to avoid product losses. Therefore more important than 10% breakthrough levels or static binding capacities are 1% breakthrough levels in order to enable a praxis-relevant comparison of different protein A resins. These 1% breakthrough levels are typically significantly lower than SBC and 10% breakthrough levels.

Starting with the first generation of protein A affinity sorbents that used native protein A bound onto an agarose matrix, two main development routes have been followed: the increased mechanical stability of the base bead and the increased chemical stability of the protein A ligand. To achieve an increased mechanical stability of the base bead, a very difficult trade-off between the high rigidity of the backbone and still large enough pore size had to be done. Besides agaroses with different degrees of cross-linker, polymethacrylate beads have been introduced along with polyacrylamide gels in a ceramic macrobead shell ("gel in a shell" approach). The large-throughpore material developed by Perseptive (now part of Thermo Fisher Scientific) is based on polystyrene, which has to be hydrophilized to be used in protein chromatography. Even though this material shows a low static binding capacity, it maintains a large percentage of that capacity even at high linear flow rates. A large-pore but rigid base material is CPG. The ProSep A materials developed by Millipore (now Merck Millipore) are available in 700 and 1000 Å pore sizes depending on the total capacity to be achieved.

Table 3.14 Commercially available protein A affinity sorbents.

Name	Manufacturer	Base material (particle size, μm)	Protein A selector alkaline stabilized = A/domain/repeat units; native protein A = N	*SBC (Q_{max}) **DBC 1%, 5%, or 10% bt
Praesto® AC	Purolite	HF agarose, highly cross-linked	—/—/—	**45[a)] 10% bt
Praesto® APc	Purolite	HF agarose, highly cross-linked	A/—/—	**50[a)] 10% bt
Praesto® AP	Purolite	HF agarose, highly cross-linked (85 μm)	A/—/	**55[a)] 10% bt
Protein A Sepharose® 4 FF	GE Healthcare	Highly cross-linked 4% agarose (60–165)	N	*61.6[b)]
rProtein A Sepharose® 4 FF	GE Healthcare	Highly cross-linked 4% agarose (60–165)	N	*55.1[b)]
MabSelect™	GE Healthcare	HF agarose, highly cross-linked (85 μm)	N	*67.3[b)]
MabSelect™ Xtra	GE Healthcare	HF agarose, highly cross-linked (85 μm)	N	**50.0[c)], 10% bt
MabSelect™ SuRe™	GE Healthcare	HF agarose, highly cross-linked (85 μm)	A/Z/4	**43[c)] 1% bt **51[c)] 10% bt
MabSelect™ Sure™ LX	GE Healthcare	HF agarose, highly cross-linked (85 μm)	A/Z/4	**60[a)] 10% bt
MabSelct™ Sure™ PCC	GE Healthcare	HF agarose, highly cross-linked (50 μm)	A/Z/4	**70[a)] 10% bt
MabSelect™ PrismA	GE Healthcare	HF agarose, highly cross-linked (60 μm)	A/Z/6	**80[a)] 10% bt

(Continued)

Table 3.14 (Continued)

Name	Manufacturer	Base material (particle size, µm)	Protein A selector alkaline stabilized = A/domain/repeat units; native protein A = N	*SBC (Q_{max}) **DBC 1%, 5%, or 10% bt
POROS® 50 A High Capacity	Thermo Fisher Scientific/Life Technologies	Poly(styrene-divinylbenzene), hydrophilized (50 µm)	—/—/—	*42.2[b] **31[c]1% bt **32[c]10% bt
POROS® MabCapture A Select	Thermo Fisher Scientific/Life Technologies	Poly(styrene-divinylbenzene), hydrophilized	A/—/—	**37[a]5% bt
ProSep®-vA High Capacity	Merck Millipore	Controlled pore glass, 1000 Å pore	N	**24[c]
ProSep®-vA Ultra Capacity	Merck Millipore	Controlled pore glass, 1000 Å pore	N	**35[c]
ProSep® A Ultra Plus	Merck Millipore	Controlled pore glass, 700 Å pore (60 µm)	N	**65.0[c] **42[c]1% bt **46[c]10% bt
Eshmuno® A	Merck Millipore	Hydrophilic polyvinylether (50 µm)	A/C/5	*85 **50[a]5% bt
Protein A Ceramic HyperD® F	BioSepra	Polyacrylamide gel in ceramic macrobead	N	*41.7[b]

TOYOPEARL® AF-rProtein A-650M	Tosoh Bioscience	Polymethacrylate	A/Y/4	**28[c] 10% bt
TOYOPEARL® AF-rProtein A HC-650F	Tosoh Bioscience	Polymethacrylate (45 µm)	A/Y/6	**70[c] 10% bt *68
Amsphere™ Protein A JWT203	JSR Life Sciences	Polymethacrylate (50 µm)	A/—/—	**44[a] 10% bt
Amsphere™ A3	JSR Life Sciences	Polymethacrylate (50 µm)	A	**60[a] 10% bt
MabSpeed™ rP202	Mitsubishi	Polymethacrylate (45 µm)	A/C/—	**50[a] 10% bt
CaptivA®	Repligen	Highly cross-linked 4% agarose	N	**44[a] 10% bt
KanCapA™	Kaneka	Highly cross-linked cellulose (65–85 µm)	A/C/5	**50[a] 5% bt
KanCapA™ 3G	Kaneka	Highly cross-linked cellulose (65–85 µm)	A/C/5	**65[a] 5% bt
UNOsphere SUPrA™	Bio-Rad Laboratories	Highly cross-linked polymer (53–61 µm)	N	**25–30[a] 10% bt
Monofinity A	Genscript	Agarose (90 µm)	A/—/—	**50[a]

a) **Manufacturer data at six minutes residence time.**
b) **Hahn, Schlegel, and Jungbauer** (2003)**.**
c) **Merck data at six minutes residence time.**

In the field of protein A variations, the first products used native protein A from *S. aureus*, while later products introduced recombinant and thus more controllable protein A. Merck Millipore introduced the first product with a recombinant protein A produced without any animal-derived component in production ("vegane" protein A, ProSep® vA) following the trend to avoid any mammalian fermentation compound that might bear a risk of a contamination with human pathogens. The latest development is the use of engineered protein A subunits with the goal to increase both the capacity and the caustic stability. The number of subunits is another product feature to be optimized, but it has to be taken into account that the protein A ligand density as well as the binding chemistry, e.g. spacer length, has a great influence on the binding capacity (Müller and Vajda 2016).

3.3.7.2   Other IgG Receptor Proteins: Protein G and Protein L

Besides the dominating protein A affinity sorbents, two other IgG binding receptor proteins have been introduced as affinity chromatography sorbents: protein G and protein L. Protein G is a cell surface protein from group G *Streptococcus* species. It exhibits two Fc binding sites as protein A and has an overall similar binding spectrum with a clear focus on IgG. Its advantage over protein A is that it also binds human IgG3-subtype antibodies, which are not bound by protein A. On the other hand, protein G in its native form also binds albumin and α2-macroglobulin, so a recombinant form is developed, which avoids the undesirable retention of these proteins. The commercial products on the market differ considerably in their properties. Their price is typically higher than the price for protein A sorbents. A hybrid protein A/G sorbent is described in literature.

Protein L from *Peptostreptococcus magnus* is able to bind whole antibodies as well as single-chain variable fragments (scFv) and Fab fragments as long as they contain kappa light chains onto which protein L binds. One of its prominent features is the binding of IgM, a class of antibodies not well retained by proteins A and G. Table 3.15 lists the properties of IgG affinity resins with protein G and L selectors.

3.3.7.3   Sorbents for Derivatized/Tagged Compounds: Immobilized Metal Affinity Chromatography (IMAC)

Certain natural amino acids, especially histidine, exhibit a high complexation affinity toward two-and three-valent transition metals, for example, Ni(II), Cu(II), Zn(II), Co(II), and Fe(III). When those transition metals are fixed via complexation onto a solid support, these sorbents can be used as affinity resins for proteins naturally rich in histidines or those with genetically engineered oligo-histidine tags (Hochuli, Doebeli, and Schacher 1987; Hochuli et al. 1988). When expression vectors became available that attach 6 or 10 histidine units at the N- or C-terminus of a protein immobilized metal affinity chromatography (IMAC) using the metal-iminodiacetic acid (IDA) or metal-nitrilotriacetic acid (NTA) affinity, the IMAC technique could be used in a very selective way. Since an oligo-histidine end of a protein is not common in nature, the selectivity over host cell or process-related protein impurities is large, making it possible to achieve a protein purity of >90% in a single chromatographic step.

Table 3.15 Protein G and L sorbents.

Name	Manufacturer	Base material	Affinity selector	Specific binding purposes
Protein G				
UltraLink™ Immobilized Protein G Plus	Thermo Scientific	Azlactone-activated polyacrylamide (50–80 μm)	Recombinant Protein G in *Escherichia coli* (22 kDa)	>25 mg of human IgG ml^{-1} of gel
Protein A/G recombinant fusion protein	Thermo Scientific	Beaded agarose, 6% cross-linked or azlactone-activated polyacrylamide (50–80 μm)	Recombinant protein in *E. coli* (50 kDa)	Maximum 3000 cm h^{-1} for polyacrylamide
POROS® Protein G	Thermo Scientific	Polystyrene-divinylbenzene coated with hydroxylated polymer (20 Åm, 800–1500 Å pore size)	Recombinant Protein G	Binding capacity 15–30 mg ml^{-1} IgG
Protein G Agarose, Fast Flow	Merck Millipore	Highly cross-linked 4% agarose beads	Protein G	20 mg ml^{-1} human IgG
Protein G Sepharose Fast Flow	GE Healthcare	Highly cross-linked agarose, 4% (45–165 μm)	Recombinant streptococcal **p**rotein G lacking the albumin binding region produced in *E. coli* (17 kDa)	Multipoint attachment to minimize leakage, protein G lacks albumin binding site, 17 mg ml^{-1} human IgG
Protein G Sepharose High Performance	GE Healthcare	Highly cross-linked agarose, 6% (34 μm)	Recombinant protein G lacking albumin binding region	1 mg ml^{-1} IgG/column

(Continued)

Table 3.15 (Continued)

Name	Manufacturer	Base material	Affinity selector	Specific binding purposes
CIM r-Protein G 8f ml Tube Monolithic Column	BIA Separations	Poly(glycidyl methacrylate-*co*-ethylene glycol dimethacrylate) monolith, 8000 Å pore size	Recombinant protein G	Maximum 1340 cm h^{-1}
KanCap G	Kaneka	Highly cross-linked cellulose	Recombinant protein G	20–30 mg ml^{-1}
Protein L				
Protein L	Thermo Scientific	Beaded agarose, 6% cross-linked (45–165 μm)	Recombinant protein from *Peptostreptococcus magnus* in *E. coli* (36 kDa)	
Capto L	GE Healthcare	Rigid, highly cross-linked agarose (85 μm)	Recombinant protein L (*E. coli*), mammalian-free	25 mg ml^{-1} human Fab at 4 min residence time
KanCap L	Kaneka	Highly cross-linked cellulose	Recombinant **p**rotein L	20–30 mg ml^{-1} SBC; 25–50 mg ml^{-1} DBC at residence time 4 min
TOYOPEARL AF-rProtein L-650F	Tosoh Bioscience	Polymethacrylate	4xB4 domain of recombinant protein L	50 mg ml^{-1} DBC at 10% BT, 6 min residence time
CaptureSelect® CH1-XL	Thermo Scientific	Agarose, epoxy activated (65 μm)	13 kDa llama antibody fragment	19 mg ml^{-1} polyclonal human Fab/L of matrix (10% breakthrough at 2 min residence time)

To achieve a good retention of the target proteins, the imidazole nitrogens in the histidyl residues have to be in their nonprotonated form, and therefore the loading buffer has to be neutral to slightly basic. By using a high-ionic-strength buffer of 0.1–1.0 M NaCl, nonspecific electrostatic interactions are suppressed. For the elution of the target protein, the pH of the elution buffer has to be low. If the target protein is not stable in low pH, alternative elution modes can be applied. Ligand exchange with imidazole as a buffer additive at neutral pH can be used as can the application of a strong chelating agent, for example, ethylene-diaminetetraacetic acid (EDTA). Both methods have their drawbacks. For the imidazole elution, the column has to be saturated and equilibrated with imidazole prior to the separation. After the elution with EDTA, the sorbent has to be recharged with metal ions as the application of EDTA results in an elution of the metal ions as well as the bound protein. IMAC resins are reported to exhibit capacities of 5–10 mg protein ml^{-1} measured for the purified proteins. Commercially available IMAC resins are listed in Table 3.16. They have been reviewed by Gaberc-Porekar and Menart (2001).

The process of tagging a protein is today compatible with most of the used expression systems, for example, prokaryotic and eukaryotic organisms that produce the protein intracellularly or secrete it.

The advantages of IMAC are the good specificity, high binding strength, and simple structure of the selector. The good stability of the chemical ligand allows using IMAC resins under denaturing conditions with urea or guanidinium–HCl. There are a few examples in literature where His-tagged proteins are bound to the IMAC resin under denaturing conditions, renatured while still bound to the solid phase by simply lowering the concentration of the chaotropic agent and later eluted in their active forms (Rogl et al. 1998). This approach is of importance especially for *Escherichia coli* expression systems where the target proteins are secreted into inclusion bodies and have to be refolded to obtain their full biological activity.

IMAC offers the possibility to modulate the binding strength of a protein by varying the metal ion and the selector. The binding strength of different metal chelators is normally in the order Cu(II) > Ni(II) > Zn(II) > Co(II), while tetradentate ligands such as NTA bind stronger compared with tridentate ligands, for example, IDA. The modulation of binding strength can be used in two ways: first to obtain mild binding and thus mild elution conditions. If the binding with the classical His6 or His10-tags is too strong, the use of a His2-tag might even be considered. On the other hand, the protein can be immobilized on the IMAC column if the binding is strong enough and a reactive column with a certain enzyme activity can be achieved. For rather stable proteins, the strong binding can be used to apply harsh washing conditions using detergents, high imidazole concentrations, and organic solvents to get rid of host cell proteins (HCPs), while the target protein is bound to the sorbent.

It has to be pointed out that IMAC suffers from two severe drawbacks limiting its use especially in the production of therapeutic proteins: two artificial compounds, the His-tag and the chelating metal, are introduced into the production process and have to be completely removed from the final product.

Table 3.16 Commercially available IMAC resins.

Name	Manufacturer	Base material	Ligand/metals
IMAC			
Fractogel® EMD Chelate 650	Merck Millipore	Polymethacrylate, M (65 μm) and S (30 μm)	Tentacle-iminodiacetic acid (IDA) for H6-tagged proteins
TOYOPEARL® AF-Chelate-650M	Tosoh Bioscience	TOYOPEARL HW (65 μm)	Iminodiacetic acid (IDA) for H6 tagged proteins
XpressLine Prep Metal Chelate	Upfront Chromatography A/S	HP (70 μm, 165 μm)	Iminodiacetic acid (IDA) for H6-tagged proteins
Chelating Sepharose® FF, High Performance	GE Healthcare	Sepharose 6 FF (90 μm), Sepharose HP (34 μm)	Iminodiacetic acid (IDA) for H6-tagged proteins
Nickel Sepharose® HP	GE Healthcare	Highly cross-linked agarose, 6% (34 μm)	Precharged chelating group with Ni^{2+} for H6-tagged proteins
Nickel Sepharose® 6 FF	GE Healthcare	Highly cross-linked agarose, 6% (90 μm)	Precharged chelating group with Ni^{2+} for H6-tagged proteins
Ni Sepharose® excel	GE Healthcare	Highly cross-linked agarose, 6% (90 μm)	Precharged chelating group with Ni^{2+} for H6-tagged proteins, EDTA resistant and outstanding binding capacity
IMAC Sepharose® High Performance	GE Healthcare	Highly cross-linked agarose, 6% (34 μm)	Precharged chelating group with Ni^{2+} for H6-tagged proteins
POROS™ MC	Thermo Scientific	20 μm	Iminodiacetic acid (IDA) for H6-tagged proteins
BD TALON® Sepharose 6B	BD Biosciences		Nitrilotriacetic acid (NTA) for H6-tagged proteins
Profinity™ IMAC	Bio-Rad Laboratories	Hydrophilic polymer (60 μm)	Iminodiacetic acid (IDA +/− Ni^{2+} precharged for H6-tagged proteins
Nuvia™ IMAC	Bio-Rad Laboratories	38–53 μm	Nitrilotriacetic acid (NTA) for H6-tagged proteins
IMAC HyperCel	Pall Corporation	90 μm	Tridentate IDA for H6-tagged proteins
Cellufine® Chelate	JNC Corporation	Cellulose (125–200 μm)	Iminodiacetic acid (IDA) for H6-tagged proteins

Nickel, especially, is a metal with high human toxicity and has shown carcinogenicity in animal experiments. The problem of metal contamination of the final product is even more difficult as the metal might be incorporated inside the protein and is not easily removed by any subsequent purification step, for example, dialysis or IEX.

The removal of the His-tag after the chromatography is the second big challenge. Chemical cleavage of the tag often leads to loss in protein activity; therefore, only enzymatical cleavage can be applied, but these methods are often inefficient with a cleavage rate between 60% and 90% only. Remaining tagged protein has to be regarded as an impurity and has to be removed by chromatographic polishing steps. This is an additional effort and reduces the overall process yield.

The integration of the His-tag might in addition reduce the expression level of the protein, and oxidative reductive conditions inside the column might lead to metal-induced cleavage of the protein. The number of large-scale applications of IMAC is therefore limited, and the biggest potential should be seen in proteins not intended for human use.

Some proteins might be purified in their native, nontagged forms, avoiding at least the problem of the His-tag cleavage. Single-chain antibody Fv fragments could especially benefit from IMAC chromatography as their capture is not possible with standard protein A affinity resins (Casey et al. 1995; Freyre et al. 2000).

One potential use of IMAC might arise in the area of vaccine purification. In vaccines, the attached His-tag might add some additional antigenicity and serve as an adjuvant, which is not to be removed from the final product. This approach has been shown by Kaslow for a malaria-transmission-blocking vaccine candidate (Kaslow and Shiloach 1994). Due to the fact that a large volume of cell culture supernatant had to be purified rapidly, a Ni–NTA agarose was used as a batch adsorbent as the product offered a too low flow rate in a packed column. By using sorbents with better pressure/flow characteristics, this problem should be overcome in large-scale production.

3.3.7.4 Other Tag-Based Affinity Sorbents

Other tag-based affinity system have been developed, which exhibit high affinities and other favorable features, e.g. elution under physiological conditions, but it has to be pointed out that their use is limited for production purposes as the removal of the tag after elution of the protein of interest is adding substantial complexity to the downstream process. Therefore, those tag systems are often only used to isolate small amounts of proteins where a cleavage of the tag is not necessary.

The by far most prominent of these systems is the streptavidin/biotin system. The vitamin biotin (vitamin B7 or H) has a high affinity against the natural tetrameric form of the avidin protein from *Streptomyces avidinii*, with each protein monomer binding one biotin molecule. This affinity has been used mainly for the purification of proteins from *E. coli* fermentation as mammalian cell culture expresses several biotinylated protein species that interfere with the purification system.

As an alternative but easier system using the streptavidin/biotin affinity, the Strep-tag® and Strep-tag II systems have been developed. These tags are peptides

consisting of eight or nine amino acid, which bind to the same pocket as biotin. In addition, the streptavidin protein was reduced to its binding core (Strep-Tactin). The Strep II Tag does not interfere with protein folding or secretion. In its native form, it is resistant to cellular proteases, but a protease recognition site can be introduced, allowing the cleavage of the tag. As the affinity of biotin is still higher to both the natural from of streptavidin and the Strep-Tactin, it can be used to displace the protein of interest and elute it from the column.

A second polypeptide tag is the FLAG-tag, which consists of eight amino acids (DYKDDDDK; D = aspartic acid, Y = tyrosine, K = lysine). It serves as an epitope against a special mAb bound to a resin and capturing the tagged protein with high specificity. Elution is accomplished by low pH, EDTA (as the binding is Ca^{2+} dependent), or the FLAG peptide as a displacing agent. An enterokinase can cleave the FLAG-tag, which might be expressed at the N- or C-terminus (Kimple, Brill, and Pasker 2013).

Table 3.17 gives an overview on commercialized systems for Strep-tag and FLAG affinity systems, and Table 3.18 summarizes other tag-based affinity systems.

A recent overview on more purification tags is given by Wood (2014).

A special class of purification tags is the self-cleaving tag. The purification system is consisting of a tag, which is co-expressed with the protein of interest, and a complementary purification tag attached to a purification resin. The two protein tags bind to each other and bring the self-cleaving active reaction into vicinity. While the protein of interest is bound to the resin via the tag, all contaminants can be washed off from the column. With a stimulus in the eluent system, e.g. a shift in the buffer pH, the cleavage site is activated, and the protein of interest is released from the column and eluted in pure, tag-less form. The tag, which is still bound to the column, can be eluted by another change in the buffer system, and the purification column is ready to be reused.

Compared to standard tags, which have to be removed with proteases after the affinity purification step, the on-column self-cleaving tag does not introduce another impurity (the cleaved tag) and therefore does not need an additional purification step.

Several systems of split-intein self-cleaving systems are currently under evaluation and developed for market introduction, e.g. Splittera from ZIP Solutions or systems developed by the group of David Wood (Warren, Coolbaugh, and Wood 2013) or Zhilei Chen (Guan, Ramirez, and Chen 2013)

3.3.8 Customized Adsorbents

Customized adsorbents are the resins synthesized for the purification of one specific component. They are usually made by sophisticated chemistry to perfectly fit into the three-dimensional structure of the target molecule. Due to the advent of combinatorial ligand-synthesis techniques and high-throughput screening, a variety of different customized synthetic and biologically derived ligands have been introduced in preparative chromatography. For customized adsorbents, it is important to consider aspects such as stability, production of the sorbent, costs, intellectual property, and regulatory needs besides the performance.

Table 3.17 Streptavidin and FLAG®-based affinity resins.

Name	Manufacturer	Base material	Ligand
Strep-Tactin® Superflow®	IBA Lifesciences	Highly cross-linked agarose, 6%	Streptactin for purification of Strep-tagged (Trp-Ser-His-Pro-Gln-Phe-Glu-Lys) proteins)
Strep-Tactin® MacroPrep	IBA Lifesciences	Highly cross-linked agarose, 6%	Streptactin for purification of Strep-tagged (Trp-Ser-His-Pro-Gln-Phe-Glu-Lys) proteins)
Strep-Tactin® Superflow® high capacity	IBA Lifesciences	Highly cross-linked agarose, 6%	Streptactin for purification of Strep-tagged (Trp-Ser-His-Pro-Gln-Phe-Glu-Lys) proteins)
Streptavidin Sepharose® High Performance	GE Healthcare	Highly cross-linked high-flow agarose 6% (34 μm)	Streptavidin removal of biotinylated proteins 6 mg ml^{-1} biotinylated bovine serum albumin
Strep-Tactin® XT	IBA Life Sciences	Highly cross-linked agarose, 6%	Streptactin for purification of Strep-tagged (Trp-Ser-His-Pro-Gln-Phe-Glu-Lys) proteins)
Strep-Tactin® Superflow® Agarose	Merck Millipore	Cross-linked agarose	Streptactin for purification of Strep-tagged (Trp-Ser-His-Pro-Gln-Phe-Glu-Lys) proteins)
S-protein Agarose	Merck Millipore	Cross-linked agarose	Streptactin for purification of Strep-tagged (Trp-Ser-His-Pro-Gln-Phe-Glu-Lys) proteins)
Anti-FLAG® M1 Agarose Affinity Gel	Merck Millipore	Agarose (45–165 μm)	M1 anti-FLAG® mouse antibody
Anti-FLAG® M2 Affinity Gel	Merck Millipore	Agarose (45–165 μm)	M2 anti-FLAG® mouse antibody
EZ view™ Red ANTI-FLAG® M2 Affinity Gel	Merck Millipore	Agarose (45–165 μm)	M2 anti-FLAG® mouse antibody, red dye for better visibility of binding

Table 3.18 Other tag-based affinity resins.

Other tags	Manufacturer	Base material	Ligand
Dextrin Sepharose® High Performance MBP	GE Healthcare	Highly cross-linked agarose, 6% (34 μm)	Dextrin for capture of proteins with maltose binding protein (MBP)
Glutathione Sepharose® 4 Fast Flow	GE Healthcare	Highly cross-linked 4% agarose (90 μm)	Glutathione for capture of glutathione S-transferase (GST)-tagged proteins
Glutathione Sepharose® 4B	GE Healthcare	Highly cross-linked 4% agarose (90 μm)	Glutathione for capture of glutathione S-transferase (GST)-tagged proteins
Glutathione Sepharose® High Performance	GE Healthcare	Highly cross-linked 6% agarose (34 μm)	Glutathione for capture of glutathione S-transferase (GST)-tagged proteins
GST•Bind™ Resin	Merck Millipore	Cross-linked agarose	Glutathione for tagged glutathione-S-transferase (GST) fusion proteins
CaptureSelect™ C-tagXL	Thermo Scientific	Agarose, epoxy activated (65 μm)	Camelid-derived single domain antibody fragments for 4 amino acid peptide tag (E-P-E-A, glutamic acid–proline–glutamic acid–alanine)
Profinity eXact™	Bio-Rad Laboratories	Superflow agarose (6% cross-linked), 60–160 μm	Engineered subtilisin protease for EEDKLFKAL (prodomain) tagged proteins
Chitin Resin	New England Biolabs	Not provided	Chitin for CBD-tagged proteins, used for intein-mediated protein ligation (IPL)

The main aspect of small chemical ligands is their higher stability especially toward harsh sanitization conditions and the fact that they do not introduce any additional material of biological origin into the production process.

For customized adsorbents, it is necessary to first define a separation target. The separation target can be defined in positive mode (the compound of interest is bound) as well as in negative mode (a critical impurity is bound and the compound of interest is eluted in flow-through mode). After the target is fixed, a suitable ligand library is tested with respect to its binding affinity toward the pure compound. Two major problems have to be overcome in this stage:

(1) For the screening experiments, sufficient target compound in pure form has to be available. Therefore, the screening procedure should be done in an automated and downscaled way.
(2) As the affinity has to be screened against the pure compound, it has to be tested if the same binding capacity and strength that can be achieved once the compound of interest is subjected to the resin in the original feed composition. Often, other feed components have a drastic influence on the binding kinetics of the target compound.

Once the selector is identified, the binding chemistry on the base resin has to be optimized, and the whole adsorbent scaled up. Finally, the large-scale production under controlled conditions and the registration of the final adsorbent have to be ensured.

Customized adsorbents are available with low molecular weight chemical ligands as well as with natural (proteins, polynucleotides) or artificial polymers.

3.3.8.1 Low Molecular Weight Ligands

The obvious way to reduce the complexity of affinity ligands and bring them down to the absolute essential structure is the use of small peptide fragments. If the binding region of a target molecule is known, it can be modeled by MD calculations. The other way is through the use of diverse peptide libraries and identifying the best binding selector. In the 1980s, Dyax (now acquired by Shire) developed and patented the phage display technology (Smith 1985). By the introduction of additional genetic information into the genome of small bacterial viruses (bacteriophages), different peptides with 6–13 amino acids, antibody fragments, or proteins will be displayed on the surface of the bacteriophages. By variations in the sequence of the 13 amino acid positions using 19 different amino acids, a library of approximately 100 million different selectors is achieved. The library of bacteriophages can be subjected to a screening procedure, and the best binding structure is identified. The best selector molecule can be easily identified, and in the case of peptides, the selector is chemically synthesized later. Kelley et al. published a process for the blood coagulation factor FVIII from Wyeth (Xyntha®/ReFacto AF), which is produced using a Dyax customized affinity sorbent (Kelley, Jankowski, and Booth 2009). With this immunoaffinity chromatographic step based on a peptide, it is possible to generate a downstream process, which is completely free of animal-derived materials.
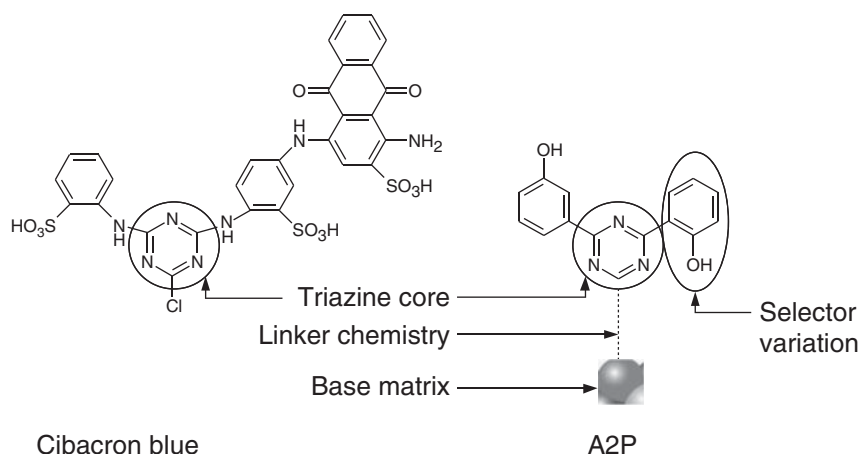
Figure 3.20 Structure of Cibacron blue and the affinity ligand A2P.

One of the oldest and best known small molecular ligands is Cibacron blue, initially a textile dye, which was found to have a certain affinity in staining experiments. Simplification and further development of the aromatic selectors attached to the triazine core element by the Canadian company Prometic Bioseparations lead to the affinity ligand A2P, which mimics the Phe-132,Tyr-133 binding site of protein A. (Lowe, Lowe, and Gupta 2001, Figure 3.20). A2P is known to bind IgG especially well when isolated from blood plasma. Different products under the label MAbsorbent™ have been developed, for example, in cooperation with GlaxoSmithKline, Boehringer Ingelheim, and Abbott for the capture of monoclonal antibodies and antibody fragments (FAB). Table 3.19 lists mimetic affinity adsorbents.

Another approach based on peptides is used by the Italian company Xeptagen (www.xeptagen.com). The D-PAM ligand optimized from a peptide library of 5832 randomized tripeptides is a tetramer of tripeptides linked together by a tetradentate lysine core [structure formula: ([NH$_2$–(*R*)Arg–(*R,S*)Thr–(*R*)Tyr)4–(*S*)Lys2–(*S*)Lys–Gly]. All amino acids are in their artificial D-form, giving the selector a higher proteolytic stability (Fassina et al. 2001).

The binding affinity is supposed to be especially good for IgM so that under selected conditions, the isolation of IgM from IgG-containing feed streams can be achieved. For pure samples, the capacities for different classes of immunoglobulins are claimed to be 10–25 mg ml^{-1} support for IgG, 10 mg ml^{-1} for IgM, and 30–60 mg ml^{-1} for IgY. The high variation in binding capacity for IgG is supposed to be related to the different types of base matrix. The high influence of the support as well as the linker could be verified by MD calculations. Within the frame of the EU-funded project Advanced Interactive Materials (AIMs) by Design , it could be shown that the ligands A2P and D-PAM bind to the same region as protein A between the CH$_2$ and CH$_3$ domains of IgG (Busini et al. 2006; Zamolo et al. 2008; Moiani et al. 2009). This region is not easily accessed, and binding needs a high sterical flexibility of the ligand. Binding of the ligand with the target

Table 3.19 Mimetic affinity sorbents.

Name	Ligand	Base material/maximum flow rate	Capacity
MAbsorbent A2P HF (for human Mab) and HF LL (for IVIG)	A2P Triazine	Agarose (90 μm, 200 cm h^{-1})	35 mg ml^{-1} IVIG, 20–30 mg ml^{-1} Mab
Fabsorbent™ FAP HF		Agarose (90 μm, 200 cm h^{-1})	Fab 20 mg ml^{-1}, IgG1 up to 60 mg ml^{-1}
p-Aminobenzamidine AP6XL	p-Aminobenzamidine	Agarose (45–165 μm, 50–150 cm h^{-1})	25–40 mg ml^{-1} serine proteases
Mimetic Blue® AP A6XL	Anthraquinone	Agarose (45–165 μm, 200 cm h^{-1})	18 000 U alkaline phosphatase/ml
EtoxiClear™		Agarose (100 μm, 200 cm h^{-1})	1 000 000 EU endotoxin/ml
Insulin		Agarose (90 μm, 500 cm h^{-1})	25 mg insulin/ml
Aminophenylboronate		Agarose (100 μm, 200 cm h^{-1})	10–20 mg glycoproteins/ml
Mimetic Blue® 1 P6XL,	Anthraquinone	Agarose (100 μm, 200 cm h^{-1})	25 mg albumin/ml
SA HL P6XL,		Agarose (100 μm, 200 cm h^{-1})	60 mg ml^{-1}
SA P6XL,		Agarose (100 μm, 200 cm h^{-1})	30 mg ml^{-1}
SA P6 HF		Agarose (90 μm, 500 cm h^{-1})	30 mg ml^{-1}
AlbuPure®	Triazine	Agarose (90 μm, 600 cm h^{-1})	35 mg albumin fusion proteins/ml

molecule is always in competition with binding of the ligand with its linker or the surface of the base material. For the high flexibility of a small ligand, a long linker is preferred although with a too long linker a reorientation of the ligand toward the linker can be observed. For the D-PAM ligand, it could be shown that two of the four arms are directed toward the binding site of the protein, while the other two are directed more to the linker and the surface. As a conclusion, it can be stated that the simple optimization of the ligand is only one part of the design work. Only if the linker and the base matrix are carefully adjusted a good customized sorbent can be achieved. Some design criteria can be concluded from the MD calculations:

- A too high hydrophobicity of the base material surface leads to a decrease of the interaction between the affinity ligand and the target protein.
- The linker influences the binding as well. A certain length of the linker is needed to give the ligand enough sterical freedom to bind to the target molecule. The hydrophilicity or hydrophobicity of the linker has to be carefully monitored as a back-orientation of the ligand toward the base material surface has to be avoided. This phenomenon might occur if the ligand and the base matrix exhibit a certain hydrophobicity and the linker is too hydrophilic.

Another small ligand approach has been developed by Heath and Agnew and commercialized by IndiMolecular (Agnew et al. 2009).

The technology uses the *in situ* click chemistry and starts with the synthesis of an epitope of interest, e.g. a peptide sequence of 8–20 amino acids. On the one end of the epitope peptide, a biotin ligand is attached for detection purposes, and on the other end, an alkyne group is coupled, which is able to react with an azine. The synthetic epitope is mixed with a library of two million cyclic peptides, called protein-catalyzed capture (PCC) agent and consisting of D-amino acids, which are immobilized on beads. Those peptides that bind the synthetic epitope in the right conformation form a covalent bond between the epitope alkyne and the azide on the ligand. The ligands, which have bound the epitope, are identified via the biotin linker and further developed as affinity ligands. Following this route, Lai et al. recently reported the identification of a peptide ligand with picomolar cooperative binding to interleukin-17F (Lai et al. 2018).

3.3.8.2 Natural Polymers (Proteins, Polynucleotides)

The Dutch company BAC B.V. (now part of Thermo Fisher Scientific) has developed a technology using Camelidae heavy-chain antibodies (CaptureSelect®) (Table 3.20). The technology is based on the identification of stable and specific affinity ligands by using immune llama antibody libraries and the expression of resulting heavy-chain antibody fragments of 129 amino acids (approximately 12 kDa) in the yeast *Saccharomyces cerevisiae*. It is claimed that the ligand has a high affinity, specificity, and capacity in combination with a good caustic stability. In addition, it should bind all IgG subclasses compared to protein A that does not bind IgG3. In a similar approach, the vNAR domain of shark antibodies can be used as affinity ligands. The group of Kolmar (Zielonka et al. 2014) describes the *in vitro* affinity maturation via yeast surface display as a platform technology.

Table 3.20 Cammelidae antibody-based affinity sorbents.

Target protein	Product, manufacturer	Base material	Affinity selector	Specific binding purposes
Follicle-stimulating hormone (FSH)	CaptureSelect® Follicle Stimulating Hormone (FSH), Thermo Scientific	Agarose, aldehyde activated (65 μm)	Camelid-derived single domain antibody fragments	3 mg ml^{-1}
Human chorionic gonadotropin (hCG)	CaptureSelect® hCG, Thermo Scientific	Agarose, aldehyde activated (65 μm)	Camelid-derived single domain antibody fragments	4 mg ml^{-1} hCG
Human growth hormone (hGH)	CaptureSelect® Human Growth Hormone (hGH), Thermo Scientific	Agarose, aldehyde activated (65 μm)	Camelid-derived single domain antibody fragments	3 mg ml^{-1}
Thyroid-stimulating hormone (TSH)	CaptureSelect® TSH, Thermo Scientific	Agarose, epoxy activated (65 μm)	Camelid-derived single domain antibody fragments	5 mg ml^{-1} TSH

In principle all stable and divers proteins scaffolds can be used as affinity ligands for chromatographic purifications. Therefore a number of companies have been recently established with the goal of developing smaller and simpler molecules compared to full-size monoclonal antibodies that can be used either as a therapeutic protein or as an affinity ligand (Table 3.21). The advances as therapeutics have been reviewed by Azhar et al. (2017).

The Nanofitins developed by the French company Affilogic consist of 66 amino acids (7 kDa). The protein Sac7d has been identified in a Yellowstone National Park geyser in 1974 and exhibits extremely good stabilities against heat and acids as its natural environment is at 85 °C and pH 2. Via randomization of the natural binding site, a library of Nanofitins® has been developed, which gives high affinity binding toward selected targets while maintaining the original stability features. The protein is bound via a thiol group onto base materials, e.g. the polyvinylether beads Eshmuno. In the frame of the EU-funded project DiVine (https://divineproject.eu/), the project partners Affilogic, GSK Vaccines, Merck Millipore, and IBET developed an affinity resin for the capture of CRM197, a nontoxic mutant of the diphtheria toxin. This protein is used as a carrier for polysaccharides and haptens to make them immunogenic. It could be shown that the affinity resin is able to increase the purity in a single step from 37% to 96% (SE-HPLC, 99% in RP-HPLC) (Nissum 2018).

The second approach to using novel protein scaffolds for bioseparation is the use of Affilin™ molecules developed by Navigo Proteins (formerly Scil Proteins).

Table 3.21 Small protein-based affinity ligands.

Name	Company	Structure	Application
Affilin	Navigo Proteins	10 kDa	Precision Capturing™ affinity chromatography
Nanofitin	Affilogic	12 kDa	Protein capturing affinity chromatography
Anticalin	Pieris	20–22	Therapeutic only
Affibody	Affibody SA		Only therapeutic
DARPin	Molecular Partners	14–21	Only therapeutic
Tetranectin	Borean Pharma		
Avimer	Avidia acquired by Amgen	9–18	
Knottin	MedImmune	3–6 kDa	
Dual affinity retargeting (DART)	MacroGenics	50	
Tetravalent tandem antibodies	Affimed	110	
Evibodies	Arana (acquired by Cephalon)		
Fynomer	Covagen (acquired by Janssen)		
mTCR	Immunocore IMTECH™		
Small modular immunopharmaceuticals (SMIPs)	Emergent Biosolutions	Binding domain from annexin	

These proteins exhibit good thermal, proteolytic, and caustic stability. After incubation in 0.1 M NaOH for 20 hours, the resin exhibits still 80% of the initial static binding capacity. As for other small proteins, the production can be done using cost-effective *E. coli* systems (Fiedler et al. 2006).

Besides proteins also polynucleic acids can be used as affinity ligands. The uniform genetic coding system of DNA or RNA polymers can be used to bind any given target molecule just via its three-dimensional structure. The so-called aptamers are short-chain oligonucleotides of 25–70 base pairs that are selected by systematic evolution by exponential enrichment (SELEX process) (Jaysene 1999). Those libraries are subjected to a high-throughput screening to find optimum binding properties for the target molecules. Binding strength and chemical and enzymatical stability can be tuned via modification at the $2'$-position of the sugar or the C-5 position of the pyrimidine bases.

The use of aptamers as affinity chromatography ligands has been evaluated as early as 1999 (Romig, Bell, and Drolet 1999) Today four companies mainly

develop aptamers for diagnostic and separation purposes: Aptagen (www .aptagen.com), Noxxon with their Spiegelmer® technology, BasePair, and SomaLogic (SOMAmer). Rohloff described the development of SOMAmers as diagnostic agents with the potential to be further scaled up to be used as affinity chromatography materials (Rohloff et al. 2014).

LFB reported the use of aptamer ligands for the purification of different plasma proteins, e.g. blood coagulation factor VII, IX. factor H, and glutamic acid (GLA) domain of factor VII (Forier et al. 1489) All aptamers have been between 40 and 50 nucleotides and are attached to NHS-activated Sepharose by a proprietary coupling procedure (Boschetti and Perret 2011) Using the affinity resins, the plasma proteins could be isolated from different sources with high specificity.

3.3.8.3 Artificial Polymers

A molecular recognition technology known in the literature for more than 40 years and often supposed to be of great potential for preparative chromatography too is the design of special polymers that function as an artificial keyhole for the target molecule. The so-called molecular imprinting (MIP) technology introduced by Mosbach and Wulff in the 1970 has to overcome some challenges to be used in preparative mode. Besides the complex polymerization process, the resulting chromatographic phases showed a serious diffusion limitation. This diffusion limitation leads to low loadings and long peak tailing, reducing the throughput to very low numbers (Alexander et al. 2006). Tables 3.22 and 3.23 list the designed and customized resins for specific targets.

3.4 Advective Chromatographic Materials

Advection (often used as a synonym for convection) is defined as the movement of materials by a fluid. It is way faster compared with diffusion, the movement of materials, e.g. proteins in the pore system of a bead-based material. As speed is one of the parameters to be maximized in chromatography, advective materials offer advantages. In addition, both the breakthrough front and the dispersive front of the elution are steeper in advective materials. For the dispersive front, this will result in smaller fraction volumes and higher concentrations of the product of interest. It is obvious that for the development of an advective material, pores with long diffusive pathways have to be avoided. On the other hand, the pores and the inner surface area they are generating are necessary to obtain a certain binding capacity as the capacity is linear to the available surface area. Over several decades, materials scientists have therefore tried to optimize the ratio between the large advective pores in the chromatographic material and the inner geometry of the material generating the adsorptive surface. With classical porous beads on the one end of the spectrum, on the other extreme are flat sheet membranes with consisting of only advective flow-through pores. As illustrated in Figure 3.21, there is a variety of different architectures trying to simultaneously maximizing speed and capacity.

Table 3.22 Customized resins for plasma protein purification.

Taget protein	Product (manufacturer)	Base material	Selector	Capacity
Albumin	CaptureSelect® Human Albumin, Thermo Scientific	Agarose, aldehyde activated (65 μm)	Camelid-derived single domain antibody fragments	15 mg ml^{-1}
Albumin	Capto Blue (high sub), GE Healthcare	Highly cross-linked agarose (75 μm)	Cibacron blue 3G	30 mg ml^{-1} HAS (human serum albumin), Qb10 at 4 min residence time
Albumin	Blue Sepharose 6 FF; GE Healthcare	Highly cross-linked Agarose, 6% (90 μm)	Cibacron Blue 3G	Purification of interferon, albumin
Tissue plasminogen activator (tPA)	CaptureSelect® tPA, Thermo Scientific	Agarose, epoxy activated (65 μm)	Camelid-derived single domain antibody fragments	6 mg ml^{-1} tPA (human tissue plasminogen activator)
Anti-A and B IgG	Eshmuno® P anti-A and anti-B resin Merck Millipore	Hydrophilic polyvinylether	Trisaccharide blood group antigens A, resp B	90% anti-A or B removal and 97% yields in flow-through at IgG load of 3 kg l^{-1} at 6 min residence time
Anti-A and B IgG	Isoclear™ A and B, Prometic Bioseparations	Polymethacrylate 65 μm	Trisaccharide blood group antigens B, resp. B	
Antithrombin (ATIII)	Capto Heparin, GE Healthcare	Highly cross-linked agarose (90 μm)	Heparin	1.4 mg ml^{-1} ATIII
ATIII	Heparin HyperD M, Pall Corporation	Porous rigid mineral bead with hydrogel filled pores (80 μm)	Heparin	25 mg ml^{-1} ATIII
Plasminogen	Lysine Sepharose 4B, GE Healthcare	Highly cross-linked agarose, 4% (90 μm)	ʟ-lysine	Isolation of plasminogen, separation of ribosomal RNA (rRNA)
Plasminogen	ECH-Lysine Sepharose 4 Fast Flow, GE Healthcare	Highly cross-linked agarose, 4% (90 μm)	L-lysine	1.5 mg ml^{-1} Plasminogen
α-1 antitrypsin (AAT)	α-1 antitrypsin Select, GE Healthcare	Highly cross-linked spherical agarose (75 μm)	Recombinant single domain antibody fragment	10 mg ml^{-1} α-1 antitrypsin (AAT)
Factor IX	IXSelect, GE Healthcare	Highly cross-linked agarose (75 μm)	Factor IX ligand	6 mg ml^{-1} factor IX

Table 3.23 Customized affinity resins for generic recombinant proteins.

Taget protein	Product (manufacturer)	Base material	Selector	Capacity
Thyroglobulin	Capto Lentil Lectin, GE Healthcare	Highly cross-linked agarose, 4% (90 µm)	Lentil lectin	>16 mg ml^{-1} porcine thyroglobulin/ml medium
Heparin	Heparin Sepharose 6 FF, GE Healthcare	Highly cross-linked agarose, 6% (90 µm)	Porcine heparin	4 mg ml^{-1} heparin
Proteases and factor Xa	Benzamidine Sepharose 4 FF (high sub), GE Healthcare	Highly cross-linked agarose, 4% (90 µm)	p-Amino benzamidine (pABA)	Purification of trypsin, trypsin-like serine proteases, zymogens, thrombin, and factor Xa
Calmodulin binding proteins	Calmodulin Sepharose 4B, GE Healthcare	Highly cross-linked Agarose, 4% (90 µm)	Calmodulin	Calmodulin binding proteins
Protein A	IgG Sepharose 6 FF	Highly cross-linked agarose 6% (90 µm)	Human IgG	3 mg ml^{-1} protein A
Gelatin	Gelatin Sepharose 4 Fast Flow, GE Healthcare	Highly cross-linked agarose 4%, 90 µm	Bovine gelatin derivative	5 mg ml^{-1} gelatin
Gelatin	Gelatin Sepharose 4B, GE Healthcare	Highly cross-linked agarose 6%, 90 µm	Bovine gelatin	4.5–8 mg ml^{-1} gelatin
Granulocyte-colony stimulating factor (G-CSF)	GCSFSelect, GE Healthcare	Highly cross-linked high-flow agarose, 75 µm	Recombinant protein, produced in S. cerevisiae	3.9 mg ml^{-1} G-CSF (Granulocyte-colony stimulating factor)

Beads	Advective chromatography	Membranes

- o Flow: diffusional
- o Flow rate: low to medium
- o Surface area: high
- o Capacity for large molecules: low

- o Flow: adjective
- o Flow rate: high
- o Surface area: medium
- o Capacity for large molecules: high

- o Flow: adjective
- o Flow rate: high
- o Surface area: low
- o Capacity for large molecules: medium
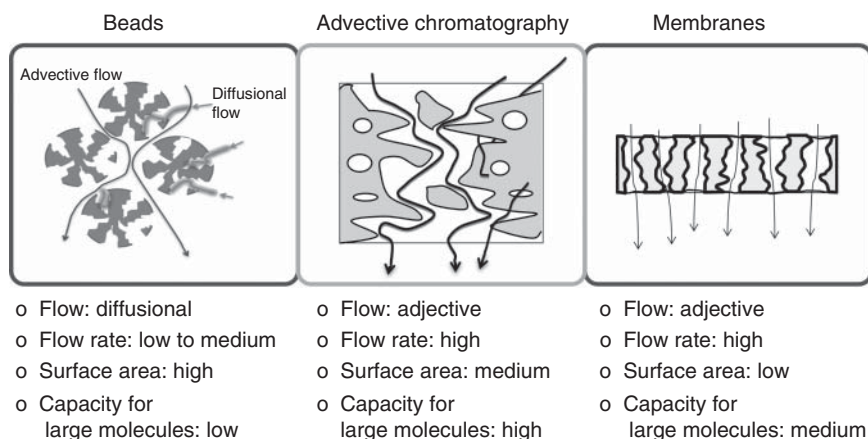
Figure 3.21 Different architectures of adsorptive materials.

The different materials can be grouped into:

1) Adsorptive membranes and grafted polymer membranes;
2) Adsorptive nonwovens;
3) Fiber/particle composites;
4) Area-enhanced fibers;
5) Monolith.

3.4.1 Adsorptive Membranes and Grafted-Polymer Membranes

The two most prominent adsorptive membrane products on the market are based on regenerated cellulose flat sheets (Sartobind® from Sartorius) or polyethersulfone (PES) (Mustang® from Pall; review in Orr et al. 2013).

The regenerated cellulose of the first-generation Sartobind membrane has a hydrophilic cross-linker with hydroxyl groups and a nominal pore width of 3–5 μm at a membrane thickness of 275 μm. IEX groups are attached on one side of the membrane via graft polymerization. This concept has been used for the strong Q- and S-type adsorber and a weak type D adsorber. With this architecture, binding capacity of 29 mg ml^{-1} of BSA can be achieved. The most recent housing of the membranes for scale-up are 0.8 and 1.6 l cassettes with a membrane height of 4 mm equivalent to 15 membrane layers. The cassettes can be stacked into stainless steel holders to result in maximum membrane volumes of 100 l. Besides the grafted-polymer layer, a direct binding of a primary amine ligand over the whole cross section of the membrane has been developed (Sartobind STIC® PA) (Faber, Yang, and Gottschalk 2009; Fischer-Frühholz, Zhou, and Hirai 2010). This ligand shows a higher salt tolerance and an increased capacity of 50 mg ml^{-1} BSA. Maximum flow rates of 40 bed volumes/min can be achieved using this kind of membrane adsorber.

The Mustang membrane adsorber developed by Pall is based on a PES membrane. They differ in pore size with 0.8 μm pores for the Q type, 0.65 μm for the S type, and 0.2 μm for a quaternized amine polymer called E for the removal

of endotoxins. The geometry of an adsorber unit consists of 16 layers with a single layer membrane thickness of approximately 100 μm. The Q membrane is specified to bind 70 mg BSA ml^{-1}. The largest capsule volume is 780 ml and is typically operated with a flow rate of 10 CV/min at a pressure drop of 1 bar (Pall 2009).

Besides IEX surface modifications, a variety of affinity selectors have been attached to membrane supports. They have been reviewed by Gosh (2002)) and Orr et al. (2013).

3.4.2 Adsorptive Nonwovens

Nonwoven fabrics consist of fibers of different length bonded together by chemical, mechanical, or physical treatment. They exhibit a random structure with large pores, which allow a high flow rate if used in biopharmaceutical processes as an adsorptive medium. Due to the low outer surface area of the fibers, nonwovens have to be modified by grafting polymerization or polymerization in the pore system to obtain a material with a surface area large enough to result in a useful binding capacity.

Liu et al. (2013) described an affinity membrane based on a polybenzophenone (PBT) nonwoven, which has been hydrophilized and used for the removal of prion proteins from blood plasma.

The non-modified nonwoven has a fiber diameter of approximately 3 μm and a medium pore size of 8 μm, with a layer thickness of the nonwoven of 300 μm. PBT is a cheap base material for the production of nonwovens but is hydrophobic in nature, therefore showing a high nonspecific protein binding. To hydrophilize the fibers and to serve as an anchor group for the attachment of an affinity ligand a UV-induced graft polymerization is used to equip the fibers with a coating. Glycidyl methacrylate (GMA) is used in a ratio of 2 : 100 GMA to PBT to form a layer of approximately 75 nm thickness on the surface of the PBT nonwoven. The epoxy function of the GMA is ring-opened with diethylene glycol or diluted sulfuric acid. The resulting hydroxyl function can be used to attach ligands to the fiber material. A proprietary ligand binding the prion protein developed by Prometic and previously described for bead-based systems (Gregori et al. 2006) has been attached to the activated nonwoven.

Another alternative to obtain a higher surface area for ligand attachment is the reduction of the fiber diameter of the nonwoven. In contrast to the melt-blown or dry-spun fibers, electrospinning offers an alternative for the production of nanofiber nonwovens, with a fibers diameter of a few hundred nanometers. Electrospinning has already been developed in the nineteenth century and is today used in different application areas, e.g. textile manufacturing, filtration materials, and composite materials used as catalytic layers, e.g. for fuel cells (Kas et al. 2014).

The systems used for electrospinning consist of a needle with small diameter connected to a solvent or suspension reservoir. Between the needle tip and a substrate plate, a high-voltage electrical field is created. The suspension is pumped through the needle tip and first leaves the needle as a straight jet stream (Tailor cone). Along the spinning direction, an electrical instability occurs, and the straight jet is transformed into a highly accelerated whipping motion. When the jet hits the substrate plate, fibers with nanometer diameters are forming a

nonwoven structure on the plate. Modern systems are using a needle-free design as the scale-up of the needle system is difficult. In addition, the substrate plate is constantly moved so that a continuous roll-to-roll production is possible.

Hardick, Stevens, and Bracewell (2011) used cellulose acetate as the base material spun from a mixture of acetone/dimethylformamide/ethanol (2 : 2 : 1) to form fibers of nanometer-scale diameter. Depending on the relative humidity (20–70%) and temperature (17.5–32.5 °C), average fiber diameter of 280–400 nm has been obtained with a remaining pore opening of approximately 0.5 μm.

The cellulosic material has been modified with 2-chloro-*N,N*-diethylethylamine to obtain a weak anion-exchange DEAE group on the nanofibers. The material is reported to have a dynamic binding capacity of 5 mg BSA ml^{-1} tested in a 0.15 ml device. Calculated maximum velocities from the 0.15 ml device (25 mm diameter, nonwoven bed height 300 μm, consisting of six layers) are an astonishing high 2400 cm h^{-1} (Hardick et al. 2013).

This work let to the spin out of the company Puridify from the University College London in 2013, which has been acquired by GE Healthcare in November 2017.

Natrix Separations, a Canadian start-up company acquired by Merck Millipore in 2017, is using a different technology to enlarge the surface area of a nonwoven base material: based on a nonwoven matrix, 3-acrylamidopropyl-trimethylammonium chloride (ATPAC) is polymerized to form a three-dimensional microporous hydrogel, which is incorporated into the open pore structure of the nonwoven. The degree of cross-linking of the formed hydrogel can be varied from 9% to 12%. The functionalized hydrogel gives a much higher binding capacity compared to adsorptive membranes (200 mg ml^{-1} BSA for Natrix$^{®}$ Q compared with 50–70 mg ml^{-1} for adsorptive membranes) (Childs et al. 2012).

Besides the Q-type strong anion-exchange membrane a mixed-mode cation-exchange membrane has been developed (Natrix$^{®}$Sb) consisting of a sulfo group containing strong CEX ligand in combination with a butyl hydrophobic ligand. In contrast to the Q-module, which is often used in flow-through polishing mode for monoclonal antibody production, the Sb type is used for the capture step in a polio vaccine process. Funded by the Bill and Melinda Gates Foundation, a vaccine manufacturing platform has been designed by the three project partners: Univercells, Batavia Biosciences, and Merck Millipore. The goal of this project is the production of a trivalent polio vaccine at very low cost (US$0.30 per dose) (Univercells 2019). Applying affinity ligands is an additional option for the capture and purification of vaccines using advective chromatographic materials. Zhao et al. (2019) recently presented an overview of affinity chromatography for vaccine manufacturing showing the variety of different affinity ligands and vaccine targets.

For sure, the most prominent affinity ligand to be attached to advective chromatographic materials is protein A for monoclonal antibody capturing. Following the industry trend of modular continuous single-use purification systems, protein A membrane adsorber is developed, offering a perfect fit for the purification of up to 10 kg batches of mAbs. Using single-use adsorbers, the validation, packing, cleaning, and storage efforts are drastically reduced. In the case of the

expensive protein A resins, this can only be achieved with high-throughput resins available in a perfect system scale so that at the end of the purification of one batch, no unused resin capacity is left over, which would be a waste in money or would result in higher efforts if the affinity resin has to be stored and revalidated (Xenopoulos 2015).

A combination of a polypropylene nonwoven with an AEX hydrogel and an asymmetric 0.2 μm multilayer depth filter has been developed by 3M™ (3M Emphaze™ AEX Hybrid Purifier). Including adsorptive charged layers in the clarification step of the downstream cascade results in the reduction of HCPs and DNA – levels prior to the protein A capture step. Therefore this approach can be regarded as a guard filter for the expensive affinity resin and can in addition reduce the necessary size of the anion exchange polishing step in a classical 3-step mAb purification process (Castro-Forero et al. 2015; Li 2017).

3.4.3 Fiber/Particle Composites

A composite material as a mixture of large surface area beads with high porosity fibers has been described by Herigstad, Gurgel, and Carbonell (2010).

To produce the material, polymethacrylate beads of 65–90 μm bead size with a pore diameter of 100 nm have been dried. These beads were placed on top of a polypropylene nonwoven with an average fiber diameter of 20 μm and a nominal pore diameter of 15 μm and covered with a second layer of the nonwoven. An ultrasonic edge sealer sealed the sandwich structure of the particle impregnated membrane (PIM). Seventy-two layers of the membrane with a single layer thickness of 550 μm were placed into a column and could be operated with velocities of up to 1260 cm h^{-1} or 5.3 CV/min. Adsorption experiments showed that the adsorption of BSA was only taking place at the porous particles and not on the nonwoven. The main application is the depletion of prion proteins. For this purpose an affinity ligand has been attached to the beads. The adsorbent is commercialized by Macopharma under the name P-CAPT® (Gregori et al. 2006).

Another combination of a filter material with adsorptive particles has been developed by Merck Millipore and is called Millistak+ HC Pro X0SP. The depth filter consists of a nonwoven made of polyacrylic fibers with a nominal pore width of 0.1 μm. It is intended to be used as a secondary clarification filter. Precipitated silica particles are incorporated into the nonwoven ensuring a higher adsorption capacity for contaminants of fermentation products. Nguyen et al. (2019) showed that the filter had a higher binding capacity for critical impurities from a CHO mAb process compared to previously used diatomaceous earth filters. In addition, the new filter material consists of totally synthetic raw materials in contrast to the natural product diatomaceous earth.

3.4.4 Area-Enhanced Fibers

Nonporous beads or cutted fibers are another option to generate a packed bed consisting of advective materials. The drawback of these materials is their limited surface area, which is influenced only by the size of the bead or the diameter of the fiber. To enlarge the surface area of a fiber, different structures have been realized,

which decorate the round fibers with wings or arms. Schwellenbach et al. (2016) have attached a cation-exchange hydrogel layer on top of a wing-shaped polyethylene terephthalate (PET) fiber of 6 mm cut length. Those fibers exhibit a specific surface area of $2 \, m^2 \, g^{-1}$ and a fiber diameter of approximately 15 µm. After surface modification, the SO_3-modified fibers have been packed into a standard column with a packing density of 0.35 g fibers/ml column volume and showed a static binding capacity for hIgG of $92 \, mg \, ml^{-1}$. The permeability of the packed fiber column was compared to a membrane adsorber (Sartobind S) and a porous bead material (Fractogel® EMD SO3). With 500 /mDa, the permeability for the winged fiber was 10 times higher compared to the membrane adsorber but 4 times lower compared to the packed column (500 /mDa versus 2.100 /mDa).

It could be shown for the membrane adsorber and the winged fiber that the drop in binding capacity at a very low residence time of 10 seconds is smaller compared to the bead-based material; nevertheless, even at the shortest residence time, the capacity for the Fractogel EMD SO3 was still higher.

Winderl, Spies, and Hubbuch (2018) examined the packing behavior of similar shaped fibers made of polyamide-6 (PA-6).

They could show that homogeneously packed columns of 6.6 mm i.d. column could be obtained when a slurry packing method was applied. The packed column showed a reduced plate height of 0.09 cm. Columns were packed with porosities of 0.2–0.4 and column length of 1–4 cm. The best columns with respect to low plate height and symmetric peak shape could be obtained for lower packing densities and longer packing length, which on the other hand reduces the binding capacity and increases the process time.

3.4.5 Monolith

Starting with the pioneering work of Hjertén and Svec for polymeric (Hjertén, Liao, and Zhang 1989; Svec and Fréchet 1992) and Tanaka (Minakuchi et al. 1996) for silica-based, monolithic columns have been developed as an alternative to porous bead chromatography for a certain application area.

Monolithic columns are used in similar column hardware compared with packed columns, and their main performance-determining parameter is the throughpore diameter. Both silica and polymeric monolith are surface modified with the same functionalities compared to porous bead materials. The synthesis of the monolithic material is limited to a certain column diameter as it is rather difficult to control the column homogeneity beyond a certain point. Due to the high efficiency at high flow rates, the use of monolithic columns allows high productivities. Schulte and Dingenen (2001) have shown that an simulated moving bed (SMB) system of six monolithic Chromolith® normal phase silica columns with 25 mm i.d. was able to separate as much as 2.6 kg of a diastereomeric mixture per day and liter of column volume.

The fast flow rates of the monolithic columns allow to use them for at-line analytics, which is highly desired for intensified biopharmaceutical downstream processes. Kupfer et al. (2017) showed that the quantification of a monoclonal antibody can be done with high precision in less than two minutes (Figure 3.22). The Chromolith rSPA, a protein A modified monolithic silica column, showed
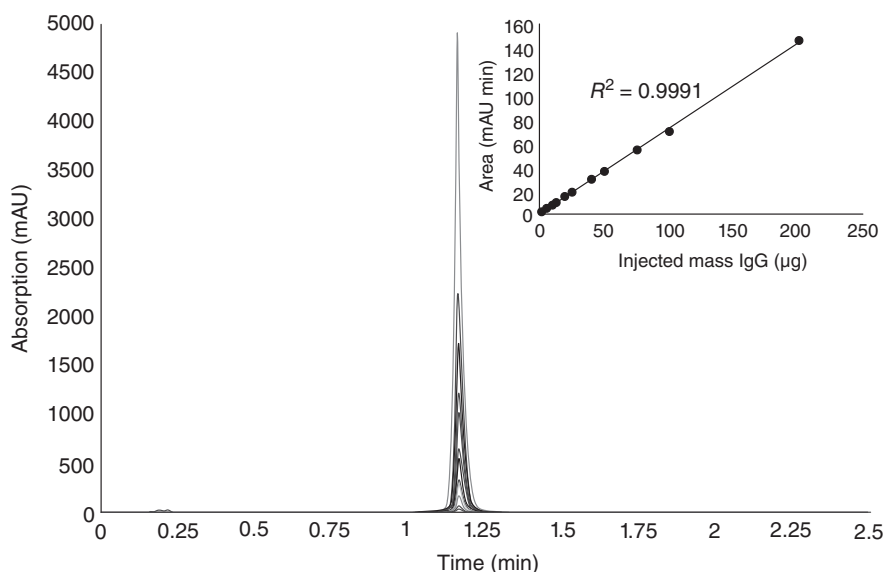
Figure 3.22 Calibration curve of cetuximab on rSPA silica monolith ranging from 1.25 to 200 μg. Chromatographic conditions: stepwise gradient: 100 mM sodium phosphate pH 7.4/100 mM sodium phosphate pH 2.5; 0.25 min 100/0, 0.25–0.26 min 0/100, 1.00 min 0/100, 1.00–1.01 100/0, 1.01–2.50 min 100/0; flow rate: 2.0 ml min^{-1}; detection: 280 nm; injection: 20 μl; temperature: 25 °C. Source: Reprinted with permission of Kupfer et al. (2017).

no changes in performance even after 10 000 injections with pH shift in each injection.

In a recent review, Lynch et al. compared the advances and applications of monolithic columns for the separation of proteins (Lynch et al. 2019). They list more than 30 different surface modifications, which have been applied to monolithic columns covering all types of chromatographic modes from RP over IEX to affinity separations.

Monolithic columns prepared from organic polymers have been introduced into the market by Bio-Rad and BIA Separations. The Bio-Rad UNO® monolith is based on a polyacrylamide polymer modified with strong cation- and anion-exchange groups. Besides the problem of homogeneity in the production of monolith, an additional difficulty in the synthesis of monolith from organic monomers is the swelling behavior in different process conditions applied during the synthesis. This effect limits the maximum size of a preparative device. UNO columns are available up to a volume of 12 ml (15 mm i.d.; column length: 68 mm). The monolith can be operated at maximum 48 bar allowing a linear flow rate of up to 350 cm h^{-1}. The Slovenian company BIA Separations has developed the CIM® (Convective Interaction Media) columns. These columns are based on a polymethacrylate polymer modified with a variety of different ligands for IEX, hydrophobic interaction, and affinity, especially protein A, chromatography. The macropore system of the monolith can be varied from 1.3 up to 6 μm with a mean diameter of 2 μm for the standard products. The recently introduced CIMmultus™ product line uses a chromatographic bed in form of an annular

Table 3.24 Properties of different monolithic columns of the CIMmultus™ series.

	1 ml	8 ml	80 ml	800 ml	8000 ml
Bed height (cm)	0.60	0.43	0.95	2.0	2.25
Column length (cm)	0.40	0.42	0.95	2.00	2.20
Column volume (ml)	1.42	0.6	7	106	793
Maximum. flow rate (ml min^{-1})	16	100	400	2000	8000
Linear flow rate (cm h^{-1})	438	4368	3462	2290	2400
Pressure drop (bar)	18	20	20	14	7

gap, with the solvent flow in radial direction (Table 3.24). The largest available module has a bed volume of close to 800 ml and can be operated with a flow rate of 8000 ml min^{-1} equivalent to 2400 cm h^{-1}. Due to the curvature of the packed bed, the average linear velocity u_{av} has to be calculated according to Eq. (3.3), as the linear velocity differs from column inlet to outlet:

$$u_{av} = \frac{F}{\pi \times L} \frac{\ln\left(\frac{D_o}{D_i}\right)}{(D_o - D_i)} \tag{3.3}$$

where F is flow rate (ml min^{-1}), L is bed height (in radial direction), and D_o and D_i are the outer and inner diameter of the column.

The pore geometry of the monolith with large throughpores and no inner pores makes them best suited for the chromatography of large molecules. While for standard proteins the adsorption capacity is limited, the large throughpores are adventitious for larger biological products, e.g. plasmids, viruses, and exosomes. Jungbauer and Hahn have been calculated for different molecular weights of proteins theoretical adsorption capacities on monolithic columns. In a monolithic material, large molecules can access the entire area of the channels; therefore the capacity in mg/ml for a product with assumed spherical form increases with the molecular weight of the product. For the CIM monolith, Jungbauer and Hahn calculated the theoretical capacity for a 150 kDa molecule (typical mAb size) to be 32 mg ml^{-1}, while for a product of 950 kDa (IgM) the capacity increases to 80 mg ml^{-1} and for a large polymer of 10 000 kDa to even 131 mg ml^{-1}, still assuming spherical shape of the product (Jungbauer and Hahn 2008).

The purification of virus-like particles (VLPs) has been demonstrated by Zaveckas et al. (2015). The porcine circovirus has a diameter of 20 nm, and its capsid protein can form VLPs of up to 200 nm. SP Sepharose XL, Heparin Sepharose CL-6B, and an SO$_3$ CIMMultus monolith have been compared with the no retention on the SP Sepharose beads. Purity and yield on the heparin-based affinity gel were also quite low, while the monolith gave a purity of 40% and a recovery of up to 18%. Still these values are far from being optimal, but they show the potential for advective-type media especially for the purification of larger products.

3.4.6 Chromatographic Materials for Larger Molecules

Besides the dominating market of mAbs, a new generation of therapeutics is currently entering the clinic. One common denominator of these macromolecules is their increased size. Classical therapeutic proteins range from 10 to 1000 kDa and hydrodynamical radii of 2–12 nm with IgM being one of the largest products (970 kDa, 12.7 nm). The new types of products to be purified are viruses and virus particles (20–200 nm), e.g. adeno-associated viruses (AAVs) (22 nm) or lentiviruses (80–120 nm) used for viral vector transfer in gene therapy. Extracellular vesicles (20–200 nm), DNA plasmids (50–200 nm), and exosomes (30–180 nm) are further examples for large therapeutic products.

For this type of products, new bead architectures are developed, e.g. core–shell or restricted access materials (RAM). The concept of RAM has been developed in the 1980s for the analysis of small drug molecules in biological fluids. A porous bead with hydrophobic modifications in the pores has been coated with a hydrophilic layer at the outer surface to prevent plasma proteins from unspecific adsorption. The small drug molecules or their metabolites penetrate into the RAM and are captured while the plasma proteins are washed away. The RAM sorbents allowed an easier and faster evaluation of drug blood levels without sample preparation (recent review in Faria et al. 2017).

A reciprocal concept is applied for the purification of large products from small-size impurities. Capto Core 700 resins exhibit a mixed-mode anion-exchange/hydrophobic surface modification within the pores of an 85 μm bead. The outer layer of the bead is hydrophilic and non-modified and excludes all molecules with a size of 700 kDa. It can therefore be used for the separation of DNA, large proteins, or protein complexes in flow-through mode from smaller-size HCPs and small molecule impurities (Blom et al. 2014).

AAVs, which are used as viral vectors for gene therapy and which exhibit a size of 20 nm, are an upcoming challenge for biochromatographic resins. For the capture of the different subtypes, affinity ligands have been developed and attached to standard agarose particles as well as flow-through perfusive polystyrene particles. Table 3.25 lists the currently available materials and their binding specificity toward different AAV subclasses. Besides the capturing step, the separation of full viral capsids containing the DNA to be transfected from empty one is a most challenging task. As the two types of capsids differ slightly in their pI, IEX chromatography can be applied but need to be optimized if the number of gene therapeutic concepts is increasing and the costs for these therapies have to be lowered. Besides the affinity chromatography-based purification sequence, there are also processes exploited, which omit affinity and use combinations of different IEX steps or IEX in combination with hydrophobic interaction chromatography or SEC (Robert et al. 2017).

3.5 Chiral Stationary Phases

Chiral stationary phases (CSPs) for preparative use have been optimized tremendously over the past two decades. After the introduction of the first commercially

Table 3.25 Affinity resins for the capturing of adeno-associated viral (AAV) vectors.

Material	Supplier	Base matrix	Binding capacity (AAV subtypes)
POROS® CaptureSelect AAV8	Thermo Scientific	Large pore, 50 µm, poly(styrene-divinylbenzene), hydrophilized	$>10^{13}$ vg ml^{-1} [AAV8]
POROS CaptureSelect® AAV9	Thermo Scientific	Large pore, 50 µm, poly(styrene-divinylbenzene), hydrophilized	$>10^{14}$ vg ml^{-1} [AAV9]
POROS® CaptureSelect AAVX	Thermo Scientific	Large pore, 50 µm, poly(styrene-divinylbenzene), hydrophilized	$>10^{13}$ vg ml^{-1} [AAV1, AAV2, AAV3, AAV4, AAV5. AAV6, AAV7, AAV8, AAV9, AAVrh10]
AVB Sepharose High Performance	GE Healthcare	Cross-linked agarose, 4%, 34 µm	10^{12} vg ml^{-1} [AAV 1,2,3,5]

available phases in the early 1980s, the reproducible synthesis of those phases in large quantities has improved significantly, so today several multi-ton productions of enantiopure drugs are operated applying chiral chromatography. CSPs most often used in preparative chromatography are listed in Table 3.26.

The breakthrough in the application of CSPs for preparative use came with the controlled bonding or coating of the chiral selector onto mesoporous silica offering both a better thermodynamic control due to the optimized silica pore system and much higher pressure stability. With these types of stationary phases, the efficient packing of large-scale columns became possible. The only known application for one of the natural or synthetic soft polymers is the preparative separation of a precursor of the cholesterol-lowering drug Lipobay (which was later withdrawn from the market due to side effects) on a polyacrylamide phase produced by Bayer (Angerbauer et al. 1993). Other types of full polymer phases are the cellulose fibers cellulose triacetate (CTA) and cellulose tribenzoate (CTB) and the later developed cross-linked cellulosic beads (Francotte and Wolf 1991). Even though they offer in principle the advantage of high loadability, they are not easy to handle in large columns and thus have never been commercialized (Franco et al. 2001; Ikai et al. 2007).

3.5.1 Cellulose- and Amylose-Based CSP

The CSPs based on cellulose and amylose derivatives coated onto silica, which have been developed by the pioneering work of Okamoto, Kawashima, and Hatada (1984), are by far the most often used ones in preparative chromatography and, especially, SMB applications. These adsorbents offer good productivities

Table 3.26 Commercial packings with enantioselective properties.

Name or class	Trade name	Manufacturer
(1) Natural polymers or derivatives		
Cellulose triacetate	CTA	Merck Millipore
Cellulose tribenzoate	CTB	Riedel-de Haen
(2) Synthetic polymers		
Poly(triphenylmethyl methacrylate)	Chiralpak® OP/OT	Daicel Chiral Technologies
(3) Silica with monomolecular ligands (brush-type CSP)		
3-[N-(3,5-Dinitrobenzoyl)phenylglycine-amido] propyl-silica	ChiraSep® DNBPG	Merck Millipore
3-[1-(3,5-Dinitrobenzamido)-1,2,3,4-tetrahydrophenanthrene-2-y1]-propyl-silica	Chirex 3001 Whelk-O 1®	Phenomenex Regis, Merck Millipore
11-[2-(3,5-Dinitrobenzamido)-1,2-diphenylethylamino]-11-oxoundecyl-silica	ULMO®	Regis
3-{3-{N-[2-(3,5-Dinitrobenzamido-1-cyclohexal)]-3,5-dinitrobenzamido}-2-hydroxy-propoxy}-propyl-silica	DACH-DNB®	Regis
3,5-Dinitrobenzamido-4-phenyl-β-lactam	Pirkle 1-J®	Regis
N-3,5-Dinitrobenzoyl-a-amino-2,2-dimethyl-4-pentenyl phosphonate	α-Burke® 2	Regis
R®-3-[N-(3,5-Dinitrobenzoyl)-1-naphthylglycine-amido]-propyl-silica	Sumichiral 2500	Sumitomo
(S)-$tert$-Leucine and (R)®-1-(α-naphthyl)ethylamine urea linkage	Chirex 3005, Sumichiral® OA-4700	Phenomenex Sumitomo
(S)-Indoline-2-carboxylic acid and (R)®-1-(α-naphthyl)ethylamine urea linkage	Chirex 3020, Sumichiral® OA-4900	Phenomenex Sumitomo
	Chirex 3022	Phenomenex
O-9-($tert$-Butylcarbamoyl) (8 R,9 S)-Quinine	Chiralpak QN-AX	Daicel (Chiral Technologies)
O-9-($tert$-Butylcarbamoyl) (8 R,9 S)-Quinidine	Chiralpak QD-AX	Daicel (Chiral Technologies)

(Continued)

Table 3.26 (Continued)

Name or class	Trade name	Manufacturer
Native cyclofructan 6	FRULIC N	Merck Millipore, AZYP
Charged cyclofructan 6	FRULIC C	Merck Millipore, AZYP
Alkyl-derivatized cyclofructan 6	LARIHC CF6-P	Merck Millipore, AZYP
R-Naphthylethyl cyclofructan 6	LAHRIC CF6-RN	Merck Millipore, AZYP
3,5-Dimethylphenyl functionalized cyclofructan 7	LAHRIC CF7-DMP	Merck Millipore, AZYP
(4) Silica with natural selector derivatives		
Cellulose and amylose derivatives (see Table 3.1)		
β-Cyclodextrin	ChiraDex®, Cyclobond®	Merck Millipore, Astec
Vancomycin	Chirobiotic® V1 and V2	Astec
Teicoplanin	Chirobiotic® T1 and T2	Astec
Teicoplanin aglycone	Chirobiotic® TAG	Astec
(5) Silica with synthetic polymer		
Poly[(*S*)-*N*-acryloylphenylalanine ethyl ester]	ChiraSpher®	Merck Millipore
Cross-linked *O,O′*-bis-(3,5-dimethylbenzoyl-L-diallyltartaramide	Kromasil® CHI-DMB	Eka Chemicals
Cross-linked *O,O′*-bis-(4-tert-butylbenzoyl)-L-diallyltartaramide	Kromasil® CHI-TTB	Eka Chemicals
(*R,R*) or (*S,S*) Poly-(trans-1,2-diamino-1,2-diphenylethane)-*N*, *N*-diacrylamide, *trans*-1,2-diaminocyclohexane)-*N*, *N*-diacrylamide	P-CAP DP, P-CAP	Astec
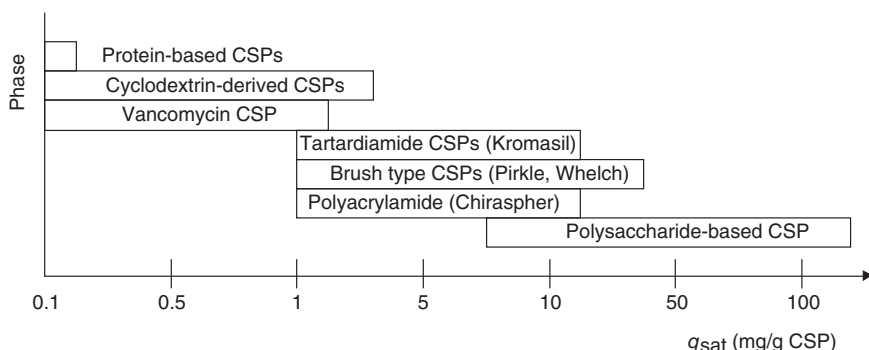
Figure 3.23 Typical saturation capacity of the most used commercially available CSPs. Source: Franco et al. (2001). Reproduced with permission of Elsevier.

because of their high loadabilities (Figure 3.23). In addition, the four most commonly used CSPs of this type separate a broad range of different racemates (Borman et al. 2003). The major problem of these adsorbents was their limited solvent stability, especially toward medium-polar solvents such as acetone, ethyl acetate, or dioxane. In the past, their use in conjunction with aqueous mobile phases was also not recommended by the manufacturer. This problem had been overcome when Ishikawa and Shibata (1993) as well as McCarthy (1994) reported good stabilities for the use of polysaccharide-type phases with aqueous mobile phase systems. The stability of the adsorbent after switching to RP conditions has been reported by Kummer and Palme (1996) to be at least 11 months and by Ning (1998) to be 3 years. No peak deviation is observed after switching to RP mode.

A breakthrough in stability was the chemical bonding of the chiral selector onto the silica backbone of the CSP, which was achieved by cross-linking of the selector adsorbed onto the silica matrix or by modification of the cellulose or amylose selector with a cross-linking agent. Table 3.27 lists the different approaches described in the literature. The covalent bonding of the cellulose or amylose polymer opens the door to the use of medium-polar solvents, which are otherwise widely used in preparative chromatography and which offer good solubilities for a lot of important racemates. However, compared to the coated phases where only a limited number of solvent combinations could be used, the mobile phase selection process for a separation on the immobilized phases could be more challenging. The immobilized polysaccharide phases have been reviewed by Franco et al. (2001), Ikai et al. (2006), and Padró and Keunchkarian (2018).

The advantages of the solvent-resistant CSPs were shown in an impressive way by Zhang, Schaeffer, and Franco (2005a) for the Ca-sensitizing drug candidate EMD53986. The major obstacle for the development of an enantiopure form of this drug substance was always its limited solubility in solvents that could be used in preparative chromatography. Even though good selectivities were found on different CSPs, none of them could be used in preparative mode with sufficient economy (Schulte et al. 1997). Using the new chemically bonded immobilized cellulose/CSP dichloromethane/THF as the solvent increased the solubility

Table 3.27 Different approaches to prepare bonded cellulose chiral phases on silica.

Method	Cross-linker	Support	Literature
Diisocyanate cross-linking	Diisocyanate	3-Aminopropyl silica	Okamoto et al. (1987)
	4,4′-Methylenediphenyl diisocyanate	3-Aminopropyl silica	Yashima (1994)
Polymerization of vinyl cellulose derivatives	Cellulose tris-(*p*-vinylbenzoate), benzoyl peroxide = radiacal initiator	Acrylamide-modified silica	Kimata et al. (1993)
	10-Undecenoate (0.3 per glucose unit)/3,5-DMP carbamate	Different silicas: unmodified, allyl, endcapped	Oliveros et al. (1995)
Photopolymerization, cross-linking	Photochemical insolubilization with and without photopolymerizable group (dimethylmaleimide)	3-Aminopropyl silica	Francotte (1996), Francotte and Zhang (1997, 1467)
Thermal cross-linking	Thermal treatment (120 °C), high amount of AIBN		Francotte (1997)
Copolymerization with a vinyl monomer	3,5-DMP carbamate/4-vinylphenylcarbamate 7/3	3-Aminopropyl and methacryloyl silica	Kubota et al. (2001)

tremendously and thus improved the productivity for the preparative separation 6.5-fold from 430 g enantiomer/kg CSP/d to 2834 g $(kg\,d)^{-1}$ (Zhang, Schaeffer, and Franco 2005a). Descriptions of the immobilized CSPs as well as recommendations for their use and special screening protocols can be found in Cox and Amoss (2004) and Zhang et al. (2005b, 2006, 2008). Table 3.28 lists the commercially available cellulose- and amylose-based CSPs.

After the first patents of the coated cellulose- and amylose-type CSPs expired in 2006, a series of generic CSPs have been introduced into the market. The main arguments for choosing one of these phases for a preparative separation process should be the loadability and stability of the stationary phase besides the price per kilogram and also the batch-to-batch reproducibility records and the availability in large batch sizes.

For method development and separation optimization, straightforward methods are described in the literature mainly for analytical purposes (Perrin et al. 2002a,b; Matthijs, Maftouh, and Vander-Heyden 2006; Ates, Mangelings, and Vander-Heyden 2008; Zhou et al. 2009). For preparative separations, it should be always kept in mind that some process parameters have a tremendous influence on the economy of the separation compared with analytical separations, for example, the cost, reusability, and toxicity of the mobile phase.

Table 3.28 Cellulose- and amylase-based chiral stationary phases.

Selector	Coated	Immobilized
Cellulose		
Tris(4-methyl-benzoate)	Chiralcel OJ, Eurocel 03, Lux Cellulose-3, CHIRAL ART Cellulose-SJ	
Tris(3-methyl-benzoate)	Chiralcel CMB	
Triphenylcarbamate	Chiralcel OC, Eurocel 04	
Tris(3,5-dimethyl-phenylcarbamate)	Chiralcel OD, Lux Cellulose-1,CHIRAL ART Cellulose-C, Sepapak-1, Astec Cellulose DMP, Reprosil Chiral-OM, CelluCoat, RegisCell, Reflect™ C-Cellulose B Nucleocell delta, Eurocel 01	Chiralpak IB, Reflect™ I-Cellulose B
Tris-(4-chlorophenylcarbamate)	Chiralcel OF	
Tris-(4-methylphenylcarbamate)	Chiralcel OG	
Tris(3,5-dichlorophenylcarbamate)	Sepapak-5	Chiralpak IC, Lux i-Cellulose-5 CHIRAL ART Cellulose-SC, Reflect™ I-Cellulose C
Tris(4-chloro-3-methylphenylcarbamate)	Chiralcel OX, Lux Cellulose-4, Sepapak-4	
Tris(3-chloro-4-methylphenylcarbamate)	Chiralcel OZ, Lux Cellulose-2, Sepapak-2	
Amylose		
tris(3,5-dimethylphenylcarbamate)	Chiralpak AD	Chiralpak IA
	Kromasil AmyCoat, Lux Amylose-1, CHIRAL ART Amylose-C, Reprosil Chiral-AM, AmyCoat, RegisPack, Reflect™ C-Amylose A, Nucleocel α, Europak 01	Lux I-Amylose-1, CHIRAL ART Amylose-SA, Reflect™ I-Amylose A
Tris([S]-à-methylbenzylcarbamate)	Chiralpak AS	
Tris(2-chloro-5-methylphenylcarbamate)	Chiralpak AY, Lux Amylose-2, Sepapak-3, RegisPack CLA-1,	
Tris(5-chloro-2-methylphenylcarbamate)	Lux Amylose-2	
Tris-[(R)1-phenylethylcarbamate]	Chiralpak AR	
Tris-(3-chloro-4-methylphenylcarbamate)	Chiralpak AZ	Chiralpak IF
Tris-(3-chlorophenylcarbamate)		Chiralpak ID
Tris-(3,5-dichlorophenylcarbamate)		Chiralpak IE
Tris-(3-chloro-5-methylphenylcarbamate)		Chiralpak IG

Chiralcel® and Chiralpak® are products of Daicel Chemical Industries/Chiral Technologies; Eurocel of Knauer; Lux® of Phenomenex; CelluCoat and AmyCoat of Kromasil®; RegisCell®, RegisPack®, and Reflect™ of Regis Technologies Inc.; CHIRAL ART of YMC Europe GMBH; Sepapak of Sepaserve; Astec® Cellulose DMP of Merck Millipore; and Reprosil Chiral of Dr. Maisch GmbH.

3.5.2 Antibiotic CSP

Macrocyclic glycopeptide antibiotics have been introduced as natural chiral selectors in a variety of commercially available CSPs (Armstrong et al. 1994). Initially, they have been critically reviewed due to the fact that they are potent drug molecules, which are introduced as part of the production process of other pharmaceutical compounds and leaching of the antibiotic selector might occur. The manufacturers of the chiral phases have reacted by optimizing the binding chemistry in the phases. The CSPs can be operated in normal phase as well as RP mode and additionally in SFC mode. Besides this classical mode of operation, it is also possible to operate them in the polar organic mode (POM) or polar ionic mode (PIM). The POM mode uses neat organic polar solvents, e.g. methanol, while the polar ionic mode (PIM) in addition adds organic acids or bases to the neat organic solvent. Especially for the macrocyclic antibiotic phases, this improves the separation as shown by Wang, Jiang, and Armstrong (2008). The main field of application of macrocyclic glycopeptide antibiotics is the separation of underivatized amino acids (Berthod et al. 1996) and small peptides (Ilisz, Berkecz, and Peter 2006). As especially underivatized amino acids and small chiral acids are difficult to be separated, there has been some effort put into an integrated separation approach by first using SMB chromatography to obtain an enantiomerically enriched fraction and later obtaining the final purity by fractionated crystallization. An example for the separation of L,D-threonine and L,D-methionine on a teicoplanin CSP is given by Gedicke et al. (2007). More recently, Berthod reviewed the use of these types of CSPs and shows a lot of separation examples (Berthod 2012).

3.5.3 Cyclofructan-Based CSP

Cyclofructans are cyclic carbohydrates derived from inulins and first described by Kawamura and Uchiyama (1989).

The use of the CF6, a cyclic molecule consisting of 6 D-fructofuranose units as a new chiral selector, has been reported by the group of Armstrong in 2009 (Sun et al. 2009). Besides the native cyclofructan 6, derivates have been prepared bearing isopropyl, naphthylethyl, and 3,5-dimethylphenyl groups. The isopropyl phase shows selectivity especially for primary amines, such as amino alcohols, amino esters, and amino amides. The separation of a simple aliphatic racemic amine bearing no other functional group is astonishing (Sun and Armstrong 2010).

The FRULIC and LRIHC phases are typically operated in normal phase mode. As the chiral selector is covalently bonded, they exhibit a high stability, allowing the use in SFC chromatography.

3.5.4 Synthetic Polymers

The synthetic polymers based on *N*-acryloyl amino acid derivatives developed by Blaschke in the 1970 and transferred to silica-bonded phases in the 1980 are especially useful for the separation of five-and six-membered N- and

O-heterocycles with chiral centers (Review in Kinkel 1994). Their wide chemical variety has been intensively exploited by Bayer HealthCare for their portfolio of chiral molecules. One example of this approach has been published in a joint work of Merck and Bayer (Schulte, Devant, and Grosser 2002). This work explicitly shows how important it is to screen different intermediates in addition to the final drug compound. Due to different selectivities and solubilities, the productivity for the preparative separation can be dramatically different.

New types of synthetic polymeric CSP are those based on tartaramide as the selector (Andersson et al. 1996) and those based on (*R,R*) or (*S,S*) trans-1,2-diaminocyclohexane (Zhong et al. 2005). The first one shows its best performance for strongly hydrophobic molecules, when a high alkane content in the mobile phase can be used. The second one has moderate selectivities and resolutions and a comparable loading to the cellulose-based CSP (Barnhart et al. 2008). It offers the possibility to reverse the elution order by choosing the other enantiomer of the chiral selector (Figure 3.24).
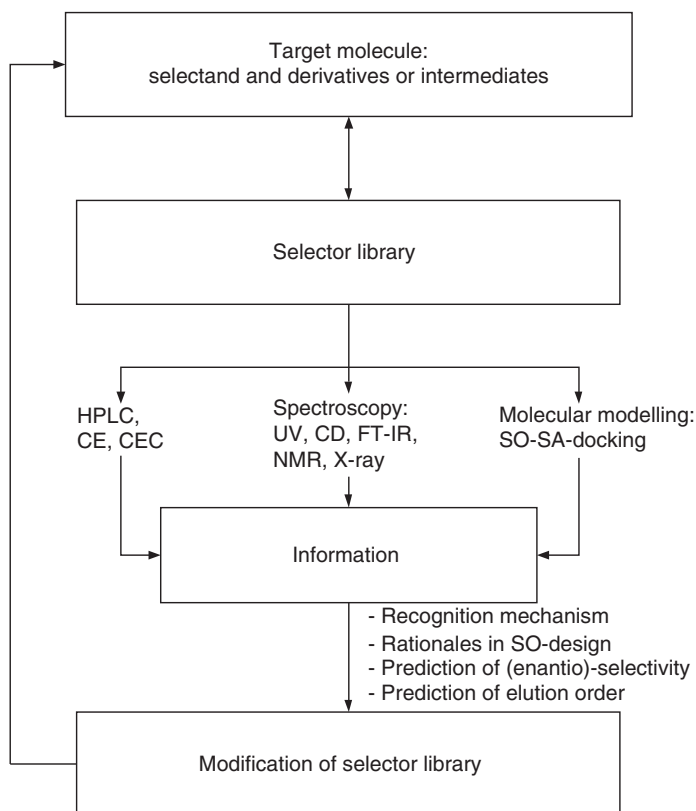
Figure 3.24 Rational screening process for enantioseparation by applying targeted selector design.

3.5.5 Targeted Selector Design

Besides the general approach of polysaccharide-type phases, more and more chiral phases are designed for special separation problems (Figure 3.11). The targeted selector or reciprocal design approach first used by Pirkle and Däppen (1987) can offer good productivities for the desired enantiomers. For the reciprocal design approach, one enantiomer of the target molecule is fixed via a spacer to a silica support. A series of racemic compounds, which can be used as chiral selectors (the selector library), are subjected onto a column packed with the target enantiomer CSP. The chiral selector, which is separated on that column with the highest selectivity, is then used to prepare the actual phase for the preparative separation of the target enantiomer. Screening for useful selectors can be automated in a combinatorial high-throughput approach (Wu et al. 1999).

The classical Pirkle-type phases are the most stable CSPs. They are mainly operated in normal phase mode and can be used to their full extent with $scCO_2$ (Macaudiere et al. 1986; Kraml et al. 2005). As the chiral selector is rather small and synthetically available, chiral phases with both enantiomers of the selector are often available, offering the possibility to choose the elution order (Welsch, Dornberger, and Lerche 1993; Dungelova et al. 2004). If this possibility is given, it is always advisable to elute the target molecule first. If a displacement effect can be observed in the separation, this choice will lead to an enormous gain in productivity.

A special subclass of brush-type CSPs are the IEX CSPs developed by Lämmerhofer and Lindner (1996). By introducing an additional ionic moiety, a strong interaction between the selector and the selectand can be achieved. The first commercial available phases are based on the cinchona alkaloids quinine and quinidine with an additional weak anion-exchange function offering good separation possibilities for chiral acids. A strong dependence of the capacity from the counterion of the mobile phase could be demonstrated by Arnell et al. (2009).

In a complementary approach, chiral cation exchangers as well as zwitterionic phases have been developed but not yet commercialized. The good separation properties for a chiral amine with only small side groups next to the chiral center (R1 = −H, R2 = −CH$_3$) have been recently published by Merck (Helmreich et al. 2010). By screening different selectors in a reciprocal approach, an optimized CSP could be developed to separate a molecule that has so far not been separated by all other known and commercially available chiral phases.

It has to be once again stressed that it is not always the best choice to separate the final chiral molecule. By screening intermediates as well as easy obtainable derivatives, a dramatically better productivity might be achieved. A better solubility of the feed can especially lead to a much higher overall process performance. The approach of derivative screening is shown in more detail in Strube, Arlt, and Schulte (2006).

As a summary, Table 3.29 lists the features of the main groups of commercially available CSPs used for preparative chromatography.

Table 3.29 Product features of different classes of chiral stationary phases.

CSP	Application range	Solvent use	Loadability (mg g^{-1} CSP)	Stability, restrictions for use	Availability (>10 kg)
Cellulose fibers CTA and CTB	Broad	Alkanes, alcohols, water	10–100	Good, large column packing difficult	Yes
Brush-type columns	Small, but focused	Unlimited including scCO$_2$	1–40	Very good	Major types; yes, several manufacturers
Cellulose and amylose derivatives coated on silica	Very broad	Alkanes, alcohols, acetonitrile, scCO$_2$	5–100	Good, but solvent restrictions	Yes, several manufacturers
Cellulose and amylose derivatives immobilized on silica	Very broad	Unrestricted	5–100	Good	Yes
Cyclodextrin-CSP	Broad	Reversed phase, alcohols	0.1–3	Limited	No
Antibiotic-CSP	Broad	Mainly polar organic mode	0.1–1	Limited	Yes
Polymer–silica composites (ChiraSpher, Kromasil)	Limited	Mainly alkanes + alcohols	1–20	Very good	Yes

Source: Loadability data from Franco et al. (2001)**.**

3.5.6   Further Developments

The development of new chiral phases for preparative use is still an important topic even though more than a hundred phases are commercially available (recent review in Lämmerhofer 2010). The main features to be still improved are selectivity, capacity, and mechanical and chemical stability, especially against a wide variety of different solvents. Optimization of the selectivity for chromatographic phases is necessary only up to a certain value. Process SMB applications are usually operated with selectivities between 1.3 and 2.0. Using too high a selectivity results in high eluent consumption needed to desorb the extract compound from the stationary phase. Conversely, phases with much higher selectivities would make it possible to use easy adsorption–desorption procedures.

The increase in capacity should always be combined with a high chemical stability against a wide variety of different solvents. The high capacities of CSPs can be used to their full extent only if a good solubility of the racemate can be found.

A third field of improvement would be the development of CSPs that combine a low pressure drop with a good efficiency and stability; for example, the pressure stability requirements for the SMB systems could be reduced. In that context, monolithic stationary phases may offer some possibilities.

3.6   Properties of Packings and Their Relevance to Chromatographic Performance

The relevant packing properties are divided into bulk and column properties. The former pertain to the bulk powder before it is packed into the column, while the latter characterize the chromatographic properties of the packed column.

3.6.1   Chemical and Physical Bulk Properties

The bulk composition and the bulk structure depend on the type and chemical composition of the adsorbent and are largely determined by the manufacturing process. Parameters that characterize the bulk structure are the phase composition, phase purity, degree of crystallinity, long- and short-range order, defect sites, and so on. Special care has to be taken with regard to the purity of the adsorbents. Metals incorporated in the bulk and present at the surface of oxides often give rise to additional and undesired retention of solutes. Remaining traces of monomers and polymerization catalysts in cross-linked polymers are leached during chromatographic operation and may affect column performance. Thus, high-purity adsorbents are aimed for during the manufacturing processes for the isolation of value-added compounds, for example, pharmaceuticals.

Among the physical properties of stationary phases, the skeleton density and the bulk density of an adsorbent are of major interest, in particular when the column packing is considered. Skeleton density is assessed as the apparent density due to helium from helium-penetration measurements. For silica, the skeleton density varies between 2.2 and 2.6 g cm^{-3} depending on the bulk structure. The bulk density of a powder is simply determined by filling the powder in a cylinder

under tapping until a dense bed is obtained. The bulk density is inversely proportional to the particle porosity: the higher the specific pore volume of the particles, the lower is the bulk density. In column chromatography, the packing density is a commonly used parameter, expressed in gram packing per unit column volume. The packing density varies between 0.2 and 0.8 g cm^{-3}. The low value holds for highly porous particles, and the high value for particles with a low porosity.

3.6.2 Morphology

The morphology of the adsorbent controls the hydrodynamic and kinetic properties in the separation process, for example, the pressure drop, mechanical stability, and column performance in terms of number of theoretical plates. In classical applications, granules of technical products were applied with irregularly shaped particles. The desired particle size was achieved by milling and grinding and subsequent sieving. Irregular chips were successively replaced by spherical particles. The latter generate a more stable column bed with adequate permeability. For crude separations, low-cost irregular particles can be used, for example, in flash chromatography.

3.6.3 Particulate Adsorbents: Particle Size and Size Distribution

Especially when beading processes are applied, the final material has to be subjected to a sizing process to obtain a narrow size distribution. The sized fractions are characterized by the average particle diameter and the size distribution. Figure 3.25 shows a differential size distribution based on the volume average particle diameter of the as-made product (Figure 3.25a) and the sized product (Figure 3.25b). As expected, the amount of small and very large particles is reduced by the sizing process. The particle size distribution of the sized material has a near-Gaussian appearance.
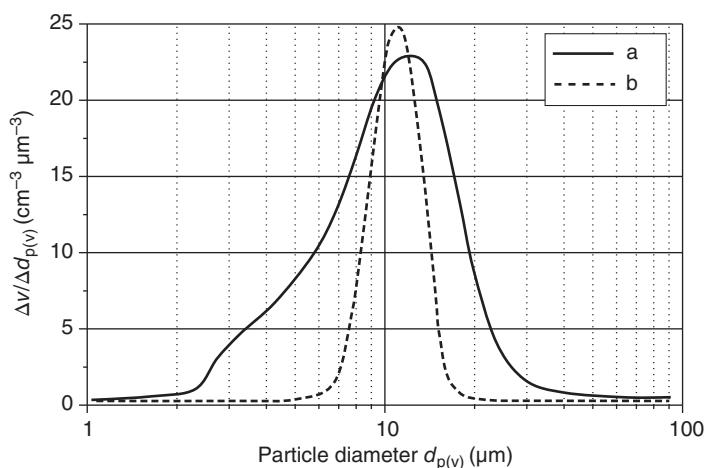
Figure 3.25 Particle size distribution of silica spheres before (a) and after (b) size classification.
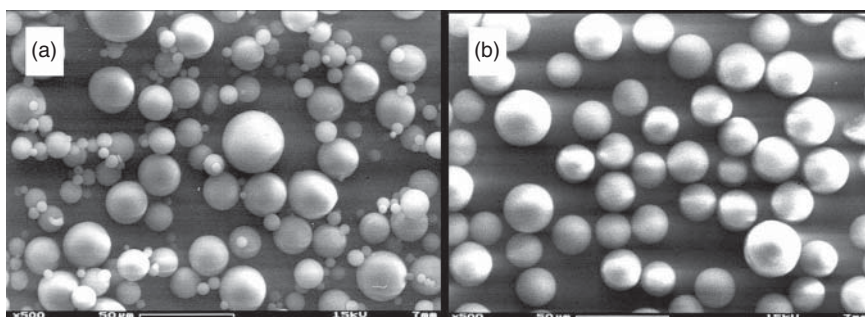
Figure 3.26 SEM pictures of silica spheres before (a) and after (b) size classification.

Usually, the width of the distribution is expressed by the ratio of d_{p90}/d_{p10}, which should be lower than 2.5 for the chromatographic application; d_{p90} (d_{p10}) equals to the average particle diameter at 90% (10%) of the cumulative size distribution. Figure 3.26a,b visualizes the effect of size classification and efficient removal of fine particles.

The particle size is given by an average value: d_p. The average particle diameter can be expressed as a number average, $d_{p(n)}$; a surface area average, $d_{p(s)}$; a weight average, $d_{p(w)}$; and a volume average, $d_{p(v)}$. Based on statistics, the following sequence is achieved: $d_{p(n)} > d_{p(s)} > d_{p(w)} < d_{p(v)}$.

Usually, in chromatography, the volume average particle diameter is employed. For comparison, the particle size distribution based on the number and the volume average is shown for the same silica measured by the same technique (Table 3.30).

Apart from the respective value, the distribution expressed as the ratio of $d_{p(90)}/d_{p(10)}$ is different. Based on the volume average, $d_{p(90)}/d_{p(10)}$ is calculated to be 1.66; for the number average, it is 3.52.

The particle size of a packing affects two major chromatographic properties: the column pressure drop and the column performance in terms of plate number per column length. For simplicity:

- Δp is inversely proportional to the square of the average particle diameter of the packing, and
- the plate number is inversely proportional to the particle diameter.

The optimum average particle size of preparative stationary phases with respect to pressure drop, plate number, and mass loadability is between 10 and 15 μm.

3.6.4 Pore Texture

The pore texture of an adsorbent is a measure of how the pore system is built. The pore texture of a monolith is a coherent macropore system with mesopores as primary pores that are highly connected or accessible through the macropores. Inorganic adsorbents often show a corpuscular structure; cross-linked polymers exhibit a network structure of interlinked hydrocarbon chains with distinct domain sizes. Porous silicas made by agglutination or solidification of silica sols

Table 3.30 Comparison of the particle size distribution data of a LiChrospher® Si 100 silica.

	Volume statistics	Number statistics
Calculation range (%)	0.96–33.5	0.96–33.5
Volume (%)	100	100
Mean (µm)	8.267	6.240
Median (d_{p50}) (µm)	8.236	7.138
Mean/median ratio	1.04	0.874
Mode (µm)	8.089	7.341
Standard deviation	0.091	0.221
Variance	0.0082	0.049
Skewness (left skewed)	462.5	−2.010
Size analysis		
d_{p5}	6.067	1.545
d_{p10}	6.475	2.865
d_{p50}	8.236	7.138
d_{p90}	10.740	9.344
d_{p95}	11.540	10.090
d_{p90}/d_{p10}	1.66	3.52

Source: Kindly supplied by Dr. K.-F. Krebs, Merck KGaA, Darmstadt, Germany.

in a two-phase system are aggregates of chemically bound colloidal particles (Figures 3.27 and 3.28).

The size of the colloidal nonporous particles determines the specific surface area of an adsorbent (Eq. (3.4)), and the porosity of particles is controlled by the average contact number of nonporous primary particles:

$$a_s = \frac{6}{d_p \cdot \varrho_{app(He)}} \tag{3.4}$$

The average pore diameter is given by Eq. (3.5) and shows that pore structural parameters such as the specific surface area, pore diameter, and specific pore volume are interrelated and, therefore, can be varied independently only to a certain extent:

$$d_{pore} = \gamma \left(\frac{v_{sp}}{a_s} \right) \tag{3.5}$$

As an example, spray drying of nanosized porous particles yields spherical agglomerates with a bimodal pore size distribution: the pores according to the primary particles (intraparticle pores) and the secondary pores (interparticle pores) made by the void fraction of the agglomerated nanobeads. Figure 3.15 shows spherically agglomerated nanoparticles that build up a porous bead. For a given size d_p of the nanoparticles, the pore diameter of the interstitial pores corresponds to about 40% of d_p. According to porosimetry experiments, this rule of thumb was verified, showing a mean pore size at 300 nm in the case of 750 nm nanoparticles.
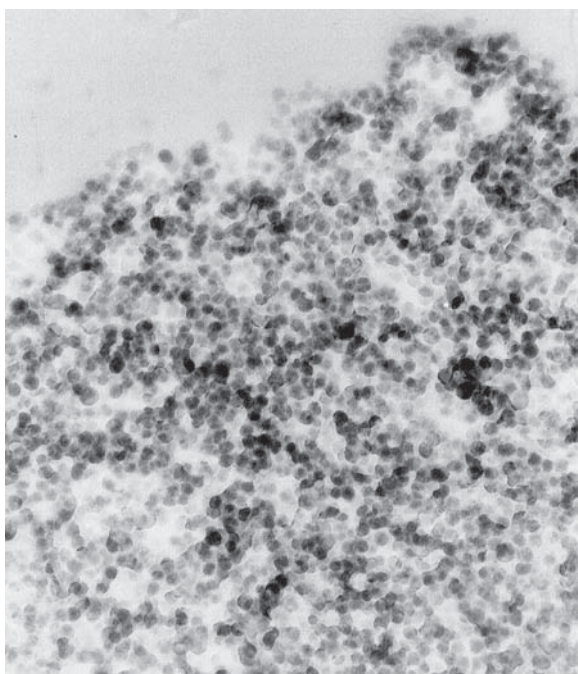
Figure 3.27 TEM image of a silica xerogel (diameter of the primary particles approximately 10 nm).
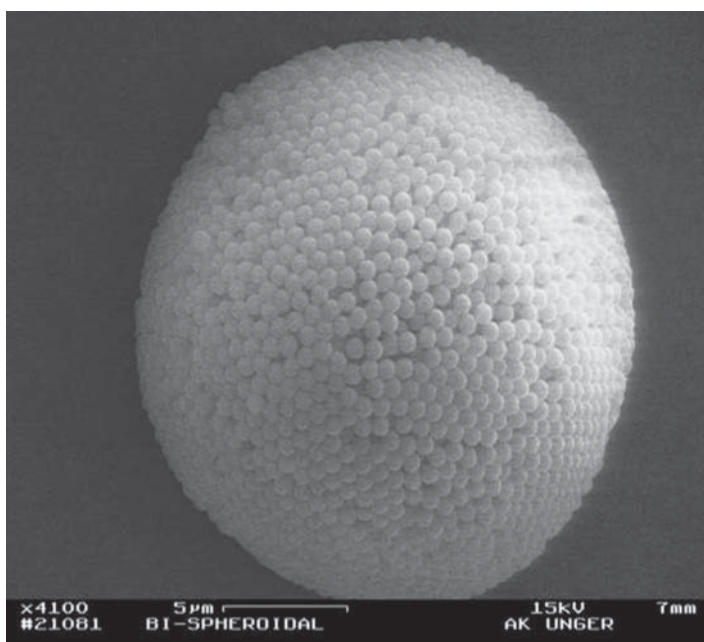
Figure 3.28 SEM picture of a 20 µm spherical agglomerate consisting of 750 nm particles.

3.6.5 Pore Structural Parameters

The pore structure of an adsorbent is characterized by the dimensionality of the pore size (unidimensional channels, three-dimensional pore system), pore size distribution, pore shape, pore connectivity, and porosity. The specific surface area is related to the average pore size. Micropores generate high specific surface areas in excess of $500\,m^2\,g^{-1}$, mesopores have values between 100 and $500\,m^2\,g^{-1}$, and macropores of d_{pore} larger than $50\,nm$ possess values of less than $50\,m^2\,g^{-1}$. Micropores of d_{pore} smaller than $2\,nm$ possess low specific pore volumes of smaller than $0.2\,cm^3\,g^{-1}$. Mesopores have specific pore volumes on the order of $0.5–1.5\,cm^3\,g^{-1}$, whereas macropores generate much higher porosities. Porosity can change due to swelling with cross-linked organic polymers. Porous oxides exhibit a permanent porosity at common conditions. The pore size distribution of adsorbents with a permanent porosity is determined either by nitrogen sorption at $77\,K$ (micropore size and mesopore size range) or by mercury intrusion (macropore size and mesopore size range). The pore size distribution can be expressed as a number or volume distribution. However, the pore size distribution does not give any indication of how the pores are interconnected across a porous particle. The most useful parameter in this context is the (dimensionless) pore connectivity η_T, which is derived from the pore network model applied to the experimental nitrogen sorption isotherm (Meyers and Liapis 1998, 1999). Pore connectivity describes the number of pore channels meeting at a node at a fixed lattice size. Low η_T values indicate a low interconnectivity; n_T can be as high as 18 for highly interconnected pore systems. Such a high interconnectivity leads to fast mass transfer kinetics and favorable mass transfer coefficients (Unger et al. 2002).

3.6.6 Comparative Rating of Columns

The rating of columns is performed according to two aspects:

(1) Assessment of column performance data obtained under analytical conditions. This includes:
   - *Plate height of the column*: The plate height should correspond to two to three times the average particle diameter of the packing.
   - *Plate height of the column as a function of the linear velocity of mobile phase*: The flow rate should have an optimum where the plate height is at a minimum.
   - *Number of plates per column length*: Commonly, the plate number is between 5000 and 10 000 to sufficiently separate mixtures.
   - Retention coefficient of a solute.

All these parameters depend on the mass loadability of the column and change significantly when a critical loadability is reached. The critical mass loadability of analytical columns is usually reached at a 10% reduction of the retention coefficient or at 50% decrease of column plate number. At higher values, the column is, in chromatographic terms, overloaded.

(2) Assessment of parameters under preparative conditions.

Preparative columns are compared with regard to the column productivity, yield, purity, and cost. Productivity is defined as the mass of isolate per kilogram of packing per day at a set purity and yield. It depends, essentially, on the applied technical chromatographic process. For example, the productivity for the separation of racemates into enantiomers by the simulated bed technology has increased from 2 kg per kg packing per day to about 10 kg of product per kg packing per day. The yield can be low provided the purity is high. Desired purities are sometimes 99.9% and higher. The overall cost is the only measure that is taken for chromatographic production processes. The main cost contributions come from costs related to the productivity (column size, amount of stationary and mobile phase), yield losses of the product, and work-up costs linked to the product dilution.

3.7 Sorbent Maintenance and Regeneration

Preparative chromatography in the nonlinear range of the isotherm means applying a high mass load of substance onto the adsorbent. Some compounds from the feed mixture may alter the surface of the adsorbent and change its separation activity. Therefore, regular washing procedures and reactivation should be performed to ensure a long column lifetime. Different goals for washing procedures can be distinguished:

Removal of highly adsorptive compounds (CIP);
Reconditioning of silica surfaces;
Sanitization in place (SIP) of adsorbents;
Column and adsorbent storage conditions.

3.7.1 Cleaning in Place (CIP)

Highly adsorptive compounds should always be removed before subjecting the feed onto the main column. This can be achieved by a pre-column, which has to be changed at regular intervals. Sometimes, simple filtration of the feed over a small layer of the adsorbent is sufficient to remove sticking compounds. Nevertheless, it has to be checked that the feed composition is not drastically changed after the prepurification step so that the simulation of the chromatogram and thus the process parameters are still valid. If compounds stick to the adsorbent (irreversible adsorption) and if the performance of the column in terms of efficiency and loadability decreases, a washing procedure has to be carried out (CIP). For this washing procedure, two general considerations have to be kept in mind:

- The flow direction should be always reversed so that the sticking compounds are not pushed through the whole column.
- As the adsorbent has to be washed with solvents of very different polarity, care has to be taken that all solvents used in a row are miscible. Especially when a solvent with a different viscosity is introduced into the column or the mixture of two solvents results in a higher viscosity than the single solvents, for example, methanol and water, the pressure drop can rapidly increase and

damage the packing. Therefore, a maximum pressure should be set in the system control, and the flow rate for the washing procedure should be reduced if the resulting pressure drop is unknown.

If the column can be opened at the feed injection side, which is not always possible for technical or regulatory (good manufacturing practice [GMP]) reasons, the first one or two centimeters of packing can be removed. The top of the bed is then reslurried, fresh adsorbent added, and the column recompressed. Up to a column diameter of 200–300 mm, this procedure might make it possible to avoid repacking of a column and ensures the further use of the packed column for some time. Table 3.31 shows some CIP regimes for silica-based adsorbents with different functionalities.

As a rule of thumb, at least 5–10 column volumes of each washing solvent should be pumped through the column. No general rules can be given as to whether column washing and regeneration is more economic than replacing the packing material as this strongly depends on the nature of the components to be removed and the type of the packing material. Naturally, if coarse, cheap packing materials are used, the solvent and time consumption for washing and regenerating a column is more expensive than unpacking and repacking with new adsorbent.

A detailed procedure for the acidic CIP of silica used in an insulin production process has been published by Larsen, Schou, and Rasmussen (2004). The column is first washed with 1.5 column volumes (CV) of ethanol/water 80/20 followed by 1.1 CV pure ethanol. Both washing steps are conducted at a flow rate of 4.5 CV/h. Afterward the flow rate is reversed, and 1.1 CV of neat formic acid is pumped into

Table 3.31 CIP procedures for silica-based adsorbents after Majors (2003a) and Rabel (1980).

Reversed phase (Procedure 1)	Reversed phase (Procedure 2)	Normal phase	Ion exchange	Protein removal
C18, C8, C4, phenyl, CN		Si, NH_2, CN, Diol	SAX, SCX, DEAE, NH_2, CM on silica	C18, C8, C4, phenyl
Distilled water (up to 55 °C)	Distilled water (up to 55 °C)	Heptane– methylene chloride	Distilled water (upto 55 °C)	Distilled water (up to 55 °C)
Methanol	Methanol	Methylene chloride	Methanol	0.1% trifluoroacetic acid
Acetonitrile	Isopropanol	Isopropanol	Acetonitrile	Isopropanol
THF	Heptane	Methylene chloride	Methylene chloride	Acetonitrile
Methanol	Isopropanol	Mobile phase	Methanol	Distilled water
Mobile phase with buffer removed	Mobile phase with buffer removed		Mobile phase with buffer removed	Mobile phase

the column at a velocity of 2.1 CV/h. The flow rate is stopped and the cleaning solution is left in the column for 30 minutes, followed by 1.1 CV of ethanol and 1.1 CV ethanol/water 80/20 at a flow rate of 4.5 CV/h. The flow rate is reversed again, and additional 4 CV ethanol/water is pumped through the column. This procedure has been applied to production-scale columns of more than 30 cm i.d. packed with a 15 μm RP-18 silica. The cleaning procedure is repeated after each 16th injection. The authors claim that it was possible to use the packed column for 2000 runs following this procedure.

Most insulin producers nevertheless prefer alkaline cleaning protocols. As stated earlier alkaline conditions will over time deteriorate the silica-based stationary phases, so the conditions have to carefully chosen. Figure 3.29 shows a protocol for the alkaline cleaning of PharmPrep® P 100 RP-18e, 10 μm silica. The two chromatograms show that after 100 CV of 0.1 M NaOH in 50% methanol, the separation efficiency is still sufficient. Assuming a volume of 2 CV of CIP solution per CIP cycle and an interval of eight injections between two CIP runs, this results in 400 runs. At an injection of 15 g insulin per kilogram silica, this leads to a lifetime factor of 6 kg insulin per kilogram silica.

3.7.2 CIP for IEX

The CIP protocols for IEX and affinity resins are of even greater importance due to the risk of contamination from the fermentation broth to be purified.

The classical CIP solution for IEX resins typically consists of up to 1 M NaOH solution, which is also accepted by the regulatory authorities. Classical resins show only little loss in capacity and performance if the resins are stored in the NaOH solution. Modern-type resins can be operated for a longer time even when CIP is done in a flow-through mode. Figure 3.30 shows the selectivity in standard protein separations for Eshmuno® S when operated in alternating cycles of 1 M NaOH cleaning solution for one hour and running buffer for the chromatographic separation. No variations in selectivity or retention time of the eluted proteins are being observed.

In most cases, quaternary ammonium-based anion-exchange resins show a reduced alkaline stability due to the Hofmann elimination reaction. As an additional buffer additive, which is breaking up hydrogen bonds, urea, arginine, or guanidium hydrochloride can be used.

Table 3.32 lists some recommended conditions for Fractogel IEX sorbents.

3.7.3 CIP of Protein A Sorbents

Stability of the expensive protein A resins is a crucial point. Protein A in its native form has only a limited stability toward caustic conditions. Therefore, careful CIP procedures have to be followed.

Füglistaller (1989) reported protein A leakage of 1.8 up to 88 ppm (weight/−weight). Caustic and acidic steps as well as treatments with detergents are described in the literature for column hygiene, for example, 0.4 M acetic acid, 0.5 M NaCl, and 0.1% Tween 20. For cleaning the affinity resin, short washing times (contact time maximum 15 minutes) with 50 mM NaOH and 1 M NaCl are
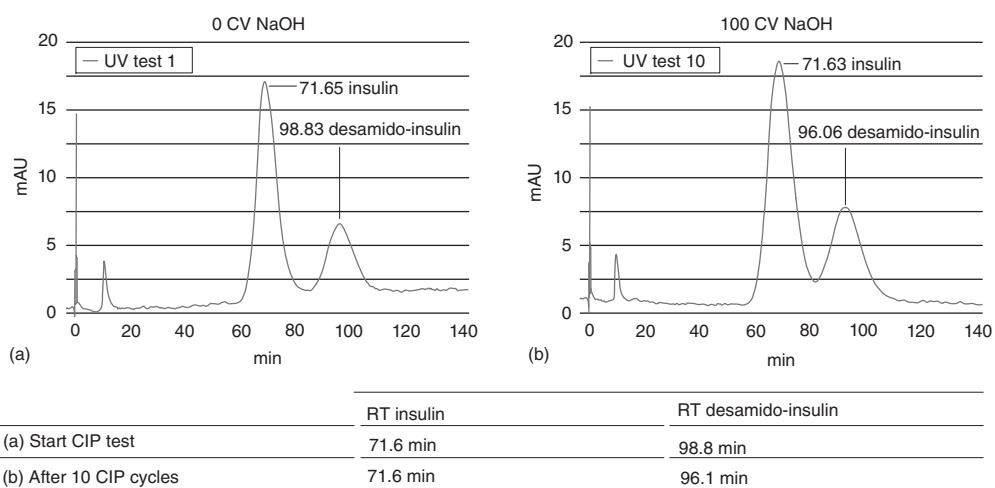
Figure 3.29 Separation of insulin and A21-desamido insulin before and after introduction of 100 CV 0.1 M NaOH in 50% methanol on PharmPrep® P 100 RP-18e, 10 μm silica.
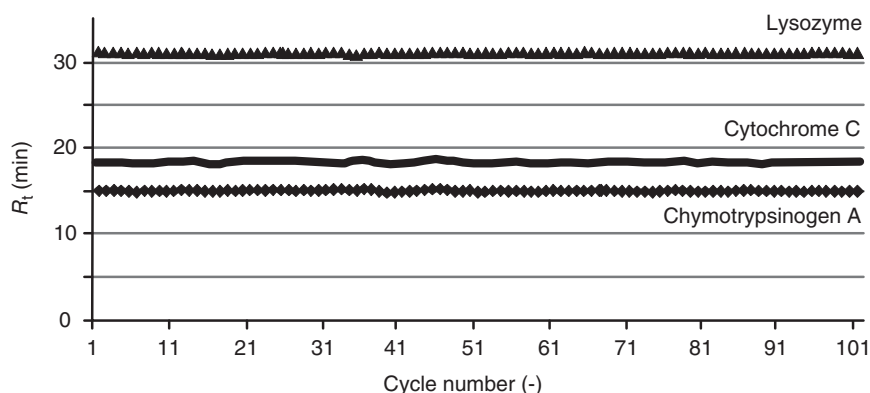
Figure 3.30 Variation of retention time for test protein mixture after 100 cycles, each cycle consisting of 1 hour 1 M NaOH treatment.

Table 3.32 Recommended cleaning and regeneration steps for Fractogel® IEX resins.

Reagent	Concentration	Column volumes (CV)
NaCl	Up to 2 M	2
NaOH	0.1–1 N	1–5
HCl	1–2 N	1–5
Pepsin/HCl	0.1%/0.01 N HCl	1–2
Sodium lauryl sulfate (SLS)/NaCl	2%/0.25 M NaCl	1–2
Isopropanol, acetonitrile, or ethanol	20%	1–2
Urea	6 M	1–2

recommended with a cleaning run every 1–10 separation runs and a sanitization run in between different product batches.

O'Leary et al. (2001) estimated the column lifetime of carefully maintained protein A columns with 225 cycles at production scale. Even though the capacity of the resin was significantly reduced, it was still able to reduce the HCP and DNA content to the required minimum (O'Leary et al. 2001). Jiang et al. (2009) reported the same behavior for the purification of an Fc fusion protein on either rProtein A Sepharose or MabSelect. Sanitization with 3 CV of 0.1 N NaOH led to a drop in yield of 30% after 66 cycles for rProtein A Sepharose. Using even milder sanitization conditions (50 mM NaOH + 500 mM NaCl) on MabSelect showed the same trend. When Q_{max} of the isotherm was determined for both resins, it declined by 38% (rProtein A Sepharose) and 43% (MabSelect), respectively, after 100 cycles of cleaning with 0.1 N NaOH. To improve column lifetime, two approaches have been followed: the addition of stabilizing excipients, for example, NaCl or Na_2SO_4, and the integration of a stripping step following column elution with the same elution conditions (low pH in the case of protein A). Three different regimes have been compared (Table 3.33).

Table 3.33 Different purification regimes for protein A sorbents.

Strip	Regeneration	Salt (stabilizing excipient)	% of initial yield (at cycle #)
No	0.1 N NaOH	No	70% (cycle 68)
0.1 M phosphoric acid	50 mM NaOH	0.5 M NaCl	68% (cycle 95)
No	50 mM NaOH	0.5 M NaCl	88% (cycle 95)

As the addition of a stabilizing agent showed the biggest influence, different additional agents were tested. Sucrose, xylitol, and ethylene glycol showed the greatest stabilizing influence, while urea, EDTA, glycerol, and L-arginine had little or no effect. The capacity of MabSelect protein A with 1 M xylitol and 1 M NaCl in the regeneration solution was still at a resin capacity of $25\,mg\,ml^{-1}$ after an incubation time of 41 hours in 50 mM NaOH compared with $17\,mg\,ml^{-1}$ for a resin incubated with 0.5 M NaCl as the stabilizing excipient. A similar trend could be observed for rProtein A Sepharose as well (Jiang et al. 2009). The most recently introduced protein A resins with stability-optimized protein A ligands exhibit a higher alkaline stability. MabSelect PrismA remains stable for 100 cycles when 0.5 M NaOH at a contact time of 15 minutes is applied, while MabSelect SuRe LX loses 10% DBC and MabSelect SuRe 30% of DBC. When cleaning with 1.0 M NaOH, MabSelect PrismA loses 10% capacity over 150 cycles, while MabSelect SuRe LX is dropping to 50% of the initial capacity.

3.7.4 Conditioning of Silica Surfaces

One of the drawbacks of chromatography with normal phase silica is the strong and changing interactions the silica surface can undergo with the mobile phase and feed components. In contrast to RP adsorbents, where the interaction takes place with the homogeneously distributed alkyl chains bonded to the surface, the silica surface has a lot of energetically different active groups such as free, germinal, and associated silanol groups, incorporated metal ions in the silica surface, and water, which might be physisorbed or chemisorbed. It is of great importance to condition the silica before using it in a preparative separation. Especially, the activity, which is determined by the amount of water, and the surface pH have to be controlled to ensure constant conditions from one column packing to another. The surface pH of a silica adsorbent depends heavily on its production process and is especially influenced by the applied washing procedures (Hansen, Helböe, and Thomasen 1986). The apparent surface pH is measured in a 10% aqueous suspension of the silica. The dramatic influence of different surface pH is illustrated in Figure 3.31 where the surface pH of a LiChroprep® Si adsorbent has been adjusted with sulfuric acid and ammonia, and two test compounds (2-aminobenzophenone and 4-nitro-3-aminobenzophenone) have been injected onto the columns. The retention time of 4-nitro-3-aminobenzophenone is strongly influenced by the surface pH. Even a reversal of the elution order can be achieved at low pH. The adjustment of surface pH is possible even in large batches
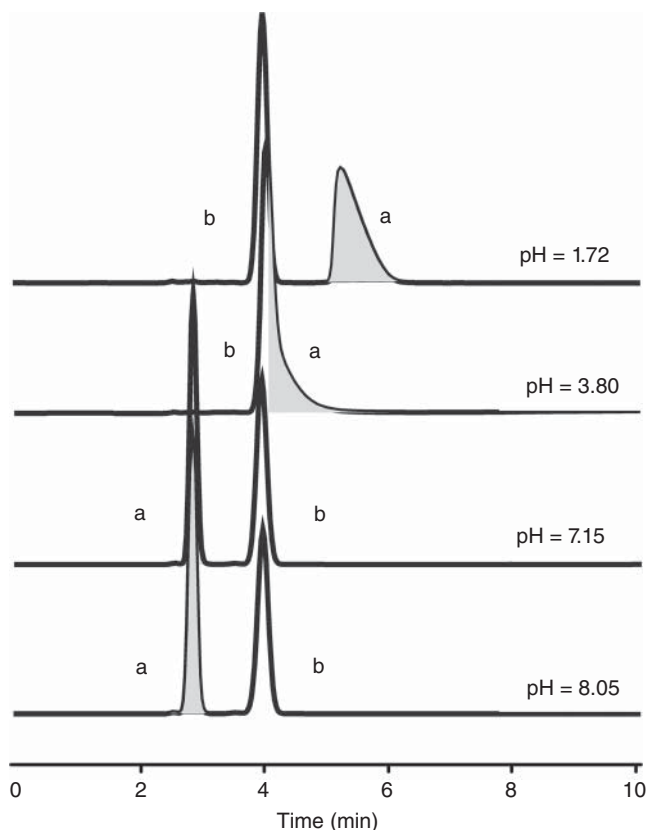
Figure 3.31 Influence of surface pH on the retention time of two test compounds: 2-aminobenzophenone (b) and 4-nitro-3-aminobenzophenone (a).

by washing the silica with diluted acids, removal of the water, and subsequent operation of the column with nonpolar solvent systems. Under these conditions, the apparent surface pH is remarkably stable during the operation of the column.

A second adsorbent characteristic that should be controlled is the water content of the silica. The water content can vary from 0 to 10 wt%. As silica is a well-known desiccant (drying agent), care has to be taken with adsorbent types that are adjusted with low amounts of water. Here, significant uptake of water from the air might influence the chromatographic conditions. Silica should therefore generally be stored in well-closed containers. The adjustment of silica to certain water contents is a necessary standard procedure in large batch sizes for most large-scale silica manufacturers. If water has to be removed from a column, a chemical drying procedure can be applied. Dimethoxypropane reacts with water, resulting in methanol and acetone (Figure 3.32).

For this procedure, the column should be flushed with 10 column volumes of a mixture of dichloromethane, glacial acetic acid, and 2,2-dimethoxypropane (68 : 2 : 30 v/v/v). Later, the column should be subsequently washed with 20 column volumes of dichloromethane and 20 column volumes of *n*-heptane.
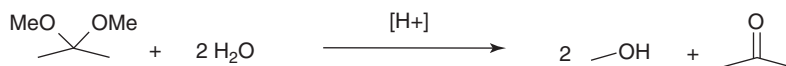
Figure 3.32 Reaction of dimethoxypropane for chemical removal of water from silica adsorbents.

Table 3.34 SIP procedures.

Solvent	Composition
Acetic acid	1% in water
Trifluoroacetic acid	1% in water
Trifluoroacetic acid + isopropanol	(0.1% TFA)/IPA 40 : 60 (v/v) viscous → reduce flow rate
Triethylamine + isopropanol	40 : 60 (v/v), adjust 0.25 N phosphoric acid to pH 2.5 with triethylamine before mixing
Aqueous urea or guanidine	5–8 M (adjusted to pH 6–8)
Aqueous sodium chloride, sodium phosphate, or sodium sulfate	0.5–1.0 M (sodium phosphate pH 7)
DMSO–water or DMF–water	50:50 (v/v)

3.7.5 Sanitization in Place (SIP)

For purification of recombinant products from fermentation broth, care has to be taken to prevent microbial growth on adsorbents. Therefore, regular SIP procedures have to be applied. When adsorbents based on organic polymers or Sepharose are used (for IEX and adsorption chromatography), decontamination is performed at high pH, for example, by using 0.1–1 M NaOH. With silica-based adsorbents, procedures based on salts, solvents, or acids are commonly used due to the chemical instability of silica above pH 8–9. Some recommended washing procedures are listed in Table 3.34.

3.7.6 Column and Adsorbent Storage

If packed columns or adsorbents removed from columns are to be stored for a period of time, the adsorbent should be carefully washed and then equilibrated with a storage solvent. Compounds strongly adsorbed to the adsorbent and, especially, any source of microbial growth have to be carefully removed before the adsorbent is stored. In addition, any buffer substances or other additives, which might precipitate during storage, have to be washed out. For flushing and storage, different solvents are recommended (Table 3.35).

IEX resins are typically stored in either diluted NaOH solution or ethanolic salt solutions (e.g. 150 mM NaCl, 20% EtOH). Cool storage is an additional requirement for the storage or protein A resins.

Table 3.35 Recommended solvents for storage and flushing.

Adsorbent type	Flushing solvent	Storage solvent
Normal phase	Methanol or other polar solvent	Heptane + 10% polar compound (isopropanol, ethyl acetate)
Reversed phase	Methanol or acetonitrile, THF, or dichloromethane for oily samples	>50% organic in water
IEX (silica based)	Methanol	>50% organic in water

References

Adams, B.A. and Holmers, E.L. (1935). Adsorbtive properties of synthetic resins. *J. Soc. Chem. Ind. London* 54: 1T.

Agnew, H., Rohde, R., Millward, S. et al. (2009). Iterative in situ-click chemistry creates antibody-like protein capture agents. *Angew. Chem. Int. Ed.* 48 (27): 4944–4948.

Alexander, C., Andersson, H.S., Andersson, L.I. et al. (2006). Molecular imprinting science and technology: a survey of the literature for the years up to and including 2003. *J. Mol. Recognit.* 19: 106–180.

Andersson, S., Allenmark, S., Moeller, P. et al. (1996). Chromatographic separation of enantiomers on *N,N'*-diallyl-L-tartardiamide-based network-polymeric chiral stationary phases. *J. Chromatogr. A* 741: 23–31.

Angerbauer, R., Grosser, R., Hinsken, W., and Rehse, J. (1993). Process for preparing sodium 3*R*,5*S*-(+)-erythro-(*E*)-7–7-[4-(4-fluorophenyl)-2,6-diisopropyl-5-methoxy-methyl-pyrid-3-yl]-3,5-dihydroxy-hept-6-enoate. DE 4309553, 24 Mar 1993.

Armstrong, D.W., Tang, Y., Chen, S. et al. (1994). Macrocylcic antibiotics as a new class of chiral selectors for liquid chromatography. *Anal. Chem.* 66: 1473–1484.

Arnell, R., Forssen, P., Fornstedt, T. et al. (2009). Adsorption behaviour of a quinidine carbamate-based chiral stationary phase: role of the additive. *J. Chromatogr. A* 1216: 3480–3487.

Arnott, S.A., Fulmer, A., Scott, W.E. et al. (1974). Agarose double helix and its function in agarose gel structure. *J. Mol. Biol.* 90: 269–284.

Ates, H., Mangelings, D., and Vander-Heyden, Y. (2008). Chiral separations in polar organic solvent chromatography: updating a screening strategy with new chlorine-containing polysaccharide selectors. *J. Chromatogr. B* 875: 57–64.

Azhar, A., Ahmad, E., Rauf, M. et al. (2017). Recent advances in the development of novel protein scaffolds based therapeutics. *Int. J. Biol. Macromol.* 102: 630–641.

Bangs, L.B. (1987). Uniform latex particles. *Am. Biotechnol. Lab.* 5 (3): 10, 12–16.

Barnhart, W., Gahm, K., Hua, Z., and Goetzinger, W. (2008). Supercritical fluid chromatography comparison of the poly(trans-1,2-cyclohexanediyl-bis-acrylamide) (P-CAP) column with several derivatized polysaccharide-based stationary phases. *J. Chromatogr. B* 875: 217–229.

Berthod, A. (2012). Chromatographic separtions and analysis: macrocyclic glycopeptide chiral stationary phases. *Compr. Chiral.* 8: 227–262.

Berthod, A., Liu, Y., Bagwill, C., and Armstrong, D.W. (1996). Facile liquid chromatographic enantioresolution of native amino acids and peptides using a teicoplanin chiral stationary phase. *J. Chromatogr. A* 731: 123–137.

Blom, H., Akerblom, A., Kon, T. et al. (2014). Efficient chromatographic reduction of ovalbumin for egg-based influenza virus purification. *Vaccine* 32: 3721–3724.

Borman, P., Boughtflower, B., Cattanach, K. et al. (2003). Comparative performances of selected chiral HPLC, SFC, and CE systems with a chemically diverse sample set. *Chirality* 15: 1–12.

Boschetti, E. and Perret, G. (2011). Method for immobilizing nucleic ligands. WO2012090183, priority date 30 December 2010.

Brockmann, H. and Schodder, H. (1941). Aluminiumoxid mit abgestuftem Adsorptionsvermögen zur chromatographischen Adsorption. *Chem. Ber.* 74: 73–78.

Busini, V., Molani, D., Moscatelli, D. et al. (2006). Investigation of the influence of spacer arm on the structural evolution of affinity ligands supported on agarose. *J. Phys. Chem. B* 110: 23564–23577.

Carroll, K.K. (1963). Acid-treated Florisil® as an adsorbent for column chromatography. *J. Am. Oil Chem. Soc.* 40: 413–419.

Casey, J.L., Keep, P.A., Chester, K.A. et al. (1995). Purification of bacterially expressed single chain Fv antibodies for clinical applications using metal chelate chromatography. *J. Immunol. Methods* 179: 105–116.

Castro-Forero, A., Jokondo, Z., Voloshin, A., and Hester, J. (2015). Anion-exchange chromatographic clarification. *Bioprocess Int.* 13 (6): 52–57.

Cavalloti, C. (2008). Univ Milano, personal communication in the frame of AIMs.

Chang, C. and Lenhoff, A.M. (1998). Comparison of protein adsorption isotherms and uptake rates in preparative cation-exchange materials. *J. Chromatogr. A* 827: 281–293.

Childs, R., Filipe, C., Gosh, R. et al. (2012). Composite materials comprising supported porous gel containing functional groups and method of separating substance. US Patent 8, 211, 682, filed 3 October 2008.

Cox, G. and Amoss, C. (2004). Extending the range of solvents for chiral analysis using a new immobilized polysaccharide chiral stationary phase CHIRALPAK® IA. LC GC North America Application Handbook.

Curling, J. and Gottschalk, U. (2007). Process chromatography: five decades of innovation. *BioPharm Int.* 20: 10–19.

Dave, N., Hazra, P., Khedkar, A. et al. (2008). Process and purification for manufacture o a modified insulin intended for oral delivery. *J. Chromatogr. A* 1177: 282–286.

DePhillips, P. and Lenhoff, A.M. (2000). Pore size distributions of cation-exchange adsorbents determined by inverse size-exclusion chromatography. *J. Chromatogr. A* 883: 39–54.

Dungelova, J., Lehotay, J., Krupcik, J. et al. (2004). Selectivity tuning of serially coupled (*S*,*S*) whelk-O 1 and (*R*,*R*) whelk-O 1 columns in HPLC. *J. Chromatogr. Sci.* 42: 135–139.

Eblinger, K. and Weller, H. (2013). Comparison of chromatographic techniques for diastereomer separation of a diverse set of drug-like compounds. *J. Chromatogr. A* 1272: 150–154.

Engelhardt, H., Grüner, R., and Scherer, M. (2001). The polar selectivities of non-polar reversed phases. *Chromatographia* 53: 154–161.

Epton, R. (1978). Hydrophobic, ion exchange and affinity methods. In: *Chromatography of Synthetic and Biological Polymers (ed. Epton, R.)*, vol. 2, 1–9. Chichester: E. Horwood.

Faber, R., Yang, Y., and Gottschalk, U. (2009). Salt tolerant interaction chromatography for large-scale polishing with convective media. *BioPharm Int. Suppl.*: 11–14.

Faria, H., Abrao, L., Santos, M. et al. (2017). New advances in restricted access materials for sample preparation: a review. *Anal. Chim. Acta* 959: 43–65.

Fassina, G., Ruvo, M., Palombo, G. et al. (2001). Novel ligands for the affinity-chromatographic purification of antibodies. *J. Biochem. Biophys. Methods* 49: 481–490.

Fiedler, E., Fiedler, M., Proetzel, G. et al. (2006). Affilin™ molecules novel ligands for bioseparation. *Food Bioprod. Process.* 84 (C1): 3–8.

Fischer-Frühholz, S., Zhou, D., and Hirai, M. (2010). Sartobind STIC® salt-tolerant membrane chromatography. *Nat. Methods* 7: 1026.

Forier, C., Boschetti, E., Ouhammouch, M. et al. (2017). DNA aptamer ligands for highly selective purification of human plasma-related proteins from multiple sources. *J. Chromatogr. A* **1489**: 39–50.

Franco, P., Senso, A., Oliveros, L., and Minguillón, C. (2001). Covalently bonded polysaccharide derivatives as chiral stationary phases in high-performance liquid chromatography. *J. Chromatogr. A* 906: 155–170.

Francotte, E. (1996). Photochemically crosslinked polysaccharide derivatives as supports for the chromatographic separation of enantiomers. PCT WO 096/27615, priority date 7 March 1995.

Francotte, E. (1997). Thermally immobilized polysaccharide derivatives. WO 097/049733.

Francotte, E. and Wolf, R.M. (1991). Benzoyl cellulose beads in the pure polymeric form as a new powerfull sorbent for the chromatographic resolution of racemates. *Chirality* 3: 43–55.

Francotte, E. and Zhang, T. (1997). Photochemically cross-linked polysaccharide derivatives having no photopolymerisable functional groups. WO 097/004011.

Francotte, E. and Zhang, T. (1467). Preparation and evaluation of immobilized 4-methylbenzoylcellulose stationary phases for enantioselective separations. *J. Chromatogr. A*: 214–220.

Freyre, F.M., Vazquez, J.E., Ayala, M. et al. (2000). Very high expression of an anti-carcinoembryonic antigen single chain Fv antibody fragment in the yeast *Pichia pastoris*. *J. Biotechnol.* 76: 157–163.

Füglistaller, P. (1989). Comparison of immunoglobulin binding capacities and ligand leakage using eight different protein a affinity chromatography matrices. *J. Immunol. Methods* 124: 171–177.

Gaberc-Porekar, V. and Menart, V. (2001). Review – perspectives of immobilized-metal affinity chromatography. *J. Biochem. Biophys. Methods* 49: 335–360.

Gedicke, K., Kaspereit, M., Beckmann, W. et al. (2007). Conceptual design and feasibility study of combining continuous chromatography and crystallisation for stereoisomer separations. *Chem. Eng. Res. Des.* 85: 928–936.

Ghethie, V. and Schell, H.D. (1967). Electrophoresis and immunoelectrophoresis of proteins on DEAE-agarose gels. *Rev. Roum. Biochim.* 4: 179–184.

Glowniak, K. (1991). Comparison of selectivity of silica and Florisil in the separation of natural pyranocoumarins. *J. Chromatogr.* 552: 453–461.

Gosh, R. (2002). Protein separation using membrane chromatography, opportunities and challenges. *J. Chromatogr. A* 952: 13–27.

Gregori, L., Lambert, B., Gurgel, P. et al. (2006). Reduction of transmissible spongiform encephalopathy infectivity from human red blood cells with prion protein affinity ligands. *Transfusion* 46 (7): 1152–1161.

Guan, D., Ramirez, M., and Chen, Z. (2013). Split Intein mediated ultra-rapid purification of tagless proteins (SIRP). *Biotechnol. Bioeng.* 110 (9): 2471–2481.

Hahn, R., Schlegel, R., and Jungbauer, A. (2003). Comparison of protein a affinity sorbents. *J. Chromatogr. B* 790: 35–51.

Hansen, S.H., Helböe, P., and Thomasen, M. (1986). Agar derivates for chromatography, electrophoresis and gel-bound enzymes – VII. Influence of apparent surface pH of silica compared with the effects in straight-phase chromatography. *J. Chromatogr.* 368: 39–47.

Hardick, O., Stevens, B., and Bracewell, D. (2011). Nanofibre fabrication in a temperature and humidity controlled environment for improved fibre consistency. *J. Mater. Sci.* 46: 3890–3898.

Hardick, O., Dods, S., Stevens, B., and Bracewell, D. (2013). Nanofiber adsorbents for high productivity downstream processing. *Biotechnol. Bioeng.* 110 (4): 1120–1128.

Hasanuzzaman, M., Rafferty, A., and Olabi, A.G. (2014). Effects of zircon on porous structure and alkali durability of borosilicate glasses. *Ceram. Int.* 40: 581–590.

Heitz, W. (ed.) (1970). Gel chromatography. *Angew. Chem. Int. Ed.* 9: 689–702.

Helmreich, M., Niesert, C.P., Schulte, M. et al. (2010). Process for separating enantiomers of 3,6-dihydro-1,3,5-triazine derivatives. WO WO/2010/108583, 30 September 2010.

Herigstad, M., Gurgel, P., and Carbonell, R. (2010). Transport and binding characterization of a novel hybrid particle impregnated membrane material for bioseparations. *Biotechnol. Progr.* 27 (1): 129–139.

Hjelm, H., Hjelm, K., and Sjoquist, J. (1972). Protein a from *Staphylococcus aureus* its isolation by affinity chromatography and its use as an immunosorbent for isolation of immunoglobulins. *FEBS Lett.* 28: 73–76.

Hjerten, S. (1964). Preparation of agarose spheres for chromatography of molecules and particles. *Biochim. Biophys. Acta* 79: 393–398.

Hjerten, S. (1983). *Protides of Biological Fluids*, vol. 30 (ed. H. Peeters), 9–17. Oxford: Pergamon Press.

Hjertén, S., Liao, J., and Zhang, R. (1989). High-performance liquid chromatography on continuous polymer beds. *J. Chromatogr.* 473: 273–275.

Hochuli, E., Doebeli, H., and Schacher, A. (1987). New metal chelate adsorbent selective for proteins and peptides containing neighbouring histidine residues. *J. Chromatogr.* 411: 177–184.

Hochuli, E., Bannwarth, W., Doebeli, H. et al. (1988). Genetic approach to facilitate purification of recombinant proteins with a metal novel chelate adsorbent. *Bio/Technology* 6: 1321–1325.

http://www.ema.europa.eu/docs/en_GB/document_library/Scientific_guideline/2009/09/WC500002674.pdf

Ikai, T., Yamamoto, C., Kamigaito, M., and Okamoto, Y. (2006). Immobilized polysaccharide-based chiral stationary phases for HPLC. *Polym. J.* 38 (2): 91–108.

Ikai, T., Yamamoto, C., Kamigaito, M., and Okamoto, Y. (2007). Preparation and chiral recognition ability of crosslinked beads of polysaccharide derivatives. *J. Sep. Sci.* 30: 971–978.

Ilisz, I., Berkecz, R., and Peter, A. (2006). HPLC separation of amino acid enantiomers and small peptides on macrocyclic antibiotic-based chiral stationary phases: a review. *J. Sep. Sci.* 29: 1305–1321.

Ishikawa, A. and Shibata, T. (1993). Cellulosic chiral stationary phase under reversed-phase condition. *J. Liq. Chromatogr.* 16 (4): 61–68.

Janowski, F. and Heyer, W. (1982). *Poröse Gläser*. Leipzig: VEB Deutscher Verlag für Grundstoffindustrie.

Janson, J.-C. (1987). On the history of the development of Sephadex. *Chromatographia* 23: 361.

Jaysene, S. (1999). Aptamers: an emerging class of molecules that rival antibodies in diagnostics. *Clin. Chem.* 45 (9): 1628–1650.

Jiang, C., Liu, J., Rubacha, M., and Shukla, A. (2009). A mechanistic study of protein a chromatography resin lifetime. *J. Chromatogr. A* 1216: 5849–5855.

Johansson, B.I., Belew, M., Eriksson, S. et al. (2003a). Preparation and characterisation of prototypes for multimodal separation aimed for capture of negatively charged biomolecules at high salt concentrations. *J. Chromatogr. A* 1016: 21–33.

Johansson, B.I., Belew, M., Eriksson, S. et al. (2003b). Preparation and characterisation of prototypes for multimodal separation aimed for capture of positively charged biomolecules at high salt concentrations. *J. Chromatogr. A* 1016: 35–49.

Jungbauer, A. (2005). Chromatographic media for bioseparation. *J. Chromatogr. A* 1065: 3–12.

Jungbauer, A. and Hahn, R. (2008). Polymethacrylate monolith for preparative and industrial separation of biomolecular assemblies. *J. Chromatogr. A* 1184: 62–79.

Kas, O., Tkacik, G., Moore, A., and Sylvia, R. (2014). Method for the preparation of fibers from a catalyst solution, and articles comprising such fibers. US20170073843A1, Priority date 20 February 2014.

Kaslow, D. and Shiloach, J. (1994). Production, purification and immunogenicity of a malaria transmission-blocking vaccine candidate: TBV25H expressed in yeast and purified using nickel-NTA Agarose. *Biotechnology* 12: 494–499.

Kato, Y., Nakamura, K., and Hashimoto, T. (1987). High-performance hydroxyapatite chromatography of proteins. *J. Chromatogr. A* 398: 340–346.

Kawamura, M. and Uchiyama, K. (1989). Formation of a cycloinulo-oligosaccharide from inulin by an extracellular enzyme of *Bacillus circulans* OKUMZ 31B. *Carbohydr. Res.* 192: 83–90.

Kelley, B., Jankowski, M., and Booth, J. (2009). An improved manufacturing process for Xyntha/ReFacto AF. *Haemophilia* 2009: 1–9.

Kimata, K., Tsuboi, R., Hosoya, K., and Tanaka, N. (1993). Chemically bonded chiral stationary phase prepared by the polymerization of cellulose-vinylbenzoate. *Anal. Methods Instrum.* 1: 23–29.

Kimple, M., Brill, A., and Pasker, R. (2013). Overview of affinity tags for protein purification. *Curr. Protoc. Protein Sci.* 73 (Unit 9): 9.

Kinkel, J.N. (1994). Optivally active polyacrylamide / silica composites and related packings and their applications. In: *A Practical Approach to Chiral Separations by Liquid Chromatography* (ed. G. Subramanian), 217–277. Weinheim: Wiley-VCH.

Kirchner, M. (1893). Unters, ü. d. Brauchbarkeit d. "B.-Filter" ausgebrannter Infusorienerde. In: *Zs. f. Hygiene* 14 H.2.

Kirkland, J., van Straten, M., and Claessens, H. (1995). High pH mobile phase effects on silica-based reversed-phase high-performance liquid chromatographic columns. *J. Chromatogr. A* 691 (1–2): 3–19.

Kopaciewicz, W., Fulton, S., and Lee, S.Y. (1987). Influence of pore and particle size on the frontal uptake of proteins: implications for preparative anionexchange chromatography. *J. Chromatogr.* 409: 111–124.

Kraml, C., Zhou, D., Byrne, N., and McConnell, O. (2005). Enhanced chromatographic resolution of amine enantiomers as carbobenzyloxy derivatives in high-performance liquid chromatography and supercritical fluid chromatography. *J. Chromatogr. A* 1100: 108–115.

Kronvall, G. (1973). Purification of staphyllococcus protein a using immunosorbents. *Scand. J. Immunol.* 2: 31–36.

Kubota, T., Kusano, T., Yamamoto, C. et al. (2001). Cellulose 3,5-dimethylphenylcarbamate immobilized onto silica gel via copolymerization with a vinyl monomer and its chiral recognition ability as a chiral stationary phase for HPLC. *Chem. Lett.* 30: 724–725.

Kummer, M. and Palme, H.J. (1996). Resolution of enantiomeric steroids by high-performance liquid chromatography on chiral stationary phases. *J. Chromatogr. A* 749 (1–2): 61–68.

Kupfer, T., Peters, B., Machtejevas, E. et al. (2017). Faster analysis of monoclonal antibodies using silica monoliths designed for bioanalysis. *Chromatogr. Today* 2017: 14–17.

Laas, T. (1975). Agar derivates for chromatography, electrophoresis and gel-bound enzymes – IV. Benzylated dibromopropanol cross-linked sepharose as an amphophilic gel for hydrophobic salting-out chromatography of enzymes with special emphasis on denaturing risks. *J. Chromatogr.* 111: 373–387.

Lai, B., Wilson, J., Loredo, J. et al. (2018). Epitope targeted macrocyclic peptide ligand with picomolar cooperative binding to interleukin-17F. *Chem. Eur. J.* 24 (15): 3760–3767.

Lämmerhofer, M. (2010). Chiral recognition by enantioselective liquid chromatography: mechanisms and modern chiral stationary phases. Review article. *J. Chromatogr. A* 1217: 814–856.

Lämmerhofer, M. and Lindner, W. (1996). Quinine and quinidine derivatives as chiral selectors I. Brush type chiral stationary phases for high-performance liquid chromatography based on cinchonan carbamates and their application as chiral anion exchangers. *J. Chromatogr. A* 741: 33–48.

Larsen, P., Schou, O., and Rasmussen, E. (2004). Regeneration of chromatographic stationary phases. WO04/089504, priority date 21 October 2004.

Lea, D.J. and Sehon, A.H. (1962). Preparation of synthetic gels for chromatography of macromolecules. *Can. J. Chem.* 40: 159–160.

Li, Y. (2017). Effective strategies for host cell protein clearance in downstream processing of monoclonal antibodies and Fc-fusion proteins. *Protein Expr. Purif.* 134: 96–103.

Liu, H., Zheng, Y., Gurgel, P., and Carbonell, R. (2013). Affintiy membrane development from PBT nonwoven by photo-induced graft polymerization, hydrophilization and ligand attachment. *J. Membr. Sci.* 428: 562–575.

Lowe, C., Lowe, A., and Gupta, G. (2001). New developments in affinity chromatography with portential application in the production of biopharmaceuticals. *J. Biochem. Biophys. Methods* 49: 561–574.

Lu, X., Claus, J., and Bell, D. (2013). Enrichment of phospholipids from biological matrices with zirconium oxide-modified silica sorbents (accessed: 24/11/2019). https://www.sigmaaldrich.com/content/dam/sigma-aldrich/docs/Supelco/Posters/1/T413042H.pdf.

Lynch, K., Ren, J., Beckner, M. et al. (2019). Monolith columns for liquid chromatographic separtions of intact proteins: a review of recent advances and applications. *Anal. Chim. Acta* **1046**: 48–68.

Maa, Y.-F. and Horvath, C. (1988). Rapid analysis of proteins and peptides by reversed-phase chromatography with polymeric microcellular sorbent. *J. Chromatogr.* 445: 71–86.

Macaudiere, P., Tambute, A., Caude, M., and Rosset, R. (1986). Resolution of enantiomeric amides on a Pirkle-type chiral stationary phase. A comparison of subcritical fluid and liquid chromatographic approaches. *J. Chromatogr.* 371: 177–193.

Macquarrie, D.J., Tavener, S.J., Gray, G.W. et al. (1999). The use of Reichardt's dye as an indicator of surface polarity. *New J. Chem.* 23: 725–731.

Majors, R.E. (2003a). The cleaning and regeneration of reversed-phase HPLC columns. *LC-GC Eur.* 16 (7): 404–409.

Matthijs, N., Maftouh, M., and Vander-Heyden, Y. (2006). Screening approach for chiral separation of pharmaceuticals. Part IV: Polar organic solvent chromatography. *J. Chromatogr. A* 1111: 48–61.

McCarthy, J.P. (1994). Direct enantiomeric separation of the 4 stereoisomers of nadolol using normal-phase and reversed-phase high performance liquid chromatography with Chiralpak AD. *J. Chromatogr. A* 685 (2): 349–355.

Meyers, J.J. and Liapis, A.I. (1998). Network modeling of the intraparticle convection and diffusion of molecules in porous particles packed in a chromatographic column. *J. Chromatogr. A* 827: 197–213.

Meyers, J.J. and Liapis, A.I. (1999). Network modeling of the convective flow and diffusion of molecules adsorbing in monoliths and in porous particles packed in a chromatographic column. *J. Chromatogr. A* 852: 3–23.

Mikes, O. (1988). *High-Performance Liquid Chromatography of Biopolymers and Biooligomers Parts A and B*, Journal of Chromatography Library, vol. 41A and B. Amsterdam: Elsevier.

Mikeš, O., štrop, P., Zbrožek, J., and Čoupek, J. (1976). Chromatography of biopolymers and their fragments on ionexchange derivates of the hydrophilic macroporous synthetic gel spheron. *J. Chromatogr.* 119: 339–354.

Minakuchi, H., Nakanishi, K., Soga, N. et al. (1996). Octacdecylsilylated porous silica rods as separation media for reversed-phase liquid chromatography. *Anal. Chem.* 68: 3498–3501.

Moiani, D., Salvalaglio, M., Cavallotti, C. et al. (2009). Structural characterization of a protein a mimetic peptide denrimer bound to human IgG. *J. Phys. Chem. B* 113: 16268–16275.

Moore, J.C. (1964). Gel permeation chromatography. I. A new method for molecular weight distribution of high polymers. *J. Polymer. Sci., Part A* 2: 835.

Muhammad, S., Hussain, S.T., Waseem, M. et al. (2012). Surface charge properties of zirconium dioxide. *Iran. J. Sci. Technol.* A4: 481–486.

Müller, E. and Vajda, J. (2016). Routes to improve binding capacities of affinity resins demonstrated for protein a chromatography. *J. Chromatogr. B* 1021: 159–168.

Nawrocki, J. (1997). The silanol group and its role in liquid chromatography. *J. Chromatogr. A* 779: 29–71.

de Neuville, B., Thomas, H., and Morbidelli, M. (2013). Simulation of porosity decrease due to protein adsorption using the distributed pore model. *J. Chromatogr. A* 1314: 77–85.

Nguyen, H.C., Langland, A.L., Amara, J.P. et al. (2019). Improved HCP reduction using a new, all-synthetic depth filtration media within an antibody purification process. *Biotechnol. J.* 14: e1700771.

Ning, J.G. (1998). Direct chiral separation with Chiralpak AD converted into the reversed-phase mode. *J. Chromatogr. A* 805 (1–2): 309–314.

Nissum, M. (2018). Affintiy chromatography for vaccines purification. *World Vaccine Congress*, Europe (30 October 2018).

Okamoto, Y., Kawashima, M., and Hatada, K. (1984). Usefull chiral packing materials for high-performance liquid chromatographic resolution of enantiomers: phenylcarbamates of polysaccharides coated on silica gel. *J. Am. Chem. Soc.* 106: 5357–5359.

Okamoto, Y., Aburatani, R., Miura, S., and Hatada, K. (1987). Chiral stationary phases for HPLC: cellulose tris(3,5-dimethylphenylcarbamate) and tris(3,5-dichlorophenylcarmacate) chemically bonded to silica gel. *J. Liq. Chromatogr.* 10: 1613–1628.

O'Leary, R.M., Feuerhelm, D., Peers, D. et al. (2001). Determining the useful lifetime of chromatography resins. *BioPharm* 14 (9): 10–17 O'Leary 2003.

Oliveros, L., López, P., Minguillón, C., and Franco, P. (1995). Chiral chromatographic discrimination ability ofa cellulose 3,5-dimethylphenylcarbamate/10-undecenoate mixed derivative fixed on several chromatographic matrices. *J. Liq. Chromatogr.* 18: 1521–1532.

Orr, V., Zhong, L., Moo-Young, M., and Chou, C. (2013). Recent advances in bioprocessing application of membrane chromatography. *Biotechnol. Adv.* 31: 450–465.

Padró, J. and Keunchkarian, S. (2018). State-of-the-art and recent developments of immobilized polysaccharide-based chiral stationary phases for enantioseparations by high-performance liquid chromatography (2013–2017). *Microchem. J.* 140: 142–157.

Pall (2009). Mustang capsules improve biotechnology process economics. *Membr. Technol.* 2009 (12): 2.

Perrin, C., Vu, V.A., Matthijs, N. et al. (2002a). Screening approach for chiral separation of pharmaceuticals. Part I. Normal-phase liquid chromatography. *J. Chromatogr. A* 947: 69–83.

Perrin, C., Matthijs, N., Mangelings, D. et al. (2002b). Screening approach for chiral separation of pharmaceuticals. Part II. Reversed-phase liquid chromatography. *J. Chromatogr. A* 966: 119–134.

Peterson, E. and Sober, H. (1956). Chromatography of proteins. I. Cellulose ion-exchange adsorbents. *J. Am. Chem. Soc.* 78 (4): 751–755.

Pirkle, W.H. and Däppen, R. (1987). Reciprocity in chiral recognition – comparison of several chiral stationary phases. *J. Chromatogr.* 404: 107–115.

Porath, J. and Flodin, P. (1959). Gel filtration: a method for desalting and group separation. *Nature* 183: 1657.

Porath, J., Janson, J.C., and Laas, T. (1971). Agar derivates for chromatography, electrophoresis and gel-bound enzymes – I. Desulphatet and reduced cross-linked agar and agarose in spherical bead form. *J. Chromatogr.* 60: 167–177.

Porath, J., Laas, T., and Janson, J.-C. (1975). Agar derivates for chromatography, electrophoresis and gel-bound enzymes – III. Rigid agarose gels cross-linked with divinyl sulphone (DVS). *J. Chromatogr.* 103: 49–62.

Rabel, F. (1980). Use and maintenance of microparticle high performance liquid chromatography columns. *J. Chromatogr. Sci.* 18: 394.

Regnier, F.E. (1987). HPLC of biological macromolecules: the first decade. *Chromatographia* 24: 241–251.

Reichardt, C. (2003). *Solvents and Solvent Effects in Organic Chemistry*, 3e. VCH: Weinheim.

Rigney, M.P., Funkenbusch, E.F., and Carr, P.W. (1990). Physical and chemical characterization of microporous zirconia. *J. Chromatogr.* 499: 291–304.

Robert, M., Chahal, P., Audy, A. et al. (2017). Manufacturing of recombinant adeno-associated viruses using mammalian expression platforms. *Biotechnol. J.* 12 (3): 1600193.

Rogl, H., Kosemund, K., Kühlbrandt, W., and Collinson, I. (1998). Refolding of *Escherischia coli* produced membrane protein inclusion bodies immobilised by nickel chelating chromatography. *FEBS Lett.* 432: 21–26.

Rohloff, J., Gelinas, A., Jarvis, T. et al. (2014). Nucleic acid ligands with protein-like side chains: modified aptamers and their use as diagnostic and therapeutic agents. *Mol. Ther. Nucleic Acids* 3: e201.

Romig, T., Bell, C., and Drolet, D. (1999). Aptamer affinity chromatography: combinatorial chemistry applied to protein purification. *J. Chromatogr. B* 731: 275–284.

Ruthven, D.M. (ed.) (1997). *Encyclopedia of Separation Technology*, vol. 1. New York: Wiley.

Salvalaglio, M., Paloni, M., Guelat, B. et al. (2015). A two level hierarchical model of protein retention in ion exchange chromatography. *J. Chromatogr. A* 1411: 50–62.

Schnabel, R. and Langer, P. (1991). Controlled-pore glass as a stationary phase in chromatography. *J. Chromatogr.* 544: 137–146.

Schulte, M. and Dingenen, J. (2001). Monolithic silica sorbents for the separation of diasteromers by means of simulated moving bed chromatography. *J. Chromatogr. A* 923: 17–25.

Schulte, M., Ditz, R., Devant, R. et al. (1997). Comparison of the specific productivity of different chiral stationary phases used for simulated moving bed – chromatography. *J. Chromatogr.* 769: 93–100.

Schulte, M., Devant, R., and Grosser, R. (2002). Enantioseparation of Gantofiban precursors on chiral stationary phases of the poly-(N-acryloyl amino acid derivative)-type. *J. Pharm. Biomed. Anal.* 27: 627–637.

Schwellenbach, J., Taft, F., Villain, L., and Strube, J. (2016). Preparation and characterization of high capacity, strong cation-exchange fiber based adsorbents. *J. Chromatogr. A* 1447: 92–106.

Seidl, J., Malinsky, J., Dušek, D., and Heitz, W. (1967). Macroporöse styrol-divinylbenzol-copolymere und ihre Verwendung in der chromatographie und zur darstellung in ionenaustauschern. *Adv. Polym. Sci.* 5: 113–213.

Smith, G.P. (1985). Filamentous fusion phage: novel expression vectors that express cloned antigenes on the virion surface. *Science* 228: 1315–1317.

Staby, A., Sand, M.-B., Hansen, R.G. et al. (2004). Comparison of chromatographic ion-exchange resins: III. Strong cation-exchange resins. *J. Chromatogr. A* 1034 (1–2): 85–97.

Stanislawski, B., Schmit, E., and Ohser, J. (2010). Imaging of fluorophores in chromatographic beads, reconstruction of radial density distributions and characterisation of protein uptaking processes. *Image Anal. Stereol.* 29: 181–189.

Strube, J., Arlt, W., and Schulte, M. (2006). Technische chromatographie. In: *Fluidverfahrenstechnik: Grundlagen, Methodik, Technik, Praxis* (ed. R. Gödecke), 381–495. Weinheim: Wiley-VCH.

Sun, P. and Armstrong, D. (2010). Effective enantiomeric separations of racemic primary amines by the isopropyl carbamate-cyclofructan 6 chiral stationary phase. *J. Chromatogr. A* 1217: 4904–4918.

Sun, P., Wang, C., Breitbach, Z. et al. (2009). Development of new HPLC chiral stationary phases based on native and derivatized cyclofructans. *Anal. Chem.* 81: 10215–10226.

Svec, F. and Fréchet, J. (1992). Continuous rods of microporous polymer as high-performance liquid chromatography separation media. *Anal. Chem.* 64: 820–822.

Tanaka, N., Hashizume, K., and Araki, M. (1987). Comparison of polymer-based stationary phases with silica-based stationary phases in reversed-phase liquid chromatography. *J. Chromatogr.* 400: 33–45.

Thomas, H., Storti, G., Joehnck, M. et al. (2013). Role of tentacles and protein loading on pore accessibility and mass transfer of proteins in cation exchange materials. *J. Chromatogr. A* 1285: 48–56.

Tian, P., Han, X., Ning, G. et al. (2013). Synthesis of porous hierarchical MgO and its superb adsorption properties. *ACS Appl. Mater. Interfaces* 5: 12411–12418.

Tweeten, K.A. and Tweeten, T.N. (1986). Reversed-phase chromatography of proteins on resin-based wide-pore packings. *J. Chromatogr.* 359: 111.

Ugelstad, J. (1984). Monodisperse polymer particles and dispersions thereof. US Patent 4, 459, 378.

Ugelstad, J., Mørk, P.C., Kaggernd, K.H. et al. (1980). Swelling of oligomer–polymer particles. New methods of preparation of emulsions and polymer dispersions. *Adv. Colloid Interface Sci.* 13: 101–140.

Unger, K.K. (1990). *Packings and Stationary Phases in Chromatographic Techniques*. New York: Marcel Dekker.

Unger, K. and Schick-Kalb, J (1971). Poröses siliciumdioxid. DE 2155281, 6 November 1971.

Unger, K.K., Janzen, R., and Jilge, G. (1987). Packings and stationary phases for biopolymer separations by HPLC. *Chromatographia* 24: 144–154.

Unger, K.K., Bidlingmaier, B., du Fresne von Hohenesche, C., and Lubda, D. (2002). Evaluation and comparison of the pore structure and related properties of particulate and monolithic silicas for liquid phase separation processes, COPS VI Proceedings. *Stud. Surf. Sci. Catal.* 144: 115–122.

Univercells (2019). Press Release (11 January 2019).

Urmann, M., Graalfs, H., Joehnck, M. et al. (2010). Cation-exchange chromatography of monoclonal antibodies – characterization of a novel stationary phase designed for production-scale purification. *mAbs* 2: 395–404.

Wang, C., Jiang, C., and Armstrong, D. (2008). Considerations on HILIC and polar organic solvent based separtions: use of cyclodextrin and macrocyclic glycopeptide stationary phases. *J. Sep. Sci.* 31 (11): 1980–1990.

Wang, Q., Li, J., Yang, X. et al. (2014). Investigation on performance of zirconia and magnesia-zirconia statioinary phases in hydrophilic interaction chromatography. *Talanta* 129: 438–447.

Warren, T., Coolbaugh, M., and Wood, D. (2013). Ligation independent cloning and self-cleaving intein as a tool for high-throughput protein purification. *Protein Expr. Purif.* 91: 169–174.

Welsch, T., Dornberger, U., and Lerche, D. (1993). Selectivity tuning of serially coupled columns in high-performance liquid-chromatography. *HRC J. High Resoult. Chromatogr.* 16 (1): 18–26.

Wenzel, B., Fischer, S., Brust, P., and Steinbach, J. (2010). Accessible silanol sites – beneficial for the RP-HPLC separation of constitual and diastereomeric azaspirovesamicol isomers. *J.Chromatogr. A* 1217: 7884–7890.

Winderl, J., Spies, T., and Hubbuch, J. (2018). Packing characteristics of winged shaped polymer fiber supports for preparative chromatography. *J. Chromatogr. A* 1553: 67–80.

Winkler, J. and Marmé, S. (2000). Titania as a sorbent in normal-phase liquid chromatography. *J. Chromatogr. A* 888: 51–62.

Wood, D. (2014). New trends and affinity tag designs for recombinant protein purification. *Curr. Opin. Struct. Biol.* 26: 54–61.

Wu, Y., Wang, Y., Yang, A., and Li, T. (1999). Screening of mixture combinatorial libraries for chiral selectors: a reciprocal chromatographic approach using enantiomeric libraries. *Anal. Chem.* 71: 1688–1691.

Xenopoulos, A. (2015). A new, integrated, continuous purification process template for monoclonal antibodies: process modeling and cost of goods studies. *J. Biotechnol.* 213: 42–53.

Xu,, F., Wu,, D., Fu, R., Wei, B. (2017). Design and Preparation of porous carbons from conjugated polymer precursors. *Mater. Today* 20: 629–656.

Yashima, E., Fukaya, H., Okamoto, Y. (2017). 3,5-Dimethylphenylcarbamates of cellulose and amylose regioselectively bonded to silica gel as chiral stationary phases for high-performance liquid chromatography. *J. Chromatogr. A* 677: 11–19.

Zamolo, L., Busini, V., Moiani, D. et al. (2008). Molecular dynamic investigations of the interaction of supported affinity ligands with monoclonal antibodies. *Biotechnol. Progr.* 24: 527–539.

Zamolo, L., Busini, V., Moiani, D. et al. (2008). Molecular dynamic investigations of the interaction of supported affinity ligands with monoclonal antibodies. *Biotechnol. Progr.* 24: 527–539.

Zaveckas, M., Snipaitis, S., Pesliakas, H. et al. (2015). Purification of recombinant virus-like particles of porcine circovirus type 2 capsid protein using ion-exchange monolith chromatography. *J. Chromatogr. B* 991: 21–28.

Zhang, T., Schaeffer, M., and Franco, P. (2005a). Optimization of the chiral separation of a Ca-sensitizing drug on an immobilized polysaccharide-based chiral stationary phase. Case study with a preparative perspective. *J. Chromatogr. A* 1083: 96–101.

Zhang, T., Kientzy, C., Franco, P. et al. (2005b). Solventversatility of immobilized 3,5-dimethylphenyl-carbamate of amylose in enantiomeric separations by HPLC. *J. Chromatogr.* 1075: 65–75.

Zhang, T., Nguyen, D., Franco, P. et al. (2006). Cellulose 3,5-dimethylphenyl-carbamate immobilised on silica. A new chiral stationary phase for the analysis of enantiomers. *Anal. Chim. Acta* 557: 221–228.

Zhang, T., Nguyen, D., Franco, P. et al. (2008). Cellulose tris-(3,5-dichlorphenyl-carbamate) immobilised on silica: a novel chiral stationary phase for resolution of enantiomers. *J. Pharm. Biomed. Anal.* 46: 882–891.

Zhao, M., Vandersluis, M., Stout, J. et al. (2019). Affinity chromatography for vaccines manufacturing: finally ready for prime time? *Vaccine* https://doi.org/10.1016/j.vaccine.2018.02.090.

Zhong, Q., Han, X., He, L. et al. (2005). Chromatographic evaluation of poly (trans 1,2-cyclohexanediyl-bis-acrylamide) as a chiral stationary phase for HPLC. *J. Chromatogr. A* 1066: 55–70.

Zhou, L., Welsh, C., Lee, C. et al. (2009). Development of LC chiral methods for neutral pharmaceutical related compounds using reversed phase and normal phase liquid chromatography with different types of polysaccharide stationary phases. *J. Pharm. Biomed. Anal.* 49: 964–969.

Zielonka, S., Weber, N., Becker, S. et al. (2014). Shark attack: high affinity binding proteins derived from shark vNAR domains by stepwise in vitro affinity maturation. *J. Biotechnol.* 191: 236–245.

Zizkovsky, V., Kucera, R., and Klimes, J. (2007). Potential employment of non-silica based stationary phases in pharmaceutical analysis. *J. Pharm. Biomed. Anal.* 44: 1048–1055.

4

Selection of Chromatographic Systems*

Michael Schulte

Merck KGaA, Life Science – Bioprocessing, Purification R&D, Frankfurter Str. 250, 64293 Darmstadt, Germany

This chapter aims to provide guidelines for the selection of chromatographic systems, as a combination of stationary and mobile phase, related to different key issues of the whole process in preparative chromatography. These key issues do not only focus on the engineer's point of view. Along with engineering parameters such as productivity, yield, and recovery, we have to take into account economy, scale of the separation, speed, time pressure, hardware requirements and availability, automation and legal aspects toward documentation, safety, and others. Obviously, rules of thumb related to these criteria may not cover all possible practical scenarios, but they may be useful in avoiding pitfalls.

The selection of chromatographic systems is critical for process productivity and thus also impacts process economy. While the selection of the chromatographic system must be regarded as holding the biggest potential for optimizing a separation process, it is also a source of severe errors. The choice of the chromatographic system includes the selection of the adsorbent and the mobile phase for a given sample.

Some general recommendations can be given for the selection of a chromatographic system to be scaled up to large scale:

(1) Choose a stationary phase that is manufactured reproducibly in large (kg to ton) quantities and is allowed to be used under regulatory issues.
(2) Prefer native and simple adsorbents to those with a sophisticated surface chemistry.
(3) Use stationary phases whose retention and selectivity can be adjusted by simple solvents. Solvent removal and solvent recovery can become an expensive step.
(4) Follow carefully the recommendations of the packing manufacturer with respect to solvent use, washing, and regeneration.
(5) Apply easy prepurification steps, e.g. pre-columns packed with the same material or adsorptive depth filters for removing highly adsorptive

---

*Matthias Jöhnck, Romas Skudas, Klaus K. Unger, Cedric du Fresne von Hohenesche, Wolfgang Wewers, Jules Dingenen, and Joachim Kinkel have contributed to the first and/or second edition.

compounds. The easier the actual separation task, the more efficient it will be economically.

Besides the pure chromatographic behavior of the stationary phase, some further features with regard to the sorbent performance as well as the supplier's reliability should be taken into account especially for a large-scale separation project. For the sorbent related features, these are:

- High dynamic capacity;
- Good product recovery;
- Straight scalability;
- Good cleanability;
- Long shelf life;
- High mechanical and chemical stability;
- Sufficient selectivity;
- Appropriate pore size.

In terms of the most important points, a reliable supplier has to fulfill one would list:

- Good documentation (regulatory support files);
- High lot-to-lot consistency;
- Long-term supply potential, e.g. financial stability;
- Large batch sizes;
- Certificates of analysis;
- Possibility to do vendor audits (initially and periodically);
- Reasonable costs;
- Technical support.

The selection of a chromatographic system can be based on a systematic optimization of the system through extensive studies of solubility, retention, and selectivity, but, sometimes, the use of generic gradient runs with standard systems is sufficient.

One source of severe mistakes in system development is a common misunderstanding about preparative chromatography. The classical differentiation between analytical and preparative chromatography is based on the size of the equipment, the size of adsorbent particles, or the amount of sample to be separated. This old view of preparative chromatography leads to a geometric scale-up of systems that are dedicated for analytical applications. Scale-up from analytical to preparative systems is problematic because the goal and restrictions for the two operation modes are different (Table 4.1), and thus the parameters to be optimized are also different. The goal of analytical separations is to generate information, whereas preparative applications aim to isolate a certain amount of purified product. For these reasons, preparative and analytical chromatography should be differentiated on the basis of the goal and not the geometric size of the system.

For analytical separations, the sample can be processed, handled, and modified in any way suitable to generate the required information (including degradation, post-column derivatization, or otherwise changing the nature of the compounds

Table 4.1 Differentiation between analytical and preparative chromatography.

Goal	Analytical information	Preparative material
Restrictions	Fast information generation	Optimal product recovery
	All separation modes allowed	Recovery of unchanged solutes must be guaranteed
Optimization parameters	• Necessary separation sensitivity • Retention factor ($1 < k < 5$) • Speed • Selectivity	• Purity • Yield • Productivity • Economics

under investigation). In preparative mode, the product has to be recovered in the same condition that it was in before undergoing the separation (i.e. no degrading elution conditions, no reaction, etc.). This determines the chromatographic process and chromatographic system far more than any consideration of process size.

Preparative high-performance liquid chromatography (HPLC) separations are used in all stages of process development. The three main stages in process development as well as examples for the tasks and corresponding criteria for process development are described in Figure 4.1. They differ in time pressure, frequency of the separations, and amount of target products, which dominate the economic structure of the process. At the laboratory and technical scale, the development of the separation is dominated by the time pressure, and the separation problem includes only a limited amount of sample and a limited number of repetitions. Process optimization in this small scale to semi-scale is not helpful, because the effort for optimization will not be repaid in reduced operational costs.

In the early stages of process development, too little sample is available for extensive optimization studies. These studies are not needed and are counterproductive to economic success because separation costs in these early stages are dominated by the time spent developing the separation and not by the operational costs. If purified products are needed for further research (e.g. lead finding), time delays are problematic. Furthermore, the number of different separation problems at this early stage is quite high, while the number of repetitions of one separation is low. In this case, generic gradient runs, which can separate a broad range of substances, provide a quick and effective means of separation.

In production-scale processes, economic pressure comes to the fore. Next to economic pressure, it is very often not possible to separate the huge amounts involved with noneffective chromatographic separations. Although the time pressure is still present, an optimization of the chromatographic system with extensive studies is required. The investment in an optimized system will be repaid though by the reduced operation costs of a subsequent production process.

However, due to the vast number of variables and the restrictions regarding the environment of the preparative separation one may say: "There is no universal chromatographic system to meet all requirements."
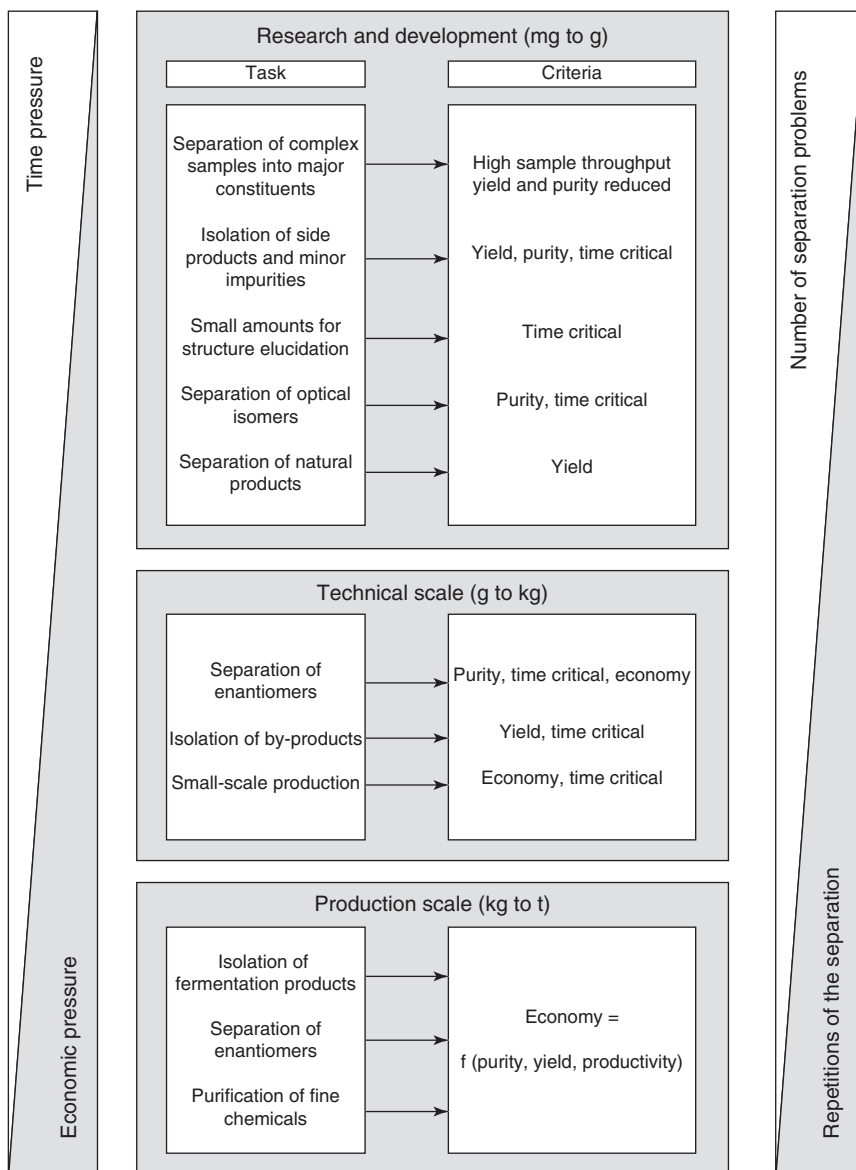
Figure 4.1 Tasks for preparative chromatography in different development stages.

Comparable to the different scales of processes (Figure 4.1), the users of preparative separations can also be distinguished by their tasks and differentiated into the following groups.

There are users who have to solve many different separation problems in a short time. These users represent the laboratory-scale production of chromatography. The frequency of changes in their tasks and thus the time pressure are high, and rules of thumb for a fast selection of suitable chromatographic systems

are needed. Other users have to develop the separation for one production-scale process. This group is interested in guidelines for the systematic optimization of the chromatographic system and for the choice of the process concept. Rules of thumb are only used for a first guess of the system.

The development of a chromatographic separation can be divided into three stages, which are discussed here and in Chapter 5. As shown in Figure 4.2, the first step is to define the task (Section 4.1), meaning nothing else than a reflection and classification of the separation problem. After the task is defined, a suitable chromatographic system must be found. For this purpose, the general properties of chromatographic systems are discussed in Sections 4.2 and 4.3, while criteria for the selection of different categories of chromatographic systems are given in
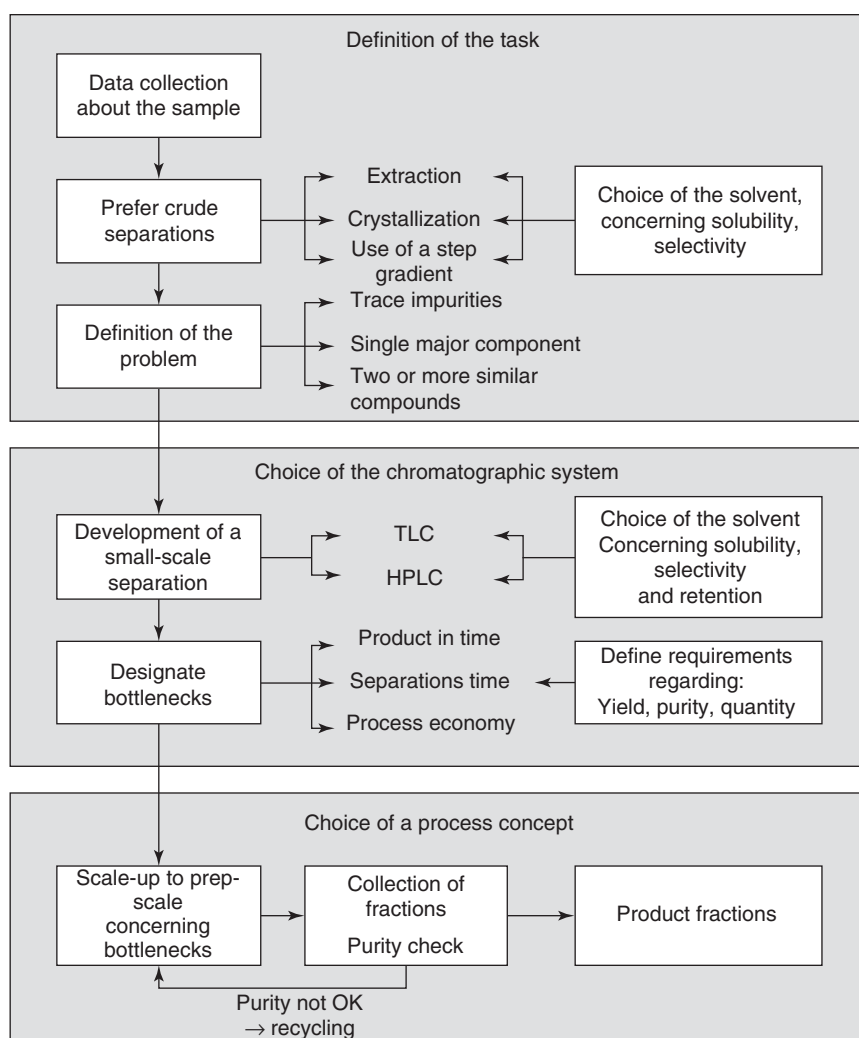
Figure 4.2 Development of a chromatographic method.

Sections 4.3–4.8. The last step of method development is the choice of the process concept, which depends on the given task and chosen chromatographic system as well as the available equipment. Different process concepts are introduced in Sections 5.1 and 5.2, while Section 5.3 gives guidelines for the selection of the chromatographic method. The whole development process is exemplified there, and thus Section 5.3 can be regarded as a conclusion resulting from Chapters 4 and 5.

4.1 Definition of the Task

Any selection of a chromatographic system for preparative isolation of individual components should start with a definition of the task. The starting point can be described as careful reflection of the main criteria influencing the separation.

Good advice for primary actions is to collect all available data describing the nature of the sample. Information exchange is especially important if synthesis and separation of the products are done by different departments. For this purpose, a rough characterization of the sample and the preparative task made by following the questionnaire of Table 4.2 eases the planning of experimental procedures.

Before starting the selection of any chromatographic system, the use of crude separation steps such as extraction, crystallization, or flash chromatography should be checked. The separation task can be simplified by the use of these crude separations if impurities or the target product is removed in the first capture steps.

An example of these steps of downstream processing is the isolation of paclitaxel, an anticancer drug that is extracted for example from the Pacific yew tree. This is a very challenging task due to the low concentration (0.0004–0.08%) in the bark (Pandey 1997; Pandey et al. 1998). The target product is extracted from the herbal material by Soxhlet extraction. The concentrated extract contains a large range of impurities, which is shown in the first chromatogram of Figure 4.3. Many prepurification steps are necessary before the separation is downsized to a separation problem of paclitaxel and closely related taxanes. Owing to the difficulty of this last separation step, paclitaxel is isolated by preparative chromatography.

Table 4.2 Questionnaire for the collection of the information.

- What is the consistency of the sample (solid, liquid, suspension, etc.)?
- What is the source of the sample (chemical synthesis, fermentation, extraction from natural products, etc.)?
- Which possible solvents for the sample as well as solubilities are known?
- Is the sample a complex mixture of unknown composition?
- Which chemical or physical properties of the sample are available (stability [chemical, oxidative], structures, UV spectra as well as toxic and biohazard data)?
- Is the structure, for example, physical or chemical behavior of the target compound(s) known?
- Is the structure, for example, the physical or chemical behavior of the impurities known?
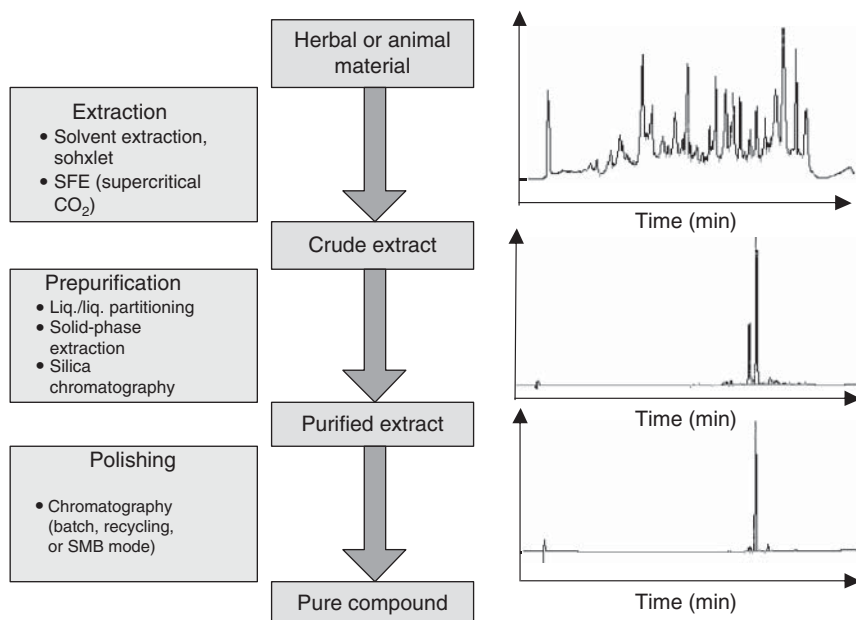- Is any kind of chromatographic data available?

Figure 4.3 Purification of paclitaxel out of a crude extract. Complexity of separation is reduced by several chromatographic steps.

The isolation of paclitaxel exemplifies that most preparative separations must be downsized to a level where a limited number of individual compounds are present to ease the final purification steps. This downsizing of the separation problem can be done by crude separations or by a cascade of consecutive chromatographic separation steps. One finally ends up at a point where a multicomponent mixture with a broad concentration range of the different substances has to be fractionated to a series of mixtures. This approach is described in Figure 4.4. In general, a mixture can be split into three types of fractions, where each represents a specific separation problem. These three fractions exemplify possible separation scenarios that differ with regard to the ratio of target products and impurities.

The first separation scenario is the most comfortable problem. The target product is the major component in the mixture, and thus it is easy to reach a yield and purity in the desired range. Thermodynamic effects can be used to displace impurities during the separation process.

In the second scenario, target products and impurities are present in similar amounts. The separation of racemic mixtures exemplifies this scenario. The problem of racemic mixture formation often occurs during chemical synthesis, where 50% of the mixture consists of the wanted enantiomer (eutomer) and 50% is the unwanted enantiomer (distomer). In this case, competitive adsorption and the elution order of the enantiomers are of special interest (Section 4.6).

The last scenario represents the most difficult separation problem. The concentration of the target product is quite small, and thus it is very important to reach, simultaneously, high yield and high purity. Because of these special constraints,
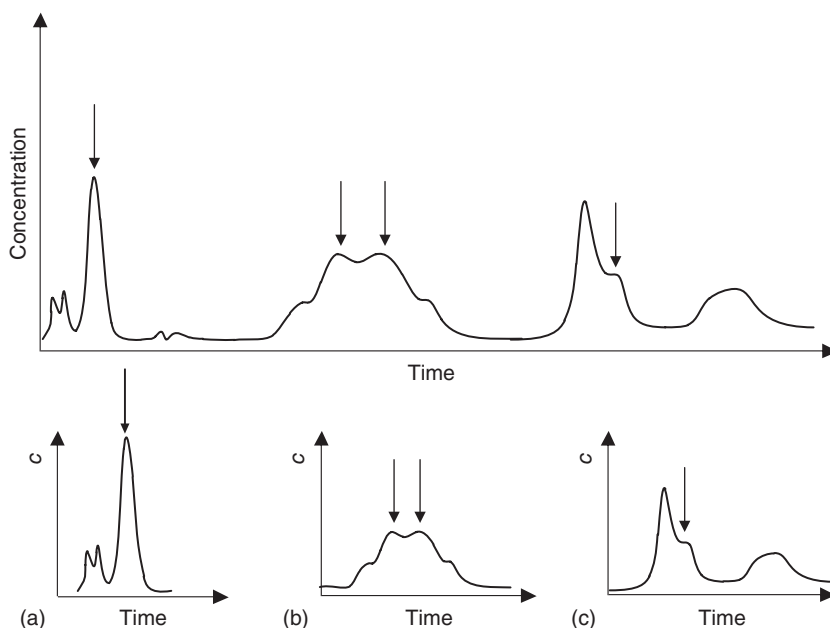
Figure 4.4 Main types of preparative chromatographic separation scenarios. (a) Target products are the dominating components. (b) Target products and impurities are of similar amount. (c) Impurities and by-products are dominating the desired products.

the chromatographic system must be selected carefully. An impropriate system may result in a wrong elution order and thus prevent separation of the products.

The choice of chromatographic system and the process concept are influenced by the classification of the separation problem into one of the three scenarios of Figure 4.4. This section focuses on the influence of the chromatographic system, while the influence on the process concept is explained in Section 5.3. Here, it should be kept in mind that the elution order of the components is essential for the whole process and the elution order is determined by the chromatographic system. Especially if one component is in excess, as in scenarios (a) and (c) in Figure 4.4, the use of thermodynamic effects such as displacement or tag-along are a special source for optimization as well as for severe errors and mistakes (Section 2.5).

Before a chromatographic system is selected, its attributes have to be defined. As described in Section 2.1, a chromatographic system consists of the adsorbent (stationary phase), mobile phase (eluent, solvent, desorbent), and solutes (samples, analyte, etc.). Figure 4.5 illustrates the interrelationship of these three constituents. The selection of the chromatographic system is influenced by their properties and their interaction. These properties are described in this section, while rules and criteria for the selection of the chromatographic system are explained in Sections 4.4–4.8.

The solute is the product of the prepurification steps. It contains the target product and the impurities. Although the solute is a part of the chromatographic
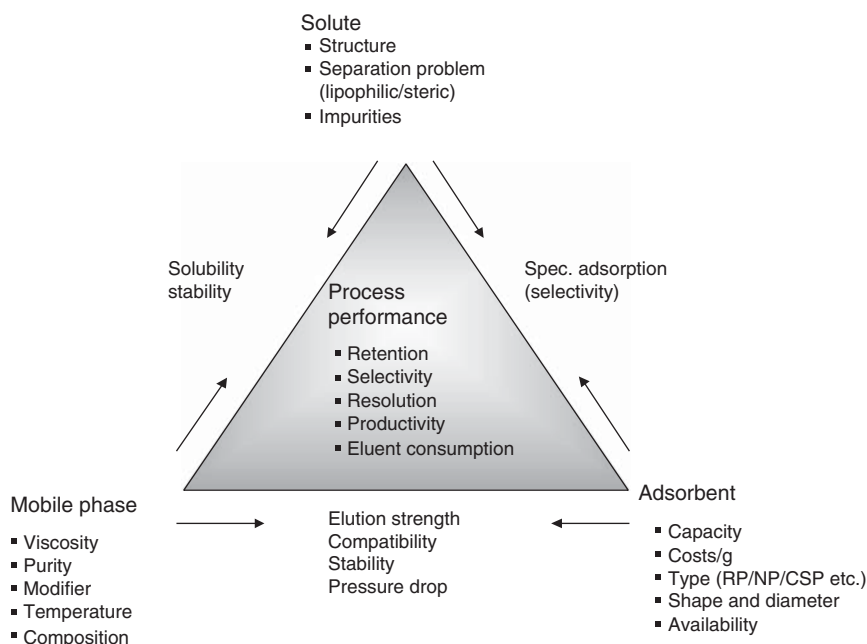
Figure 4.5 Elements of the chromatographic system.

system, it is not a free parameter like the eluent or the adsorbent. Subsequent to previous crude separations, the composition of the feedstock is fixed, and the chromatographic system is completed by the choice of mobile phase and adsorbent.

4.2 Mobile Phases for Liquid Chromatography

The first step of system development is the choice of the mobile phase. While the use of neat solvents is preferred, very often, a mixture of solvents must be used to obtain good results. The selection of the mobile phase should be based on:

- Throughput;
- Stability;
- Safety concerns;
- Operating conditions.

The most important criterion for solvent selection is throughput, which mainly depends on a sufficient solubility of the solutes and the corresponding selectivity of the separation. Because solubility and selectivity depend on the interaction between the three elements of the chromatographic system, the selection of the mobile phase dependent on these parameters is further discussed in Sections 4.3–4.8.
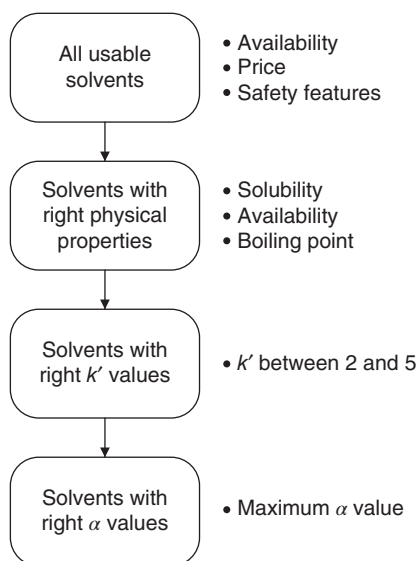
Figure 4.6 Decision tree for the choice of mobile phases.

A useful decision tree for the determination of the best mobile phase is shown in Figure 4.6. From all solvents, which are considered appropriate for preparative chromatography, the first screen is based on the right physical properties, e.g. solubility and boiling point. With this selection, the retention should be adjusted to a k'-value between 2 and 5, and finally the selectivity should be maximized by fine-tuning the mobile phase composition.

Along with these interactions, there are a lot of properties of the neat solvents, with regard to stability, safety, and operation conditions, which help to decrease the number of suitable solvents for preparative chromatography. In contrast to analytical separations, the number of applicable solvents for preparative use is decreased by these limitations. Snyder has examined the behavior of 74 different solvents for general use in liquid chromatography (Snyder and Kirkland 1979). Forty-one of them are most often used in preparative separations (Table 4.3). Restrictions in terms of use have come up for some solvents in recent years due to toxicity (*n*-hexane), safety (tetrahydrofuran [THF]), or environmental (chlorinated solvents) reasons. This has limited the choice further down.

4.2.1 Stability

The stability of all components of the chromatographic system must be assured for the complete operation time. The solvent must be chemically inert toward all kinds of reactions. Neither an instable solvent, which, for example, tends to form peroxides, nor a solvent that reacts with the sample or the adsorbent is suitable for an economically successful solution of the separation problem. Of course, corrosion of the HPLC unit must be prevented, too.

In chromatographic systems operated with a high percentage of water or buffer, the microbial contamination of the solvent has to be carefully monitored.

Table 4.3 Properties of solvents frequently used in preparative chromatography.

Solvent	Polarity[a]	ET(30)[b]	Boiling point (°C)	Viscosity 25 °C (cP)	RI (–)	UV cutoff (nm)	LD 50 (mg kg^{-1})	ICH class[c]	Vapor pressure 25 °C (bar)	Explosion limit (vol%)
Cyclohexane	0.006	30.9	81	0.898	1.426	200	12.705	2	0.104	1.3–8
Cyclopentane			49	0.44	1.400	200	11.400		0.346	1.1–8.7
n-Hexane[d]	0.009	31.0	69	0.31[e]	1.375	195	28.710	2	0.202	1.2–7.8
n-Pentane	0.009	31.0	36	0.24	1.358	200	5.000	3	0.562	1.5–7.8
n-Heptane	0.012	31.1	98	0.386	1.3855	200	17.986	3	0.533	1.05–6.7
Diisobutylene (isooctane, 2,2,4-trimethylpentane)			105	0.5[e]	1.3884	210	5.000	[c]	0.103	0.9-5.5
Cyclohexene		32.2	83	0.67[e]	1.446	214	2.000	—	0.09[e]	1.09–7.7
Di-n-butyl ether		33.0	142	0.64	1.397	220	7.400	—	0.006[e]	0.9–8.5
Toluene	0.099	33.9	111	0.59[e]	1.497	284	636	2	0.038	1.27–7.1
Diisopropyl ether		34.1	69	0.58	1.365	220	8.470	[c]	0.200	1.4–7.9
Benzene[d]	0.111	34.3	80	0.6	1.498	280	930	1	—	1.4–8
Diethyl ether	0.117	34.5	35	0.24	1.35	218	1.213	3	0.669	1.8–48
Methyl tertiary butyl ether	0.124	34.7	55	0.27[e]	1.369	210	3.870	3	0.27	1.6–8.4
1,4-Dioxane	0.164	36.0	101	1.2	1.42	215	5.200	2	0.050	2–22
2-Methyltetrahydrofuran		36.5	80	0.55	1.4059	200	890	[c]	0.136[e]	1.2–5.7
Tetrahydrofuran[d]	0.207	37.4	66	0.55[e]	1.407	212	1.650	2	0.216	1.8–11.8
Ethyl acetate	0.228	38.1	77	0.45[e]	1.372	256	5.620	3	0.126	2–12
Methoxyethanol (methyl glycol, ethylene glycol monomethyl ether)			125	1.6	1.4	210	2.370	2	0.013	2.5–14

(Continued)

Table 4.3 (Continued)

Solvent	Polarity[a]	ET(30)[b]	Boiling point (°C)	Viscosity 25°C (cP)	RI (–)	UV cutoff (nm)	LD 50 (mg kg^{-1})	ICH class[c]	Vapor pressure 25°C (bar)	Explosion limit (vol%)
Dimethoxyethane (monoglyme)	0.231	38.2	85	0.46	1.379	220	3.200	2	0.064[e]	1.6–10.4
Chloroform[d]	0.259	39.1	61	0.53	1.443	245	908	2	0.259	
Methyl acetate	0.253	38.9	57	0.36	1.3614	260	3.700	3	0.228	3.1–16
1,2-Dichloroethane[d]	0.269	39.4	83	0.78	1.442	228	670	1	0.105	5.6–11.4
Isobutyl methyl ketone		39.4	117	0.55	1.396	334	2.080	2	0.019	1.2–8
Pyridine[d]	0.302	40.5	115	0.88	1.507	330	891	2	0.028	1.8–12.4
Dichloromethane[d]	0.309	40.7	40	0.44[e]	1.424	233	1.600	2	0.573	—
Methyl ethyl ketone (2-butanone)	0.327	41.3	80	0.38	1.376	329	2.600	3	0.103[e]	1.8–10
Acetone	0.355	42.2	56	0.36[e]	1.359	330	5.800	3	0.306	2.2–13
Dimethylformamide	0.386	43.2	153	0.8	1.428	268	2.800	2	0.005	2.2–15.2
Acetonitrile	0.460	45.6	82	0.38[e]	1.344	190	2.460	2	0.118	3–16
2-Propanol	0.546	48.4	82	2.4[e]	1.377	205	5.045	3	0.05	2–13
1-Pentanol	0.568	49.1	138	3.68[e]	1.4101	220	4.590	3	0.001	1.2–10
n-Butanol	0.586	49.7	118	2.6	1.397	210	790	3	0.009	1.4–11.3

2-Butoxyethanol		50.0	171	2.9	1.418		470		0.001	1.1–12.7
1-Propanol	0.617	50.7	97	1.9	1.385	240	1.870	3	0.028	2.1–13.5
Acetic acid	0.648	51.7	118	1.16	1.37	230	—	3	—	4–17
Ethanol	0.654	51.9	78	1.2[e]	1.361	195	7.060	3	0.079	3.4–19
Ethylene glycol	0.790	53.8	197	16.13	1.4385	210	786	2	—	3.2-15.2
2-Methyl-2,4-pentanediol (hexylene glycol)			197	36	1.427		3.692		0.066[e]	1.3–7.4
Methanol	0.762	55.4	65	0.55[e]	1.328	205	5.628	2	0.169	5.4–44
Formamide		55.8	210	3.3	1.447	210	5.800	2	0.004[e]	—
Water	1.000	63.1	100	1[e]	1.333	< 190			0.032	—

a) Polarity estimation according to Reichardt (2003).
b) $E_T(30)$ values measured with the solvatochromic pyridinium-N-phenolate betaine dye $E_T(30)$ according to Reichardt and Schäfer (1995); available online: https://www.uni-marburg.de/fb15/ag-reichardt/et_home ET30.
c) ICH Harmonized Guideline Category 4.4: Solvents for which no adequate toxicological data was found.
d) Severe ecological or toxicological restrictions, banned in many companies.
e) Value for 20 °C.
f) Value for 30 °C.

4.2.2 Safety Concerns

The safety of preparative processes depends on the flammability and toxicity of the solvent. Owing to the huge amounts of solvents handled in preparative chromatography, low flammability should be preferred. Flammability is described by the vapor pressure, the explosion limits, or the temperature class of the solvent. Generally, the use of flammable solvents cannot be avoided, and thus the risk must be minimized by good ventilation and other precautions in the laboratory.

Using higher amounts of alcohols in aqueous buffers may require specific attention regarding explosion protective equipment and environment. The regulations given by the authorities differ from country to country.

The toxicity of the solvent is important with reference to safety at work and product safety. Toxicity is classified, for example, by the LD_{50} value. If no alternative solvent is available, any danger of toxification of the employees during the production process has to be avoided by precautions in the laboratory. The safety of the product is another concern linked to the choice of certain eluents. A contamination of the product might occur through the inclusion of solvent in the solid product due to inadequate drying of the product. The residual amount of solvents in the product is regulated by the different pharmacopoeia as well as the International Guidelines for Harmonization (ICH Guideline Q3C Impurities: Residual Solvents www.fda.gov/cber). Class 1 solvents should be avoided by any means, while the use of class 2 solvents cannot be avoided and, therefore, has to be carefully optimized. If possible, class 3 solvents with low toxic potential should be used. The ICH classification as well as the classification limit of the single solvents in pharmaceutical products is given in Table 4.3. It should be pointed out for those solvents, which are not (yet) listed in the ICH Q3C, the data situation is still insufficient. This does not mean that those solvents are of less concern. It is often better to work with solvents with known, but well-evaluated restrictions instead of solvents, which might be banned in the future due to new findings.

4.2.3 Operating Conditions

For operational reasons, it is important to look at detection properties, purity, recycling ability, and viscosity of the mobile phase. If solvent mixtures are used as mobile phase, the miscibility of the solvents is an absolute condition for their use, which has to be guaranteed for the whole concentration range of the solute as well. For example, acetonitrile and water are miscible, but when sugars are added at high concentrations (e.g. fructose), the system demixes. Table 4.4 lists the major immiscibilities of solvents often used in preparative chromatography. Acetonitrile, methanol, and ethylene glycol are not miscible with the alkanes *n*-pentane, *n*-hexane, isooctane, cyclohexane, cyclopentane, and petroleum ether. The alternative for a mixture of a nonpolar solvent with methanol is *n*-heptane, which has the additional benefit of being an ICH class 3 solvent compared to *n*-hexane, which is categorized in class 2.

The detection system is another boundary condition for the choice of the mobile phase. In most cases, ultraviolet (UV) absorbance or refractive index (RI) detectors are used. An imprecise detection leads to insufficient recognition of

Table 4.4 Limited miscibilities of solvents for preparative chromatography.

Solvent	Not miscible with
Acetonitrile, methanol, ethylene glycol, and water	*n*-Pentane, *n*-hexane, isooctane, cyclohexane, cyclopentane, petroleum ether
Water	Toluene
Solvent	Limited miscibility (solubility g organic solvent/l water)
Water	Diisopropyl ether $2\,g\,l^{-1}$
	Methyl isobutyl ketone (MIBK) $19\,g\,l^{-1}$
	Pentanol $22\,g\,l^{-1}$
	MTBE $48\,g\,l^{-1}$
	EtAc $83\,g\,l^{-1}$
	Methyl acetate $250\,g\,l^{-1}$
	EMK $275\,g\,l^{-1}$

the target substances as well as the impurities, thus causing purity problems. To avoid these problems, the UV cutoff value and the RI are given in Table 4.3 for different pure solvents.

UV detection is based on the UV absorption of the solutes, and, thus, the detection wavelength is determined by the UV spectra of the solutes. The mobile phase must be highly transparent at the detection wavelength. This is most important for solutes with low UV activity, due to missing double bonds. To detect these solutes, it might be necessary to choose a wavelength below 220 nm. In this range, most solvents absorb UV light significantly as well. The UV absorbance of the solvent is described by the UV cutoff value or by plots and tables of absorbance at different wavelengths, which are documented in the technical data sheet of the solvent. The UV cutoff, which is given in Table 4.3 for the most common solvents, is defined as the wavelength at which the absorbance of the pure solvent measured in a 1 cm cell against air reaches 1 absorbance unit (Poole 2003). It represents the lower limit for the wavelength, at which the solvent absorbance is getting problematic. Due to this definition, the solute should have a significant UV absorbance at wavelengths higher than the UV cutoff value. Otherwise, only the absorbance of the solvent is measured, while the solutes cannot be detected. Since the UV cutoff values in Table 4.3 are measured for pure solvents, these data should be regarded as a criterion for the exclusion of UV detection if certain solvents, for example, acetone, are used. For technical solvents, it is advisable to rely on absorbance data in the technical data sheet, because the detection limits of different solvents are influenced by impurities within the solvents. Traces of impurities can increase the UV cutoff by 50–100 nm. For example, saturated hydrocarbons such as *n*-hexane are reasonably transparent down to 190 nm, but even "research-grade" solvents often contain a few tenths of a percent of olefins of similar boiling point (e.g. 1-hexene). This contamination is already sufficient to make the solvent opaque at wavelengths below 260 nm (Snyder and Kirkland 1979). In addition, some

solvents, e.g. ethers, are stabilized with butylhydroxytoluene (BHT), which has a quite high UV activity and has an influence on the solvent transparency as well.

It has to be mentioned that for some separation tasks, also those solvents should be considered, which are not UV transparent below 300 nm. Acetone and other ketones are quite good solvents for a wide variety of compounds and exhibit an elution strength in the medium polarity region. For a preparative separation it could be a good approach to cut fractions during the chromatographic run and analyze them at-line or offline. With modern fast chromatographic methods using monolith or Ultra-High Performance LC (UHPLC), the purity of the fractions can be evaluated in less than one minute, which can be sufficient for fractionation decisions. Combined with an automated fractionation system, real-time monitoring of chromatographic runs is possible. Tiwari et al. have showed one implementation for cation-exchange chromatography (Tiwari et al. 2018).

RI detection depends on the difference in RI of the solute and the solvent. If the RI of the solute is known, a solvent with a significantly different RI, and thus high detection selectivity, should be chosen.

As mentioned before, detection problems can result from impurities in the solvents. For the production of pure substances, nonvolatile impurities in the solvent are also problematic. In most cases, the solvent is removed after separation by evaporation, and thus nonvolatile impurities accumulate in the product fraction. For these reasons, the use of HPLC-grade solvents is recommended, and the availability of appropriate amounts has to be assured.

Dependent on economic pressure, the recycling ability of the solvent is becoming ever more important. Especially in case of production-scale processes, the recycling of the mobile phase is essential for economic success. For solvent recycling, the following rules should be taken into account:

- Prefer pure solvents to binary or ternary mixtures.
- With binary mixtures prefer azeotropic mixtures (as they can be more easily recovered by distillation without readjustment of the composition).
- Prefer solvents with low boiling points and enthalpies of evaporation.

The last decision parameter concerning process operation is the viscosity. Process economy is influenced by the viscosity in two ways. The pressure drop of the system is proportional to the viscosity of the eluent, and, in most cases, the pressure drop is the limiting factor for the flow rate and, thus, productivity. High viscosity mobile phases also show low diffusion of the solutes and thus a worse mass transfer inside the pore system.

Table 4.3 lists the viscosities of pure solvents. For nonaqueous solvent mixtures, they can be calculated with Eq. (4.1) from the viscosities of the pure solvents and their mole fractions X_A and X_B (Snyder, Kirkland, and Glajch 1997):

$$\log(\eta) = X_A \cdot \log(\eta_A) + X_B \cdot \log(\eta_B) \tag{4.1}$$

Especially with strongly associating solvent mixtures (alcohol–water, acetonitrile–water), the viscosity shows anomalous variations with composition. The viscosity of the mixture is very often larger than the viscosity of the pure solvents (Figure 4.7). For example, the maximum viscosity of an ethanol–water mixture is more than twofold higher compared with the pure solvents. Next to
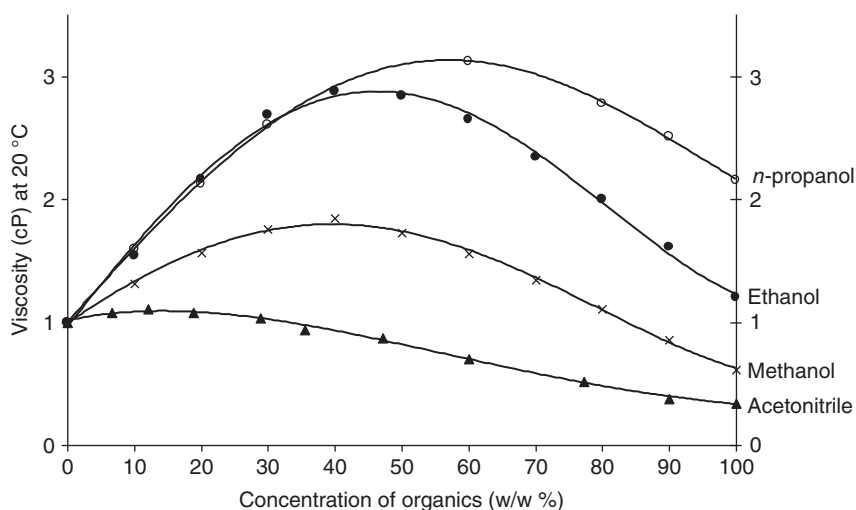
Figure 4.7 Viscosity of different mixtures of water and organic solvents.

the composition, the viscosity is strongly influenced by temperature. At higher temperatures the viscosity reduces dramatically. However, chromatographic processes are very often operated at ambient temperature, because it is difficult and expensive to guarantee a constant elevated process temperature. Gant, Dolan, and Snyder (1979) give further information for a few solvent mixtures.

Table 4.5 shows the retention of human recombinant insulin on PharmPrep® 100 P RP-18, 10 μm at constant conditions with six different organic solvents. Insulin is eluted using a gradient of water with the organic solvent. The retention time of insulin is recorded as well as the amount of the organic solvent at the time of elution and the pressure drop of the system. The flash point of the neat solvent is shown as well. From the data, it can be seen that (if the selectivity for the separation is given) *n*-propanol would be the best solvent. The pressure drop is moderate, the flash point is higher compared to 2-propanol, and the elution

Table 4.5 Elution of recombinant human insulin on PharmPrep® P100 RP-18 using different organic modifiers.

Solvent	Retention time insulin (min)	Percentage organic solvent at elution (%)	Pressure drop at elution (bar)	Flash point (of the neat solvent) (°C)
Acetonitrile	23.6	39	46	2
Methanol	43.96	67	70	15
Ethanol	28.42	45	110	13
1-Propanol	15.36	27	85	25
2-Propanol	18.97	32	108	12
Hexylene glycol	21.67	36	139	98
Hexylene glycol (at 50 °C)	19.85	33	78	98

is the fastest; therefore only 27% of organic solvent is needed for elution of the main peak.

One interesting alternative could be hexylene glycol (2-methyl-2,4-pentanediol) if the separation can be operated under elevated temperature. Hexylene glycol has a boiling point of 197 °C, but with molecules of 1000 or more Dalton, the product recovery can be easily achieved by tangential flow filtration (TFF), avoiding the need for solvent evaporation (EMD Millipore 2017) or by crystallization using 2 mg of $ZnCl_2$ per mg of insulin.

4.2.4 Aqueous Buffer Systems

The choice of aqueous buffer systems depends on different factors: protein stability, resin performance, wastewater treatment, and standard operation conditions, for example, standardization of solvents in a production facility.

The most common buffer systems used in biochromatography are listed in Table 4.6.

Positively charged buffering ions should be used on anion exchangers to avoid an interaction or binding to the functional group. Therefore, Tris (pK_a 8.2) is preferred with Cl^- as counterion. For cation exchangers, the buffering ion should be negatively charged, for example, carbonate, acetate, or MES, and the counterion is K^+ or Na^+. Phosphate buffers are generally used on both exchanger types. The buffer concentration is in the range of 10–50 mM.

In addition to the buffering salts, special additives are used in some cases to stabilize the target protein or to enhance the elution and selectivity. Table 4.7 lists

Table 4.6 Common buffer compounds used in biochromatography.

Common name	pK_a at 25 °C	Buffer range	Molecular weight	Full compound name
Phosphate	2.15	1.7–2.9	94.9	
Glycylglycine	3.14	2.5–3.8	132.1	2-[(2-Aminoacetyl)amino]acetic acid
Acetate	4.76	3.6–5.6	60.05	
Maleate	5.13	4.0–6.0	116.05	
MES	6.15	5.5–6.7	195.2	2-(*N*-Morpholino)ethanesulfonic acid
Citrate	6.40	5.5–7.2	192.1	
PIPES	6.76	6.1–7.5	302.4	Piperazine-*N*,*N*′-bis(2-ethanesulfonic acid)
SSC	7.0	6.5–7.5	189.1	Saline sodium citrate
MOPS	7.20	6.5–7.9	209.3	3-(*N*-Morpholino)propanesulfonic acid
HEPES	7.55	6.8–8.2	238.3	4-2-Hydroxyethyl-1-piperazineethanesulfonic acid
Tricine	8.05	7.4–8.8	179.2	*N*-Tris(hydroxymethyl)methylglycine
Tris	8.06	7.5–9.0	121.14	Tris(hydroxymethyl)methylamine
Bicine	8.35	7.6–9.0	163.2	*N*,*N*-Bis(2-hydroxyethyl)glycine
TAPS	8.43	7.7–9.1	234.3	3-{[(Tris(hydroxymethyl)methyl]amino} propanesulfonic acid

Table 4.7 Buffer additives.

Additive	Typical concentration	Effect
2-Mercaptoethanol	10 mM	Prevent protein oxidation
Dithiothreitol (DTT)	1 mM	Prevent protein oxidation
Glycerol	20%	Polarity reductant, reduces hydrophobic interactions
MgCl$_2$	5 mM	Chaotropic salt; enhances solubility for hydrophobic proteins
Benzamidine-HCl	1 mM	Serine protease inhibitor
Chymostatin	10 µg ml^{-1}	Peptide protease inhibitor
Ethylenediaminetetraacetic acid (EDTA)	2 mM	Bind heavy metals, avoid poisoning of sensitive proteins, deactivate metalloproteases, reduce sulfhydryl oxidation
Triton	0.5%	Nonionic detergent, relaxing hydrophobic interactions
Sodium cholate	0.25%	Ionic detergent, relaxing hydrophobic interactions
α-Methyl mannoside	0.25 M	Elution buffer, esp. for Con A affinity chromatography
Sodium azide	0.02%	Prevent bacterial growth (not to be used with peroxidases and heme proteins)

some of these additives together with the effect they are offering. As any additive is increasing the complexity of the chromatographic system, it should be carefully considered if the result is justifying its introduction.

Especially for the expensive protein A resins, an intermediate wash might be used to elute host cell proteins from the capture column and thus increase the number of cycles the protein A resin can be used. Li summarized eight different reagents, which are listed in Table 4.8 (Li 2017).

Table 4.8 Reagents used for the intermediate wash of protein A resins.

Additive	Concentration	References
Arginine	0.1–1 M	Chollangi et al. (2015) and Holstein, Cotoni, and Bian (2015)
Guanidinium HCl	1 M	Holstein, Cotoni, and Bian (2015)
Isopropanol	5–20%	Shukla and Hinckley (2008)
NaCl	0.1–2 M	Holstein, Cotoni, and Bian (2015)
Propylene glycol	5–20%	Chollangi et al. (2015)
Triton X-100	<1%	Chollangi et al. (2015)
Tween-80	1%	Shukla and Hinckley (2008)
Urea	0.5–3 M	Shukla and Hinckley (2008) and Chollangi et al. (2015)

4.3   Adsorbent and Phase Systems

The last two sections (4.1 and 4.2) characterized the elements of a chromatographic system and discussed different separation tasks. This section provides guidelines to develop the chromatographic system for a given separation problem. The classical recommendation for preparative separations performed by elution chromatography is as follows:

Find a mobile phase with high solubility, a compatible stationary phase, and then optimize selectivity, capacity, and efficiency followed by a systematic increase in column load.

This is certainly true for the technical and production scale domain, but for high-throughput separations or other projects, where time dominates productivity, other solutions have to be applied based on limited or even not optimized methods.

These two main fields of application for chromatography result of course in a dissimilar approach to selecting the chromatographic system. If time pressure minimizes the possible number of experiments, the use of generic gradient systems (Section 4.3.4) is recommended. In such cases, solubility problems are also important, but they should be solved quickly (Section 4.3.2) and not by extensive solubility studies.

For production-scale processes, economic pressure arises, and thus a successive optimization of the chromatographic system will pay off by a reduction in operating costs. Therefore, the development of the chromatographic system has to start with the search for a suitable mobile phase with high solubility for the given solute (Section 4.3.1) and a compatible adsorbent. Dependent on the nature of the phase system, the separation is optimized by adjusting the mobile phase composition (Sections 4.4–4.6).

4.3.1   Choice of Phase System Dependent on Solubility

The most important step in developing a chromatographic system is the choice of mobile phase. Although the mobile phase influences the separation process in many ways, the main decision parameters for the choice of the mobile phase are the maximum solubilities c_s of the target components and the selectivity of the separation. Solubility is essential for the productivity of the chromatographic separation process, because it is a precondition for exploiting the whole range of column loadability.

An old alchemist maxim, "similia similibus solvuntur" ("like dissolves like"), is the oldest rule for selecting suitable solvents, meaning that the nature of the solute determines the nature of the solvent. Due to the classification of phase systems in Section 4.3, organic and aqueous solvents are distinguished. Nonpolar to medium-polar substances show best solubility in typical organic solvents, while medium-polar to polar substances show best solubility in aqueous solvents.

Referring to this differentiation in the nature and the polarity of suitable solvents, a first classification concerning the adsorbent and thus the phase system can be made. Figure 4.8 describes how the solvent and the nature of the separation
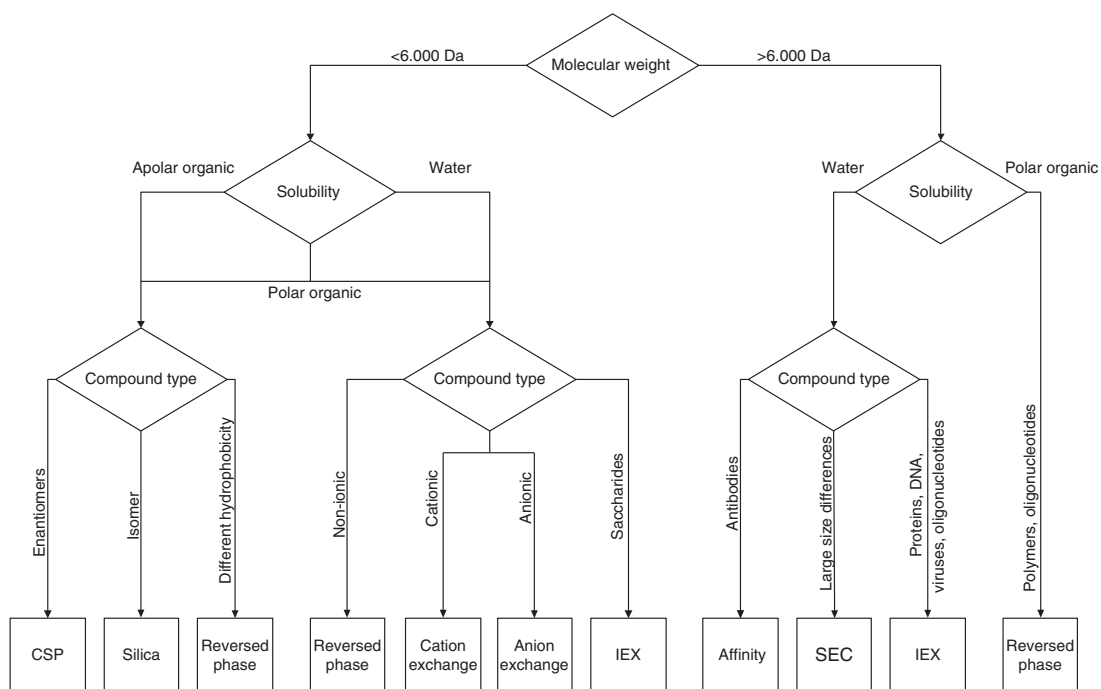
Figure 4.8 Selection of phase systems dependent on the separation problem.

problem influence the choice of adsorbent. Separation of enantiomers needs chiral stationary phases (CSPs), which will be discussed in Section 4.6.

Normal phase (NP) systems are used for the separation of nonionic, apolar to medium-polar samples. If the sample is soluble in organic solvents, an NP system should be applied as a first test system (e.g. silica and organic mobile phase). However, if the sample shows best solubility in aqueous solvents, the sample is quite polar. In this case, reversed phase (RP) systems with semipolar (cyano, amino, or diol) or apolar packings such as alkyl silica should be used.

Solvent mixtures are often used to obtain a desirable chromatographic separation. For this reason, the elution strength of the strong solvent with high solubility is adjusted by a weaker solvent. Water is used in RP chromatography, while heptane, hexane, or cyclohexane is used for NP systems. For solvent mixtures, the dependency of the solubility on the solvent composition is very important. Good solubility results, in most cases, in low retention and thus poor separation. Usually, the weaker solvent according to the elution strength possesses less solubility, and thus the choice of the solvent is a compromise between retention and solubility.

For example, in RP chromatography, very often organic solvents and water are used. The solubility in the organic solvent is higher and water is used to adjust retention and selectivity. Figure 4.9 shows a typical plot for the dependence of the solubility of a pharmaceutical intermediate on both the volume fraction ϕ of methanol in a mixture with water and the temperature. Generally, solubility increases with temperature, and, in most cases, it increases for high fractions of methanol.

4.3.2 Improving Loadability for Poor Solubilities

Although high solubility should be preferred for good productivities, time pressure and thermodynamics can require the acceptance of poor solubilities.
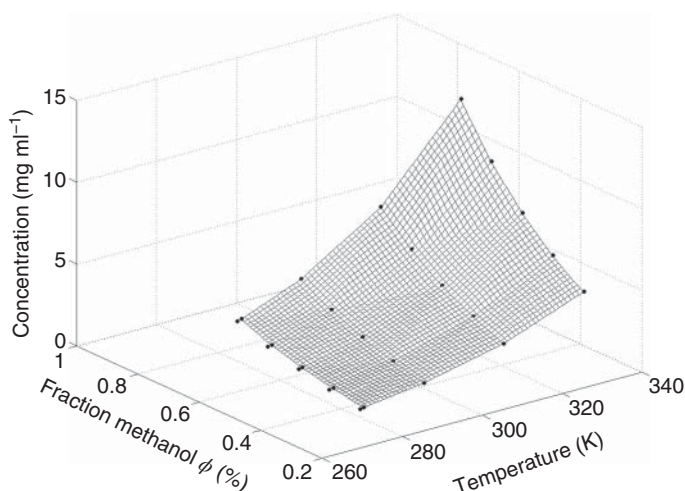

Figure 4.9 Influence of methanol content and temperature on solubility.

Nearly half of R&D laboratories involved in preparative chromatography examine 10–100 samples per day, and the number of candidates for preparative separation is still increasing (Neue et al. 2003). Obviously, time and large amounts of sample cannot be spent for systematic evaluations and tedious solubility studies. Very often, the amount of sample is also too small to carry out extensive experiments.

Cases of severe solubility limitations (<5 g l^{-1}) are handled in different ways. First, the sample may be dissolved in a solvent different from the mobile phase, for example, the sample solvent may be 100% organic and quite different from the mobile phase. In most cases, this solvent is, in addition to its high solubility, also a much stronger chromatographic solvent than the mobile phase. In such a case, large sample injections into the mobile phase may have an adverse effect on the separation process. Peak shapes may be badly distorted, and the sample may even precipitate in the mobile phase, if it is only slightly soluble in the mobile phase.

Figure 4.10 shows the separation of a pharmaceutical agent on an analytical alkyl-silica column (Purospher® STAR RP-18e, 100 mm long, internal diameter 4 mm). The sample was dissolved in pure methanol and between 5 and 250 µl was injected, while the mobile phase consists of methanol and water (60 : 40 volumetric ratio). At small injection volumes, no peak distortion is observed, but with 30 µl the chromatogram shows a distortion of the main peak and band splitting. A small part of the sample elutes unretained with the dead time of the column. The strong injection solvent displaces the sample until the sample and the solvent are sufficiently diluted with the mobile phase solvent. At high injection volumes, methanol and the sample are no longer diluted, and, thus, a front of both migrates through the bed. This behavior is can be seen between 40 and 80 s elution time in Figure 4.10.
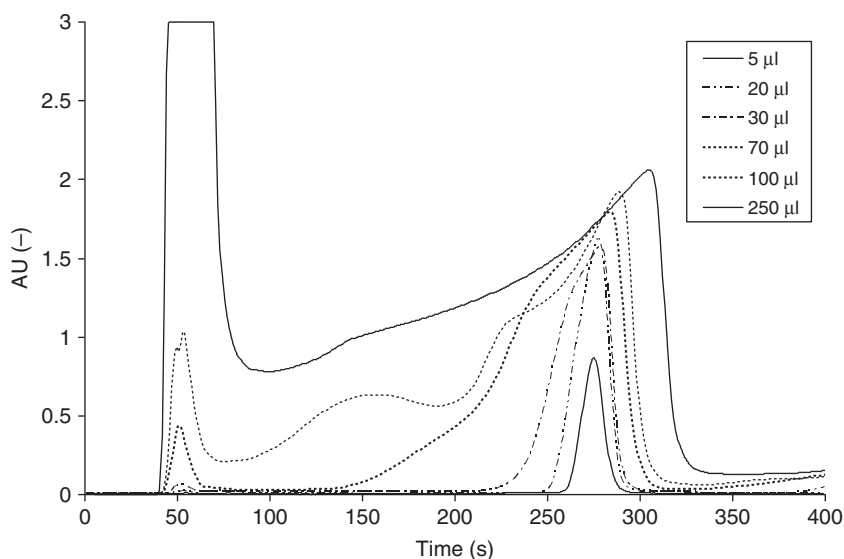

Figure 4.10 Peak distortion due to injection of sample dissolved in pure methanol (Purospher STAR RP-18; methanol–water, 60 : 40).

These problems are intensified if the sample is dissolved in a solvent completely dissimilar to the mobile phase solvents. Many samples delivered for preparative separations are dissolved in common universal organic solvents such as dimethyl sulfoxide, dimethylformamide, or other polar organic solvents (Neue et al. 2003). Guiochon and Jandera have examined the influence of sample solvent and advise avoiding injections with a solvent of higher elution strength than the mobile phase, especially at high sample loads (Jandera and Guiochon 1991). Injection of a large volume of the saturated mobile phase is preferred.

Peak distortion and precipitation problems due to injection of solvents of high solubility (Fig 4.11a) can be defused by changing the injection technique. Figure 4.11b shows the principle of the at-column-dilution (ACD) technique. Sample is dissolved in a strong solvent, but, before it is injected into the column, it is mixed with the weak solvent to adjust the solvent strength to the mobile phase. The solubility of the sample in the mixture is of course decreased, but due to the short path between the mixing point and the packed bed, the growth of particles large enough to clog the frits can be excluded, especially since precipitate formation is preceded by a supersaturated solution (Neue et al. 2003). ACD significantly increases the amount of sample that can be purified relative to conventional injection methods. A desirable peak shape is obtained for the ACD technique although the separation is performed at mass loadings more than 10 times greater than conventional loading where the conventional chromatographic separation already fails (Szanya et al. 2001).

Another method for separating low-solubility samples, which is well known in the downstream processing of biopolymers, starts with a large volume of sample dissolved in a chromatographically weak solvent. This solution is fed to the column. As the solute has a relatively strong affinity to the stationary phase, for example, silica, it is adsorbed and concentrated at the column inlet. This has the effect of introducing the sample as a concentrated plug.
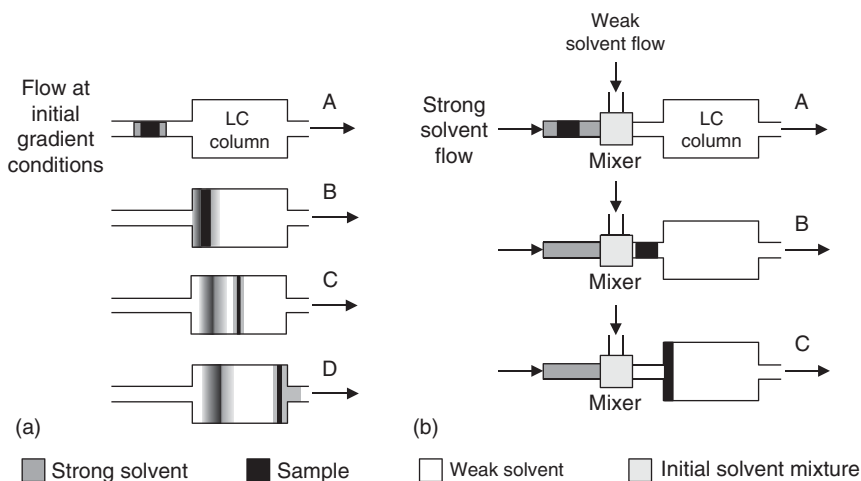

Figure 4.11 Scheme of conventional column loading (a) and at-column dilution (b).

When enough sample solution has been injected, the solvent is changed to a chromatographically stronger mobile phase. The sample is thus eluted with a high concentration in a step-gradient-type procedure. When this technique is used, coarse filtration of the original sample solution is advisable to prevent solid material entering the system.

4.3.3 Dependency of Solubility on Sample Purity

During scale-up of a multistep chemical synthesis, the chemical purity of samples is often very variable. This is a major issue for process optimization of chromatographic processes as chemical impurities can strongly influence a sample's solubility. The solubility of the sample can decrease dramatically when it becomes purer.

Figure 4.12 shows the quantitative analysis of the racemic pharmaceutical intermediate HG290 to determine its maximum solubility. Two different samples, with 90% and 100% purity, have been available. For both samples, a big excess of the solid compound was dissolved under slight agitation for 24 hours in the solvent. It has to be assured that a residue remains at the bottom of the sample vial to achieve a saturated solution. After 24 hours a sample of the clear supernatant is taken and analyzed by HPLC. The peak areas in Figure 4.12 show that the solubility is about two times higher for the sample with 90% purity.

In production-scale processes, the purity of the samples also depends on the quality of the raw material (e.g. educts for chemical reactions) as well as on the equipment used. To avoid problems in the subsequent separation process, the influence of purity on solubility must be checked after the first amounts of the actual sample are available.
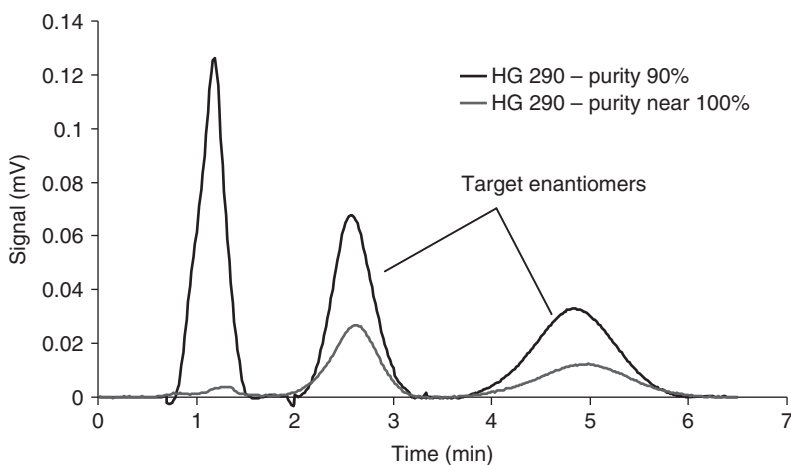

Figure 4.12 Maximum solubility of a sample for two different purities; sample volume 20 μl. Source: Courtesy of H. Gillandt SiChem GmbH, Bremen.

4.3.4 Generic Gradients for Fast Separations

For components to be isolated in the milligram to gram range, tedious method development is not advisable as these components have to be delivered under time pressure and not with maximum economy. Specialized laboratory units that perform high-throughput purification are often operated within the pharmaceutical industry.

A fast solution for these separation problems is the use of generic gradients. Table 4.9 lists typical solvents and conditions for gradient runs for RP and NP systems.

Gradient separations always start with a mobile phase composition of 90–100% of the solvent with low elution strength (weak solvent). This leads to the highest possible retention at the beginning. For instance, RP systems start with 100% water, if the stationary phase can tolerate this high amount of water without any collapse of the alkyl chains. Otherwise, water has to be mixed with a small amount of an organic solvent. Section 4.5.2 describes the development of a typical RP gradient. The sample should be injected in a solvent composition with weak elution strength. Otherwise the sample breaks through with the front of the injection solvent. Solvent strength is now increased linearly by increasing the volume fraction of the solvent with high elution strength. The mobile phase composition is linearly changed to 100% of the strong solvent during the so-called gradient time, t_g. This gradient time should be adjusted to 10- to 15-fold of the dead time of the column.

4.4 Criteria for Choosing Normal Phase Systems

NP systems consist of a polar adsorbent and a less polar mobile phase. Because these were the first available chromatographic systems, they were named NP systems. They are, for instance, silica gels or other oxides in conjunction with a nonpolar solvent such as heptane or hexane or some slightly polar solvents such as dioxane. Semipolar adsorbents such as cyano or diol phases can be operated in the NP mode as well. NP systems have excellent separating power characteristics for samples with low to moderate polarity and intermediate molecular weight (<1000 Da). As long as the sample to be separated does not contain extremely polar or dissociating functional groups, it is the method of choice for preparative

Table 4.9 Typical gradient runs for reversed and normal phase systems.

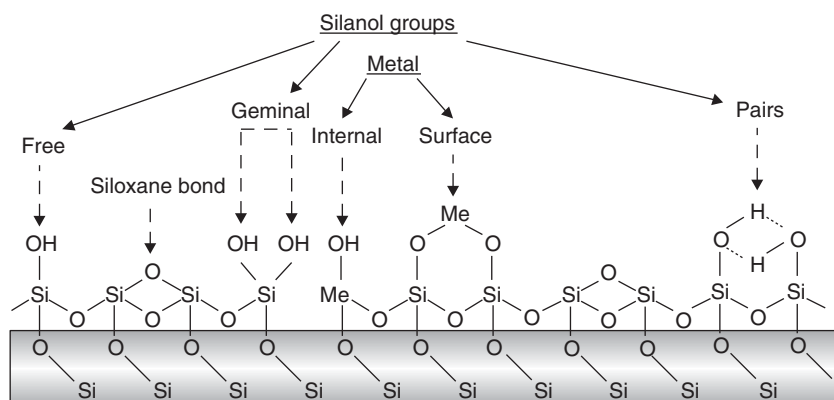| Phase system	Adsorbent	Weak solvent	Strong solvent
Reversed phase	RP-18, RP-8	Water	Acetonitrile
Reversed phase	RP-18, RP-8	Water	Methanol
Reversed phase	RP-18, RP-8	Dichloromethane	Acetonitrile
Normal phase	Silica	Heptane	Ethyl acetate
Normal phase	Silica	Dichloromethane	Methanol

Figure 4.13 Surface groups on silica.

chromatographic applications. In general, small organic molecules have better solubility in organic solvents than in the water-based mobile phases used in RP chromatography.

In addition, more product can be loaded on a silica gel than on RP materials. Furthermore, the separated products are readily recovered by simple evaporation procedures, while the isolation of products from an RP separation process often requires additional work-up steps. These steps include the removal of salts or other aqueous phase additives and extraction of the target product after evaporation of the organic phase (Section 4.5.5).

The combination of water and silica is not recommended due to the strong interaction between water and adsorbent. Furthermore, silica is slightly soluble in water (strongly depending on the pH value!), which results in a shortened lifetime of the adsorbent. NP systems are limited to organic solvents, and thus the solutes have to be soluble in these solvents.

The interaction mechanism in NP chromatography is adsorption on the polar surface of the adsorbent. Because silica is the most widespread NP adsorbent, the following focuses on the use of silica. As mentioned in Section 3.2.4, active centers for adsorption are statistically spread over the surface of the silica. Generally, these are siloxane groups and different kinds of silanol groups (Figure 4.13). The silanol groups appear as single (free) or as pairs. Single silanol groups have the strongest polarity, while the polarity of silanol pairs is reduced. Impurities such as metal atoms (Ca, Al, or Fe) produce a disturbed surface chemistry and the formation of polarity hot spots, resulting in unwanted strong adsorption on these sites.

Obviously, due to the polar surface, only polar parts of solutes interact with the adsorbent, while nonpolar groups such as alkyls are not adsorbed. This behavior determines the range of applications for NP chromatography. For instance, it is not suitable for the separation of homologues that only differ in the length of an alkyl group. Conversely, solutes that differ in the number, nature, or configuration of their substituents are mainly separated by NP chromatography. This includes the separation of stereoisomers, if they are not enantiomeric. This

stereoselectivity can be explained by the isotropic nature of the adsorption on silica. Silanol groups are rigidly fixed on the surface, and due to the short bond length of the silanol groups, the interaction between the solute and surface is very isotropic.

Aqueous mobile phases are not used because the interaction between water and the polar stationary phase would be too strong. However, a minimal amount of water is needed to saturate the abovementioned hot spots of polarity due to metal atoms. For these two reasons the water content of the solvents should be controlled very carefully. Changes in the range of a few ppm, resulting, for example, from air humidity or the quality of the used solvent, can cause significant changes in retention time and peak shape. As a result of this sensitivity to changes in water content, the equilibration time for the system is very high, particularly when nonpolar solvents such as *n*-hexane are employed. A constant baseline and system behavior is reached after about 50 column volumes, while Poole (2003) remarked that column equilibration for mobile phases of different hydration level takes at least 20 column volumes.

4.4.1 Retention in NP Systems

Different models have been developed to describe the retention of substances in adsorption chromatography. The Snyder model (Figure 4.14) assumes that in liquid–solid chromatography the whole adsorbent surface is covered with a monolayer of solvent molecules and the adsorbent together with the adsorbed monolayer has to be considered as the stationary phase (Snyder 1968; Snyder and Kirkland 1979; Snyder, Kirkland, and Glajch 1997). Adsorption of the sample occurs by the displacement of a certain volume of solvent molecules from the monolayer by an approximately equal volume of sample, by which these molecules can adsorb on the adsorbent and become part of the monolayer. In
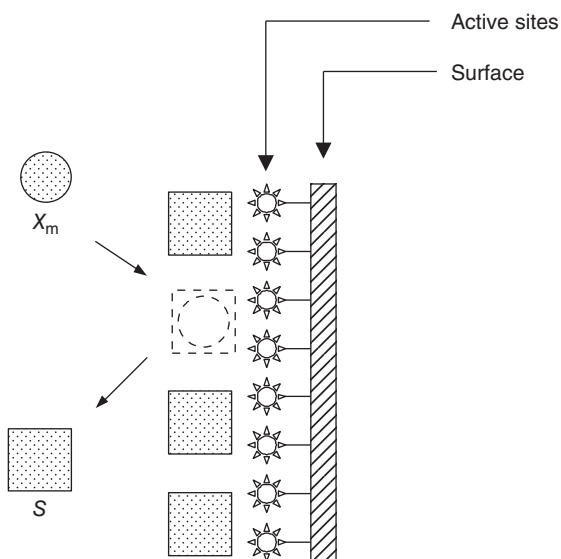

Figure 4.14 Graphical representation of the adsorption process.

this model, product retention is always caused by the displacement of solvent molecules from the monolayer.

Snyder's model provides a good understanding of separations on alumina as the adsorbent and is fairly good at explaining separations on silica gel using weak solvents. An almost similar model developed by Soczewinski (1969) is more suitable for separations on silica gel using strong eluents.

In contrast, the Scott–Kucera model considers a solvent system composed of an apolar solvent A and a polar solvent B (Scott and Kucera 1975). When this mixture is pumped through a column, a monolayer of the most polar solvent B is formed by adsorption of B on the adsorbent. Sample molecules are adsorbed on this monolayer instead of on the adsorbent surface. In other words, there is no displacement of adsorbed solvent molecules, and interaction between the molecules of the monolayer and the sample molecules determines the retention of the component. This theory has been adapted by saying that the model is only valid for medium-polar mobile phases and solutes with a polarity lower than the most polar solvent in the eluent. These medium-polar solvents are called hydrogen bonding solvents (esters, ethers, ketones). A monolayer of these solvents behaves as a hydrogen-bonding phase. Interaction between this monolayer and the product molecules takes place mainly by means of hydrogen bonding. When the monolayer of strong solvent B is completely formed, a second layer comes into being. Advancement in the buildup of this second layer determines whether the sample can displace solvent molecules. However, product molecules will never displace solvent molecules from the monolayer as long as the sample molecules are less polar than the strongest solvent in the eluent.

As already described, molecules of the mobile phase and solute compete for the active sites of the adsorbent. The competition is represented by Eq. (4.2) (Snyder 1968):

$$X_{\mathrm{m}} + n S_{\mathrm{ads}} = X_{\mathrm{ads}} + n S_{\mathrm{m}}. \tag{4.2}$$

Here X_{m} and X_{ads} represent the sample molecule in the mobile phase and the adsorbed state, respectively. S_{m} and S_{ads} represent the corresponding states of the mobile phase molecules; n is the number of solvent molecules that have to be displaced to accommodate the sample molecule.

Equation (4.3) gives the equilibrium, which shows that the relative interaction strength of the solvent and the sample molecules for the active sites of the adsorbent determine the retention of a product:

$$K = \frac{(X_{\mathrm{ads}}) \cdot (S_{\mathrm{m}})^{n}}{(X_{\mathrm{m}}) \cdot (S_{\mathrm{ads}})^{n}}. \tag{4.3}$$

Both silica and aluminum oxide contain surface hydroxyl groups and possess some possibilities of Lewis acid–base type interaction, which determine their adsorption characteristics. The more the hydroxyl groups, the stronger a solute molecule will be retained. The number and the topographical arrangement of these groups determine the activity of the adsorbent.

Silica and alumina have the highest surface activity when the adsorbents are free of physisorbed water. Addition of water blocks the most active sites on the surface since water as a polar adsorptive is preferentially adsorbed. Other polar

compounds such as alcohols can also adsorb irreversibly at the surface. Consecutive adsorption of water deactivates the adsorbent surface and the solute retention will decrease concurrently. For this reason, the water content of the mobile phase solvents should be controlled carefully if an apolar mobile phase is used (Unger and Weber 1999). The water content only influences retention when apolar eluents such as hexane or heptane are used. When these solvents are mixed with 10% or more of a moderately polar solvent (e.g. acetone, ethyl acetate), the dependency disappears. The influence can be decreased by the addition of a small amount of acetonitrile to the mobile phase.

The steric orientation of the functional groups in the solute molecule in relation to the spatial arrangement of the hydroxyl groups on the surface enables silica and alumina to separate isomeric components (e.g. cis–trans/positional isomers).

4.4.2 Solvent Strength in Liquid–Solid Chromatography

Knowing that the solvent and the solute compete for active sites of the adsorbent, it is easily understood that the more the mobile phase interacts with the adsorbent, the less a solute molecule is retained. Therefore, the major factor determining product retention in adsorption chromatography is the relative polarity of the solvent compared with the solute.

It is possible to set up a polarity scale by empirically rating solvents in order of their strength of adsorption on a specific adsorbent. A solvent of higher polarity will displace a solvent with a lower rank on the polarity scale. Solvents ranked according to such a polarity scale form an eluotropic series.

Table 4.10 gives an eluotropic series developed for different NP sorbents. The ε^0 value in Table 4.10 called the "solvent strength parameter" is a quantitative representation of the solvent strength and can be used for the calculation of retention factors for different solvent compositions. Assuming that the adsorbent surface is energetically homogeneous and the solute–solvent interaction mechanism in the mobile phase does not influence interactions in the adsorbent phase, Poole (2003) recommends the following empirical equation (Eq. (4.4)) for binary mixtures:

$$\log k_2' = \log k_1' + aA_s(\varepsilon_1^0 - \varepsilon_2^0) \tag{4.4}$$

Here ε_1^0 and ε_2^0 are the solvent strength parameters for the mixture, while k_1' and k_2' represent the retention factors for the solute S, which occupies the surface cross section A_s at the stationary phase; a stands for the activity parameter of the adsorbent phase (Eq. 4.5).

Values in the table only serve as a guide because the relative polarity can change, depending on the type of sample and adsorbent.

An eluotropic series is a tool to adjust the retention of sample components. If the retention of a product has to be reduced, a solvent of higher ranking in the eluotropic series is chosen. Due to increased competition between product and solvent molecules for the active sites on the adsorbent, the retention factor of the product will automatically decrease. The same holds true for the opposite situation.

Table 4.10 Eluotropic series for alumina and silica.

Solvent	$\varepsilon^0_{Al_2O_3}$	$\varepsilon^0_{SiO_2}$
n-Pentane	0.00	0.00
n-Hexane	0.01	0.01
Isooctane	0.01	0.01
Cyclohexane	0.04	0.03
iso-Propyl ether	0.28	
Toluene	0.29	0.22
Diethyl ether	0.38	0.43
Dichloromethane	0.42	0.32
Methyl *iso*-butyl ketone	0.43	
Methyl ethyl ketone	0.51	
Triethylamine	0.54	
Acetone	0.56	0.53
Methyl acetate	0.60	
Dioxane	0.61	0.51
1-Pentanol	0.61	
Tetrahydrofuran	0.62	0.53
Ethyl acetate	0.62	
Methyl-*t*-butyl ether	0.62	0.48
Diethyl amine	0.63	
Acetonitrile	0.65	0.52
2-Methoxyethanol	0.74	
1-Propanol	0.82	
2-Propanol	0.82	0.60
Ethanol	0.88	
Methanol	0.95	0.73
Ethylene glycol	1.11	
Acetic acid	Large	

According to Snyder (1968), it is possible to calculate the solvent strength of binary mixtures using Eq. (4.5):

$$\varepsilon^0_{ab} = \varepsilon^0_a + \frac{\log[N_b \cdot 10^{a \cdot n_b} \cdot (\varepsilon^0_b - \varepsilon^0_a) + 1 - N_b]}{a \cdot n_b}. \tag{4.5}$$

Here n_b describes the molecular cross section occupied on the adsorbent surface by the solvent molecule b in units of $0.085\,nm^2$ (which is 1/6 of the area of an adsorbed benzene molecule, corresponding to the effective area of an aromatic carbon atom on the adsorbent surface), while the parameter a describes the activity parameter of the adsorbent surface. The adsorbent activity parameter is a measure of the adsorbent's ability to interact with adjacent molecules of solute

or solvent and is constant for a given adsorbent. For silica gel a value of 0.57 is given by Poole (2003). The molar solvent ratio is calculated by Eq. (4.6) with the molar volumes of the molecules (Eq. (4.7)):

$$N_b = \text{molar solvent ratio} = \frac{\text{Volume \% } B \cdot \left(\frac{1}{V_b}\right)}{\text{Volume \% } B \cdot \left(\frac{1}{V_b}\right) + \text{Volume \% } A \cdot \left(\frac{1}{V_a}\right)} \quad (4.6)$$

$$\left(\frac{1}{V_a}\right) \text{ and } \left(\frac{1}{V_b}\right) = \frac{\varrho(\text{density})}{MW(\text{molecular} - \text{weight})} \quad (4.7)$$

In the following example, the solvent strength of a mixture of dichloromethane and methanol with 90% (v/v) dichloromethane is calculated.

Dichloromethane		Methanol
$\varepsilon_a^0 = 0.42$	and	$\varepsilon_b^0 = 0.95$
$n_a = 4.1$	and	$n_b = 8$
$a = 0.7$		

$$\left(\frac{1}{V_a}\right) = \frac{1.325(\text{g ml}^{-1})}{84.93 \text{ g mol}^{-1}} = 0.0157 \text{ mol ml}^{-1} \text{ and}$$

$$\left(\frac{1}{V_b}\right) = \frac{0.79 \text{ g ml}^{-1}}{32 \text{ g mol}^{-1}} = 0.0249 \text{ mol ml}^{-1}$$

$$N_b = \frac{10 \times 0.0249}{10 \times 0.0249 + 90 \times 0.00157} = 0.1489$$

$$\varepsilon_{ab}^0 = 0.42 + \frac{\log(0.1498 \times 10^{0.78} \times (0.95 - 0.42) + 1 - 0.1498)}{0.7 \times 8}$$

$$= 0.42 + 0.38 = 0.80$$

For practical use, nomograms have been calculated, which show the equivalent solvent strength for different binary mixtures. Figure 4.15 shows the nomograms for NP chromatography using *n*-hexane or dichloromethane as the main solvent with different solvent modifiers. If, for example, a solvent strength of 0.4 is achieved with a binary mixture of 17% 2-propanol in dichloromethane, the same solvent strength can be achieved with 25% THF in *n*-hexane or only 1% methanol in dichloromethane, leading to totally different solubilities for the mixture to be separated.

4.4.3 Pilot Technique Thin-Layer Chromatography Using the PRISMA Model

Thin-layer chromatography (TLC) is a simple, fast technique that often provides complete separation of fairly complex mixtures. Any sample type that has been successfully separated by TLC on silica or alumina plates can be separated by means of liquid chromatography.
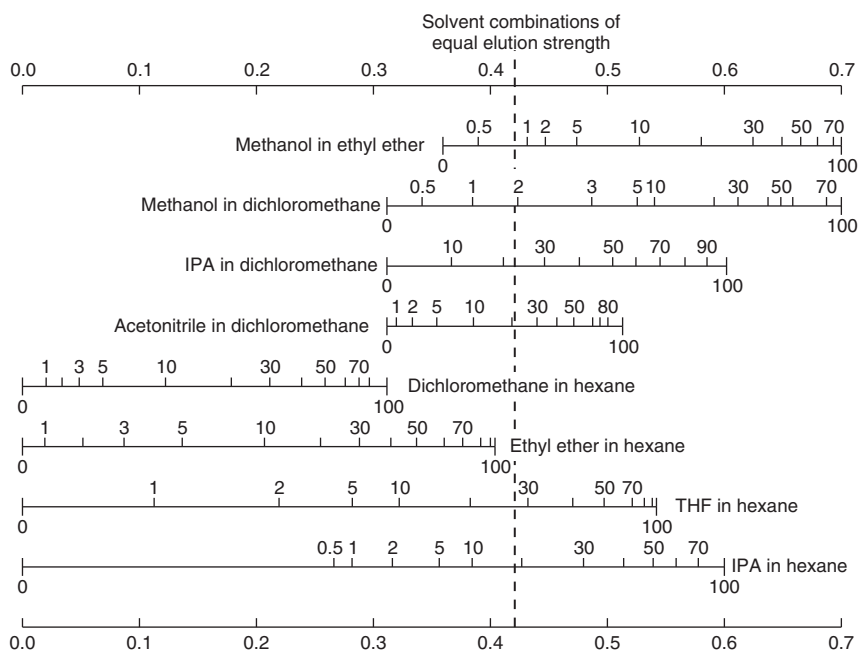
Figure 4.15 Nomograms for binary mixtures of *n*-hexane and dichloromethane with different solvent modifiers. (Source: Sadek (2002). Reproduced with permission of John Wiley and Sons).

Mobile phase optimization using HPLC can easily be carried out using fully automated instruments, but this approach is extremely time consuming. Conversely, modern thin-layer chromatographic techniques allow several mobile phases to be tested in parallel within a very short period of time. Furthermore, different methods are available to visualize the sample components, and the thin-layer chromatogram immediately provides information about the presence of products in the sample that remain at the point of application.

Taking some basic rules into account, the mobile phase composition established by means of TLC can be used directly for preparative chromatographic applications. A pragmatic approach using TLC as a pilot technique for NP preparative chromatographic separations is elucidated in this chapter.

Similar to the retention factor in HPLC, the retardation factor R_f describes retention behavior during TLC experiments. It represents the ratio of the distance migrated by the sample to the distance traveled by the solvent front. Boundaries are $0 < R_f < 1$. For $R_f = 0$, the product does not migrate from the origin, and for $R_f = 1$, the product is not retained. R_f values are calculated to two decimal places, while some authors prefer to tabulate values as whole numbers, as hR_f values (equivalent to $100R_f$) (Poole 2003).

Before starting extensive experiments, a procedure recommended by Kaiser and Oelrich (1981) to rule out adsorbents by fast experiments should be employed. Each elution experiment takes about 20 seconds. For this purpose, samples are applied on a 50×50 mm TLC plate at nine points, which are exactly

10 mm apart. Five microliters of methanol is drawn into a microcapillary with a platinum−iridium point. By applying the point of the filled capillary on one of the sample points on the plate, methanol is introduced onto the plate. A miniature radial chromatogram of about 7 mm diameter is produced. If the sample components remain at the point of application, the use of this adsorbent type is ruled out for HPLC usage. To make sure, the procedure is repeated with 5 μl of acetonitrile and THF, respectively. If the products still remain at the point of application, the situation will not be changed by using any other mobile phase that is suitable for preparative chromatography work.

However, if the entire sample migrated to the outer ring with methanol, the test is repeated with *n*-heptane. If the entire sample still migrates to the outer ring, then the used adsorbent is again ruled out as stationary phase. If, with *n*-heptane, the entire sample or part of it remains at the starting point, the unlimited possibilities of combining solvents can be exploited to further optimize the method (Kaiser and Oelrich 1981).

The PRISMA model developed by Nyiredy and coworkers Nyiredy et al. (1985), Dallenbach-Tölke et al. (1986), Nyiredy and Fater (1995), and Nyiredy (2002) for use in over pressured layer chromatography is a three-dimensional model that correlates solvent strength and the selectivity of different mobile phases. Silica is used as the stationary phase, and solvent selection is performed according to Snyder's solvent classification (Table 4.11).

The PRISMA model is a structured trial-and-error method that covers solvent combinations for the separation of compounds from low to high polarity. Initial experiments are done with neat solvents, covering the eight groups of the Snyder solvent classification triangle (Figure 4.16). The solvents are grouped according to their proton acceptor and donor functionality as well as their dipole moment into eight groups. To obtain improved selectivities, mobile phase mixtures should consist of solvents from different groups instead of mixing two solvents from the same group.

The PRISMA model (Figure 4.17a) has three parts: an irregular truncated top prism, a regular middle part with congruent base and top surfaces, and a platform symbolizing the modifier. The model neglects the contribution of the modifier to the solvent strength, because modifiers are usually only present in a low and constant concentration. In NP chromatography, the upper frustum is used in optimizing mobile phases for polar and/or semipolar substances. The regular central part of the prism is used in solvent optimization for apolar and semipolar components.

The three top corners of the model represent the selected undiluted neat solvents. The corner to the longest edge of the prism (A) represents the solvent with the highest strength, while the solvent with the lowest strength (C) corresponds to the corner of the shortest edge. Because the three selected solvents have unequal solvent strengths, the length of the edges of the prism are unequal, and the top plane of the prism will not be parallel and congruent with its base. If the prism is intersected at the height of the shortest edge and the upper frustum is removed, a regular prism is obtained (Figure 4.17b). The height of this prism corresponds to the solvent strength of the weakest solvent. All the points of the equilateral triangle formed by the cover plate of the prism have equal solvent strength.

Table 4.11 Classification of the solvent properties of common liquids.

Solvent	S_t	Acidity α	Basicity β	$\Pi *$	Group
Cyclohexane	0.2	0.0	0.0	0.0	—
Cyclopentane	0.1				—
n-Hexane	0.1	0.0	0.0	−0.08	—
n-Pentane	0.0	0.0	0.0	−0.087	—
n-Heptane	0.1	0.0	0.0	−0.08	—
Isooctane	0.1				—
Di-n-butyl ether					I
Diisopropyl ether		0.0	0.49	0.27	I
Diethyl ether	2.8	0.0	0.47	0.27	I
Methyl tertiary butyl ether	2.5				I
2-Propanol	3.9	0.76	0.95	0.48	II
n-Butanol	3.9	0.79	0.88	0.47	II
1-Propanol	4.0	0.78		0.52	II
Ethanol		0.83	0.77	0.54	II
Methanol	5.1	0.93	0.62	0.60	II
Tetrahydrofuran	4.0	0.0	0.55	0.58	III
Methoxyethanol	5.5			0.71	III
Pyridine	5.3	0.0	0.64	0.87	III
Dimethylformamide	6.4	0.0	0.69	0.88	III
Acetic acid				0.64	IV
Ethylene glycol		0.90	0.52	0.92	IV
Dichloromethane	3.1	0.30	0.0	0.82	V
1,2-Dichloroethane	3.5	0.0	0.0	0.81	V
1,4-Dioxane	4.8			0.71	VIa
Ethyl acetate	4.4				VIa
Methyl ethyl ketone	4.7	0.06	0.48	0.67	VIa
Acetone	5.1	0.08	0.48	0.71	VIa
Isobutyl methyl ketone	4.2				VIa
Acetonitrile	5.8	0.19	0.31	0.75	VIb
Benzene	2.7	0.0	0.10	0.59	VII
Toluene	2.4	0.0	0.11	0.54	VII
Chloroform	4.1	0.44	0.0	0.58	VIII
Water	10.2	1.17	0.18	1.09	VIII

S_t = solvent strength, hydrogen bond acidity.
α, hydrogen bond basicity.
β, dipolarity.
$\pi*$ Solvent Group according to Snyder and Kirkland (1979) and Sadek (2002).

Group	Solvents
I	Aliphatic ethers, trialkylamines
II	Aliphatic alcohols
III	Pyridines, tetrahydrofuran, amides
IV	Glycols, glycol ethers, benzyl alcohol, formamide, acetic acid
V	Methylene chloride, ethylene chloride
VIa	Ketones, esters, nitriles, dioxane
VIb	Nitro compounds, aromatic hydrocarbons
VII	Halobenzenes, diphenyl ether
VIII	Fluoroalkanols, chloroform, water

Figure 4.16 Solvent characterization according to proton acceptor and donor characteristic as well as dipole moment. Source: Redrawn from Snyder and Kirkland (1979).
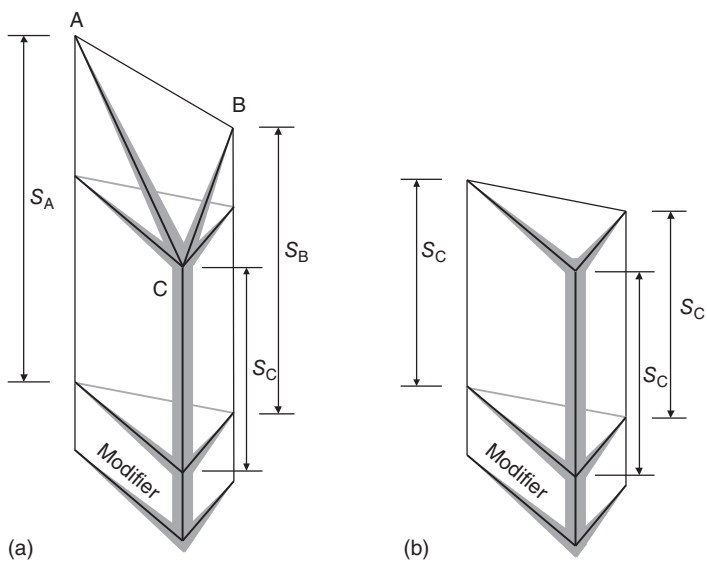
Figure 4.17 Graphic representation of the PRISMA model: (a) complete model and (b) regular part of the model.

One of the corners (C) represents the neat solvent with the lowest strength. The composition of the two other corners can be obtained by diluting these solvents with a solvent of zero strength (*n*-hexane for NP and water for RP applications).

In the regular prism, horizontal intersections parallel to the base can be prepared by further diluting the selected solvents with solvent of zero strength (represented by the line from P_s^* to P_s^{**} in Figure 4.18). All points on the obtained triangles represent the same solvent strength, while all points on a vertical straight line correspond to the same selectivity points (P_s).

Points along the edges of the irregular part of the model, which represents mixtures of two solvents (AB, BC, and AC), are shown in Figure 4.19b, while Figure 4.19a describes the selectivity points of mixtures of the three solvents.

Each selectivity point can be characterized by a coordinate, defined by the volume ratio of the three solvents. The ratio is written in the order of decreasing solvent strength of the undiluted solvent (A, B, C). 100% solvent A with the highest solvent strength is represented by $P_s = 10–0–0$, and the solvent with the lowest strength (C) by $P_s = 0–0–10$.

From these data, a three-digit number can define all other basic selectivity points. For example, the selectivity point with coordinates 325 means 30 vol% A, 20 vol% B, and 50 vol% C (Figure 4.20). Finer adjustment of the volume fractions can be expressed by three two-digit numbers ($P_s = 55–25–20$):

The whole strategy of solvent optimization via the PRISMA model includes the following steps:

- Start – Selection of neat solvents.
- Step 1 – Solvent strength adjustment.
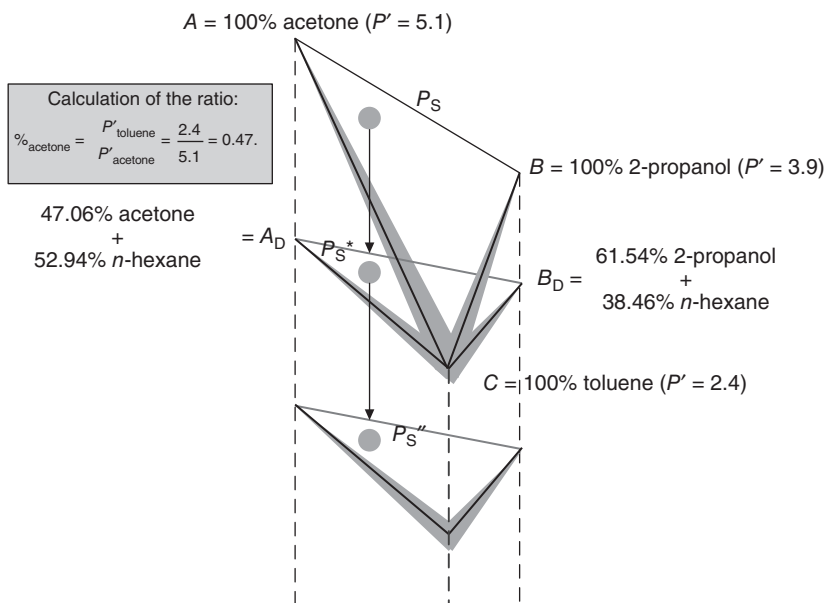
Figure 4.18 Example calculation of mobile phase composition.
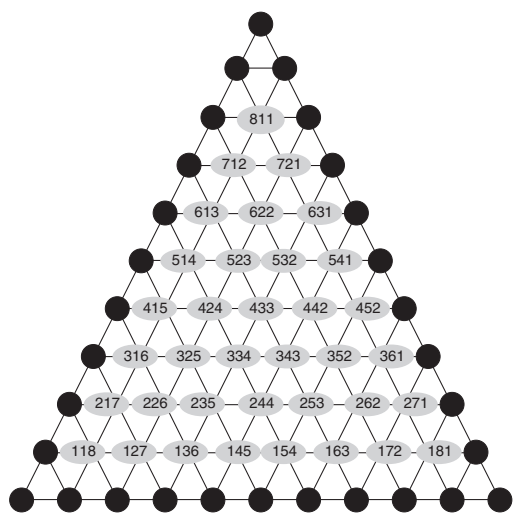
(a)
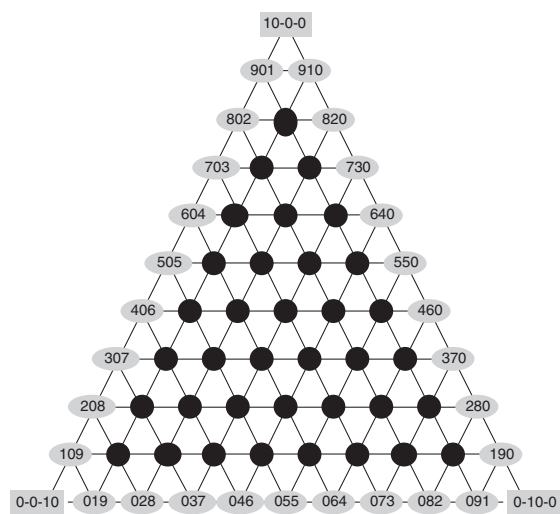
(b)

Figure 4.19 Basic selectivity points of the PRISMA model.

Figure 4.20 Combination of three neat solvents in the irregular part of the model.
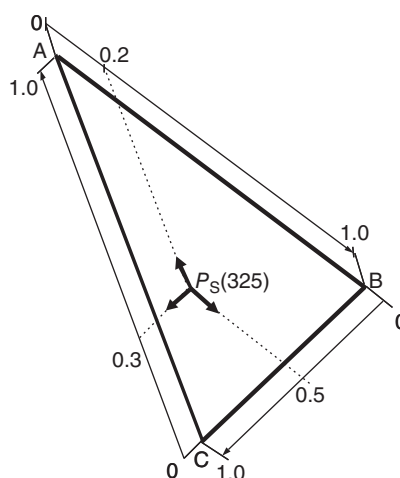
- Step 2 – Optimization of selectivity.
- Step 3 – Final optimization of solvent strength.
- Step 4 – Determination of optimal mobile phase composition.

The optimization strategy will be exemplified by a rather difficult isomer separation. The product to be separated was a relatively strong base and first experiments using neat solvents on different types of stationary phases (silica gel and amino-, cyano-, and diol-modified silica gel) revealed that it would be very difficult to separate the two isomers on a larger scale. Therefore, synthetic chemists were contacted to modify one of the secondary base functions with an easily removable BOC (tert-butoxycarbonyl) group.

Preliminary TLC experiments in unsaturated chromatographic chambers were performed using ten neat solvents. Solvents listed in Table 4.12 represent the most common starting solvents from each group of the Snyder model. For the example of the isomers, this list was modified slightly to fit the experience of previous experiments. Figure 4.21 shows the results of the solvent-selection experiments.

Based on experience (R_f values, selectivity, and spot shape), one to three solvents were selected. Preferentially, solvents are chosen that demonstrate small, well-defined spot shapes for the title components. Binary mixtures or

Table 4.12 Solvents for preliminary TLC experiments.

Solvent	Group	Solvent	Group
Diethyl ether	I	Dichloromethane	V
2-Propanol	II	Ethyl acetate	VI
Ethanol	II	Dioxane	VI
Tetrahydrofuran	III	Benzene	VII
Acetic acid	IV	Chloroform	VIII
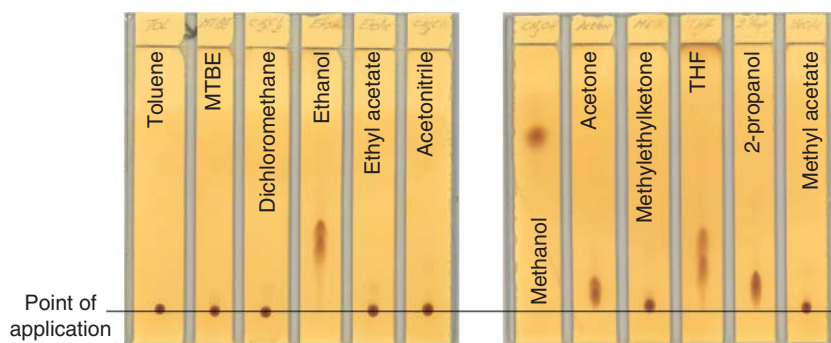
Figure 4.21 TLC experiments for the separation of two isomers using neat solvents.

single solvents that result in round finite spots have to be selected for the first set of experiments.

Figure 4.21 clearly demonstrates that only ethanol, acetone, and THF showed some selectivity between the two isomers, while only methanol gave a nice round spot. This example shows the practical usefulness of screening with TLC experiments. Because the experiment with each plate took roughly 20 minutes, the use of 12 different solvents could be examined in 40 minutes.

As a standard approach for preparative chromatography, binary solvent combinations are always investigated before considering ternary mixtures. Figure 4.22 shows the results of experiments with binary mixtures where selectivity was obtained. Other binary combinations were tested, but none resulted in a good spot shape and an acceptable separation between the isomers. Therefore, some additional tests were performed with ternary solvent combinations.
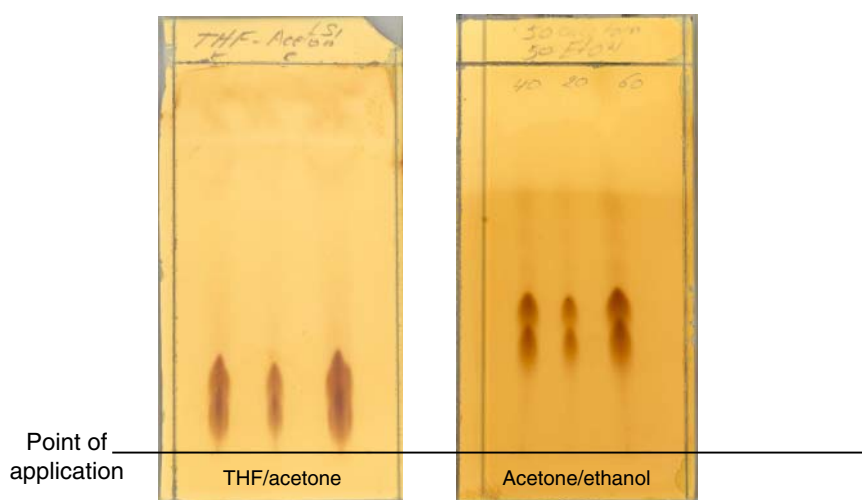
Figure 4.22 Screening of binary mixtures (50 : 50 v/v) of selected neat solvents.

4.4.3.1 Step (1): Solvent Strength Adjustment

Once the different solvents have been selected, a first experiment is done using the mobile phase composition corresponding to the center of the cover triangle ($^1/_3$ solvent A, $^1/_3$ solvent B, and $^1/_3$ solvent C). If the observed R_f values are too high, additional experiments are performed to adjust the solvent strength by the addition of zero strength solvent.

4.4.3.2 Step (2): Optimization of Selectivity

In the triangle with the desired solvent strength, three selectivity points near the edges of the triangle, (**811** (80% A–10% B–10% C)), (**181** (10% A–80% B–10% C)), and (**118** (10% A–10% B–80% C)), are the mobile phase compositions for the following three experiments (Figure 4.23).

For binary mixtures the selectivity points (75% A–25% B–0% C), (25% A–75% B–0% C), (75% A–0% B–25% C), (25% A–0% B–75% C), (0% A–75% B–25% C), and (0% A–25% B–75% C) were investigated.

The obtained chromatograms and chromatograms of step 1 serve as guidelines for the next experiments. If necessary, selectivity is further optimized by choosing new points in the triangle near the coordinate or between coordinates that gave the best resolution. Generally, a limited number of additional experiments
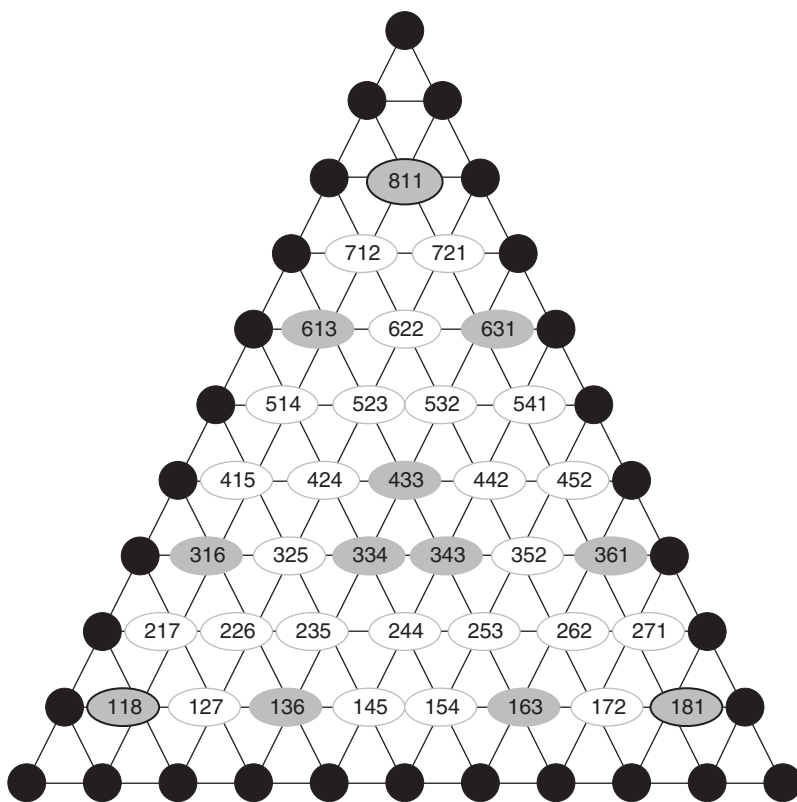
Figure 4.23 Starting points for selectivity optimization.

are required to obtain optimum conditions for separation. The resulting selectivity point (P_s) is used in the final optimization step. To separate the isomers the following solvent combinations were chosen for steps 1 and 2:

- Acetonitrile, methanol, and ethanol.
- Acetone, methanol, and ethanol.
- Acetone, ethyl acetate, and ethanol.
- Acetone, methyl acetate, and methanol.
- Acetonitrile, methyl acetate, and methanol.

First experiments were done with equal volumes of the three neat solvents as described in step 1. Based on this data some additional experiments were performed using different volume ratios of the most promising solvent mixtures.

Figure 4.24 shows the results of this optimization. The R_f values are in a promising range and thus a zero strength solvent is not needed. The TLC chromatograms clearly illustrate that different ternary solvent combinations separate the isomers well. Both spot shape and resolution are better than for the binary solvent mixtures (Figure 4.22).

4.4.3.3 Step (3): Final Optimization of the Solvent Strength

This step is used for the final optimization of solvent strength. It corresponds to a vertical shift in the regular part of the prism, starting from the optimal selectivity point (P_s) established in step 2. If all products of interest are sufficiently separated, the solvent strength can be increased or decreased to reach the desired goal.

4.4.3.4 Step (4): Determination of the Optimum Mobile Phase Composition

After the basic tests, where suitable solvents are selected and the desired solvent strength is established, the effect of eluent changes at a constant solvent strength are further investigated to find the optimum mobile phase composition.

To obtain reliable results the TLC measurements have to be carried out in saturated chambers, because in unsaturated chambers the reproducibility of R_f may
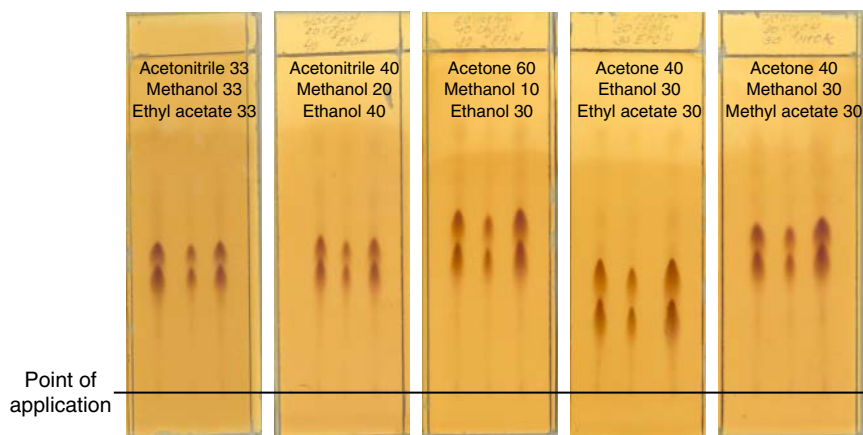
Figure 4.24 Screening of ternary solvent mixtures.

be poor and the formation of secondary and tertiary solvent fronts can affect the interpretation of the generated results. The most versatile TLC chamber in which to perform such experiments is the Vario-KS chamber developed by Geiss, Schlitt, and Klose (1965). This chamber is suitable for evaluating the effect of different solvents, solvent vapors, and relative humidity. In this type of chamber, the chromatoplate is placed face down over a conditioning tray containing several compartments to hold the required conditioning solvents. The design of the chamber ensures that saturating and developing solvents are completely separated. The chamber's major advantage is that for the purpose of solvent optimization, up to 10 activity and/or saturating conditions can be compared on the same plate using the same eluent.

To formulate a mathematical model for the dependence of hR_f on mobile phase composition, the obtained hR_f are displayed against the selectivity points, which symbolize the composition of the eluent.

Correlations were tested along the axes of the triangle and from the three basic selectivity points (118–811–181) across the middle point to the opposite side of the triangle.

A minimum of 12 experiments are required to determine a local optimum. By measuring hR_f for the selectivity points 118–316–613–811–631–361–181–163–136–433–334 and 343 (Figure 4.23), hR_f for the selectivity points 217–415–514–712–721–541–451–271–172–154–145–127–235––253–325–352, 523, and 532 can be calculated using the mathematical functions obtained from the measured values.

Functions along the axes:

- 811–613–316–118 (solvent A) (calculation of 217–415–514–712)
- 181–361–631–811 (solvent B) (calculation of 271–451–541–721)
- 118–136–163–181 (solvent C) (calculation of 127–145–154–172)

In general, the correlation between hR_f and the selectivity points at a constant solvent strength level can be expressed by Eq. (4.8):

$$hR_f = a \cdot (P_s)^2 + b \cdot (P_s) + c. \tag{4.8}$$

$$\ln hR_f = a(S_t) + b. \tag{4.9}$$

To obtain a global solvent optimum, the vertical relationship between the solvent strength and hR_f values has also to be investigated, and, therefore, some additional tests are required. Using quaternary solvents, the correlation was found to be described by Eq. (4.9). Because a linear mathematical function requires a minimum of three measured data points, the vertical relationship between solvent strength and hR_f values has to be tested at three different solvent strength levels. To collect accurate data, the chosen solvent strength levels have to differ individually by 5–10%.

To determine accurately the vertical relationship function, the following selectivity points were investigated:

- Solvent strength level 1: 811–631–118–343–334–181
- Solvent strength level 2: 811–433–118–316–361–181
- Solvent strength level 3: 811–613–118–334–163–181

4.4.4 Strategy for an Industrial Preparative Chromatography Laboratory

The effort required to develop a separation method strongly depends on several factors:

(1) Recurrence of a separation problem (repeatedly or only once).
(2) Amount of product to be separated.
(3) Do we have to isolate a single target component or all relevant peaks in the mixture?
(4) Quality requirements.
(5) Purpose of the purification process.
   - Purification of key intermediates or separation of a final product.
   - Preparation of reference standards for analytical purposes.
   - Isolation and purification of impurities in the $0.05–0.1$ mg ml^{-1} concentration range.
   - Current good manufacturing practice (cGMP)-related investigations.

Obviously, when separating small quantities of many different products, standard separation methods using gradient elution are preferred. Conversely, for larger-scale separations, it is important to design a robust separation process that can run fully automated 24 hours a day. Clearly, for a production-scale process, that has to be performed under cGMP conditions. Many experiments are required to be able to design a reproducible, robust process that can be transferred from one production location to another without the need for substantial modifications. For this reason, two examples covering both separations are exemplified.

Example 4.1 *Separation of Large Numbers of Different Products in the Range of up to 10 g*

As mentioned before, for this type of work, standard procedures using gradient elution are the method of choice, and there are two possible approaches:

- Normal phase chromatography on silica.
- Reversed phase chromatography.

For such products, HPLC chromatograms using a standardized method and mass spectrometry (MS) data are usually available, and, therefore, it is very tempting to perform a preparative chromatographic purification using these experimental conditions.

The major advantage of this approach is that for mixtures containing several peaks of approximately equal size, the analytical high-performance liquid chromatography-mass spectrometry (HPLC-MS) data allow immediate recognition of the desired product in the preparative run, and, therefore, no additional structural analyses are required to identify the isolated product. However, the major disadvantage of reversed phase applications is often the limited solubility of the samples in eluents having high water content. Furthermore, due to the relatively high viscosity of the eluents used in reversed phase chromatography, the flow rate that can be pumped through a preparative chromatography column

is generally lower than that for the pure organic solvent mixtures used in normal phase chromatography. Another point that certainly has to be considered is the loading capacity of a C18 reversed phase material, which is generally only $1/2 - 1/3$ of the loading capacity of bare silica gel.

However, is it possible to run, reproducibly, solvent gradients on bare silica? Many people have their doubts, especially concerning the necessity of very long equilibration times when returning to the initial solvent composition. Furthermore, it was impossible to perform gradient elutions on the first generation of silica using very polar solvents, for example, methanol, because these solvents washed out the silica dust originating from the production process, which was electrostatically attached onto the particles. This phenomenon certainly is not very convincing. Nonetheless, new spherical materials prepared from ultrapure silica no longer demonstrate this pronounced problem. On these materials, gradient runs ending up with 100% of very polar organic solvent are easily performed. The problem of activity changes when going from an intermediate polarity to a relatively polar solvent is also nonexistent when, for two or more injections in succession, exactly the same procedure is followed, that is, same gradient profile, same rinsing time with polar solvent, same time to go back to the start solvent composition, and, very important, same time at the initial composition of the gradient to start the next injection. Only when, for the next series of samples, the gradient has to start with a zero strength solvent (*n*-heptane) equilibration problems can be expected, and then some measures may have to be taken to reactivate the stationary phase.

4.4.4.1 Standard Gradient Elution Method on Silica

To select suitable gradient conditions, TLC experiments are performed using an eluotropic series based on dichloromethane–methanol mixtures. By means of a Camag Vario chamber (Figure 4.25), the eluent combinations following Table 4.13 have been tested.

The mixture dichloromethane–methanol (50 : 50 v/v) has been chosen based on experience that products remaining in the point of application with solvents of lower strength often can be moved more easily to higher R_f values with this mixture than with pure methanol as the eluent. Probably, this phenomenon is

Figure 4.25 Vario chamber with accessories.
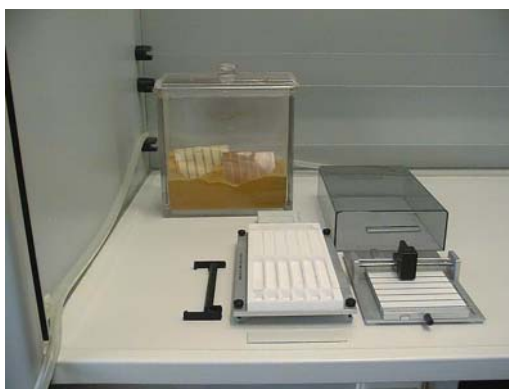
Table 4.13 Solvent series based on dichloromethane–methanol mixtures.

Dichloromethane–*n*-heptane (50–50 v/v) ($S_T = 1.55$)
Dichloromethane ($S_T = 3.1$)
Dichloromethane–methanol (98–2 v/v) ($S_T = 3.14$)
Dichloromethane–methanol (95–5 v/v) ($S_T = 3.195$)
Dichloromethane–methanol (90–10 v/v) ($S_T = 3.3$)
Dichloromethane–methanol (50–50 v/v) ($S_T = 4.1$)

due to the very good solubility characteristics of this solvent mixture for a broad variety of products.

Based on the observed chromatographic profile, the start and end conditions for a preparative gradient run are selected. The solvent composition that corresponds to the solvent mixture where the product of interest just leaves the point of application is used as the starting composition for the gradient. The solvent mixture moving the product of interest closely to the solvent front is the final composition of the gradient.

4.4.4.2 Simplified Procedure

Instead of testing the whole dichloromethane–methanol eluotropic series, only one TLC run is performed using a 90 : 10 volume ratio mixture of dichloromethane–methanol. The location of the product of interest on this plate is then used to establish the preparative gradient conditions. This procedure is shown in Figure 4.26.

The type of silica selected to perform this type of preparative gradient elutions is a 5–10 μm good quality spherical material with excellent mechanical stability
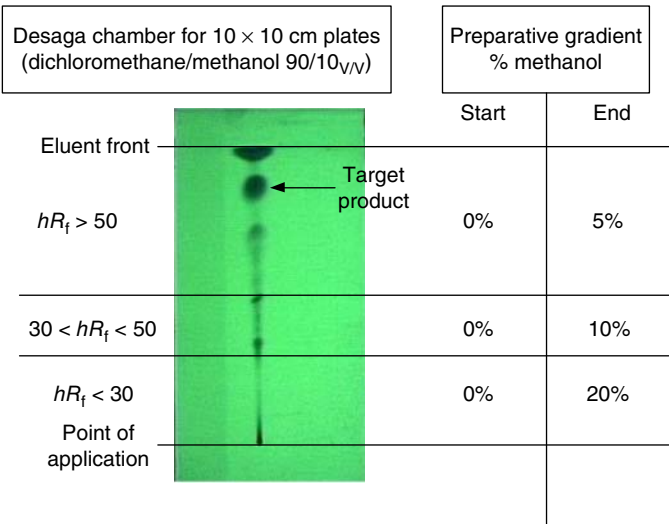
Figure 4.26 Simplified procedure to establish the start and end composition for a preparative gradient elution on native silica.

(Kromasil®, AkzoNobel, Sweden). About 200–250 g is packed at 100–150 bar in a 50 mm internal diameter dynamic axial compression (DAC) column. Chromatography is executed at a flow rate of 110–125 ml min⁻¹, and the average sample amount applied is about 3 g. This gradient approach on native silica has proven to be a very versatile and robust method as long as the sample and eluent are carefully filtered prior to their use, thus avoiding partial blockage of the porous metal plates in the top flange and the piston of the column.

Example 4.2 *Pilot Chemistry Laboratories and Pilot Plant-Scale Separations (a Few Hundred Grams to Tenths of Kilograms Scale)*

For this type of problem, time constraints generally dominate. Very often, the scale-up of a chemical reaction without extensive optimization work results in low yields and bad qualities. The necessity to deliver a certain amount of product within a very narrow time frame, in general, does not allow preparative chromatography workers to thoroughly optimize the separation method. Therefore, a standard approach is required.

At first the polarity of the product is investigated by means of a TLC analysis using an eluotropic series based on dichloromethane–methanol mixtures such as described in Table 4.13.

Very often, one of the tested mixtures can be used to perform the separation, or a few additional experiments using the same solvent combination have to be performed to fine-tune the chromatography process.

Simultaneously, two additional silica TLC plates are made to test 12 neat solvents that, from a safety, health, environmental, and practical point of view, are acceptable for use on a larger scale.

From the series of solvents proposed in Table 4.12, diethyl ether, dioxane, benzene, and chloroform are excluded. Instead, the following solvents are used:

Plate 1: Toluene–*tert*-butyl methyl ether (TBME)–dichloromethane–ethanol–ethyl acetate–acetonitrile.
Plate 2: Methanol–acetone–methyl ethyl ketone–tetrahydrofuran–2-propanol–acetic acid.

Toluene, acetone, and methyl ethyl ketone are, due to their cutoff values, not the first choice if UV detection is used to control the process. THF has to be avoided because for larger scale use it has to be stabilized with an antioxidant (butylated hydroxytoluene) that will finally end up in the product, often making an additional purification step necessary.

However, for a broad variety of substances, some solvent mixtures based on toluene or acetone or THF have proven to be universally applicable:

- Toluene–2-propanol
- Toluene–ethyl acetate–ethanol
- Toluene–2-propanol–25% ammonia in water
- *n*-Heptane–methyl ethyl ketone (or acetone)
- Acetone–ethanol
- Acetone–ethanol–ethyl acetate
- Dichloromethane (or acetonitrile)–THF

Based on the chromatographic profiles observed on both plates, suitable binary solvent mixtures are chosen. Using another TLC plate, an eluotropic series of these solvents is prepared and tested. The start and end composition of this eluotropic series depends on the R_f values measured for the strongest solvent of the mixture.

If, on silica, no satisfactory results are obtained with the neat solvents, the two solvent series (except acetic acid) are, respectively, tested on an amino-, cyano- and diol-modified TLC plate.

Most problems can be solved on silica gel as the stationary phase. If either some specific selectivities or the addition of a basic modifier is required, amino-modified silica gel (90 : 10 v/v) often brings the solution.

Clearly, this solvent-selection procedure will not always result in optimal preparative chromatographic conditions, but it offers a method that can be applied immediately.

Direct application of a TLC method for preparative chromatography requires consideration of some basic differences between the techniques:

(1) Driving force for solvent transport:
   - Capillary forces (TLC)
   - External force (pump) in HPLC
(2) Specific surface area of silica gel used to prepare a TLC plate can differ from the packing material in the column.
(3) Organic or inorganic binders are used to fix the silica layer on the surface of a glass plate. Furthermore, the layer generally contains an inorganic fluorescence indicator.
(4) TLC starts from a dry layer, and we have to deal with a mobile phase gradient over the whole migration distance.

Preferential adsorption of the most polar component of the solvent mixture in TLC means that the use of the same mobile phase composition in an HPLC experiment will always result in shorter retention times. (In HPLC, the solvent mixture is continuously pumped through the column, and, after some time, the active surface spots are occupied with polar solvent molecules.)

Therefore, it is advisable to perform a test injection of the sample on the HPLC column using a mobile phase containing a somewhat smaller amount of the polar component.

4.5 Criteria for Choosing Reversed Phase Systems

The demand for separation of water-soluble solutes that differ in their nonpolar part led to the development of adsorbents for RP chromatography. In RP systems, the polarities of the adsorbent and mobile phase are inverted compared with NP systems. Therefore, RP chromatography should be better termed as reversed polarity chromatography. Nonpolar or weak polar adsorbents are used together with polar solvents. The transition to polar mobile phases affords the use of water. A typical solvent for RP systems consists of a mixture of water and a miscible

organic solvent, such as methanol or THF. Due to the aqueous solvents, precise control of the water content as in NP chromatography working with nonpolar solvents is not necessary. The nonpolar packing material consists, for instance, of a porous silica support coated with a monolayer of alkyl groups (C_2–C_{18}), aryl groups, or hydrophobic polymers. Alternatives to these RP silicas are hydrophobic cross-linked organic polymers or porous graphitized carbons. One important property is the hydrophobicity of this surface. It is mainly afforded by the carbon content and the endcapping of the silica (see also Section 3.2.6.9).

Adsorption–desorption mechanisms of RP systems are a turnaround from NP systems (reversed polarity). In this case, the nonpolar, or hydrophobic, portion of solute molecules adsorbs to the surface of the stationary phase, while the polar part of the molecule is solvated by the mobile phase solvent. The result is a reversed elution order – polar before less polar solutes (Figure 4.27).

RP silicas are called brush type because of their structure. Numerous alkyl groups point from the surface into the mobile phase, and thus the surface is similar to a brush, with bristles of alkyl groups. To describe the adsorption process, a simple two-layer model of the system has been proposed (Galushko 1991), which means that the surface layer of the alkyl groups is assumed to be quasi-liquid. The retained solutes penetrate into the surface layer and retention can be regarded as partitioning between hydrophobic stationary phase and mobile phase, similar to liquid–liquid chromatography.
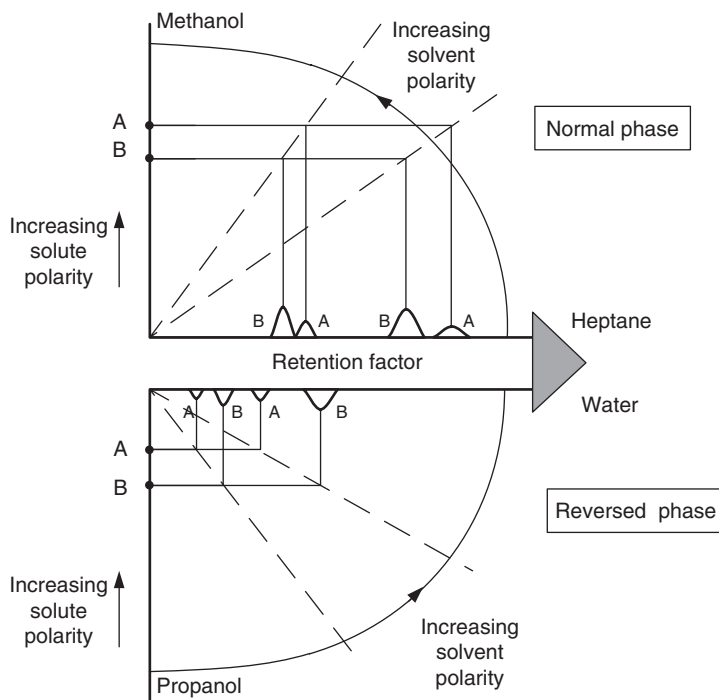
Figure 4.27 Retention behavior in both normal and reversed phase chromatography.

RP chromatography is mainly used to separate substances that differ in their lipophilic part or in the number of C atoms, for example, the separation of homologues. However, due to the anisotropic nature of the interaction between surface layer and solute, RP systems reach lower selectivities for the separation of stereoisomers than NP systems.

The elution order in NP and RP systems is described in Figure 4.27. The retention time and thus the elution order for two solutes of different polarity are exemplified for RP in the lower part of Figure 4.27 and for NP in the upper part. Component A is more polar than B, which results in A eluting before B in RP systems and an inverted elution order for NP systems. The influence of solvent polarity is shown by the two diagonal lines from the origin. Each line illustrates a solvent with a certain polarity. Retention times are given by the point of intersection with the horizontal line, which describes the solute polarity.

Most analytical separations are performed by RP systems, while most preparative separations are performed using an NP system. For example, 84% of the analytical separations at the former Schering AG, now part of Bayer Healthcare, are done in RP mode, while 85% of the preparative separations are performed on NP silica gels (Brandt and Kueppers 2002).

RP systems dominate analytical applications because of their robustness and reduced equilibration time. This fast column equilibration makes RP applicable for gradient operation. For preparative chromatography, NP systems are preferred because of some disadvantages of the RP systems. Although water is a very cheap eluent, it is not an ideal mobile phase for chromatography because it evaporates at higher temperatures, the enthalpy for evaporation is quite high, and the viscosity of aqueous mixtures is much higher than the viscosity of mixtures of organic solvents.

Since the polarity range of adsorbents is bordered by silica on the polar side and RP-18 or hydrophobic polymeric phases on the nonpolar side, it is easy to assign these absorbents to NP or RP systems. Medium-polar packings possess polar properties because of the functional group as well as hydrophobic properties contributed by the spacer (Unger and Weber 1999). Owing to this mixed nature, these phases cannot be directly assigned to a certain type of phase system.

4.5.1 Retention and Selectivity in RP Systems

RP liquid chromatography is used in separating polar to medium-polar components. Their separation is based on the interaction of the lipophilic part of the solutes with the nonpolar surface groups. Retention depends on the nature of the active groups bonded on the silica surface as well as the functional groups of the solute. The hydrophobicity of RP packings differs in the relative sequence:

Porous graphitized carbon > polymers made from cross-linked styrene-divinylbenzene > n-octadecyl (C18) bonded silicas > n-octyl (C8) bonded silicas > phenyl-bonded silicas > n-butyl (C4) bonded silicas > n-propylcyano-bonded silicas > diol-bonded silicas.

The retention time in RP chromatography increases with the surface hydrophobicity. Therefore, for instance, C18 groups cause higher retention times than C8 groups at constant ligand density, as demonstrated in Figure 4.28, which
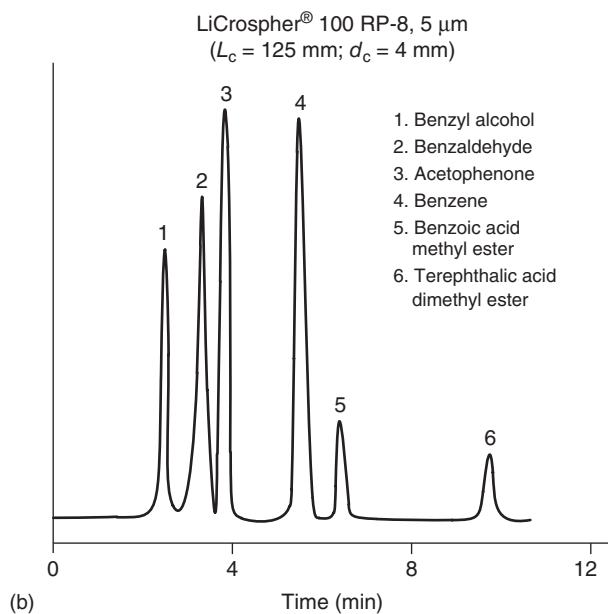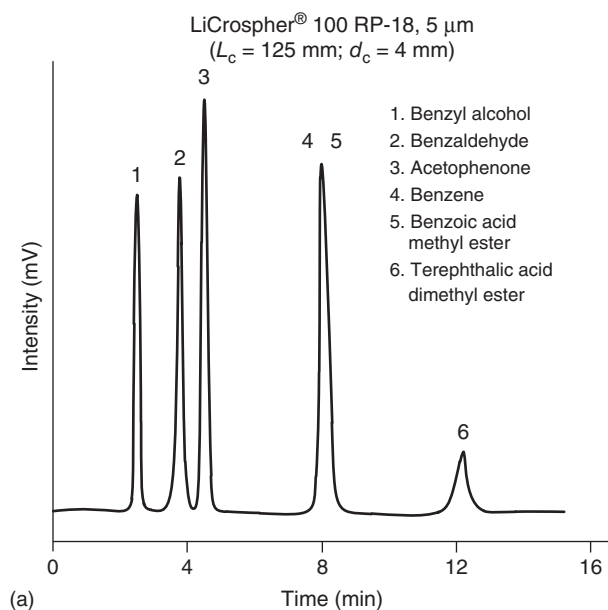
Figure 4.28 Retention of aromatic components on RP-8 and RP-18 columns with water–methanol (50 : 50 v/v); flow rate 1 ml min^{-1}. (Source: Unger and Weber (1999). Reproduced with permission of John Wiley and Sons).

compares the retention on RP-8 and RP-18 phases. Apart from a higher retention time, RP-18 silicas also exhibit different selectivities.

In addition to the surface groups of the adsorbent, the nature of the functional groups of the solutes determines the interaction and, thus, the retention time as well. The following sequence shows the elution order for solutes of similar size with different functional groups (Unger and Weber 1999):

Amine/alcohols/phenols < acids < esters < ethers < aldehydes/ketones < aromatic hydrocarbons < aliphatic hydrocarbons.

Figure 4.28 presents the influence of functional groups on the retention time. Benzene and some aromatic derivates are separated by RP chromatography. Compared with benzene the retention time is decreased for derivates with polar aldehyde or hydroxyl groups, while it is increased for the more bulky apolar esters, for example, benzoic or terephthalic methyl esters.

In RP chromatography, mixtures of organic solvents such as methanol, acetonitrile, and THF with water are used as mobile phases. The organic (more hydrophobic) solvent also interacts with the nonpolar surface groups of the packing and thus is in competition with the solutes for the nonpolar adsorption sites on the adsorbent. Consequently, the retention time of the solutes decreases with increasing fraction of the organic solvent in the mobile phase. The dependency of the retention factor on the volume fraction ϕ of the organic solvent is described by Eq. (4.10) for medium values of W. In this equation, $k'_{0,S}$ is the retention factor for pure water, and ε^0 is the elution strength of the organic modifier (Snyder and Kirkland 1979; Snyder, Kirkland, and Glajch 1997; Snyder and Dolan 1998):

$$\ln k' = \ln k'_{0,S} - \varepsilon^0 \cdot \phi \tag{4.10}$$

Owing to the exothermic behavior of the adsorption, the retention time increases at lower temperatures. An Arrhenius-type equation describes the retention factor's dependence on temperature (Eq. (4.11)):

$$\ln k' = \ln k'_{0,T} - \frac{b}{T} \tag{4.11}$$

The impact of the mobile phase composition and the temperature is unique for each component, and thus the selectivity can be optimized by these parameters.

The choice of organic modifier for an RP system can have a drastic influence on the selectivity and retention order. Lobsten-Guth, Briancon-Scheid, and Anton (1983) showed for a dried ethanol extract of *Ginkgo biloba* leafs a drastic change in elution order when acetonitrile, methanol, and THF are used as organic modifiers. Figure 4.29a shows the separation with acetonitrile as the organic modifier. Ginkgolides A (2) and B (3) are co-eluting, while bilobalide (4) is eluting as the first compound. Changing to methanol in Figure 4.29b gives a fist partial separation between ginkgolides A and B. Drastic changes can be seen in Figure 4.29c with THF as the organic modifier: ginkgolides A and B show a drastic increase in selectivity, but bilobalide (4) has a much longer retention time now and is co-eluting with ginkgolide A (2). Using a mixture of water with two organic modifiers (methanol and THF) resulted in a chromatogram with nicely separated peaks of all four terpenes (Figure 4.29d).
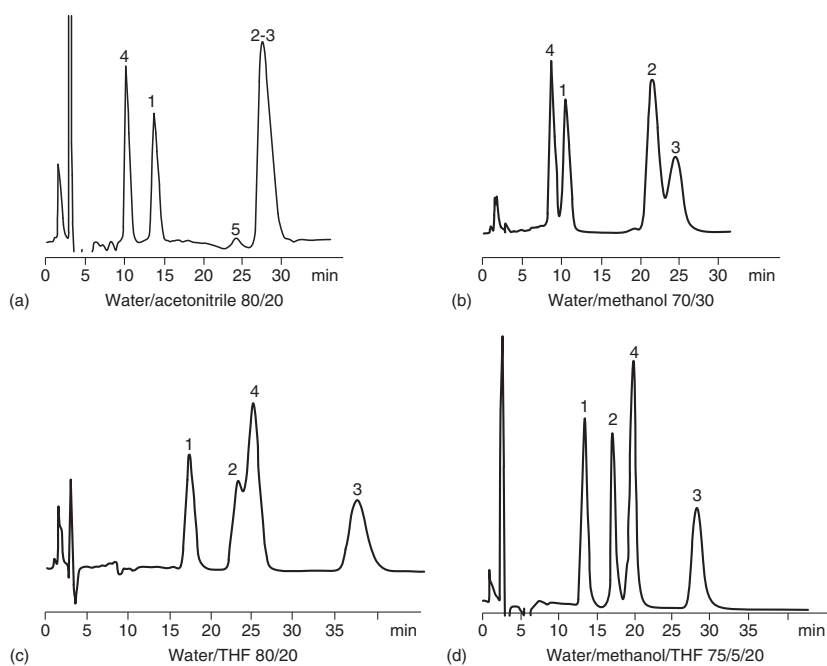
Figure 4.29 Separation of *Ginkgo biloba* terpenes on RP chromatography with different organic modifier. (a) acetonitrile (b) methanol (c) THF (d) methanol and THF, Sorbent: LiChrosorb® RP-18, 10 μm, column dimension 250 mm × 4 mm i.d., dried ethanol extract of *G. biloba L.* leafs in MeOH, compounds: 1 ginkgolide C, 2 ginkgolide A, 3 ginkgolide B, 4 bilobalide. (Source: Lobsten-Guth, Briancon-Scheid, and Anton (1983). Reproduced with permission of Elsevier).
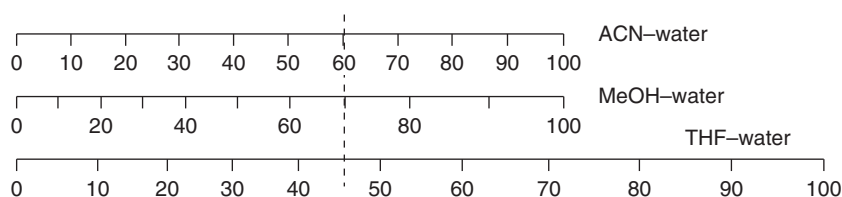
Figure 4.30 Nomogram for the elution strength of acetonitrile, methanol, and THF in RP chromatography.

To adjust the solvent strength in between the three most common used organic modifiers in RP chromatography, the nomogram in Figure 4.30 can be used. It shows that for equal retention parameters when 60% acetonitrile is used, only 45% of THF would be equivalent, but 70% of methanol is needed.

4.5.2 Gradient Elution for Small Amounts of Product on RP Columns

RP chromatography is widely used to isolate small amounts of target molecules in automated high-throughput systems. Due to good reproducibility, stability, and a broad application range, RP instead of NP chromatography is preferred for this task. For RP separations, TLC is seldom used as a pilot technique, mainly due to the large difference in the degree of derivatization between RP materials used in column chromatography and the materials that can be used for TLC applications. With the now ready availability of MS detection and since MS is coupled to columns with diameters of up 25 mm by splitting systems, compound isolation is often directly combined with its identification. The structure of the molecules to be separated largely determines the type of mobile phases that can be used in RP chromatography. For some product types, mixtures of water and organic solvents can be used as the mobile phase. However, in this case, one has to deal with basic or acidic molecules, and so, in general, the aqueous phase has to be buffered to obtain acceptable peak shapes. It is common practice in HPLC-MS identification to add an ammonium salt to the aqueous phase.

Figure 4.31 gives experimental conditions that can be used as a standard HPLC-MS analysis procedure. After the column has been equilibrated, the operation starts with a 10 minute gradient separation (from 70% A, 15% B, and 15% C to 50% B and 50% C) followed by 5 minute washing and 5 minute re-equilibration.

The obtained analytical results can be directly transferred to a preparative chromatography column. For the standard method depicted in Figure 4.31, a combination of acetonitrile and methanol is used as the organic modifier. Therefore, some additional experiments, investigating the effect of each type of organic modifier individually, are advisable because, very often, large differences in selectivity can be observed.

Owing to microbiological growth, a solution of ammonium acetate in water cannot be stored for a long period. In other words, when for preparative chromatographic applications larger volumes of an ammonium acetate solution have to be stored, some measures have to be taken to avoid this microbiological
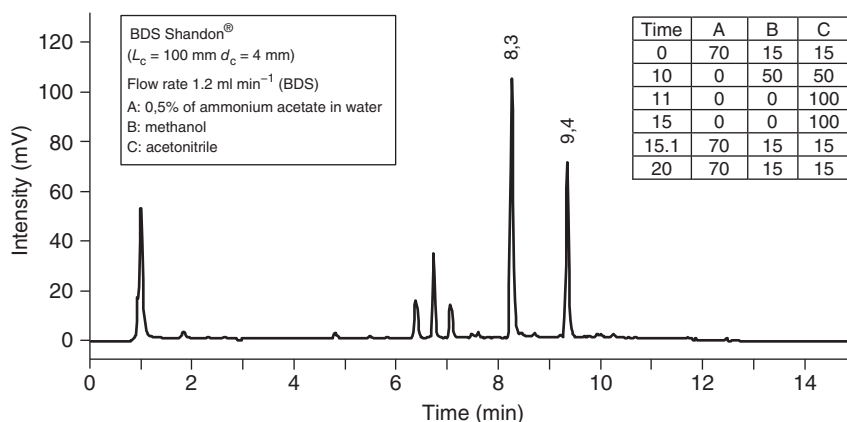
Figure 4.31 Standard HPLC mass spectrometric reversed phase analysis procedure.

growth. Different remedies are possible, one of which is to add 5–10 vol% acetonitrile to the mixture of ammonium acetate and water. Obviously, the presence of this amount of organic modifier has to be taken into account when transferring data from an analytical to a preparative column.

Therefore, the standard gradient for HPLC-MS analysis is modified by using an aqueous ammonium acetate solution containing 10 vol% acetonitrile. Care has to be taken that the polarity at the start of the gradient remains approximately equal. Chromatograms in Figure 4.32 depict the separation using this modified weak solvent.

4.5.3 Rigorous Optimization for Isocratic Runs

After developing a first gradient method, the optimization of an isocratic method should be considered for process-scale separations. Gradient runs help to find optimal conditions for isocratic operation, which should be preferred for preparative purposes as the advantages for large-scale separations are obvious:

– Easier equipment can be used (only one pump, lower number of eluent tanks). No re-equilibration time necessary (touching band methods as well as closed-loop recycling and simulated moving bed (SMB) chromatography can be applied).
– Easier eluent recycling due to constant eluent composition.

In the following paragraph, the development of a separation method is explained in detail by the separation of a pharmaceutical sample consisting of three intermediates.

The general tasks during optimization are:

– Minimize total elution time.
– Minimize cycle time (=time between first and last peak).
– Optimize selectivity.
– Use isocratic conditions.
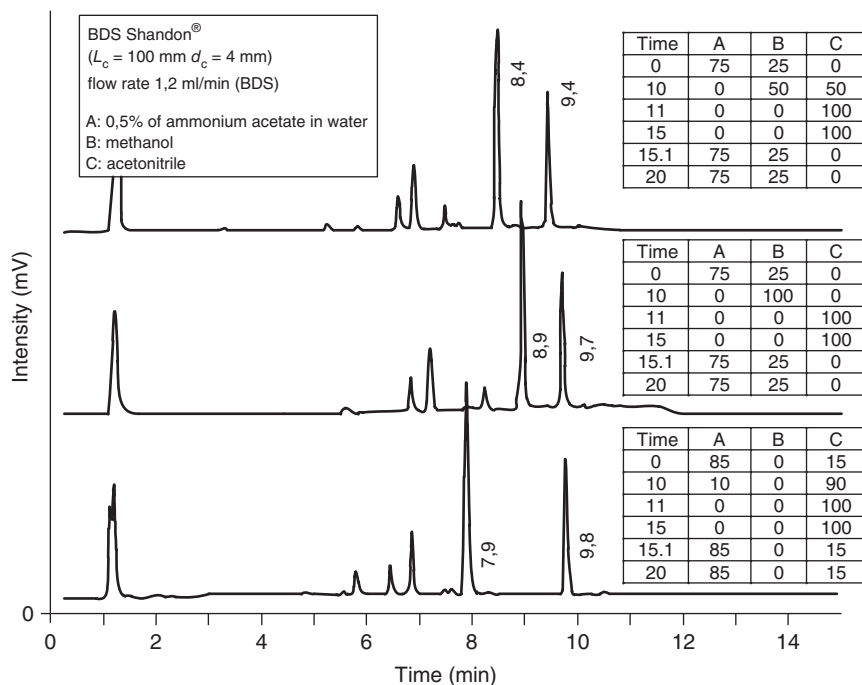
Figure 4.32 Standard gradient with modified weak solvent.

Minimization of the total elution and cycle time results in higher productivity and lower eluent consumption. Optimizing the selectivity can be contradictory to these parameters. However, if the cycle time is minimized, the productivity for touching band operation increases.

Figure 4.33 presents a procedure for optimizing RP chromatography by isocratic experiments. It usually begins with gathering solubility data for the sample using water-miscible solvents. The solvent with highest solubility for the sample is the first mobile phase. A test run is made on an alkyl silica, and the retention factor k and the selectivity are determined. In most cases, this solvent (e.g. methanol) will not separate the solutes, and they elute unretained within the dead time of the column. Solvent strength is then decreased by successively adding water to the mobile phase. As the polarity of the mobile phase solvent is increased, the retention factors also increase.

When the selectivity α is inadequate for preparative purposes, the stronger solvent, in this case methanol, is substituted by another water-miscible organic solvent, such as THF or acetonitrile. The optimization of k is then repeated by adjusting the water–organic ratio. This approach works well for most polar to moderately polar compounds that remain nonionic in the solution.

As an example, Figure 4.34 shows the separation of three pharmaceutical intermediates on LiChrospher® RP-18 with a mobile phase composition of acetonitrile–water (80 : 20). Intermediate 1 elutes at 2.28 minutes, while intermediates 3 and 2 co-elute at 3.16 minutes. Obviously, the separation problem
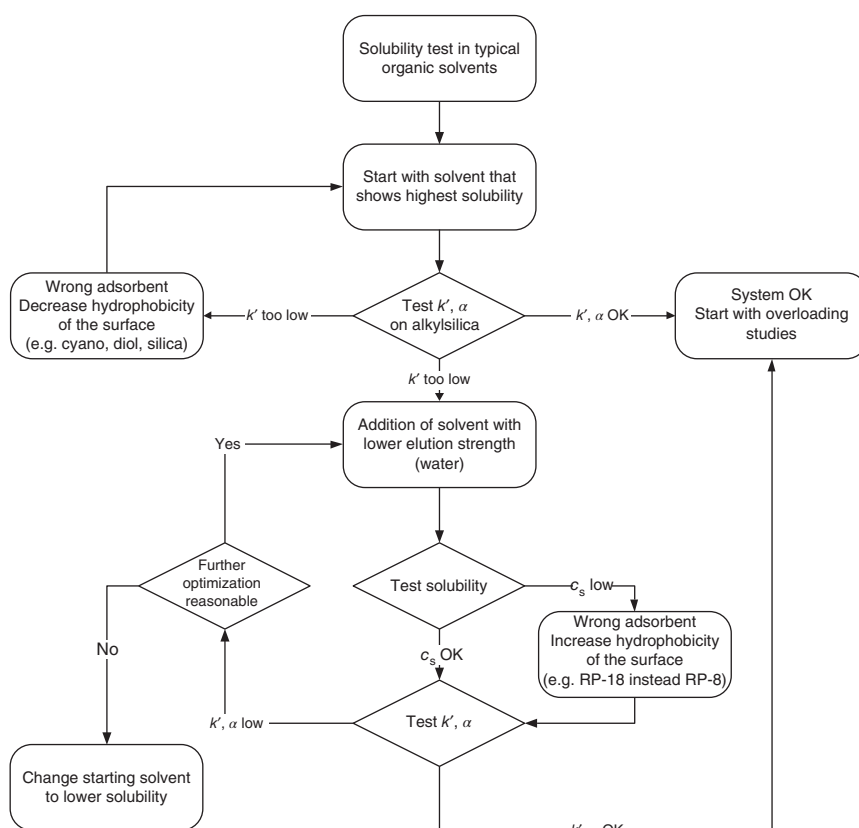
Figure 4.33 Choice of optimal solvent mixture for RP chromatography.
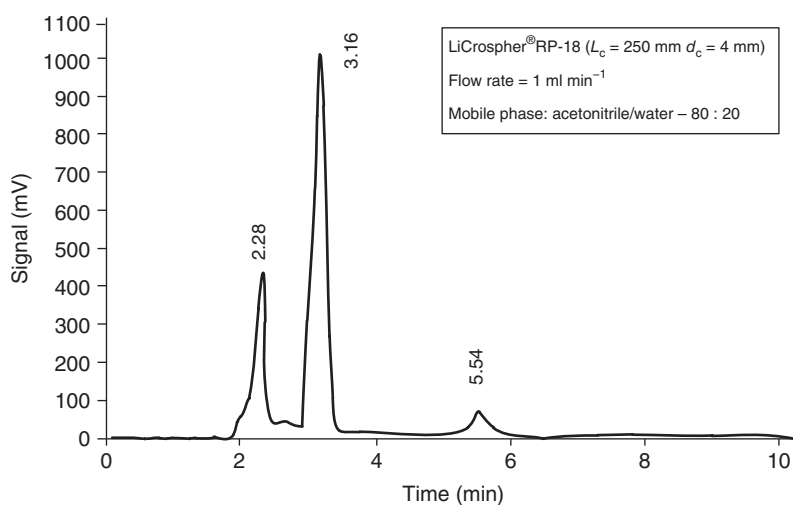
Figure 4.34 Separation with LiChrospher® RP-18 with acetonitrile–water (80 : 20).

is not solved, and, thus, the mobile phase composition must be adjusted in subsequent batch runs with higher water fractions.

Table 4.14 gives the selectivities and retention factors for increased water fractions, while Figure 4.35 shows the plot of ln k' versus ϕ. Corresponding to Eq. (4.10), the influence of ϕ on the retention factor of the intermediates is described by the slopes of these straight lines.

The parameters of Eq. (4.10) are determined from Figure 4.35, and thus the selectivity can be calculated for the whole range of mobile phase composition by Eq. (4.12). The influence of ϕ on selectivity is mainly determined by the difference between slopes S_1 and S_2. If the difference is positive ($S_2 < S_1$), the selectivity increases for higher fractions of the organic solvent:

$$\alpha_{2,1} = \frac{k_2'}{k_1'} = \frac{e^{(\ln\,k_{0,S2}-\varepsilon_2^0\cdot\phi)}}{e^{(\ln\,k_{0,S1}-\varepsilon_1^0\cdot\phi)}} = \frac{k_{0,S2}}{k_{0,S1}}e^{((\varepsilon_1^0-\varepsilon_2^0)\cdot\phi)} \tag{4.12}$$

The mobile phase composition can now be adjusted to the needs of the separation. For example, if intermediate 1 must be isolated with high purity, its retention

Table 4.14 Optimization of an RP separation with LiChrospher® RP-18 and different volume fractions ϕ of acetonitrile.

ϕ(%)	k_1	k_2	k_3	$\alpha_{2,1}$	$\alpha_{3,2}$
40	1.34	4.80	10.23	3.58	2.13
50	0.46	2.22	3.51	4.78	1.58
60	0.19	1.23	1.63	6.42	1.33
80	0.04	0.45	0.45	12.13	1.00
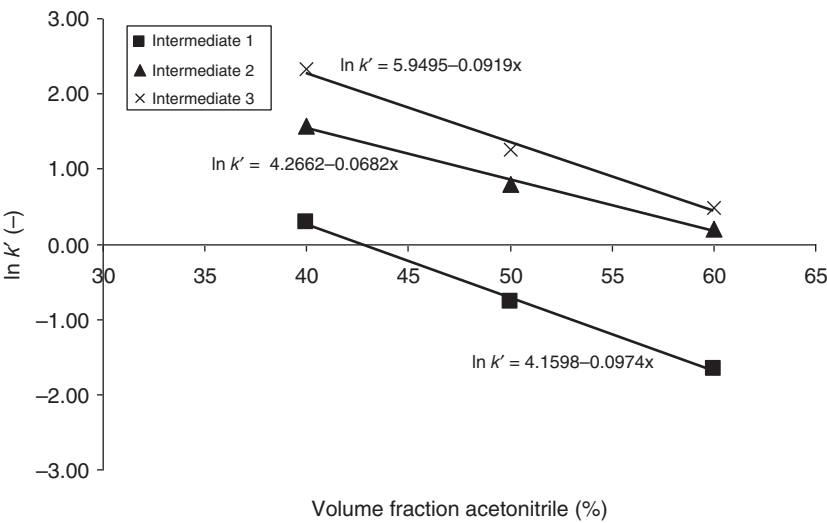
Figure 4.35 Dependency of retention factor on mobile phase composition.

factor should not be too small ($k > 1$; $\ln k > 0$), and thus the volume fraction should not exceed 43% acetonitrile.

The selectivities $\alpha_{2,1}$ and $\alpha_{3,2}$ show a contrary behavior: $\alpha_{2,1}$ increases with ϕ, while $\alpha_{3,2}$ decreases at higher volume fractions of acetonitrile. This is due to the differences in slopes in the plot of Figure 4.35; $S_1 > S_2$ and thus $S_1 - S_2$ is positive, while $S_3 > S_2$ and thus $S_2 - S_3$ is negative.

Selection of the optimal mobile phase composition has to take into account the desired product components. If there are more than two product components in the sample, a crucial separation must be defined. In the example case, a volume fraction of 60% acetonitrile shows best results for the three-component separation because a good selectivity $\alpha_{2,1}$ is observed at low retention times and the reduced k_1' is still acceptable (Table 4.14).

4.5.4 Rigorous Optimization for Gradient Runs

The optimization of RP separation by gradient runs is sometimes unavoidable even in process scale. Mobile phase gradients can reduce the development time dramatically as the solvent strength is varied during the chromatographic separation by changing the mobile phase composition. Figure 4.36 shows the development scheme for optimizing mobile phase composition by gradient operation.

The optimization by gradient operation starts with a linear gradient over the whole range of 100% water to 100% organic. If the solubility in different solvents is unknown, methanol or acetonitrile can be taken as starting solvents. Gradient time is adjusted to 10–15-fold the dead time of the column. If the target solutes elute at retention factors <1, the solutes are either polar or they ionize in aqueous solvents. Here, the interaction of polar solutes with the nonpolar adsorbent is very low, and a polar solvent with low interaction (e.g. 100% water) is recommended. Ionization must be suitably suppressed (Section 4.5.5), or the solutes should be separated by ion-exchange (IEX) chromatography.

If the retention time is much higher than the time of the initial gradient (retention factor $\gg 10$), the substances seem to be too lipophilic for RP separation on the initial adsorbent. The polarity of the adsorbent should be increased by the use of amino or diol phases. If the adsorbent is already polar, the phase system must be changed to NP chromatography (Section 4.4).

If the retention times are in a suitable range ($1 < k < 10$–15), solvent composition is adjusted by further gradient runs. Conditions for subsequent gradient runs are derived from the retention times of the solutes during the previous run. Mobile phase composition at the elution point of the first target solute is a good starting point for the mobile phase composition of the following gradient run, while the mobile phase composition at the elution point of the last peak can be taken as the final composition of the mobile phase.

The following example for the optimization of mobile phase composition by gradient runs refers to a separation of the same pharmaceutical mixture as specified in Figure 4.34. LiChrospher RP-18 ($L_c = 250$ mm; $d_c = 4$ mm) is used as adsorbent, and the mobile phase is a mixture of acetonitrile and water. Figure 4.37 shows the initial gradient from 0% to 100% acetonitrile over 30 minutes and a
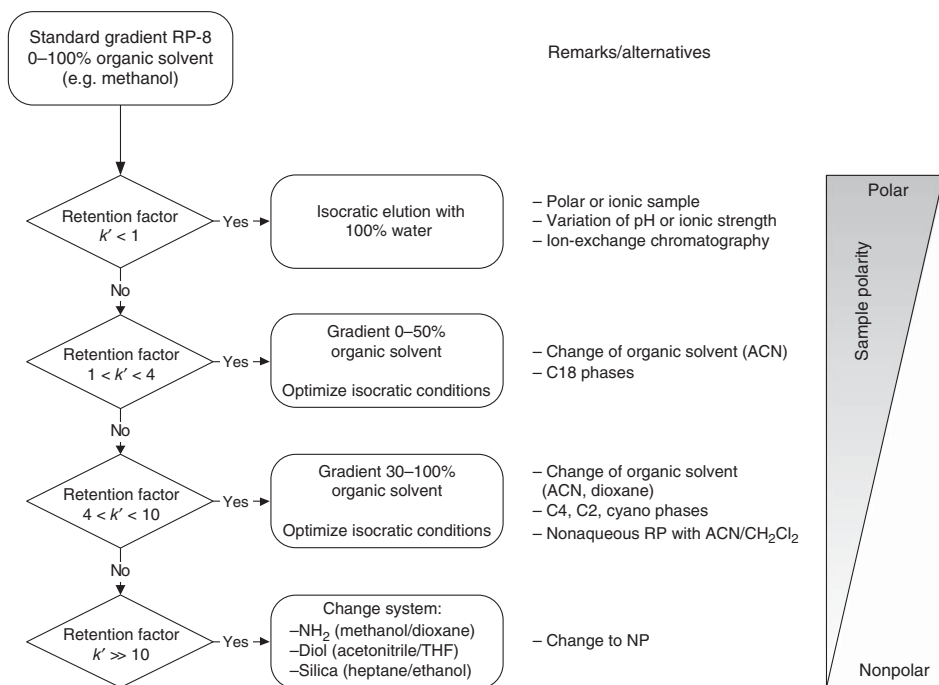
Figure 4.36 Optimization of mobile phase composition by gradient operation.
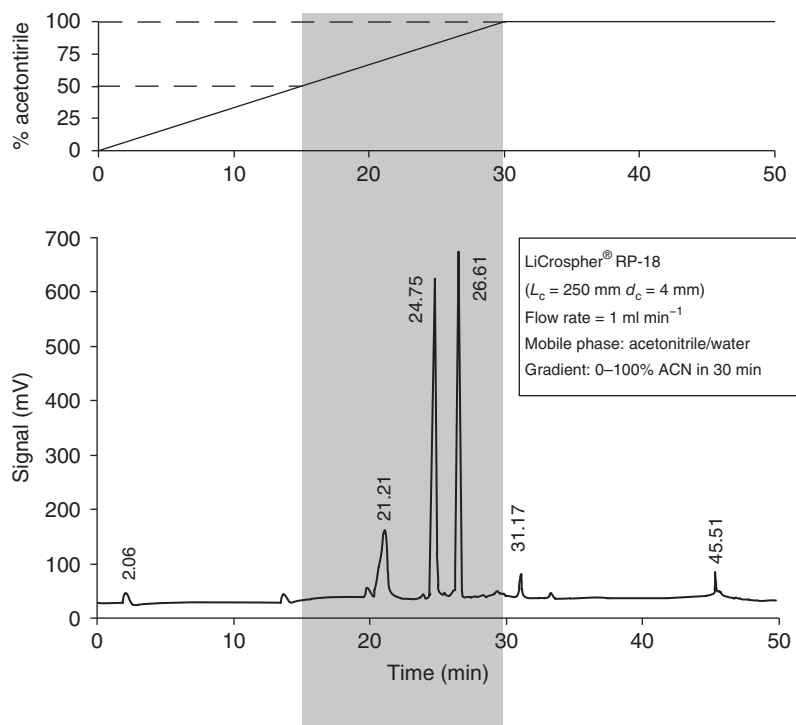
Figure 4.37 Initial gradient for the separation of three intermediates.

flow rate of 1 ml min^{-1}. The three target intermediates elute at 21.21, 24.75, and 26.61 minutes. The range of the elution times of the three intermediates is marked by the gray box in the chromatogram. It exceeds the above recommended starting and ending points by a few minutes. Corresponding to this time range, the gradient conditions for further optimization are determined according to the upper part of Figure 4.37.

The first mobile phase composition for the subsequent gradient run corresponds to ϕ at the beginning of the gray marked time range (50%), while the final composition is equal to ϕ at the end of this range (100%). By this strategy, the gradient (and thus the mobile phase) is optimized step by step.

Table 4.15 shows the gradient optimization. The initial gradient is followed by a second gradient from 50% to 100% acetonitrile. A third gradient from 70% to 100% has been examined, but the retention times are too low and, therefore, the components were not separated.

To check the selectivity with different chromatographic systems, the separation with LiChrospher RP-18 is compared with the gradient separation with two different adsorbents. For LiChrospher RP-8 the separation with methanol–water is shown in Figure 4.38a, while Figure 4.38b shows the separation with acetonitrile–water. With methanol the elution order of the first two peaks was inverted compared with the separation with acetonitrile. However, this change of the elution order results in decreased selectivities, and thus only

Table 4.15 Optimization of RP separation of three intermediates by gradient operation and resulting isocratic conditions.

Adsorbent	Organic solvent	Gradient	t_G (min)	Cycle time (min)	$k_1(-)$		$k_3(-)$	$\alpha_{2/1}$	$\alpha_{3/2}$
RP-18	Acetonitrile	0–100	30	5.40	8.64	10.26	11.10	1.19	1.08
RP-18	Acetonitrile	50–100	30	5.99	0.46	2.00	3.18	4.35	1.59
RP-18	Acetonitrile	70–100	30	1.24	0.07	0.07	0.64	1.00	8.71
RP-18	Acetonitrile	60	Isocratic	3.16	0.19	1.23	1.63	6.42	1.33
RP-8	Methanol	0–100	30	2.29	11.54[a]	12.35[a]	12.58	1.07	1.02
RP-8	Methanol	50–100	30	6.27	4.17[a]	6.73[a]	7.02	1.62	1.04
RP-8	Methanol	70–100	30	0.99	0.81[a]	1.12[a]	1.26	1.39	1.12
RP-8	Acetonitrile	0–100	30	5.02	8.52	9.78	10.80	1.15	1.10
CN	Acetonitrile	0–100	30	7.58	5.83	8.44	9.28	1.45	1.10
CN	Acetonitrile	30–100	30	8.49	0.56	3.45	4.42	6.22	1.28
CN	Acetonitrile	60	Isocratic	1.77	0.06	0.63	0.87	9.80	1.38

a) Elution order between intermediates 1 and 2 inverted due to the use of methanol.
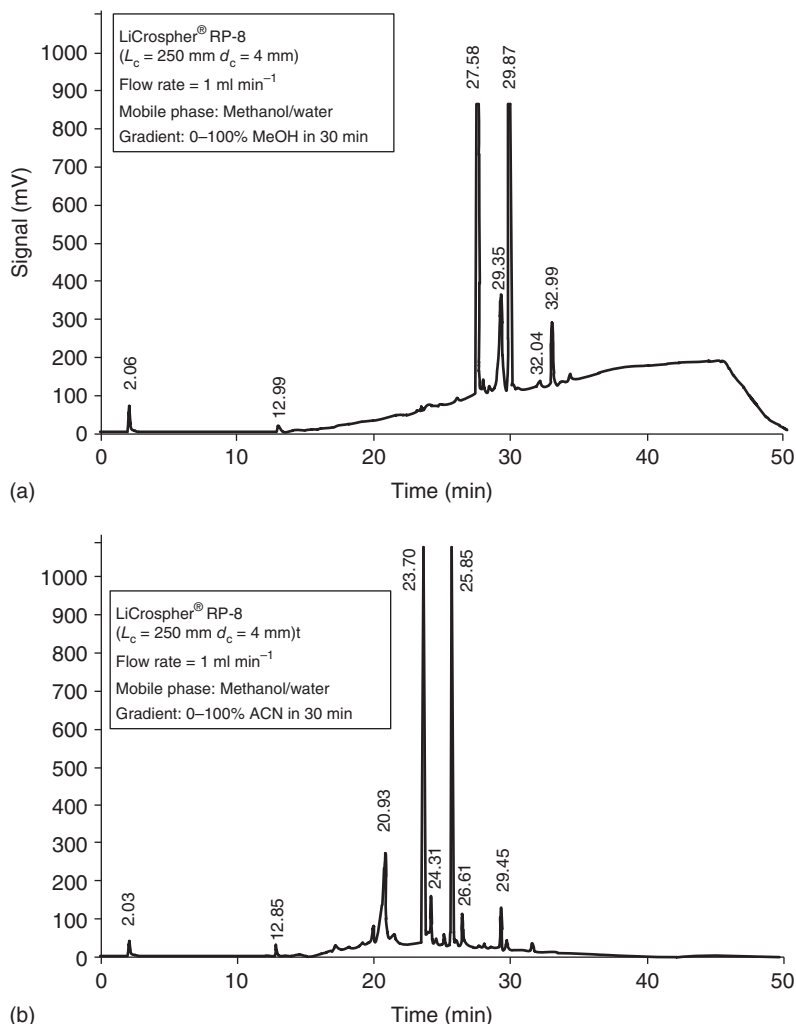
Figure 4.38 Gradient runs for two different organic solvents with LiChrospher® RP-8: (a) methanol and (b) acetonitrile.

acetonitrile is further tested as organic solvent. The third tested adsorbent is LiChrospher CN. Retention factors and selectivities are shown in Table 4.15. For the RP-8 phase no suitable system was found, while the selectivity for the RP-18 and CN phase was satisfying and appropriate gradient conditions could be identified. Based on the good selectivities on these two adsorbents, isocratic conditions in the medium polarity region of the gradient composition were also tested and gave good results. The two isocratic separations on RP-18 and CN silica would be preferred for large-scale separations of these feed mixtures as they show short cycle times and still have good separation factors. Isocratic mobile phase compositions for both phases are also presented in Table 4.15.

4.5.5 Practical Recommendations

Although RP systems are quite robust, different sources of practical problems during the operation exist:

- Solutes might ionize in aqueous mobile phases.
- Effects of residual silanol groups of the RP packing.
- Operational problems due to high fractions of water in the mobile phase.

Since retention in RP systems depends on the interaction between hydrophobic groups of the solutes and the adsorbent surface, ionization of the solutes can result in severe peak distortion. Ions are very hydrophilic and are thus poorly retained in RP systems even if the nonionized solute shows good retention. Because ionization reactions (e.g. dissociation of organic acids) are determined by their chemical equilibrium, solutes are present in both forms. This leads to broad peaks with poor retention. The ionization reaction must be suppressed by buffering the system. Thus, the stability of the adsorbent for the pH range must be checked. Especially for alkaline mobile phases, silica-based materials are problematic, and the use of polymeric phases should be checked. If ionization of the solutes is suppressed by adding salts to the aqueous mobile phases, a second effect occurs since the salt increases the polarity of the mobile phase, thereby increasing retention times.

Residual silanol groups on the adsorbent surface are a source of secondary interaction different from the bonded groups. Next to hydrogen bonding and dipole interactions, silanol groups can be regarded as weak ion exchangers (Arangio 1998). Especially for basic solutes, the IEX effect dominates. Secondary interactions result in significant changes in retention time and, very often, peak tailing. The IEX mechanism can be suppressed by protonation of the silanol groups at low pH. At pH 3 roughly all residual silanols are protonated and no ionic interactions are observed. At pH > 8 nearly all residual silanol groups are present in ionic form. Along with suppression of ionization by adding buffer, chromatographic efficiency is increased by reducing the number of residual silanol groups by endcapping.

Endcapping of adsorbents is very important if high volume fractions (even 100%) of water are used as mobile phase. Due to the hydrophobicity of the adsorbent surface, problems with moistening of the adsorbent can occur, and, as a result, the surface groups can collapse. Standard RP-18 alkyl chains are not wetted and are thus not stable at 100% water. The alkyl chains, which should point into the mobile phases like bristles from a brush, will collapse and stick together on the surface. As a result, solutes in the mobile phase will not migrate into the surface of the adsorbent, and the retention time will change dramatically. This behavior depends strongly on the endcapping of the surface. If nonpolar groups are used for endcapping, the hydrophobicity of the alkyl silica increases, and thus the stability for 100% water mobile phases gets worse. For this reason, special adsorbents with polar groups for the endcapping or embedded polar groups in the alkyl chain have been designed for use in 100% water. Nevertheless, wherever possible nonendcapped adsorbents should be used in process-scale applications, because they are cheaper and less sophisticated.

Owing to the practical problems with RP chromatography, very often aqueous solvents with buffers are used as mobile phase. Because of the high boiling point of water and the presence of salts in the mobile phase, recovery with high purity of the target solutes from the fractions can be simplified with one more adsorption step. A short RP column with a large diameter (so-called pancake column) can be used for a solid-phase extraction step. The target fraction is diluted with water to decrease the solvent strength of the mobile phase. The diluted fraction is then pumped onto the column, and the sample is strongly adsorbed at the column inlet. After the complete fraction is collected in the column, it is washed with a mobile phase of low solvent strength to remove the salts. In the last step, the sample is eluted with a low volume of a solvent with high elution strength (e.g. methanol). The concentration of the sample is now much higher, the salt is removed, and the more volatile strong solvent is easier to evaporate.

4.6 Criteria for Choosing CSP Systems

In contrast to NP and RP separations, one critical difference with chromatographic enantioseparations on CSP is that rational development of selectivities on one given stationary phase is nearly impossible. Optimization of the chromatographic parameters for enantioseparation is much more difficult than for nonchiral molecules and involves the screening of several mobile–stationary phase combinations. As a general guide to successful enantioseparation, the process should be developed using the following steps (Figure 4.39):

- Suitability of preparative CSP.
- Development of enantioselectivity.
- Optimization of separation conditions.

4.6.1 Suitability of Preparative CSP

Before starting to screen for a suitable CSP, some general considerations have to be taken into account to optimize the separation in the best direction right from the beginning. The required purity and amount and time frame should be known along with some limitations with regard to solvents or other process conditions, for example, temperature range. In addition, it should be known if only one or both enantiomers have to be delivered in purified form.

Over 100 CSPs are now commercially available (Section 3.5). Not all of them are designed and suited for preparative purposes. Certainly, every CSP might be used to isolate some milligram amounts of an enantiomer in case of urgent need, but to develop a production process, the CSP should fulfill some critical requirements. The main parameters are:

- Selectivity (range).
- Reproducibility.
- Stability.
- Availability.
- Price.
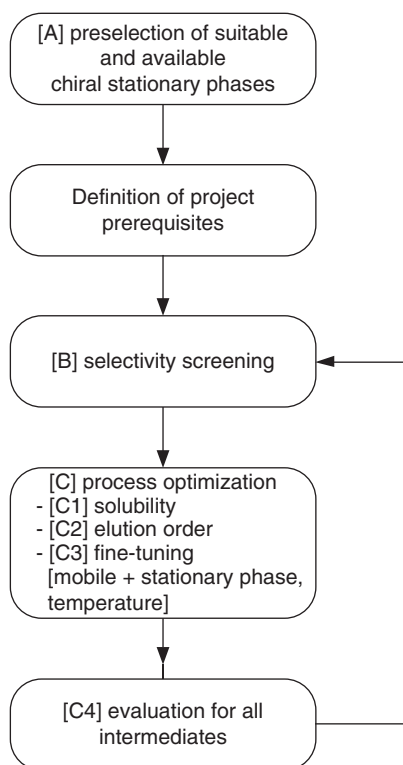
Figure 4.39 Screening strategy for chiral separations.

A certain selectivity range should be given for the individual CSP. The selectivity range is of great importance for laboratories where moderate amounts (maximum in the gram range) of a multitude of different racemates are separated in a short time. Chiral phases with the broadest selectivity range are the cellulose and amylose derivatives. With the chiral phases Chiralcel® OD and OJ and Chiralpak® AD and AS, selectivities for about 70% of all screened racemates are found (Daicel Application Guide 2003). For production purposes, a broad selectivity range is not necessary if only the desired racemate is well separated. Even tailor-made adsorbents could be used if the production is well controlled and the regulatory and reproducibility issues of the phase are well addressed. The main parameters for overall suitability are related to the mechanical and chemical stability of the adsorbents. Chemical stability is mainly linked to the range of solvents that can be used. As solubility is often an issue for pharmaceutical compounds, the chosen CSP should have a good stability against solvents with different polarities so that the whole spectrum of retention adjustment can be used. For production processes, the availability of the CSP in bulk quantities at a reasonable price should also be taken into account.

4.6.2 Development of Enantioselectivity

For CSPs, the mobile phase selection has to aim first for enantioselectivity α (D, L). The molecules to be separated show identical chemical (same functional

groups) and chromatographic behavior (same retention on the bare stationary phase; chiral recognition of enantiomers only by the bonded chiral selector). Therefore, the separation is based on very small differences in complexation energies of the transient diastereomer complexes formed, and similar strategies as for the selections of solvents for liquid–solid chromatography are helpful. Take a good solvent, in which the sample readily dissolves (e.g. ethanol for cellulose- or amylose-based packings) and increase retention until enantioseparation may be observed.

As pointed out above, no selectivity guarantee can be given for the separation on a certain CSP. Therefore, screening routines have to be followed to obtain the appropriate adsorbent. The first possibility is the knowledge-based approach. Some CSP exhibit a certain group specificity, for example, the quinine-based CSPs for N-derivatized amino acids or the poly(N-acryloyl amide derivatives) for five-membered heterocycles. The most advanced statistical and knowledge-based approach is the chiral separation database ChirBase®, developed by Christian Roussel at the University of Marseille (http://chirbase.u-3mrs.fr/). Based on more than 20 000 separations integrated into the database, software has been developed by Chiral Technologies in cooperation with the University of Marseille to suggest the most successful starting conditions for a racemate based on its functional groups. More general predictions have been made by the Marseille group based on correspondence analysis of the graphical representation of single CSPs and 15 empirical molecular descriptors of the racemates included in the database (Roussel, Piras, and Heitmann 1997).

If no rational starting point for the separation of a racemate can be found, a random screening procedure has to be applied. In most cases 250 mm × 4 or 4.6 mm columns are used for this purpose. Modern HPLC systems often include a column switching device with up to 12 columns. Most systems have programmable software options for the set of different mobile phase compositions. Combination of UV and polarimetric detection allows even very small selectivities to be found and used as a starting point for further optimization. Commercial systems with deconvolution and optimization options are available, together with a given set of 12 different CSPs (http://scientex.com.au/pdr-chiral/). After an initial detection of selectivity on a CSP, the mobile phase composition and additives as well as temperature have to be varied either manually or by means of an automated system.

For large-scale separations even the design of a new CSP might be economically advisable. The most prominent CSP design approach is the reciprocal approach developed by Pirkle and Däppen (1987). One pure enantiomer of the racemate to be separated is bound via a spacer to silica as chiral selector. Onto this CSP, various racemates are subjected whose pure enantiomers are readily available in sufficient amounts. One enantiomer of the racemate with the highest selectivity is chosen as the chiral selector for the CSP. After manufacturing this reciprocal CSP, the production of the desired enantiomer can take place. This approach has been used to obtain a very good stationary phase for the separation of nonsteroidal anti-inflammatory drugs, for example, ibuprofen and naproxen (Pirkle, Welch, and Lamm 1992).

Now that combinatorial and parallel syntheses are available, the number of possible selectors for CSPs can be drastically increased. Selector synthesis on solid phases and the testing in 96-well plate format have been used to make the CSP screening process more efficient (Welch, Protopopova, and Bhat 1998; Murer et al. 1999; Bluhm, Wang, and Li 2000; Svec, Wulff, and Fréchet 2001).

The history of columns used for screening racemates for large-scale production purposes should be carefully documented. Cellulose and amylose derivative CSPs, especially, sometimes show strong reactions on small amounts of acids and bases. These compounds might not only be mobile phase additives but also racemates bearing acidic or basic functions that have been previously injected. For large-scale projects, it is advisable to use new columns to avoid disappointments if selectivities cannot be reproduced on other or larger columns.

4.6.3 Optimization of Separation Conditions

4.6.3.1 Determination of Racemate Solubility

The solubility of the racemate in the mobile phase is the first parameter to be optimized. Several solvents should be screened for solubility and selectivity at the CSP that showed the highest selectivity. Notably, once again, not all CSPs can be operated with all solvents. The instability of the coated cellulose and amylose derivative CSPs against medium-polar solvents such as dichloromethane, ethyl acetate, and acetone is widely known. Improved phases with immobilized chiral selectors have been recently developed and made available in bulk quantities (Section 3.5.1).

4.6.3.2 Selection of Elution Order

With chromatographic production processes, the elution order of the enantiomers is of importance. In SMB processes, the raffinate enantiomer can often be obtained with better economics as it is recovered at higher purities and concentrations. If the CSP offers the possibility of choosing one of the two optically active forms of the selector, the adsorbent on which the desired enantiomer elutes first should be chosen. This option can be used especially with the brush-type phases with monomolecular chiral selectors. Even if the CSP is not available in both forms, the elution order should be checked carefully as the elution order might be reversed on two very similar adsorbents or with two similar mobile phase combinations. Okamoto and Nakazawa (1991) and Dingenen (1994) have shown that by changing only from 1-propanol to 2-propanol, respectively, with 1-butanol, the elution order on a cellulose-based CSP might reverse.

4.6.3.3 Optimization of Mobile/Stationary Phase Composition, Including Temperature

It should be taken into account that the highest enantioselectivity is observed at the lowest degree of nonchiral interactions, that is, at the level of a nearly nonretained first enantiomer. Moreover, enantioselectivity increases with lower

temperature according to Eq. (4.13):

$$\alpha = \frac{1}{e^{\left(\frac{\Delta\Delta G_{D,L}}{R\bullet T}\right)}} \tag{4.13}$$

This effect on resolution may be counterbalanced by increased viscosity, leading to lower efficiency of the system. Therefore, fine tuning of mobile phase composition and temperature should be carefully taken into account for production-scale systems as some economic benefits have to be considered against a higher complexity of the separation system, for example, in terms of controlling temperature and small amounts of modifier.

4.6.3.4 Determination of Optimum Separation Step

Notably, in the synthetic route toward the final enantiomerically pure compound, all intermediates should be taken into account for a chromatographic separation step. After introducing the chiral center, the intermediates might differ substantially in solubility and selectivity. No general guidelines can be given as to whether separation on an early or final stage is better economically. Good project coordination involving synthetic chemists and chromatography specialists is the best way to ensure that the optimum separation stage is found. Following this approach, Zhou et al. showed the separation of six different intermediates of the semisynthetic carcinostatic drug homoharringtonine on Chiralpak IC. Using isopropanol as the solvent modifier, five of the six intermediates show a low to medium enantioselectivity between 1.1 and 1.8. Intermediate five however is standing out with an enantioselectivity of 2.24, making this intermediate the obvious choice for a preparative separation (Zhou et al. 2015).

4.6.4 Practical Recommendations

When optimizing the temperature of a chiral separation, it should be noted that some chiral compounds tend to racemize at elevated temperatures. On-column racemization might be seen as a typical plateau between the two peaks of single enantiomers (Trapp and Schurig 2002). Acidic or basic mobile phase additives might even catalyze such racemization. Conversely, on-column racemization can be used to optimize the yield of a chiral SMB separation. If only one enantiomer is of interest and the other is considered as "isomeric ballast," on-column racemization could be used to enhance the separation yield by transferring the undesired enantiomer into the racemate again. This might be done in an on- or offline chromatographic reactor (Section 5.2.10).

In chiral chromatography, especially in SMB production systems, the quite sensitive CSPs are subjected to a high mass load of compounds to be separated – which might cause some conformational changes of the chiral selector. Once the column is rinsed with pure solvent and checked by a pulse injection, severe changes might be observed. Figure 4.40a shows enantioseparation on a column continuously loaded with feed mixture for several hours. Afterward, the column was washed with pure eluent and checked with a pulse injection (Figure 4.40b).
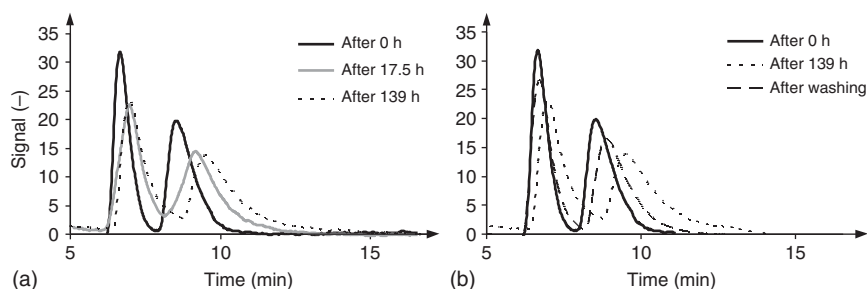
Figure 4.40 Effect of high feed loading on achiral stationary phase. (a) without column washing (b) with column washing

Clearly, some severe changes have occurred during the 139 hours of operation. The retention time of both peaks has shifted, and, especially, the tailing of the second peak has increased tremendously with time. After washing the chiral phase with a solvent of high polarity, the changes are only partly reversible. This behavior is shown in Figure 4.40b, where the chromatograms at the beginning 0 hours and after 139 hours of separation are compared with that after washing. Obviously, after the washing step, the column does not reach the original condition at the beginning of the separation. For SMB chromatography, the increased tailing had to be adjusted by changing the flow rates. However, finally, the separation had to be stopped because no stable conditions were found under which the change in stationary phase behavior could be compensated by small flow rate changes or short washing procedures.

CSPs are also used for the separation of positional isomers. Isomers are normally well separated on straight-phase silica or medium-polar silica phases, for example, cyano-modified silica. However, if two or more chiral centers are a certain distance apart, they might behave on the columns as if they were pairs of enantiomers. Therefore, it is also worth testing CSPs if difficult isomer separations have to be performed. Figure 4.41a–c shows optimized separations of a pair of diastereomers on a straight-phase silica (LiChrospher Si60), an RP silica (Purospher RP-18e), and a CSP (Chiralpak AD), respectively. Clearly, the separation with the CSP is much better and simplifies the preparative separation so that the higher costs of the stationary phase are compensated by improved overall process economics.

Derivatization of racemates is widely used for analytical purposes to enhance detection or reduce the interference of the target compound with the matrix (Schulte 2001), but derivatization might also be used for preparative purposes. Francotte (1998) showed that the reaction of different chiral alcohols with a benzoyl ester functionality results in a series of racemates that are well separated on benzoylcellulose-type CSPs. With difficult enantioseparations for a given target molecule, it can be worthwhile derivatizing the racemate with different achiral side groups and testing the series of racemates for optimum selectivity.

Table 4.16 shows the results of this approach for a series of derivatives of a chiral C3 building block. This building block is widely used in medicinal chemistry. As the side chain is cleaved off during the following synthesis step, the derivatization group might be chosen from a wide range of available components.
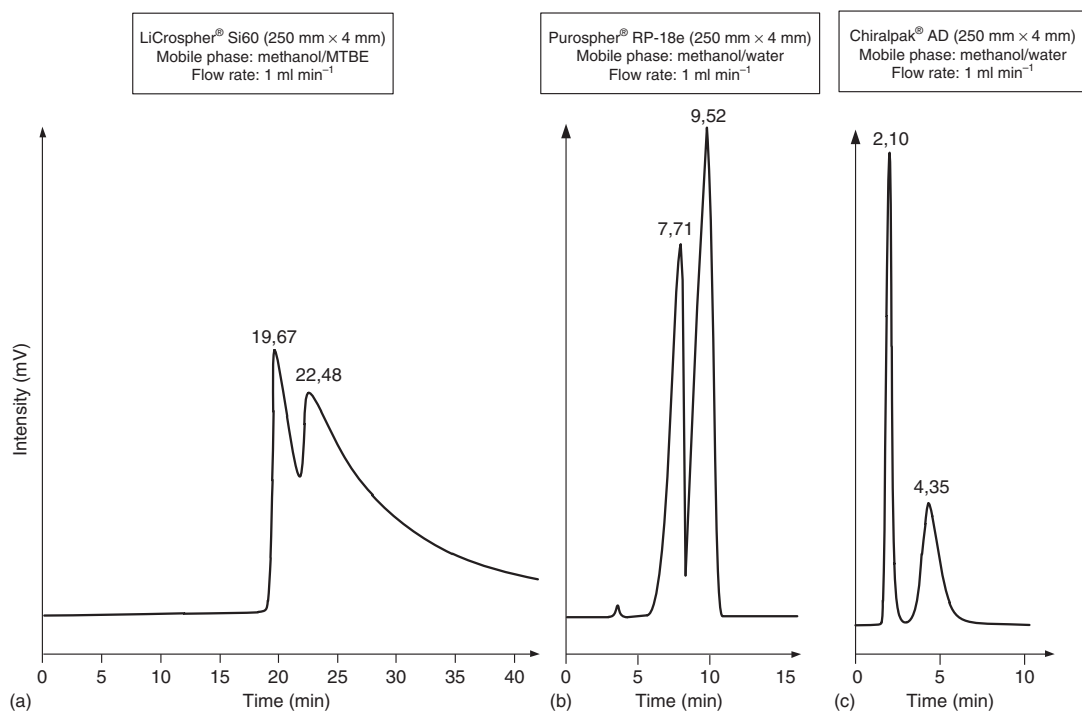
Figure 4.41 Separation of a pair of diastereomers on different nonchiral and chiral stationary phases (a–c).

Table 4.16 Derivatization of a chiral C3 building block and corresponding chromatographic results.

C3 moiety				
X	**R3**	**CSP**	k_1'	α
—O—	—H	Several	n.a.	1.0
—O—		Several	n.a.	1.0
—O—		Chiralpak® AS	0.52	1.08
—O—		Whelk-O-1®	1.19	1.08
—O—		Whelk-O-1®	1.39	1.11
—O—		Chiralcel® OJ	1.26	1.21
—O—		Whelk-O-1®	0.69	1.05
—O—		Whelk-O-1®	2.27	1.07
—O—		Whelk-O-1®	1.17	1.24
—O—		Exp. poly (*N*-acryloyl amide)	1.26	1.11
—OH, —OH		Chiralcel® OD	3.69	1.25

Table 4.16 shows that substantial differences in enantioselectivity can be observed for the single compounds. Nevertheless, it should be taken into account that the derivatization group is ballast in terms of the mass balance of the total synthetic route. The molecular mass of the group should be kept as low as possible to keep the total amount of components to be separated small. This strategy has, for example, been successfully implemented by Dingenen (1994) for α-(2,4-dichlorophenyl)-1*H*-imidazole-1-ethanol derivatives.

4.7   Downstream Processing of mAbs Using Protein A and IEX

The separation tasks for IEX chromatography differ mainly by the type of expression system used. The most abundant systems are mammalian cells, microbial cells (yeast), and the bacterial organism *Escherichia coli*. All expression systems have a common feature that they not only generate the target protein but also process-related impurities, such as host cell proteins, DNA, viruses, and endotoxins. In addition, the downstream process has to isolate the active form of the target molecule from all its derivatives, for example, oxidated, deamidated, and acetylated forms, dimers, aggregates, and unfolded proteins.

Impurities and excipients stemming from the production process are another group of molecules to be removed during the purification process. These process-related molecules can be of low molecular weight, for example, antibiotics, antifoaming agents, inducing and refolding agents, sugars, solvents, salts, and water, or molecules of high molecular weight, for example, insulin or albumin.

It is clear that this difficult separation task cannot be done with a single chromatographic step. Therefore, the typical downstream process, for example, a monoclonal antibody consists of three distinct chromatographic steps: capturing, intermediate purification, and polishing.

Figure 4.42 a shows one very typical mAb downstream process, which is focused here on the chromatography steps. The assumption for this downstream process is a fermentation titer of $2\,g/l^{-1}$ mAb in a $12\,m^3$ bioreactor. Following centrifugation and filtration, the so-called clarified cell culture supernatant is loaded to a protein A affinity resin. The mAb in the protein A eluted fraction is concentrated by about a factor of 4, and the total volume to be processed is also significantly reduced to almost the same factor. The following steps are virus removal by a low pH step in the virus hold tank, followed by a cation-exchange step, performed in a bind and elute modus, followed by a hold tank where the cation elution pool is adjusted to be pumped over an anion-exchange (AEX) column in a flow-through or nonbinding mode, respectively. Volumes to be processed and concentration of the target molecule are given in Figure 4.42a.

It is obvious that not only the chromatographic columns are adding costs to the overall process but also the vast number of liquid handling steps, e.g. buffer preparation and product holding tanks, are creating great complexity as well as high costs. For new downstream processes, there is a clear trend to integrate process steps and to intensify the use of single unit operations as shown in Figure 4.42b. The capture step is often implemented as a multicolumn capture step with a higher utilization of the expensive affinity resins. Virus inactivation should be done in a continuous flow-through mode instead of a hold tank. For the further downstream processing, integrated polishing trains are under development with the goal to have only minimum buffer adjustments in between the two chromatographic steps and to run both steps if possible in a flow-through (negative) mode. Negative chromatographic steps are only binding the impurities, e.g. host cell DNA and remaining viruses in case of the AEX step
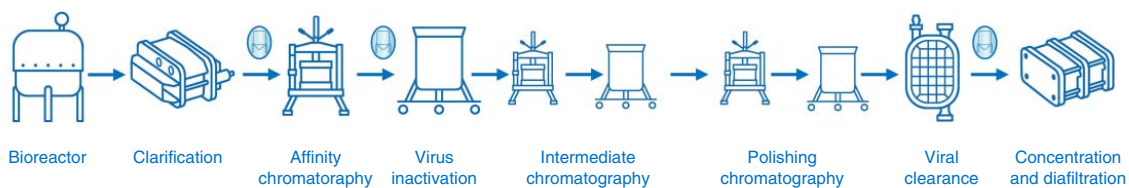
	Prot A	Virus hold	CEX	Hold tank	AEX	Hold tank
Input	12 000 l	2 850 l	3 280 l	1 530 l	3 060 l	3 060 l
	2 g l^{-1}	8.2 g l^{-1}	7.1 g l^{-1}	13.7 g l^{-1}	6.9 g l^{-1}	6.9 g l^{-1}

(a)
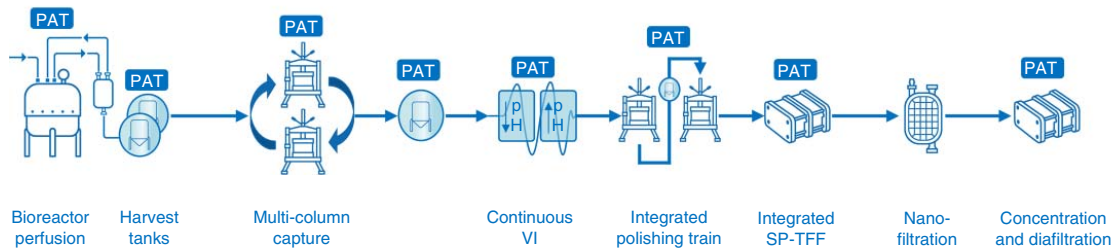
(b)

Figure 4.42 mAb purification platform. (a) standard process (b) intensified process

but let the target molecule always in solution. For sure, this complex task can only be fulfilled with rigorous process development. For IEX chromatography, the main criteria to be optimized include type of IEX group (weak or strong, cation or anion) and on the mobile phase side the pH, nature, and concentration of the buffer. Some additives might be required in addition.

Chromatographic IEX process development is more and more using high-throughput methods. Three different approaches are mainly used to obtain the necessary information:

(1) Static binding capacity as a function of salt and pH.
(2) Pseudo-dynamic binding capacity from static deep well plate experiments.
(3) Pseudo-gradient elution using automated miniaturized chromatographic columns.

A typical result demonstrating the static binding characteristics of three different cation-exchange resins for a monoclonal antibody as function of pH and salt concentration in the load buffer is shown in Figure 4.43. As it can be seen from the different plots, the static binding capacity is influenced by the number of ionic ligands so that the different IEX resins can be used according to their binding profile, e.g. in high or low salt environment.

For static binding experiments, 96-well plates are typically filled with 10–20 μl of settled resin volume and equilibrated. The plates are then incubated with the protein-containing buffers for up to two hour to reach full saturation of the beads. The robotic system shakes the plates at defined time intervals. At the end of the incubation time, the supernatant is separated from the resin by a vacuum suction step. The protein concentration in the supernatant is analyzed by an online UV detection system. Following a washing and elution step and the determination of the protein concentration in the washing and elution fractions, also the recovery and the elution binding capacity can be determined. This method gives results that are in good accordance with column experiments but basically are being used to compare different operating conditions (Stein and Kiesewetter 2007). It has to be pointed out that the measurement of the UV signal cannot distinguish between the target protein and any impurity. The integration of an offline analytical system, for example, by HPLC or ELISA techniques to analyze the impurities is possible but needs a quite substantial investment.

A solution for quasi-dynamic high-throughput analysis using deep well plates has been developed by Boehringer Ingelheim and named Rapptor® (Eckermann et al. 2007; Rathjen et al. 2009). Samples are taken in defined incubation intervals representing different residence times and analyzed for their protein content (Figure 4.44). By closing the mass balance of the fractions taken, a breakthrough curve can be calculated from the UV signal of the fractions.

More recently also high-throughput screening systems in flow-through mode have been developed, enabling dynamic binding and elution experiments. These systems use prepacked arrays of chromatographic scout columns, for example, Opus® MiniColumns or RoboColumns® from Atoll (acquired by Repligen in 2016) (Schulze-Wierling et al. 2007). The packed columns are operated by the liquid handling system that presses a defined amount of mobile phase under predefined linear velocities through the single scout columns (Wiendahl et al. 2008).
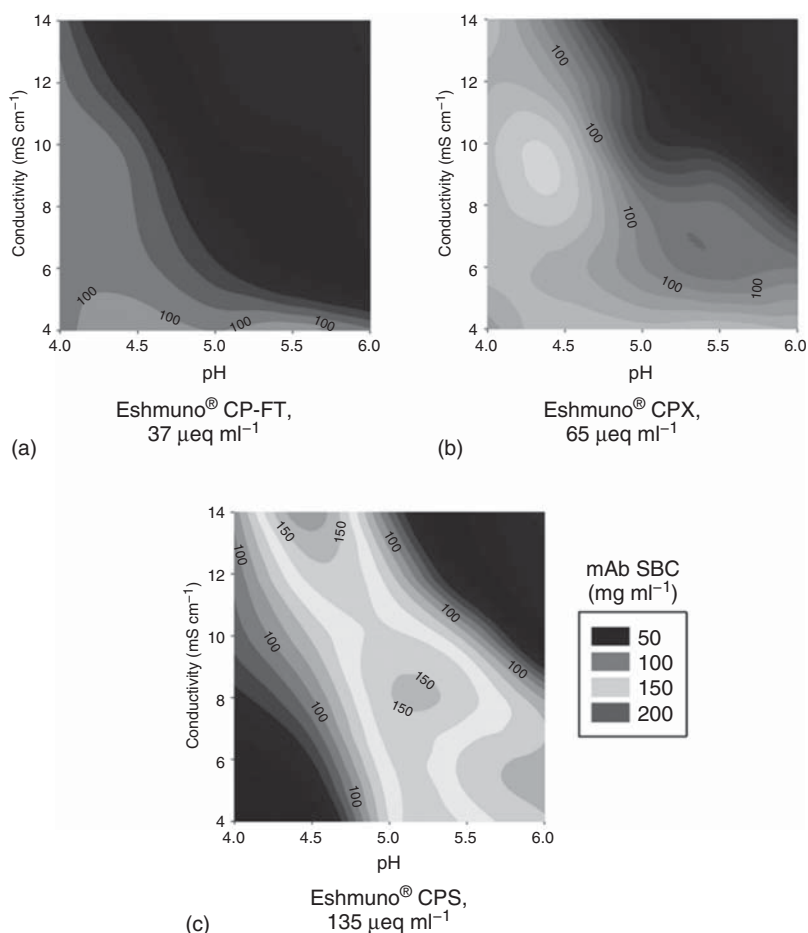
Figure 4.43 Static binding capacity of mAb on cation-exchange (CEX) resins having the same base bead and strong CEX group (SO_3) but different ionic capacities (37, 65, and 135 µeq ml^{-1}) at different pH and NaCl concentrations.(a) Eshmuno® CP-FT, (b) Eshmuno® CPX and (c) Eshmuno® CPS

As for each new mobile phase composition, the needle of the robot has to be replaced and filled again, only step gradients can be applied.

Using these miniaturized columns, it is possible to apply pseudo-linear gradient elution (LGE) in a high-throughput format. This approach offers the possibility to exploit the selectivity of different IEX resins in a fast and parallel way (Kiesewetter et al. 2016). The methodology of LGE has been introduced into IEX chromatography by Yamamoto, Nakanishi, and Matsuno (1988). It is the goal of the LGE to obtain plots of the Peak salt concentration I_R for the different proteins versus the normalized gradient slope GH. The GH value is representing the gradient slope times the stationary phase volume and is determined at different pH values. From the GH versus I_R plot, the relation between the protein distribution coefficient K versus the ionic strength can be derived. Using Eq. (4.14), the dimensionless
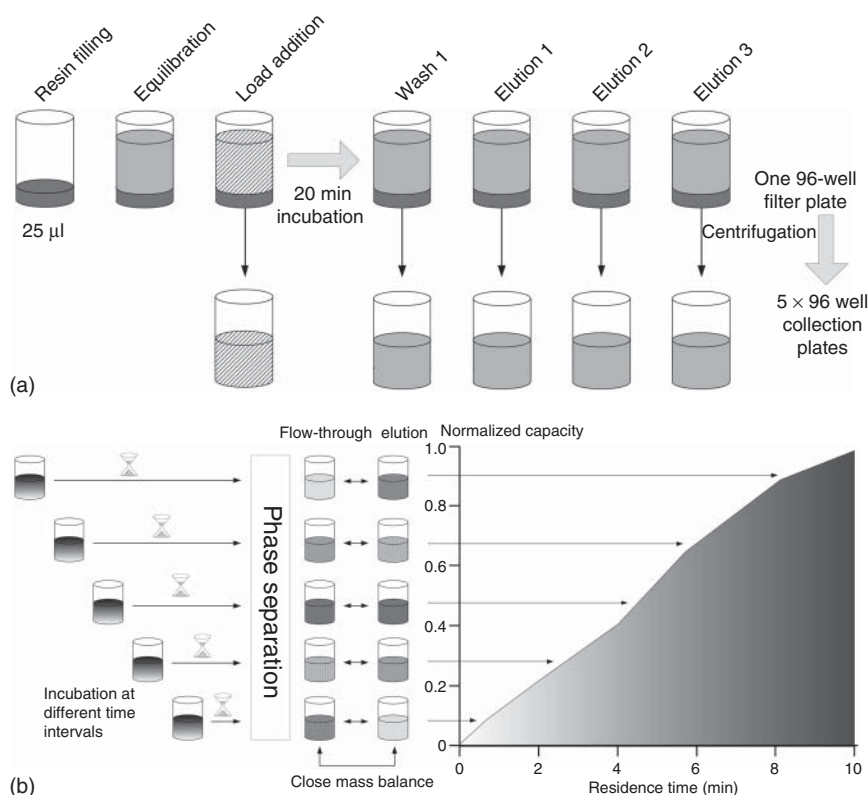
Figure 4.44 Principle of the Rapptor® robotic platform. Samples are incubated for different time intervals and filtered, and the flow-through as well as bounded protein analyzed. (a) Robotic examination steps: 1. resin incubation and 2. analytical assays; 32 variables in triplicate in a 96-well plate. Four different resins with eight different conditions, 20 minutes incubation time, load, one washing step, three elution steps. (b) Quasi-dynamic examination of different resins with the robotic system.

number O representing the resolution can be introduced:

$$O = (ZI_a)/(G(\text{HETP})_{\text{LGE}}) \tag{4.14}$$

where Z is the column length in cm, I_a is a dimensionless constant having a numerical value of 1 (M), G is the gradient slope normalized with respect to column void volume, and HETP_{LGE} is the plate height in the LGE. Identical elution curves can be achieved with different column geometries, gradient volumes, and linear velocities as shown in Table 4.17.

The LGE model can be applied on dual gradients as well, where pH and salt concentration are modified in different parallel and antiparallel ways. This tool has recently been applied successfully to anion- and cation-exchange chromatography as well as mixed-mode chromatography (Lee et al. 2015; Wittkopp et al. 2018).

It can be seen from Table 4.17 that completely different processes with respect to the amount of stationary and mobile phase and the column dimension have

Table 4.17 Process parameters for the separation of egg white proteins on the strong cation exchanger Fractogel SO_3 with identical *O*-values of 10 000.

Value	Parameter set 1	Parameter set 2	Parameter set 3
Column length (cm)	5.4	25.0	24.3
Column diameter (cm)	1	1	2.6
Gradient volume	5.3	5.1	5.5
Linear velocity (cm h^{-1})	100	240	150

Source: Jacob and Frech (2007). Reproduced with permission of John Wiley and Sons.

to be compared to obtain the process with the best economy. By calculating iso-resolution curves (Yamamoto and Kita 2005), the optimization of protein separations in the linear range of the adsorption isotherm can be achieved. For nonlinear conditions, more sophisticated calculation methods taking into account the competitive effects have to be used.

4.8 Size-Exclusion Chromatography (SEC)

Size-exclusion resins in their ideal form do not exhibit any adsorption. For protein purification, they should be as hydrophilic and inert as possible. The separation principle is a complete partitioning process in between the pore system of the matrix (Yau, Kirkland, and Bly 1979; Cutler 2004). Therefore, the separation efficiency is solely based on the column length, and for a good resolution of compounds with only minor differences in molecular weight (or better molecular volume), a long column length is needed. As a consequence, the matrix of the sorbent has to be quite rigid, so a high degree of cross-linking is preferred, without reducing the accessible pore volume too much. As no adsorption is taking place, the load of a size-exclusion column is quite low, and the injection volume is restricted to <5% of the column volume if high resolution should be achieved. To maximize throughput, the protein concentration should be high in the range of 2–20 mg ml^{-1} depending on the solubility of the protein and the maximum viscosity the chromatographic system can tolerate.

In addition, the flow rate in size-exclusion chromatography (SEC) is quite low to ensure complete diffusion of the feed into the pore system. From these facts, it can be clearly seen that SEC in preparative mode is a quite difficult technology: long columns up to 1 m in length were packed with semirigid sorbents and operated with low flow rates. Nevertheless, it is quite often used for special purposes, for example, the removal of protein aggregates, vaccine purification, or the fractionation of blood plasma fractions. As an example, Octapharma has shown the use of SEC for the separation of the clotting factor FVIII and the associated von Willebrand factor (vWF) in preparative scale using the polymethacrylic SEC

resin Fractogel® BioSEC in a column of 10 cm i.d. and 90 or 100 cm length (Josic et al. 1998).

It can be observed with certain SEC matrices that a certain adsorption occurs. Remaining residual charges might come from sulfate groups in agarose gels or carboxyl residues in dextrans. To overcome these adsorptive effects, the ionic strength of the buffer should be kept at 0.15–0.2 M to suppress electrostatic or van der Waals forces. Cross-linking agents in polymeric gels may introduce a certain hydrophobicity to the matrix, which can especially lead to the adsorption of smaller proteins rich in aromatic amino acids. The additional adsorptive effects can be used to tune the selectivity of the separation, but they might be also the reason for incomplete yield due to strong adsorption.

Preparative size-exclusion matrices are either cross-linked cellulose, agarose, or dextrans or hydrophilic polymers. Table 4.18 lists the most common sorbents with their fractionation range and pH stability.

As SEC is a per se isocratic conditions, there have been several attempts to use it in the classical SMB setup. Several benefits are quite obvious: only shorter columns have to be packed and the low loadability and productivity due to the long retention times can be overcome. Britsch, Schulte, and Strube showed for the separation of whey proteins an increase in productivity by a factor of 95 while simultaneously the eluent consumption was reduced by a factor of 40 (Britsch, Schulte, and Strube 2003). Other examples have been published including the isolation of insulin (Mun et al. 2003), the separation of lactose from human milk oligosaccharides (Geisser et al. 2005), and the integration of refolding and purification of proteins using size-exclusion chromatography-simulated moving bed (SEC-SMB) (Wellhoefer et al. 2014).

4.9 Overall Chromatographic System Optimization

4.9.1 Conflicts During Optimization of Chromatographic Systems

Up to now many different criteria for the choice of an optimized chromatographic system have been given. Many of these parameters are not independent. For example, a high solubility should always be preferred, but the retention time is very often too low with solvents that provide high solubilities. The most important parameter is high throughput at the desired purity and yield. The resolution gives useful hints for the optimization of a separation, because it merges different effects into one parameter:

$$R_S = \underbrace{\left(\frac{\alpha - 1}{\alpha} \right)}_{\substack{\text{influence} \\ \text{of the} \\ \text{selectivity}}} \cdot \underbrace{\left(\frac{k_2'}{1 + k_2'} \right)}_{\substack{\text{dependent} \\ \text{on the} \\ \text{retention time}}} \cdot \underbrace{\frac{\sqrt{N_2}}{4}}_{\substack{\text{efficiency} \\ \text{of the column}}} \tag{4.15}$$

Resolution can be increased if one of the three terms in Eq. (4.15) is increased. As mentioned in Section 2.2.4, the first term describes the influence of selectivity. This term should be maximized by maximizing α in a selectivity screening

Table 4.18 Commercially available preparative SEC sorbents.

Name (nature)	Manufacturer	Type	Fractionation range (kDa)	pH stability	Organic solvent stability
Sephadex (dextran)	GE Healthcare	G25	1–5	2.0–10.0	
		G50	1.5–30		
		G75	3–80		
		G100	4–100		
		G150	5–150		
		G200	5–600		
Sepharose (agarose)	GE Healthcare	6B	10–4000	3.0–13.0	
		4B	60–20 000		
		2B	70–40 000		
Superdex (agarose/dextran)	GE Healthcare	30	0–10	3.0–12.0	
		75	3–70		
		200	10–600		
Sephacryl (dextran/bis-acrylamide)	GE Healthcare	S100HR	1–100	3.0–11.0	
		S200HR	5–250		
		S300HR	10–1500		
Bio-Gel P (polyacrylamide)	Bio-Rad	P-2	0.1–18	2.0–10.0	
		P-4 gel	0.8–41		
		P-10 gel	1.5–20		
		P-60 gel	3–60		
		P-100 gel	5–100		
Bio-Gel A (agarose)	Bio-Rad		10–500/100–50 000	4.0–13.0	
TOYOPEARL (methacrylate)	TosoHaas		0.1–10/400–30 000	1.0–14.0	Yes
Fractogel EMD BioSEC 650 (methacrylate)	Merck Millipore		0.1–10/500–50 000	1.0–14.0	Yes
Matrex Cellufine (cellulose)	Merck Millipore		0.1–3/10–3000	1.0–14.0	
Ultrogel AcA (acrylamide/agarose)	BioSepra		1–15/100–1200	3.0–10.0	
Trisacryl GF (acrylamide)	BioSepra		0.3–7.5/10–15 000	1.0–11.0	

with different adsorbents and mobile phases. The second term should be kept in a certain range and not be maximized, because the maximum value of 1 is reached for an infinite retention factor. At infinite retention, the productivity would decrease due to the high cycle time. The last term of Eq. (4.15) describes the efficiency of the column in terms of the number of plates. Resolution can be increased by selecting efficient adsorbents with small particle size and appropriate narrow particle size distribution. For these adsorbents, fluid dynamic and mass transfer resistances are minimized. Conversely, the backpressure of the column and the stability of the packing must also be taken into account for process-scale separations. Very small particles with a narrow particle size distribution result in high backpressure and may show reduced efficiency due to packing imperfections. Figure 4.45 illustrates the effect of the optimization of the three individual terms of the resolution equation, where it can be clearly seen that the maximization of the selectivity gives the largest benefit.

Next to these practical problems of high efficient column packings, a high number of plates are very often not needed if peak broadening results from thermodynamic effects. Seidel-Morgenstern (1995) has discussed the effects of high column loading (Section 2.5) and showed that separation efficiency is not dependent on the number of plates, if isothermal effects come to the fore. A typical isothermal effect is the decreasing retention time for high concentration in the Langmuir range of the isotherm. Highly efficient adsorbents (with high number of plates) are not useful for separations with dominant isothermal effects. Only for separations with low selectivities at low loadings must the number of plates be high to reach a sufficient resolution (Figure 2.12).

This behavior is demonstrated by the different working areas defined in Figure 4.46. Assuming that a certain selectivity can be reached, the influence of the retention factor and the solubility is shown. The working range of process chromatography should have medium retention factors and medium to high solubilities for the feed compounds. For low feed solubilities, the influences of thermodynamics and fluid dynamics dominate. In this range, adsorbents with high numbers of plates per meter should be used. At high solubilities, high
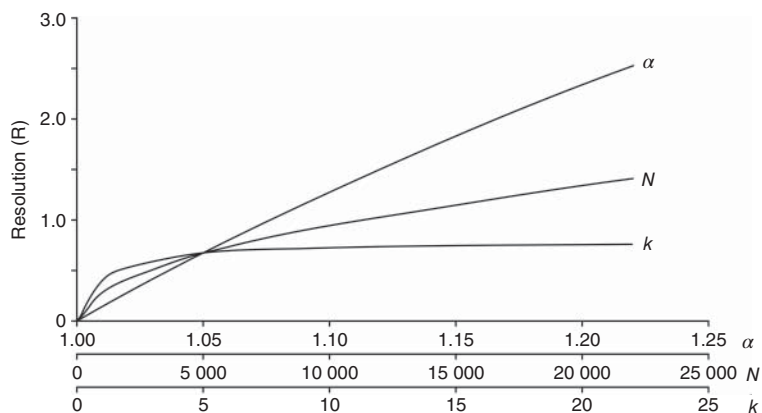
Figure 4.45 Influence of the single equation parameters on resolution.
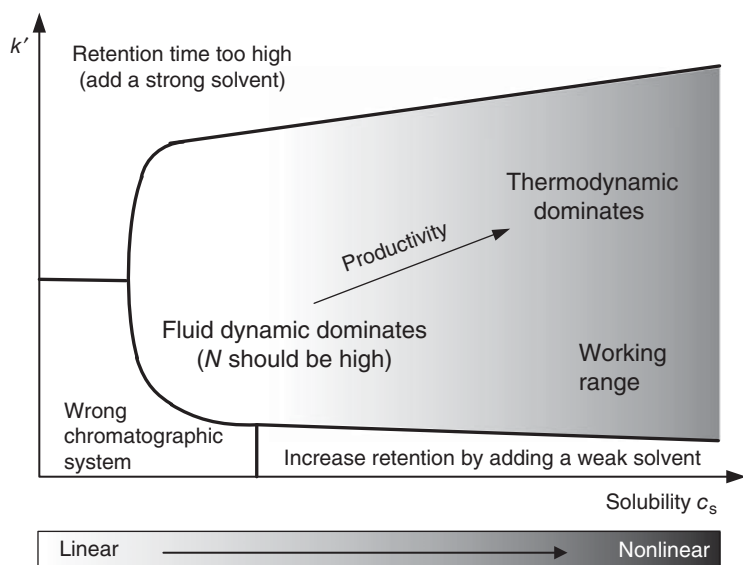
Figure 4.46 Working ranges of chromatographic separations.

column loading is possible, and thermodynamic effects come to the fore. In this range, less efficient adsorbents for high flow rates can be used.

In preparative chromatography, the systems are mainly operated at high feed solubilities, and thus thermodynamic effects dominate. If separations with low feed solubilities have to be operated, high-efficiency adsorbents should be used, and the ad-column dilution (ACD) injection technique could be applied.

Thermodynamic effects are the main source of increasing productivity in preparative chromatography. The most important parameter is the selectivity, which describes the ratio of the initial slopes H of the adsorption isotherms for both components (Eq. (2.15)).

Especially for feed mixtures with different ratios of the single components, the elution order must be considered. The major component should elute as the second peak, because in this case the displacement effect can be used to ease the separation (Section 2.4.3). If the minor component elutes as the second peak, the tag-along effect reduces the purity and loadability of the system.

If the components to be separated are present in a similar amount (e.g. as for racemic or diastereomeric mixtures), the target component should elute first, because the first peak is normally obtained at higher productivity and concentration.

Very often, the cycle time of isocratic batch chromatography is high due to extensive peak tailing of the second peak, which can be explained by a Langmuir-type isotherm. The black line in Figure 4.47 shows a typical chromatogram of an enantioseparation with a polysaccharide adsorbent with n-hexane–ethanol as the mobile phase. Here ethanol is the solvent with higher elution strength. The second peak shows tailing due to the Langmuir shape of the isotherm and high concentrations. The cycle time (time between the starting
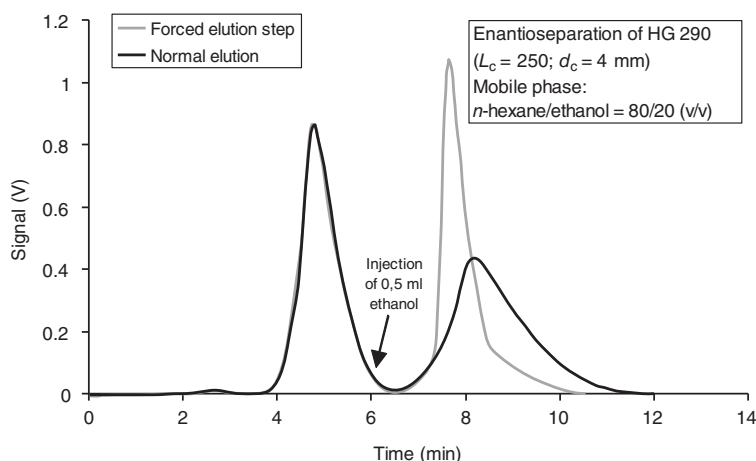
Figure 4.47 Increase in productivity due to forced elution step (injection of a strong eluent) during enantioseparation of HG290. (Source: Courtesy of H. Gillandt SiChem GmbH, Bremen).

point of the first peak and the ending point of the last peak) for the isocratic elution mode is 8.2 minutes.

The gray line in Figure 4.47 shows the separation when a forced elution step is used. After the first peak has eluted from the column, a second injection is made with the strong solvent (in this case ethanol). If the volume of this second injection is large enough, the strong solvent displaces the second peak. Owing to this displacement, the second peak elutes much faster and at higher concentrations. The cycle time is decreased from 8.2 to 6.7 minutes, and, thus, productivity is increased by 22%. Eluent consumption is also decreased as well, but recycling of the solvent becomes slightly more problematic because the eluent composition is no longer constant over the whole cycle time. When using the forced elution step method, it should be ensured that the column is in equilibrium at the end of the cycle time. If only small amounts of eluent with high elution strength are used for this method, isocratic process concepts can still be applied, for example, touching band elution.

4.9.2 Stationary Phase Gradients

From the aforementioned optimization strategies, it can be seen that the solubility of the feed and the target compound in a suitable solvent is of utmost importance for productive preparative chromatographic separations. Therefore, it is of consequence to choose the best solvent for the separation first and later try to optimize the separation by adjusting the selectivity of the stationary phases. This stationary phase selectivity optimization can be achieved by developing a new stationary phase with an optimized selector or simply by mixing or combining stationary phases with different selectors to stationary phase gradients. The concept has been exploited in analytical chromatography by Eppert and Heitmann (2003) as well as Nyiredy, Szucs, and Szepesy (2006, 2007) with the goal to minimize the analysis time and to maximize the peak capacity.

The concept of stationary phase gradients is similar to 2D chromatography, which is used in analytical chromatography to increase the peak capacity, but as always in preparative chromatography, the concept of stationary phase gradients tries to keep the system much more simple. In 2D chromatography, the chromatogram in the first dimension (on the first stationary phase) is cut into fractions and submitted to a second type of stationary phase with an orthogonal selectivity. During the process of fractionation, the fractions can be stored and solvents can be adjusted. Using stationary phase gradients, the goal is to end up with a system where simple isocratic chromatography can be applied and gives the best selectivity and capacity for a given separation task.

The optimization procedure follows quite a simple strategy:

(1) Setting of boundary conditions, especially in the choice of appropriate solvents.
(2) Single runs on the individual stationary phases.
(3) Optimization of the combination of stationary phases using the PRISMA model.
(4) Combination of the stationary phases and verification of the separation.

For the choice of the mobile phase as a starting point, several important criteria should be fulfilled: First of all the solubility of the feed in the solvent should be high enough to ensure a good injection concentration. In addition, the boiling point of the solvent should be in a moderate temperature range (ideally between 60 and 80 °C), and the solvent should show a low viscosity. Low UV adsorption is not as important as in analytical chromatography because detection methods other than UV adsorption can be used. For reasons of production costs and regulatory constraints, the solvent should be available in good quality for a reasonable price and should be of low toxicity. It should definitely fall into the ICH classes 2 or 3 of residual solvents (ICH Harmonized Guideline 2016).

By restricting the choice of mobile phases, the regulatory impact of chromatographic processes might be significantly reduced. For cosmetic or food ingredients, the restriction to ethanol–water mixtures could be a viable option, as natural extracts from those solvents are generally regarded as safe. If, in a second step, only chromatographic adsorption of impurities is applied, the whole process is considered as purely "physical" (in contrast to "chemical") and the product is thus a "natural" one.

After the choice of the solvent has been optimized, the screening of different stationary phases can start. The phases should be of similar particle size and show similar pore diffusivities to exhibit similar chromatographic properties. The surface modifications should cover different molecular interaction principles, but the phases in general should be able to interact with the chosen mobile phase without problems. It has to be especially taken into account that problems might occur with hydrophobic RP phases due to insufficient wetting of the stationary phase surface by the mobile phase or collapse of the surface modifications due to insufficient solubility in the mobile phase.

Figure 4.48a–c shows the single chromatograms of a three-component mixture on three different stationary phases: a highly nonpolar RP-18e phase, a combined reversed phase/weak anion-exchange phase (RP/WAX), and a cyano-modified
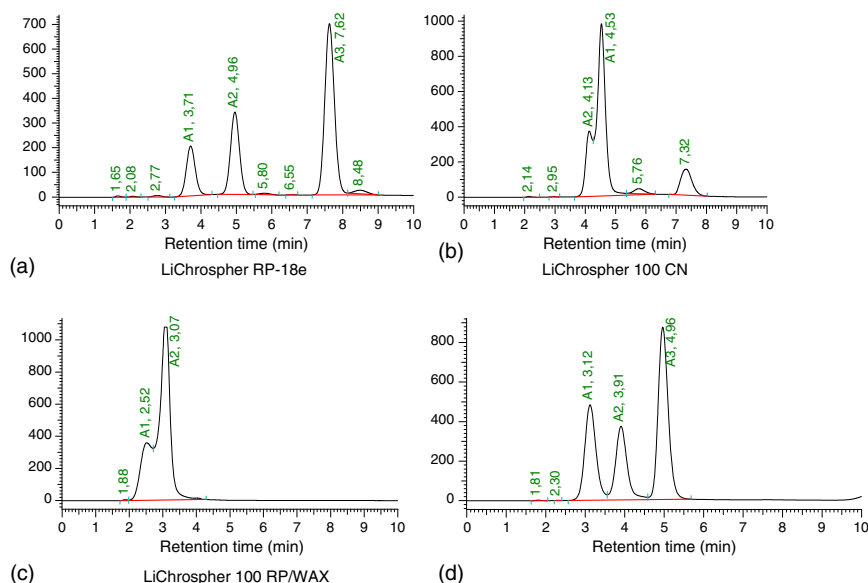
Figure 4.48 (a–c) Chromatograms on the single sorbents. (d) Chromatogram on a combined sorbent of LiChrospher RP-18e/LiChrospher RP/WAX 2 : 3.

phase. All three stationary phases have been prepared on the same base silica, a 12 μm, 100 Å LiChrospher. While on the RP-18e phase the mixture can be separated, the retention on the other two phases is shorter and insufficient for complete resolution. Through the combination of the different stationary phases, the retention time of a single run with sufficient resolution can be reduced from five to three minutes, which is equivalent to a capacity increase of the system of 40%. This can be achieved by a selection of RP-18e and RP/WAX phases in a 2 : 3 combination (Figure 4.48d) (Horn 2004).

The optimization of the stationary phase combination can be approached by following the PRISMA model (Section 4.4.3). Instead of using different solvents, in this case, the solvent is fixed, and the different selectivities are obtained by using different surface modifications on the stationary phases.

For the combination of the stationary phases in a preparative system, the stationary phase particles can be either packed together in one column or used in segmented columns. In the first case, care has to be taken that no demixing of the particles occur and that the slurry solvent is equally suited for both types of packings. In the latter case, there should be a minimum dead volume between the two or more columns to avoid any backmixing. Sreedhar and Seidel-Morgenstern (2008) have shown that the serial coupling of single-column segments have benefits. In addition, it has to be taken into account that the order of coupling is of importance for the separation if the whole system is operated in the nonlinear range of the adsorption isotherm. In that case the optimal length of the column segments is also different from the one used for a simple analytical separation.

The prejudices faced for preparative chromatography are often related to the mobile phase, for example, they are expensive, toxic, explosive, difficult to

remove, and yielding only low concentrations. By choosing an optimized mobile phase and later developing the appropriate stationary phase gradient, a lot of simplification in the phase system can be achieved. The concept of stationary phase gradients is thus a so far underutilized tool to improve preparative chromatography economics.

The following example illustrates the usefulness of the combination of stationary phases to solve a separation problem on production-scale level. An intermediate used in the last step of a drug synthesis contained small levels of three highly unwanted process critical impurities, resulting in side reaction products in the final product, which could not be removed using the generally applied purification methods. The relatively apolar product showed both on bare silica and on a polar modified silica a good retention using a hydrocarbon as the mobile phase. Therefore, preparative chromatographic experiments were performed on both types of stationary phases to study the behavior of the unwanted impurities. The experiments were immediately performed on a somewhat larger scale to provide the process research chemists with sufficient material to immediately evaluate the final reaction step using the purified material.

The results of these experiments are summarized in Table 4.19. Chromatograms of a 50 g crude product injection on a column filled with 2000 g of cyano-modified silica and on a combination of two columns filled with 500 g of silica gel and 2000 g of cyano-modified silica gel, respectively, are depicted in Figures 4.49 and 4.50.

The experiments performed indicated that silica gel was highly effective in separating impurity number 1 from the main component, while the cyano-modified silica gel was more selective in the separation of impurities numbers 2 and 3 from the target product. After further optimization work with regard to the most efficient ratio of silica gel to cyano-modified silica gel, an amount of 100 g of silica gel and 1250 g of cyano-modified silica gel was chosen to fill the 110 mm i.d. test columns.

For the production-scale purification of about 600 kg of this intermediate, a 110 mm i.d. DAC column filled with 350 g of 10 μm Kromasil 60 Å–silica gel was

Table 4.19 Summary of the purification results for an API and its impurities on different stationary phases.

		IMP-1	IMP-2	IMP-3
	Specification limit	0.35%	0.10%	0.10%
	Starting material	1.25%	0.17%	0.11%
10 μm Si 60 Å	Injection amount (g)	% impurity in the purified product		
	10	0.00	0.19	0.12
	30	0.00	0.17	0.11
	60	0.00	0.18	0.11
	100	0.50	0.16	0.10
60 Å Cyano-modified silica gel	20	0.86	0.00	0.00
	50	1.17	0.00	0.00
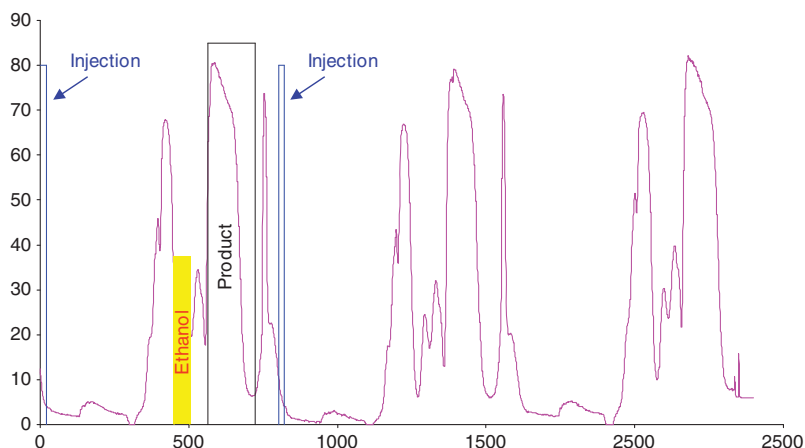
Figure 4.49 Injection of 50 g of product on a cyano-modified silica. Column: 110 mm i.d. DAC filled with 2000 g of 10 µm Kromasil 60 Å–cyano-modified silica, mobile phase: *n*-heptane, flow rate: 750 ml min−1, temperature: eluent: 28 °C Column: 30 °C, sample amount: 50 g dissolved in 292 ml of *n*-heptane.
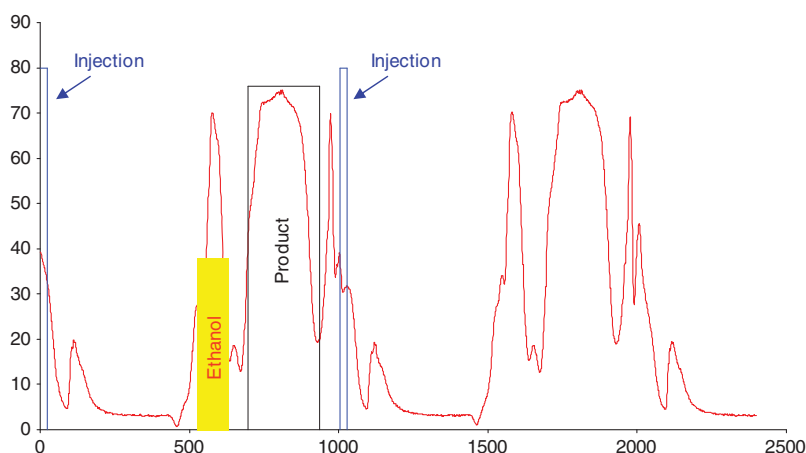
Figure 4.50 Injection of 50 g on a column filled with silica connected with a column filled with a cyano-modified silica. Pre-column: 110 mm i.d. DAC filled with 500 g of 10 µm Kromasil 60 Å–silica gel. Main column: 110 mm i.d. DAC filled with 2000 g of 10 µm Kromasil 60 Å–cyano-modified silica, mobile phase: *n*-heptane, flow rate: 750 ml min^{-1}, temperature: eluent: 28 °C, column: 30 °C, sample amount: 50 g dissolved in 292 ml of *n*-heptane.

combined with a 200 mm i.d. DAC column filled with 4150 g of 10 µm Kromasil 60 Å–cyano-modified silica. To speed up the purification process, a 40 seconds rinsing plug of pure ethanol was introduced after detection of the impurities eluting in front of the main peak to fasten the elution of the impurities eluting behind the target component. Using this methodology, it was possible to very easily remove the unwanted impurities.

This example clearly illustrates that column coupling is not only a tool to be used in analytical chemistry but can certainly be very convenient and efficient to solve challenging separation problems.

References

Arangio, M. (1998). Chromatographische Charakterisierung von Umkehrphasen. Dissertation. Saarbrücken: Mathematisch Naturwissenschaftliche Fakultät.

Bluhm, L.H., Wang, Y., and Li, T. (2000). An alternative procedure to screen mixture combinatorial libraries for selectors for chiral chromatography. *Anal. Chem.* 72: 5201–5205.

Brandt, A. and Kueppers, S. (2002). Practical aspects of preparative HPLC in pharmaceutical and development production. *LCGC Eur.* 15 (3): 147–151.

Britsch, L., Schulte, M., and Strube, J. (2003). Continuous method for separating substances according to molecular size. US Patent 6, 551, 512, 22 April 2003.

Chollangi, S., Parker, R., Singh, N. et al. (2015). Development of robust antibody purification by optimizing protein A chromatography in combination with precipitation methodologies. *Biotechnol. Bioeng.* 112: 2292–2304.

Cutler, P. (2004). Size exclusion chromatography in protein purification protocols. *Methods Mol. Biol.* 244: 239–252.

Dallenbach-Tölke, K., Nyiredy, S., Meier, B., and Sticher, O. (1986). Optimization of overpressured layer chromatography of polar, naturally occurring compounds by the PRISMA model. *J. Chromatogr. A* 365: 63–72.

Daicel Application Guide (2003). (accessed24/11/2019). https://www.daicelchiral.com/en/application-guide.html.

Dingenen, J. (1994). Polysaccharide phases in enantioseparations. In: *A Practical Approach to Chiral Separations by Liquid Chromatography* (ed. G. Subramanian), pp. 115–181.. Weinheim: Wiley-VCH.

Eckermann, C., Ebert, S., Rubenwolf, S., and Ambrosius, D. (2007).Process for Optimizing Chromatographic Purification Processes for Biomolecules. Patent WO2007144353.

EMD Millipore (2017). Small Molecule Processing by Tangential Flow Filtration. Technical Brief, Lit. No. TB1800EN00 Ver. 1.

Eppert, G.J. and Heitmann, P. (2003). Selectivity optimization of stationary phases. *LCGC Eur.* 16 (10): 698–705.

Francotte, E. (1998). Achiral derivatization as a means of improving the chromatographic resolution of racemic alcohols on benzoylcellulose CSPs. *Chirality* 10: 492–498.

Galushko, S.V. (1991). Calculation of retention and selectivity in reversed-phase liquid chromatography. *J. Chromatogr. A* 552: 91–102.

Gant, J.R., Dolan, J.W., and Snyder, L.R. (1979). Systematic approach to optimizing resolution in reversed phase liquid chromatography, with emphasis on the role of temperature. *J. Chromatogr. A* 185: 153–177.

Geiss, F., Schlitt, H., and Klose, A. (1965). Reproducibility in thin-layer chromatography: influence of humidity, chamber form, and chamber atmosphere. *Z. Anal. Chem.* 213: 5.

Geisser, A., Hendrick, T., Boehm, G., and Stahl, B. (2005). Separation of lactose from human milk oligosaccharides with simulated moving bed chromatography. *J. Chromatogr. A* 1092: 17–23.

Holstein, M., Cotoni, K., and Bian, N. (2015). Protein A intermediate wash strategies. *Bioprocess Int.* 13: 56–62.

Horn, F. (2004). *Selektivitätsoptimierung von Festphasen in der HPLC*. Diploma thesis. Fachhochschule Lippe und Höxter, Fachbereich Lebensmitteltechnologie.

ICH Harmonized Guideline (2016). Impurities: Guideline for Residual Solvents Q3C(R6), version 20 October 2016. https://www.ich.org/fileadmin/Public_Web_Site/ICH_Products/Guidelines/Quality/Q3C/Q3C__R6___Step_4.pdf.

Jacob, L. and Frech, C. (2007). Ion exchange chromatography in biopharmaceutical manufacturing. In: *Bioseparation and Bioprocessing* (ed. G. Subramanian), 127–149. Weinheim: Wiley-VCH.

Jandera, P. and Guiochon, G. (1991). Effect of the sample solvent on band profiles in preparative liquid chromatography using non-aqueous reversed-phase high performance liquid chromatography. *J. Chromatogr. A* 588: 1–14.

Josic, D., Horn, H., Schulz, P. et al. (1998). Size-exclusion chromatography of plasma proteins with high molecular masses. *J. Chromatogr. A* 796: 289–298.

Kaiser, R.E. and Oelrich, E. (1981). *Optimisation in HPLC*. Heidelberg: Dr. Alfred Hüthig Verlag.

Kiesewetter, A., Menstell, P., Peeck, L., and Stein, A. (2016). Development of pseudo-linear gradient elution for high-throughput resin selectivity screening in RoboColumn® format. *Biotechnol. Progr.* 32 (6): 1503–1519.

Lee, Y., Schmidt, M., Graalfs, H. et al. (2015). Modeling of dual gradient elution in ion exchange and mixed-mode chromatography. *J. Chromatogr. A* 1417: 64–72.

Li, Y. (2017). Effective strategies for host cell protein clearance in downstream processing of monoclonal antibodies and Fc-fusion proteins. *Protein Expression Purif.* 134: 96–103.

Lobsten-Guth, A., Briancon-Scheid, F., and Anton, R. (1983). Analysis of terpenes from *Ginkgo biloba* L. by high-performance liquid chromatography. *J. Chromatogr. A* 267: 431–438.

Mun, S., Xie, Y., Kim, J.-H., and Wang, L. (2003). Optimal design of a size-exclusion tandem simulated moving bed for insulin purification. *Ind. Eng. Chem. Res.* 42: 1977–1993.

Murer, P., Lewandowski, K., Svec, F., and Frechet, J.M. (1999). On-bead combinatorial approach to the design of chiral stationary phases. *Anal. Chem.* 71: 1278–1284.

Neue, U.D., Mazza, C.B., Cavanaugh, J.Y. et al. (2003). At-column dilution for improved loading in preparative chromatography. *Chromatographia* 57: 121–127.

Nyiredy, S. (2002). Planar chromatographic method development using the PRISMA optimization system and flow charts. *J. Chromatogr. Sci.* 40 (10): 553–563.

Nyiredy, S. and Fater, Z. (1995). Automatic mobile phase optimization, using the "PRISMA" model for the TLC separation of apolar compounds. *JPC J. Planar Chromatogr. - Mod. TLC* 8 (5): 341–345.

Nyiredy, S., Meier, B., Erdelmeier, C.A.J., and Sticher, O. (1985). PRISMA: a geometrical design for solvent optimization in HPLC. *J. High Resolut. Chromatogr. Chromatogr. Commun.* 8: 186–188.

Nyiredy, S., Szucs, Z., and Szepesy, L. (2006). Stationary phase optimized selectivity LC (SOS-LC) separation examples and practical aspects. *Chromatographia* 63: S3–S9.

Nyiredy, S., Szucs, Z., and Szepesy, L. (2007). Stationary phase optimized selectivity liquid chromatography: basic possibilities of serially connected columns using the "PRISMA" principle. *J. Chromatogr. A* 1157 (1–2): 122–130.

Okamoto, M. and Nakazawa, H. (1991). Reversal of elution order during direct enantiomeric separation of pyriproxyfen on a cellulose-based chiral stationary phase. *J. Chromatogr. A* 588: 177–180.

Pandey, R.C. (1997). Isolation and purification of paclitaxel from organic matter containing paclitaxel, cephalomannine and other related taxanes. US patent 5,654,448.

Pandey, R.C., Yankov, L.K., Poulev, A. et al. (1998). Synthesis and separation of potential anticancer active dihalocephalomannine diastereomers from extracts of *Taxus yunnanensis*. *J. Nat. Prod.* 61 (1): 57–63.

Pirkle, W.H. and Däppen, R. (1987). Reciprocity in chiral recognition – comparison of several chiral stationary phases. *J. Chromatogr. A* 404: 107–115.

Pirkle, W.H., Welch, C.J., and Lamm, B. (1992). Design, synthesis and evaluation of an improved enantioselective naproxen selector. *J. Organomet. Chem.* 57: 3854–3860.

Poole, C.F. (2003). *The Essence of Chromatography*. Amsterdam: Elsevier.

Rathjen, T., Wenzel, D., Studts, J.M., and Ambrosius, D. (2009). High-throughput downstream development. *Innov. Pharm. Technol.* **29:** 56–60.

Reichardt, C. (2003, 2003). *Solvents and Solvent Effects in Organic Chemistry*, 3e. Wiley-VCH Publishers.

Reichardt, C. and Schäfer, G. (1995). Determination of new and correction of old ET(30) values as empirical measures of solvent polarity for 40 organic solvents. *Liebigs Ann.* 1995 (8): 1579–1582.

Roussel, C., Piras, P., and Heitmann, I. (1997). An approach to discriminating 25 commercial chiral stationary phases from structural data sets extracted from a molecular database. *Biomed. Chromatogr.* 11: 311–316.

Sadek, P. (2002). *The HPLC Solvent Guide*, 2e. New York: Wiley Interscience.

Schulte, M. (2001). Chiral derivatization chromatography. In: *Chiral Separation Techniques* (ed. G. Subramanian), pp. 187-204. Weinheim: Wiley-VCH.

Schulze-Wierling, P., Bougmil, P., Knieps-Griinhagen, E., and Hubbuch, J. (2007). High-throughput screening of packed-bed chromatography coupled with SELDI-TOF MS analysis: monoclonal antibodies versus host cell protein. *Biotechnol. Bioeng.* 98 (2): 440–450.

Scott, R. and Kucera, P. (1975). Solute interactions with the mobile and stationary phases in liquid-solid chromatography. *J. Chromatogr. A* 112: 425–442.

Seidel-Morgenstern, A. (1995). *Mathematische Modellierung der präparativen Flüssigchromatographie*. Wiesbaden: Deutscher Universitätsverlag.

Shukla, A. and Hinckley, P. (2008). Host cell protein clearance during protein A chromatography: development of an improved column wash step. *Biotechnol. Progr.* 24: 1115–1121.

Snyder, L.R. (1968). *Principles of Adsorption Chromatography*. New York: Marcel Dekker.

Snyder, L.R. and Dolan, J.W. (1998). The linear-solvent-strength model of gradient elution. *Adv. Chromatogr.* 38: 115–187.

Snyder, L.R. and Kirkland, J.J. (1979). *Introduction to Modern Liquid Chromatography*. New York: Wiley.

Snyder, L.R., Kirkland, J.J., and Glajch, J.L. (1997). *Practical HPLC Method Development*. New York: Wiley.

Soczewinski, E. (1969). Solvent composition effects in thin-layer chromatography systems of the type silica gel-electron donor solvent. *Anal. Chem.* 41 (1): 179–182.

Sreedhar, B. and Seidel-Morgenstern, A. (2008). Preparative separation of multi-component mixtures using stationary phase gradients. *J. Chromatogr. A* 1215: 133–144.

Stein, A. and Kiesewetter, A. (2007). Cation exchange chromatography in antibody purification: pH screening for optimized binding and HCP removal. *J. Chromatogr. B* 848: 151–158.

Svec, F., Wulff, D., and Fréchet, J.M. (2001). Combinatorial approaches to recognition of chirality: preparation and use of materials for the separation of enantiomers. In: *Chiral Separation Techniques* (ed. G. Subramanian), pp. 57-93. Weinheim: Wiley-VCH.

Szanya, T., Argyelan, J., Kovats, S., and Hanak, L. (2001). Separation of steroid compounds by overloaded preparative chromatography with precipitation in the fluid phase. *J. Chromatogr. A* 908 (1–2): 265–272.

Tiwari, A., Kateja, N., Chanana, S., and Rathore, A. (2018). Use of HPLC as an enabler of process analytical technology in process chromatography. *Anal. Chem.* 90: 7824–7829.

Trapp, O. and Schurig, V. (2002). Novel direct access to enantiomerization barriers from peak profiles in enantioselective dynamic chromatography: enantiomerization of dialkyl-1, 3-allene-dicarboxylates. *Chirality* 14: 465–470.

Unger, K.K. and Weber, E. (1999). *A Guide to Practical HPLC*. Darmstadt: GIT Verlag.

Welch, C., Protopopova, M.N., and Bhat, G. (1998). Microscale synthesis and screening of chiral stationary phases. *Enantiomer* 3: 471–476.

Wellhoefer, M., Sprinzl, W., Hahn, R., and Jungbauer, A. (2014). Continuous processing of recombinant proteins: integration of refolding and purification using simulated moving bed-size exclusion chromatography with buffer recycling. *J. Chromatogr. A* 1337: 48–56.

Wiendahl, M., Schulze-Wierling, P., Nielsen, J. et al. (2008). High throughput screening for the design and optimization of chromatographic processes – miniaturization, automation and parallelization of breakthrough and elution studies. *Chem. Eng. Technol.* 31: 893–903.

Wittkopp, F., Peeck, L., Hafner, M., and Frech, C. (2018). Modeling and simulation of protein elution in linear pH and salt gradients on weak, strong and mixed cation exchange resins applying an extended Donnan ion exchange model. *J. Chromatogr. A* 1545: 32–47.

Yamamoto, S. and Kita, A. (2005). Theoretical background of short chromatographic layers. Optimization of gradient elution in short columns. *J. Chromatogr. A* 1065: 45–50.

Yamamoto, S., Nakanishi, K., and Matsuno, R. (1988). *Ion-Exchange Chromatography of Proteins*. New York: Marcel Dekker.

Yau, W.W., Kirkland, J.J., and Bly, D.D. (1979). *Modern Size-Exclusion Chromatography*. New York: Wiley.

Zhou, J., Du, Q., Sun, F. et al. (2015). Enantioseparation of the six important intermediates of Homoharringtonine with immobilized cellulose chiral stationary phase. *Chirality* 27: 538–542.

5

Process Concepts*

Malte Kaspereit[1] and Henner Schmidt-Traub[2]

[1] *Friedrich-Alexander-Universität Erlangen-Nürnberg, Lehrstuhl für Thermische Verfahrenstechnik, Egerlandstr. 3, 91058 Erlangen, Germany*
[2] *TU Dortmund, Fakultät für Bio- und Chemieingenieurwesen, Lehrstuhl für Anlagen- und Prozesstechnik, Emil-Figge-Str. 70, 44227 Dortmund, Germany*

The basis for every preparative chromatographic separation is the proper choice of the chromatographic system. The most important aspects in this context are selectivity, capacity, and solubility, which are influenced and can be optimized by the deliberate selection of stationary and mobile phases, as is discussed extensively in Chapter 4.

Besides the selection of the chromatographic system, its implementation in a preparative process concept plays an important role in serving the different needs not only for the performance achievable but also in terms of, for example, system flexibility and production amount. Depending on the operating mode, several features distinguish chromatographic process concepts:

- Pulse-wise or continuous feed introduction;
- Operation in a single- or multicolumn mode;
- Elution under isocratic or gradient conditions;
- Co-, cross-, or countercurrent flow of mobile and stationary phases;
- Withdrawal of two or a multitude of fractions.

Starting with the description of the main components of a chromatographic unit, this chapter gives an overview of process concepts available for preparative chromatography. Process design and engineering aspects are discussed in Chapters 8–10. The introduction is followed by some guidelines to enable a reasonable choice of the concept, depending on the production rate, separation complexity, and other aspects.

*Michael Schulte, Klaus Wekenborg, and Wolfgang Wewers have contributed to the first and/or second edition.

5.1 Discontinuous Processes

5.1.1 Isocratic Operation

The simplest chromatographic setup consists of one solvent reservoir, one pump that can deliver the necessary flow rate against the pressure drop of the packed column, a selection valve that alters between eluent and feed (alternatively, an injection valve can be used), the column, and one or more valves for the collection of fractions (Figure 5.1).

With a proper choice of the operating conditions, such as injected amount and flow rate, an efficient operating scenario can be achieved in which the stationary phase is utilized very efficiently. As illustrated in Figure 5.2, highest product recovery is achieved by "baseline separation," where the component peaks of the same injection (e.g. A_1 and B_1) do not overlap when leaving the column. If these two peaks just "touch," this is denoted as "touching band" situation. Moreover, by minimizing the time between two injections, a "stacked injections" situation can be achieved, wherein the latest and the earliest eluting peaks of two consecutive injections just "touch" each other (e.g. B_1 and A_2) in Figure 5.2. It is worth noting that productivity and eluent consumption may be further improved – at the cost of lower recovery – by waiving baseline separation and instead allowing for waste fractions collected between the product fractions or between the elution profiles of consecutive injections.
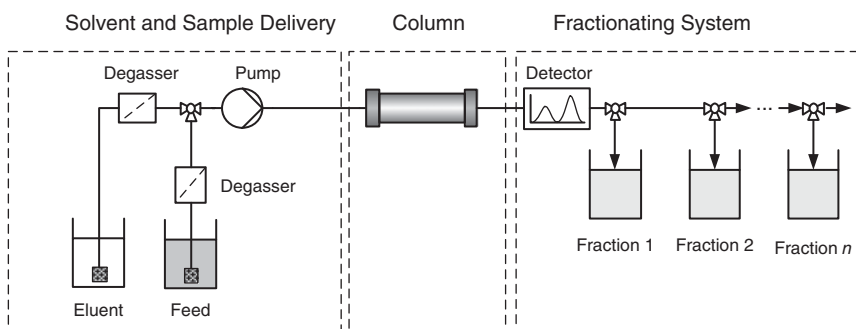
Figure 5.1 General setup of a preparative chromatographic plant.
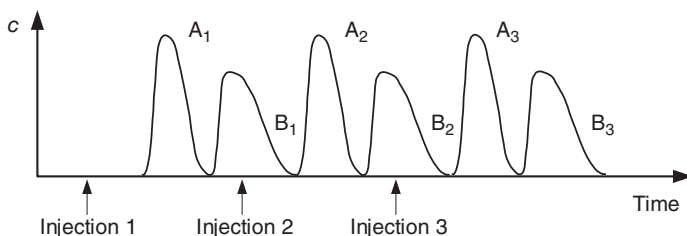
Figure 5.2 Separation of two components under touching band and stacked injections conditions for three consecutive injections.

Section 8.2 gives a detailed description of design and optimization strategies for isocratic chromatographic separations that aim at maximizing productivity and minimizing eluent consumption or total separation costs.

Processes where the composition of the solvent is not altered during elution, as is the case for the one described above, are called *isocratic*. They exhibit the following benefits:

- Simplicity of setup – the number of pumps and reservoirs is reduced to the absolute minimum;
- Cycle times are short, since no reconditioning of the column is necessary;
- Work-up and reuse of the solvent is easier due to its constant composition.

Whenever possible the development of a chromatographic separation should start with an isocratic elution mode. Its economic feasibility has to be checked afterward.

If the feed mixture contains late-eluting impurities and their adsorption in the main column has to be avoided, the implementation of a short precolumn might be helpful (Figure 5.3). The only purpose of this guard column is to keep late-eluting impurities from entering the column by strongly retaining them. As soon as a breakthrough of the bound impurities is imminent, the precolumn is regenerated, replaced, or emptied and repacked. Repacking with a cheap, coarse adsorbent is often more advisable than attempting a regeneration. If the separation must not be interrupted, a second precolumn and a switching valve are installed allowing for easy replacement or offline treatment.

Further options to separate mixtures with late-eluting components using a single-column setup are, for example, the use of gradients (Section 5.1.2) or the flip-flop concept (Section 5.1.5).

5.1.2 Gradient Chromatography

Under isocratic conditions, the most retained component might take a very long time to elute. This leads to low productivity and high eluent consumption. In addition, work-up costs for such late-eluting components are high since they are typically strongly diluted. In extreme cases, some components do not even elute under the chosen conditions. These drawbacks can be avoided by implementing gradients that manipulate (i.e. increase) the elution strength of the mobile phase (Section 2.5.2) during the elution process. An illustration is given in Figure 5.4.
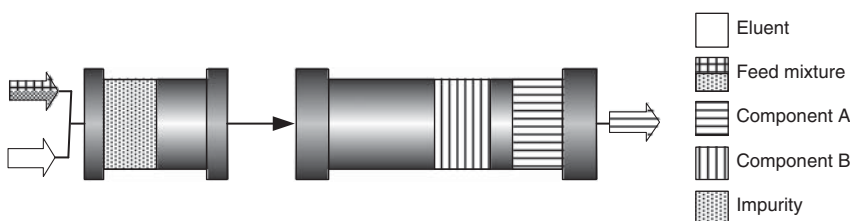
Figure 5.3 Pre-column for the adsorption of late-eluting impurities.
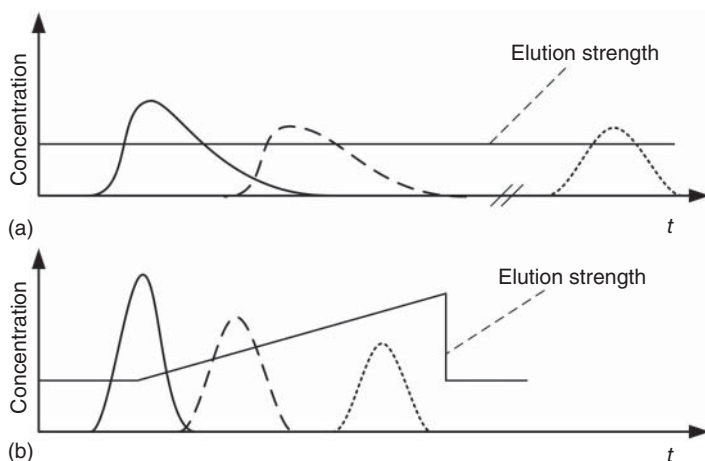
Figure 5.4 Principles of isocratic operation (a) and a simple gradient elution (b).

Process conditions that might be altered during elution are:

- mobile phase composition (in terms of organic modifier, buffer amount or strength, salt concentration, or pH value);
- mobile phase flow rate;
- temperature;
- pressure (in supercritical fluid chromatography [SFC]).

Most common are gradients of the mobile phase composition. These are established using gradient pumps (Section 10.4.3.4) that mix before the column two solvents with different elution strengths and vary their ratio during the run.

Figure 5.5 illustrates typical elution modes. The simplest option is the step gradient in Figure 5.5b. It is mostly used if a single target component (or a class of closely related compounds) can be adsorbed selectively and strongly by using at first a weak mobile phase. Non-bound impurities are "washed off" the column, until the target fraction is eluted by the stepwise-increased mobile phase strength. Instead of binding the target compound, also the impurities might be "captured" while the product passes the column in dead time. This approach is denoted as flow-through chromatography or negative chromatography. It was suggested, for instance, for polishing a final product like a monoclonal antibody or for the recovery of viruslike particles (Lee, Chan, and Tey 2014; Iyer et al. 2011; Lee et al. 2015).

A continuous increase in elution strength (Figure 5.5c) offers the best resolution of several mixture components with very different affinities to the stationary phase. If, under isocratic conditions, the retention times of the first and the last components differ by more than 30% (Unger 1994), gradient elution should be applied, or the whole separation should be divided into several process steps. As indicated in Figure 5.4, linear gradients give good resolution at reduced peak width, allowing the isolation of pure fractions at higher product concentrations within a shorter cycle time.

Also combinations of linear and step gradients are used. The option shown in Figure 5.5d combines a shallow gradient for the part of the chromatogram where
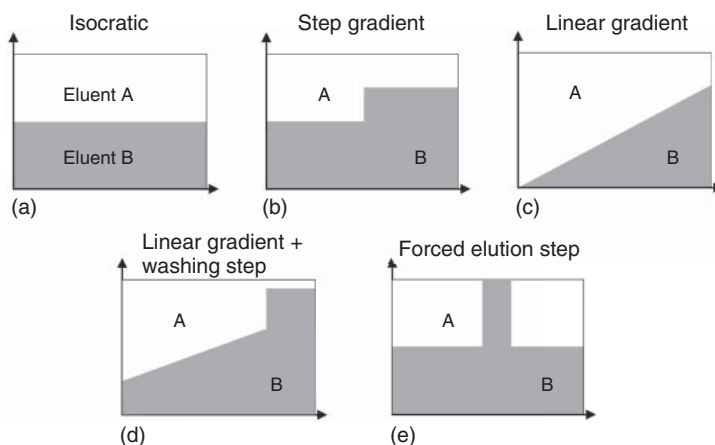
Figure 5.5 Isocratic and gradient elution modes realized by varying mobile phase strength. The picture shows eluent composition versus time. A denotes the eluent with the lower elution strength (i.e. the "weak" eluent), and B the one with the high elution strength ("strong" eluent).

the highest separation power is needed, with a step gradient for the quick removal of all impurities that elute after the component of interest.

An efficient form of a step gradient can be the injection of a "plug" of mobile phase with high elution strength into the part of the chromatogram where the component of interest elutes (Figure 5.5e). Such forced elution step (Section 4.9.1, Figure 4.47) can desorb the component of interest more efficiently, leading to higher fraction concentration at equal or even shorter cycle time without an additional solvent readjustment step (Section 4.3). A similar approach is often applied if the sample has a poor solubility in the mobile phase. Here process performance can be improved significantly by injecting a more concentrated mixture dissolved in a stronger solvent (Gedicke, Antos, and Seidel-Morgenstern 2007).

A typical goal of gradient elution is the reduction of the overall cycle time. However, the design must consider also the additional time needed for readjusting the mobile phase and re-equilibrating the column before the next injection. Moreover, the feed may contain components with so high adsorptivity that their elution would take very long when pushing them through the whole column. Such components "stick" close to the column's inlet. They may be eluted faster by reversing the flow direction to withdraw them at the column's inlet (Section 5.1.5).

Gradients are standard tools in biochromatography. They are applied in various chromatographic modes. A standard task is, for example, to separate a product molecule like a protein from a variety of impurities. In the case of batch chromatography, this is performed in a bind–wash–elute operation with the following process steps (Figure 5.6):

1. Equilibration of the column;
2. Injection of the feed mixture;
3. Washing out unbound impurities;
4. Eluting weakly bound impurities, the product, and strongly bound impurities as individual peaks by a (linear or nonlinear) gradient;
5. Eluting and washing off tightly bound impurities by a step gradient.
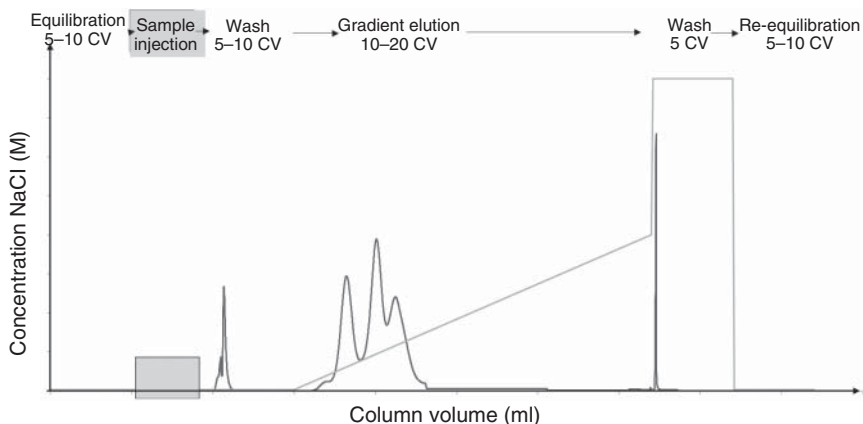
Figure 5.6 Typical ion-exchange separation using linear gradient elution.

Further steps for washing, cleaning in place (Section 3.7.1), etc. may be implemented.

It should be mentioned that such operation is often suboptimal in terms of solvent consumption and productivity. While this may be justified against the typically high value of the product, more efficient as well as continuous operating modes are available (Section 5.2.9).

Sreedhar and Seidel-Morgenstern (2008) suggested the use of gradients of the stationary phase for preparative chromatography. In this concept, column segments packed with different stationary phases are arranged in series. Type, order, and length of these segments can be optimized to enhance performance. This has in common some aspects with multidimensional and "orthogonal" methods known in analytical chromatography.

5.1.3 Closed-Loop Recycling Chromatography

Major constraints in preparative chromatography are the inherent interdependencies of purity and yield as well as column efficiency and pressure drop. If a given separation needs to be improved, column capacity and efficiency (i.e. plate number) would have to be increased. Using a longer column or a stationary phase with smaller particles is often not possible due to too high pressure drop. One possible work-around is to increase the number of plates *virtually*. By connecting the column's outlet to its inlet, the partially separated chromatogram is recycled back into the column, and the separation proceeds during a second or more passages through the column. This process concept is called closed-loop recycling chromatography (CLRC).

The CLRC concept is easy to implement as shown in Figure 5.7. Its main advantage is the possibility of isolating components with good purity and yield even at very low selectivity. A second interesting aspect is that the consumption of mobile phase is not increased by this concept. During the closed-loop operation, no eluent is consumed as the complete mobile phase is circulated
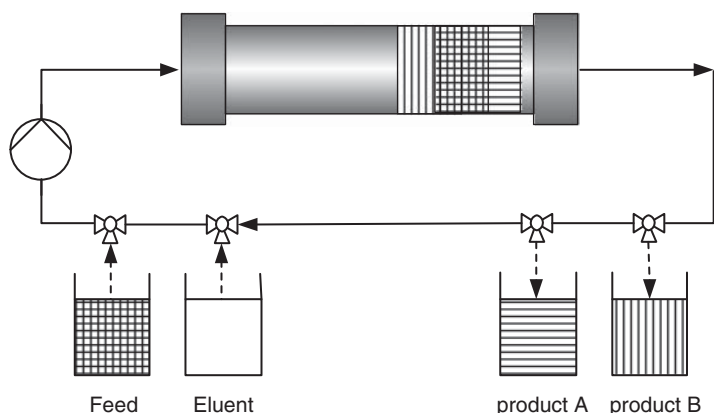
Figure 5.7 Principle of closed-loop recycling chromatography (CLRC). In conventional CLRC, products A and B are collected after several cycles when separation is complete. Alternatively, when combined with peak shaving, during each cycle sufficiently pure parts of the chromatogram are collected as product fractions. A corresponding chromatogram is shown in Figure 5.8.

within the system. Fresh eluent is introduced only with the original feed and during fraction collection.

To enhance its performance further, CLRC can be combined with "peak shaving" wherein sufficiently pure parts of the front and the tail of the chromatogram are collected ("shaved off") during each cycle (Figure 5.8). This eases separation and allows separation within fewer cycles. However, after a few cycles, only small amounts of the original feed mixture are left in the column, and last the product fractions are strongly diluted.

The most critical point in CLRC is the increase in axial dispersion within the additional holdup volumes of the recycle line (i.e. pump head, additional piping
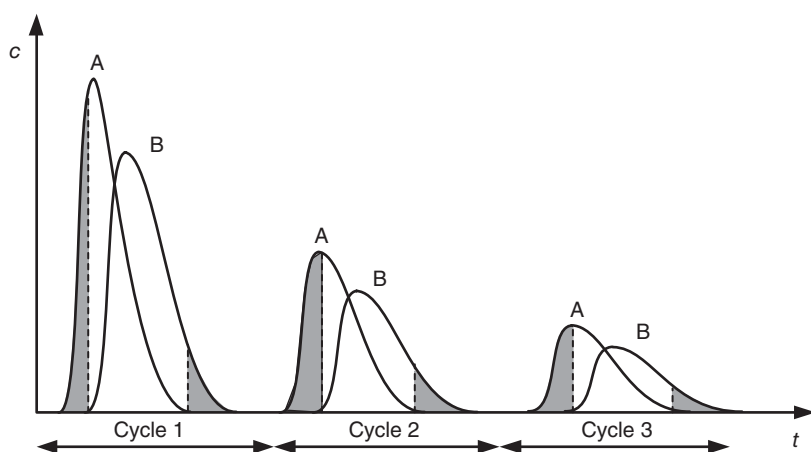
Figure 5.8 Development of concentrations during closed-loop recycling chromatography operation with peak shaving.

and valves). This can be minimized by the "alternate pumping" approach that employs two columns (Duvdevani, Biesenberger, and Tan 1971), also denoted as "twin-column recycling separation process" (TCRSP) (Gritti et al. 2017).

5.1.4 Steady-State Recycling Chromatography (SSRC)

An interesting option to improve the performance of recycling operations is steady-state recycling chromatography (SSRC) (Bailly and Tondeur 1982; Grill and Miller 1998; Grill, Miller, and Yan 2004). SSRC is based on recycling with peak shaving, but during each recycling interval, also a limited amount of fresh feed mixture is introduced to the column. By this operating policy, the process attains a periodic steady state characterized by high product concentrations and improved productivity. Several process variants exist that differ in the way the fresh feed is injected. The recycle fraction may be mixed with fresh feed and then re-injected; it may be fractionated itself, and these subfractions are injected in an optimized order; or the fresh feed may be placed after the recycle fraction or in its middle. The latter version is marketed as "CycloJet" process.

The basic setup for SSRC is similar to the CLRC concept in Figure 5.7. Figure 5.9 shows a chromatogram of a single cycle during periodic steady state. While the first component A elutes from the column in sufficient purity ($t_{A,1} \leq t \leq t_{A,2}$), the first fraction of purified product is collected. The region of nonseparated mixture eluting between $t_{A,2}$ and $t_{B,1}$ is recycled and re-injected together with fresh feed. Component B is obtained in the second fraction in the interval ($t_{B,1} \leq t \leq t_{B,2}$).

The exact time points for fractionation and recycling as well as for the fresh feed injection depend on the specific operating policy and are a question of optimal design. In modes with a direct closed-loop recycling, the column length should be optimized in order to attain a stacked injection scenario and to prevent unnecessary periods in which only mobile phase elutes from the column. If column length cannot be varied, additional external holdup volumes may be used to optimize the time point for reintroduction of the recycle (Scherpian and Schembecker 2009). More flexible and easier to design are mixed-recycle modes where before re-injection the recycle fraction is collected and mixed with the fresh feed. While
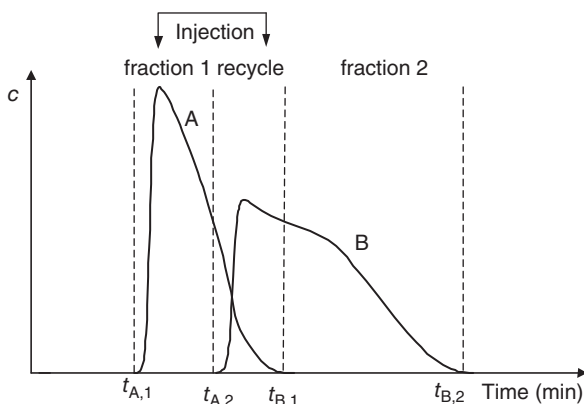
Figure 5.9 Steady-state recycling chromatography (SSRC) in mixed-recycle mode.

the achieved partial separation of the recycle fraction is given up by this, the time point for re-injection can be chosen freely. Designing a so-called mixed-recycle SSRC is possible based on simple shortcut methods for any purity requirement (Bailly and Tondeur 1982; Sainio and Kaspereit 2009; Kaspereit and Sainio 2011). Furthermore, instead of simple mixing also further operations can be performed in the recycle line. For example, performance is enhanced strongly when removing solvent from the recycle fraction (Siitonen, Sainio, and Kaspereit 2011). Nimmig and Kaspereit (2013) developed an SSRC-based process that completely converts a racemic mixture into a single pure enantiomer. Here, a reactor placed in the recycle performed a chemical racemization of the undesired enantiomer enriched in the recycle fraction, while excess solvent was removed by nanofiltration.

Concerning its performance, SSRC always allows for lower solvent consumption than in batch chromatography. For systems with significant dispersion and/or difficult separations, it also achieves higher productivity (Sainio and Kaspereit 2009; Kaspereit and Sainio 2011). Overall, the performance of SSRC lies between batch chromatography or CLRC operation and continuous simulated moving bed (SMB) processes (Section 5.2) while having much lower equipment requirements than SMB systems.

5.1.5 Flip-Flop Chromatography

A concept capable of dealing with mixtures containing highly adsorptive as well as fast-eluting components is the so-called flip-flop chromatography developed by Martin et al. (1979) and further elaborated by Colin, Hilaireau, and Martin (1991). As shown in Figure 5.10, the feed mixture is injected at the one end of the column, and the early-eluting components are pushed through the column (Figure 5.10a) and collected at the other end (Figure 5.10b). When these fast-eluting components have been withdrawn from the column, the flow direction is reversed. The late-eluting component(s) still in the column is now transported back toward the other end of the column (Figure 5.10c). After a certain time a new portion of feed mixture is injected, and the elution proceeds in the reversed flow direction (Figure 5.10d). At the end of the column, the late-eluting impurity from the previous injection is now eluted (Figure 5.10e), followed by the early-eluting components of the last injection. When the latter have been withdrawn, the flow direction is reversed again, and a new injection is performed.

The flip-flop concept is an elegant way of dealing with feed mixtures consisting of components with very different adsorption behavior. It may be an alternative to or may be combined with gradient elution (Section 5.1.2). Nicoud (2015) presented design criteria for identifying situations in which the flip-flop mode is advantageous. However, apparently this mode is not used very frequently, which may be due to concerns regarding design or suitability of the packing integrity during flow reversal. Alternatives to be considered are the abovementioned concepts of pre-columns (Section 5.1.1), gradients (Section 5.1.2), or to divide the whole separation process into two steps: a simple adsorption of the late-eluting impurities (see above) and the main separation.

(a)

(b)

(c)

(d)

(e)

(f)

☐ Eluent   ▦ component A   ▨ Impurity I

▦ Feed mixture   ⦀ component B
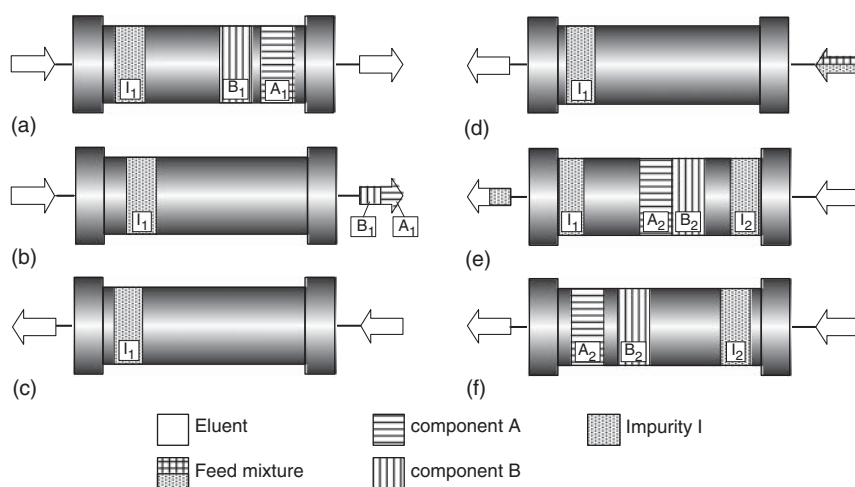
Figure 5.10 Flip-flop concept.

5.1.6 Chromatographic Batch Reactors

In conventional chemical productions, a reaction unit is followed by one or more separations. If conversion is limited by an unfavorable reaction equilibrium, unreacted educts can be isolated and recycled back to the reaction. Such recycle, however, may increase load on the separation, equipment size, and investment costs.

An elegant option for enhancing reaction yield and separation is to perform reaction and separation simultaneously within one apparatus. Examples for such reactive separations are reactive distillation, extraction, absorption, membrane separations, crystallization, and adsorption (Kulprathipanja 2002; Sundmacher, Kienle, and Seidel-Morgenstern 2005). A chromatographic reactor performs a chemical or biochemical reaction within a chromatographic column. Figure 5.11 explains the principle for the example of a reversible reaction of the type $A \leftrightarrows B + C$. Reactant A is injected as a pulse into the column and reacts during its propagation along the column to give B and C. A has intermediate adsorptivity, while products B and C are the more strongly and weakly adsorbed components.
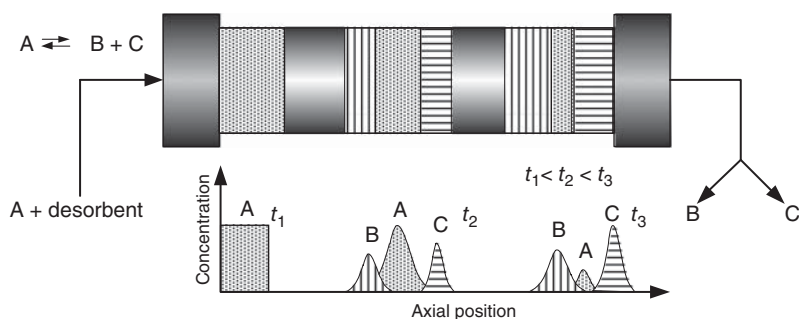
Figure 5.11 Principle of the chromatographic batch reactor.

Owing to their different affinities, all components propagate with different velocities. This leads to complete conversion of A and complete separation of the products – without the need for an additional separation unit.

Generally, the reaction performed can be spontaneous, homogeneously catalyzed, or heterogeneously catalyzed. A homogeneous catalyst has to be recovered after the chromatographic reactor. One option for heterogeneous catalysis is to apply catalytically active stationary phases like ion-exchange resins as used for esterifications. Alternatively, a catalytically active compound like an enzyme can be bound covalently to the stationary phase. Also mixed beds of catalyst and stationary phase may be used. De-mixing of the different particles can be avoided by alternating layers of adsorbent and catalyst (Meurer et al. 1997).

While process integration can obviously be attractive, operating parameters of reaction and separation must match and have to fulfill restrictions related to equipment design. These requirements reduce the degrees of freedom, i.e. they result in a reduced window of possible operating points. Of particular relevance for chromatographic reactors is the order of adsorptivities. Grüner and Kienle (2004) and Vu et al. (2005) demonstrated that, for instance, the reaction $A \leftrightarrows B + C$ allows total conversion and separation for any order of adsorptivity (however, intermediate affinity of A as assumed in Figure 5.11 is most favorable). In contrast, for reactions of the type $2A \leftrightarrows B + C$, reactant A must have intermediate adsorptivity to allow for complete conversion and separation. For multiple reactants, the separation factor should be close to unity to prevent the reactants separating from each other. More detailed discussions of relevant aspects are given in Sardin, Schweich, and Villermaux (1993) and Sundmacher, Kienle, and Seidel-Morgenstern (2005).

Since the late 1950s, analytical chromatographic reactors have been applied to studies of reactions (Coca et al. 1993), determination of reaction kinetics (Bassett and Habgood 1960), characterization of stationary phases (Jeng and Langer 1989), or examination of interactions between mobile and stationary phases (Coca et al. 1989). Examples for preparative-scale developments include the production of instable reagents at lab scale (Coca et al. 1993), the racemic resolution of amino acid esters (Kalbé, Höcker, and Berndt 1989), acid-catalyzed sucrose inversion (Lauer 1980), and production of dextran (Zafar and Barker 1988). The majority of studies focused on ester hydrolysis, esterification, or trans-esterification reactions using ion-exchange resins; to give only a few examples, see Sardin, Schweich, and Villermaux (1993); Falk and Seidel-Morgenstern (2002); Ströhlein et al. (2006a); Sainio et al. (2007); Pereira, Silva, and Rodrigues (2009); and Oh et al. (2016).

Apart from the chromatographic batch reactor, also reactive continuous multicolumn concepts were suggested that should overcome limitations regarding process performance (Section 5.2.10).

5.2 Continuous Processes

In the separation processes mentioned so far, the introduction of the feed mixture is realized in a batchwise manner onto one single column only. Especially for

separations in a preparative scale, modes for continuous operation have to be considered to increase productivity and product concentration and to save fresh eluent.

5.2.1 Column Switching Chromatography

The easiest way of transforming a batch separation into a (pseudo-)continuous one is the column switching approach, which can be applied for relatively simple adsorption–desorption processes. The feed is pumped through a column until, for example, a breakthrough of the target component is observed. At that moment, the injection is switched to a second column, while the first one is desorbed by introducing a (strong) eluent by a second pump. After desorption is finished the initial eluent conditions are readjusted before the first column is again used for adsorption. Obviously, this setup can be used only for relatively simple separations, where either the impurities or the target component can be bound strongly to the stationary phase, while the other is easily eluted. A straightforward extension of this is the use of multiple columns as described in Section 5.2.3

5.2.2 Annular Chromatography

For complex feed mixtures, other approaches for continuous separation have to be considered. One example is annular chromatography with a rotating stationary phase as anticipated already by Martin (1949). Solms (1955) developed this concept in the 1950s as a continuous method for paper chromatography. In annular chromatography, the stationary phase is packed between two concentric cylinders and rotates around a central axis (Figure 5.12).

At the top of the column, the feed injection is performed at a fixed position. Over the whole remaining circumference of the packed bed, the eluent is introduced into the column. The fluid phase moves toward the bottom while the annular column rotates slowly. This operation corresponds to a crosscurrent movement of packing material and mobile phase. The components of the feed mixture migrate in helical bands downward through the bed and are separated into several product streams eluting at different angles at the bottom of the bed. From a design point of view, annular chromatography is a continuous alternative
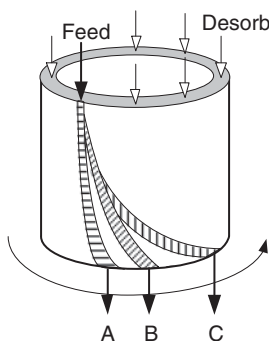
Figure 5.12 Annular chromatographic separation.

to batch chromatography. Its performance is comparable with multiple batch columns arranged in a circle. In fact, a batch chromatogram can be transferred to an annular chromatographic system by a coordinate transform that replaces the retention time by corresponding angular positions. However, it is underlined that the concept allows for a truly continuous separation of multicomponent mixtures.

As in batch chromatography, the solvent strength can be altered along the circumference by introducing further solvents, resulting in gradients for improved process performance. In addition, reactive variants were suggested (Sarmidi and Barker 1993a,b).

One drawback of annular chromatography is the difficulty of packing efficient columns. Because of the angular rotation, axial and tangential dispersions affect the peak broadening. In order to decrease tangential dispersion, Brozio and Bart (2004) recommend building apparatuses with a thicker diameter and a smaller annular width. They also discuss criteria for a simplified scale-up from batch chromatography to annular chromatography. To operate annular chromatography only rigid adsorbents should be used to obtain an improved distribution of the target components over the different withdrawal ports (Schmidt et al. 2003). The tolerable pressure drop is limited by the quality of the sealing. Wolfgang and Prior (2002) have given a detailed overview of principles, technical aspects, and industrial applications.

5.2.3 Multiport Switching Valve Chromatography (ISEP/CSEP)

As mentioned above, the concept of an annular chromatographic system can be realized by a multicolumn setup where several single columns are mounted to a rotating "column carrousel." The distribution of the different liquid streams as well as the collection of all outlet streams is realized by one central multiport switching valve (Figure 5.13). The inlet and outlet lines of the unit are connected to the stationary part of the valve, while the columns are connected to the rotating part. In contrast to annular chromatography, where the bed rotates with a constant velocity, the switching valve performs this movement in discrete steps, from one position to the next, at given switching intervals. The approach is also known as ion separator (ISEP) or chromatographic separator (CSEP) concept.

The introduction of this valve and the fact that the stationary phase is packed into fixed beds offer a great variety of possible column interconnections. Besides performing the mentioned crosscurrent flow, columns can be connected very flexibly in series or parallel, allowing a multitude of different process setups (Figure 5.14). Different sections can be realized to fulfill special tasks within the process. Common tasks for such sections are:

- Introduction and adsorption of feed mixture;
- Washing of the columns and removal of impurities;
- Desorption of target component by a different mobile phase;
- Reconditioning of columns with the mobile phase of the adsorption step.

The number of columns in certain sections and their interconnection can be chosen according to the process needs. To ensure continuous operation of the
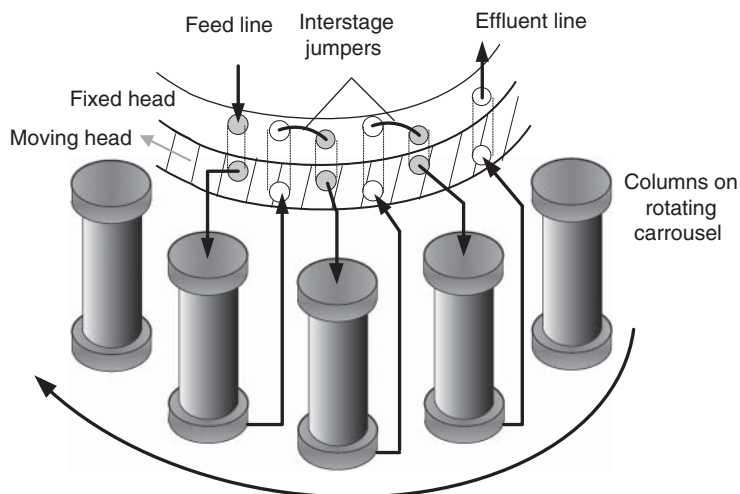
Figure 5.13 ISEP principle; the rotating valve.

system, the number of columns has to be adjusted to the time needed for the operation of each individual step. Many systems are known, for example, for the purification of amino acids and sugars on ion-exchange resins.

As mentioned before, the complete parallel interconnection of the columns is similar to annular chromatography. The second border case is to connect all beds in series, which corresponds to the SMB chromatography discussed in Section 5.2.4.

5.2.4 Isocratic Simulated Moving Bed (SMB) Chromatography

In general, a countercurrent operation can achieve a more efficient separation than the crosscurrent operation considered above. In chromatography, this is realized by the SMB technology. Chromatographic countercurrent operation requires the mobile and stationary phases to move in opposite directions. Figure 5.15 illustrates the more or less hypothetical concept of an ideal countercurrent system, denoted as true moving bed (TMB). This concept utilizes an actual circulation of the solid phase with a constant flow rate.
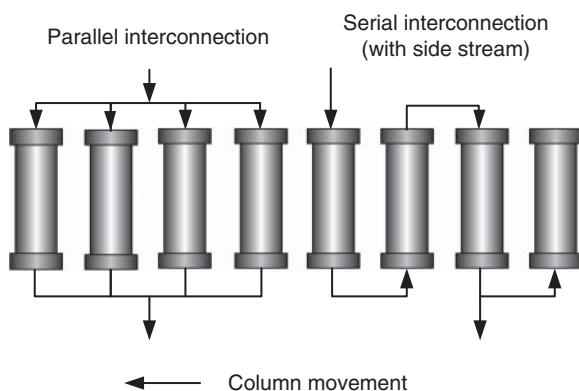
Figure 5.14 ISEP principle involving parallel and serial column interconnection.
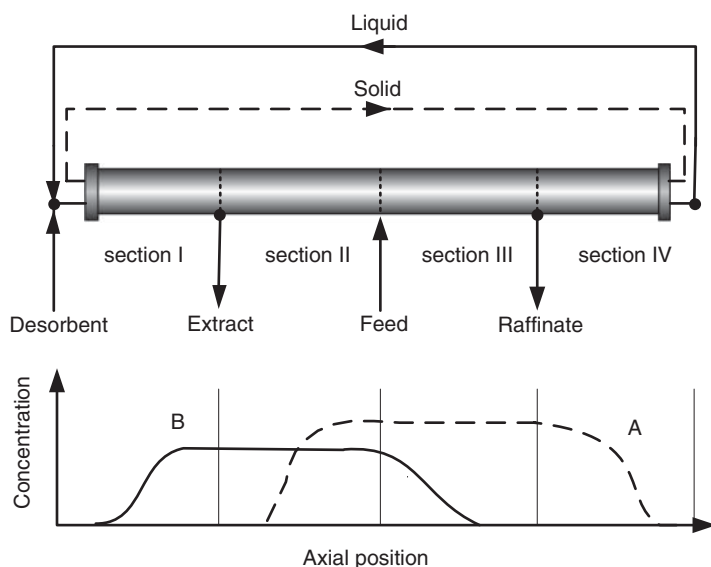
Figure 5.15 True moving bed (TMB) chromatography with internal concentration profiles.

For the chromatographic separation, four external streams are present:

- Feed inlet containing the components to be separated;
- Desorbent inlet;
- Extract outlet containing the more retained component B;
- Raffinate outlet enriched with the less retained component A.

These streams divide the system into four sections or zones with different flow rates of the liquid phase. Each of the sections plays a specific role in the process. Separation is performed in Sections II and III, where the more retained component B has to be adsorbed and carried toward the extract port by the moving solid, while the less retained component A has to be desorbed and carried by the mobile phase toward the raffinate port. In Section I, the solid phase is regenerated by a fresh eluent stream that desorbs the strongly adsorbed component and transports it to the extract outlet. Finally, in Section IV the liquid is regenerated by adsorbing the amount of less retained component not collected in the raffinate. In this way both the solid phase and the liquid phase can be recycled to Sections IV and I, respectively. In summary, the four sections have to fulfill the following tasks:

- *Section I*: Desorption of the strongly adsorptive component;
- *Section II*: Desorption of the less adsorptive component;
- *Section III*: Adsorption of the strongly adsorptive component;
- *Section IV*: Adsorption of the less adsorptive component.

With a proper choice of all individual internal fluid flow rates in Sections I–IV and the velocity of the stationary phase, the feed mixture can be completely separated into two pure products. Complete separation corresponds to axial concentration profiles at steady state as displayed in Figure 5.15.

Unfortunately, an efficient, dispersion-free movement of a stationary phase, which in most cases consists of porous particles in the micrometer range, is technically not possible. Therefore, other technical solutions had to be developed. The breakthrough was achieved with SMB systems, which were developed by Universal Oil Products (UOP) for the petrochemical industry in the 1960s (Broughton and Gerhold 1961). Here the stationary phase is packed into single, discrete columns, which are connected to each other in a circle.

Figure 5.16 illustrates the principle of SMB processes. The mobile phase passes the fixed bed columns in one direction. Countercurrent flow of both phases is achieved theoretically by switching the columns periodically upstream in the direction opposite to the liquid flow. Practically, not the columns are shifted but all ports are moved in the direction of the liquid flow by means of valves. Either way, the periodic switching "simulates" a true countercurrent movement of the two phases, giving the process its name. The countercurrent character of the process becomes more obvious when the relative movement of the packed beds to the inlet and outlet streams during several switching intervals is observed. After a number of switching events or shifting intervals equal to the number of columns in the system, one so-called cycle is completed, and the initial positions for all external streams are reestablished. The analogy to the TMB concept above becomes even clearer when considering an SMB process with a large number of very short columns shifted in very short intervals.

The total number of columns and their distribution over the different sections are not fixed to eight with two columns per zone (2/2/2/2) as assumed in Figure 5.16. Another quite common setup is 1/2/2/1 with only one column in Sections I and IV. Naturally, this reduction in total number of columns can
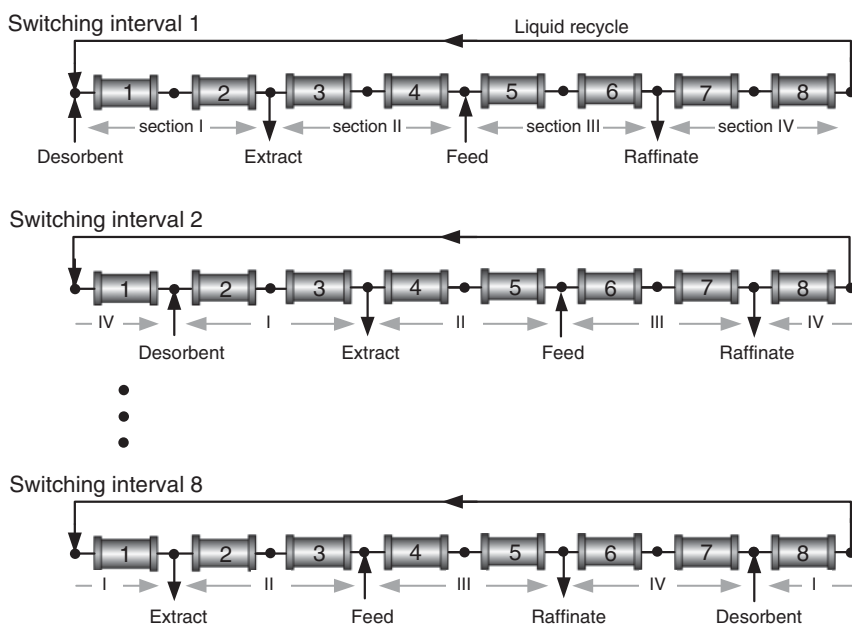
Figure 5.16 Simulated moving bed (SMB) chromatography.

reduce investment costs. A further decrease of column number is possible by other continuous process concepts like Varicol or iSMB (Section 5.2.5).

In general, the SMB concept is realized for pharmaceutical and fine chemical separation purposes in two different ways. In the first alternative, one central rotating valve, as introduced in Section 5.2.3, is used to distribute and collect all inlet and outlet streams. The second design concept switches the ports by means of two-way valves between all columns. While the first approach corresponds to a less complex setup, the advantage of the second is that higher pressures can be realized and the switching of the individual ports can be handled very flexibly, allowing for implementations like the Varicol process (Section 5.2.5).

Another characteristic of the SMB setup is the implementation of a so-called recycle pump to ensure the liquid flow in one direction. In general, four cases can be distinguished (Figure 5.17).

In the first case (Figure 5.17a), the recycle pump is at a fixed position between two columns. Since all columns are moving upstream according to the SMB principle, the recycle pump performs the same migration. This means that the flow rate of this pump has to be adjusted depending on which section it is currently located in. This design results in a locally increased dead volume because of the recycle line and the pump itself. Asynchronous shifting of the external ports, as introduced by Hotier and Nicoud (1995), can compensate such an unequal distribution of the dead volume.
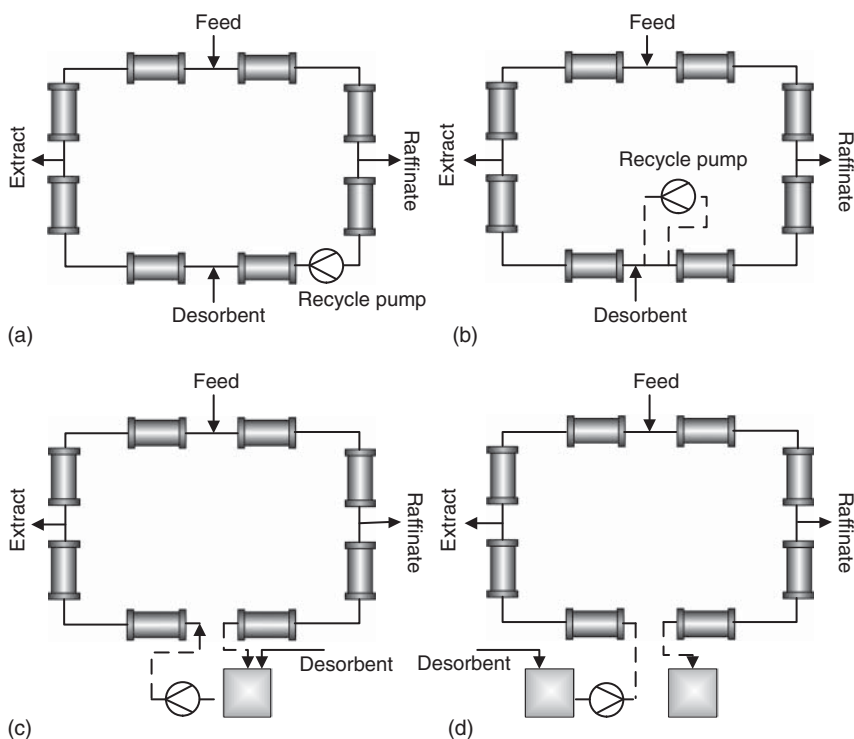
Figure 5.17 Possible setups of SMB units with an additional recycle pump.
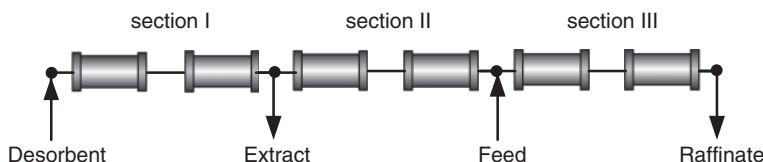
Figure 5.18 Three-section SMB concept.

The second approach (Figure 5.17b) is characterized by a "moving" recycle pump that is always located near the desorbent line. This has the advantage that the recycle pump never comes into contact with the products to be separated and is operated at a constant flow rate. However, this design requires additional valves.

Besides these options, more approaches exist that do not require an additional recycle pump. In the third case (Figure 5.17c), the outlet of Section IV is not directly recycled to Section I but introduced to the desorbent tank instead. Figure 5.17d shows another possibility where no recycling of the solvent takes place (Ruthven and Ching 1989). This method is applied when the regeneration of the desorbent turns out to be very difficult and fresh solvent is rather inexpensive. In such case, the regeneration of the fluid is no longer necessary, and, consequently, Section IV is no longer required. This leads to a three-section SMB concept without solvent recycle, as depicted in Figure 5.18. Finally, also two recycle pumps may be used that are positioned in zones II and IV, respectively.

In addition to three- and four-section SMBs, a system with five or more sections can be used if a third fraction is required; see Section 5.2.8. For very strongly retained components, a second solid regeneration section can be implemented by introducing a second desorbent stream with higher solvent strength.

The technology of SMB chromatography has been widely used in the petrochemical (Parex process for xylene isomer separation) and food industries (glucose–fructose separation) in a multi-ton scale. Since the 1990s, with the advent of stable chiral stationary phases for enantioseparations, the SMB technology is applied successfully by the pharmaceutical industry. Today it is possible to build SMB systems with column sizes from 4 to 1000 mm inner diameter and to produce pharmaceuticals at small scale as well as up to a 100 ton scale.

An empirical design of SMB systems is quite difficult and is practically impossible for the further advanced SMB setups and operating strategies explained in the next section. Therefore, modeling and simulation are important tools for design and optimization of SMB processes. Corresponding modeling approaches are presented in Chapter 6, while model-based design and optimization are discussed in Section 8.4.

5.2.5 SMB Chromatography with Variable Process Conditions

Continuous countercurrent separation by SMB chromatography can improve process economics. Nevertheless, more advanced processes have been developed. They are all based on the standard SMB technology but operated

under variable process conditions to reduce the costs of column hardware and stationary phase as well as for fresh eluent and eluent work-up. Trends and suggestions to improve the operation of SMB processes have been reviewed, for example, by Seidel-Morgenstern, Kessler, and Kaspereit (2008) and Kaspereit (2009).

5.2.5.1 Varicol

Classical SMB systems are characterized by the synchronous and constant downstream shift of all inlet and outlet lines after a defined switching period. In that case four defined sections can be distinguished over the complete cycle time (Figure 5.19a). Within these sections the columns are distributed equally (e.g. 2/2/2/2) or in any other given configuration. The number of columns per section is constant and an integer number (e.g. 1/2/2/1). At periodic steady state, the same process conditions are always reached after one switching interval (t_{shift}).

The Varicol approach, as introduced by Ludemann-Hombourger, Bailly, and Nicoud (2000), increases the flexibility of the continuous separation system by an asynchronous movement of the injection and withdrawal ports. Within a complete process cycle, this leads to mean numbers of columns per section that are typically non-integer. As the minimum number of columns per section in an SMB system is 1, it is possible in Varicol systems to reduce the mean number to virtually any value less than 1. Owing to the asynchronous shift of the inlet and outlet lines in a Varicol process, it may even happen that, during a certain interval, there are no columns in a section. In this case, the inlet and outlet lines of this section
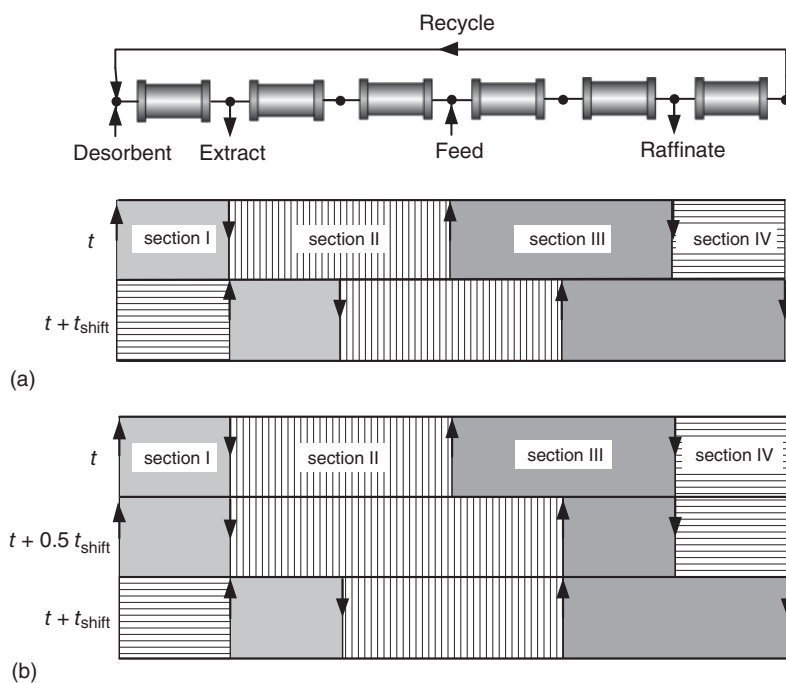
Figure 5.19 Switching strategies for (a) SMB and (b) Varicol.

coincide in one valve block. By placing the outlet lines upstream from the inlet lines, a pollution of the product lines is avoided.

As a simple example, the initial column configuration of a Varicol process at time t might be 1/2/2/1 (Figure 5.19a). After a predetermined time interval (e.g. $t + 0.5\, t_{shift}$), only the feed line is shifted to the next downstream position (Figure 5.19b). Now Section II contains three columns for the rest of the time interval, while only one column remains in Section III. Thus, the new configuration is 1/3/1/1. At the end of the switching time ($t + t_{shift}$), all other ports are shifted, and the initial setup is reestablished. The section configuration can now be calculated according to the number of columns and their residence time within a section. In our example, the overall distribution of columns within one process cycle is 1/2.5/1.5/1. These figures demonstrate that the Varicol process offers high flexibility, especially for systems with a low number of columns (five or less columns). The main goal of the Varicol process is to decrease the amount of stationary phase and the number of columns, e.g. decreasing investment costs for column hardware and stationary phase.

5.2.5.2 PowerFeed

Another multicolumn process based on the SMB principle is the so-called Power-Feed approach proposed by Kloppenburg and Gilles (1999) and Zhang, Mazzotti, and Morbidelli (2003). In contrast to the Varicol process, the switching is the same as in a classical SMB plant. The main idea of the PowerFeed approach is the variation of the internal ($\dot{V}_I - \dot{V}_{IV}$) and external flow rates ($\dot{V}_{feed}$, $\dot{V}_{des}$, $\dot{V}_{ext}$, $\dot{V}_{raf}$) within one switching interval t_{shift}. In the example illustrated in Figure 5.20, the flow rate in Section IV $\dot{V}_{IV}$ is lowered during the second part of the switching interval for improved adsorption of the less retained component. However, as a consequence, also other flow rates may change and might have to be manipulated to maintain, for example, a constant flow rate in Section I. Designing the various flow rates during the subintervals is an optimization problem.
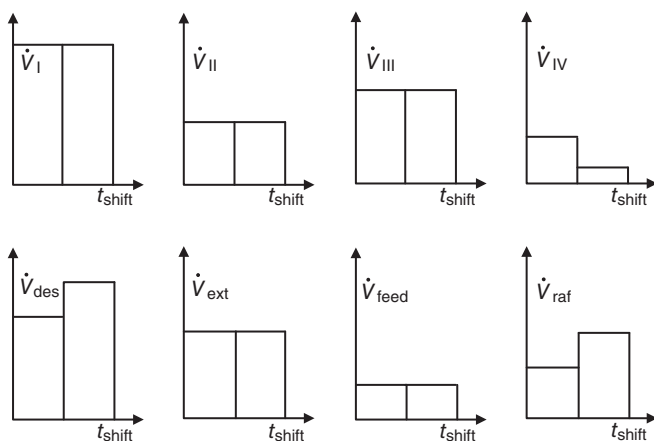
Figure 5.20 Flow rates during PowerFeed operation (illustrative example).

As reported by Zhang, Mazzotti, and Morbidelli (2003), the performance of the PowerFeed process is similar to Varicol and significantly improved with respect to classical SMB processes. Furthermore, the extent of improvement is particularly increasing for more difficult separations. However, this improved performance is paid for by the increased complexity of operation and design; for more details see Section 8.5.

5.2.5.3 Partial-Feed, Partial-Discard, and Fractionation-Feedback Concepts

Similar to the PowerFeed concept explained above, the Partial-Feed approach introduced by Zang and Wankat (2002a,b) exploits the feed duration and feed time as degrees of freedom. Figure 5.21a compares the feed flow of classical SMB and Partial-Feed processes. Because of this operation strategy, the raffinate flow rate changes during each switching interval according to the change in the feed flow (Figure 5.21b). In comparison with a conventional SMB process, the feed interval is shorter, but its flow rate can be higher. This procedure process can improve performance for the same throughput.

The Partial-Feed concept seems promising for applications where the separation is difficult particularly due to significant band broadening effects. Another option for such problem is the Partial-Discard strategy proposed by Bae and Lee (2006). Here, purity is improved by fractionating off impurities that elute at the outlet ports in the beginning or toward the end of a switching interval. This allows to choose more productive operating points. The resulting reduction of the recovery yield can be acceptable in certain cases.

An extension of the above is the Fractionation-Feedback approach (FF-SMB; see Section 5.2.5.6) suggested by Keßler and Seidel-Morgenstern (2008), wherein collected fractions with insufficient purity are collected, recycled, and refed into the SMB unit, which overcomes yield limitations.

Besides the concepts discussed above, there are ongoing activities in the development of further refined operating modes for SMB systems. A complete review is out of scope here.

5.2.5.4 Improved/Intermittent SMB (iSMB)

Partial-Feed processes switch the feed stream on and off within one time interval, while the other inlet and outlet lines are active all the time. The improved or
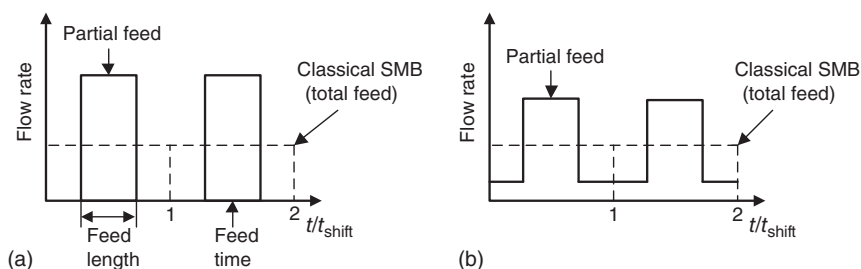
Figure 5.21 Flow rates during Partial-Feed operation. (a) Feed flow rate. (b) Raffinate flow rate. Source: From Zang and Wankat (2002a,b).
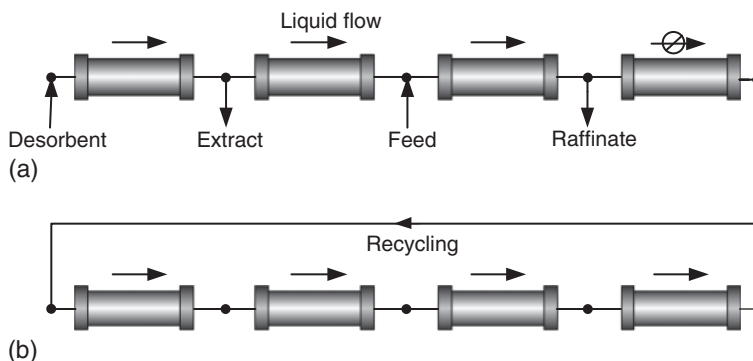
Figure 5.22 Flow rates during iSMB operation. (a) Injection period. (b) Recirculation period.

intermittent SMB (iSMB) process (Tanimura, Tamura, and Teshima 1995) partitions the switching interval in a different way. In the first part of the period (Figure 5.22a), the unit is operated basically as a conventional SMB process; hence all external streams (desorbent and feed inlets as well as extract and raffinate outlets) are in operation. However, in contrast to a classical SMB unit, the outlet of Section IV is not recycled during this part of the switching interval, and, consequently, the flow rate in Section IV is zero. This first "injection period" is followed by a recirculation period in the second part of the switching interval (Figure 5.22b). During this interval, all external ports are closed, and recirculation is performed with a constant flow rate in all sections of the plant. The aim is to reposition the internal concentration profiles in an optimal manner. This operating procedure allows a separation to be carried out with a rather small number of columns, which of course has a positive impact on investment costs. Furthermore, the concept has been demonstrated to achieve a superior performance (Katsuo and Mazzotti 2010a,b). The main application area of the iSMB concept is so far the sugar industry.

Obviously the forth section is not in use during the injection period. Based on this, Jermann and Mazzotti (2014) suggested further improvements of the iSMB process. They found that at the end of the recirculation period, the first column is almost completely regenerated and therefore can be used to adsorb the weakly retained component. This leads to a three-column iSMB process (3C-iSMB) in which the first column fulfills the function of the fourth column of the classical iSMB process. The process can be designed by means of the triangle theory (Section 8.4.2).

Furthermore, Jermann, Meijssen, and Mazzotti (2015) developed a design method for 3C-SMB cascades for center-cut separations. Figure 5.23 illustrates this for the ternary separation of two impurities (A, B) from a product. In this example, the impurity A is separated from the product and B in step 1a. The latter two are withdrawn together as an intermediate fraction. They are later separated from each other in step 2a. A buffer tank is necessary for decoupling the semicontinuous steps of the iSMB concept.

Jermann, Alberti, and Mazzotti (2014) confirmed also experimentally that 3C-iSMB outperforms a corresponding iSMB or SMB process. Besides saving
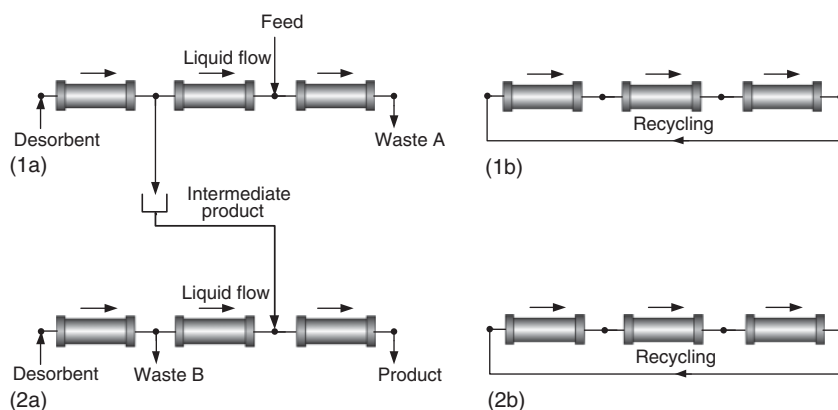
Figure 5.23 3C-iSMB cascade separation. (1a, 2a) Injection period. (1b, 2b) Recirculation period.

investment costs, the reduced number of columns allows higher flow rates that results in higher productivity at the same purity level.

5.2.5.5 Modicon

Another modification of the classical SMB process is the Modicon (*mod*ulated feed *con*centration) approach by Schramm et al. (2003). In contrast to the Partial-Feed process, where the feed flow rate is varied during one switching interval, in Modicon the concentration of the feed is altered instead of its flow rate. Figure 5.24 illustrates this variation of the feed concentration during the switching interval t_{shift}. In the example shown, which is suitable for systems with favorable isotherms, at the beginning only pure solvent is fed to the plant, while in the second part feed at a rather high concentration is used. Provided the modulation of the feed concentration is not limited by solubility constraints, the concept allows for improved performance for systems with nonlinear adsorption isotherms.

5.2.5.6 FF-SMB

Another modification of SMB technology, referred to as fractionation and feedback SMB (FF-SMB), is based on fractionating of one or both outlet streams and feeding the off-spec fractions back into the unit alternatively with the original feed mixture. Based on results of an extensive optimization study,

Figure 5.24 Feed concentration during Modicon operation.
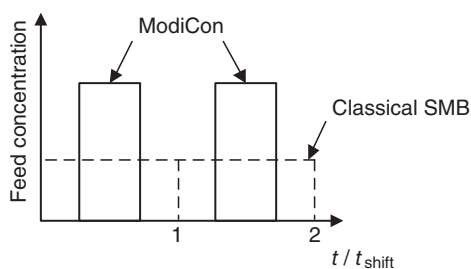
Li et al. (2010a,b) point out that the simultaneous fractionation of both outlet streams is the most efficient operating scheme in terms of maximum throughput while already the single outlet fractionation mode can be significantly superior to the classical SMB process.

5.2.6 Gradient SMB Chromatography

One restriction of SMB chromatography as described so far is the operation under isocratic conditions. When selecting the stationary and the fluid phases, it is one of the main goals to find a separation method where the first component is fairly well adsorbed on the stationary phase, while the second one is still eluting under those conditions. This is quite often a tedious task in which a number of compromises have to be made. In many cases, isocratic elution conditions lead to a severe tailing of the second component. However, similar to batch chromatography, a gradient can improve the SMB separation if the selectivity of the components is very large, the product concentrations should be increased, or a separation under isocratic conditions is impossible.

The easiest and most adopted way to adjust different elution strengths within an SMB plant is a two-step gradient (Figure 5.25). This is achieved, for example, by using a desorbent with high elution strength while the feed stream contains a "weaker" eluent. Such solvent gradient SMB operation leads to the formation of a step gradient with a regime of high desorption power in Sections I and II and a region of improved adsorption in Sections III and IV. According to the tasks of the different sections (Section 5.2.4), it becomes obvious that such gradient in an SMB process can improve its performance with respect to productivity, eluent consumption, and product concentration.

The cost for the improved performance can be a more complex operation and layout of the process, requiring precise process design and control – especially when a recycling of the Section IV outlet is applied. An open-loop operation without eluent recycling between Sections I and IV is more robust and allows for more pronounced gradients, which is particularly attractive when regeneration of the adsorbent is difficult.
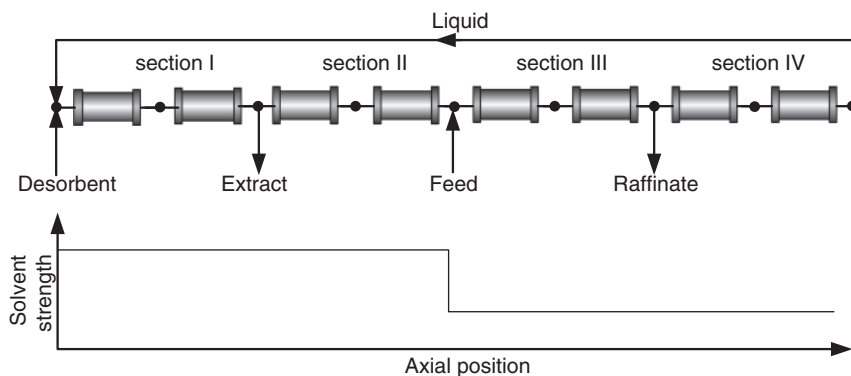
Figure 5.25 Solvent gradient operation of a SMB unit.

Some prerequisites for the choice of solvent and stationary phase should be considered when developing the chromatographic system. The solvents used for the gradient should exhibit low viscosities, high diffusivity, and thus good miscibility. In addition, heat of mixing as well as volume changes should be low. Several research projects have investigated the application of gradient SMB processes (Jensen et al. 2000; Antos and Seidel-Morgenstern 2001; Abel, Mazzotti, and Morbidelli 2002; Beltscheva, Hugo, and Seidel-Morgenstern 2003; Abel, Mazzotti, and Morbidelli 2004). The concept is of special interest in the separation of bioproducts, such as the separation of proteins by ion exchange (Houwing, Billiet, and van der Wielen 2002; Wekenborg, Susanto, and Schmidt-Traub 2004; Wekenborg 2009) or based on hydrophobic interaction (Palani et al. 2011; Gueorguieva et al. 2011).

Manipulating adsorption strength is most readily achieved by variation of solvent composition (or column pressure in the case of SFC-SMB; Section 5.2.7.2). However, there exist further options for implementing gradients. In particular, the use of salt and pH gradients is attractive in the context of bioseparations (Sections 5.1.2 and 5.2.9.2). Another, obvious option is to introduce temperature gradients (e.g. Eagle and Rudy 1950; Ching and Ruthven 1986; Ching, Ho, and Ruthven 1986; Kim et al. 2005). For example, a dedicated heating of Section I of the SMB process enhances desorption and solid regeneration (Migliorini et al. 2001). A drawback is here the heat capacity of the system (including valves and pipes) and the slow change of temperature. This is particularly critical since the columns eventually enter another section where its temperature is to be lowered again. A useful alternative is to manipulate the temperature of the mobile phase (Jin and Wankat 2007).

5.2.7 Supercritical Fluid Chromatography (SFC)

SFC systems are operated above the critical pressure and usually also above the critical temperature of the mobile phase. In most cases, the main component of the mobile phase is carbon dioxide, for which the critical point is reached at 31 °C and 74 bar.

In the supercritical state, the density and, therefore, the solvating power of the fluid are highly dependent on pressure and temperature, and so is the affinity of a given solute for the supercritical fluid phase itself. With a higher operating pressure, and thus a density increase, the elution strength is improved, and smaller retention times can be realized. Supercritical fluids can be seen as intermediates between gases and liquids with liquid-like solvating powers in combination with gas-like viscosities and diffusivities in between a liquid and a gas. This results in the following main benefits: low mobile phase viscosity and high diffusivity, which promote fast mass transfer and high throughput, easy recovery of substances from the eluent stream by simple solvent expansion, and low cost and nontoxicity of the mobile phase ("green solvent"). Because of the favourable transport parameters, SFC is a rather fast separation technique compared with high-performance liquid chromatography (HPLC). On the other hand, such a system is more complex, and the solubility of most pharmaceutical components in pure CO_2 is rather limited, because drug substances often exhibit

a certain hydrophilicity to achieve solubility and resorption in the gastrointestinal tract. This drawback is often overcome by introducing an additional modifier, in most cases an alcohol or ether (Dai, Li, and Rajendran 2015; Saito 2013). Lesellier and West (2015) point out that in the course of gradient conditions, the mixture of carbon dioxide with a modifier will transfer from a supercritical fluid into a subcritical fluid, and as long as the backpressure is maintained above critical pressure, the temperature may remain below the critical temperature in order to preserve instable solutes. The extensive review of Lesellier and West (2015) is recommended for detailed information on SFC even though they focus predominately on analytical scale. Guiochon and Tarafder (2011) published another review worth reading on fundamentals and opportunities for preparative SFC. Speybrouck and Lipka (2016) discuss benefits of preparative SFC versus benefits of HPLC. Recently, Rossé (2019) edited a two-volume book on SFC, which gives a comprehensive overview on the field.

5.2.7.1 Supercritical Batch Chromatography

Figure 5.26 illustrates the flow sheet and different thermodynamic states of an SFC batch process. At the inlet of the main pump, CO_2 is in liquid state (40 bar and $-5\,°C$) and compressed at the outlet to the operating pressure. Modifier (e.g. methanol) is added to adjust the polarity of the solvent. After heating, the solvent is in supercritical state and feed is injected. At the outlet of the column, a decompression turns the mobile phase to a biphasic system: gaseous mobile phase (CO_2 and traces of the modifier) and droplets of solute (products and modifier). As the gaseous phase makes up the majority of the mobile phase, the final product has to be separated from only a low amount of solvent. In the case of temperature-sensitive compounds, this has the advantage to limit the risk of degradation and enantiomerization. The different fractions of the solute are collected by separate cyclones. The precipitator allows the recovery not only of
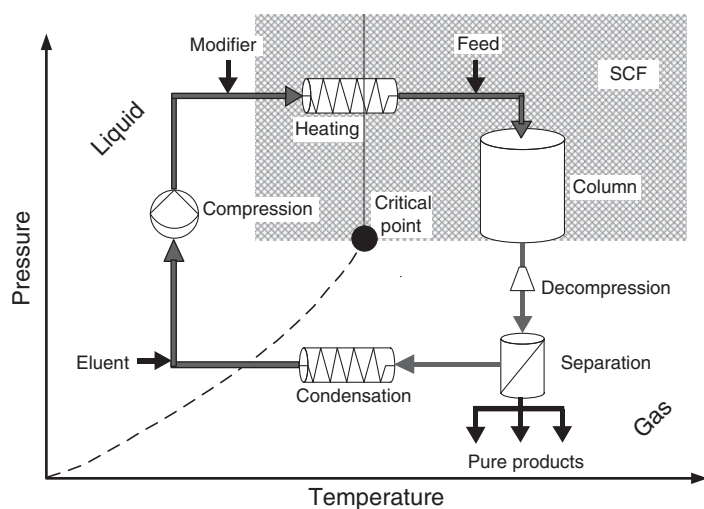
Figure 5.26 Supercritical batch chromatography with CO_2 recycling.
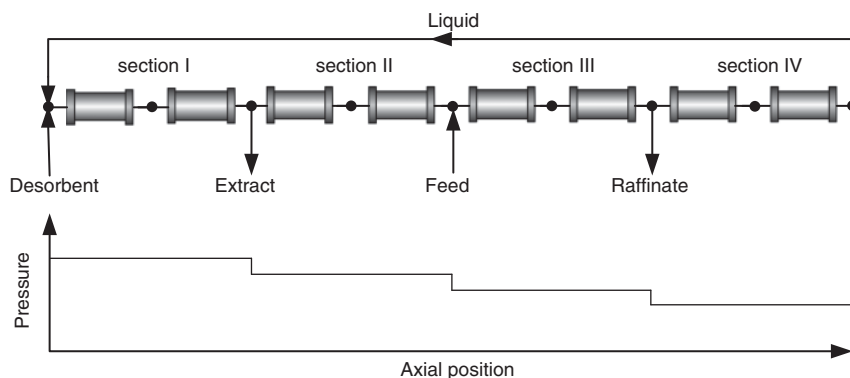
Figure 5.27 Supercritical fluid operation of a SFC-SMB unit.

the solute but also of the gaseous CO_2 that can be recycled after condensation. Finally, CO_2 is introduced to compensate the amount lost during the separation step. At the end of this process, the mobile phase has "experienced" a complete turn around its critical point. Alternatively, CO_2 can pass the SFC process in an open loop.

5.2.7.2 Supercritical SMB processes

Pressure influences the elution strength of the supercritical mobile phase; therefore, a pressure gradient is an additional degree of freedom in supercritical SMB processes (SFC-SMB). The pressure gradient is adjusted across the different sections (Figure 5.27). In Section I desorption of the more adsorptive component has to take place; therefore, the elution capability should be the highest, and thus the system pressure is also the highest. Through Sections II and III toward IV, the pressure can be constantly lowered due to adsorption and desorption requirements in the single sections. More detailed information about this process concept can be found in Clavier, Nicoud, and Perrut (1996); Denet et al. (2001); Depta et al. (1999); Giovanni et al. (2001); Peper et al. (2002); Brunner and Johannsen (2006); Cristancho, Peper, and Johannsen (2012); Lin et al. (2015); and Johannsen and Brunner (2018).

So far, supercritical SMB has attracted mainly scientific research; the industrial utilization of production-scale units is unclear and still in discussion according to West (2014).

5.2.8 Multicomponent Separations

The classical SMB process has two outlet ports and is, thus, limited to binary separations. A number of approaches have been suggested to perform separations of multicomponent mixtures based on SMB technology. A straightforward attempt is to implement several SMB units in series as shown in Figure 5.28a. Wankat (2001) investigated a number of corresponding options. Another way is to increase the number of zones of the SMB unit and to perform an internal recycling of partially separated streams as is the case, for example, in the nine-zone
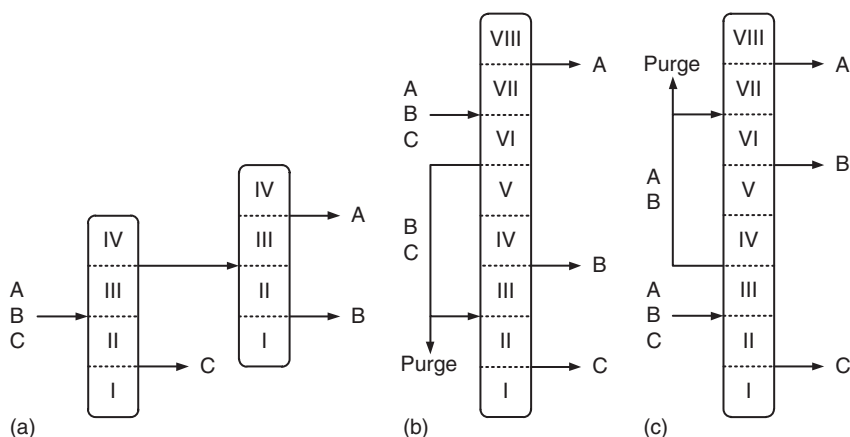
Figure 5.28 Examples for possible approaches for multicomponent separations by SMB chromatography for the case of separating a three-component mixture of A, B, and C. (a) Interconnected SMB units. (b, c) Different eight-zone setups with internal recycle streams. Source: Reproduced with permission of Kaspereit (2009).

system proposed by Wooley, Ma, and Wang (1998) and the eight-zone setup by Keßler and Seidel-Morgenstern (2006); see Figure 5.28b,c. An overview on such and further possible multicomponent setups is given in, for example, Chin and Wang (2004).

The mentioned concepts exhibit a higher degree of integration making necessary some specific design considerations. Interconnected SMB processes might require a partial solvent removal between the units to balance the dilution of the product delivered by the upstream SMB unit. In systems with internal recycles, usually purge streams or solvent removal steps are necessary, as indicated in Figure 5.28b,c. Furthermore, a restrictive design aspect of such multizone processes is the identical switching time applied to all zones.

5.2.9 Multicolumn Systems for Bioseparations

Above sections already describe plant concepts where chromatographic columns can be arranged very flexible according to process needs and optimization. Also for bioseparations there exists a multitude of process options, because in comparison to fine chemicals, the separation of bioproducts is characterized by a wide range of the adsorption strength. Hence, it is standard to change the eluent compositions, that is, the solvent strength within the process (Carta and Jungbauer 2010).

The challenges inherent to separation and purification of biotechnological products are explained best for the example of monoclonal antibodies (mAbs). mAbs such as immunoglobulin (IgG) play an important role among new pharmaceutical drugs. An established method to purify mAbs is protein A affinity batch chromatography, but these stationary phases are insensitive to mAb variants. An alternative to purify charged mAb variants is ion-exchange batch chromatography, which has the drawback to achieve high purities at
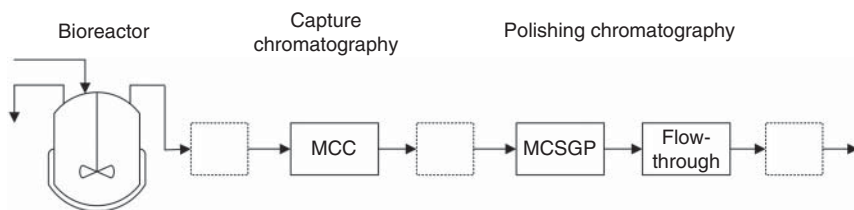
Figure 5.29 Integrated continuous process for protein production.

low yield or vice versa. A general principle to increase productivity and yield of separation processes is a countercurrent mass transport that, for instance, characterizes SMB processes. The purification of proteins from clarified cell culture supernatants normally requires the separation of impurities, especially host cell impurities and mAb variants that are, respectively, weaker and stronger adsorbing than the product.

Improved technologies, cost reduction, and the rapidly growing market are stimulating the intensification of the production of biotherapeutics, especially mAbs. A major challenge in this context is the change from step-by-step batch operations to continuous processes. Increasing titers and perfusion operations of bioreactors are demanding continuous downstream processes. Figure 5.29 illustrates an example of a process scheme for continuous production of proteins. The supernatant of a continuously operating bioreactor enters a multicolumn capture chromatography (MCC) where the product protein is captured and clarified from the majority of contaminants. In the following, the product has to be purified from similar weak and strong adsorbing components by a polishing step. MCSGP- and flow-through chromatography are options for these steps. In between and downstream of these separation steps, other units like centrifugation, virus inactivation, buffer exchange, or filtration will complete the process.

Steinebach, Müller-Späth, and Morbidelli (2016) review different processes for capture and polishing chromatography. In the following, different MCC processes are described. For modeling and experimental results of MCC processes, see Section 8.7.

5.2.9.1 Multicolumn Capture Chromatography (MCC)

Capture chromatography is a high-quality alternative to multicolumn gradient separations. While gradient separation uses ion exchange resins for protein separation, capture chromatography is mostly based on protein A affinity sorbents. These provide a highly selective binding capacity, but they are also a magnitude more expensive than other non-affinity sorbents. Thus, process design has to reduce costs by achieving high specific productivity as well as high mAb yield. In conjunction with continuously operated bioreactors, continuous countercurrent processes, therefore, increasingly replace batch chromatography.

Against this background, in the recent past various MCC processes with different numbers of columns have been suggested (Figure 5.30) (Warikoo et al. 2012; Ng et al. 2014; Gjoka et al. 2015; Angarita et al. 2015; Steinebach et al. 2017; Girard et al. 2015).
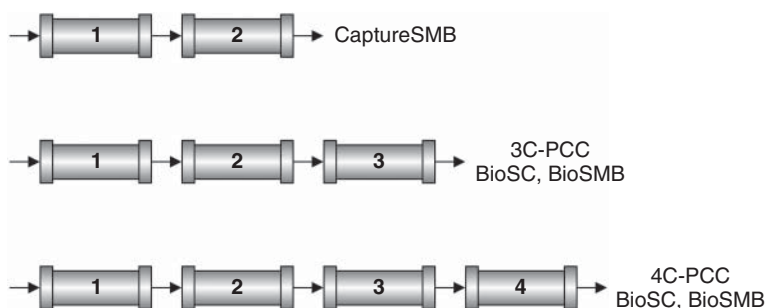
Figure 5.30 2–4 column MCC processes, commercialized by ChromaCon (CaptureSMB®), GE Healthcare (3C-PCC, 4C-PCC), Novasep (BioSC®), and Pall (BioSMB®). Source: Pfister et al. (2017). Reproduced with permission of Elsevier.

As illustrated in Figure 5.31, the basic concept of all these processes is to capture the main product during a loading period followed by a refresh period that includes separate steps for washing, elution, regeneration, and equilibration (Pfister et al. 2017). In the case of a single column batch process, this would be a sequential process so that the cycle time is given by the sum of the loading and the refresh period. In MCC processes, these steps can be operated simultaneously or sequentially, which offers numerous degrees of freedom for process design.

Figure 5.31 illustrates the principle of a three-column MCC process. The main point is that target product is captured in two columns (1 and 2) while a third column is refreshed. The loading period ends just before a product breakthrough at the outlet of the column 2. This allows maximum "overloading" of column 1, while column 2 simply prevents a loss of product. Next, after a switching step, loading continues onto column 2, and a refreshed column takes over the function of preventing product breakthrough. During this second period, the loaded first column is refreshed. Different buffers are used for washing out remaining impurities, eluting the product, and regenerating and equilibrating the sorbent for repeated capturing. To ensure a continuous operation, the time intervals for the loading period and the refresh period have to be synchronized. The processes named in Figure 5.30 fulfill all these functionalities by different process schemes.

In comparison with single-column batch chromatography, the main advantage of MCC processes is that they realize a much higher binding capacity per column and, correspondingly, a significantly higher productivity at high yields. This becomes clear when considering that in a single-column batch process, the load
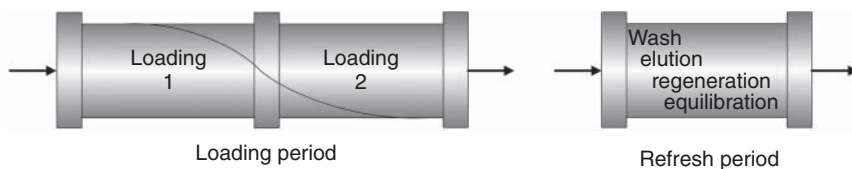
Figure 5.31 Process steps of capture chromatography.
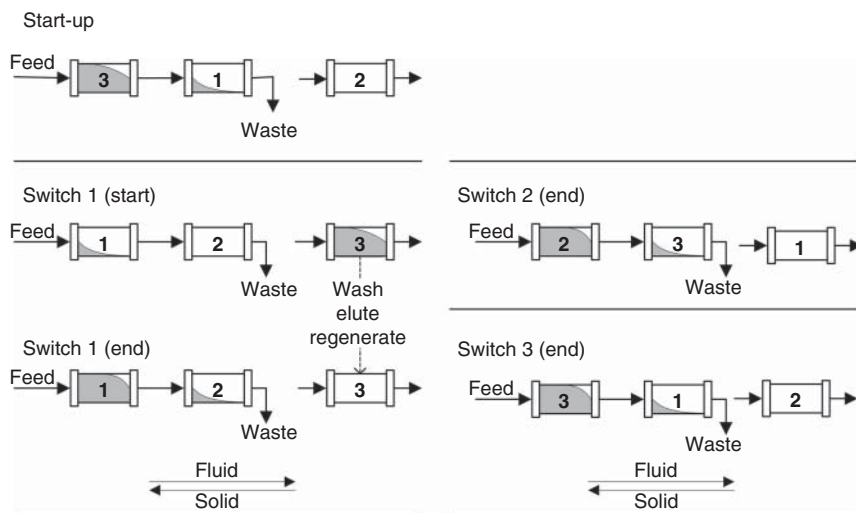
Figure 5.32 Three-column PCC chromatography with hypothetical countercurrent switching of columns. Source: Reproduced with permission of Gjoka et al. (2015).

profile in columns 1 and 2 shown in Figure 5.31 has to be confined within a single column. This is possible only by much shorter loading cycles, which limits performance.

Periodic Countercurrent Chromatography (PCC) One group of MCC processes is operating with a continuous feed stream. These processes are, for instance, known as 3C-PCC, 4C-PCC, or BioSMB®. In the following, a "switch" refers to a discrete switching of the columns countercurrently to the fluid direction. A "step" indicates that the fluid connections of the columns are changed during a switching period.

Figure 5.32 depicts a three-column countercurrent periodic countercurrent chromatography (PCC) process for mAb purification as described by Gjoka et al. (2015). In the example, a countercurrent flow is realized by periodically switching the columns opposite to the fluid flow.

The process realizes the operating principle described above by corresponding column switching events. During start-up of the process (top of Figure 5.32), columns 3 and 1 are interconnected, and loading is stopped just before product breaks through the column 1. Column 2 is regenerated and in standby modus. The subsequent continuous operation comprises the following periods:

1. After start-up, columns 1 and 2 are switched countercurrently to the fluid flow. Now column 1 is "overloaded," while column 2 captures the breakthrough product. Column 3 is isolated and washed, eluted, and regenerated during this switching period. For switch 1 the product load at the beginning and the end of this switching period is shown in Figure 5.32.
2. Switches 2 and 3 are operated in the same manner as switch 1.
3. With switch 3 the process cycle is completed and the process starts the next cycle.
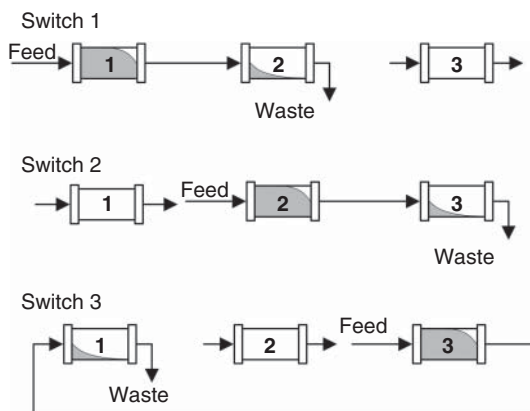
Figure 5.33 Three-column PCC chromatography: practical process scheme, where process nodes are switched in the direction of liquid flow. Source: Reproduced with permission of Gjoka et al. (2015).

The corresponding practical realization of the countercurrent movement is shown in Figure 5.33. Here the columns are locally fixed and their ports are switched in the direction of the fluid flow. Similar to the SMB process as described in Section 10.4.5.1, the complexity of the pipework of a PCC plant depends on the type of valves that are switching the fluid flow (Mahajan, Anupa, and Wolk 2012; Faria and Rodrigues 2015).

Warikoo et al. (2012) have published a comparable process design. Here the switching period is additionally subdivided into two steps. Referring to Figure 5.33 the feed goes first into column 1 only, while column 2 is at rest. In a following step, columns 1 and 2 are linked as shown in Figure 5.33. Meanwhile column 3 is refreshed until the columns are switched again.

The PCC processes can be expanded to more than 3 columns; commercial plants are offered with 3–8 or even 10 columns (Steinebach, Müller-Späth, and Morbidelli 2016). An increasing number of columns offer more flexibility in process design, for instance, in parallelization of the process steps of the refreshing period (washing, elution, regeneration, and equilibration). Optimal design will also depend on thermodynamics, i.e. the shape of the breakthrough curve, which can be shallow or steep. However, it has to be kept in mind that a higher number of columns also result in a higher complexity of the plant as the number of valves and connecting pipes are increasing, which raises costs and influences the stability of plant operation.

CaptureSMB When reducing the number of columns to a twin-column MCC, the feed has to be supplied discontinuously. The group of Morbidelli (Angarita et al. 2015; Ulmer et al. 2015) has intensively investigated this process design. Figure 5.34 illustrates the principles of this process called "twin-column CaptureSMB." Because of the reduced number of columns, every switch is subdivided into two steps.

As shown in Figure 5.34 both columns are separated at the beginning of the periodic capture process. The saturated column 2 is refreshed by washing, eluting the product, and finally regenerating and equilibrating the resin. Meanwhile
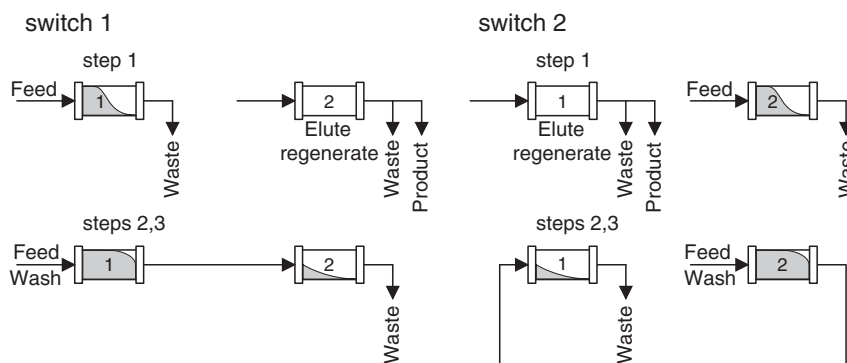
Figure 5.34 Schematic diagram of the CaptureSMB process. Source: Reproduced with permission of Ulmer et al. (2015).

column 1 is loaded without any product breakthrough. During this process step, the operating time of both columns should be the same; therefore the process conditions of both columns have to match to each other. Step 2 links both columns, and now column 1 is loaded up to maximum binding capacity, while column 2 captures the product breakthrough. At the end of step 2, the feed is interrupted, and by a third step the first column is washed in order to capture in the second column the residual product solved within the mobile phase. These three process steps form a process switch, which is followed by a corresponding second switch as shown in Figure 5.34, after which the process cycle starts again.

Sequential Multicolumn Chromatography (SMCC) Figure 5.35 illustrates the sequential multicolumn chromatography (SMCC) with four columns (Holzer, Osuna-Sanchez, and David 2008). As already explained in Section 5.2.9.1 a countercurrent movement between the mobile and stationary phases is achieved by switching the connecting nodes in the direction of the liquid flow. Due to the periodic countercurrent switching, a process cycle is subdivided into different switches and is completed if the process scheme has reached its starting point again. The number of process switches is equivalent to the number of columns. During each switching period, different process steps (feed, wash, elution, etc.) take place.

Figure 5.35 illustrates the switching periods of a four-column SMCC process as it is commercialized under the designation BioSC® by Novasep. After a quasi-steady state has been reached, the process is operated in the following steps:

Switch 1:
- *Step 1*: Column 1 is eluted, regenerated, and finally equilibrated, while columns 2–4 are loaded without a breakthrough of the product.
- *Step 2*: Column 2 is washed until all product molecules within the liquid phase of column 2 are transferred into the subsequent columns.
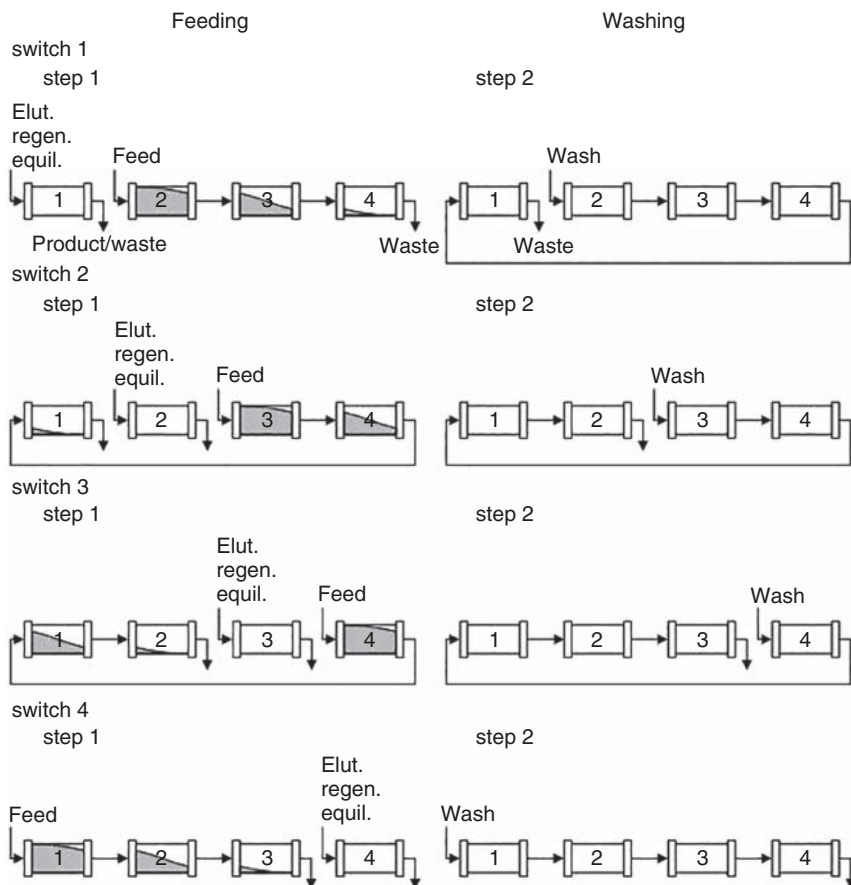
Figure 5.35 Sequential multicolumn chromatography (SMCC). (a) Step 1. (b) Step 2. Source: Reproduced with permission of Holzer, Osuna-Sanchez, and David (2008).

Switch 2:
- *Step 1*: As shown in Figure 5.35, the process scheme is changed again. Now column 2 is eluted, regenerated, and equilibrated, while columns 3, 4, and 1 are loaded.
- *Step 2*: Now column 3 is washed until all product molecules within the liquid phase of column 3 are transferred into the subsequent columns.

Switches 3 and 4:
- *Steps 1 and 2*: The process scheme is changed corresponding to steps of switches 1 and 2.
- The process cycle starts again if the switching period 4 is finished.

It is characteristic for SMCC processes that the loading of feed is not continuous during all process steps. For example, in Figure 5.35 the feed stream enters the process during step 1, while it is stopped during step 2.

Depending on feed composition, flow rates, thermodynamics, and conditions for wash, elution, regeneration, and equilibration, SMCC processes may vary in
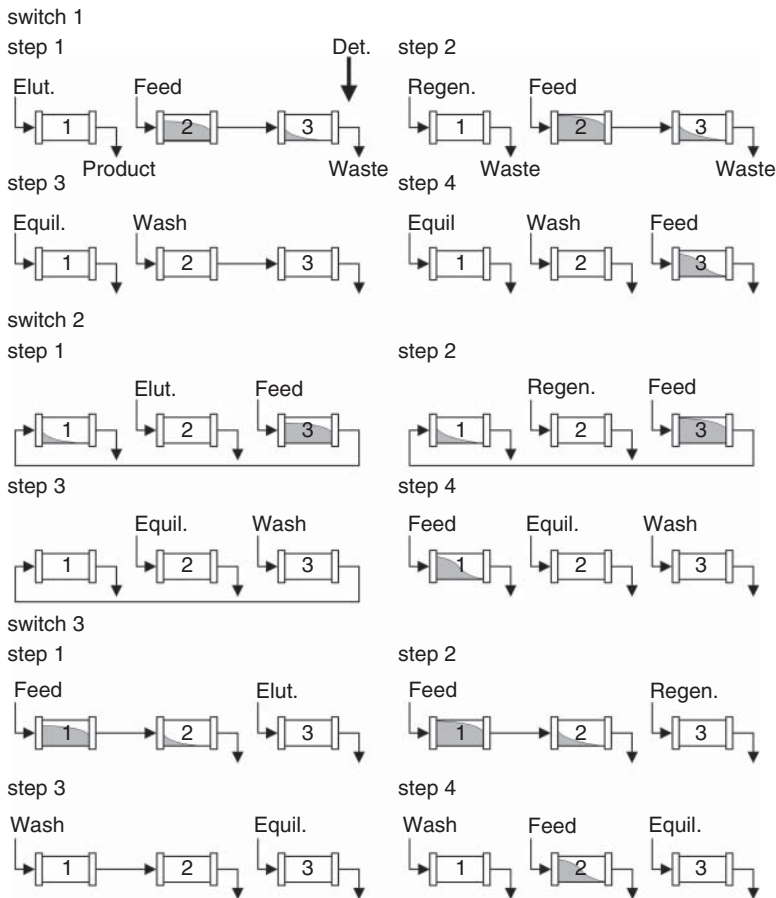
Figure 5.36 SMCC process with three columns. Source: Reproduced with permission of Ng et al. (2014).

the number of columns and details of the process steps. For instance, Ng et al. (2014) describe a three-column SMCC process as illustrated in Figure 5.36. This process consists of three switches per cycle and is subdivided into four steps per switching period.

The different steps within the first switch are as follows:

- *Step 1*: Column 1 is eluted while the feed stream enters columns 2 and 3.
- *Step 2*: Elution is finished and column 1 is regenerated, while columns 2 and 3 are still fed continuously without product breakthrough.
- *Step 3*: Column 1 is equilibrated while the feed stream is stopped, and columns 2 and 3 are washed until all product molecules within the mobile phase of column 2 is transferred into the subsequent column.
- *Step 4*: Column 1 is equilibrated, and column 2 is washed continuously, while the feed stream now enters column 3 until maximum binding capacity without breakthrough is reached.

The other switches are operated analogously. Note that in this process scheme the continuous feed stream is interrupted during step 3.

5.2.9.2 Multicolumn Countercurrent Solvent Gradient Purification (MCSGP)

The multicolumn countercurrent solvent gradient purification (MCSGP) process (Ströhlein et al. 2006b) aims at the purification of biomolecules from earlier- and later-eluting impurities. It takes advantage of the reduction of the overall retention time by nonisocratic elution strength and the efficiency of countercurrent flow separation (Aumann, Ströhlein, and Morbidelli 2007a,b).

In contrast to PCC processes, MCSGP elutes three defined fractions. These are – depending on the feed composition – three product factions or one product and an earlier- and later-eluting waste fraction. Mixed fractions are internally recycled. Compared with SMB processes, the MCSGP concept offers extended flexibility of process design. In particular, a linear gradient allows separating of close eluting components, whereas an SMB process enables step gradients only (Section 5.2.6). The feed loading is discontinuous during certain process steps. Driven by process economics, the number of columns associated with the number of valves and tubing, the process scheme with initially six columns has been simplified later to a three-column or even a twin-column MCSGP (Steinebach, Müller-Späth, and Morbidelli 2016).

Figure 5.37b shows the principle of a six-column MCSGP process (Müller-Spath et al. 2010). Like in SMB processes, the countercurrent flow of the stationary and liquid phases is achieved theoretically by switching the column periodically upstream, that is, in the opposite direction of the liquid flow. Practically all ports are shifted downstream. Solvent pumps in front of each column adjust the solvent gradient. The solvent strength is the highest at the
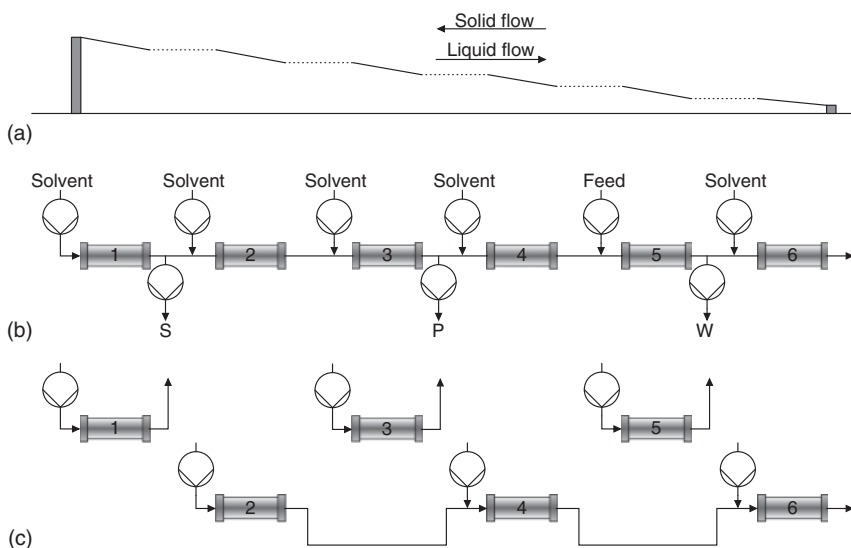
Figure 5.37 Continuous multicolumn countercurrent solvent gradient purification (MCSGP) process. Source: Reproduced with permission of Aumann, Ströhlein, and Morbidelli (2007a).

inlet of column 1 and decreases until the outlet of column 6. For the example shown in Figure 5.37a, the solvent concentration at the adjoining inlets and outlets of the columns is equal. However, this is not mandatory; depending on thermodynamics, stepwise or other forms of the overall gradient may be chosen. While the operation of the concept is relatively complex, in principle it places a gradient in an optimized fashion such that the strongly adsorbing component S is transported and eluting on the left, while the product P is retained in the middle and the weakly adsorbed component W elutes on the right.

Aumann, Ströhlein, and Morbidelli (2007a) describe the process operation as follows: "Only weak impurities W and product P are present in column 6, where they strongly adsorb. In column 5, the feed that also contains strongly adsorbing impurities S is added to the unit. P and S strongly adsorb in column 5, so that they never leave column 5 with the liquid flow. However, the conditions in column 5 are designed, so that W leaves the system after several switches through the outlet of column 5. In column 4, all W has to leave the column before it switches to the position 3. The mobile phase conditions are designed so that P and S adsorb, but W desorbs. After W has left completely, column 4 is switched to position 3 and pure product can be collected. No W is present in column 3 and S adsorbs strongly. Before S starts to contaminate the product outlet flow $Q_{3,out}$, column 3 is switched to position 2 from where the side fraction containing P is washed for recycling into column 4. When column 2 does not contain product anymore, it is switched to position 1 to clean out S and to perform some cleaning in place if required."

Figure 5.37c shows the real scheme of the MCSGP process. Columns 1, 3, and 5 operate in batch mode, while columns 2, 4, and 6 are interconnected. It is not necessary to operate all columns at the same time; therefore the operation time of the batch columns as well as the interconnected columns can be chosen individually, which offers additional parameters for process optimization. Aumann and Morbidelli (2008) also point out that in order to reduce investment cost, the number of columns can be halved. In this case, columns 1, 3, and 5 are operated in batch mode. Afterward, the column switching takes place so that the former columns 1, 3, and 5 are now the interconnected columns 2, 4, and 6.

Steinebach et al. (2017) and Angarita et al. (2015) describe a twin-column MCSGP configuration. The principles of this process are to withdraw the product as central fraction and to recycle within the process mixtures of product and weak and strong adsorbing waste components for further fractionation (Figure 5.38).

The cut strategy for column 1 with increasing gradient elution is shown on the right of Figure 5.38:

1. At the beginning column 1 is loaded with components W, P, and S. By increasing gradient elution (dashed line), a mixture of product P and the weak adsorbing component W (cut 1) passes column 1, is diluted by a second stream of lower elution strength, and is recycled for further separation to column 2.
2. During the second time step, the columns are disconnected. Because of the increasing gradient, pure P (cut 2) is eluted from column 1, while new solution is fed to column 2.
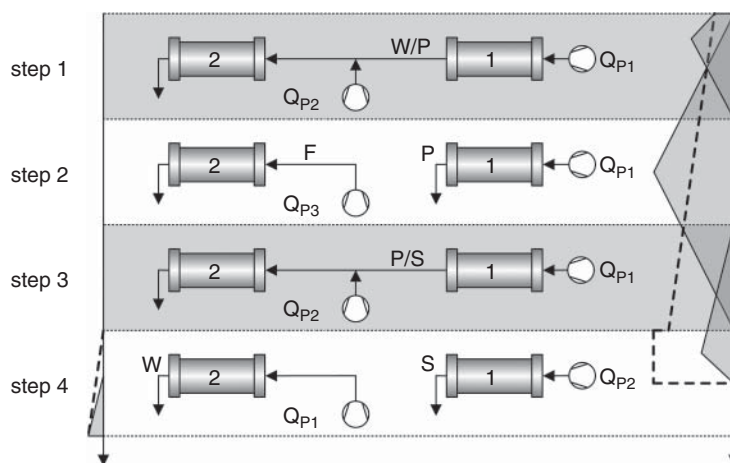
Figure 5.38 Process steps during a switching period of the twin-column MCSGP process. Source: Reproduced with permission of Pfister et al. (2017).

3. Both columns are connected to each other again, and by further increasing the gradient, the rest of product P and accompanying strong binding component S are leaving column 1 (cut 3) and are diluted before entering column 2 where S and P are captured.
4. During the fourth step S is separated from column 1 (cut 4) by a step gradient, while in column 2 W is eluted by a low gradient.

After the fourth step columns 1 and 2 are switching their position, and steps 1–4 are repeated in corresponding manner to accomplish one process cycle. Three different pumps are installed in this process: P1 is forming the elution gradient, P2 is changing the elution strength, and P3 is loading the feed.

Two columns are the minimum number for the separation of three components by such schemes. Krättli, Müller-Späth, and Morbidelli (2013) describe how to realize an MCSGP process if more than one product has to be separated with a minimum number of columns. Because of pressure drop considerations, they conclude that more than five fractions are unlikely in practice.

5.2.10 Countercurrent Chromatographic Reactors

5.2.10.1 SMB Reactor

The simulated moving bed reactor (SMBR) based on the SMB process is a practical alternative for implementing countercurrent continuous reactors. Countercurrent movement of the phases is simulated by sequentially switching the inlet and outlet ports located between the columns in direction of the liquid flow (Figure 5.39) or by moving the columns in the opposite direction. Owing to the periodic switching, the process reaches a cyclic steady state. Depending on the stoichiometry of the reaction and the adsorptivity of the components, at most two pure products can be withdrawn. The concept is usually proposed in the context of increasing conversion for equilibrium-limited reactions.
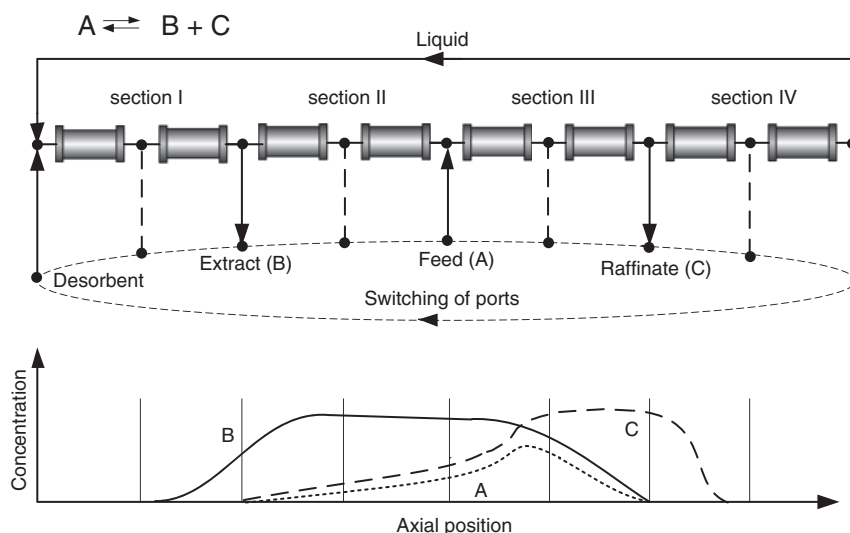
Figure 5.39 Chromatographic simulated moving bed reactor.

The design of SMBR processes has to take into account the requirements of different types of reactions. Therefore, different types of flowsheets and operating modes can be chosen. As with a semicontinuous operation, a process without Section IV (regeneration of the solvent), a five-section process, or a four-section process without recycle of the eluent may be advantageous.

SMB reactors have been examined for various reaction stoichiometries, with the main focus on reactions of the type $A + B \rightleftarrows C + D$. Examples are esterifications of acetic acid with methanol (Lode et al. 2003; Ströhlein, Mazzotti, and Morbidelli 2005), ethanol (Mazzotti et al. 1996a; Mazzotti, Storti, and Morbidelli 1996b), and β-phenethyl alcohol (Kawase et al. 1996) as well as the production of bisphenol A (Kawase et al. 1999). The same reaction type can also be found for various hydrocarbons, such as the transfer reaction of sucrose with lactose to lactosucrose (Kawase et al. 2001) and the hydrolysis of lactose (Shieh and Barker 1996). Barker et al. (1992), Kurup et al. (2004), and Ströhlein, Mazzotti, and Morbidelli (2005) focused on reactions of the type $A \rightleftarrows B + C$, such as enzyme-catalyzed sucrose inversion and the production of dextran.

Reactions of the type $A \rightleftarrows B$ have been investigated, for example, the isomerization of glucose to fructose, by Fricke (2005) as well as Toumi and Engell (2004). However, for isomerizations conventional SMB reactors are suitable only if the purity requirements are moderate. In other cases, a spatial distribution of the reaction and separation is necessary as discussed below.

Based on the triangle theory for TMB reactors, Lode et al. (2003) as well as Fricke and Schmidt-Traub (2003) and Fricke (2005) developed shortcut methods for the preliminary design of SMB reactors. They derived analytical solutions for different types of reactions by taking into account the conditions for different subdivisions of the separation region.

5.2.10.2 SMB Reactors with Distributed Functionalities

Conventional chromatographic SMB reactors as described in Section 5.2.10.1 are not well suited for reactions of the type A $\rightleftarrows$ B. Due to the reaction proceeding throughout the whole unit, it is only possible to slightly overcome the chemical equilibrium; total conversion is not possible. However, specially designed processes can overcome this limitation.

Hashimoto et al. (1983) proposed a reactive countercurrent chromatographic process for the production of higher fructose syrup. This process, denoted as the three-section Hashimoto process, is based on a partial de-integration of reaction and separation. Columns and reactors are arranged alternately in one or several sections of the SMB process (Figure 5.40a). Characteristic for this process is that the reactors remain stationary in the assigned section. For the example shown in Figure 5.40a after shifting the nodes, the reactors will be located in front of the columns numbered 6, 7, 8, and 1. Movement of the reactors is also responsible for the characteristic internal axial concentration profiles and process dynamics of the Hashimoto process. By shifting the reactors, their liquid content is moved from the inlet to the outlet of the column. At the reactor outlet, a much higher concentration level results than at the inlet of the following column. Therefore, a discontinuity in the axial concentration profile arises, which is balanced over the switching interval by adsorption and hydrodynamic effects. To obtain high product purity, a considerable number of reactors and columns are required in the "reactive" zone, in particular if the weaker adsorbing component should be produced. Michel et al. (2003) and Michel (2007) proposed electrochemical side reactors for producing arabinose. Several modifications of the concept were proposed, including four-zone processes aiming at the removal of side products or improved performance. Figure 5.40b depicts such process variant where the raffinate stream is recycled over an external reactor to the feed stream.
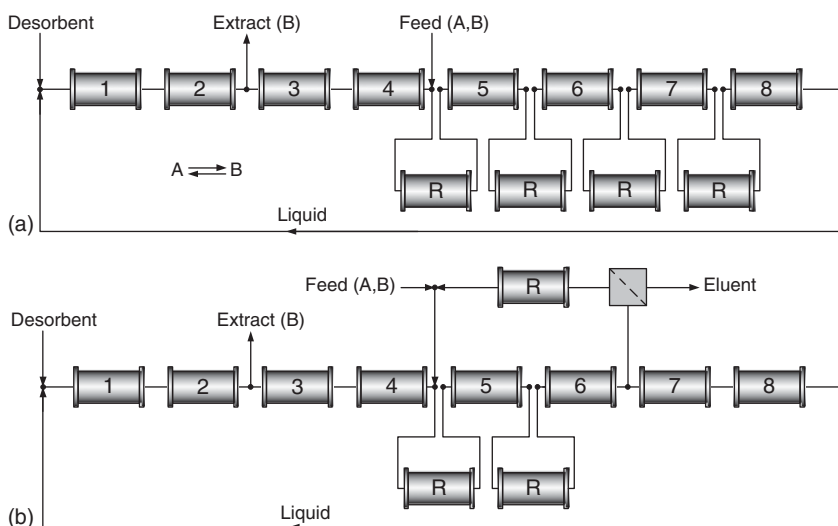
Figure 5.40 (a) Three-section Hashimoto process. (b) Four-section process variant with raffinate recycle. Reactors are labeled with "R."

The strength of the Hashimoto process stems from the fact that it separates the functionalities separation and reaction as well as its flexibility. Various types of (bio)chemical reactions can be carried out in the side reactors. The concept offers the possibility of exchanging adsorbent and catalyst (e.g. immobilized enzymes) separately after different operating times. It also allows for different operating conditions (e.g. temperatures) for reaction as well as separation. An interesting application of this kind is the thermal racemization of enantiomers (Borren 2007) if the stronger adsorbed enantiomer should be produced. Several authors investigated the isomerization of glucose to fructose (Hashimoto et al. 1983; Borren and Schmidt-Traub 2004; Borges da Silva et al. 2006; Zhang, Hidajat, and Ray 2007). A possible economic benefit is also expected for *p*-xylene isomerization using four-zone schemes similar to Figure 5.40b (with a product outlet instead of the recycle) as proposed by Minceva et al. (2008) and Bergeot et al. (2010).

An application for reactive systems with more than two components is also possible if special catalysts or operating conditions are required. However, an even more complex design, as well as control of the process, has to be taken into account.

The Hashimoto concept is particularly suited for separations with low to moderate purity requirements but has limited performance for very high product purities (Palacios, Kaspereit, and Kienle 2009). As regards isomers, it is not capable of producing the weaker adsorbing species at high purity and 100% yield. A possible work-around for such systems is to replace the side reactors by chromatographic reactors in the corresponding zone as suggested by Palacios, Kaspereit, and Kienle (2009, 2011a). The reaction in the column may be triggered by a step gradient of, for example, the pH value, the temperature, or a homogeneous catalyst. Goal is to accelerate the reaction in one zone, while it should be suppressed in the other zones, that is, to spatially distribute reaction and separation functionalities. Figure 5.41 explains the approach, which can be adapted to produce either the weaker or stronger adsorbing isomer. Such setup
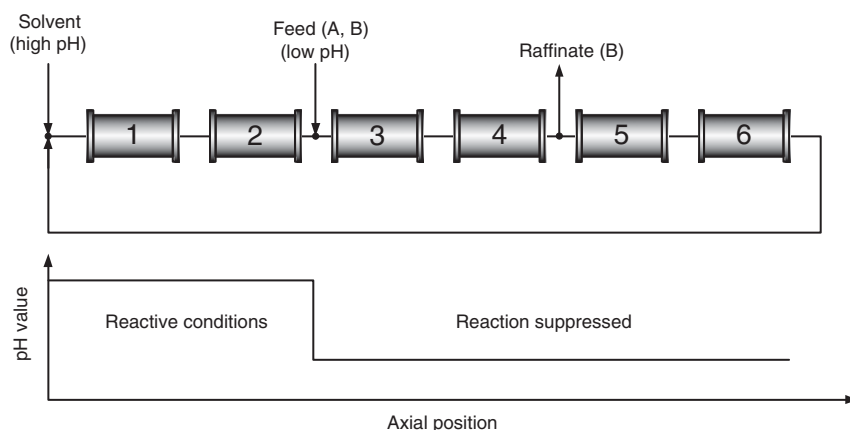
Figure 5.41 Reactive SMB process with a pH gradient for the production of the weaker adsorbing enantiomer B from a racemic mixture at 100% purity and yield.

was successfully applied to produce the weaker adsorbing enantiomer from a racemic mixture at 100% yield (Palacios, Kaspereit, and Kienle 2011a; Palacios et al. 2011b). In practical applications, the major challenge related to this concept is certainly to find a suitable variable to manipulate sufficiently the reaction rate.

5.3 Choice of Process Concepts

Every new separation is an individual task. Skilled experts are needed to find the optimal chromatographic system and to scale up the process according to proven routes for successful process development. Developing a new separation based on routines can ensure a trouble-free development but might also risk not finding the optimum process economy and thus endanger the whole project. Therefore, every separation should be developed as open-mindedly as possible.

This section provides some guidelines to assist the decision for an appropriate process concept. The main decision criteria of the approach, as shown in Figure 5.42, are "scale," "range of k'," and "number of fractions." These criteria will be briefly discussed below. Subsequently, a series of examples is used to demonstrate how processes are derived from this decision tree. Each example comprises an analytical chromatogram typical for the early stage of process development and a chromatogram for the finally realized preparative process.

5.3.1 Scale

The main criterion to be considered is the "scale" of the project, which distinguishes between large or production scale ($\mathrm{kg\,a^{-1}}$ to $\mathrm{t\,a^{-1}}$) and small or laboratory scale ($\mathrm{mg\,a^{-1}}$ to $\mathrm{g\,a^{-1}}$). This implies the question of whether the separation justifies a time-consuming method development and process design to improve process performance in terms of productivity, eluent consumption, and yield.

Influencing aspects in this context are, for instance:

- total amount of feed mixture to be separated;
- duration and frequency of the project;
- equipment available in the laboratory or at the production site;
- experience and knowledge about certain process concepts.

5.3.2 Range of k'

Chromatographic processes show their best performance when the adsorption behavior of the components to be separated is not too different. Target components of the feed mixture should elute within a certain window. Under optimized conditions, k' is in the range of 2–8. Within that window, the selectivity between the target component and the impurities should be optimized (Chapter 4).

If early- or late-eluting components are present in the feed, simple prepurification steps can remove the front- or rear-end components. These steps need not be chromatographic separations. Alternatives are extraction techniques, as the components normally differ substantially in their polarity and, thus, solubility behavior.
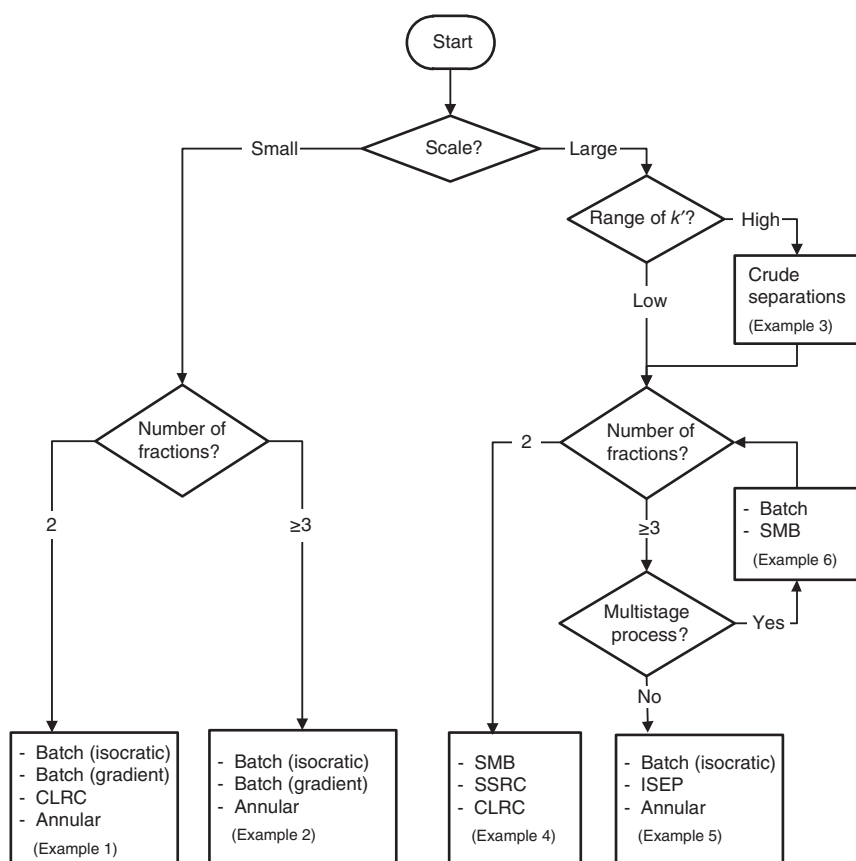
Figure 5.42 Guidelines for the choice of a process concept.

5.3.3 Number of Fractions

To find a suitable process concept, the final differentiation is given by the number of fractions to be collected. Notably, one fraction can contain either one single component (e.g. one target product) or a group of many similar components (e.g. several impurities). Some process concepts, such as conventional SMB and SSRC chromatography, can only separate a feed mixture into two fractions. In contrast, batch elution chromatography, annular chromatography, ISEP, and so on separate feed streams into three or more fractions.

Multistage processes should be considered for production-scale processes with three or more fractions. An intermediate step by SMB or batch separation reduces the separation problem, finally, to a two-fraction problem that can be performed by applying one of the abovementioned concepts.

5.3.4 Example 1: Lab Scale; Two Fractions

A racemic mixture had to be separated to produce several grams of a pure enantiomer for further investigations. By optimizing the batch conditions, a good

Table 5.1 Example 1.

	Analytical scale	Production scale
Sample	Chiral sulfoxide	
Adsorbent	Chiralcel® OD, 20 μm	
Mobile phase	Heptane–isopropanol (85 : 15) isocratic	
Column	250 × 4.6 mm, stainless steel	200 × 50 mm, stainless steel
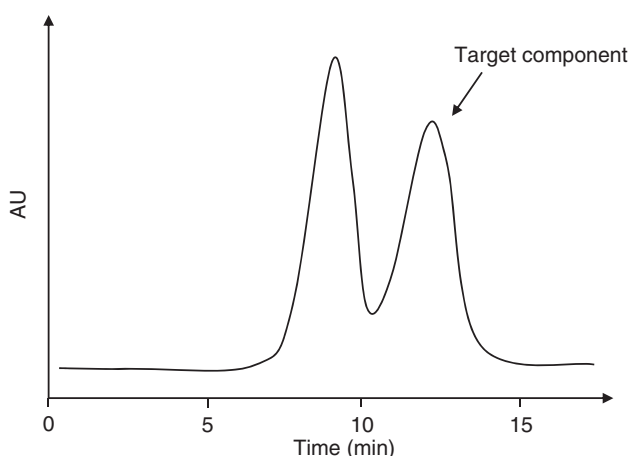
Figure 5.43 Example 1: Analytical conditions.

selectivity but no baseline separation was obtained. Details are given in Table 5.1 and Figure 5.43.

Because only a small amount of the target component was available, the yield of the chromatographic separation should be as high as possible. Therefore, CLRC (Section 5.1.3) with peak shaving was chosen to avoid fractions with insufficient purity, which otherwise had to be reworked. Figure 5.44 depicts the resulting chromatogram of the preparative process with four cycles. Both enantiomers were collected directly during the first cycle. In cycle 2, the main part of the second eluting component could be withdrawn in sufficient purity so that in cycle three nearly no second enantiomer was left.

5.3.5 Example 2: Lab Scale; Three or More Fractions

Only a few milligram of a drug metabolite had to be separated from a patient's urine for structure elucidation purposes. Table 5.2 summarizes the conditions of orienting experiments.

In the resulting chromatogram, the target component is surrounded by other components (Figure 5.45). In addition, all components elute within a wide range of k'. However, since the total amount to be separated was very small, no additional preseparation steps were implemented. For the same reason no
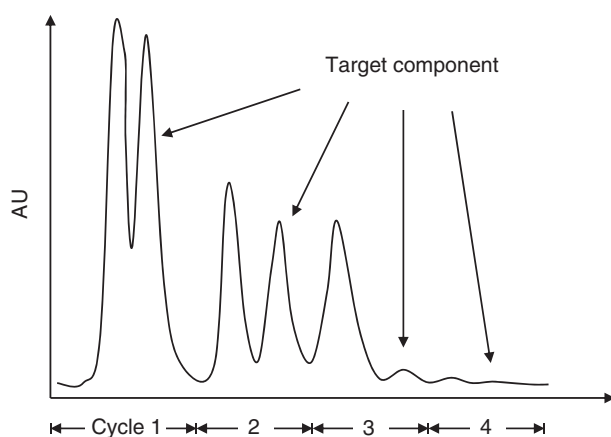
Figure 5.44 Example 1: Preparative conditions.

Table 5.2 Example 2.

	Analytical scale	**Production scale**
Sample	Drug metabolites from urine	
Adsorbent	LiChrospher® 100 RP-18, 5 μm	Superspher® 100 RP-18, 4 μm
Mobile phase	Acetonitrile–water; gradient	Acetonitrile–water; gradient
Column	250 × 4 mm, stainless steel	200 × 50 mm, stainless steel
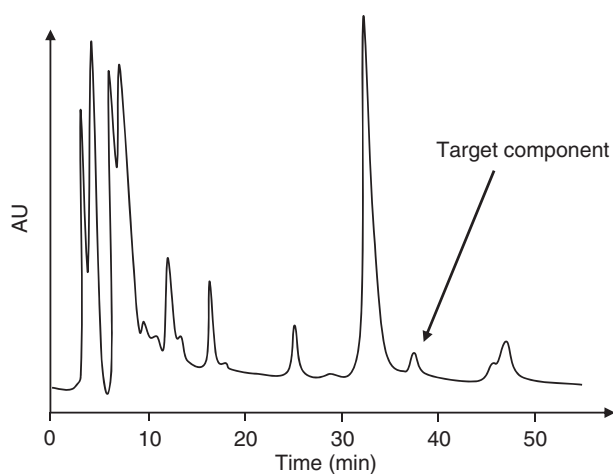
Figure 5.45 Example 2: Analytical conditions.
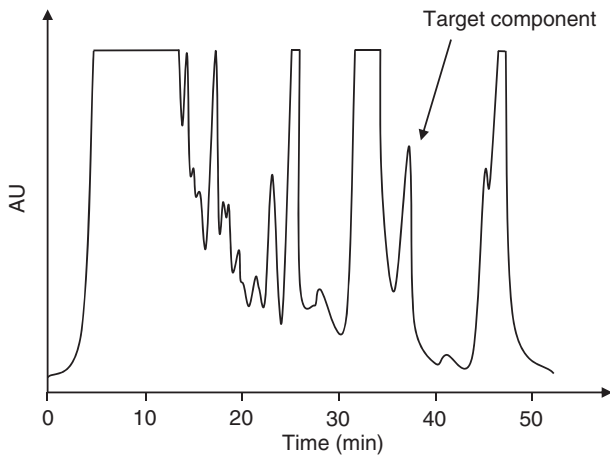
Figure 5.46 Example 2: Preparative conditions.

further effort was made to improve the chromatographic system. The elution conditions were linearly transferred to a larger column (Table 5.2), and the loading factor increased until the target component eluted immediately behind the earlier-eluting impurity (Figure 5.46). In this case, a smaller adsorbent particle diameter was chosen for the preparative column to achieve the necessary plate number in the column.

As only milligrams or grams of product were to be purified in the above examples, relatively little effort was made to optimize the chromatographic system, and quite simple concepts were applied. This is completely different to processes with production rates of $100 \, \text{kg a}^{-1}$ or higher.

5.3.6 Example 3: Production Scale; Wide Range of k′

Several flavonoids had to be separated from a plant extract with the desired production rate in the range of several tons per year. At the very beginning of the project, the complete feedstock had been analyzed under the conditions listed in Table 5.3.

The resulting chromatogram (Figure 5.47) reveals a rather wide range of retention times for the multiple components in the mixture, even though a gradient had been applied. This indicates that the components have very different physical

Table 5.3 Example 3.

	Analytical scale	Production scale
Sample	Flavonoids from plant extract	
Adsorbent	LiChrospher® 100 RP-18, 5 µm	LiChroprep® 100 RP-18, 40–63 µm
Mobile phase	Acetonitrile–water; gradient	Water–ethanol (90 : 10), isocratic
Column	250 × 4 mm, stainless steel	125 × 25 mm, stainless steel
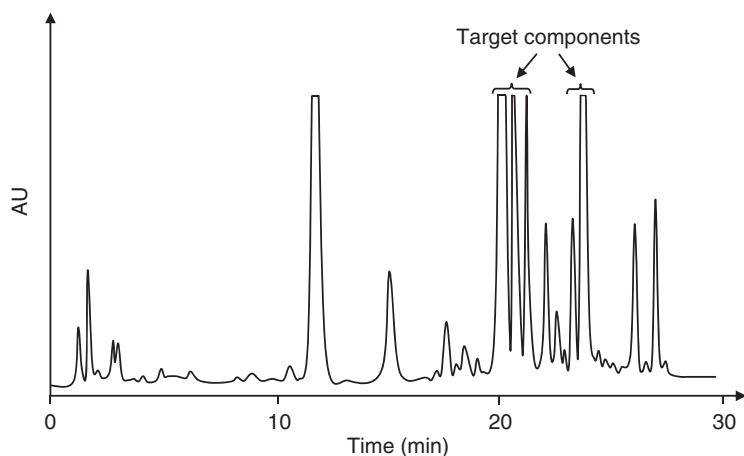
Figure 5.47 Example 3: Analytical conditions.
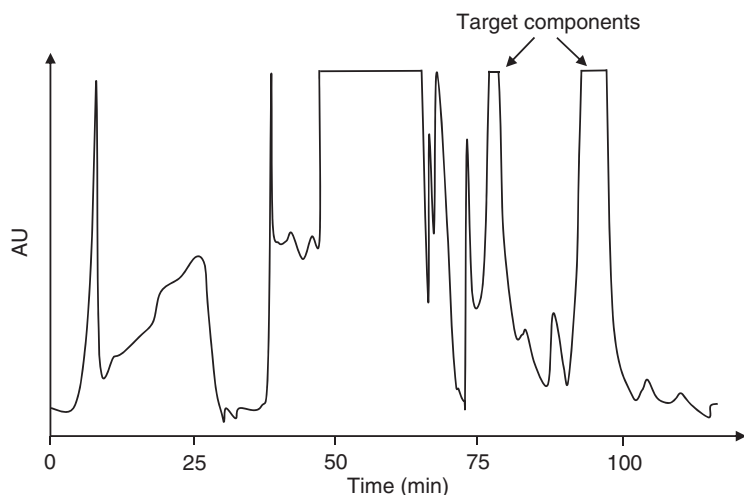
Figure 5.48 Example 3: Preparative conditions.

properties and a crude separation at the beginning should be sufficient to remove the main impurities.

A simple adsorption step under isocratic conditions was chosen for crude separation with a water–alcohol solvent on a coarse RP-18 silica (40–63 μm). Figure 5.48 shows the corresponding chromatogram. Using this prepurification step, the components of interest were obtained at high concentrations. In subsequent polishing steps, single flavonoids could be purified further.

5.3.7 Example 4: Production Scale; Two Main Fractions

A pharmaceutical component had to be isolated from a multicomponent mixture at a production rate of more than $100\,kg\,a^{-1}$. After adjusting conditions for

Table 5.4 Example 4.

	Analytical scale	Production scale
Sample	Pharmaceutical component	
Adsorbent	LiChrospher® Si 60, 15 µm	
Mobile phase	*n*-Heptane/ethylacetate, isocratic	
Column	250 × 4 mm, stainless steel	250 × 25 mm, stainless steel
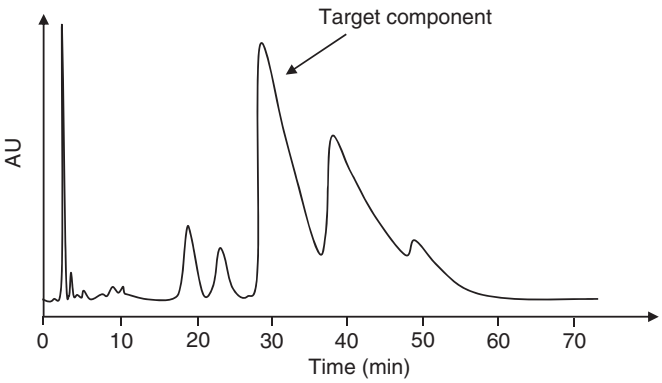
Figure 5.49 Example 4: Analytical conditions.

the preparative separations (Table 5.4), a chromatogram was obtained on a small column (Figure 5.49).

This analytical chromatogram indicates that some early-eluting impurities were present in the feed mixture as well as two main impurities that elute after the target component. No baseline separation could be obtained between the component of interest and the late-eluting impurities. CLRC was applied to avoid intermediate fractions with insufficient purities, which would have to be stored and reworked. As shown in Figure 5.50, therefore early-eluting impurities were sent to waste during the first cycle, which reduced the separation problem to a two-component separation. By only one additional cycle, the target component was obtained in good purity and yield.

5.3.8 Example 5: Production Scale; Three Fractions

For the production scale separation of a prostaglandine derivative (about $100 \, \text{kg} \, \text{a}^{-1}$), the chromatographic system in terms of stationary and mobile phases had been optimized in advance according to the considerations described in Chapter 4 (Table 5.5).

Figure 5.51 indicates that, besides the target product, early- and late-eluting impurities are also present. Following the considerations made in the beginning of this section, the decision had to be made as to whether the separation should be performed by a process concept that allows a multifraction withdrawal or
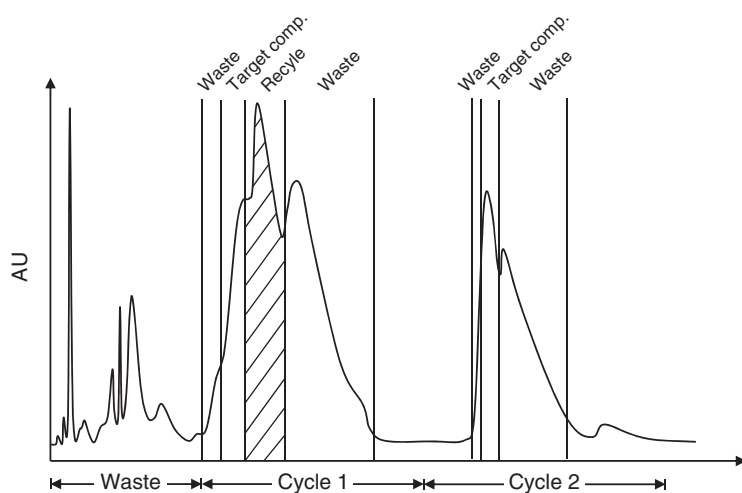
Figure 5.50 Example 4: Preparative conditions.

Table 5.5 Example 5.

	Analytical scale	**Production scale**
Sample	Prostaglandine	
Adsorbent	LiChrosorb® Si 60, 10 μm	LiChroprep® Si 60, 25–40 μm
Mobile phase	*n*-Heptane–isopropanol–methanol–THF (96/2.4/1/0.6)	
Column	250 × 4 mm, stainless steel	600 × 200 mm, stainless steel
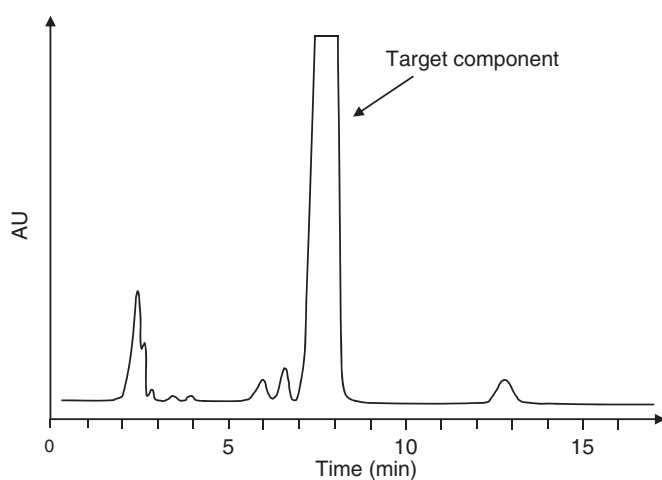
Figure 5.51 Example 5: Analytical conditions.
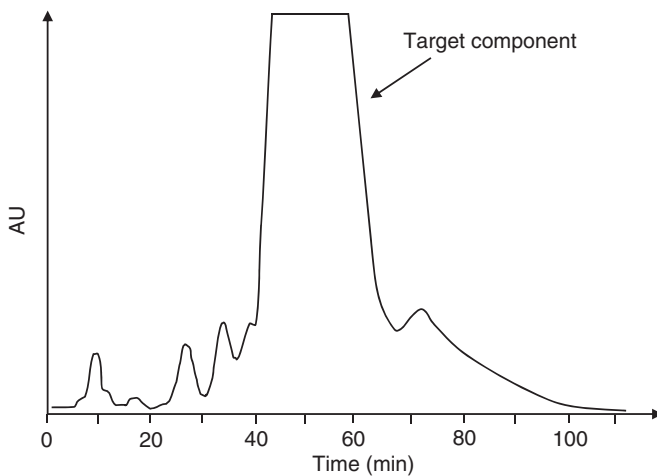
Figure 5.52 Example 5: Preparative conditions.

by a multistage process. In the present case, isocratic batch chromatography on an existing process-scale HPLC system had been used. During scale-up, the chromatographic system was kept constant with regard to stationary and mobile phase. Only the particle diameter of the silica sorbent was increased. As the stationary phases were manufactured by the same production process, the different particle sizes did not change the adsorbent's properties in terms of selectivity. Figure 5.52 shows the chromatogram under preparative conditions.

For problems as described in this example, alternatives to the chosen batch process are also preparative annular or ISEP chromatographic processes.

5.3.9 Example 6: Production Scale; Multistage Process

A $100 \, \text{kg} \, \text{a}^{-1}$ cyclic peptide had to be separated from a fermentation broth. Analytical experiments (Table 5.6) afforded an initial chromatogram (Figure 5.53).

Again, the target component was surrounded by both early- and late-eluting impurities. However, in contrast to the previous example, here a multistage process was applied consisting of a batch separation followed by two SMB separations. The first batch unit divided the complete feed into two fractions.

Table 5.6 Example 6.

	Analytical scale (step 1)	**Analytical scale (step 2)**
Sample	Cyclic peptide from fermentation broth	
Adsorbent	LiChrospher® 100 RP-18e, 5 μm	LiChrospher® 100 RP-18, 12 μm
Mobile phase	Acetonitrile–water; gradient	Acetonitrile–water, isocratic
Column	$250 \times 4 \, \text{mm}$, stainless steel	$250 \times 4 \, \text{mm}$, stainless steel
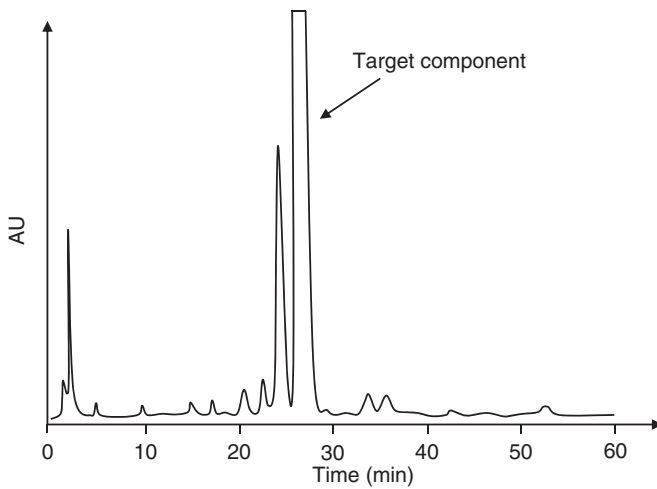
Figure 5.53 Example 6: Analysis of the complete feed stock.
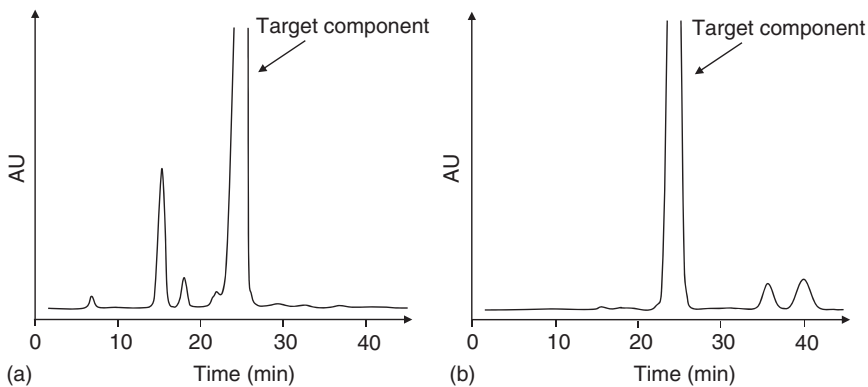
Figure 5.54 Example 6: Analysis of the two fractions obtained by the initial batch separation.

The first fraction contained early-eluting impurities and approximately half of the target component, while the rest of the main product and late-eluting impurities were collected in the second fraction. Figure 5.54 shows an analysis of these two fractions.

Both fractions obtained from the first separation can be processed in subsequent SMB units where, again, the respective portion is split into two fractions. In this case fraction (a) is fed to a SMB unit and the target product is collected as extract. An SMB separation of fraction (b) leads to a raffinate stream containing the main product and the extract line where all impurities are collected.

Even though three chromatographic steps are now involved instead of just one batch separation, the overall process economy is increased because a higher yield is achieved and no intermediate fractions with lower purities have to be collected and reworked (Voigt, Hempel, and Kinkel 1997).

References

Abel, S., Mazzotti, M., and Morbidelli, M. (2002). Solvent gradient operation of simulated moving beds I: Linear isotherms. *J. Chromatogr. A* 944: 23–39.

Abel, S., Mazzotti, M., and Morbidelli, M. (2004). Solvent gradient operation of simulated moving beds II: Langmuir isotherms. *J. Chromatogr. A* 1026: 47–55.

Angarita, M., Müller-Späth, T., Baur, B. et al. (2015). Twin-column CaptureSMB: a novel cyclic process for protein A affinity chromatography. *J. Chromatogr. A* 1389: 85–95.

Antos, D. and Seidel-Morgenstern, A. (2001). Application of gradients in simulated moving bed processes. *Chem. Eng. Sci.* 56: 6667–6682.

Aumann, L. and Morbidelli, M. (2008). A semicontinuous 3-column countercurrent solvent gradient purification (MCSGP) process. *Biotechnol. Bioeng.* 99: 728–733.

Aumann, L., Ströhlein, G., and Morbidelli, M. (2007a). Parametric study of a 6-column countercurrent solvent gradient purification (MCSGP) unit. *Biotechnol. Bioeng.* 98: 1029–1042.

Aumann, L., Ströhlein, G., and Morbidelli, M. (2007b). A continuous multicolumn countercurrent solvent gradient purification (MCSGP) process. *Biotechnol. Bioeng.* 98: 1043–1055.

Bae, Y.-S. and Lee, C.-H. (2006). Partial-discard strategy for obtaining high purity products using simulated moving bed chromatography. *J. Chromatogr. A* 1122: 161–173.

Bailly, M. and Tondeur, D. (1982). Recycle optimization in non-linear productive chromatography – I Mixing recycle with fresh feed. *Chem. Eng. Sci.* 37: 1199–1212.

Barker, P.E., Ganetsos, G., Ajongwen, J., and Akintoye, A. (1992). Bioreaction-separation on continuous chromatographic systems. *Chem. Eng. J.* 50: B23–B28.

Bassett, D.W. and Habgood, H.W. (1960). A gas chromatographic study of the catalytic isomerisation of cyclopropane. *J. Phys. Chem.* 64: 769–773.

Beltscheva, D., Hugo, P., and Seidel-Morgenstern, A. (2003). Linear two-step gradient counter-current chromatography: analysis based on a recursive solution of an equilibrium stage model. *J. Chromatogr. A* 989: 31–45.

Bergeot, G., Le-Cocq, D.L., Wolff, L. et al. (2010). Intensification of paraxylene production using a simulated moving bed reactor. *Oil Gas Sci. Technol.* 65: 721–733.

Borges da Silva, E., de Souza, A., de Souza, S., and Rodrigues, A. (2006). Analysis of high-fructose syrup production using reactive SMB technology. *Chem. Eng. J.* 118: 167–181.

Borren, T. (2007). Untersuchungen zu chromatographischen Reaktoren mit verteilten Funktionalitäten. Fortschritt-Berichte VDI: Reihe 3 Nr. 876. Düsseldorf: VDI Verlag GmbH.

Borren, T. and Schmidt-Traub, H. (2004). Vergleich chromatographischer Reaktorkonzepte. *Chem. Ing. Tech.* 76 (6): 805–814.

Broughton, D.B. and Gerhold, C.G. (1961). Continuous sorption process employing fixed bed of sorbent and moving inlets and outlets. US Patent 2, 985, 589.

Brozio, J. and Bart, H.-J. (2004). A rigorous model for annular chromatotography. *Chem. Eng. Technol.* 27: 962–970.

Brunner, G. and Johannsen, M. (2006). New aspects on adsorption from supercritical fluid phases. *J. Supercrit. Fluids* 38: 181–200.

Carta, G. and Jungbauer, A. (2010). *Protein Chromatography: Process Development and Scale-Up*. Weinheim: Wiley-VCH Verlag.

Chin, C.Y. and Wang, N.-H.L. (2004). Simulated moving bed equipment designs. *Sep. Purif. Rev.* 33: 77–155.

Ching, C.B. and Ruthven, D.M. (1986). Experimental study of a simulated counter-current adsorption system – IV. Non-isothermal operation. *Chem. Eng. Sci.* 41: 3063–3071.

Ching, C.B., Ho, C., and Ruthven, D.M. (1986). An improved adsorption process for the production of high-fructose syrup. *AIChE J.* 32: 1876–1880.

Clavier, J.-Y., Nicoud, R.M., and Perrut, M. (1996). A new efficient fractionation process: the simulated moving bed with supercritical eluent. ProcessTechnology Proceedings 12: 429–434.

Coca, J., Bravo, M., Abascal, E., and Adrio, G. (1989). Dicyclopentadiene dissociation in a chromatographic reactor – effect of the liquid phase polarity on the reaction rate. *Chromatographia* 28: 300–302.

Coca, J., Adrio, G., Jeng, C.Y., and Langer, S.H. (1993). Gas and liquid chromatographic reactors. In: *Preparative and Production Scale Chromatography* (eds. G. Ganetsos and P.E. Barker), 449–475. New York: Marcel Dekker Inc.

Colin, H., Hilaireau, P., and Martin, M. (1991). Flip-flop elution concept in preparative liquid chromatography. *J. Chromatogr. A* 557: 137–153.

Cristancho, C.A.M., Peper, S., and Johannsen, M. (2012). Supercritical fluid simulated moving bed chromatography for the separation of ethyl linoleate and ethyl oleate. *J. Supercrit. Fluids* 66: 129–136.

Dai, Y., Li, G., and Rajendran, A. (2015). Peak distortion arising from large-volume injection in supercritical fluid chromatography. *J. Chromatogr. A* 1392: 91–99.

Denet, F., Hauck, W., Nicoud, R.M. et al. (2001). Enantioseparation through supercritical fluid simulated moving bed (SF-SMB) chromatography. *Ind. Eng. Chem. Res.* 40: 4603–4609.

Depta, A., Giese, T., Johannsen, M., and Brunner, G. (1999). Separation of stereoisomers in a simulated moving bed-supercritical fluid chromatography plant. *J. Chromatogr. A* 865: 175–186.

Duvdevani, I., Biesenberger, J.A., and Tan, M. (1971). Recycle gel permeation chromatography. III. Design modifications and some results with polycarbonate. *J. Polym. Sci., Part B: Polym. Lett.* 9: 429–434.

Eagle, S. and Rudy, C.E. Jr., (1950). Separation and desulfurization of cracked naphtha. Application of cyclic adsorption process. *Ind. Eng. Chem.* 42: 1294–1299.

Falk, T. and Seidel-Morgenstern, A. (2002). Analysis of a discontinuously operated chromatographic reactor. *Chem. Eng. Sci.* 57: 1599–1606.

Faria, R.P.V. and Rodrigues, A.E. (2015). Instrumental aspects of simulated moving bed chromatography. *J. Chromatogr. A* 1421: 82–102.

Fricke, J. (2005). Entwicklung einer Auslegungsmethode für chromatographische SMB-Reaktoren. Fortschritt-Berichte VDI: Reihe 3 Nr. 844. Düsseldorf: VDI Verlag GmbH.

Fricke, J. and Schmidt-Traub, H. (2003). A new method supporting the design of simulated moving bed chromatographic reactors. *Chem. Eng. Process.* 42: 237–248.

Gedicke, K., Antos, D., and Seidel-Morgenstern, A. (2007). Effect on separation of injecting samples in a solvent different from the mobile phase. *J. Chromatogr. A* 1162: 62–73.

Giovanni, O.D., Mazzotti, M., Morbidelli, M. et al. (2001). Supercritical fluid simulated moving bed chromatography. II Langmuir isotherm. *J. Chromatogr. A* 919: 1–12.

Girard, V., Hilbold, N.-J., Ng, C. et al. (2015). Large-scale monoclonal antibodies purification by continuous chromatography, from process design to scale-up. *J. Biotechnol.* 213: 65–73.

Gjoka, X., Rogler, K., Martino, R.A. et al. (2015). A straightforward methodology for designing continuous monoclonal antibody capture multi-column chromatography processes. *J. Chromatogr. A* 1416: 38–46.

Grill, C.M. and Miller, L. (1998). Separation of a racemic pharmaceutical intermediate using closed-loop steady state recycling. *J. Chromatogr. A* 827: 359–371.

Grill, C.M., Miller, L., and Yan, T.Q. (2004). Resolution of a racemic pharmaceutical intermediate – a comparison of preparative HPLC, steady state recycling, and simulated moving bed. *J. Chromatogr. A* 1026: 101–108.

Gritti, F., Leal, M., McDonald, T., and Gilar, M. (2017). Ideal versus real automated twin column recycling chromatography process. *J. Chromatogr. A.* 1508: 81–94.

Grüner, S. and Kienle, A. (2004). Equilibrium theory and nonlinear waves for reactive distillation columns and chromatographic reactors. *Chem. Eng. Sci.* 59: 901–918.

Gueorguieva, L., Palani, S., Rinas, U. et al. (2011). Recombinant protein purification using gradient assisted simulated moving bed hydrophobic interaction chromatography. Part II: process design and experimental validation. *J. Chromatogr. A* 1218: 6402–6411.

Guiochon, G. and Tarafder, A. (2011). Fundamental challenges and opportunities for preparative supercritical fluid chromatography. *J. Chromatogr. A* 1218: 1037–1114.

Hashimoto, K., Adachi, S., Noujima, H., and Ueda, Y. (1983). A new process combining adsorption and enzyme reaction for producing higher-fructose syrup. *Biotechnol. Bioeng.* 25: 2371–2393.

Holzer, M., Osuna-Sanchez, H., and David, L. (2008). Multicolumn chromatography. *Bioprocess Int.* 6 (8): 74–82. https://www.novasep.com/media/articles-and-publications/18multicolumnchromatography-bioprocess.pdf.

Hotier, G. and Nicoud, R.M. (1995). Separation by simulated moving bed chromatography with dead volume correction by desynchronization of periods. European Patent EP 688589 A1.

Houwing, J., Billiet, H.A.H., and van der Wielen, L.A.M. (2002). Optimization of azeotropic protein separation in gradient and isocratic ion-exchange simulated moving bed chromatography. *J. Chromatogr. A* 944: 189–201.

Iyer, G., Ramaswamy, S., Asher, D. et al. (2011). Reduced surface area chromatography for flow-through purification of viruses and virus particles. *J. Chromatogr. A* 1218: 3973–3981.

Jeng, C.Y. and Langer, S.H. (1989). Hydroquinone oxidation for the detection of catalytic activity in liquid chromatographic columns. *J. Chromatogr. Sci.* 27: 549–552.

Jensen, T.B., Reijns, T.G., Billiet, H.A., and van der Wielen, L.A. (2000). Novel simulated moving-bed method for reduced solvent consumption. *J. Chromatogr. A* 873: 149–162.

Jermann, S. and Mazzotti, M. (2014). Three column intermittent simulated moving bed chromatography: 1. Process description and comparative assessment. *J. Chromatogr. A* 1361: 125–138.

Jermann, S., Alberti, A., and Mazzotti, M. (2014). Three column intermittent simulated moving bed chromatography: 2. Experimental implementation for the separation of Tröger's base. *J. Chromatogr. A* 1364: 107–116.

Jermann, S., Meijssen, M., and Mazzotti, M. (2015). Three column intermittent simulated moving bed chromatography: 3. Cascade operation for center-cut separations. *J. Chromatogr. A* 1378: 37–49.

Jin, W. and Wankat, P.C. (2007). Thermal operation of four-zone simulated moving beds. *Ind. Eng. Chem. Res.* 46: 7208–7220.

Johannsen, M. and Brunner, G. (2018). Supercritical fluid chromatographic separation on preparative scale in continuous mode. *J. Supercrit. Fluids* 134: 61–70.

Kalbé, J., Höcker, H., and Berndt, H. (1989). Design of enzyme reactors as chromatographic columns for racemic resolution of amino acid esters. *Chromatographia* 28: 193–196.

Kaspereit, M. (2009). Advanced operation concepts for simulated moving bed processes. In: *Advanced Chromatography*, vol. 47 (eds. E. Grushka and N. Grinberg), 165–192. Boca Raton, FL: CRC Press.

Kaspereit, M. and Sainio, T. (2011). Simplified design of steady-state recycling chromatography under ideal and nonideal conditions. *Chem. Eng. Sci.* 66: 5428–5438.

Katsuo, S. and Mazzotti, M. (2010a). Intermittent simulated moving bed chromatography: 1. Design criteria and cyclic steady-state. *J. Chromatogr. A* 1217: 1354–1361.

Katsuo, S. and Mazzotti, M. (2010b). Intermittent simulated moving bed chromatography: 2. Separation of Tröger's base enantiomers. *J. Chromatogr. A* 1217: 3067–3075.

Kawase, M., Suzuki, T.B., Inoue, K. et al. (1996). Increased esterification conversion by application of simulated moving-bed reactor. *Chem. Eng. Sci.* 51 (11): 2971–2976.

Kawase, M., Inoue, Y., Araki, T., and Hashimoto, K. (1999). The simulated moving-bed reactor for production of bisphenol A. *Catal. Today* 48: 199–209.

Kawase, M., Pilgrim, A., Araki, T., and Hashimoto, K. (2001). Lactosucrose production using a simulated moving bed reactor. *Chem. Eng. Sci.* 56: 453–458.

Keßler, L.C. and Seidel-Morgenstern, A. (2006). Theoretical study of multicomponent continuous countercurrent chromatography based on connected 4-zone units. *J. Chromatogr. A* 1126: 323–337.

Keßler, L.C. and Seidel-Morgenstern, A. (2008). Improving performance of simulated moving bed chromatography by fractionation and feed-back of outlet streams. *J. Chromatogr. A* 1207: 55–71.

Kim, J.K., Abunasser, N., Wankat, P.C. et al. (2005). Thermally assisted simulated moving bed systems. *Adsorption* 13: 579–584.

Kloppenburg, E. and Gilles, E.D. (1999). A new concept for operating simulated moving-bed processes. *Chem. Eng. Technol.* 22 (10): 813–817.

Krättli, M., Müller-Späth, T., and Morbidelli, M. (2013). Multifraction separation in countercurrent chromatography (MCSGP). *Biotechnol. Bioeng.* 110: 2436–2444.

Kulprathipanja, S. (2002). *Reactive Separation Processes*. New York: Taylor & Francis.

Kurup, A., Subramani, H., Hidajat, K., and Ray, A. (2004). Optimal design and operation of SMB bioreactor for sucrose inversion. *Chem. Eng. J.* 108: 19–33.

Lauer, K. (1980). Technische Herstellung von Fructose. *Starch/Stärke* 32: 11–13.

Lee, M.F.X., Chan, E.S., and Tey, B.T. (2014). Negative chromatography: progress, application and future perspectives. *Process Biochem.* 49: 1005–1011.

Lee, M.F.X., Chan, E.S., Tan, W.S. et al. (2015). Negative chromatography purification of hepatitis B virus-like particles using poly(oligo(ethylene glycol) methacrylate) grafted cationic adsorbent. *J. Chromatogr. A* 1415: 161–165.

Lesellier, E. and West, C. (2015). The many faces of packed column supercritical fluid chromatography – a critical review. *J. Chromatogr. A* 1382: 2–46.

Li, S., Kawajiri, Y., Raisch, J., and Seidel-Morgenstern, A. (2010a). Optimization of simulated moving bed chromatography with fractionation and feedback: Part I. Fractionation of one outlet. *J. Chromatogr. A* 1217: 5337–5348.

Li, S., Kawajiri, Y., Raisch, J., and Seidel-Morgenstern, A. (2010b). Optimization of simulated moving bed chromatography with fractionation and feedback: Part II. Fractionation of both outlets. *J. Chromatogr. A* 1217: 5349–5357.

Lin, C.-H., Lin, H.-W., Wu, J.-Y. et al. (2015). Extraction of lignans from the seed of *Schisandra chinensis* by supercritical fluid extraction and subsequent separation by supercritical fluid simulated moving bed. *J. Supercrit. Fluids* 98: 17–24.

Lode, F., Francesconi, G., Mazzotti, M., and Morbidelli, M. (2003). Synthesis of methylacetate in a simulated moving bed reactor: experiments and modelling. *AIChE J.* 49 (6): 1516–1524.

Ludemann-Hombourger, O., Bailly, M., and Nicoud, R.-M. (2000). The VARICOL-process: a new multicolumn continuous chromatographic process. *Sep. Sci. Technol.* 35: 1829–1862.

Mahajan, E., Anupa, G., and Wolk, B. (2012). Improving affinity chromatography resin efficiency using semi-continuous chromatography. *J. Chromatogr. A* 1227: 154–162.

Martin, A.J.P. (1949). Summarizing paper. *Discuss. Faraday Soc.* 7: 332–336.

Martin, A.J.P., Halász, I., Engelhardt, H., and Sewell, P. (1979). "Flip-flop" chromatography. *J. Chromatogr. A* 186: 15–24.

Mazzotti, M., Kruglov, A., Neri, B. et al. (1996a). A continuous chromatographic reactor: SMBR. *Chem. Eng. Sci.* 51 (10): 1827–1836.

Mazzotti, M., Storti, G., and Morbidelli, M. (1996b). Robust design of countercurrent adsorption separation processes: 3. Nonstoichiometric systems. *AIChE J.* 42: 2784–2796.

Meurer, M., Altenhöner, U., Strube, J., and Schmidt-Traub, H. (1997). Dynamic simulation of simulated moving bed chromatographic reactors. *J. Chromatogr. A* 769: 71–79.

Michel, M. (2007). Integration elektrochemischer Mikroreaktoren in chromatographische Trennverfahren. Fortschritt-Berichte VDI: Reihe 3 Nr. 869. Düsseldorf: VDI Verlag GmbH.

Michel, M., Schmidt-Traub, H., Ditz, R. et al. (2003). Development of an integrated process for electrochemical reaction and chromatographic SMB-separation. *J. Appl. Electrochem.* 33: 939–949.

Migliorini, C., Wendlinger, M., Mazzotti, M., and Morbidelli, M. (2001). Temperature gradient operation of a simulated moving bed unit. *Ind. Eng. Chem. Res.* 40: 2606–2617.

Minceva, M., Gomes, P.S., Meshko, V., and Rodrigues, A.E. (2008). Simulated moving bed reactor for isomerization and separation of *p*-xylene. *Chem. Eng. J.* 140: 305–323.

Müller-Spath, T., Krattli, M., Aumann, L. et al. (2010). Increasing the activity of monoclonal antibody therapeutics by continuous chromatography (MCSGP). *Biotechnol. Bioeng.* 107: 652–662.

Ng, C.K.S., Rousset, F., Valery, E. et al. (2014). Design of high productivity sequential multi-column chromatography for antibody capture. *Food Bioprod. Process.* 92: 233–241.

Nicoud, R.-M. (2015). *Chromatographic Processes – Modeling, Simulation, and Design*. Cambridge: Cambridge University Press.

Nimmig, S. and Kaspereit, M. (2013). Continuous production of single enantiomers at high yields by coupling single column chromatography, racemization, and nanofiltration. *Chem. Eng. Process.* 67: 89–98.

Oh, J., Sreedhar, B., Donaldson, M.E. et al. (2016). Transesterification of propylene glycol methyl ether in chromatographic reactors using anion exchange resin as a catalyst. *J. Chromatogr. A* 1466: 84–95.

Palacios, G.J., Kaspereit, M., and Kienle, A. (2009). Conceptual design of integrated chromatographic processes for the production of single (stereo-)isomers. *Chem. Eng. Technol.* 32: 1392–1402.

Palacios, G.J., Kaspereit, M., and Kienle, A. (2011a). Integrated simulated moving bed processes for the production of single enantiomers. *Chem. Eng. Technol.* 34: 688–698.

Palacios, G.J., Kramer, B., Kienle, A., and Kaspereit, M. (2011b). Experimental validation of a new integrated simulated moving bed for the production of single enantiomers. *J. Chromatogr. A* 1218: 2232–2239.

Palani, S., Gueorguieva, L., Rinas, U. et al. (2011). Recombinant protein purification using gradient assisted simulated moving bed hydrophobic interaction chromatography. Part I: selection of chromatographic system and estimation of adsorption isotherms. *J. Chromatogr. A* 1218: 6396–6401.

Peper, S., Lübbert, M., Johanssen, M., and Brunner, G. (2002). Separation of ibuprofen enantiomers by supercritical fluid simulated moving bed chromatography. *Sep. Sci. Technol.* 37: 2545–2566.

Pereira, C.S.M., Silva, V.M.T.M., and Rodrigues, A.E. (2009). Fixed bed adsorptive reactor for ethyl lactate synthesis: experiments, modelling, and simulation. *Sep. Sci. Technol.* 44: 2721–2749.

Pfister, D., David, L., Holzer, M., and Nicoud, R.-M. (2017). Designing affinity chromatographic processes for the capture of antibodies. Part I: A simplified approach. *J. Chromatogr. A* 1494: 27–39.

Rossé, G. (ed.) (2019). *Supercritical Fluid Chromatography*. Berlin, Boston, MA: de Gruyter.

Ruthven, D.M. and Ching, C.B. (1989). Counter-current and simulated counter-current adsorption separation processes. *Chem. Eng. Sci.* 44: 1011–1038.

Sainio, T. and Kaspereit, M. (2009). Analysis of steady state recycling chromatography using equilibrium theory. *Sep. Purif. Technol.* 66: 9–18.

Sainio, T., Kaspereit, M., Kienle, A., and Seidel-Morgenstern, A. (2007). Thermal effects in reactive liquid chromatography. *Chem. Eng. Sci.* 62: 5674–5681.

Saito, M. (2013). History of supercritical fluid chromatography: Instrumental development. *J. Biosci. Bioeng.* 115: 590–599.

Sardin, M., Schweich, D., and Villermaux, J. (1993). Preparative fixed-bed chromatographic reactor. In: *Preparative and Production Scale Chromatography* (eds. G. Ganetsos and P.E. Barker), 477–521. New York: Marcel Dekker Inc.

Sarmidi, M.R. and Barker, P.E. (1993a). Saccharification of modified starch to maltose in a continuous rotating annular chromatograph. *J. Chem. Technol. Biotechnol.* 57: 229–235.

Sarmidi, M.R. and Barker, P.E. (1993b). Simultaneous biochemical reaction and separation in a rotating annular chromatograph. *Chem. Eng. Sci.* 48: 2615–2623.

Scherpian, P. and Schembecker, G. (2009). Scaling-up recycling chromatography. *Chem. Eng. Sci.* 64: 4068–4080.

Schmidt, S., Wu, P., Konstantinov, K. et al. (2003). Kontinuierliche Isolierung von Pharmawirkstoffen mittels annularer Chromatographie. *Chem. Ing. Tech.* 75: 302–305.

Schramm, H., Kienle, A., Kaspereit, M., and Seidel-Morgenstern, A. (2003). Improved operation of simulated moving bed processes through cyclic modulation of feed flow and feed concentration. *Chem. Eng. Sci.* 58: 5217–5227.

Seidel-Morgenstern, A., Kessler, L.C., and Kaspereit, M. (2008). New developments in simulated moving bed chromatography. *Chem. Eng. Technol.* 31: 826–837.

Shieh, M.T. and Barker, P.E. (1996). Combined bioreaction and separation in a simulated counter-current chromatographic bioreactor-separator for the hydrolysis of lactose. *J. Chem. Technol. Biotechnol.* 66: 265–278.

Siitonen, J., Sainio, T., and Kaspereit, M. (2011). Theoretical analysis of steady state recycling chromatography with solvent removal. *Sep. Purif. Technol.* 78: 21–32.

Solms, J. (1955). Kontinuierliche Papierchromatographie. *Helv. Chim. Acta* 38: 1127–1133.

Speybrouck, D. and Lipka, E. (2016). Preparative supercritical fluid chromatography: a powerful tool for chiral separation. *J. Chromatogr. A* 1467: 33–55.

Sreedhar, B. and Seidel-Morgenstern, A. (2008). Preparative separation of multicomponent mixtures using stationary phase gradients. *J. Chromatogr. A* 1215: 133–144.

Steinebach, F., Müller-Späth, T., and Morbidelli, M. (2016). Continuous counter-current chromatography for capture and polishing steps in biopharmaceutical production. *Biotechnol. J.* 11: 1126–1141.

Steinebach, F., Ulmer, N., Decker, L., and Morbidelli, M. (2017). Experimental design of a twin-column countercurrent gradient. *J. Chromatogr. A* 1492: 19–26.

Ströhlein, G., Mazzotti, M., and Morbidelli, M. (2005). Optimal operation of simulated-moving-bed reactors for nonlinear adsorption isotherms and equilibrium reactions. *Chem. Eng. Sci.* 60: 1525–1533.

Ströhlein, G., Assuncao, Y., Dube, N. et al. (2006a). Esterification of acrylic acid with methanol by reactive chromatography: experiments and simulation. *Chem. Eng. Sci.* 61: 5296–5306.

Ströhlein, G., Aumann, L., Mazzotti, M., and Morbidelli, M. (2006b). A continuous, counter-current multicolumn chromatographic process incorporating modifier gradients for ternary separations. *J. Chromatogr. A* 1126: 338–346.

Sundmacher, K., Kienle, A., and Seidel-Morgenstern, A. (eds.) (2005). *Integrated Chemical Processes – Synthesis, Operation, Analysis, and Control*. Weinheim: Wiley-VCH.

Tanimura, M., Tamura, M., and Teshima, T. (1995). Chromatographic Separation Method. Japanese Patent JP-B-H07–046097.

Toumi, A. and Engell, S. (2004). Optimization-based control of a reactive simulated moving bed process for glucose isomerization. *Chem. Eng. Sci.* 59: 3777–3792.

Ulmer, N., Müller-Späth, T., Neunstöcklin, B. et al. (2015). Affinity capture of F(ab')$_2$ fragments: using twin-column countercurrent chromatography. *BioProcess Int.* http://www.bioprocessintl.com/downstream-processing/chromatography/affinity-capture-fab2-fragments-using-twin-column-countercurrent-chromatography/.

Unger, K.K. (ed.) (1994). *Handbuch der HPLC, Teil 2: Präparative Säulenflüssig-Chromatographie*. Darmstadt: GIT Verlag.

Voigt, U., Hempel, R., and Kinkel, J.N. (1997). Chromatographic process for obtaining very pure cyclosporin and related cyclosporins. German Patent DE 196 11 094 A1.

Vu, T., Seidel-Morgenstern, A., Grüner, S., and Kienle, A. (2005). Analysis of ester hydrolysis reaction in a chromatographic reactor using equilibrium theory and a rate model. *Ind. Eng. Chem. Res.* 44: 9565–9574.

Wankat, P.C. (2001). Simulated moving bed cascades for ternary separations. *Ind. Eng. Chem. Res.* 40: 6185–6193.

Warikoo, V., Godawat, R., Brower, K. et al. (2012). Integrated continuous production of recombinant therapeutic proteins. *Biotechnol. Bioeng.* 109: 3018–3029.

Wekenborg, K., Susanto, A., and Schmidt-Traub, H. (2004). Nicht-isokratische SMB-Trennung von Proteinen mittels Ionenaustauschchromatographie. *Chem. Ing. Tech.* 76: 815–819.

Wekenborg, K. (2009) Kontinuierliche Trennung von Proteinendurch nicht-isokratische SMB-Chromatographieprozesse, Shaker-Verlag, Aachen.

West, C., (2014) Enantioselective Separation with Supercritical Fluids – Review, Current Analytical Chemistry, 10, 99–120.

Wolfgang, J. and Prior, A. (2002). Modern advances in chromatography. *Adv. Biochem. Eng./Biotechnol.* 76: 233–255.

Wooley, R., Ma, Z., and Wang, N.H.L. (1998). A nine-zone simulating moving bed for the recovery of glucose and xylose from biomass hydrolyzate. *Ind. Eng. Chem. Res.* 37: 3699–3709.

Zafar, I. and Barker, P.E. (1988). An experimental and computational study of a biochemical polymerisation reaction in a chromatographic reactor separator. *Chem. Eng. Sci.* 43: 2369–2375.

Zang, Y. and Wankat, P.C. (2002a). SMB operation strategy – partial feed. *Ind. Eng. Chem. Res.* 41: 2504–2511.

Zang, Y. and Wankat, P.C. (2002b). Three-zone simulated moving bed with partial feed and selective withdrawal. *Ind. Eng. Chem. Res.* 41: 5283–5289.

Zhang, Z., Mazzotti, M., and Morbidelli, M. (2003). PowerFeed operation of simulated moving bed units: changing flow-rates during the switching interval. *J. Chromatogr. A* 1006: 87–99.

Zhang, Y., Hidajat, K., and Ray, A. (2007). Modified reactive SMB for production of high concentrated fructose syrup by isomerisation of glucose to fructose. *Biochem. Eng. J.* 35: 341–351.

6

Modeling of Chromatographic Processes*

Andreas Seidel-Morgenstern

Otto-von-Guericke-Universität, Lehrstuhl für Chemische Verfahrenstechnik, Universitätsplatz 2, 39106 Magdeburg, Germany
Max-Planck-Institut für Dynamik komplexer technischer Systeme, Sandtorstraße 1, 39106 Magdeburg, Germany

6.1 Introduction

Essential steps in the design of production-scale chromatographic processes are the selection of the chromatographic system and the most suitable process concept as well as the scale-up from laboratory-scale experiments to economically relevant plant sizes. The complex nonlinear system behavior makes an empirical design difficult and time consuming. Predictions based on approximations and numerical simulations can considerably reduce material and time needed for process analysis and optimization. Validated process models can be used for optimal plant design and identification of suitable operating parameters. Other clear benefits offered by process simulation are an improved process understanding and the possibility for efficient training of operators.

In this chapter, established concepts of modeling chromatographic separation processes will be summarized. In addition to describing the phenomena occurring in the separation columns, also extra-column elements of the plant will be considered. A short introduction into numerical methods typically required to solve the model equations is also given.

6.2 Models for Single Chromatographic Columns

There is a large spectrum of references available devoted to describe the state of the art of modeling chromatographic processes, mainly in order to predict effluent profiles of chromatographic columns (Ruthven 1984; Bellot and Condoret 1991; Seidel-Morgenstern 1995; Guiochon and Lin 2003; Guiochon et al. 2006).

---

* Henner Schmidt-Traub, Mirko Michel, Achim Epping, and Andreas Jupke have contributed to the first and/or second edition.

Since the second edition of this book and the second edition of the book by Gu (2015), two excellent new summaries were published by Nicoud (2015) and Pfister, Nicoud, and Morbidelli (2018) .

A quantitative description of band propagation phenomena is possible using suitable mathematical models. These are typically based on material, energy, and momentum balances, in addition to equations that quantify the thermodynamic equilibria of the distribution of the solutes between the different phases. Since the evolution of chromatographic profiles is time and space dependent, dynamic and microscopic balances must be employed to describe the process behavior. Hereby, the basic physical phenomena that occur during a chromatographic separation process (Chapter 2) need to be represented.

Related to the precision of a model, the engineering rule holds true: that a good model should be not only as detailed as necessary but also as simple as possible.

An important modeling approach capable of quantifying chromatographic processes exploits the stochastic theory of chromatography, which is based on fundamental molecular dynamic considerations introduced by Giddings and Eyring (1955). There are numerous later developments of this powerful theory, as documented, e.g. by McQuarrie (1963), Giddings (1991), and Felinger et al. (1999).

Another group of models, which is the focus of this book, is those models that solve in a rigorous manner the well-established component mass balance equations for the chromatographic particles and the column as a whole. In this field, there is large spectrum of chemical engineering approaches devoted to describe fixed beds. An essential classification of the models distinguishes between two types. In one case the whole columns are considered as a series connection of a certain number of discrete parts of the column (cells or stages). In the other case, continuous formulations are used to describe the time-dependent local concentration profiles. The various partial differential equation (PDE) formulations differ with respect to the nature of the balance spaces considered. Macroscopic balances are applied if all physical quantities are assumed to be constant throughout the whole volume of interest, whereas microscopic balances are necessary in the case of spatial changes of the state variables. If various sub-steps are resolved, a proper connection of the corresponding sub-models is essential.

The next chapter will first describe the widely used equilibrium stage models.

6.2.1 Equilibrium Stage Models

Regarding discrete stage models of chromatography, there are often equilibrium stage models considered. Thus, the solution requires knowledge of the underlying equilibrium functions introduced in Chapter 2. A very successful equilibrium stage model was proposed by Martin and Synge (1941), which considers the column essentially as a series connection of well-mixed stages, through which a continuous flow of the liquid phase occurs. This model corresponds to the well-known cascade of stirred tanks often applied in chemical reaction engineering (Levenspiel 1999). Before describing this model in a bit more detail, we will introduce below an even simpler fully discrete model of chromatography suggested in 1944 by Craig.
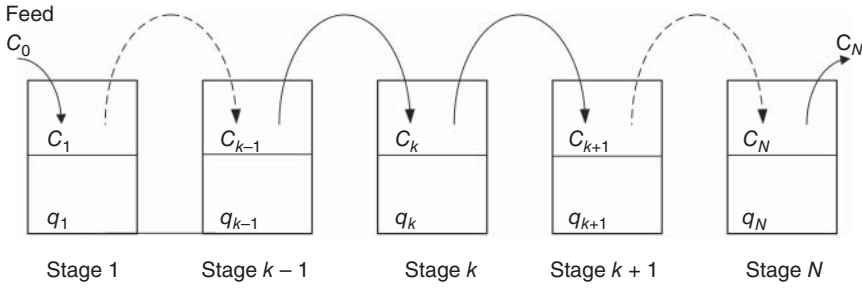
Figure 6.1 Illustration of the discrete equilibrium stage model according to Craig (1944).

6.2.1.1 Discontinuous Model According to Craig

The column is modeled as a sequence of a finite number N of similar stages. Each stage is filled with liquid and solid and the two phases are completely mixed. The so-called Craig model is based on the assumption of a constant residence time in each stage, which is sufficient to achieve equilibrium, and a subsequent discrete exchange of the liquid phase in the flow direction (Craig 1944). The various exchange steps are illustrated in Figure 6.1.

The quantification of the Craig process is simple. The total mass balance for a specific component present in a process step j in stage k is

$$m_{\text{tot}}^{k,j} = m_{\text{liq}}^{k,j} + m_{\text{sol}}^{k,j} = \varepsilon_t V_k c^{k,j} + (1 - \varepsilon_t) V_k q^{k,j}(c^{k,j}) \quad k = 1, N; \ j = 1, j_{\text{end}}$$

(6.1)

Hereby, the volume of a single stage V_k out of N stages is $(V_k = V_c/N)$, and ε_t and q are the consistently connected total column porosity and the equilibrium loadings, respectively (Section 2.4.1).

In the next step $j + 1$, the liquid phase moves one stage on, i.e. there is a loss of the current fluid phase and an input from stage $k - 1$ as expressed by Eq. (6.2):

$$m_{\text{tot}}^{k,j+1} = m_{\text{tot}}^{k,j} + \varepsilon_t V_k (c^{k-1,j} - c^{k,j}) \quad k = 1, N; \ j = 1, j_{\text{end}}$$

(6.2)

After equilibration holds in analogy to Eq. (6.1) at the end of step $j + 1$,

$$m_{\text{tot}}^{k,j+1} = \varepsilon_t V_k c^{k,j+1} + (1 - \varepsilon_t) V_k q^{k,j+1}(c^{k,j+1}) \quad k = 1, N; \ j = 1, j_{\text{end}}$$

(6.3)

Exploiting Eqs. (6.1)–(6.3) leads to the final mass balance of the Craig model:

$$\varepsilon_t (c^{k,j+1} - c^{k-1,j}) + (1 - \varepsilon_t)(q^{k,j+1}(c^{k,j+1}) - q^{k,j}(c^{k,j})) = 0 \quad k = 1, N; \ j = 1, j_{\text{end}}$$

(6.4)

In this equation the equilibrium loading $q^{k,j+1}$ is the unknown quantity. Provided the equilibrium function $q(c)$ is known, the algebraic equation (6.4) can be solved. For nonlinear isotherms, well-established numerical solution methods (e.g. the Newton–Raphson method (Deuflhard 2004)) need to be applied.

In the case of mixtures of n components for any component i, the mass balance equation (6.4) has to be respected, i.e.

$$\varepsilon_t (c_i^{k,j+1} - c_i^{k-1,j}) + (1 - \varepsilon_t)(q_i^{k,j+1}(\overline{c}^{k,j+1}) - q_i^{k,j}(\overline{c}^{k,j})) = 0$$
$$i = 1, n; \ k = 1, N; \ j = 1, j_{\text{end}}$$

(6.5)

After specifying the competitive isotherms, i.e. the dependences of q_i on (c_1, c_2, ..., c_n), the solution of the system of nonlinear algebraic equations (Eq. (6.5)) requires numerical techniques.

To complete and apply the Craig model, an adjustment of the discrete steps to the real time is needed. This can be done by assuring that a nonretained component introduced at $t = 0$ into the first stage, which is known to elute after the column dead time $t_{0,t}$, leaves the last Craig stage N after $j = N$ exchange steps. This leads to the following equations:

$$\Delta t^{j \to j+1} = \frac{t_{0,t}}{N} \quad \text{with } t_{0,t} = \frac{\varepsilon_t V}{\dot{V}} \text{ and } t_j = j \cdot \Delta t^{j \to j+1} \tag{6.6}$$

In the case of linear isotherms, $q = H\,c$, the Craig model leads for a single component to the following well-known analytical solution, which is a binomial distribution (Guiochon et al. 2006):

$$c_N(t_j = j * \Delta t) = \frac{m_{inj}}{\dot{V}\, t_R} \frac{N(j)!}{N!(j-N)!} R_t^N (1-R_t)^{j-N} \quad \text{with } t_j = j \cdot \Delta t, j = 1, j_{end} \tag{6.7}$$

The mean retention time t_R corresponds to the expression given in Eq. (2.73).

For a rectangular pulse injection, the injected amount m_{inj} is related to the volumetric flow rate, the injection time, and the injection concentration:

$$m_{inj} = \dot{V} \cdot t_{inj} \cdot c_{inj} \tag{6.8}$$

For reversible adsorption processes, this amount must completely leave the column over the outlet stage N, i.e.

$$m_N = \dot{V} \cdot \int_0^\infty c_N(t)\mathrm{d}t = m_{inj} \tag{6.9}$$

In Eq. (6.7) the R_t represent the liquid-phase mass fractions that are stepwise exchanged. For any stage k holds

$$R_t^{k,j} = \frac{\varepsilon_t V_k c^{k,j}}{\varepsilon_t V_k c^{k,j} + (1-\varepsilon_t) V_k q^{k,j}} \tag{6.10}$$

Rearrangement provides a simple relation between R_t and the capacity factor k_t' (Eq. (2.14)):

$$R_t^{k,j} = R_t = \frac{1}{1 + \frac{(1-\varepsilon_t)}{\varepsilon_t} \frac{q^{k,j}}{c^{k,j}}} = \frac{1}{1 + k_t'} \tag{6.11}$$

Equation (6.7) converges for large values of N into a continuous Gaussian distribution (Guiochon et al. 2006):

$$c_N(t) = \frac{m_{inj}}{\dot{V}} \frac{e^{-\frac{(t-\mu_1)^2}{2\sigma^2}}}{\sigma\sqrt{2\pi}} \tag{6.12}$$

Hereby, the first moment μ_1 corresponds to the mean retention time t_R (Eq. (2.17)), i.e.

$$\mu_1 = t_R = t_{0,t}(1 + k_t') \tag{6.13}$$

The variance of the outlet concentration profile, i.e. the second moment σ^2, is related to the number of equilibrium stages N as follows (Guiochon et al. 2006):

$$\sigma^2 = \frac{t_R^2}{N} \frac{k_t'}{1 + k_t'} \tag{6.14}$$

A widely used method to estimate quickly the column stage number N is to extract it from the retention time of the peak maximum, $t_{R,max}$, and the peak width at half height, $w_{0.5}$, of measured responses generated by small amounts injected. The approximation assumes the elution profile to be Gaussian. This leads to the following approximation (Eq. (2.20)):

$$N \approx 5.54 * \left(\frac{t_{R,max}}{w_{0.5}} \right)^2 \tag{6.15}$$

6.2.1.2 Continuous Model According to Martin and Synge

Another stage model concept was introduced already in 1941 by Martin and Synge. It exploits the assumption that a column can be represented by a cascade of stirred tanks (stages) through which the fluid moves continuously with a constant flow rate and in which the two phases are permanently equilibrated. As in the Craig model, each tank has a total volume equal to V_c/N. Inside each stage, a fraction $(1 - \varepsilon_t)$ is occupied by the solid phase. This leads to the following mass balance for a component i and stage k, where overall accumulation is balanced by the difference between the inlet stream from stage $k - 1$ and the outlet stream:

$$\frac{V_c}{N} \cdot \left(\varepsilon_t \cdot \frac{\partial c^k}{\partial t} + (1 - \varepsilon_t) \cdot \frac{\partial q^k(c^k)}{\partial t} \right) = \dot{V} \cdot (c^{k-1} - c^k) \quad i = 1, n; \ \ k = 1, N \tag{6.16}$$

This model leads to a system of N ordinary differential equations (ODEs). For linear isotherms and the injection of an ideal Dirac pulse of a single component, the resulting equation can be solved analytically. The resulting Poisson distribution describing the effluent profile of stage N exploits the mean retention time t_R (Eq. (6.13)):

$$c_N(t) = \frac{m_{inj}}{\dot{V} t_R} \left(\frac{t}{t_R} \right)^{N-1} \cdot \frac{N^N}{(N - 1)!} \cdot \exp \left\{ -\frac{N \cdot t}{t_R} \right\} \tag{6.17}$$

For larger values of N, the solution of this cascade model (Eq. (6.17)) reduces also into the Gaussian distribution (Eq. (6.12)).

In Section 6.2.9 illustrative results and a comparison will be provided for the two discrete equilibrium stage models just introduced (Craig and Martin/Synge): the Gaussian distribution and one of the widely used continuous models introduced below.

A problem in applying both the discrete equilibrium stage models is the fact that both exploit just a single stage number N. To take component-specific band broadenings into account, in principle, different numbers of stages must be used for each component. The lack of this degree of freedom is a disadvantage of these

simple equilibrium stage models and limits the potential to properly describe the elution behavior of all components in multicomponent mixtures. However, if the N_i are sufficiently large for all components, this disadvantage is negligible and exploitation of an averaged plate number provides good results.

6.2.2 Derivation of Continuous Mass Balance Equations

Powerful and flexible models capable to describe the dynamics of chromatographic processes exploit differential component specific and total mass balances for the fluid mobile phase as well as the stationary adsorbent phase. These balances are valid in differential (small) volume elements of the space of interest. Since integral concentration profiles at specific positions (typically at the column outlets) are of main interest, there is an integration of PDE required. This typically is possible only numerically. Depending on the degree of details considered or neglected, numerous continuous dynamic models of chromatography have been developed (Guiochon et al. 2006).

In addition to forced convection required to introduce the mobile phase and the feed, the continuous models take into account one or more of the following effects (Figure 6.2):

- Dispersion in the fluid phase outside the particles;
- Mass transfer from the bulk phase into the boundary layer of the adsorbent particle;
- Diffusion inside the pores of the particle (pore diffusion);
- Diffusion along the surface of the solid phase ("surface diffusion");
- Finite rates of the adsorption and desorption steps.
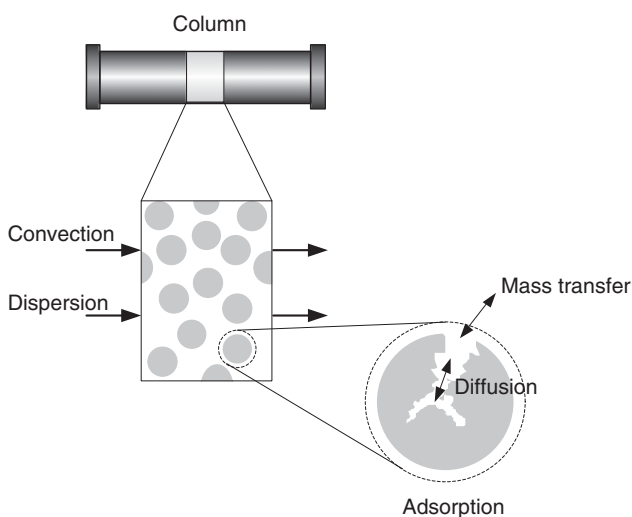
Figure 6.2 Principle of differential mass balances for a chromatographic column.

To simplify the modeling of liquid chromatographic processes, the following assumptions are frequently justified:

- The adsorbent bed is homogeneous and packed with spherical particles of constant diameter.
- Fluid density and viscosity are constant.
- Gradients over the radius of the column are negligible.
- The process is isothermal.
- The eluent is inert. Its influence on the adsorption process is taken into account only implicitly by the parameters of the adsorption isotherm.
- There is no convection inside the particles.

Consequently, standard models describing chromatographic columns consist typically of spatially one-dimensional mass balances. Only such models will be introduced below.

Figure 6.3 shows a possible classification of the various continuous chromatography models developed based on the number and type of band broadening effects considered.
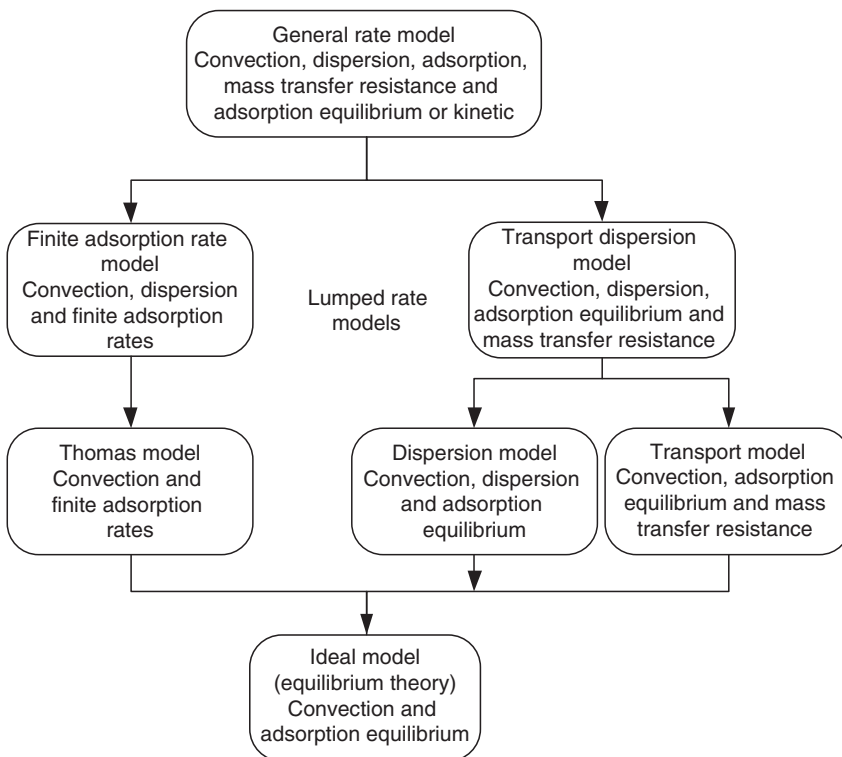
Figure 6.3 Classification of different continuous models capable of describing chromatographic processes. Source: Adapted from Klatt (1999).
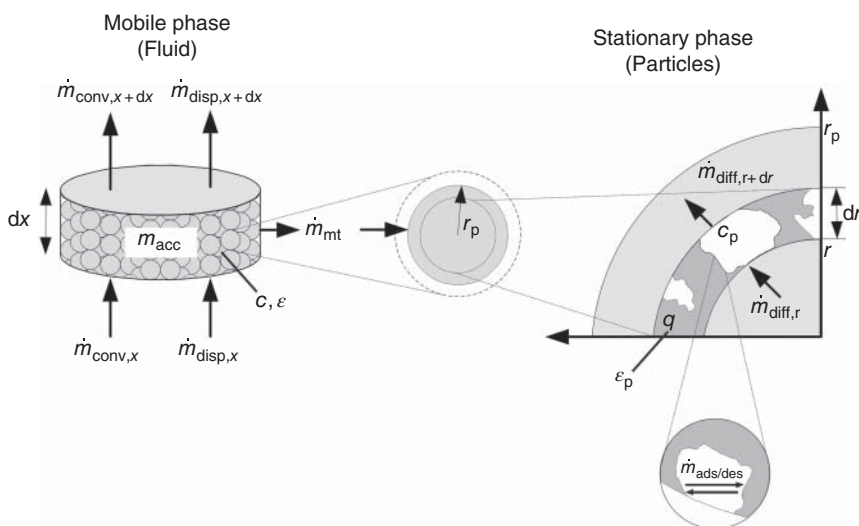
Figure 6.4 Differential model elements required to derive continuous models of chromatography.

6.2.2.1 Mass Balance Equations

In Figure 6.4 are visualized possible ingoing and outgoing streams as well as source and sink terms for a differential volume element. Such elements exist and need to be accounted for in both the mobile and the stationary phases. Hereby, the stationary phase can be split additionally into a range of stagnant fluid inside the particle pores and the actual solid structure of the particles (Chapter 2).

In the following, we will provide first the mass balance for different types of volume elements. Then we will introduce the additionally needed expressions quantifying different possible types of mass transport mechanisms (Chapter 2).

The general mass balance for one component i in the mobile phase of a differential volume dV_c is (see Figure 6.4, left)

$$\frac{\partial}{\partial t}(m_{\text{acc},i}(x,t)) = \dot{m}^x_{\text{conv},i}(x,t) - \dot{m}^{x+dx}_{\text{conv},i}(x,t) + \dot{m}^x_{\text{disp},i}(x,t)$$
$$- \dot{m}^{x+dx}_{\text{disp},i}(x,t) - \dot{m}_{\text{mt},i}(x,t) \tag{6.18}$$

Equation (6.18) includes mass accumulation in a specific differential volume, the mass transport by ingoing and outgoing convection and dispersion, and the mass transfer into the particles. Using a first-order Taylor series approximation for the outgoing streams

$$\dot{m}^{x+dx} \approx \dot{m}^x + \frac{\partial \dot{m}^x}{\partial x}dx \tag{6.19}$$

Equation (6.18) can be written as

$$\frac{\partial}{\partial t}(m_{\text{acc},i}) = -\frac{\partial(\dot{m}^x_{\text{conv},i} + \dot{m}^x_{\text{disp},i})}{\partial x}dx - \dot{m}_{\text{mt},i} \tag{6.20}$$

The superscript x marking the axial position is dropped in the following.

The mass transfer into the particle needs to be equal to the overall accumulation of component i in the adsorbent:

$$\frac{\partial}{\partial t}(\overline{m}_{\text{acc,ads},i}) = \dot{m}_{\text{mt},i} \tag{6.21}$$

Inside the adsorbent particles, mass transport is assumed to take place due to pore and/or surface diffusion. The resulting mass balances for the two reservoirs in the adsorbent include finite adsorption–desorption kinetics on the solid surface (Figure 6.4, right):

$$\frac{\partial}{\partial t}(m_{\text{acc,pore},i}) = -\frac{\partial}{\partial r}(\dot{m}_{\text{diff,pore},i})\mathrm{d}r - \dot{m}_{\text{ads/des}} \tag{6.22}$$

$$\frac{\partial}{\partial t}(m_{\text{acc,solid},i}) = -\frac{\partial}{\partial r}(\dot{m}_{\text{diff,solid},i})\mathrm{d}r + \dot{m}_{\text{ads/des}} \tag{6.23}$$

Alternatively, either Eq. (6.22) or (6.23) can be replaced by the sum of the two (Eq. (6.24)):

$$\frac{\partial}{\partial t}(m_{\text{acc,pore},i} + m_{\text{acc,solid},i}) = -\frac{\partial}{\partial r}(\dot{m}_{\text{diff,pore},i} + \dot{m}_{\text{diff,solid},i})\mathrm{d}r \tag{6.24}$$

If adsorption equilibrium is assumed, the reaction kinetics are infinitively fast and the term $\dot{m}_{\text{ads/des}}$ vanishes. Thus, the consideration of two independent balances (Eqs. (6.22) and (6.23)) is no longer required.

To transfer the equations derived above into mass balances based on concentrations and loadings, it is necessary to introduce and apply the characteristic volumes introduced in Chapter 2.2.1. The overall differential volume $\mathrm{d}V_{\text{c}}$ is the sum of the mobile phase volume $\mathrm{d}V_{\text{int}}$ and the stationary phase volume $\mathrm{d}V_{\text{ads}}$. By means of the external void fraction ε_{e} (Eq. (2.3)) and the cross section A_{c} of the column, those volumes can be calculated as

$$\mathrm{d}V_{\text{int}} = \varepsilon_{\text{e}} \cdot A_{\text{c}} \cdot \mathrm{d}x \tag{6.25}$$

$$\mathrm{d}V_{\text{ads}} = (1 - \varepsilon_{\text{e}}) \cdot A_{\text{c}} \cdot \mathrm{d}x \tag{6.26}$$

Thus, it holds:

$$\mathrm{d}V_{\text{c}} = A_{\text{c}} \cdot \mathrm{d}x = \mathrm{d}V_{\text{int}} + \mathrm{d}V_{\text{ads}} \tag{6.27}$$

The same splitting can be applied for the differential pore phase volumes $\mathrm{d}V_{\text{pore}}$ and solid phase volumes $\mathrm{d}V_{\text{solid}}$ of the adsorbent using the internal porosity ε_{p} (Eq. (2.4)) of the adsorbent:

$$\mathrm{d}V_{\text{pore}} = \varepsilon_{\text{p}} \cdot \mathrm{d}V_{\text{ads}} = \varepsilon_{\text{p}} \cdot (1 - \varepsilon_{\text{e}}) \cdot A_{\text{c}} \cdot \mathrm{d}x \tag{6.28}$$

With these volumes the masses accumulated can be expressed using corresponding concentrations in the liquid (bulk) phase c_i, mean pore concentrations $\bar{c}_{\text{p},i}$, mean solid loadings $\bar{q}_i$, and mean overall adsorbent loadings $\bar{q}_i^*$ (Section 2.4.1):

$$\mathrm{d}V_{\text{solid}} = (1 - \varepsilon_{\text{p}}) \cdot \mathrm{d}V_{\text{ads}} = (1 - \varepsilon_{\text{p}}) \cdot (1 - \varepsilon_{\text{e}}) \cdot A_{\text{c}} \cdot \mathrm{d}x \tag{6.29}$$

$$m_{\text{acc},i} = c_i \cdot \mathrm{d}V_{\text{int}} = c_i \cdot \varepsilon_{\text{e}} \cdot A_{\text{c}} \cdot \mathrm{d}x \tag{6.30}$$

$$\overline{m}_{\text{acc,pore},i} = \bar{c}_{\text{p},i} \cdot \mathrm{d}V_{\text{pore}} = \bar{c}_{\text{p},i} \cdot \varepsilon_{\text{p}} \cdot (1 - \varepsilon_{\text{e}}) \cdot A_{\text{c}} \cdot \mathrm{d}x \tag{6.31}$$

$$\overline{m}_{\text{acc,solid},i} = \overline{q}_i \cdot \mathrm{d}V_{\text{solid}} = \overline{q}_i \cdot (1 - \varepsilon_{\text{p}}) \cdot (1 - \varepsilon_{\text{e}}) \cdot A_{\text{c}} \cdot \mathrm{d}x \tag{6.32}$$

$$\overline{m}_{\text{acc,ads},i} = \overline{q}_i^* \cdot \mathrm{d}V_{\text{ads}} = \overline{q}_i^* \cdot (1 - \varepsilon_{\text{e}}) \cdot A_{\text{c}} \cdot \mathrm{d}x \tag{6.33}$$

The bar above the symbols in Eqs. (6.31)–(6.33) denotes average values. The overall balance (Eqs. (6.33)) has to be in agreement with the particle mass balances that take into account internal radial distributions – the average concentrations and loadings within spherical particles of radius r_{p} can be calculated with the following integrals:

$$\overline{c}_{\text{p},i} = \frac{1}{(4/3) \cdot \pi \cdot r_{\text{p}}^3} \int_0^{r_{\text{p}}} c_{\text{p},i}(r) \cdot 4\pi \cdot r^2 \, \mathrm{d}r = \frac{3}{r_{\text{p}}^3} \int_0^{r_{\text{p}}} r^2 \cdot c_{\text{p},i}(r) \, \mathrm{d}r$$

$$\overline{q}_i = \frac{3}{r_{\text{p}}^3} \int_0^{r_{\text{p}}} r^2 \cdot q_i(r) \, \mathrm{d}r \tag{6.34}$$

Hereby, in addition to the loadings q_i valid for V_{solid}, again also local and averaged overall adsorbent loadings q_i^* valid for V_{ads} can be used, which are the sums of the pore concentrations and the solid loadings (Eq. (2.38)):

$$q_i^*(r) = \varepsilon_{\text{p}} \cdot c_{\text{p},i}(r) + (1 - \varepsilon_{\text{p}}) \cdot q_i(r) \tag{6.35}$$

$$\overline{q}_i^* = \varepsilon_{\text{p}} \cdot \overline{c}_{\text{p},i} + (1 - \varepsilon_{\text{p}}) \cdot \overline{q}_i \tag{6.36}$$

To match mass transfer occurring over the particle surfaces and accumulation occurring in the particle volumes, the mass balances can also take into account the number of particles present in the volume element. For spherical particles holds:

$$N_{\text{p}} = \frac{\mathrm{d}V_{\text{ads}}}{\text{particle volume } (r_{\text{p}})} = \frac{(1 - \varepsilon_{\text{e}}) \cdot A_{\text{c}} \cdot \mathrm{d}x}{(4/3) \cdot \pi \cdot r_{\text{p}}^3} \tag{6.37}$$

After having defined above the accumulation terms of the general mass balances, we will now derive the transport and source terms.

6.2.2.2 Convective Transport

The mass transport in the mobile phase due to convection is proportional to the volumetric flow rates applied. The latter define the interstitial velocities, which are related to the overall column cross-sectional area and the fraction in which fluid phase is present. There are again the two options, depending on how the phase boundary is drawn (Chapter 2, Eqs. (2.2)–(2.6)):

$$\dot{m}_{\text{conv},i} = \dot{V} \cdot c_i \quad \text{with } \dot{V} = A_{\text{c}} \cdot \varepsilon_{\text{e}} \cdot u_{\text{int,e}} \text{ or } \dot{V} = A_{\text{c}} \cdot \varepsilon_{\text{t}} \cdot u_{\text{int,t}}^{\text{hypo}} \tag{6.38}$$

6.2.2.3 Axial Dispersion

It is assumed that axial dispersion (Eq. (6.39)) in the external (bulk) liquid phase can be defined in analogy to Fick's first law of diffusion:

$$\dot{m}_{\text{disp},i} = -\varepsilon_{\text{e}} \cdot A_{\text{c}} \cdot D_{\text{ax}} \cdot \frac{\partial c_i}{\partial x} \tag{6.39}$$

The axial dispersion coefficient D_{ax} depends on the quality of the packing and captures deviations of the fluid dynamics from plug flow (Section 7.6.2, Rastegar and Gu 2017).

In preparative chromatography, where one is typically interested in applying larger flow rates, contributions of molecular diffusion to D_{ax} are often small.

6.2.2.4 Intraparticle Diffusion

Diffusion inside the adsorbent particles can also be quantified using Fick's law. As for the accumulation terms, size and number of particles per unit volume (Eq. (6.37)) are taken into account:

$$\dot{m}_{\text{diff,pore},i}(r) = -N_p \cdot \varepsilon_p \cdot 4\pi \cdot r^2 \cdot D_{\text{pore},i} \frac{\partial c_{p,i}(r)}{\partial r} \tag{6.40}$$

$$\dot{m}_{\text{diff,solid},i}(r) = -N_p \cdot (1 - \varepsilon_p) \cdot 4\pi \cdot r^2 \cdot D_{\text{solid},i} \frac{\partial q_i(r)}{\partial r} \tag{6.41}$$

In Eq. (6.40) the transport in the pore fluid is modeled as free diffusion in the macropores and mesopores, but the diffusion coefficient $D_{\text{pore},i}$ is usually smaller than the molecular diffusivity characterizing transport in the liquid mobile phase due to the random orientations and variations in the diameter of the pores (tortuosity) (Section 7.6).

In Eq. (6.41) transport is assumed to occur by micropore or surface diffusion, where the molecules are under the influence of a force field of the inner adsorbent surface. The surface diffusion concept is applied to quantify the transport in the adsorbed phase.

6.2.2.5 Mass Transfer Between Phases

Figure 6.5 illustrates a typical intraparticle concentration profile that can be quantified with the equations given in Section 6.2.2.4. Also given is a concentration drop at the outer surface of the particles where the mass transfer between the solid and fluid phases takes place.

A common method introduces an external mass transfer $\dot{m}_{\text{mt},i}$ as a linear function of the concentration difference between the concentration in the bulk phase and that on the adsorbent surface, which are separated by a film of stagnant liquid (boundary layer). This so-called liquid phase linear driving force (LDF) model has proven to be often suitable to describe chromatographic processes (Ruthven 1984; Bellot and Condoret 1991; Guiochon et al. 2006).

In the corresponding equation for the mass transfer rate of component i, calculated by Eq. (6.41), the film transfer coefficient k_{film} is related to the overall surface

Figure 6.5 Concentration profile assumed in liquid film linear driving force models.
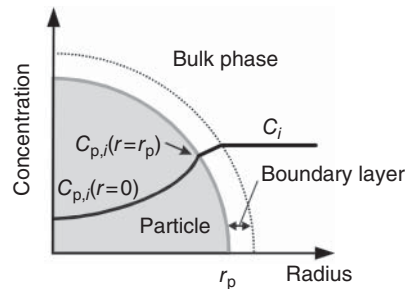
area dA_s of the adsorbent of all particles in the finite volume element (Eqs. (6.37) and (6.43)):

$$\dot{m}_{\mathrm{mt},i} = k_{\mathrm{film},i} \cdot (c_i - c_{\mathrm{p},i}(r = r_\mathrm{p})) \cdot dA_s \tag{6.42}$$

$$dA_s = N_\mathrm{p} \cdot 4\pi \cdot r_\mathrm{p}^2 = \frac{3}{r_\mathrm{p}} \cdot (1 - \varepsilon_\mathrm{e}) \cdot A_\mathrm{c} \cdot dx \tag{6.43}$$

A characteristic value is the specific surface area a_s of the particles per unit volume, which can be derived from Eq. (6.43):

$$a_s = \frac{dA_s}{dV} = \frac{3}{r_\mathrm{p}} \cdot (1 - \varepsilon_\mathrm{e}) \tag{6.44}$$

Combining Eqs. (6.42) and (6.43) yields Eq. (6.45) for the mass transfer rate:

$$\dot{m}_{\mathrm{mt},i} = k_{\mathrm{film},i} \cdot (c_i - c_{\mathrm{p},i}(r = r_\mathrm{p})) \cdot \frac{3}{r_\mathrm{p}} \cdot (1 - \varepsilon_\mathrm{e}) \cdot A_\mathrm{c} \cdot dx \tag{6.45}$$

According to Eq. (6.21), the mass flow $\dot{m}_{\mathrm{mt}}$ is generally equal to the overall accumulation in the adsorbent. This allows to use another approach to calculate $\dot{m}_{\mathrm{mt}}$. An integration of the dynamically changing concentration and loading profiles inside the particles (Eqs. (6.40) and (6.41)) over the radial coordinate (Eq. (6.34)) provides the overall solid-phase accumulation and thus also the mass flow $\dot{m}_{\mathrm{mt}}$:

$$\dot{m}_{\mathrm{mt},i} = -(\dot{m}_{\mathrm{diff,pore},i}(r = r_\mathrm{p}) + \dot{m}_{\mathrm{diff,solid},i}(r = r_\mathrm{p})) \tag{6.46}$$

To simplify the calculation of the overall solid-phase accumulation and to avoid the numerically expensive integration of the intraparticle mass balance equations, another type of linear driving force models became very popular in recent years. Core of the approach is the following expression assuming in analogy to Eq. (6.45) a linear driving force expressed by the difference of equilibrium and mean loadings combined with effective solid-phase linear driving force coefficients (Guiochon et al. 2006). Depending on the type of equilibrium loadings applied, q_i or q_i^*, the following two equivalent forms can be derived using either $k_{\mathrm{solid,t},i}^{\mathrm{eff}}$ or $k_{\mathrm{solid,e},i}^{\mathrm{eff}}$:

$$\dot{m}_{\mathrm{mt},i} = k_{\mathrm{solid,t},i}^{\mathrm{eff}} \cdot (q_i(c_i) - \bar{q}_i) \text{ or } \dot{m}_{\mathrm{mt},i} = k_{\mathrm{solid,e},i}^{\mathrm{eff}} \cdot (q_i^*(c_i) - \bar{q}_i^*) \tag{6.47}$$

6.2.2.6 Finite Rates of Adsorption and Desorption

The kinetics of the adsorption and desorption steps on the particle surfaces are another element of the mass balances. According to Eqs. (6.22) and (6.23), adsorption and desorption steps are modeled as reactions with finite rates. The mass transfer related to the net reaction rate $\psi_{\mathrm{reac},i}$ based on the solid volume of all particles in the volume element is

$$\dot{m}_{\mathrm{reac}} = (1 - \varepsilon_\mathrm{p}) \cdot N_\mathrm{p} \cdot \psi_{\mathrm{ads/des}} \cdot 4\pi \cdot r^2 \cdot dr \tag{6.48}$$

The net rates of adsorption and desorption, designated below as $\psi_{\mathrm{reac},i}$, can be defined in quite different ways. One simple and typically applied example is given in Eq. (6.49) where a second-order rate law is assumed for adsorption and

a first-order rate law for desorption introducing the two rate constants k_{ads} and k_{des} (Ma, Whitley, and Wang 1996):

$$\psi_{\text{ads/des}}(r) = k_{\text{ads},i} \cdot q_{\text{sat},i} \cdot \left(1 - \sum_{j=1}^{n} \frac{q_j(r)}{q_{\text{sat},j}}\right) \cdot c_{\text{p},i}(r) - k_{\text{des},i} \cdot q_i(r) \qquad (6.49)$$

In Eq. (6.49) it is assumed that the rate can change in the particles as a function of the radius, due to locally varying concentrations. The quantity $q_{\text{sat},i}$ represents the maximum possible loadings for each component. Competition between the different components is considered by the summation over all n components. The single-component nonequilibrium form can be obtained by neglecting the sum in Eq. (6.49), which leads to

$$\psi_{\text{ads/des}}(r) = k_{\text{ads},i} \cdot q_{\text{sat},i} \cdot c_{\text{p},i}(r) - k_{\text{des},i} \cdot q_i(r) \qquad (6.50)$$

6.2.2.7 Adsorption Equilibria

The intrinsic adsorption and desorption steps are usually very fast. In the limit of very large adsorption rate constants, $\psi_{\text{ads/des},i}$ becomes zero. Then there is an equilibrium between adsorption and desorption steps. Under this condition, Eq. (6.49) provides the multicomponent Langmuir isotherm (Eq. (2.48)), and Eq. (6.50) reduces to a linear isotherm with the following Henry coefficient:

$$H = \frac{k_{\text{ads}}}{k_{\text{des}}} q_{\text{sat}} \qquad (6.51)$$

Due to the fact of the relative fast rate of adsorption and desorption steps in general, compared with the rates of transport processes, the assumption that $\psi_{\text{ads/des}} = 0$ is typically well justified.

If the adsorption equilibria can be assumed to be established, knowledge regarding the isotherm is of large importance (Section 2.4.1), i.e. of the following generally formulated functions:

$$q_i = f(c_1, \ldots, c_n) \text{ (Option 1) or } q_i^* = f^*(c_1, \ldots, c_n) \text{ (Option 2)}$$
$$i = 1, n; \ \ T = \text{const.} \qquad (6.52)$$

In the following, the relevant continuous models for liquid chromatography are derived in a bottom-up procedure related to Figure 6.3.

To illustrate the difference between these models, their specific assumptions are discussed, and their field of application is pointed out. In all cases, the mass balances must be complemented by initial and boundary conditions (Section 6.2.7). For illustration, a dimensionless representation of one model will also be presented.

6.2.3 Equilibrium Model of Chromatography

The simplest continuous model capable of describing the propagation of concentration fronts in chromatographic columns takes into account only convective transport and assumes a permanently established local equilibrium between mobile and stationary phases. This model is frequently called the "ideal model" of chromatography (Guiochon et al. 2006). It was described first by

Wicke (1939) for the elution of a single component. Subsequently, De Vault (1943) derived in more detail the corresponding mass balances. Today there is a well-established, comprehensive, and rather complete theory available to solve the equations of the ideal model. This theory is called now predominantly the equilibrium theory of chromatography. Major contributions were made by Helfferich and Klein (1970), Helfferich and Carr (1993), Helfferich and Whitley (1996), Helfferich (1997), Rhee, Aris, and Amundson (1970, 1986, 1989), and Mazzotti and Rajendran (2013) who derived instructive analytical solutions of the resulting first-order system of nonlinear PDE. Comprehensive analytical solutions are available for multicomponent Langmuir isotherms. Interested readers will find in the excellent treatments of Rhee, Aris, and Amundson (1989) the basics of the method of characteristics applied to derive the solutions and to explain the wave phenomena that take place in chromatographic columns.

Let us summarize the assumptions of the equilibrium theory, which neglects the influences of axial dispersion and all mass transfer and kinetic effects. Thus, it holds:

$$D_{ax} = 0$$
$$D_{pore,i} = D_{solid,i} = \infty \qquad i = 1, n$$
$$k_{film,i} = \infty$$
$$\psi_{ads/des,i} = 0 \tag{6.53}$$

Consequently, the loadings and concentrations within the adsorbent are constant and not a function of the particle radius. Furthermore, the concentrations in the liquid phase are identical to that in the pores of the adsorbent:

$$\left.\begin{array}{l} c_{p,i} = \bar{c}_{p,i} \\ q_i = \bar{q} \\ q_i^* = \bar{q}_i^* \end{array}\right\} \neq f(r) \text{ and } c_i = c_{p,i} \quad i = 1, n \tag{6.54}$$

Therefore, Eqs. (6.20) and (6.21) reduce to the following balance:

$$\frac{\partial}{\partial t}(m_{acc,i}) = -\frac{\partial(\dot{m}_{conv,i})}{\partial x}dx - \frac{\partial}{\partial t}(\overline{m}_{acc,ads,i}) \tag{6.55}$$

Introducing the appropriate terms given by Eqs. (6.30)–(6.33) and (6.38) provides, depending on the loading definition applied, the following two options for the mass balances:

$$\varepsilon_e \frac{\partial c_i}{\partial t} + (1 - \varepsilon_e) \cdot \frac{\partial q_i^*(c_1, \ldots, c_n)}{\partial t} + \varepsilon_e u_{int,e} \cdot \frac{\partial c_i}{\partial x} = 0 \,(\text{Option 1}) \quad i = 1, n \tag{6.56}$$

Introducing the total porosity $\varepsilon_t = \varepsilon_e + \varepsilon_p(1 - \varepsilon_e)$ (Eq. (2.5)), the equilibrium loadings q_i, and the hypothetical effective velocity $u_{int,t}^{hypo}$ of a nonretained solute that enters the pore space (Eq. (2.8)),

$$u_{int,t}^{hypo} = \frac{\varepsilon_e}{\varepsilon_t} u_{int,e} = \frac{L_c}{t_{0,t}} = \frac{\varepsilon_e}{\varepsilon_t} \frac{L_c}{t_{0,e}} \tag{6.57}$$

instead of Eq. (6.56) holds also the following mass balance equation, which will be further used below:

$$\varepsilon_t \frac{\partial c_i}{\partial t} + (1 - \varepsilon_t) \cdot \frac{\partial q_i(c_1, \dots, c_n)}{\partial t} + \varepsilon_t u_{\text{int,t}}^{\text{hypo}} \cdot \frac{\partial c_i}{\partial x} = 0 \text{ (Option 2)} \quad i = 1, n$$

$$(6.58)$$

As discussed above (Section 2.2.1), the velocity $u_{\text{int,t}}^{\text{hypo}}$ is connected with the retention time of a nonretained but penetrating tracer and is, thus, smaller than the "real" interstitial velocity $u_{\text{int,e}}$ velocity, which is related to the retention time $t_{0,e}$ of a nonpenetrating nonretained molecules.

The additional equation required for predicting front dynamics is an explicit function for the thermodynamic equilibrium $q_i(c_1, \dots, c_n)$. Then Eq. (6.58) can be formulated as follows:

$$\frac{\partial c_i}{\partial t} \left(1 + \frac{(1 - \varepsilon_t)}{\varepsilon_t} \cdot \frac{dq_i}{dc_i}\Big|_{\bar{c}} \right) + u_{\text{int,t}}^{\text{hypo}} \cdot \frac{\partial c_i}{\partial x} = 0 \quad i = 1, n \tag{6.59}$$

Equation (6.59) is the basic mass balance equation of the equilibrium theory of chromatography.

The theory available for analyzing and solving Eq. (6.59) does not provide only a powerful tool to understand important phenomena that take place during the chromatographic process. One of the main advantages of equilibrium theory is the capability to explain some fundamental phenomena that occur in multicomponent chromatography such as the displacement effect and the tag-along effect (Section 2.4.3). An even more important application is the use of the equilibrium theory as a powerful shortcut method for preliminary process design. It is further an important starting point for several shortcut design methods. In particular, the understanding and design of the complex simulated moving bed (SMB) processes benefited in the last decades strongly from the equilibrium theory (Chapter 5).

To illustrate the strength of the results that can be obtained by applying the equilibrium theory (or the ideal model), we will consider below the case of single-component elution of a component i. Using an established adsorption equilibrium, the time derivatives of the overall loadings can be expressed by the isotherm slope and the corresponding liquid phase time derivative:

$$\frac{\partial q_i}{\partial t} = \frac{dq_i}{dc_i} \cdot \frac{\partial c_i}{\partial t} \tag{6.60}$$

Equation (6.59) can now be rearranged as follows:

$$\frac{\partial c_i}{\partial t} + \frac{u_{\text{int,t}}^{\text{hypo}}}{1 + \frac{1 - \varepsilon_t}{\varepsilon_t} \cdot \frac{dq_i}{dc_i}} \cdot \frac{\partial c_i}{\partial x} = 0 \tag{6.61}$$

Equation (6.61) predicts the current propagation velocity w of an arbitrary concentration c^+ inside the column depending on the isotherm slope:

$$w(c_i^+) = \frac{u_{\text{int,t}}^{\text{hypo}}}{1 + \frac{1 - \varepsilon_t}{\varepsilon_t} \cdot \frac{dq_i}{dc_i}\Big|_{c_i^+}} \tag{6.62}$$

This velocity is connected with an observable retention time by

$$t_{R,i}(c_i^+) = \frac{L_c}{w(c_i^+)} \tag{6.63}$$

Combining Eqs. (6.62) and (6.63) leads to one of the basic equations of chromatography:

$$t_{R,i}(c_i^+) = t_{0,t} \cdot \left(1 + \frac{1 - \varepsilon_t}{\varepsilon_t} \cdot \left. \frac{dq_i}{dc_i} \right|_{c_i^+} \right) \tag{6.64}$$

In the special case of linear isotherms, Eq. (6.64) reduces to

$$t_{R,\text{lin},i} = t_{0,t} \cdot \left(1 + \frac{1 - \varepsilon_t}{\varepsilon_t} \cdot H_i \right) \tag{6.65}$$

Thus, for linear isotherms (or diluted conditions used in analytical chromatography), the retention times do not depend on concentration (Lapidus and Amundson 1952; Van Deemter, Zuiderweg, and Klinkenberg 1956).

Already, through work by Glueckauf and Coates (1947) and Glueckauf (1949), considerable progress has been made in understanding the influences of the isotherm shapes on the shapes of elution profile for nonlinear isotherms.

For nonlinear systems, the isotherm slopes decide whether smaller or larger concentrations propagate faster. In most cases the isotherm slopes decrease with increasing concentrations, as described, for example, by the Langmuir isotherm. This behavior causes a faster movement of high concentrations. Under these conditions, Eq. (6.64) predicts that larger concentrations could overtake smaller concentrations. This would cause unrealistic discontinuities at the column outlet. In reality, shock fronts form instead, in which again all concentrations travel with the same velocity. To describe the movement of these shocks, the differentials in Eq. (6.64) have to be replaced by difference quotients Δ, which evaluate a secant in the isotherm between the two equilibrium points framing the limiting concentrations of a shock $a \to b$:

$$t_{R,i,\text{shock}}^{a \to b} = t_{0,t} \cdot \left(1 + \frac{1 - \varepsilon_t}{\varepsilon_t} \cdot \left. \frac{\Delta q_i}{\Delta c_i} \right|_{\text{shock}} \right) = t_{0,t} \cdot \left(1 + \frac{1 - \varepsilon_t}{\varepsilon_t} \frac{q_i^b - q_i^a}{c_i^b - c_i^a} \right) \tag{6.66}$$

It should be noted that the injection time t_{inj} has to be considered when evaluating measured retention times belonging to rear parts of elution bands:

$$t_{R,i}(c_i^+) = t_{\text{inj}} + t_{0,t} \cdot \left(1 + \frac{1 - \varepsilon_t}{\varepsilon_t} \cdot \left. \frac{dq_i}{dc_i} \right|_{c_i^+} \right) \tag{6.67}$$

Equations (6.64) and (6.67) are valid only for disperse parts of peaks. Depending on the shape of the isotherm, this is the rear part ("Langmuir") or the front part ("anti-Langmuir"). The description of the velocity of the opposite shock front requires Eq. (6.65). It should be mentioned that in the case of inflection points in the course of an isotherm, the situation is more complex

and composite fronts form (Rhee, Aris, and Amundson 1986; Zhang, Shan, and Seidel-Morgenstern 2006).

For large sample sizes that cause complete concentration breakthroughs, Eq. (6.66) can be directly used to calculate the position of the breakthrough curve or to determine parameters of an isotherm model from measured breakthrough times (see Section 7.5.5).

For multicomponent mixtures and competitive isotherms, total differentials of the equilibrium functions need to be used, and the analysis becomes more complicated. For two components, the following relations hold:

$$\frac{dq_1}{dc_1} = \frac{\partial q_1}{\partial c_1} + \frac{\partial q_1}{\partial c_2} \cdot \frac{dc_2}{dc_1}$$

$$\frac{dq_2}{dc_2} = \frac{\partial q_2}{\partial c_2} + \frac{\partial q_2}{\partial c_1} \cdot \frac{dc_1}{dc_2} \tag{6.68}$$

Thus, the elution behavior of the two components is coupled through the concentration dependences of both isotherm equations. To quantify the impact of the concentration of one component on the propagation velocity of other components, the so-called coherence condition introduced by Helfferich and Klein (1970) needs to be applied.

The coherence condition states that transitions of concentrations will occur for the two components coherently. This allows for a binary system connecting the two total differentials:

$$\frac{dq_1}{dc_1} = \frac{dq_2}{dc_2} \tag{6.69}$$

With Eq. (6.68) results a quadratic equation for two functional derivatives dc_1/dc_2:

$$\frac{\partial q_2}{\partial c_1} \left(\frac{dc_1}{dc_2} \right)^2 + \left(\frac{\partial q_2}{\partial c_2} - \frac{dq_1}{dq_1} \right) \frac{dc_1}{dc_2} - \frac{\partial q_1}{\partial c_2} = 0 \tag{6.70}$$

In Figure 6.6 we provide as an illustrative result the prediction of breakthrough curves for adsorption and desorption in the case of two components for which the equilibria can be described with the competitive Langmuir isotherm model. Shown is the development of the concentration profiles of the two components at the column outlet for a cycle starting from an equilibrated initial state of a fully regenerated column (init). The feed mixture considered contains an excess of the first eluting faster traveling component. The injection causes a shock wave into an intermediate state (inter_{ads}), in which the concentration of the first component is higher than the injected one and the concentration of second component is still zero. Then a complete breakthrough into the feed state (feed) occurs, which is characterized by the breakthrough of the second component. When the feeding is stopped and pure mobile phase regenerates the column after the dead time, the two components start to leave in simple waves via another intermediate plateau (inter_{des}), in which the first component has already reached zero concentration. Finally the initial state is reached again.
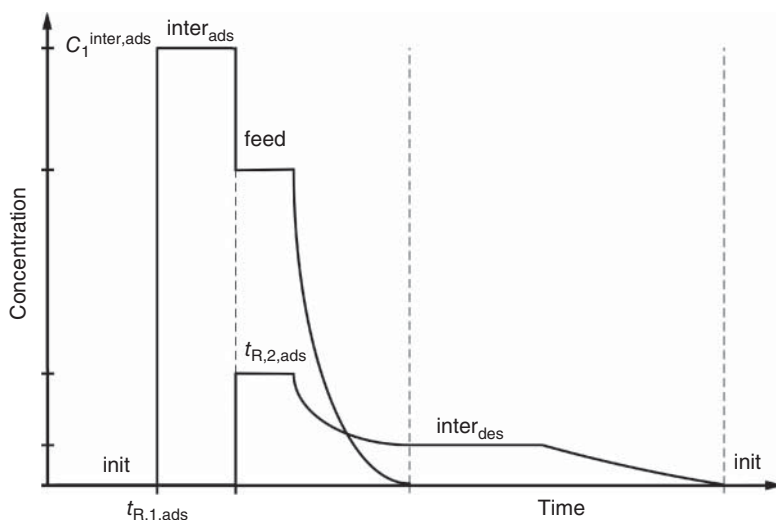
Figure 6.6 Illustration of the analytical solution of the concentration profile of a chromatographic cycle for two components obeying the Langmuir competitive isotherms.

The chromatographic cycle shown in Figure 6.6 is characterized by four important characteristic quantities, namely, the times of the two shock and the compositions of the two intermediate plateaus. The determination of these unknowns is straightforward for Langmuir isotherms. The solution can be illustrated in the so-called hodograph plane, in which the effluent concentrations c_1 are plotted over the effluent concentrations c_2. The plot corresponding to Figure 6.6 is given in Figure 6.7. The chromatographic cycle is characterized (only) for Langmuir isotherms by four straight lines connecting the three states (init, $inter_{ads}$, feed, and $inter_{des}$). The concentrations of the two intermediate states can be easily calculated from the slopes of the corresponding two roots for dc_1/dc_2 of the quadratic equation (6.70) by determining the intersections with the two axes of the diagram.

Finally, with the concentrations of the intermediate states, the two times of the characteristic transitions are readily available. For example, for the breakthrough
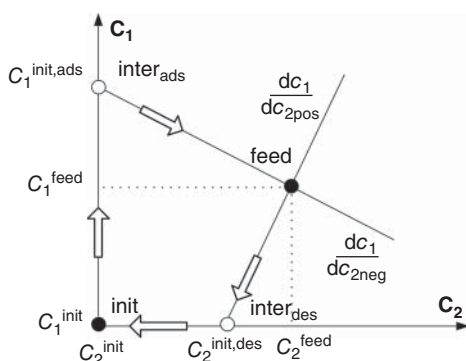
Figure 6.7 Hodograph plot corresponding to the cycle shown in Figure 6.6.

time of the first component holds:

$$t_{R,1,ads} = t_{0,t} \cdot \left(1 + \frac{1-\varepsilon_t}{\varepsilon_t} \frac{q_1^0 \left(c_1^{inter,ads} \right) - 0}{c_1^{inter,ads} - 0} \right) \tag{6.71}$$

The time for the second shock results from

$$t_{R,2,ads} = t_{0,t} \cdot \left(1 + \frac{1-\varepsilon_t}{\varepsilon_t} \frac{q_2 \left(c_1^{feed}, c_2^{feed} \right) - 0}{c_2^{feed} - 0} \right) \tag{6.72}$$

At this second characteristic time also the concentration of the first component will drop from $c_1^{inter,ads}$ to c_1^{feed}.

Figure 6.7 also illustrates the transition during the desorption cycle returning to the initial state passing the transition state $inter_{des}$. For Langmuir competitive isotherms, this desorption process will not occur in two shocks but via simple waves (Rhee, Aris, and Amundson 1986; Mazzotti and Rajendran 2013).

In the context of the equilibrium theory, a recently derived analytical solution for the prediction of the elution bands of two components in the case of shorter injection times should be mentioned. In such cases, the column outlet concentrations do not reach the feed concentrations. The explicit equations derived, which extend results earlier described by Guiochon et al. (2006), can be used for efficient optimization of batch chromatography (Siitonen and Sainio 2011).

Regarding further details of the equilibrium theory and available analytical solutions for more than two components and cases including temperature changes, we refer the reader to the references by Helfferich et al., Rhee et al., and Mazzotti and Rajendran provided in the reference list.

6.2.4 Models with One Band Broadening Effect

In addition to the information about the equilibria, the models lump all effects in only one model parameter to describe band spreading. Among these models, the most simple equilibrium dispersion model is described first.

6.2.4.1 Equilibrium Dispersion Model

This model is very often used to design and optimize chromatographic systems (e.g. Guiochon et al. 2006). Compared to the ideal model (Eq. (6.56)), a term describing axial dispersion (Eq. (6.39)) is included in the mass balance of the mobile phase together with:

$$D_{solid,i} = D_{pore,i} = \infty$$
$$k_{film,i} = \infty$$
$$\psi_{ads/des,i} = 0$$
$$\left. \begin{array}{l} c_{p,i} = \bar{c}_{p,i} \\ q_i = \bar{q} \\ c_i = c_{p,i} \end{array} \right\} \neq f(r) \tag{6.73}$$

Using these simplifications, Eqs. (6.20) and (6.21) provide

$$\frac{\partial}{\partial t}(m_{\mathrm{acc},i}) = -\frac{\partial(\dot{m}_{\mathrm{conv},i} + \dot{m}_{\mathrm{disp},i})}{\partial x}\mathrm{d}x - \frac{\partial}{\partial t}(\overline{m}_{\mathrm{acc,ads},i}) \tag{6.74}$$

which can be evaluated using Eqs. (6.30)–(6.32), (6.38), and (6.39).

As already mentioned, the effects of several parameters are often lumped into a dispersion coefficient. The so-called apparent dispersion coefficient D_{app} is used here differing from the axial dispersion coefficient, D_{ax}, which is assumed to be independent of concentration and influenced only by the quality of the packing. The lumped parameter D_{app} includes peak broadening effects caused by the fluid dynamics of the packing (axial dispersion), as well as by all other mass transfer effects that might occur:

$$D_{\mathrm{app}} = f(D_{\mathrm{ax}}, D_{\mathrm{solid}}, D_{\mathrm{pore}}, k_{\mathrm{film}}, c_i, \dots, c_n, u_{\mathrm{int}}) \tag{6.75}$$

Like most lumped parameters, the apparent dispersion coefficient is generally dependent on the interstitial velocity (Section 7.4.2). For nonlinear isotherms, it will generally also depend on the concentration.

Despite using only one parameter to describe mass transfer resistance and the fluid dynamics of the packing, experiments and simulation show good agreement for highly efficient columns ($N \gg 100$). In this region, the difference between this model and the more detailed models almost vanishes (Golshan-Shirazi and Guiochon 1992; Seidel-Morgenstern 1995; Guiochon et al. 2006).

Using this new coefficient and term, Eq. (6.74) becomes

$$\frac{\partial c_i}{\partial t} + u_{\mathrm{int,e}} \cdot \frac{\partial c_i}{\partial x} + \frac{1 - \varepsilon_{\mathrm{e}}}{\varepsilon_{\mathrm{e}}} \cdot \frac{\partial q_i^*(c_1, \dots, c_n)}{\partial t} = D_{\mathrm{app,e},i} \cdot \frac{\partial^2 c_i}{\partial x^2} \quad i = 1, n \tag{6.76}$$

As the fluid concentration is in equilibrium with the solid loading, still no differential equation for the particle phase is needed.

As discussed above, Eq. (6.76) can be derived also as

$$\frac{\partial c_i}{\partial t} + u_{\mathrm{int,t}}^{\mathrm{hypo}} \cdot \frac{\partial c_i}{\partial x} + \frac{1 - \varepsilon_{\mathrm{t}}}{\varepsilon_{\mathrm{t}}} \cdot \frac{\partial q_i(c_1, \dots, c_n)}{\partial t} = D_{\mathrm{app,t},i} \cdot \frac{\partial^2 c_i}{\partial x^2} \quad i = 1, n \tag{6.77}$$

with

$$D_{\mathrm{app,t},i} = \frac{\varepsilon_{\mathrm{e}}}{\varepsilon_{\mathrm{t}}} D_{\mathrm{app,e},i} = \frac{u_{\mathrm{int,t}}^{\mathrm{hypo}}}{u_{\mathrm{int,e}}} D_{\mathrm{app,e},i} \quad i = 1, n \tag{6.78}$$

The equilibrium dispersion model is widely applied in chromatography, owing to the equivalence with standard dispersion models well known in chemical engineering (Levenspiel and Bischoff 1963; Danckwerts 1953) and due to the availability of numerical solution techniques.

Instructive analytical solutions of Eq. (6.76) for linear isotherms and different boundary and initial conditions have been reported (Levenspiel and Bischoff 1963; Guiochon et al. 2006; Guiochon and Lin 2003). Considering a Dirac injection of mass m_{inj} and the so-called open–open boundary conditions, the following equation describes the elution profile:

$$c(t, x = L_{\mathrm{c}}) = \frac{m_{\mathrm{inj}}}{\dot{V}t_{\mathrm{R}}} \sqrt{\frac{(u_{\mathrm{int,t}}^{\mathrm{hypo}})^2 t_{0,\mathrm{t}} t_{\mathrm{R}}}{4\pi D_{\mathrm{app,t}} t}} \mathrm{e}^{-\frac{(u_{\mathrm{int,t}}^{\mathrm{hypo}})^2 t_{0,\mathrm{t}}}{4 D_{\mathrm{app,t}} t_{\mathrm{R}}} \frac{(t - t_{\mathrm{R}})^2}{t}} \tag{6.79}$$

When $D_{app,t}$ is "small" (corresponding to numbers of stages $N > 50$), also the solution of the equilibrium dispersion model can be approximated under linear conditions after matching the second moments by a Gaussian distribution (Eq. (6.12)).

6.2.4.2 Finite Adsorption Rate Model

A model that postulates the only rate-limiting step is related to the finite rate of the adsorption kinetic, was first used by Thomas (1944) to simulate ion-exchange processes. Originally, homogeneous particles without pores ($\varepsilon_p = 0$) were assumed, but this can be modified to fit in the framework presented here. It need only be stated that the concentration in the bulk phase is the same as in the particle pores. Thus, the mobile phase balance is still the same as used for the derivation of the ideal model (Eq. (6.56)). However, in the accumulation term of the stationary phase mass balance equation, a term is needed to quantify finite adsorption kinetics (which can be expressed, for example, by Eq. (6.49)) and rewritten for constant concentrations inside the particles:

$$\varepsilon_p \frac{\partial c_i}{\partial t} + (1 - \varepsilon_p) \frac{\partial q_i}{\partial t} = \widetilde{k}_{ads,i} \cdot q_{sat,i} \cdot \left(1 - \sum_{j=1}^{N_{comp}} \frac{q_j}{q_{sat,j}} \right) \cdot c_i - \widetilde{k}_{des,i} \cdot q_i \quad (6.80)$$

In Eq. (6.80) the $\widetilde{k}_{ads}$ and $\widetilde{k}_{des}$ are the lumped rate constants of the adsorption and desorption steps, respectively. Equation (6.49) is just one example how to express the kinetic equation – others have been published by Bellot and Condoret (1991) and Ma, Whitley, and Wang (1996).

Notably, for "standard" chromatography, the assumption that adsorption is the only rate-determining mechanism is unrealistic, because this step is generally much faster than other mass transfer-related effects (Guiochon et al. 2006; Ruthven 1984).

6.2.5 Continuous Lumped Rate Models

The next level of detail in the model hierarchy of Figure 6.3 is considered by the so-called lumped rate models. They are characterized by a second parameter describing rate limitations apart from axial dispersion. This second parameter subdivides the models into those where either mass transport or kinetic terms are rate limiting. No concentration distribution inside the particles is considered; only particle-averaged concentrations and loading are considered. Thus, the diffusion coefficients inside the adsorbent are assumed to be infinite:

$$D_{solid,i} = D_{pore,i} = \infty$$

$$\left. \begin{matrix} c_{p,i} = \bar{c}_{p,i} \\ q_i = \bar{q} \end{matrix} \right\} \neq f(r) \quad i = 1, n \quad (6.81)$$

The basic material balance of the mobile phase for all lumped rate models is based on Eqs. (6.20), (6.21), (6.30)–(6.33), and (6.36) and can be derived in the same manner as the equilibrium dispersion model 6.76:

$$\frac{\partial c_i}{\partial t} + u_{int,e} \cdot \frac{\partial c_i}{\partial x} + \frac{1 - \varepsilon_e}{\varepsilon_e} \cdot \frac{\partial q_i^*}{\partial t} = D_{ax} \cdot \frac{\partial^2 c_i}{\partial x^2} \quad i = 1, n \quad (6.82)$$

The dispersion coefficient D_{ax} (Section 7.4.2) is assumed to depend only on the packing properties and flow conditions (6.39) and is therefore smaller than the apparent dispersion coefficient D_{app} defined in Section 6.2.4.1.

Variants of the lumped rate models can be distinguished based on the different equations used to quantify the accumulation of the particle phase, considering in a simplifying manner either external or internal mass transfer resistances.

6.2.5.1 Transport Dispersion Models

The transport dispersion model (TDM) is an extension of the transport model (Figure 6.3) and summarizes the internal and external mass transfer resistance in one lumped transfer coefficient, k_{eff} (compare Eq. (6.45)):

$$k_{eff,i} = f(D_{solid}, D_{pore}, k_{film}, c_i, \dots, c_{N_{comp}}, u_{int}) \tag{6.83}$$

In contrast to the transport model, $k_{eff,i}$ is theoretically assumed to be independent of axial dispersion and therefore of the packing quality (Section 7.4). Compared with D_{ax}, the k_{eff} values are less dependent on the fluid velocity (Section 7.6).

The mass transfer term can be quantified by the linear driving force approach. Then, the TDM consists of a balance equation for the mobile phase (Eq. (6.82)) written with the pore concentration. Thus, in addition to Eq. (6.82), the following second mass balance holds for the stationary phase:

$$\frac{\partial q_i^*}{\partial t} = k_{eff,i} \cdot \frac{3}{r_p} \cdot (c_i - \bar{c}_{p,i}^{\ eq}(q_1^*, q_2^*, \dots, q_n^*)) \quad i = 1, n \tag{6.84}$$

which is derived from Eqs. (6.21) and (6.32)–(6.35) as well as the assumptions of Eq. (6.81). As discussed in Section 6.2.2, the driving force in Eq. (6.84) is the difference between the concentration c_i in the bulk phase and the concentration $c_{p,i}$ on the particle surface, which in the case of the lumped rate model is identical to the concentration inside the whole network of particle pores.

In Eq. (6.84), the main resistance is modeled to lie within the liquid boundary layer surrounding the walls of the particle pores.

Several modifications of this model can be found in the literature. One that is frequently used considers the mass transfer resistance in the solid phase to be rate limiting. As proposed by Glueckauf and Coates (1947), an analogue lumped kinetic model applying a linear driving force approach for the mass transfer in the solid can be derived. The driving force is modeled as the difference between the overall solid loading of Eq. (6.45) and an additional hypothetical loading q_{eq}, which is in equilibrium with the liquid-phase concentration:

$$\frac{\partial q_i^*}{\partial t} = k_{eff,s,i} \cdot \frac{3}{r_p} \cdot (q_i^{*eq}(c_1, c_2, \dots, c_n) - q_i^*) \quad i = 1, n \tag{6.85}$$

For linear isotherms ($q_i = H_i \cdot c_i$), Eqs. (6.84) and (6.85) are equivalent using the following relationships between the transport coefficients:

$$k_{eff,i} = [\varepsilon_p + (1 - \varepsilon_p) \cdot H_i] \cdot k_{eff,s,i} \tag{6.86}$$

and

$$q_i^{*eq} = [\varepsilon_p + (1 - \varepsilon_p) \cdot H_i] \cdot c_i \tag{6.87}$$

6.2.5.2 Lumped Finite Adsorption Rate Model

Another subgroup of the lumped rate approach consists of considering besides axial dispersion the reaction dispersion model where in addition the adsorption kinetics are rate limiting. It is an extension of the reaction model (Section 6.2.4.2). Like the mass transfer coefficient in the TDM, the adsorption and desorption rate constants are considered as effective lumped parameters, $k_{\mathrm{ads,eff}}$ and $k_{\mathrm{des,eff}}$. Since no film transfer resistance is considered ($c_{\mathrm{p},i} = c_i$), the solid-phase material balance can be described by Eq. (6.88):

$$\frac{\partial q_i^*}{\partial t} = k_{\mathrm{ads,eff},i} \cdot q_{\mathrm{sat},i} \cdot \left(1 - \sum_{j=1}^{n} \frac{q_j^*}{q_{\mathrm{sat},j}}\right) \cdot c_i - k_{\mathrm{des,eff},i} \cdot q_i^* \tag{6.88}$$

and the material balance of the mobile phase by: (6.83)

$$\frac{\partial c_i}{\partial t} + u_{\mathrm{int,e}} \cdot \frac{\partial c_i}{\partial x} + \frac{1 - \varepsilon_{\mathrm{e}}}{\varepsilon_{\mathrm{e}}} \cdot \left(\varepsilon_{\mathrm{p}} \frac{\partial c_i}{\partial t} + (1 - \varepsilon_{\mathrm{p}})\frac{\partial q_i}{\partial t}\right) = D_{\mathrm{ax}} \cdot \frac{\partial^2 c_i}{\partial x^2} \tag{6.89}$$

6.2.6 General Rate Models

General rate models (GRM) are the most detailed continuous models considered in this book. In addition to axial dispersion, they incorporate a minimum of two other parameters describing mass transport effects. These two parameters may combine mass transfer in the liquid film and inside the pores as well as surface diffusion and adsorption kinetics in various kinds. Only a small representative selection of the abundance of different models suggested is given here in order to provide an overview. Alternatives not considered can be easily derived in a straightforward manner.

The underlying basic equations needed within a comprehensive approach using film transport, pore diffusion, surface diffusion, and adsorption kinetics (Berninger et al. 1991; Whitley, Van Cott, and Wang 1993; Ma, Whitley, and Wang 1996) were discussed in Section 6.2.2.

In contrast to the models presented in Sections 6.2.3 to 6.2.5, radial mass transport inside the particle pores is here also taken into account, which results in concentration and loading distributions along the particle radius. Hence, averaged concentrations in Eqs. (6.31)–(6.33) have to be calculated using Eqs. (6.34) and (6.35).

The mass balance in the liquid phase (Eq. (6.20)) includes accumulation (Eq. (6.30)), convection (Eq. (6.38)), axial dispersion (Eq. (6.39)), and (external) mass transfer through the liquid film outside the particles (Eq. (6.45)):

$$\frac{\partial c_i}{\partial t} + u_{\mathrm{int,e}} \cdot \frac{\partial c_i}{\partial x} + \frac{1 - \varepsilon_{\mathrm{e}}}{\varepsilon_{\mathrm{e}}} \cdot \frac{3}{r_{\mathrm{p}}} \cdot k_{\mathrm{film},i} \cdot (c_i - c_{\mathrm{p},i}(r = r_{\mathrm{p}})) = D_{\mathrm{ax}} \cdot \frac{\partial^2 c_i}{\partial x^2} \tag{6.90}$$

The differential mass balances for the pores (Eq. (6.22)) and the solid (Eq. (6.23)) are formulated together with Eqs. (6.40) and (6.41) as well as Eqs. (6.48) and (6.49) as

$$\frac{\partial c_{\mathrm{p},i}(r)}{\partial t} = \frac{1}{r^2} \cdot \frac{\partial}{\partial r}\left(r^2 \cdot D_{\mathrm{pore},i} \cdot \frac{\partial c_{\mathrm{p},i}(r)}{\partial r}\right) - \frac{1 - \varepsilon_{\mathrm{p}}}{\varepsilon_{\mathrm{p}}} \cdot \psi_{\mathrm{ads/des},i}(r) \tag{6.91}$$

$$\frac{\partial q_i(r)}{\partial t} = \frac{1}{r^2} \cdot \frac{\partial}{\partial r}\left(r^2 \cdot D_{\text{solid},i} \cdot \frac{\partial q_i(r)}{\partial r}\right) + \psi_{\text{ads/des},i}(r) \tag{6.92}$$

The internal mass transfer is modeled with Fick's diffusion inside the (macro) pores (Eq. (6.91)) as well as surface or micropore diffusion in the solid phase (Eq. (6.92)). Note that Eqs. (6.91) and (6.92) represent the balance in one particle.

Equation (6.49) quantifies the net adsorption rate based on the solid phase volume, assuming a classical kinetic expressions with saturation capacities $q_{\text{sat},i}$.

If rapid adsorption rates can be assumed, the assumption of local adsorption equilibrium (Section 6.2.2.7) is normally valid. In this case, Eq. (6.49) formally reduces to an isotherm relationship connecting pore concentrations and solid loading. As mentioned in Section 6.2.2.7, the two balances in the stationary phase (Eqs. (6.22) and (6.23)) and the adsorption kinetics (Eq. (6.49)) can then be replaced by an isotherm equation and the overall material balance for one particle (Eq. (6.24)). The latter can be derived analogous to Eqs. (6.91) and (6.92), leading to

$$\varepsilon_{\text{p}}\frac{\partial c_{\text{p},i}}{\partial t} + (1 - \varepsilon_{\text{p}})\frac{\partial q_i}{\partial t} = \frac{1}{r^2} \cdot \frac{\partial}{\partial r}\left[r^2 \cdot \left(\varepsilon_{\text{p}} \cdot D_{\text{pore},i} \cdot \frac{\partial c_{\text{p},i}}{\partial r} + (1 - \varepsilon_{\text{p}}) \cdot D_{\text{solid},i} \cdot \frac{\partial q_i}{\partial r}\right)\right] \tag{6.93}$$

Gu, Tsai, and Tsao (1990a) and Gu et al. (1990b) proposed an even more reduced GRM, which only considers pore diffusion inside the particles (pore diffusion model). Then, Eq. (6.93) can be replaced by Eq. (6.94):

$$\varepsilon_{\text{p}}\frac{\partial c_{\text{p},i}}{\partial t} + (1 - \varepsilon_{\text{p}})\frac{\partial q_i}{\partial t} = \varepsilon_{\text{p}} \cdot \frac{1}{r^2} \cdot \frac{\partial}{\partial r}\left(r^2 \cdot D_{\text{pore},i} \cdot \frac{\partial c_{\text{p},i}}{\partial t}\right) \tag{6.94}$$

Not considering an established adsorption equilibrium between $c_{\text{p},i}$ and q_i, adsorption kinetics were included later (Gu, Tsai, and Tsao 1991, 1993; Gu 2015). The approach by Gu et al., neglecting surface diffusion, is justified for so-called "low-affinity" adsorbents in adsorption chromatography, where transport by free pore diffusion dominates surface diffusion (Furuya, Takeuchi, and Noll 1989). Only for adsorbents with a pronounced micropore system ("high-affinity" adsorbents) surface diffusion can dominate over pore diffusion, and the more comprehensive model consisting of Eqs. (6.90)–(6.92) must be used. In such high-affinity adsorbents, the loadings are several orders of magnitudes higher than in particles applied in "normal" adsorption chromatography. The resulting high loading gradients can lead to a dominance of surface diffusion (Ma, Whitley, and Wang 1996), although the transport coefficient D_{solid} is lower by orders of magnitude compared with D_{pore} (Suzuki 1990).

Note that Eqs. (6.93) and (6.94) are identical if the pore diffusion coefficient is taken as a lumped concentration-dependent parameter that includes pore and surface diffusion:

$$D_{\text{app,pore},i} = D_{\text{pore},i} + \frac{1 - \varepsilon_{\text{p}}}{\varepsilon_{\text{p}}} \cdot D_{\text{solid},i} \cdot \frac{\partial q_i}{\partial c_{\text{p},i}} \tag{6.95}$$

Applying GRM, boundary conditions for the adsorbent phase are necessary in addition to boundary conditions at the column inlet and outlet (Section 6.2.7).

The choice of appropriate boundary conditions is mathematically subtle and often a cause for discussion in the literature. The following boundary condition can be frequently used in solving the "complete" GRM (Ma, Whitley, and Wang 1996).

Owing to symmetry, the concentration and loading gradients vanish at the particle center:

$$\left.\frac{\partial c_{\mathrm{p},i}}{\partial r}\right|_{r=0} = \left.\frac{\partial q_i}{\partial r}\right|_{r=0} = 0 \tag{6.96}$$

The links between liquid, pore, and solid phase are given by mass balances at the particle boundary. Equation (6.46) connects the external mass transfer rate and the diffusion inside all particles, which after insertion of Eqs. (6.40, 6.41, 6.45), and (6.45) results in

$$k_{\mathrm{film},i} \cdot (c_i - c_{\mathrm{p},i}(r = r_\mathrm{p})) = \varepsilon_\mathrm{p} \cdot D_{\mathrm{pore},i} \left.\frac{\partial c_{\mathrm{p},i}}{\partial r}\right|_{r=r_\mathrm{p}} + (1 - \varepsilon_\mathrm{p}) \cdot D_{\mathrm{solid},i} \left.\frac{\partial q_i}{\partial r}\right|_{r=r_\mathrm{p}} \tag{6.97}$$

The set of boundary conditions is completed by recognizing that no surface diffusion exists outside the particles and, therefore, the gradient of the corresponding flux is zero:

$$\left.\frac{\partial \dot{m}_{\mathrm{diff,solid},i}}{\partial r}\right|_{r=r_\mathrm{p}} = \left.\frac{\partial}{\partial r}\left(\frac{\partial q_i}{\partial r}\right)\right|_{r=r_\mathrm{p}} = \left.\frac{\partial^2 q_i}{\partial r^2}\right|_{r=r_\mathrm{p}} = 0 \tag{6.98}$$

Considering Eq. (6.92), the corresponding boundary condition is

$$\left.\frac{\partial q_i}{\partial t}\right|_{r=r_\mathrm{p}} = D_{\mathrm{solid},i} \cdot \frac{3}{r_\mathrm{p}} \cdot \left.\frac{\partial q_i}{\partial r}\right|_{r=r_\mathrm{p}} + \psi_i|_{r=r_\mathrm{p}} \tag{6.99}$$

6.2.7 Initial and Boundary Conditions of the Column

Mathematically, all models form systems of partial differential and algebraic equations. For the solution of such systems, initial and boundary conditions for the chromatographic column are necessary. The initial conditions for the concentration and the loading specify their values at time $t = 0$. Frequently, not preloaded (fully regenerated) columns are assumed:

$$c_i = c_i(t = 0) = 0$$
$$c_{\mathrm{p},i} = c_{\mathrm{p},i}(t = 0, r) = 0$$
$$q_i = q_i(t = 0, r) = 0 \tag{6.100}$$

Since no adsorbent enters or leaves the column, suitable inlet and outlet boundary conditions have to be provided only for the mass balance of the mobile phase (Eq. (6.20)).

One condition frequently applied at the column inlet is the classical "closed boundary" condition for dispersive systems derived by Danckwerts (1953):

$$c_i(t, x = 0) = c_{\mathrm{in},i} - \frac{D_{\mathrm{ax}}}{u_{\mathrm{int,e}}} \cdot \frac{\partial c_i(t, x = 0)}{\partial x} \tag{6.101}$$

In general, the overall balance for the mass transport streams (Eqs. (6.38) and (6.39)) at the column inlet and outlet has to be fulfilled. In Eq. (6.101), the closed boundary condition is obtained by setting the dispersion coefficient outside the column equal to zero. In open systems, the column stretches to infinity, and in these limits, concentration changes are zero.

For real chromatographic systems, the dispersion coefficient is usually small as the number of stages is very high ($N > 100$) and convection dominates. Therefore, Eq. (6.101) may be simplified to the Dirichlet type of boundary conditions:

$$c_i(t, x = 0) = c_{\text{in},i}(t) \tag{6.102}$$

A common condition of the inlet function (the injection profile) is a rectangular pulse (Section 6.3.2.1), that is, an injection of a constant feed concentration c_{feed} for a given injection time period, t_{inj}:

$$c_{\text{in},i}(t) = \begin{cases} c_{\text{feed},i}, & t \leq t_{\text{inj}} \\ 0, & t > t_{\text{inj}} \end{cases} \tag{6.103}$$

For the outlet boundary condition, typically a zero gradient of the fluid concentration is assumed (Danckwerts 1953):

$$\frac{\partial c_i(t, x = L_{\text{c}})}{\partial x} = 0 \tag{6.104}$$

Notably, Eq. (6.102) is in any case the "correct" inlet condition for all models without axial dispersion and is therefore often convenient to use. In practice, the difference between the solutions for different boundary conditions is typically irrelevant for highly efficient columns (Guiochon et al. 2006). Within numerical simulations, the effect of different boundary conditions can be easily evaluated.

In the case of applying several columns, eventually operated in a periodic manner (as, e.g. in the SMB processes, described in Chapter 5), the incorporation of the process-dependent correct specific boundary and initial conditions is of large importance.

6.2.8 Dimensionless Model Equations

To reduce the number of parameters and to analyze their interdependence, it is instructive to convert the model equations as well as the boundary conditions into a dimensionless form. This is demonstrated below for the most important quantities.

Feed concentrations $c_{\text{feed},i}$ are suitable reference states for concentrations and loadings:

- Dimensionless fluid concentrations:

$$C_{\text{DL},i} = \frac{c_i}{c_{\text{feed},i}} \Rightarrow \partial C_{\text{DL},i} = \frac{1}{c_{\text{feed},i}} \cdot \partial c_i \tag{6.105}$$

- Dimensionless concentration in the pores of the particles:

$$C_{\text{p,DL},i} = \frac{c_{\text{p},i}}{c_{\text{feed},i}} \Rightarrow \partial C_{\text{p,DL},i} = \frac{1}{c_{\text{feed},i}} \cdot \partial c_{\text{p},i} \tag{6.106}$$

- One possibility to introduce dimensionless loadings:

$$Q_{\mathrm{DL},i} = \frac{q_i}{c_{\mathrm{feed},i}} \Rightarrow \partial Q_{\mathrm{DL},i} = \frac{1}{c_{\mathrm{feed},i}} \cdot \partial q_i \tag{6.107}$$

A dimensionless axial coordinate Z is obtained by division through the column length:

$$Z = \frac{x}{L_{\mathrm{c}}} \Rightarrow dx = L_{\mathrm{c}} \cdot dZ \tag{6.108}$$

and a dimensionless time t can be defined as one option using the column dead time $t_{0,\mathrm{e}}$:

$$\tau = \frac{t}{t_{0,\mathrm{e}}} = \frac{u_{\mathrm{int,e}}}{L_{\mathrm{c}}} \cdot t \Rightarrow d\tau = \frac{u_{\mathrm{int,e}}}{L_{\mathrm{c}}} \cdot dt \tag{6.109}$$

Dimensionless parameters represent ratios of different mass transport phenomena. One example is the axial Péclet number, which is the ratio of convection rate to axial dispersion:

$$Pe_{\mathrm{e}} = \frac{u_{\mathrm{int,e}} \cdot L_{\mathrm{c}}}{D_{\mathrm{ax}}} \tag{6.110}$$

Additional parameters can be useful depending on the model selected and the physical effects that are taken into account. Parameters appropriate for the GRM are given, for example, by Berninger et al. (1991) and Ma, Whitley, and Wang (1996).

Introducing Eqs. (6.105)–(6.109) into the equations of the TDM leads to the following dimensionless mass balances:

$$\frac{\partial C_{\mathrm{DL},i}}{\partial \tau} + \frac{\partial C_{\mathrm{DL},i}}{\partial Z} + \frac{1 - \varepsilon_{\mathrm{e}}}{\varepsilon_{\mathrm{e}}} \cdot \left(\varepsilon_{\mathrm{p}} \frac{\partial C_{\mathrm{DL},i}}{\partial \tau} + (1 - \varepsilon_{\mathrm{p}}) \frac{\partial Q_{\mathrm{DL},i}}{\partial \tau} \right) = \frac{1}{Pe_{\mathrm{e}}} \cdot \frac{\partial^2 C_{\mathrm{DL},i}}{\partial Z^2} \tag{6.111}$$

$$\varepsilon_{\mathrm{p}} \frac{\partial C_{\mathrm{DL},i}}{\partial \tau} + (1 - \varepsilon_{\mathrm{p}}) \frac{\partial Q_{\mathrm{DL},i}}{\partial \tau} = \frac{L_{\mathrm{c}}}{u_{\mathrm{int,e}}} \cdot \frac{6}{d_{\mathrm{p}}} \cdot k_{\mathrm{eff},i} \cdot (C_{\mathrm{DL},i} - C_{\mathrm{p,DL},i}) \tag{6.112}$$

The rate parameter in Eq. (6.112) determines the ratio of effective mass transport to convection, which is quantified by a modified effective Stanton number (St_{eff}):

$$St_{\mathrm{eff},i} = k_{\mathrm{eff},i} \cdot \frac{6}{d_{\mathrm{p}}} \cdot \frac{L_{\mathrm{c}}}{u_{\mathrm{int}}} \tag{6.113}$$

This finally leads to a system of differential equations that depend only on two dimensionless parameters, namely, the Péclet and Stanton numbers:

$$\frac{\partial C_{\mathrm{DL},i}}{\partial \tau} + \frac{\partial C_{\mathrm{DL},i}}{\partial Z} + \frac{1 - \varepsilon}{\varepsilon} \cdot \left(\varepsilon_{\mathrm{p}} \frac{\partial C_{\mathrm{p,DL},i}}{\partial \tau} + (1 - \varepsilon_{\mathrm{p}}) \frac{\partial Q_{\mathrm{DL},i}}{\partial \tau} \right) = \frac{1}{Pe} \cdot \frac{\partial^2 C_{\mathrm{DL},i}}{\partial Z^2} \tag{6.114}$$

$$\varepsilon_{\mathrm{p}} \frac{\partial C_{\mathrm{p,DL},i}}{\partial \tau} + (1 - \varepsilon_{\mathrm{p}}) \frac{\partial Q_{\mathrm{DL},i}}{\partial \tau} = St_{\mathrm{eff},i} \cdot (C_{\mathrm{DL},i} - C_{\mathrm{p,DL},i}) \tag{6.115}$$

In addition to the mass balances, the isotherm equations and the boundary conditions have to be transformed into a dimensionless form. Equation (6.116), for example, presents the dimensionless form of the multicomponent Langmuir equation (Eq. (2.48)) for a binary mixture:

$$Q_{\text{DL},i} = \frac{H_i \cdot C_{\text{p,DL},i}}{1 + b_1 \cdot c_{\text{feed},1} \cdot c_{\text{p,DL},1} + b_2 \cdot c_{\text{feed},2} \cdot c_{\text{p,DL},2}}, \quad \text{with } H_i = q_{\text{sat},i} \cdot b_i$$

(6.116)

The parameters of this equation are the Henry coefficients H_i and the dimensionless Langmuir parameters $b_1 c_{\text{feed},1}$ and $b_2 c_{\text{feed},2}$.

Conversion of the boundary condition at the column inlet (Eq. (6.103)) leads to

$$C_{\text{DL,in},i}(t) = \begin{cases} 1, \ \tau \leq \dfrac{t_{\text{inj}}}{t_{0,\text{e}}} = \dfrac{t_{\text{inj}} \cdot \dot{V}}{\varepsilon_{\text{e}} \cdot V_{\text{c}}} \\[4mm] 0, \ \tau > \dfrac{t_{\text{inj}}}{t_{0,\text{e}}} \end{cases}$$

(6.117)

where $t_{\text{inj}}/t_{0,\text{e}}$ is a dimensionless injection time.

The application of dimensionless mass balance equations significantly supports evaluating the effect of specific kinetic parameters.

6.2.9 Comparison of Different Model Approaches

The above described models for simulating chromatographic processes differ in their structure and number of free parameters. Since their essential task is to describe correctly the main features of elution profiles, a simple basis for comparison is given by evaluating a smaller number of moments corresponding to these models. Matching the moments allows identifying essential connections between the specific model parameters. Hereby, a clear and simple hierarchy holds regarding the importance of the specific moments. The lower the order of the moments, the more important it is to match by a model the corresponding experimental situation. Thus, a violation of the zeroth moments, which signify the mass balances, is least tolerable:

$$\mu_0' = \int_0^\infty c(t) \cdot \text{d}t$$

(6.118)

The very important quantity, captured by the first initial moment μ_1', is the position of fronts or the mean retention time t_{R}:

$$\mu_1' = \frac{1}{\mu_0} \int_0^\infty t^1 \cdot c(t) \cdot \text{d}t$$

(6.119)

Next, and frequently exploited in chromatography comes the peak or front dispersion captured by the second central moment μ_2 and designated frequently as the variance σ^2:

$$\mu_2 = \frac{1}{\mu_0} \int_0^\infty (t - \mu_1')^2 \cdot c(t) \cdot \text{d}t = \sigma^2$$

(6.120)

The strong and remarkable equivalence between the solution of the equilibrium dispersion model (Eq. (6.79)) and the analytical solutions introduced above for the two discrete model proposed by Craig (Eq. (6.7)) and Martin and Synge (Eq. (6.17)) is illustrated in Figure 6.8 together with depicting the corresponding Gaussian distribution (Eq. (6.12)). The parameters selected are typical for lab-scale analytical high-performance liquid chromatography (HPLC) situations. The basis for comparison is matching the plate numbers and dispersion coefficients to generate the same second moments σ, i.e. to describe the same degree of band broadening around the mean retention time t_R (which does not depend on kinetic parameters). To perform the comparison, at first the equilibrium stage numbers of the cascade model of Martin and Synge model was set. To illustrate the effect, two values were considered, namely, $N = N_{casc} = 10$ and $N = N_{casc} = 100$. The second moment is then

$$\sigma_{casc}^2 = \frac{t_R^2}{N_{casc}} \tag{6.121}$$

With this second moment, a corresponding stage numbers of the Craig model, N_{Craig}, can be specified:

$$N_{Craig} = \frac{t_R^2}{\sigma_{casc}^2} \frac{k'}{1 + k'} = N_{casc} \frac{k'}{1 + k'} \tag{6.122}$$

The corresponding apparent axial dispersion coefficients of the equilibrium dispersion model, $D_{app,t}$, result from the second moment of this model as follows:

$$D_{app,t} = \frac{u_{int,t}^{hypo} L_c}{2 N_{casc}} \tag{6.123}$$

Finally, the corresponding Gaussian distribution, which provides the limiting case for all three models discussed, simply needs to assume

$$\sigma_{Gauss} = \sigma_{casc} \tag{6.124}$$

The results in Figure 6.8 reveal the strong similarity between the different models. The still visible difference for an equilibrium stage number of $N = 10$ (top) almost completely vanishes for larger efficiencies. For $N = 100$ (bottom) the predictions can be hardly distinguished. This strongly support the fact that different models are capable of describing real elution profiles to a similar degree of precision, provided the parameters applied in the models are chosen in a way that the lower order models are captured correctly. This offers an excellent basis for estimating free parameters from experimentally determined moments as discussed below in Section 7.6.2.

Matching the second moments guarantees already a good basis for reliable modeling of chromatographic processes. Higher precision requires conserving higher moments. The general formula to calculate a moment of order m is

$$\mu_m = \frac{1}{\mu_0} \int_0^\infty (t - \mu_1')^m \cdot c(t) \cdot dt \tag{6.125}$$

Of practical relevance are typically just the central moments μ_3 and μ_4, which signify the still observable quantities skewness and kurtosis. To require from a
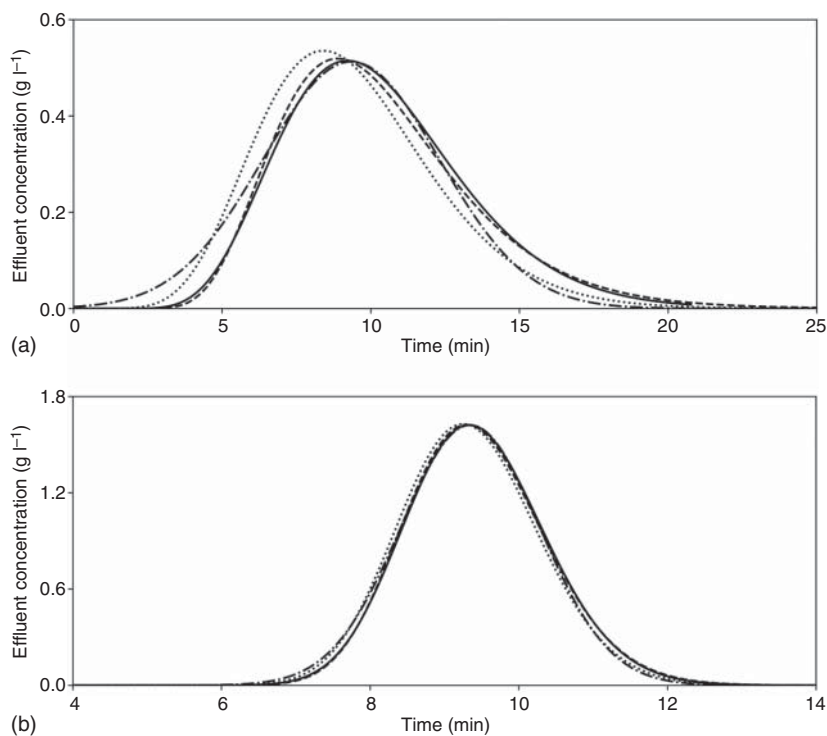
Figure 6.8 Comparison between the analytical solutions valid for linear isotherms for the two discrete equilibrium stage models (Craig, Eq. (6.7), solid line) and (Martin and Synge, Eq. (6.18), dotted line), the continuous equilibrium dispersion model (Eq. (6.79), dashed line) and the Gaussian distribution (Eq. (6.12), dotted-dashed line). Parameters: $H = 3.5$, $d_c = 0.46$ cm (or $A_c = 0.166$ cm^2), $L_c = 25$ cm, $\varepsilon_t = 0.5$, $\dot{V} = 1$ ml min^{-1}, $u_{int,t}^{hypo} = 12$ cm min^{-1}, $t_{0,t} = 2.08$ min, $t_R = 9.36$ min, $m_{inj} = 4$ mg. (a) $N = 10$ (or $D_{app,t} = 15$ cm^2 min^{-1}). (b) $N = 100$ (or $D_{app,t} = 1.5$ cm^2 min^{-1}).

model that represents correctly moments of higher order than four is very ambitious and typically not a realistic goal.

If linear adsorption isotherms are assumed, analytical solutions for the higher moments can be obtained exploiting the properties of the Laplace transform technique. After deriving for a specific model, an analytical solution for the continuous effluent concentration profile $c(t)$ in the Laplace domain as $C(s)$ the generation of explicit expressions for the initial moments is based on the following relation (Van der Laar 1958):

$$\mu_0 = \lim_{s \to 0} C(s) \text{ and } \mu'_m = (-1)^m \lim_{s \to 0} \frac{d^m C(s)}{ds^m} \tag{6.126}$$

Then, the central moments of the orders 2, 3, and 4 can be derived from the initial moments as follows:

$$\mu_2 = \mu'_2 - (\mu_2)^2$$
$$\mu_3 = \mu'_3 - 3\mu'_1\mu'_2 + 2(\mu'_1)^3$$
$$\mu_4 = \mu'_4 - 4\mu'_1\mu'_3 + 6 - 4\mu'^2_1\mu'_2 - 3(\mu'_1)^3 \tag{6.127}$$

Applying this approach it is possible to derive the moments for very general and flexible models discussed above. An example is given for the GRM assuming infinitely fast adsorption rates (Section 6.2.6), $\psi_{\text{reac}} = 0$; details are given, e.g. by Qamar et al. (2019).

For the first thermodynamically controlled initial moment holds:

$$\mu_1' = t_{\text{R}} = t_{0,\text{e}}(1 + F_{\text{e}}H^*) \tag{6.128}$$

with the adsorption equilibrium constant and the phase ratio defined as follows:

$$H^* = \varepsilon_{\text{p}} + (1 - \varepsilon_{\text{p}})H = \frac{q^*}{c}$$

$$F_{\text{e}} = \frac{1 - \varepsilon_{\text{e}}}{\varepsilon_{\text{e}}} \tag{6.129}$$

The next three higher moments corresponding to the GRM are

$$\mu_2 = \sigma^2 = \frac{2}{Pe}(1 + F_{\text{e}}H^*)^2 + 2F_{\text{e}}H^{*2}\left(\frac{F_{\text{e}}}{\xi} + \frac{1}{15\eta}\right) \tag{6.130}$$

$$\mu_3 = \frac{12}{Pe^2}(1 + F_{\text{e}}H^*)^3 + \frac{6(1 + F_{\text{e}}H^*)F_{\text{e}}}{Pe}\left(\frac{2F_{\text{e}}H^{*2}}{\xi} + \frac{2H^{*2}}{15\eta}\right)$$

$$+ F_{\text{e}}H^{*3}\left(\frac{4}{105\eta^2} + \frac{4F_{\text{e}}}{5\xi\eta} + \frac{6F_{\text{e}}^2}{\xi^2}\right) \tag{6.131}$$

$$\mu_4 = \frac{12}{Pe^4}(1 + F_{\text{e}}H^*)^4(Pe^2 + 10Pe) - \frac{4}{175}\frac{F_{\text{e}}^2 H^{*4}(2 + Pe)}{\eta^2 Pe}$$

$$+ \frac{24(1 + F_{\text{e}}H^*)^2 F_{\text{e}}H^{*2}}{Pe^4}\left(\frac{F_{\text{e}}}{\xi} + \frac{1}{15\eta}\right)(Pe^2 + 6Pe)$$

$$+ \frac{2F_{\text{e}}H^{*3}}{Pe}\left(\frac{4}{105\eta^2} + \frac{4F_{\text{e}}}{5\xi\eta} + \frac{6F_{\text{e}}^2}{\xi^2}\right)[4 + F_{\text{e}}H^*(6 * Pe)]$$

$$+ 8F_{\text{e}}H^{*4}\left(\frac{1}{525\eta^3} + \frac{9F_{\text{e}}}{175\xi\eta^2} + \frac{3F_{\text{e}}^2}{5\xi^2\eta} + \frac{3F_{\text{e}}^2}{\xi^3}\right) \tag{6.132}$$

with the three dimensionless parameters η, ξ, and Pe containing the three kinetic parameters D_{ax}, k_{film}, and $D_{\text{app,pore}}$:

$$\eta = \frac{D_{\text{app,pore}}L_{\text{c}}}{r_{\text{p}}^2 u_{\text{int,e}}}, \quad \xi = 3F_{\text{e}}\frac{k_{\text{film}}L_{\text{c}}}{r_{\text{p}}u_{\text{int,e}}}, \quad Pe = \frac{u_{\text{int,e}}L_{\text{c}}}{D_{\text{ax}}} \tag{6.133}$$

Similar expressions for the moments of other less general and even more complex 2D models are found, e.g. in Qamar et al. (2015) and Qamar and Seidel-Morgenstern (2016).

Depending on the specific kinetic parameters applied, different values for the moments will be predicted. In order to minimize the differences between the models, it is a standard approach to consider first the second central moments. This provides explicit relations, which must hold between the parameters belonging to different models. This can be illustrated considering in comparison with the GRM the simpler lumped kinetic model with a solid-phase linear

driving force (Section 6.2.5), which contains besides D_{ax} just the lumped kinetic parameters $k_{eff,s}$. The corresponding second moment of this lumped kinetic model is

$$\mu_2 = \sigma^2 = \frac{2}{Pe}(1 + F_e H^*)^2 + \frac{2F_e^{\,2}H^{*2}\varepsilon_e}{k_{eff,s}} \qquad (6.134)$$

Thus, matching the two second moments of the GRM (Eq. (6.130)) and the solid-phase lumped kinetic model (Eq. (6.134)) requires that the following relation is fulfilled between the specific model parameters:

$$k_{eff,s} = \frac{F_e^{\,*}\varepsilon_e}{H^*\left(\frac{F_e}{\xi} + \frac{1}{15\eta}\right)} = \frac{1 - \varepsilon_e}{H^*}\frac{u_{int,e}}{L_c}\left[\left(\frac{r_p}{3k_{film}} + \frac{r_p^2}{15D_{app,pore}}\right)\right]^{-1} \qquad (6.135)$$

Matching the next (but less relevant) third moments is also possible; however, it would lead to other relations between the parameters. Qamar et al. (2019) summarized this for other combinations of moments and different models.

In summary, all models presented in section 6.2 are capable of representing main feature of chromatography. Besides the adsorption isotherms, it is mainly required to represent the kinetics of the process properly by having correctly adjusted the corresponding model parameters. For this, a column can be conveniently characterized by a number of stages N, which can be obtained either from the column manufacturer or by a few simple preliminary experiments (Sections 2.2.3 and 7.6.2, Golshan-Shirazi and Guiochon 1992; Seidel-Morgenstern 1995; Guiochon et al. 2006).

Finally, the following facts should be emphasized:

- Influences of finite adsorption kinetics can be typically neglected.
- The ideal equilibrium model provides a very good accuracy only if the column efficiency is very high ($N \gg 1000$).
- The equilibrium dispersion model offers an acceptable accuracy for $N \gg 100$, which may be sufficient for many practical cases.
- For most practical applications, it is not necessary to use two parameters to describe mass transfer and a lumped rate model using only one parameter sufficient (Ludemann-Hombourger, Bailly, and Nicoud 2000).
- If the number of stages is lower than 50, more detailed models have to be applied to described the band shapes accurately.
- As increasing computational power and sophisticated numerical solvers are now available, it is no longer necessary to use oversimplified models to reduce computing time. However, it will not improve the quality of predictions if more complex models with incorrect parameters are used.

Table 6.1 provides a summary and gives recommendations for the application of the models discussed.

Table 6.1 Fields of application of different continuous models available to simulate chromatographic processes.

Model	Recommended application
Equilibrium stage models	• Attractive for low efficient columns • Accurate only for single components or it there are only small differences in N between the components
Equilibrium (ideal) model	• Considers thermodynamic effects only ($N \gg 1000$) • Useful for rapid process evaluation and design
Equilibrium dispersion model	• Adsorption chromatography for products with low molecular weights • High accuracy only if $N \gg 100$
Transport dispersion model	• Adsorption chromatography for products with low molecular weights • Generally high accuracy
General rate model	• Useful to quantify difficult chiral separations and separation of solutes with complex mass transfer and adsorption behavior (e.g. bioseparations or ion exchange chromatography)

6.3 Including Effects Outside the Columns

6.3.1 Experimental Setup and Simulation Flow Sheet

Section 6.2 presents various models capable of describing front propagation phenomena in chromatographic columns. It has to be kept in mind that these models account only for effects occurring within the packed bed. An HPLC plant, however, consists of several additional equipment and fittings besides the column. Therefore, the effect of this extra-column equipment has to be accounted for to obtain reasonable agreement between experimental results and process simulation. Peripheral equipment (e.g. pipes, injection system, pumps, and detectors) causes dead times and mixing. Thus, it can contribute considerably to the band broadening measured by the detector.

So-called extra-column or plant dispersion effects have to be taken into account by additional mathematical models rather than including them indirectly in the model parameters of the column, for example, by altering the dispersion coefficient. The combination of peripheral and column models can be implemented in a modular simulation approach. In a flow-sheeting approach, the boundary conditions of different models are connected by streams (node balances), and all material balances are solved simultaneously.

Figure 6.9a shows the standard setup of an HPLC plant. Injections of rectangular pulses are performed via a three-way valve and a subsequent pump or a six-port valve with a sample loop. The feed passes the connecting pipes and a flow
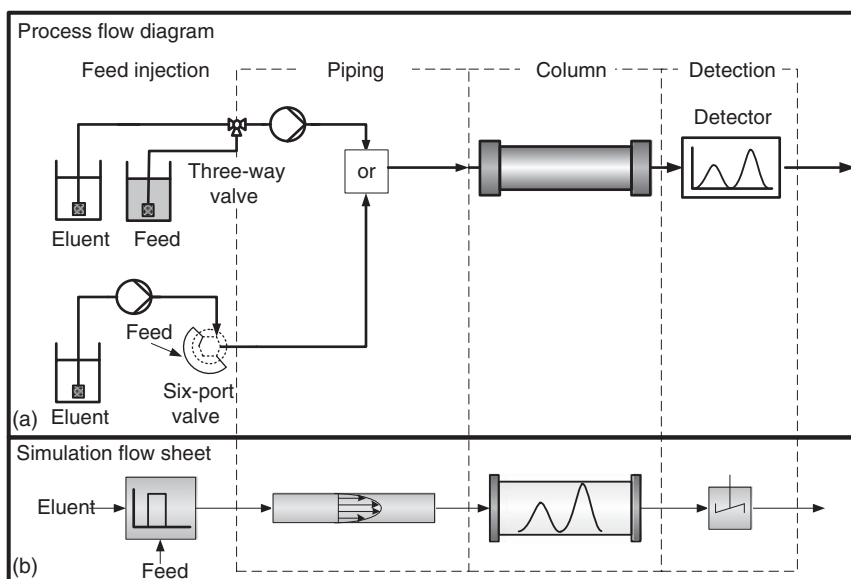
Figure 6.9 Comparison between (a) process flow diagram and (b) simulation flow sheet for an HPLC plant.

distributor before entering the packed bed. At the exit, there are another flow distributor and connecting pipes before a detector records the chromatogram. Because of these additional elements, an exact rectangular pulse will not enter the chromatographic column, and the detected chromatogram is not identical to the concentration profile at the column exit.

As mentioned in Chapters 2 and 4, peak distortion is caused by nonideal equipment not only outside the column but also inside the column. Although sophisticated measurements such as nuclear magnetic resonance (NMR) (Tallarek, Bayer, and Guiochon 1998) allow the investigation of the packed bed only, from a practical viewpoint, the observable performance of a column always includes the effects of walls, internal distributors, and filters. Using the method described in this chapter, these are always contained in certain model parameters (e.g. in D_{ax}). The column manufacturers have to ensure a proper bed packing and flow distribution (Chapter 4), and, thus, negative influence of imperfections on column performance, for example, on D_{ax}, can be assumed to be small. However, the aspect of extra-column effects should always be kept in mind when doing scale-up.

Transformation of the process diagram into a corresponding simulation flow sheet is illustrated in Figure 6.9b. In principle, all plant elements may be represented by separate sub-models. For practical applications, though, it is typically sufficient to take into account only a time delay as well as the dispersion of the peaks until they enter the column. This can be achieved by a pipe flow model that includes axial dispersion. Large volume detectors (including some connecting pipes) can be approximated, if required, by a stirred tank model.

6.3.2 Modeling Extra-Column Equipment

6.3.2.1 Injection System

The injection system is sufficiently described by setting the appropriate boundary conditions at the entry of the pipe, for example, a rectangular pulse:

$$c_{\text{pipe},i}(x = 0, 0 \leq t \leq t_{\text{inj}}) = c_{\text{feed},i}$$
$$c_{\text{pipe},i}(x = 0, t > t_{\text{inj}}) = 0 \tag{6.136}$$

Injection volume and the injection time are related by

$$V_{\text{inj}} = \dot{V} \cdot t_{\text{inj}} \tag{6.137}$$

6.3.2.2 Piping

If the piping only contributes to the dead time of the plant, the delay can be described by a pipe model assuming an ideal plug flow:

$$\frac{\partial c_{\text{pipe},i}}{\partial t} = -u_{0,\text{pipe}} \cdot \frac{\partial c_{\text{pipe},i}}{\partial x} \tag{6.138}$$

When the plant behavior without the column shows non-negligible backmixing, a dispersed plug flow model might be used (Eq. (6.139)):

$$\frac{\partial c_{\text{pipe},i}}{\partial t} = D_{\text{ax,pipe}} \cdot \frac{\partial^2 c_{\text{pipe},i}}{\partial x^2} - u_{0,\text{pipe}} \cdot \frac{\partial c_{\text{pipe},i}}{\partial x} \tag{6.139}$$

The fluid velocity u_0 inside the pipe is given by the continuity equation:

$$u_{0,\text{pipe}} = \frac{\dot{V}}{A_{\text{pipe}}} \tag{6.140}$$

The primary parameters of interest are the pipe volume (Eq. (6.141)) and the correspnding dead time (Eq. (6.142)):

$$V_{\text{pipe}} = A_{\text{pipe}} \cdot L_{\text{pipe}} \tag{6.141}$$

$$t_{0,\text{pipe}} = \frac{V_{\text{pipe}}}{\dot{V}} \tag{6.142}$$

If $t_{0,\text{pipe}}$ is determined from experiments and A_{pipe} is set, all other parameters are known from Eqs. (6.140) to (6.142).

6.3.2.3 Detector

Detectors contain measuring cells that exhibit a backmixing behavior that dominates the influence of the pipe system behind the chromatographic column. Therefore, the whole system behind the column is modeled as an ideal continuously stirred tank (CST):

$$\frac{\partial c_{\text{tank},i}}{\partial t} = \frac{\dot{V}}{V_{\text{tank}}} \cdot (c_{\text{in,tank},i} - c_{\text{tank},i}) \tag{6.143}$$

The dead time of the tank (Eq. (6.144)) is

$$t_{0,\text{tank}} = \frac{V_{\text{tank}}}{\dot{V}} \tag{6.144}$$

Note that the overall dead time of the plant (Eq. (6.145)) is the sum of the dead times of both the pipes and the detector (tank):

$$t_{\text{plant}} = t_{0,\text{pipe}} + t_{0,\text{tank}} \tag{6.145}$$

6.4 Calculation Methods and Software

6.4.1 Analytical Solutions

For the simplest column models under certain simplifying conditions, there are analytical solutions of the model equations available. Related to the equilibria this holds for problems where all components of interest are characterized by linear isotherm equations, in which the Henry constants are not affected by the presence of other component. Then all kinetic effects causing band broadening can be described by a single lumped parameter, for example, the number of theoretical plates. Consequently, the usage of two or more kinetic parameters is not justified. This field of linear or analytical chromatography has been extensively studied and is quite mature (Guiochon et al. 2006; Snyder, Kirkland, and Dolan 2010).

For a number of nonlinear and competitive isotherm models, analytical solutions of the mass balance equations can be provided for only one strongly simplified column model. This is the "ideal model" of chromatography, which considers just convection and neglects all mass transfer processes (Section 6.2.3). Using the method of characteristics within the elegant equilibrium theory, analytical expressions were derived capable to calculate single elution profiles for single components and mixtures (Helfferich and Klein 1970; Helfferich and Carr 1993; Helfferich and Whitley 1996; Helfferich 1997; Rhee, Aris, and Amundson 1970; Rhee, Aris, and Amundson 1986; Rhee, Aris, and Amundson 1989; Guiochon et al. 2006). However, these predictions are typically too optimistic since real columns are not characterized by an infinite efficiency. In many cases, they are however close to real profiles and offer the chance for rapid process design and easy process evaluation.

6.4.2 Numerical Solution Methods

6.4.2.1 Discretization

Discretization "replaces" the continuous space–time domain by a rectangular mesh or grid of discrete elements and points (Figure 6.10). Note that initial and boundary conditions of the system must also be considered.

Because of the discretization, numerical solutions are only approximations of the "true" continuous solutions at discrete points of the space–time domain. The quality of the numerical solution depends on the structure of the discretization method and the number of discretes.

An example of the "errors" introduced by the approximation is the effect of "numerical dispersion," which leads to an additional artificial band broadening. Another example is the occurrence of nonphysical oscillations in the profile. Typically holds that the finer the grid is, the more accurate the numerical approximation becomes and, finally, approaches the true solution. Naturally, a reduced
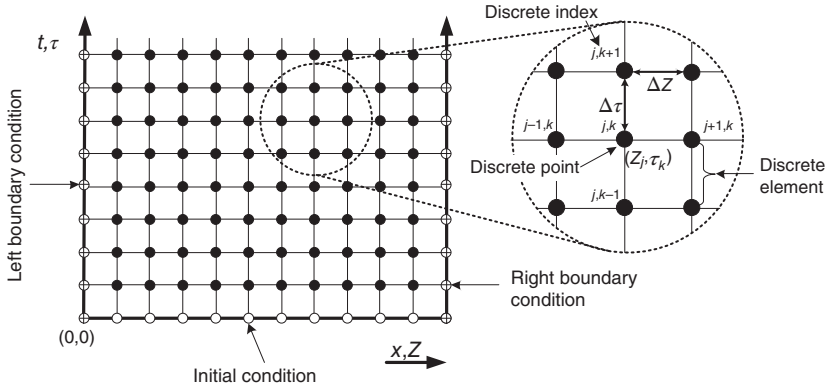
Figure 6.10 Scheme of discretized space–time domain using a uniform grid.

grid spacing requires more equations and longer calculation times. Practically, the grid is "fine enough" if the simulated elution profiles do not change noticeably on using a smaller grid size. Other simple tests for accuracy involve comparison with analytical solutions in special cases or control of fulfillment of the mass balance. Numerical integrations of simulated peaks should not deviate by more than 1% from masses injected (Guiochon and Lin 2003).

For brevity, further discussion is restricted to the spatial discretization used to obtain ODEs. Often, the choice and parameter selection for this method is left to the user of commercial process simulators, while the numerical (time) integrators for ODEs have default settings or sophisticated automatic parameter adjustment routines. For example, using finite difference methods (FDM) for the time domain, an adaptive selection of the time step is performed that is coupled to the iteration needed to solve the resulting nonlinear algebraic equation system. For additional information concerning numerical procedures and algorithms, the reader is referred to the special literature.

FDM are directly derived from the space–time grid. Focusing on the space domain (horizontal lines in Figure 6.10), the spatial differentials are replaced by discrete difference quotients based on interpolation polynomials. Using the dimensionless formulation of the balance equations (Eq. (6.111)), the convection term at a grid point j (Figure 6.10) can be approximated by assuming, for example, the linear polynomial:

$$\frac{\partial C_{\mathrm{DL}}(Z = Z_j)}{\partial Z} \approx \frac{C_{\mathrm{DL},j+1} - C_{\mathrm{DL},j}}{\Delta Z}, \quad \text{with } Z_j = j \cdot \Delta Z \tag{6.146}$$

Figure 6.11 illustrates this approach.

Equation (6.146) is a forward FDM, as grid points "after" j (here $j + 1$) are used for evaluation. It is a first-order scheme, as only one point is used. Higher order schemes involve more neighboring points for the approximation. Therefore, they are generally more accurate and have greater numerical stability. Other FD schemes involve grid points with lower indexes (backward FDM) or points on both sides of j (central FDM). Equation (6.146) illustrates only the principle of discretization. The continuous coordinates are replaced by the corresponding
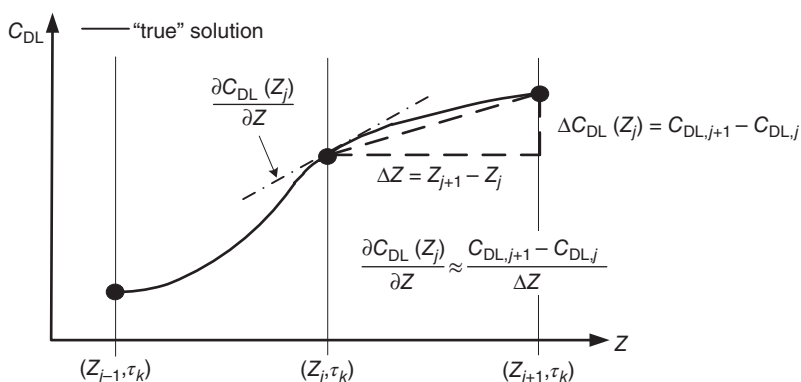
Figure 6.11 Approximation of spatial derivatives by difference quotients.

numbers of grid points (n_p) and the continuous profile $C_{DL}(Z)$ by a vector, with n_p elements $C_{DL,j}$.

The major drawback of (simple) FD schemes is that a rather fine grid, resulting in a large number of equations and hence high computational time, is necessary to obtain a stable and accurate solution, as chromatography is a convection-dominated process. Fewer grid points and shorter computational times can be realized by using UPWIND schemes for the convection term (Du Chateau and Zachmann 1989; Shih 1984). These are either higher order backward FDM or more complex schemes (Leonard 1979).

FDM are point approximations because they focus on discrete points. In contrast, finite element methods focus on the concentration profile inside one grid element. As an example of these segment methods, orthogonal collocation on finite elements (OCFE) is briefly discussed below.

The collocation method is based on the assumption that the solution of the PDE system can be approximated by polynomials of order n. In this method the whole space domain (the column), including the boundary conditions, is approximated by one polynomial using $n + 2$ collocation points. Polynomial coefficients are determined by the condition that the differential equation must be satisfied at the collocation points. This approach allows the spatial derivatives to be described by the known derivatives of the polynomials and transforms the PDE into an ODE system.

Mathematical methods exist that guarantee an "optimal" placement of the collocation points. In orthogonal collocation (OC), the collocation points are equal to the zero points of the orthogonal polynomials.

The OCFE method (Villadsen and Stewart 1967) is derived straightforwardly by dividing the column into n_e elements (Figure 6.12). For each element an own orthogonal solution polynomial is used, leading to an ODE system for the column with $(n + 2)n_e$ equations. The element boundaries are connected by setting equal values and slopes for the adjacent polynomials at the boundary points, which guarantees the continuity of the concentration profile.

Finite element methods proved to be a good choice for various column models (Guiochon, Golshan-Shirazi, and Katti 1994; Seidel-Morgenstern 1995;
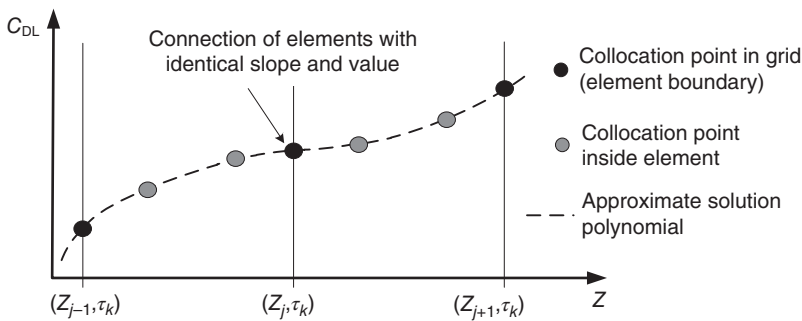
Figure 6.12 Representation of the numerical solution by the OCFE method for a second-order polynomial.

Kaczmarski et al. 1997; Lu and Ching 1997; Berninger et al. 1991). Comparisons show that they are, for the type of models discussed here, to be preferred to difference methods, especially if high accuracy is needed (Dünnebier 2000; Finlayson 1980; Guiochon and Lin 2003).

Newer works report successful application of spatial discretization using finite volumes and the weighted essentially non-oscillatory (WENO) method (von Lieres and Andersson 2010), high-resolution finite volume schemes (Javeed et al. 2011a), and a discontinuous Galerkin method (Javeed et al. 2011b).

6.4.2.2 General Solution Procedure and Software

The balance equations described in Sections 6.2 and 6.3 include both space and time derivatives. Apart from a few simple cases, the resulting set of coupled PDE cannot be solved analytically. The solution (the concentration profiles) must be obtained numerically using either self-developed programs or commercially available dynamic process simulation tools. The latter can be distinguished in general equation solvers, where the model has to be implemented by the user, or special software dedicated to chromatography. Some providers are given in Table 6.2.

The generalized numerical solution procedure typically involves the following steps:

(1) Transformation of the PDE system into ODEs with respect to time by discretization of the spatial derivatives;
(2) Solving the ODEs using numerical integration routines, which generally involve another discretization into a nonlinear algebraic equation system and subsequent iterative solution.

The stability, accuracy, and speed of the solution process depend on the choice and parameter adjustment of the individual mathematical methods in each step as well as their proper combination. Notably, in simulating a batch column, computational time is hardly an issue using today's PC systems.

Detailed discussion of discretization techniques and numerical solution methods is beyond the scope of this book. Numerical methods are discussed in detail by, for example, Finlayson (1980), Davis (1984), and Du Chateau and Zachmann

Table 6.2 Examples of dynamic process simulation tools.

Examples for dynamic process simulation tools	
Aspen Engineering Suite (e.g. Aspen Custom Modeler™) aspenONE Engineering®/Aspen Chromatography™/Aspen Plus® (Aspen Technology, Inc., USA)	http://www.aspentech.com https://www.aspentech.com/en/products/full-product-listing
gPROMS® (Process Systems Enterprise Limited (PSE), UK)	https://www.psenterprise.com https://www.psenterprise.com/products/gproms

Examples for application software for liquid chromatography	
Aspen Chromatography (Aspen Technology, Inc., USA)	http://www.aspentech.com https://www.aspentech.com/en/products/pages/aspen-chromatography
Chromulator (Tingyue Gu's Chromatography Simulation)	https://people.ohio.edu/gu/CHROM/
VERSE (The Bioseparations Group, School of Chemical Engineering, Purdue University, West Lafayette)	https://engineering.purdue.edu/~biosep/research.html
ChromWorks® and Ypso Ionic® (Ypso-Facto®, Nancy, France)	https://www.ypsofacto.com/services-chemical-process-software.php https://www.ypso-ionic.com
ChromX (GoSilico, Karlsruhe, Germany)	https://gosilico.com/chromx

Open-source software to simulate chromatography	
CADET (von Lieres and Andersson 2010): Chromatography Analysis and Design Toolkit	https://cadet-web.de or in "A fast and accurate solver for the general rate model of column liquid chromatography," Computers and Chemical Engineering 34 (2010), 1180–1191

(1989). Summaries of different discretization methods applied in the simulation of chromatography are given by Guiochon, Golshan-Shirazi, and Katti (1994) and Guiochon and Lin (2003). For an introduction into numerical programming procedures see, for example, Press et al. (2002, http://www.nr.com) or Ferziger (1998).

Examples of dynamic process simulation tools and software for simulating liquid chromatography are summarized in Table 6.2.

References

Bellot, J.C. and Condoret, J.S. (1991). Liquid chromatography modelling: a review. *Process Biochem.* 26: 363–376.

Berninger, J.A., Whitley, R.D., Zhang, X., and Wang, N.-H. (1991). Versatile model for simulation of reaction and nonequilibrium dynamics in multicomponent fixed-bed adsorption processes. *Comput. Chem. Eng.* 15 (11): 749–768.

Craig, L.C. (1944). Identification of small amounts of organic compounds by distribution studies. II: Separation by counter-current distribution. *J. Biol. Chem.* 155: 519–534.

Danckwerts, P.V. (1953). Continuous flow systems – distribution of residence times. *Chem. Eng. Sci.* 2 (1): 1–13.

Davis, M.E. (1984). *Numerical Methods and Modeling for Chemical Engineers*. John Wiley & Sons, Ltd.

De Vault, D. (1943). The theory of chromatography. *J. Am. Chem. Soc.* 65: 532.

Deuflhard, P. (2004). *Newton Methods for Nonlinear Problems. Affine Invariance and Adaptive Algorithms*, Springer Series in Computational Mathematics, vol. 35. Berlin: Springer-Verlag.

Du Chateau, P. and Zachmann, D. (1989). *Applied Partial Differential Equations*. Harper & Row.

Dünnebier, G. (2000). Effektive Simulation und mathematische Optimierung chromatographischer Trennprozesse. Dissertation (PhD thesis). Universität Dortmund, Shaker Verlag.

Felinger, F., Cavazzini, A., Remelli, M., and Dondi, F. (1999). Stochastic−dispersive theory of chromatography. *Anal. Chem.* 71 (20): 4472–4479.

Ferziger, J.H. (1998). *Numerical Methods for Engineering Applications*, 2e. Wiley-Interscience.

Finlayson, B. (1980). *Numerical Analysis in Chemical Engineering*. New York: McGraw-Hill.

Furuya, F., Takeuchi, Y., and Noll, K.E. (1989). Intraparticle diffusion of phenols within bidispersed macrorecticular resin particles. *J. Chem. Eng. Jpn.* 22 (6): 670.

Giddings, J.C. (1991). *Unified Separation Science*. New York: Wiley.

Giddings, J.C. and Eyring, H. (1955). A molecular dynamic theory of chromatography. *J. Phys. Chem.* 59: 416–421.

Glueckauf, E. (1949). Theory of chromatography: VII. The general theory of two solutes following non-linear isotherms. *Discuss. Faraday Soc.* 7: 12.

Glueckauf, E. and Coates, J.I. (1947). Theory of chromatography. Part 4. The influence of incomplete equilibrium on the front boundary of chromatogram and on the effectiveness of separation. *J. Chem. Soc.*: 1315–1321.

Golshan-Shirazi, S. and Guiochon, G. (1992). Comparison of the various kinetic models of non-linear chromatography. *J. Chromatogr. A* 603: 1–11.

Gu, T. (2015). *Mathematical Modeling and Scale-Up of Liquid Chromatography*, 2e. New York: Springer-Verlag.

Gu, T., Tsai, G.-J., and Tsao, G.T. (1990a). New approach to a general nonlinear multicomponent chromatography model. *AlChE J.* 36 (5): 784–788.

Gu, T., Tsai, G.-J., Tsao, G.T., and Ladisch, M.R. (1990b). Displacement effect in multicomponent chromatography. *AlChE J.* 36 (8): 1156–1162.

Gu, T., Tsai, G.-J., and Tsao, G.T. (1991). Multicomponent adsorption and chromatography with uneven saturation capacities. *AlChE J.* 37 (9): 1333–1340.

Gu, T., Tsai, G.-J., and Tsao, G.T. (1993). Modeling of nonlinear multicomponent chromatography. In: *Advances in Biochemical Engineering/Biotechnology*, vol. 49 (ed. A. Fiechter), 45–71. New York: Springer-Verlag.

Guiochon, G. and Lin, B. (2003). *Modeling for Preparative Chromatography*. Amsterdam: Elsevier.

Guiochon, G., Golshan-Shirazi, S., and Katti, A. (1994). *Fundamentals of Preparative and Nonlinear Chromatography*. Boston, MA: Academic Press.

Guiochon, G., Felinger, A., Shirazi, D.G., and Katti, A.M. (2006). *Fundamentals of Preparative and Nonlinear Chromatography*. Amsterdam: Elsevier.

Helfferich, F.G. (1997). Non-linear waves in chromatography III. Multicomponent Langmuir and Langmuir-like systems. *J. Chromatogr. A* 768: 169–205.

Helfferich, F.G. and Carr, P.W. (1993). Non-linear waves in chromatography, I. Waves, shocks, and shapes. *J. Chromatogr.* 629: 97–122.

Helfferich, F.G. and Klein, G. (1970). *Multicomponent Chromatography: Theory of Interferences*. New York: Marcel Dekker.

Helfferich, F.G. and Whitley, R.D. (1996). Non-linear waves in chromatography II. Wave interference and coherence in multicomponent systems. *J. Chromatogr. A* 734: 7–47.

Javeed, S., Qamar, S., Seidel-Morgenstern, A., and Warnecke, G. (2011a). Efficient and accurate numerical simulation of nonlinear chromatographic processes. *Comput. Chem. Eng.* 35: 2294–2305.

Javeed, S., Qamar, S., Seidel-Morgenstern, A., and Warnecke, G. (2011b). A discontinuous Galerkin method to solve chromatographic models. *J. Chromatogr. A* 1218: 7137–7146.

Jupke, A. (2004). Experimentelle Modellvalidierung und modellbasierte Auslegung von Simulated Moving Bed (SMB) Chromatographieverfahren. Fortschrittbericht VDI: Reihe 3 Nr. 807. Düsseldorf: VDI Verlag GmbH.

Kaczmarski, K., Mazzotti, M., Storti, G., and Morbidelli, M. (1997). Modeling fixed-bed adsorption columns through orthogonal collocation on moving finite elements. *Comput. Chem. Eng.* 21: 641–660.

Klatt, K.U. (1999). Modellierung und effektive numerische Simulation von chromatographischen Prozessen im SMB-Betrieb. *Chem. Ing. Tech.* 71: 708–713.

Lapidus, L. and Amundson, N.R. (1952). A descriptive theory of leaching: mathematics of adsorption beds. *J. Phys. Chem.* 56: 984–988.

Leonard, B. (1979). A stable and accurate convective modelling procedure based on quadratic upstream procedure. *Comput. Methods Appl. Mech. Eng.* 19: 59–98.

Levenspiel, O. (1999). *Chemical Reaction Engineering*, 3e. New York: Wiley.

Levenspiel, O. and Bischoff, K.B. (1963). Patterns of flow in chemical process vessels. *Adv. Chem. Eng.* 4: 95.

von Lieres, E. and Andersson, J. (2010). A fast and accurate solver for the general rate model of column liquid chromatography. *Comput. Chem. Eng.* 34: 1180–1191.

Lu, Z. and Ching, C.B. (1997). Dynamics of simulated moving-bed adsorption separation processes. *Sep. Sci. Technol.* 32: 1118–1137.

Ludemann-Hombourger, O., Bailly, M., and Nicoud, R.-M. (2000). Design of a simulated moving bed: optimal size of the stationary phase. *Sep. Sci. Technol.* 35 (9): 1285–1305.

Ma, Z., Whitley, R.D., and Wang, N.-H. (1996). Pore and surface diffusion in multicomponent adsorption and liquid chromatography systems. *AIChE J.* 42 (5): 1244–1262.

Martin, A.J.P. and Synge, R.L.M. (1941). A new form of chromatogram employing two liquid phases: a theory of chromatography. 2. Application to the

micro-determination of the higher monoamino-acids in proteins. *Biochem. J.* 35: 1358.

Mazzotti, M. and Rajendran, A. (2013). Equilibrium theory - based analysis of nonlinear waves in separation processes. *Annu. Rev. Chem. Biomol. Eng.* 4: 119–141.

McQuarrie, D.A. (1963). On the stochastic theory of chromatography. *J. Chem. Phys.* 38: 437.

Migliorini, C., Mazzotti, M., and Morbidelli, M. (2000). Robust design of countercurrent adsorption separation processes: 5. Nonconstant selectivity. *AlChE J.* 46: 1384–1399.

Nicoud, R.-M. (2015). *Chromatographic Processes: Modeling, Simulation, and Design*. Cambridge University Press.

Pfister, D., Nicoud, L., and Morbidelli, M. (2018). *Continuous Biopharmaceutical Processes: Chromatography, Bioconjugation, and Protein Stability*. Cambridge University Press.

Press, W.H., Flannery, B.P., Teukolsky, S.A., and Vetterling, W.T. (2002). *Numerical Recipes in C++: The Art of Scientific Computing*, 2e. Cambridge: Cambridge University Press.

Qamar, S. and Seidel-Morgenstern, A. (2016). Extending the potential of moment analysis in chromatography. *Trends Anal. Chem.* 81: 87–101.

Qamar, S., Abbasi, J.N., Mehwish, A., and Seidel-Morgenstern, A. (2015). Linear general rate model of chromatography for core–shell particles: analytical solutions and moment analysis. *Chem. Eng. Sci.* 137: 352–363.

Qamar, S., Bashir, S., Perveen, S., and Seidel-Morgenstern, A. (2019). Relations between kinetic parameters of different column models for liquid chromatography applying core-shell particles. *J. Liq. Chromatogr. Related Technol.* 42: 16–30.

Rastegar, S.O. and Gu, T. (2017). Empirical correlations for axial dispersion coefficient and Peclet number in fixed-bed columns. *J. Chromatogr. A* 1490: 133–137.

Rhee, H.K., Aris, R., and Amundson, N.R. (1970). On the theory of multicomponent chromatography. *Philos. Trans. R. Soc. London, Ser. A* 267: 419–455.

Rhee, H.K., Aris, R., and Amundson, N.R. (1986). First-order partial differential equations. In: *Theory and Application of Hyperbolic Systems of Quasilinear Equations*, vol. I. New Jersey: Prentice-Hall.

Rhee, H.K., Aris, R., and Amundson, N.R. (1989). First-order partial differential equations. In: *Theory and Application of Hyperbolic Systems of Quasilinear Equations*, vol. I. New Jersey: Prentice-Hall.

Ruthven, D.M. (1984). *Principles of Adsorption and Adsorption Processes*. New York: Wiley.

Seidel-Morgenstern, A. (1995). *Mathematische Modellierung der präparativen Flüssigchromatographie*. Wiesbaden: Deutscher Universitätsverlag.

Shih, T.M. (1984). *Numerical Heat Transfer*, Series in Computational Methods in Mechanics and Thermal Sciences. New York: Springer-Verlag.

Siitonen, J. and Sainio, T. (2011). Explicit equations for the height and position of the first component shock for binary mixtures with competitive Langmuir isotherms under ideal conditions. *J. Chromatogr. A* 1218: 6379–6389.

Snyder, L.R., Kirkland, J.J., and Dolan, J.W. (2010). *Introduction to Modern Liquid Chromatography*, 3e. Hoboken, NJ: Wiley.

Storti, G., Masi, M., and Morbidelli, M. (1988). Optimal design of SMB adsorption separation units through detailed modelling and equilibrium theory. *Proceedings of NATO Meeting*, Vimeiro, Portugal. Neuilly sur Seine, France: Research and Technology Agency.

Storti, G., Mazzotti, M., Morbidelli, M., and Carrà, S. (1993). Robust design of binary countercurrent adsorption separation processes. *AlChE J.* 39: 471–492.

Suzuki, M. (1990). *Adsorption Engineering*. Amsterdam: Elsevier.

Tallarek, U., Bayer, E., and Guiochon, G. (1998). Study of dispersion in packed chromatographic columns by pulsed field gradient nuclear magnetic resonance. *J. Am. Chem. Soc.* 120 (7): 1494–1505.

Thomas, H. (1944). Heterogeneous ion exchange in a flowing system. *J. Am. Chem. Soc.* 66: 1664–1666.

Van Deemter, J.J., Zuiderweg, F.J., and Klinkenberg, A. (1956). Longitudinal diffusion and resistance to mass transfer as causes of nonideality in chromatography. *Chem. Eng. Sci.* 5: 271–289.

Van der Laar, T. (1958). Letter to the editors on notes on the diffusion type model for longitudinal mixing in flow. *Chem. Eng. Sci.* 7: 187–191.

Villadsen, J. and Stewart, W.E. (1967). Solution of boundary-value problems by orthogonal collocation. *Chem. Eng. Sci.* 22: 1483.

Whitley, R.D., Van Cott, K.E., and Wang, N.-H. (1993). Analysis of nonequilibrium adsorption/desorption kinetics and implications for analytical and preparative chromatography. *Ind. Eng. Chem. Res.* 32: 149–159.

Wicke, E. (1939). Empirische und theoretische Untersuchungen der Sorptionsgesehwindigkeit yon Gasen an porösen Stoffen. *Kolloid Z.* 86: 295–313.

Zhang, W., Shan, Y., and Seidel-Morgenstern, A. (2006). Breakthrough curves and elution profiles of single solutes in case of adsorption isotherms with two inflection points. *J. Chromatogr. A* 1107: 216–225.

7

Determination of Model Parameters*

Andreas Seidel-Morgenstern[1,2], Andreas Jupke[3], and Henner Schmidt-Traub[4]

[1] Otto-von-Guericke-Universität, Lehrstuhl für Chemische Verfahrenstechnik, Universitätsplatz 2, 39106 Magdeburg, Germany
[2] Max-Planck-Institut für Dynamik komplexer technischer Systeme, Sandtorstraße 1, 39106 Magdeburg, Germany
[3] RWTH Aachen University, FakultätMaschinenwesen, AVT - Aachener Verfahrenstechnik, Lehrstuhl für Fluidverfahrenstechnik, Forckenbeckstraße 51, 52074 Aachen, Germany
[4] TU Dortmund, Fakultät für Bio- und Chemieingenieurwesen, Lehrstuhl für Anlagen- und Prozesstechnik, Emil-Figge-Str. 70, 44227 Dortmund, Germany

As summarized in Chapter 6, there are reliable models available for quantitatively describing front propagation processes in chromatographic columns. The same holds true regarding procedures to combine the column models with additional models describing extra-column effects as well as other extra-column process steps. Always knowledge regarding the specific model parameters is the most essential factors for reliable design and optimization of chromatographic processes. There is a need in having protocols to determine the key parameters.

7.1 Parameter Classes for Chromatographic Separations

7.1.1 Design Parameters

The models presented in Section 6.2 contain sets of independent and dependent parameters. Designing a chromatographic process starts with selecting the chromatographic system (Chapter 3) and, subsequently, the kind of the chromatographic process as well as the hardware required to realize it (Chapters 4 and 5). These selections require the specification of the design parameters:

- Stationary phase (particle diameter d_p);
- Mobile phase (type, composition);
- Length (L_c) and diameter (d_c) of the chromatographic bed;
- Maximum allowable pressure drop (Δp);
- Temperature;
- Additional process-specific design parameters (e.g. number of columns per section in simulated moving bed (SMB) processes).

*Mirko Michel and Achim Epping have contributed to the first and/or second edition.

Various design parameters specify the chromatographic plant. Hereby geometrical design parameters are typically also objects of optimization (if no already existing plants are used for the separation).

7.1.2 Operating Parameters

The second class of parameters consists of the operating parameters for a given plant, which can be changed during plant operation:

- Flow rate ($\dot{V}_{feed}$);
- Feed concentration (c_{feed});
- Amount of feed (V_{inj}, m_{inj});
- Additional degrees of freedom, for example, switch times (fraction collection) in batch chromatography or flow rates in each section of a SMB process.

Like geometrical design parameters, operating parameters are part of the degrees of freedom for optimizing chromatographic separations. Their impact will be discussed in Chapter 8.

7.1.3 Model Parameters

System inherent physical and chemical parameters that specify the chromatographic system within the column as well as the plant operation make up the third set of parameters. These model parameters are typically not known a priori:

- Packing parameters (void fraction, porosity, and pressure drop);
- Axial dispersion coefficients;
- Equilibrium isotherms;
- Mass transfer coefficients;
- Plant parameters (describing the residence time behavior in the plant peripheral).

The above list refers to the transport dispersion model (Section 6.2.5.1), and, if other models are selected, the model equations and hence the corresponding number of parameters are expanded or reduced.

Physical properties and especially the isotherms depend on temperature as well as eluent composition. Feed and eluent composition influence the viscosity and therefore the fluid dynamics. The latter effects have already to be taken into account when selecting the chromatographic system (Chapter 3). The operating temperature for preparative processes is commonly selected in liquid chromatography to be close to room temperature for cost and stability reasons. Consequently, temperature and eluent composition are early fixed parameters that are often not explicitly considered during subsequent process design.

The time and money invested in model parameter determination has to be in balance with the aim of a certain chromatographic separation. Often only sample products are needed for further studies with the pure substances, and, to evaluate a separation process, only a few milligrams of the feed mixture is available. Time is typically an important factor, and shortcut methods will be applied to find conservative operating parameter values for a safe separation. A quite different

situation is the design of commercial large-scale production plants. Here, process economics are more essential. Therefore, parameters that are more precise are necessary for process optimization. As some parameters may change during operation, repeated determination may be necessary to maintain or reestablish optimal production.

Research has a third focus. Here, results have to be as accurate and reliable as possible. Consequently, more time and money are invested to acquire the data. Research aims are, for instance, better understanding of the process and improved methods for process design, optimization, and control. This cannot be done only experimentally. Therefore, verified models are needed to perform the investigations, with the aid of process simulation as virtual plant experiments.

Against this background, both precise and straightforward shortcut methods for model parameter determination are presented below. Based on the individual task, users have to decide specifically which procedures are most adequate. In this context, it must be mentioned that the adsorption equilibrium has clearly the largest influence on the position and shape of chromatographic profiles and, therefore, the isotherms deserve the greatest care.

7.2 Concept to Determine Model Parameters

A method for consistent parameter determination is depicted in Figure 7.1. Altenhöner et al. (1997) developed this method to determine the free parameters of the transport dispersion model. The basic idea is to start with the simplest parameters and to use them subsequently to determine the ones that are more difficult to determine. The procedure is structured into the following steps:

(1) Detector selection and calibration.
(2) Estimate magnitude of extra-column effects, as dead volume and degree of backmixing in the plant to prevent that these effects falsify model parameters. This step is only necessary occasionally if the plant configuration setup has been changed.
(3) Determine void fraction, porosity, and axial dispersion of the columns as well as pressure drop parameters.
(4) Determine the adsorption equilibria of the pure components and a few selected mixtures.
(5) Determine transport coefficients for the adsorbable solutes.

The experimental techniques are mainly based on the injection of small pulses (peaks) or very large pulses (breakthrough curves) and the subsequent analysis of the obtained chromatogram. Although the presented approach tries to limit the impact of measurement errors, experimental conditions and, especially, the material (adsorbent, eluent) used should be the same or at least comparable to the envisaged preparative application to ensure reliable results. The effects of plant peripherals should be kept low. Another aspect that deserves care is the calibration of the detectors.

Probably the simplest theoretical methods for determining the parameters from the experimental data involve the use of analytical solutions of simple
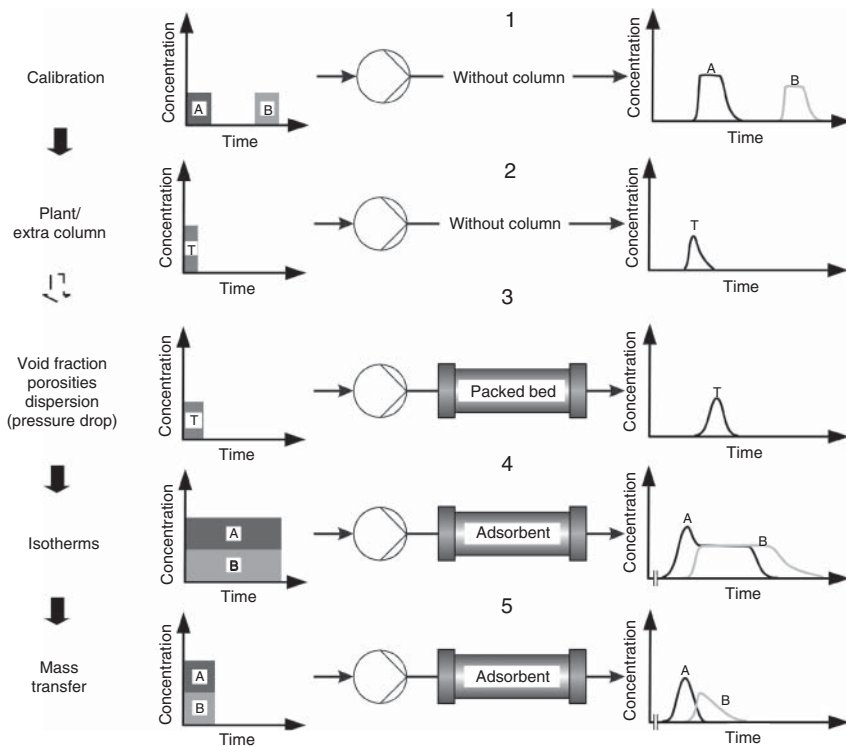
Figure 7.1 Concept to determine the model parameters (T, tracer; A and B, solutes).

column models and the analysis of the first moment of the elution profiles, for example, to determine the dead time or the Henry coefficient. In some cases where less accuracy is acceptable, parameters such as axial dispersion might be estimated by means of empirical correlations from literature. An overall kinetic coefficient can be also estimated analyzing the corresponding second moment of the elution profile.

To determine isotherms, methods based on numerical integration and differentiation of dynamic concentration profiles in combination with an analysis of mass balances can be used. A more versatile method is to use a parameter estimation tool to fit whole elution profiles ("peak fitting," "inverse method"), which is often the method of choice to obtain consistent and accurate estimates for many model parameters. Parameter estimation routines are included in some commercially available simulation programs (Section 6.4.2.2) or can be linked to one's own simulation software. By solving an optimization problem, these tools minimize the difference between the measured data and the simulation results by varying the model parameters. Thus, the result is an optimal set of parameter values. Since it is the preferred method, "parameter estimation" is typically used in the following, if not noted otherwise.

Table 7.1 gives an overview of different methods for parameter determination and illustrates the contradictory influences of accuracy and speed. Figure 7.2 describes the workflow for parameter determination. Different methods for

Table 7.1 Parameter determination methods.

General remarks			
Use for parameter estimation the same adsorbent as in the later applications			
Take care in calibrating the detectors			
Check influence of kinetic effects			
In case of fluid mixtures as eluent: check sensitivity to eluent composition fluctuations			

Method	High accuracy and experimental effort	Medium accuracy and experimental effort	Initial guess ("quick and dirty")
Plant/extra column	Experiment + moment analysis + parameter estimation: V_{pipe}, V_{tank} (t_{plant}), if necessary $D_{ax, pipe}$	Experiment + moment analysis: t_{plant}	Experiment + moment analysis: t_{plant}
Packing: void fraction and porosity	Experiment + moment analysis + parameter estimation: ε and ε_t	Experiment + moment analysis: ε_t set ε	ε_t (from manufacturer), set ε
Packing: D_{ax}	Experiment + parameter estimation	Experiment + moment analysis	Use correlation
Isotherms	Elution profiles (peak fitting), frontal analysis, perturbation analysis	Measure using ECP and peak maximum method	Measure with ECP
Mass transfer: k_{eff}	Experiment (overload injection) + parameter estimation	Experiment + moment analysis (or HETP)	Use correlation

determining individual parameters are discussed below. First, some general methods are presented, which are applicable in evaluating experimentally determined chromatograms.

7.3 Detectors and Parameter Estimation

An essential task in determining parameters is the identification of suitable detection methods. There is a choice of commercially available detectors (Section 10.4.7). These typically provide overall signals, which are influenced by the presence of the numerous components present in the mixture. To generate quantitative information typically a careful calibration of the specific detectors is needed.

7.3.1 Calibration of Detectors

Careful detector calibration is crucial, as it directly influences the accuracy of the measured data. Hereby, a major practical problem is often the limited availability of pure components.

When adsorption isotherms are determined by breakthrough experiments (Section 7.5.5), the acquired data can be directly taken for the detector calibration. Breakthrough curves should be recorded after injecting well-characterized solutions into the plant without the column. This requires considerably less sample to reach complete saturation of the detectors. Since the plateau concentrations are the known injected feed concentrations, a plot of c_{feed} versus the detector signal u provides the sought-after relationship, and a calibration function can be easily fitted to these values.

If the form of the calibration function

$$c = f_{\text{cal}}(u) \tag{7.1}$$

is known a priori, a pulse experiment may also be used to obtain the calibration curve. For a known amount of injected sample

$$m_{\text{inj}} = V_{\text{inj}} \cdot c_{\text{feed}} = \dot{V} \cdot t_{\text{inj}} \cdot c_{\text{feed}} \tag{7.2}$$

the mass balance at the column outlet provides

$$m_{\text{inj}} = \dot{V} \cdot \int_0^{\overline{\infty}} c(L_{\text{c}}, t)\mathrm{d}t = \dot{V} \cdot \int_0^{\infty} f(u(t))\mathrm{d}t \tag{7.3}$$

In the special case of a linear calibration function,

$$c = F_{\text{cal}} \cdot u \tag{7.4}$$

Equations (7.2) and (7.3) together with the numerical integration of the detector signal allow the determination of the calibration factor F_{cal}:

$$F_{\text{cal}} = \frac{V_{\text{inj}} \cdot c_{\text{inj}}}{\dot{V} \cdot \int_0^{\infty} u(t)\mathrm{d}t} = \frac{t_{\text{inj}} \cdot c_{\text{inj}}}{\cdot \int_0^{\infty} u(t)\mathrm{d}t} \tag{7.5}$$

For nonlinear detector responses, calibration curves may be also determined by curve fitting. For such more complex calibration functions with more than one unknown parameter, additional information (e.g. regarding the physical foundations of the measuring method) or pulse experiments with different concentrations are necessary. In any case, it is advised to check the validity of the calibration curves in the low and high concentration ranges by separate experiments with different feed concentrations.

7.3.2 Parameter Estimation

The analysis of two moments offers to estimate only two characteristic parameters that characterize a peak but not the whole peak shape. By "fitting" of either analytical equations or simulation results to the complete peak, this drawback might be overcome. It also allows a direct comparison between the calculated and measured concentration profiles.

As suitable analytical solutions are not available for most of the column models, simulation-based parameter estimation using simulation software

can be recommended as a powerful tool (see Chapter 6.4.2.2). This method is very versatile in terms of the number and complexity of models that can be handled. Estimation tasks can be solved, for example, with tools included in the gPROMS program package (PS Enterprise, UK). An additional advantage of the simulation-based approach is the consistency of the obtained data, if the same models and simulation tools are used for subsequent process analysis and optimization.

The fitting procedure results in a set of model parameters, minimizing the difference between theoretical and measured concentration profiles. A discussion of statistical-based objective functions and optimization procedures is beyond the scope of this book. For further information see, for example, Lapidus (1962), Barns (1994), Korns (2000), and Press et al. (2002, http://www.nr.com/).

Objective functions, *O,* are often based on least squares methods. They can be, for example, a function of the absolute or relative squared error of n_p measured concentration values, c_{exp}, and the theoretical values, c_{theo}:

$$O = f\left(\sum_{j=1}^{n_p} (c_{exp,j} - c_{theo,j})^2 \right) \quad \text{or} \quad f\left(\sum_{j=1}^{n_p} \left(\frac{c_{exp,j} - c_{theo,j}}{c_{exp,j}} \right)^2 \right) \tag{7.6}$$

In general, objective functions can capture more than one set of experimental data.

To solve the arising optimization problem, the solution (in this case the shape of the simulated chromatogram) must be sensitive to the variable in question; otherwise no meaningful parameter set can be obtained. It is not recommended to determine more than two or maximal three parameters simultaneously, because this increases the chances of being trapped in local minima or in finding more than one set of parameters that fulfills optimization criteria. The concept depicted in Figure 7.1 follows this consideration as not all column parameters are obtained from one measured chromatogram. Instead, estimation is performed step by step, using different experimental data and increasing the complexity of the model required in each step.

Another aspect to be considered is the quality of the measurement, as all errors (e.g. detector noise) affect the accuracy of the determined parameters. Notably, in contrast to these statistical errors, systematic measurement errors cannot be minimized by repeated measurements.

It should be noted that the users must provide initial guesses of the parameters. These may be based on initial tests, experience, or shortcut calculations. If the equations are nonlinear, the initial guesses influence the result of the optimization, and it is recommended to test the sensitivity of the obtained parameters with respect to the initial guesses.

In any case, the simulated profiles must be compared with the measured data to check the validity of the determined data as well as the assumed model. Statistical methods to quantify the goodness of the fit are given, for example, in Lapidus (1962), Barns (1994), Korns (2000), and Press et al. (2002).
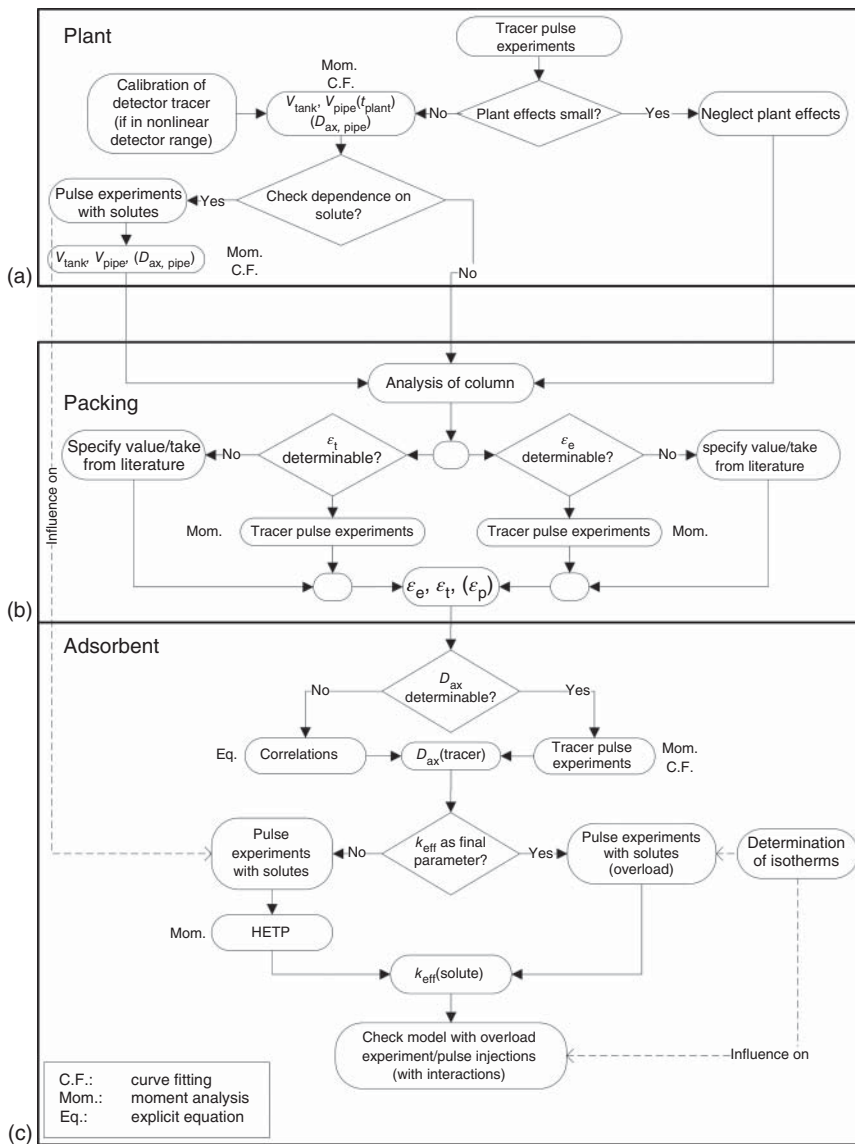
Figure 7.2 Illustration of different ways to determine the various types of model parameters.

7.3.3 Evaluation of Chromatograms

The previous section 7.2 gave an overview regarding experiments possible to determine free model parameters. This section describes general procedures for evaluating parameter values from acquired experimental data. Model parameters are defined in Chapter 2, while Section 6.2 shows how they appear in the model equations. Based on the assumptions for these models, it follows that all plant effects as well as axial dispersion, void fraction, and mass transfer resistance

are independent of the adsorption/desorption processes occurring within the column.

Figure 7.2 provides a schematic overview regarding useful methods capable to provide the most important model parameters and a possible workflow. The first step devoted to identify plant parameters is depicted separately as it has to be done only occasionally (Section 7.2).

7.4 Determination of Packing Parameters

When the model parameters of the plant are known, packing quality properties, that is, void fraction, pressure drop, and dispersion, should be evaluated (step 3 in Figure 7.1).

7.4.1 Void Fraction and Porosity of the Packing

To determine void fractions and the (total) porosity (Eqs. (2.3)—(2.6)), pulses of a nonpenetrating tracer (T1) and of a nonadsorbable tracer (T2), which penetrates into the pore system (t_0 marker), respectively, are injected. Using the definition of the dead times (Section 2.2.1), one obtains

$$\varepsilon_t = t_{0,t} \cdot \frac{\dot{V}}{V_c} \quad \text{or} \quad \varepsilon_e = t_{0,e} \cdot \frac{\dot{V}}{V_c} \tag{7.7}$$

If no suitable tracers are available, alternative methods may be used (Section 2.2.2). In the case of difficulties, a void fraction of about $\varepsilon_e = 0.4$ can be estimated, since typical values for packings of spheres are between 0.32 and 0.42.

7.4.2 Axial Dispersion

The axial dispersion coefficient can be estimated from the concentration profile of a nonpenetrating tracer (T1). An approximation regarding its velocity dependence goes back to van Deemter, Zuiderweg, and Klinkenberg (1956). The axial dispersion coefficient is seen as the sum of the contributions of molecular diffusion and eddy diffusion (Ruthven 1984; Rastegar and Gu 2017):

$$D_{ax} = \gamma \cdot D_m + \lambda \cdot d_p \cdot u_{int} \tag{7.8}$$

where D_m is the molecular diffusion coefficient while γ and λ are the (external) tortuosity and a characterization factor of the packing, respectively. For typical values the following holds:

$$\gamma \approx 0.7, \quad \lambda \approx 1$$
$$D_m \approx 10^{-6} \text{ to } 10^{-5} \text{ cm}^2\text{s}^{-1},$$
$$d_p \cdot u_{int} \approx (10^{-3} \times 0.1) \text{ cm}^2\text{s}^{-1} = 10^{-4} \text{ cm}^2\text{s}^{-1} \tag{7.9}$$

For typical chromatographic conditions, the contribution of molecular diffusion is relatively small, and D_{ax} approximately becomes a linear function of the velocity:

$$D_{ax} \approx \lambda \cdot d_p \cdot u_{int} \tag{7.10}$$

Several methods for determining D_{ax} have been described in the literature. If a suitable tracer is available, chromatograms at different flow rates should be measured.

Chung and Wen (1968) and Wen and Fan (1975) proposed a dimensionless equation using the dependency of the dispersion coefficient on the (particle) Reynolds number Re (Eq. (7.12)) for fixed and expanded beds. It is an empirical correlation, based on published experimental data and correlations from other authors, which covers a wide range of Reynolds numbers Re. Owing to two different definitions of the Reynolds number, actual forms of the correlations vary in the literature. Since the particle diameter d_p is the characteristic length scale used in Eq. (7.12) a particle Péclet number Pe_p results (Eq. (7.13)):

$$Pe_p = \frac{0.2}{\varepsilon} + \frac{0.011}{\varepsilon} \cdot (\varepsilon \cdot Re)^{0.48} \Rightarrow 10^{-3} \leq Re \leq 10^3 \tag{7.11}$$

$$Re = \frac{u_{int} \cdot d_p \cdot \varrho_1}{\eta_1} = \frac{u_{int} \cdot d_p}{\nu_1} \tag{7.12}$$

$$Pe_p = \frac{u_{int} \cdot d_p}{D_{ax}} \tag{7.13}$$

Notably, the particle Péclet number differs from the axial Péclet number defined in Eq. (6.110) by the ratio of particle diameter to column length:

$$Pe = \frac{u_{int} \cdot L_c}{D_{ax}} = Pe_p \frac{L_c}{d_p} \tag{7.14}$$

Transforming Eq. (7.11) leads to Eq. (7.15):

$$D_{ax} = \frac{u_{int} \cdot d_p \cdot \varepsilon}{0.2 + 0.011 \cdot (\varepsilon \cdot Re_p)^{0.48}} \tag{7.15}$$

which allows a rough estimation of the axial dispersion coefficient, especially for high-quality packings. For such packings, Re has little influence as the value is under chromatographic conditions typically considerably smaller than 1.

7.4.3 Pressure Drop

Pressure drop and flow rate are usually linearly related – expressed by Darcy's law (Section 2.2.5). Pressure drops are usually measured for different volume flows, once with column in the plant and once without the column, using preferably a "zero-volume" connector. The difference between the two values yields the pressure drop characteristic Δp_c of the column alone. By plotting Δp_c versus u_{int}, the unknown coefficient k_0 is readily determined from the slope of the curve by rearranging Eq. (2.33):

$$\Delta p_c = \frac{\eta L_c}{k_0 d_p^2} \cdot u_{int}$$

$$k_0 = \frac{u_{int}}{\Delta p_c} \cdot \frac{\eta L_c}{d_p^2} \tag{7.16}$$

7.5   Adsorption Isotherms

7.5.1   Determination of Adsorption Isotherms

The adsorption isotherms have the most pronounced influence on the courses of the chromatograms. They determine front propagation velocities (Section 6.2.3). Consequently, single-component and multicomponent isotherms should be determined with high accuracy in order to achieve a good agreement between simulations and experiments, including all model parameters measured so far (Figure 7.1).

This chapter discusses some of the most frequently used methods to determine isotherms and the corresponding model parameters. For further information, see reviews by Seidel-Morgenstern and Nicoud (1996) and Seidel-Morgenstern (2004) as well as the monograph by Guiochon et al. (2006). Table 7.2 summarizes the most important methods.

The techniques listed in Table 7.2. differ in terms of accuracy and experimental effort. Their application is also limited by the availability of the required equipment. Not all methods are suitable for columns with low efficiency, because peak deformations will affect the isotherm parameters. The actual setup and experimental conditions should be as close as possible to the operating conditions for later production purposes. However, to save time and solutes, the column dimensions are usually only of smaller (analytical) scale or "semipreparative" at maximum. Preparative chromatography requires typically the application of adsorbents of larger particle sizes compared to analytical applications. In isotherm measurements, temperature control is crucial, since adsorption may show significant temperature dependence. Sometimes the costs of solutes prohibit the use of methods that need larger amounts of samples.

The graphical guideline in Figure 7.3 illustrates the general steps of a comprehensive analysis of the adsorption equilibria.

7.5.2   Estimation of Henry Coefficients

Very important parameters that describe the initial slope of the adsorption isotherms are the Henry coefficients. They are most relevant in analytical chromatography where diluted solutions are processed. The Henry constants can be conveniently determined analyzing measured mean retention times after pulse injections performed with very low amounts of solutes to ensure linear isotherm behavior. The linearity can be tested by comparing two or three pulse responses belonging to different concentrations. If the results for the determined Henry coefficients are identical, the system is linear. Provided the column porosity or phase ratios are known (Section 7.4.1), the Henry constants H can be calculated in two ways:

$$H^* = \frac{t_R - t_{0,e}}{\dfrac{1 - \varepsilon_e}{\varepsilon_e} t_{0,e}} \quad \text{or} \quad H = \frac{t_R - t_{0,t}}{\dfrac{1 - \varepsilon_e}{\varepsilon_e} t_{0,t}} \tag{7.17}$$

Table 7.2 Methods and steps in isotherm determination.

General aspects
Use directly the preparative adsorbents
Use one plant for all measurements and try to keep extra-column effects low
Determine dead volumes of column and plant
Control column temperature within 1 °C
Calibrate the detectors carefully
For multicomponent systems: try to apply component-specific detectors
Favor measurement methods with packed columns
Evaluate concentration range of the application process
Check applicability of measurement method
Determine single-component parameters first
Check consistency with standard pulse tests of linear chromatography, especially Henry coefficients
Select isotherm model equation carefully
Try to simulate mixture experiments with single-component isotherms
Quantify component interactions only if necessary
Check agreement between theoretical and experimental chromatograms

Name	Methods	Isotherm type	Comments
Static methods			
Batch method (closed vessel)	• Immersion of adsorbent in solution • Mass balance	Single-component and multicomponent	• No packed column • No detector calibration necessary (only HPLC analytics) • Tedious • Limited accuracy

Method	Description	Components	Characteristics
Adsorption/ desorption method	• Loading and unloading of column • Mass balance	Single-component and multicomponent	• No detector calibration necessary (only HPLC analytics) • Tedious but accurate
Circulation method	• Closed system • Stepwise injection and circulation of components till equilibrium • Mass balance	Single-component and multicomponent	• Lower amount of sample • Accumulation of errors for the injection • Possibility for automation
Dynamic methods			
Frontal analysis	• Integration of step response (breakthrough curves) • Numerical integration and mass balance	Single-component and multicomponent	• High accuracy • Easy automation • Detector calibration necessary (directly obtainable from breakthrough experiments) • Component-specific detectors or fractionated analysis necessary for multicomponent isotherms only • High amounts of sample • Suitable for low efficient columns • No kinetic errors • Impurities must not cause significant detector signals
Analysis of disperse fronts: elution by characteristic point (ECP), frontal analysis by characteristic point (FACP)	• Pulse or step injection (high concentration) • Slope of dispersive front	Single component	• Small sample amounts • Highly efficient columns and small plant effects necessary • Phase equilibrium is required (sensitive to kinetics) • Precise detector calibration necessary
Peak maximum	• Peak injection with systematic overload • Peak maximum equal to retention time	Single component	• Small sample amounts • Less sensitive to low-efficiency columns than ECP/FACP • For special cases no detector calibration necessary

(Continued)

Table 7.2 (Continued)

Name	Methods	Isotherm type	Comments
Perturbation method (minor disturbance method)	• Determination of the retention times of small (minor) disturbances • Column with different loading states	Single-component and multicomponent	• No detector calibration necessary • Can deal with small impurities • Equilibrium is required • Can deal with low efficient columns • Isotherm models necessary to calculate multicomponent isotherms • Potential for automation
Curve fitting (peak fitting) of chromatograms	• Parameter estimation	Single and binary (difficult!) Multicomponent not feasible	• validate column and plant model necessary • Isotherm model necessary • Isotherm parameters must be sensitive
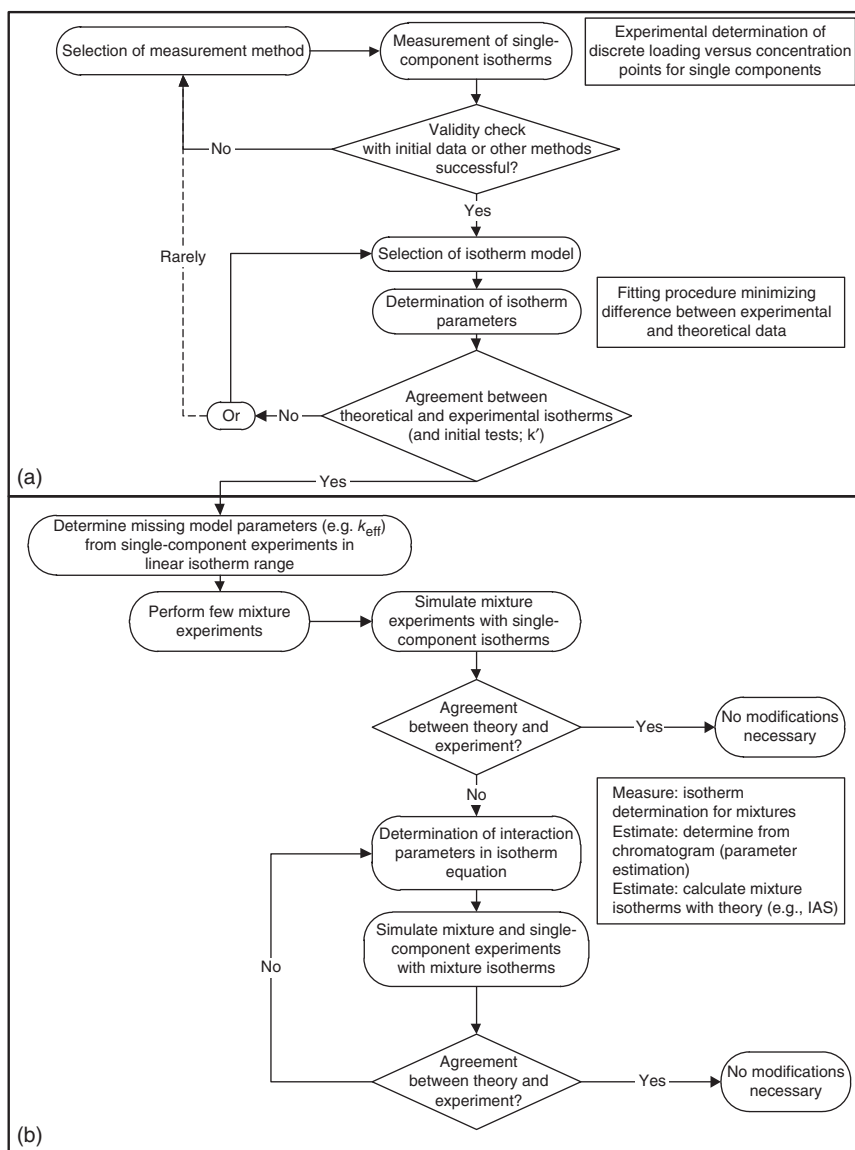
Figure 7.3 Graphical guideline for determining adsorption isotherms. (a) Single-component isotherms and (b) multicomponent isotherms.
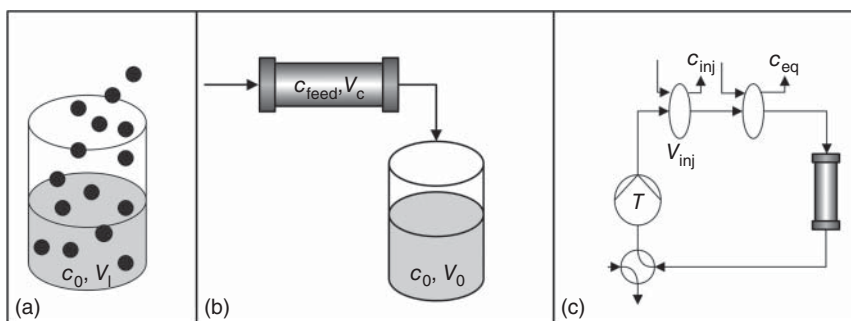
Figure 7.4 Principle of different static methods for isotherm determination.(a) Batch method, (b) adsorption/desorption method, and (c) circulation method.

In the above equation both options possible to quantify the phase ration are considered (Section 2.2.1). To estimate reliable parameters valid for the packing, possible extra-column retention times need to be subtracted from the retention times (Section 7.7)

7.5.3 Static Isotherm Determination Methods

Static methods (Figure 7.4) determine phase equilibrium data based on overall mass balances. They are often more time consuming and less accurate than dynamic methods described below:

7.5.3.1 Batch Method

A known amount of adsorbent, V_{ads}, with initially empty pores is added to a solution of the volume, V_L, containing the solute with the concentration $c_{0,i}$. The mixture is then agitated in a closed vessel until equilibrium is reached. The final concentration in the solution ($c_{eq,i}$) is determined by standard analytical methods. From the following mass balance, the appropriate equilibrium loading, $q(c_{eq,i})$, is calculated:

$$V_L \cdot c_{0,i} = V_1 \cdot c_{eq,i} + V_{ads}(1 - \varepsilon_p)q_i(c_{eq,i}) \tag{7.18}$$

Using different initial concentrations or adsorbent amounts, a relevant concentration range can be covered. The method can be easily expanded to multicomponent mixtures, where the loadings are functions of all components present. Drawbacks are the time-consuming preparations of the different mixtures and the transferability of the results to packed columns (e.g. due to uncertainties in phase ratio/porosity). Because of the numerous steps of manual work and an uncertainty when equilibrium is fully reached, the accuracy of the method is not too high.

7.5.3.2 Adsorption–Desorption Method

An initially unloaded ($q = 0$) column is equilibrated by a feed concentration, c_{feed}, which may be a single-component or multicomponent mixture. Equilibrium is achieved by pumping a sufficient quantity of feed through this column. The plant

is then flushed without the column to remove the solute solution. Afterwards, all solute is eluted from the column, collected, and analyzed to obtain the desorbed amount $m_{\text{des},i}$. The equilibrium loading $q(c_{\text{feed}})$ for each component i can be calculated according to

$$m_{\text{des},i} = \varepsilon \cdot V_{\text{c}} \cdot c_{\text{feed},i} + (1 - \varepsilon) \cdot V_{\text{c}} \cdot [\varepsilon_{\text{p}} \cdot c_{\text{feed},i} + (1 - \varepsilon_{\text{p}}) \cdot q_i(c_{\text{feed},i})]$$

(7.19)

The experimental effort to include different concentrations is considerable, but the obtained equilibrium values are typically rather reliable.

7.5.3.3 Circulation Method

Another static method is based on a closed fluid circuit that includes the chromatographic column. A known amount m_{inj} of solute or a mixture of several solutes is injected into this circuit and pumped around until equilibrium is established. Samples are taken and analyzed to determine the resulting equilibrium concentration c_{eq}. The mass balance for the equilibrium loading accounts for the holdup of the complete plant:

$$m_{\text{inj},i} = V_{\text{plant}} \cdot c_{\text{eq},i} + \varepsilon \cdot V_{\text{c}} \cdot c_{\text{eq},i} + (1 - \varepsilon) \cdot V_{\text{c}}$$
$$\cdot [\varepsilon_{\text{p}} \cdot c_{\text{eq},i} + (1 - \varepsilon_{\text{p}}) \cdot q(c_{\text{feed},i})]$$

(7.20)

With

$$m_{\text{inj},i} = V_{\text{inj}} \cdot c_{\text{inj},i}$$

(7.21)

Subsequently, new injections are made to change the concentration step by step. The successive nature of this method saves solute, but unavoidable inaccuracies accumulate.

7.5.4 Dynamic Methods

Dynamic methods extract information about the isotherms from the measured transient concentration profiles. The basic principle is to inject disturbances in an equilibrated column and to analyze the column response. Based on the type of disturbance, three major groups can be distinguished. Injection of a large sample, with a concentration different from the existing equilibrated state, results in a breakthrough curve (frontal analysis, method of step response). The complementary case induces small disturbances to an equilibrated chromatographic system. Another possibility is the injection of overloaded pulses with concentrations in the nonlinear range of the isotherm, but for injection volumes small enough not to reach breakthrough. The last two methods are sometimes also referred to as pulse response techniques.

7.5.5 Frontal Analysis

Frontal analysis is one of the most popular methods to determine isotherms. The method evaluates mean retention times of fronts neglecting kinetic phenomena. Thus, its foundation is the equilibrium theory introduced in Section 6.2.3.
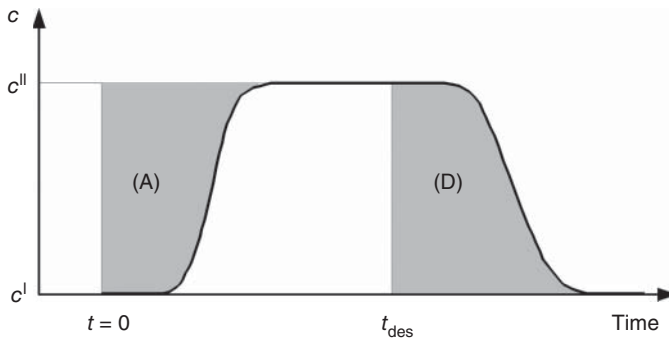
Figure 7.5 Typical breakthrough curve for adsorption and desorption of a pure component. Source: Reproduced from Seidel-Morgenstern (1995). https://pure.mpg.de/pubman/faces/ViewItemOverviewPage.jsp?itemId=item_1758552.Licensed Under CC BY 3.0.

The principle of the method can be described as follows. At $t = 0$ a step signal with concentration c^{II} is injected into a preequilibrated column until $t_{inj} = t_{des}$, where the feed concentration is once again lowered to the initial feed concentration. The outgoing concentration profiles are detected. The injected volume has to be large enough to reach a plateau concentration, resulting in a concentration profile as depicted in Figure 7.5 for a pure component and a column equilibrated initially with the concentration c^{I}. A component index i is omitted for brevity.

It takes a certain time for the outlet profile to reach a plateau. During this adsorption period, a new equilibrium is established, with a liquid concentration being the feed concentration c^{II}. Likewise, during the desorption step the initial equilibrium is restored with a delay of t_{des}. This experimental procedure is easy to implement and to automate if a gradient delivery system is available.

A very effective way to evaluate the equilibrium is to calculate the overall mass balances by numerical integration. Area "A" in Figure 7.5 is equivalent to the solute accumulated inside the plant and the column, which is split into two parts accumulated in the liquid and the adsorbent phase. The integral mass balance allows the calculation of the loading, $q^{II} = q(c^{II})$, provided the status I and the total porosity are known:

$$V_{plant} \cdot (c^{II} - c^{I}) + V_c \cdot [\varepsilon_t \cdot (c^{II} - c^{I}) + (1 - \varepsilon_t) \cdot (q(c^{II}) - q(c^{I}))]$$

$$= \dot{V} \cdot \int_0^{t_{des}} (c^{II} - c(t)) dt \tag{7.22}$$

If the solute is injected in the plant without the column, the dead time of the plant can be estimated at the inflection point of the breakthrough curve. The finally observed plateau signal also allows one to verify that the linear range of the detector was not exceeded.

Frontal analysis is straightforward when starting from an unloaded column ($c^{I} = 0$). A modification to reduce the amount of solute is the stepwise increase of the feed concentration, starting from the unloaded column. This results in successive plateaus. Desorption steps are obtained after the highest concentration plateau has passed through the column, if the concentrations are reduced
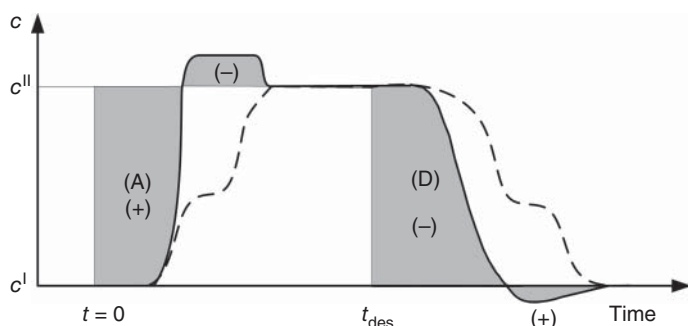
Figure 7.6 Typical breakthrough curve for adsorption and desorption of a binary mixture component (solid line, weaker retained component; dashed line, stronger retained component). Source: Reproduced from Seidel-Morgenstern (1995). https://pure.mpg.de/pubman/faces/ViewItemOverviewPage.jsp?itemId=item_1758552.Licensed Under CC BY 3.0.

inversely to the adsorption steps. To consume even less feed mixture, this procedure can be performed in closed-loop or circulation operation (Figure 7.4).

Independent of the method applied, the gray area "D" in Figure 7.5 has to be equal to the area "A." A comparison may serve as a consistency check. Another possibility to verify the results is to stop the flow after the plateau is reached and analyze the desorption front according to the adsorption–desorption method (Section 7.5.3).

An extension to multicomponent systems is straightforward, by injecting more than one component. A prerequisite is the measurement of the concentration profile of each solute during the elution. This can be achieved either by using solute-specific detectors or by collection of multiple fractions and subsequent chemical analysis. Solute-specific detection may be performed, for example, by using different wavelengths for UV detection or multidetector setups. For a binary separation, the latter must provide two independent signals. A typical breakthrough curve of a binary mixture for convex (Langmuir-type) isotherms and interaction of the solutes is given in Figure 7.6. The concentration profile of the weaker adsorbed component is denoted by a solid line, while the more strongly adsorbed component is represented by the dashed line.

The increase of the concentration of the first eluting component above feed concentration c^{II} is due to the displacement by the stronger adsorbed second component (Section 2.4.3). Calculation of the equilibrium loading is done for each component using Eq. (7.22). For the first eluting component, the areas (+) and (−) illustrate the positive and negative contributions, respectively, in the integral. As with single components, calculations can be done using the adsorption profile (A) or the desorption profile (D). For $c^{I} = 0$, no positive contribution can be found in the desorption profile.

With compressive fronts (Section 6.2.3), the integration of the steep front may be simplified, if the kinetic effects are low (large number of stages). In the case of a Langmuir-type (convex, self-sharpening) isotherm, the first front is very steep,
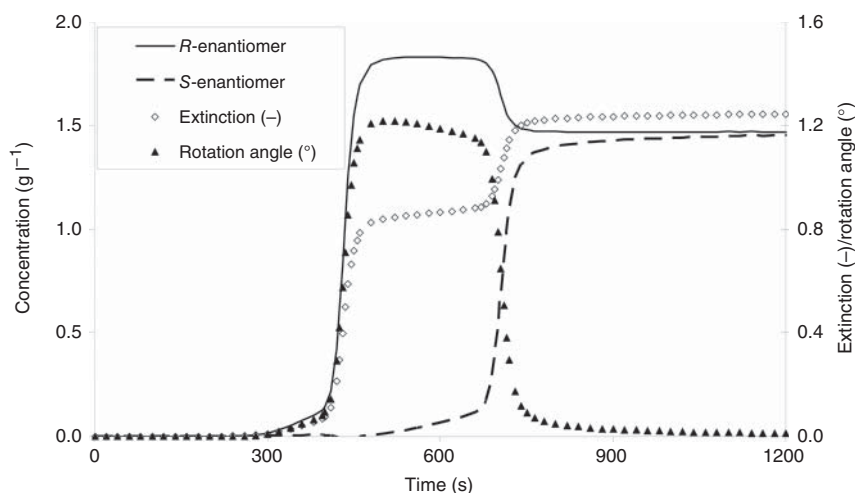
Figure 7.7 Experimental breakthrough curves of the mixture of *R*- and *S*-enantiomers of EMD53986 (lines, concentrations; symbols, detector signals; $c_{feed} = 3 \, g \, l^{-1}$, $\dot{V} = 20 \, ml \, min^{-1}$; for additional data see Appendix A.1).

originating from the formation of a shock (Section 6.2.3). Using Eq. (6.66), taking t_R as the time at the inflection point of the front profile and considering a possible delay time caused by extra-column effect taking place in the plant (Section 7.7), the loading q^{II} is obtained by Eq. (7.23):

$$t_R = t_{plant} + t_0 \cdot \left(1 + \frac{1 - \varepsilon_t}{\varepsilon_t} \cdot \frac{q^{II} \left(c^{II} \right) - q^{I} \left(c^{I} \right)}{c^{II} - c^{I}} \right) \tag{7.23}$$

Parameters of the isotherm equation can be determined from a set of experimental data using a least squares approximation (Section 7.5.10).

As an example, Figure 7.7 gives the experimental breakthrough curve for a racemic mixture of EMD53986 using Chiralpak AD ($d_p = 20 \, \mu m$, Daicel) as adsorbent and ethanol as eluent. Here, a two-detector setup of polarimeter and UV detector was used, permitting the solute-specific detection of both components (Mannschreck 1992; Jupke 2004; Epping 2005).

Breakthrough curves (lines in Figure 7.7) are calculated from the detector signals (symbols). The rotation angle detected by the polarimeter is zero if both enantiomers are present ($t > 800 \, s$) while the UV signal is additive and has the highest value there.

The two breakthrough curves of both components are described by convex isotherms with competitive adsorption and show a typical displacement effect for the weaker retained *R*-enantiomer.

The corresponding equilibrium data for pure components and different mixtures are represented in Figure 7.8 by filled rhombuses and triangles. Also shown are the results of different isotherm equations (solid and dashed lines) that have
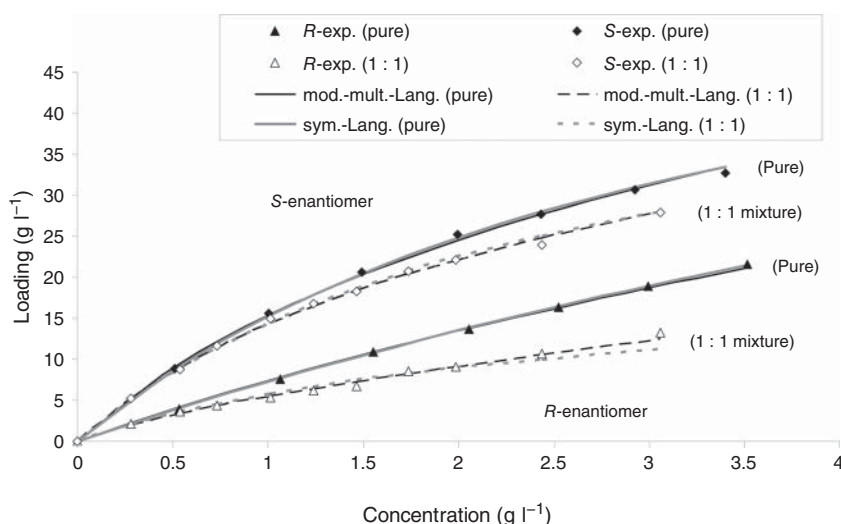
Figure 7.8 Comparison of experimental data (rhombuses and triangles) and fitted isotherm equations (lines) for *R*- and *S*-enantiomers of EMD53986 (pure components and the 1 : 1 mixture on Chiralpak AD in ethanol at 25 °C; mod-multi-Langmuir, Eq. (2.49); for additional data see Appendix A.1).

been fitted to the experimental data. In this case the modified multicomponent Langmuir isotherm (Eq. (2.49))

$$R - \text{enantiomer}: \quad q_R = 2.054 \cdot c_R + \frac{5.847 \cdot c_R}{1 + 0.129 \cdot c_R + 0.472 \cdot c_S}$$

$$S - \text{enantiomer}: \quad q_S = 2.054 \cdot c_S + \frac{19.902 \cdot c_S}{1 + 0.129 \cdot c_R + 0.472 \cdot c_S} \quad (7.24)$$

and the classical Langmuir isotherm (Eq. (2.48)) for the multicomponent system were used. Isotherms for the mixtures result in lower loadings than those of the pure components, and the interaction is stronger for the more weakly retained component, which is characteristic for competitive adsorption.

Other examples are isotherms for the isomers fructose and glucose. Figure 7.9 shows that the resulting isotherms exhibit an upward curvature and the slope of the isotherm is increased in the case of mixtures. This anti-Langmuir behavior is explained from the specific interaction between the hydrated solute molecules and the eluent (water) (Saska et al. 1991, 1992; Nowak et al. 2007). These isotherms are expressed by the following empirical correlations:

$$q_{glu} = 0.27 \cdot c_{glu} + 0.000\,122 \cdot c_{glu}^2 + 0.103 \cdot c_{glu} \cdot c_{fru}$$

$$q_{fru} = 0.47 \cdot c_{fru} + 0.000\,119 \cdot c_{fru}^2 + 0.248 \cdot c_{glu} \cdot c_{fru} \quad (7.25)$$

Another aspect to keep in mind when performing frontal analysis is that severe changes in the general shape of the breakthrough curve for different
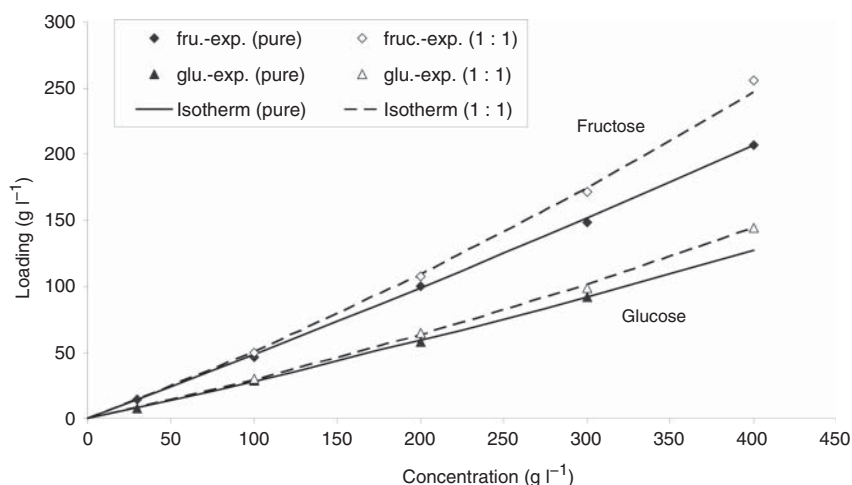
Figure 7.9 Measured and calculated isotherms for pure components and mixtures of glucose and fructose (adsorbent: ion-exchange resin Amberlite CR1320 Ca, $d_p = 325$ µm, eluent: water; for additional data see Appendix A.3).

concentrations may hint at mass transfer or adsorption kinetic effects. As similar changes occur when changing the flow rate, the variation of these two parameters can be used to further discriminate kinetic effects (Ma, Whitley, and Wang et al. 1996). Although analog changes are observed for peak injection too, breakthrough curves are easier to analyze because of the defined conditions for the equilibrium plateau.

The following list summarizes some characteristics of the frontal analysis method:

- Only equilibrium states are evaluated; therefore, errors due to kinetic effects are widely eliminated.
- Amount of solutes and experimental efforts are high, as only one equilibrium point is determined per injection. This is increasingly important if kinetic effects are strong, and thus the time needed to reach the phase equilibrium is rather long. Closed-loop operation may be used to reduce the consumption of solutes.
- Frontal analysis typically provides a high accuracy compared with the other methods mentioned.
- Detector calibration is needed but directly supported by the signal values collected at the plateaus.
- Multicomponent isotherms can be determined if suitable offline analytical methods or solute-specific detectors are available.

The frontal analysis method can be easily extended to determine equilibrium data for mixture with more than two components. An example is illustrated in Figures 7.10 and 7.11 for the determination of the isotherms of three components from ternary breakthrough curves. Details are given by Seidel-Morgenstern (2004).
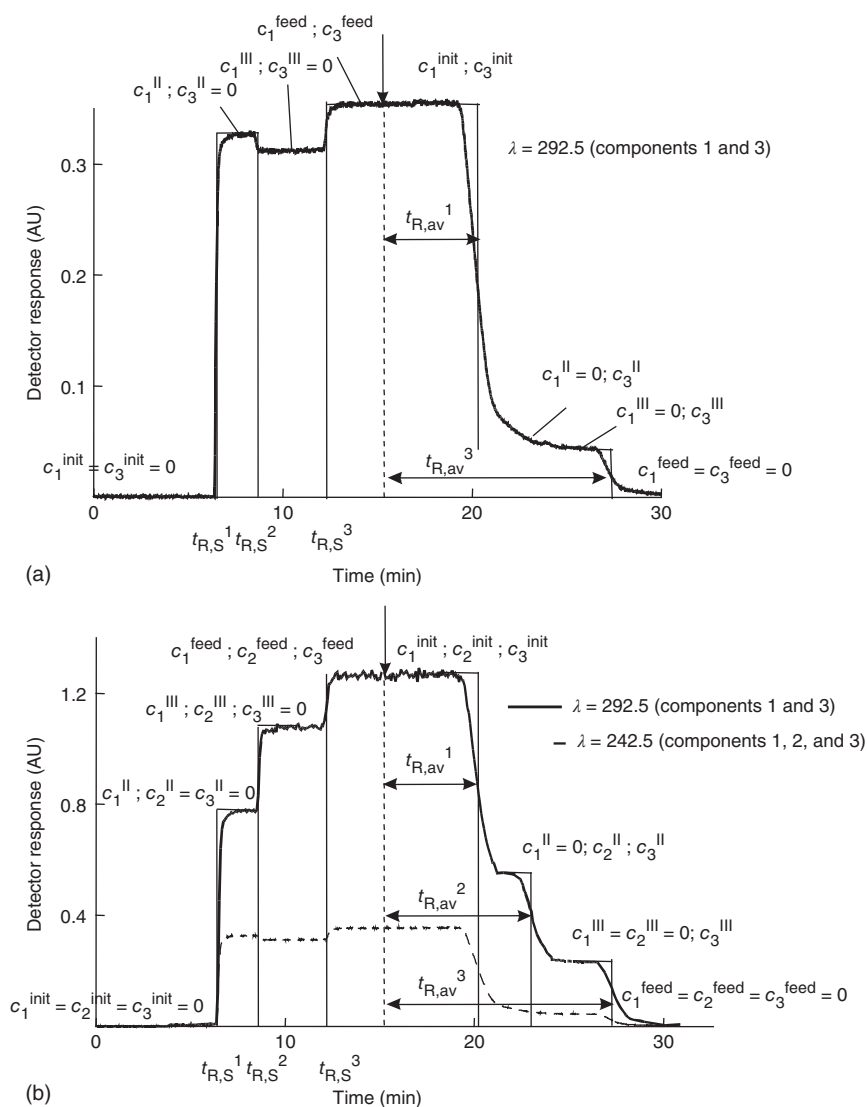
Figure 7.10 Experimental breakthrough curves of a ternary mixture 2-phenylethanol, phenol, and 3-phenyl-1-propanol (Kromasil C_{18}, methanol–water (50 : 50), $c_{PH}^{feed} = c_{PE}^{feed} = c_{PP}^{feed} = 4.7\,g\,l^{-1}$, $\dot{V} = 1\,ml\,min^{-1}$). (a) Detector response at $\lambda = 292.5\,nm$ (solid curve). (b) Detector response at $\lambda = 292.5\,nm$ (dotted curve) and $\lambda = 242.5\,nm$ (solid curve) with marked breakthrough times and plateau heights. Source: Seidel-Morgenstern (2004). Reproduced with permission of Elsevier).
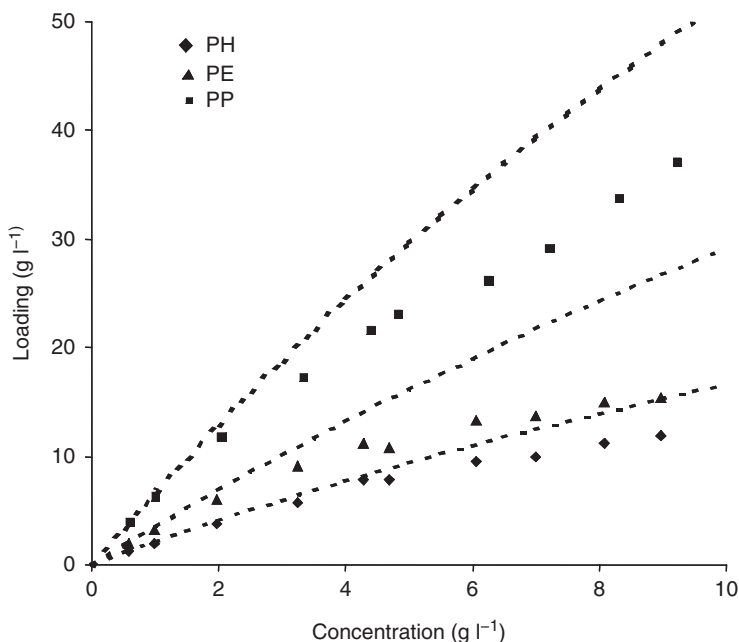
Figure 7.11 Adsorption equilibrium data (symbols) for ternary mixtures of 2-phenylethanol (PE), phenol (PH), and 3-phenyl-1-propanol (PP) (Kromasil C$_{18}$, methanol–water (50 : 50)) determined from frontal analysis. Dashed lines: single solute isotherms calculated with the Langmuir model. (Source: Seidel-Morgenstern (2004). Reproduced with permission of Elsevier).

7.5.6 Analysis of Dispersed Fronts

Analysis of disperse fronts exploits the equilibrium theory of chromatography (Section 6.2.3). It generally reduces the experimental effort as well as the sample amount needed compared with frontal analysis. Because of the complex mathematical solutions in the case of mixtures, it is only suitable for single-component isotherms. Two different forms are described in literature. After injection of a pulse that is not wide enough to cause a concentration breakthrough, the disperse part of the overloaded concentration profile is analyzed. For Langmuir-type isotherms, this is the rear part of the peak. This method is called "elution by characteristic point" (ECP). If the injected volume is high enough to get a breakthrough, it is termed "frontal analysis by characteristic points" (FACP).

The principle of both methods is explained in Figure 7.12.

According to equilibrium theory, the retention time t_R at a characteristic concentration c^+ correlates to the slope of the isotherm at this specific concentration. Rearranging Eq. (6.64), the local slope can be calculated by

$$\left.\frac{dq}{dc}\right|_{c^+} = \frac{t_R(c^+) - t_{0,t}}{t_{0,t}} \frac{\varepsilon_t}{1 - \varepsilon_t} \tag{7.26}$$

The measured retention times must be corrected by the dead time t_{plant} of the plant and for Langmuir-shaped isotherms additionally by the injection time t_{inj} (Eq. (6.67)).
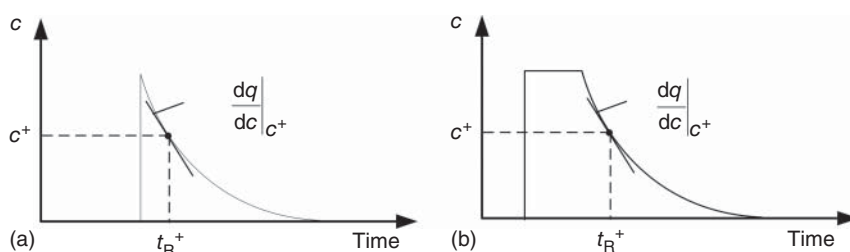
Figure 7.12 Illustration of the principle of the (a) ECP and (b) FACP methods.

If this analysis is repeated at different positions of the profile, the whole isotherm can be estimated based on analyzing a single chromatogram. The concentration range is limited up to the value at the peak maximum. Isotherm parameters can be determined from the slope versus concentration values in two ways.

First, numerical integration leads to the desired relationship between loading and concentration according to

$$q(c^+) = \int_0^{c^+} \frac{\mathrm{d}q}{\mathrm{d}c} \mathrm{d}c = \int_0^{c^+} \frac{t_R(c) - t_{0,t}}{t_{0,t}} \frac{\varepsilon_t}{1 - \varepsilon_t} \mathrm{d}c \tag{7.27}$$

The isotherm equation is then fitted as described in Section 7.5.10.

Second, the derivative of a selected isotherm model equation can be fitted directly to the measured slope values. Thus, in the optimization problem the errors of the loading values are replaced by the errors of the slopes.

Regardless of which method is used, the initial slope of the isotherm must be determined with great care. Either the lower bound for integration must be approximated with the lowest recorded concentration, or the slope for zero concentration must be determined separately. As the latter task is identical to the determination of the Henry constant, this value can be obtained from pulse experiments with very low injection concentrations using momentum analysis.

ECP and FACP are limited to single-component systems. They save time and sample as the whole isotherm is derived from one experiment only. The most severe limitation of the method is the fact that highly efficient columns are required, because kinetic effects are completely neglected. This limits the applicability to systems where the plate number is above 1000. Experimental errors hampering the application of the method are as follows:

- Imprecise detector calibration directly influences the concentration profile and thus the isotherm.
- Peak deformation through extra-column effects of the plant cannot be accounted for.
- Determination of the slopes from retention times for very low concentrations causes typically errors and provides Henry constants differing from values obtained exploiting pulse experiments.

Regarding the FACP method, complementary frontal analysis might be used to check the determined isotherms at the breakthrough concentration.

7.5.7 Peak Maximum Method

A possibility to reduce the influence of limited column efficiencies on the results obtained by the ECP method is to detect just the positions of the peak maxima. The method based on this is called consequently the peak maximum or retention time method. Chromatograms as shown in Figure 7.12a are acquired by measuring a series of pulse response injections for different injection concentrations. The concentration and position of the maximum is strongly influenced by the adsorption equilibrium due to the compressive nature of either the front or the rear of the peak. Thus, the obtained values are less sensitive to kinetic effects than in the case of the ECP method. The isotherm parameters can be evaluated in the same way as described in Section 7.5.6, but the same limitations have to be kept in mind. For some isotherm equations, analytical solutions of the ideal model can be used to evaluate the retention times of the concentration maxima (Golshan-Shirazi and Guiochon 1989; Guiochon et al. 2006). Thus, only retention times must be considered, and detector calibration can be omitted in these cases.

7.5.8 Minor Disturbance/Perturbation Method

The minor disturbance or perturbation method relies on equilibrium theory too and was suggested, for example, by Reilley, Hildebrand, and Ashley (1962). As known from linear chromatography and exploited above already frequently, the retention time of the response to a small pulse injected into a column filled with pure eluent can be used to obtain the initial slope of the isotherm. This approach can be expanded to cover the whole isotherm range. For the example of a single-component system, the procedure is as follows (Figure 7.13): the column is equilibrated with a concentration c_a, and, once the plateau is established, a small pulse is injected at a time $t_{start,a}$, and a pulse of a different concentration is detected at the corresponding retention time $t_{R,a}$.

The injected concentration can be either higher or lower than the plateau concentration, c_a. However, to maintain equilibrium conditions inside the column, the concentration should not deviate too much from c_a, and the injected volume should be small. Care has to be taken to assure that the resulting peak is large enough to be distinguishable from the signal noise. Since for that reason the injected amount must be comparatively high, it is recommended to average results obtained for more or less concentrated injections. In practice, pure eluent with very small injected volumes often provides sufficient accuracy.

According to equilibrium theory, elution of the small disturbance depends on the isotherm slope at the plateau concentration. Because the perturbation peak
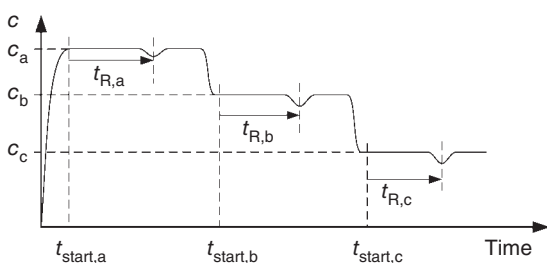
Figure 7.13 Principle of the minor disturbance method for a single-component system (lower concentrated sample injection).

is almost Gaussian, the time at the peak maximum (respectively, minimum) can be taken to estimate in a simple manner local isotherm slopes by Eq. (6.64):

$$\frac{\mathrm{d}q}{\mathrm{d}c}\bigg|_{c_a} = \frac{t_{R,a} - t_{0,t}}{t_{0,t}} \frac{\varepsilon_t}{1 - \varepsilon_t} \tag{7.28}$$

The characteristic retention times have to be corrected again by the dead time of the plant and eventually by the injected time (Section 7.6.2). Using values at different plateau concentrations, the isotherm parameters are derived similar as described in Section 7.5.6.

To determine multicomponent isotherms, the column has to be pre-equilibrated at well-defined mixture concentrations. Perturbations now trigger several recordable peaks. For example, an injection of pure mobile phase on a column pre-equilibrated with a two-component mixture results in two peaks. Their retention times are the experimental information. For exploitation, a competitive isotherm model must be assumed. Using Eq. (6.62) and the definition of the retention times (Eq. (6.64)), for two-component systems together with the coherence condition (Eq. (6.69)), the two measured retention times can be used to calculate the four partial differentials of Eq. (6.68) of the assumed isotherm model at the plateau concentrations. The complexity of these calculations increases rapidly with increasing number of components. Additionally, detector noise can make it difficult to clearly distinguish the earlier- and later-eluting peaks.

An advantage of this method, compared with ECP method, is that the perturbation method is not as sensitive to the number of stages of a column. Additionally, detector calibration is not necessary, and the analysis does not require solute-specific detectors.

The method described can be advantageously combined with the frontal analysis method, which also requires a concentration plateau and thus shares the disadvantage of high sample consumption. As indicated in Figure 7.13, the measurement procedure starts at maximum concentration. This concentration plateau is reduced step by step by diluting the solution. To reduce the amount of samples needed for the isotherm determination, the experiments can be done in a closed-loop arrangement (Figure 7.4, Blümel, Hugo, and Seidel-Morgenstern 1999). It is easily possible to automate this procedure.

As an example, Figure 7.14a gives the results of the isotherm determination for Tröger's base enantiomer on Chiralpak AD ($d_p = 20\,\mu m$) from perturbation measurements (Mihlbachler et al. 2002a). Theoretical retention times for the pure components and racemic mixtures (lines) were fitted to the measured data (symbols) by means of Eq. (7.28) to determine the unknown parameter in Eq. (7.29). Total differentials for the mixture (Eq. (6.68)) were evaluated, respecting the coherence condition (Eq. (7.69) (7.29)). Note that the Henry coefficients were independently determined by pulse experiments and were fixed during the fitting procedure:

$$R\text{-enantiomer}: \ q_R = \frac{0.0311 \cdot c_R \cdot (54 + 0.732 \cdot c_S)}{1 + 0.0311 \cdot c_R} + \frac{0.732 \cdot 0.0365 \cdot c_R \cdot c_S}{1 - 0.0365 \cdot c_R}$$

$$S\text{-enantiomer}: \ q_S = \frac{27 \cdot c_S \cdot (0.1269 + 2 \cdot 0.0153 \cdot c_S)}{1 + 0.1269 \cdot c_S + 0.0153 \cdot c_S^2} \tag{7.29}$$
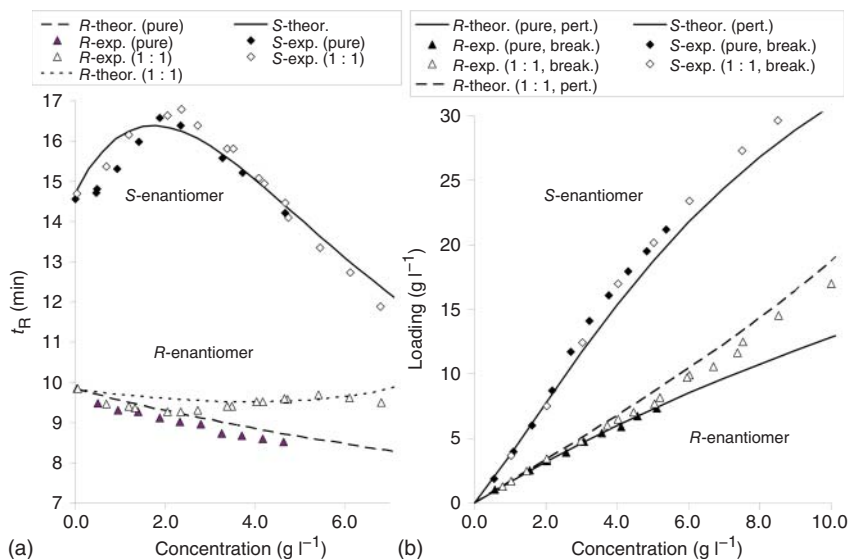
Figure 7.14 (a) Results for isotherm determination for Tröger's base on Chiralpak AD for pure components and mixtures (symbols, experimental data; lines, retention times calculated by Eqs. (7.30) and (7.31) ($t_0 = 5.144$ min, $\dot{V} = 1$ ml min^{-1}); for additional data see Appendix A.2). (b) Comparison of Eq. (7.31) with experimental data from frontal analysis. Source: Data taken from Mihlbachler et al. (2002a).

The resulting isotherms are illustrated as lines in Figure 7.14b. The stronger adsorbing *S*-enantiomer isotherm exhibits an inflection point and can be roughly assumed to be independent of the *R*-enantiomer concentration. The *R*-enantiomer isotherm shows typical Langmuir behavior and minor interaction with the *S*-enantiomers. The unusual behavior of the *R*-enantiomer can be explained with multilayer adsorption processes (Mihlbachler et al. 2002a). A more detailed discussion related to consequences of inflection points in isotherm courses is given by Arnell and Fornstedt (2006).

Figure 7.14b also shows the isotherm data obtained from frontal analysis experiments (symbols), which agree sufficiently well with those obtained using the perturbation analysis.

The determined competitive equilibrium data could be more precisely successfully fitted to a second-order model capable to describe concave isotherms with saturation (Hill 1960; Lin et al. 1989; Mihlbachler et al. 2002a; Jupke 2004):

R-enantiomer: $q_R = \dfrac{54 \cdot c_R \cdot (0.035 + 0.0046 \cdot c_S)}{1 + 0.035 \cdot c_R + 0.062 \cdot c_S + 0.0046 \cdot c_R \cdot c_S + 0.0052 \cdot c_S^2}$

S-enantiomer: $q_S = \dfrac{54 \cdot c_S \cdot (0.062 + 0.0046 \cdot c_R + 2 \cdot 0.0052 \cdot c_S)}{1 + 0.035 \cdot c_R + 0.062 \cdot c_S + 0.0046 \cdot c_R \cdot c_S + 0.0052 \cdot c_S^2}$

$$(7.30)$$

Other illustrative applications of the minor disturbance method were given by Heuer et al. (1998) and Seidel-Morgenstern (2004). Figure 7.15 shows results of
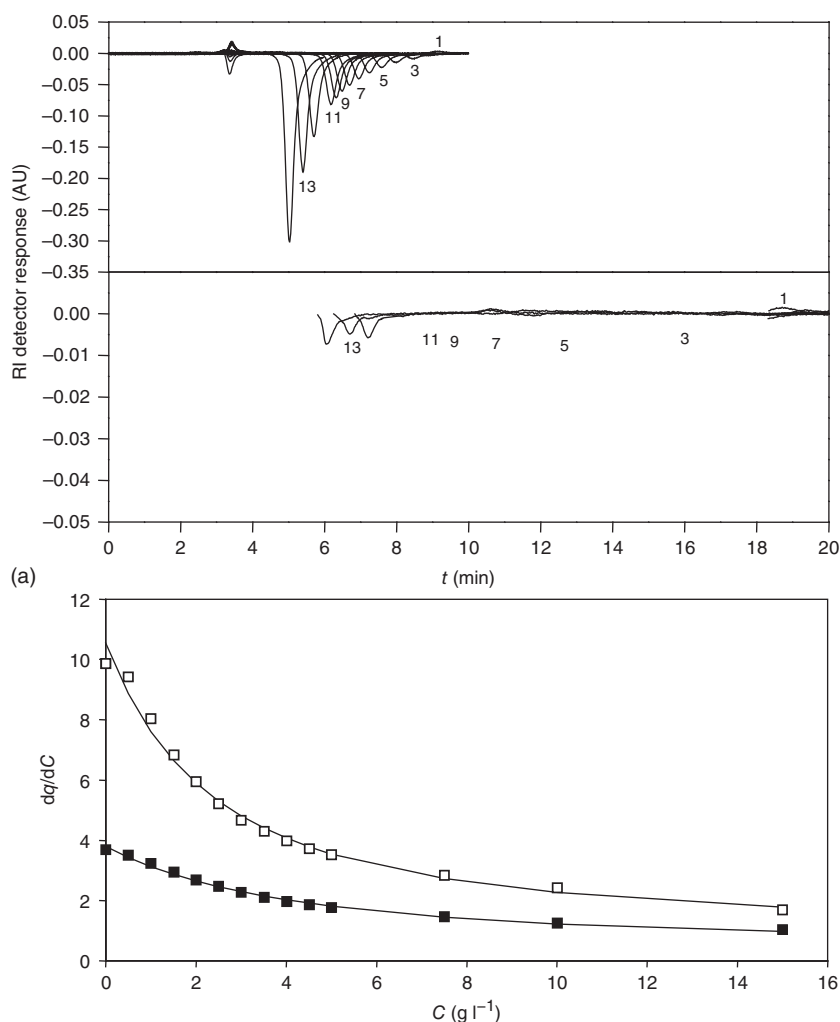
Figure 7.15 Illustration of the perturbation method. (a) Detector responses after equilibrating the column with 1 : 1 mixtures of the two enantiomers of 1-phenoxy-2-propanol (Chiralcel OD, *n*-hexane-isopropanol (90 : 10)). For each of the 14 plateaus, the smaller retention times are illustrated in the upper part, and the corresponding larger retention times in the lower part. (b) Total isotherm derivatives obtained from the determined retention times. Source: Heuer et al. (1998). Reproduced with permission of Elsevier.

performing a series of perturbation experiments on different plateau heights for two enantiomers of a chiral system using a chiral stationary phase.

7.5.9 Curve Fitting of the Chromatogram

The approach of parameter estimation exploiting dynamic process models can also be applied to determine isotherm parameters. In the framework of Figure 7.1, this requires the provision of a validated column model (Section 6.2)

and the plant model (Section 6.3.2) together with an (assumed) adsorption equilibrium model (i.e. an isotherm equation). If the plant parameters, the packing parameters, and detector calibration curves are determined, transport coefficients (Section 7.6) can be estimated from analyzing in the linear range of the isotherm responses to injected pure component pulses. These standard experiments can also provide the Henry coefficient and mass transfer parameters (Section 7.6.2). The remaining unknown isotherm parameters can then be estimated by matching model predictions to the peak shapes observed during overloading experiments (large pulses). To determine significant branches of the isotherms, the injection and thus elution concentrations should be as "high" as possible. This curve fitting method is frequently called "inverse method" (or sometimes just peak fitting). It was first applied systematically by James et al. (1999) in order to determine the competitive adsorption isotherms of the ketoprofen enantiomers on a cellulose-based chiral stationary phase. A systematic comparison of the results achieved using this method with the results of frontal analysis was published by Vajda, Felinger, and Cavazzini (2010). Cornel et al. (2010) suggested recently an attractive extension, designated as direct inverse method, which avoids the calibration of the detector.

In order to identify the correct isotherm model, the analysis has to be repeated for several potential candidate models. In each case realistic initial estimates for the free parameters have to be provided in order to facilitate convergence of the nonlinear optimization procedure required. A drawback of this curve fitting approach is that all errors of the assumed column and plant models have an effect on the quality of the isotherm parameters estimated. Thus, this approach is in particular recommended to get relatively fast a first idea about the thermodynamic properties of the chromatographic system investing only small amounts of sample.

7.5.10 Data Analysis and Accuracy

When dynamic methods are applied, the measured profiles should include enough points and sufficiently low detector noise to allow performing an accurate numerical integration and isotherm determination.

Through repetition of the same experiment and subsequent evaluation of the equilibrium data, the accuracy may be increased by averaging the values, if no systematic errors occur. Significant deviations between equivalent measurements indicate problems in either the data evaluation or the experiment itself. In the latter case, it should be checked if the pumps deliver a constant flow rate and that the temperature is constant in the range of a few tenths of $1\,°C$. If the eluent consists of a fluid mixture, possible influences of slight changes in eluent composition must be critically evaluated (Section 7.5.1).

All plant and packing parameters, as well as the calibration curve of the detector, must be determined with care to give proper results. Simulation and experiment might still agree sufficiently if the "wrong" void fractions and porosities are determined and, consequently, the isotherm parameters are

inaccurate. This is because not the isotherm but rather the isotherm multiplied by the porosities appears in the model equations, and thus both inaccuracies cancel each other out to a certain degree.

Most determination methods finally lead to discrete loading versus concentration data that have to be fitted to a continuous isotherm equation. For this purpose, it is advised to use a least squares method to obtain the parameters of the isotherm. Nonlinear optimization algorithms for such problems are implemented in standard spreadsheet programs. To select a suitable isotherm equation and obtain a meaningful fit, the number of data points should not be too low, and their distribution should be such that changes in the slope or curvature are properly represented. A suitable objective function to minimize the overall error Δ includes the sum of the weighed relative error:

$$\Delta = \sqrt{\sum_{j=1}^{n_p} f_j \cdot \left(\frac{q_{\text{exp},j} - q_{\text{theo},j}}{q_{\text{exp},j}}\right)^2} \tag{7.31}$$

where $q_{\text{theo},j}$ is the value obtained from the isotherm equation, $q_{\text{exp},j}$ is the experimental value, and f_j describes a weighting factor. Often, f_j is a constant and depends only on the number of experimentally determined points (n_p) and the number of isotherm parameters (n_{para}):

$$f_j = \frac{1}{n_p - n_{\text{para}}} \tag{7.32}$$

This allows a comparison of the fitting quality for certain isotherm equations with different numbers of adjustable parameters. Further equations for statistical analysis can be found for example in Barns (1994) and Press et al. (2002). The use of relative instead of absolute errors is necessary to increase the fit in the low concentration region of the isotherm. Otherwise, the isotherm is inaccurate in the low concentration region, and the calculated band profile is inaccurate at the rear boundary.

A problem often encountered in nonlinear optimization is the necessity to provide suitable initial guesses for the free parameters to be estimated. Therefore, it should be tested if different initial guesses lead to different final sets of the parameters. This is connected to the sensitivity problem, which is pronounced in the case of multicomponent systems where several parameters need to be fitted at once. Substantial initial guesses are often difficult to find, and the sensitivity is often low, which demands much experimental data or leads to the selection of other isotherm equations.

For the linear part of the isotherm, the Henry coefficient may be determined separately by pulse experiments (Section 7.5.2). If a significant deviation from the value obtained with the isotherm equation is encountered, additional experiments in the low concentration range should be carried out.

As the overall aim of parameter determination is mostly the (simulation-based) prediction of the process behavior, the final decision about the suitability of the isotherm equation can only be made by comparing experimental and theoretical elution profiles (Section 7.8).

7.6 Mass Transfer Kinetics

Due to numerous different possible kinetic mechanism that can contribute to band broadening and, thus, deviation for the predictions of equilibrium theory, there is a need in simple and easy to apply methods for identifying the parameters of the models summarized in Table 6.1.

Most accurate but also time consuming is the application of fitting model predictions to experimentally observed elution profiles (inverse method), which was already discussed in the context of determining the adsorption isotherms (Section 7.5.9). The application of this method to estimate certain kinetic parameters requires the provision of both a column model and the (independently determined) adsorption isotherms. If a larger number of kinetic parameters are fitted simultaneously, there might be often a problem of proper identification due to parameter correlations. Furthermore, also the model needs to be validated. This can be done by applying the inverse method with various models of increasing flexibility and complexity. Then it is advisable to pick the model, which is sufficiently accurate and does not contain too many kinetic parameters. Obviously, this approach is rather time consuming. To avoid it, there are a few alternative and simpler methods for parameter estimation:

(a) Parameter via correlations, which are partly available, based on aggregated dimensionless parameters (Section 6.2.8).
(b) If measurements under diluted conditions are available, the method of moments provides rapid access to certain model parameters.
(c) Applying neural networks

7.6.1 Correlations

Parameter prediction via correlations, which are partly available, is based on aggregated dimensionless parameters (Section 6.2.8). An illustration for this method was already given in Section 7.4.2 related to estimate the axial dispersion coefficient D_{ax}.

There is a careful selection and application of correlations needed due to typically limited range of validity. Thus, one has to check whether the same units and definitions are used during the development of the correlations as in the column models under consideration. Hereby, there are particular problems related to consistent definitions of porosities and velocities.

For illustration let us consider the effective transport coefficient k_{eff} of the transport dispersion model (Section 6.2.5.1, Eq. (6.84)). This parameter could be determined by a simulation-based parameter estimation using the inverse method that needs to be now performed with the full set of model equations. The estimated value of k_{eff} might be verified by evaluating results of measurements for different volumetric flow rates and injection amounts.

If mass transfer in the film and diffusion inside the pores are taken into account, the effective mass transfer coefficient k_{eff} can be expressed by a series connection

of the internal ($1/k_{pore}$) and external ($1/k_{film}$) mass transfer resistances:

$$\frac{1}{k_{eff}} = \frac{d_p}{10 \cdot \varepsilon_p \cdot D_{pore}} + \frac{1}{k_{film}} = \frac{1}{k_{pore}} + \frac{1}{k_{film}} \tag{7.33}$$

For the film transfer coefficient k_{film}, Wilson and Geankoplis (1966) developed the following correlations:

$$Sh = \frac{1.09}{\varepsilon} \cdot (\varepsilon \cdot Re)^{0.33} \cdot Sc^{0.33} \quad (0.0015 < \varepsilon \cdot Re < 55)$$

$$Sh = \frac{1.09}{\varepsilon} \cdot (\varepsilon \cdot Re)^{0.33} \cdot Sc^{0.33} \quad (55 < \varepsilon \cdot Re < 1050) \tag{7.34}$$

where the Sherwood number Sh and the Schmidt number Sc are defined as

$$Sh = \frac{k_{film} \cdot d_p}{D_m} \tag{7.35}$$

$$Sc = \frac{\eta_l}{\varrho_1 \cdot D_m} = \frac{\nu_1}{D_m} \tag{7.36}$$

The (particle) Reynolds number is given by Eq. (7.12):

$$Re = \frac{u_{int} \cdot d_p \cdot \varrho_l}{\eta_1} = \frac{u_{int} \cdot d_p}{\nu_l} \tag{7.12}$$

Using the same assumptions as in Section 7.4.2 and typical viscosity values ν_l of about 0.01 cm^2 s^{-1}, the Schmidt number for small molecules is of the order of 1000. The Reynolds number is about 0.01, so the first equation in Eq. (7.34) is applicable. For a typical external void fraction ε of 0.37–0.4, the Sherwood number is about 4.5, and the film transfer coefficient is then calculated by

$$k_{film} = \frac{1.09}{\varepsilon} \cdot \frac{D_m}{d_p} \cdot \left(\varepsilon \cdot \frac{u_{int} \cdot d_p}{D_m} \right)^{0.33} \tag{7.37}$$

According to the approximations mentioned above, the film transfer coefficient k_{film} is about 4.5×10^{-2} cm s^{-1} for a 10 µm particle.

The intraparticle (pore) diffusion coefficient defined in Section 6.2.2.4 can be estimated by the Mackie–Meares correlation (Mackie and Meares 1955):

$$D_{pore} = \frac{\varepsilon_p}{(2 - \varepsilon_p)^2} \cdot D_m \tag{7.38}$$

The factor in front of D_m approximates the internal tortuosity factor. For a porosity of 0.9–0.5, D_{pore} is five times smaller than D_m or even lower, so that the contribution to the effective mass transfer coefficient (Eq. (7.33)) is

$$k_{pore} = \frac{10 \cdot \varepsilon_p \cdot D_{pore}}{d_p} = \frac{10}{d_p} \frac{\varepsilon_p^2}{(2 - \varepsilon_p)^2} \cdot D_m \tag{7.39}$$

which gives a value for k_{pore} of about 1×10^{-3} cm s^{-1}. Intraparticle transport is typically an order of magnitude slower than film transfer and is, therefore, the rate-limiting step (see also Ludemann-Hombourger, Bailly, and Nicoud 2000).

Thus, k_{eff} is mainly defined by Eq. (7.39). This simplified analysis provides also a justification to take the effective transfer coefficient as independent of volumetric flow rate and inversely proportional to particle diameter.

7.6.2 Application of Method of Moments

The first moments of chromatographic response curves do not depend on any mass transfer and dispersion coefficients. They capture exclusively thermodynamic parameters and are applied to determine adsorption isotherms as indicated above in Sections 7.5.5–7.5.7.

Normalized moments of experimentally determined elution profiles can be used to estimate kinetic parameters of column models. If the detector signal is a linear function of concentration, analysis can be carried out directly with the detector signals without calibration. Recorded concentration profiles are typically available as n_p discrete concentration versus time values. The first two moments (Eqs. (2.17) and (2.18)) have to be calculated by numerical integration (summation):

$$\mu_1^{ex} = \frac{\int_0^\infty t \cdot c(t) \cdot dt}{\int_0^\infty c(t) \cdot dt} \approx \frac{\sum\limits_{j=1}^{n_p} t_j \cdot c_j \cdot \Delta t}{\sum\limits_{j=1}^{n_p} c_j \cdot \Delta t} \tag{7.40}$$

Kinetic processes as dispersion (D_{ax}), liquid film mass transfer (k_{film}), diffusion inside the particles ($D_{app,pore}$), and adsorption kinetics (k_{ads}) contribute in a complex manner jointly to the overall band broadening as captured by the second moment and to higher order moments (Eqs. (7.41) and (7.42)) quantifying skewness and kurtosis (Kubin 1965):

$$\mu_2^{ex} = \sigma^2 = \frac{\int_0^\infty (t - \mu_1'^{ex})^2 \cdot c(t) \cdot dt}{\int_0^\infty c(t) \cdot dt} \approx \frac{\sum\limits_{j=1}^{n_p} (t_j - \mu_1'^{ex})^2 \cdot c_j \cdot \Delta t}{\sum\limits_{j=1}^{n_p} c_j \cdot \Delta t} \tag{7.41}$$

$$\mu_n^{ex} = \frac{\int_0^\infty (t - \mu_1'^{ex})^n \cdot c(t) \cdot dt}{\int_0^\infty c(t) \cdot dt} \approx \frac{\sum\limits_{j=1}^{n_p} (t_j - \mu_1'^{ex})^n \cdot c_j \cdot \Delta t}{\sum\limits_{j=1}^{n_p} c_j \cdot \Delta t} \tag{7.42}$$

The signal quality (=low detector noise) and sampling rate should be sufficiently high to obtain correct results, else postprocessing of the data is necessary, such as smoothing, baseline correction, and so on. Even then, the result of the integration in Eq. (7.41) depends very much on finally reaching again the baseline. This limits in particular the precision of experimentally determining moments of higher order n with the following general equation.

Moment analysis up to the second moment and related HETP plots were already described in Section 2.2.3. More details regarding the method of

moments were then introduced later in Section 6.2.9 in order to compare higher-order theoretical moments corresponding to different column models. An easy and elegant analysis of measured moments and kinetic model parameters is only possible for response curves in the linear range of the isotherm. For the latter there is the easy way of generating corresponding theoretical expressions exploiting the moment generating properties of the Laplace transform (Kucera 1965, and Ma et al. 1996). In this section it was also already shown that in order to describe one and the same chromatogram, a certain connection between the kinetic parameters of different rate models needs to be respected. Explicit examples were given for illustration connecting the kinetic parameters of the general rate model (Section 6.2.6) and the lumped kinetic model (Section 6.2.5.1) with Eqs. (6.134) and (6.135). More details regarding parameter connections of parameters belonging to different kinetic models can be found in Qamar et al. (2015, 2019) and Qamar and Seidel-Morgenstern (2016).

7.7 Plant Parameters

Regions outside the separation column that can be relevant in interpreting chromatograms and influencing the precision of determining model parameters have been already discussed in Section 6.3.

When comparing simulated profile with measured profiles, the desired level of accuracy has to be specified by the user taking into account the relevance of the plant effects in comparison to the column effects. The dead time of the plant should always be determined. The necessity of the other parameters depends on the design of the plant. Especially for analytical-scale plants, careful parameter estimation is recommended. Finally, influences of the volumetric flow rate on the plant parameters should be checked. In the case of deviations, it should be remembered that, on changing the fluid patterns in the piping and detector cells, the finite response time of the detector and/or changes of temperature might alter the measured signal and different parameter might be obtained.

Following the general concept summarized in Figure 7.1, the parameters describing the fluid dynamic and residence time distribution of the plant peripherals can be determined by means of systematic pulse experiments. For this purpose, small amounts of tracer are injected into the plant without the column, and the output concentrations are measured.

Assuming linear conditions, the contributions to the moments from all parts of the chromatographic plant (Section 6.3.1) are additive, as well known in linear chromatography (Ashley and Reilley 1965). For plant peripherals, equations for the resulting moments can be found in standard chemical engineering textbooks (e.g. Levenspiel 1999; Baerns, Hofmann, and Renken 1999):

The overall retention time of the plant can be obtained by moment analysis of a chromatogram. Using this result together with the known volume of the injected sample V_{inj} and the volumetric flowrate $\dot{V}$, the dead volume of the plant V_{plant} and the corresponding dead time t_{plant} can be estimated. Also individual components can be characterized separately.

In the following, essential parts of a chromatographic unit through which the components to be separated dwell for a certain time are characterized via their first and second moments:

Injector (Eqs. (6.136) and (6.137)):

$$\mu_{inj} = \frac{t_{inj}}{2}, \quad \sigma^2_{inj} = \frac{t^2_{inj}}{12}, \quad t_{inj} = \frac{V_{inj}}{\dot{V}} \tag{7.43}$$

Pipe (Eq. (6.139)):

$$\mu_{pipe} = \frac{V_{pipe}}{\dot{V}}, \quad \sigma^2_{pipe} = 2\left(\frac{V_{pipe}}{\dot{V}}\right)^2 \cdot \frac{D_{ax,pipe}}{u_{0,pipe} \cdot L_{pipe}} \tag{7.44}$$

Detector (Eq. (6.143)):

$$\mu_{tank} = \frac{V_{tank}}{\dot{V}}, \quad \sigma^2_{tank} = \left(\frac{V_{tank}}{\dot{V}}\right)^2 \tag{7.45}$$

Overall plant:

$$\begin{aligned} \mu_{plant} &= \mu_{pipe} + \mu_{tank} \\ \sigma^2_{plant} &= \sigma^2_{pipe} + \sigma^2_{tank} \end{aligned} \tag{7.46}$$

Figure 7.16 illustrates the application of two different concepts of describing the periphery outside a column. The two sets of corresponding simulated concentration profiles are compared with the measurements. In one case ideal plug flow (Eq. (6.138)) and in the other case axial dispersion flow (Eq. (6.139)) was assumed for the pipe system, while both models use the CST model (Eq. (6.143)) to describe the detector system. Figure 7.16 shows that the second model using
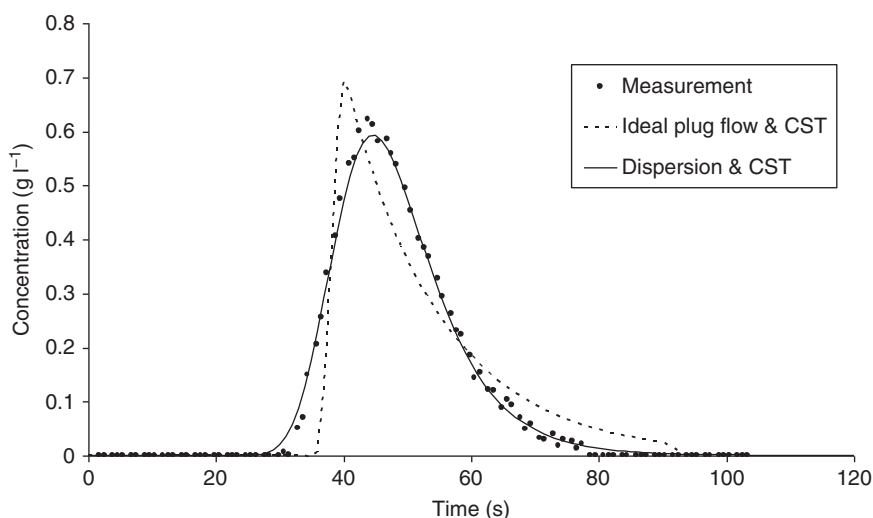
Figure 7.16 Comparison of experimental and simulated profiles (feed: *R*-enantiomer EMD53986 at 4 mg ml^{-1}, $\dot{V} = 20$ ml min^{-1}, preparative scale; for additional data see Appendix A.1).

axial dispersion provides an excellent fit for this setup, while the other does not predict the peak deformation.

A more detailed analysis of dead volume effects is difficult. To allow incorporating into the column models the correct inlet boundary conditions, this analysis needs to carefully distinguish between volumes before and after the column. In any case determined extra-column volumes and residence time characteristics should be documented well, since they are transferable to other process configurations.

7.8 Experimental Validation of Column Models and Model Parameters

After having introduced various column models and methods to estimate the free parameters, below we will shortly demonstrate based on a few examples the degree of agreement between experimental and simulation results.

Hereby the focus will be first on single-column batch elution. Single-column models are the building blocks for more the sophisticated processes described in Chapter 5. In this chapter results for the periodically operating multicolumn SMB processes will be given (Section 5.2.4). To model this periodic process, also an additional simpler steady-state model is shortly introduced, which assumes a hypothetical true countercurrent between two phases involved.

7.8.1 Batch Chromatography

The following examples illustrate a few effects encountered in model validation based on research by Epping (2005) and Jupke (2004). All process simulations are based on the transport dispersion model. Model equations were solved by the gPROMS® software (PS Enterprise, UK) using the orthogonal collocation on finite element (OCFE) method (Section 6.4.2).

Figure 7.17 compares measured and simulated profiles for the batch separation of EMD53986. Very good agreement between theory (solid lines) and experiment (symbols) is achieved using the multicomponent modified Langmuir isotherm (Figure 7.8). Also shown are the simulation results neglecting component interaction by using only the single-component isotherms (dashed line), which deviate strongly from the observed mixture behavior. Typical for competitive adsorption are the displacement of the weaker retained *R*-enantiomer and the peak expansion of the stronger adsorbed *S*-enantiomer.

Finally, selected simulated profiles using an experimentally determined multicomponent isotherm and the respective data calculated according to the ideal adsorbed solution (IAS) theory are compared. Figure 7.18 shows the very close agreement between these methods for this enantiomer system. Especially when considering the effort necessary to measure the multicomponent isotherms, IAS theory or its extensions may provide a good estimate for the component interaction in the case of competitive adsorption. Therefore, it is advisable to simulate elution profiles using the IAS theory after single-component
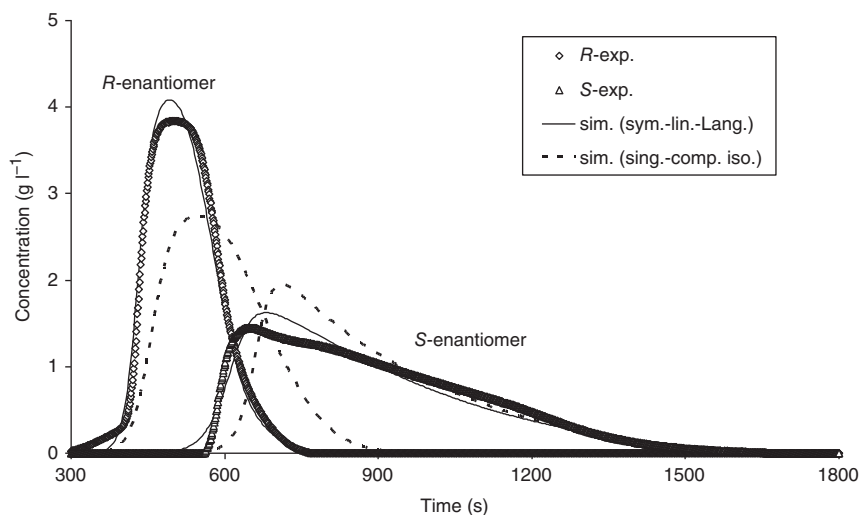
Figure 7.17 Comparison of experimental and simulated profiles for the separation of EMD53986 racemic mixture using single- and multicomponent isotherms (exp., experimental; sim., simulated; $c_{feed} = 6\,g\,l^{-1}$, $\dot{V} = 20\,ml\,min^{-1}$, $V_{inj} = 80\,ml$, $V_c = 54\,ml$; for additional data see Appendix A.1).
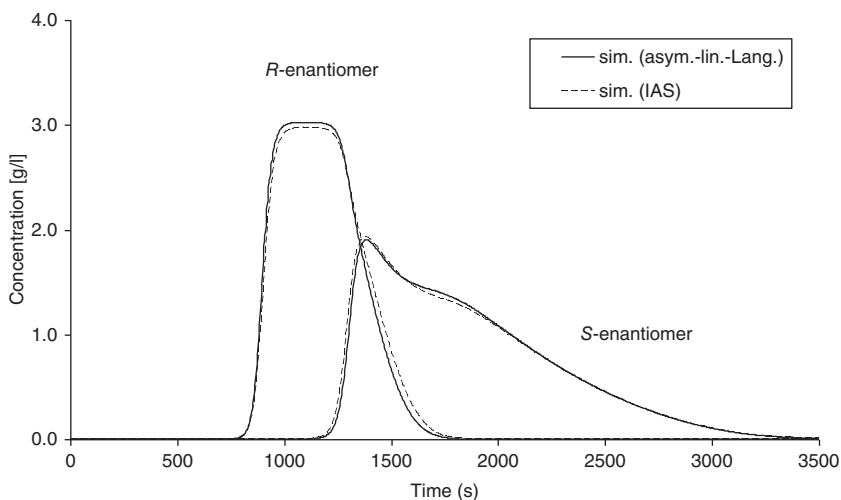
Figure 7.18 Comparison of the simulated profiles for the modified multicomponent Langmuir isotherm and the IAS equation ($c_{feed} = 4.4\,g\,l^{-1}$, $\dot{V} = 10\,ml\,min^{-1}$, $V_{inj} = 120\,ml$, $V_c = 54\,ml$; for additional data see Appendix A.1).

isotherms have been measured. These calculations should then be compared with a few separation experiments to decide if additional measurements of the multicomponent isotherm are still necessary.

The validity of the transport dispersion model was further successfully confirmed by experiments with other chromatographic systems such as Tröger's

base (Mihlbachler et al. 2002a; Jupke 2004), the WMK (Epping 2005), and fructose–glucose (Jupke 2004).

As one example, Figure 7.19 shows the results for Tröger's base using isotherm data determined from breakthrough curves (Eq. (7.30)).

Even for the fructose–glucose isomer system, with liquid phase concentrations that are an order of magnitude higher than those of the enantiomer system, the transport dispersion model is valid. As shown in Figure 7.20, the model approach is in good agreement with experimental data for an industrial-scale plant with a column diameter of about 3 m. In this case, the extra-column dead volumes were especially important to account for.
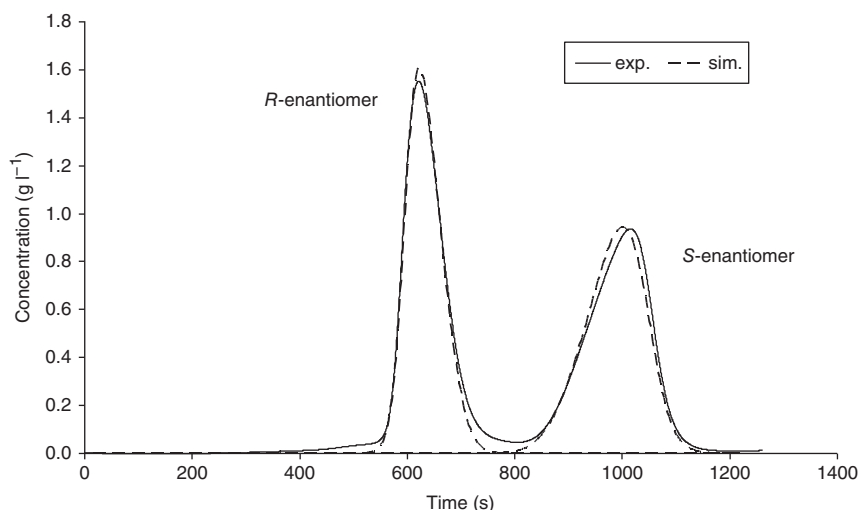
Figure 7.19 Measured and simulated pulse experiment for the Tröger's base racemate ($\dot{V} = 1$ ml min^{-1}, $V_{inj} = 1$ ml, $c_{feed} = 2.2$ g l^{-1}, $V_c = 7.9$ ml; for additional data see Appendix A.2).
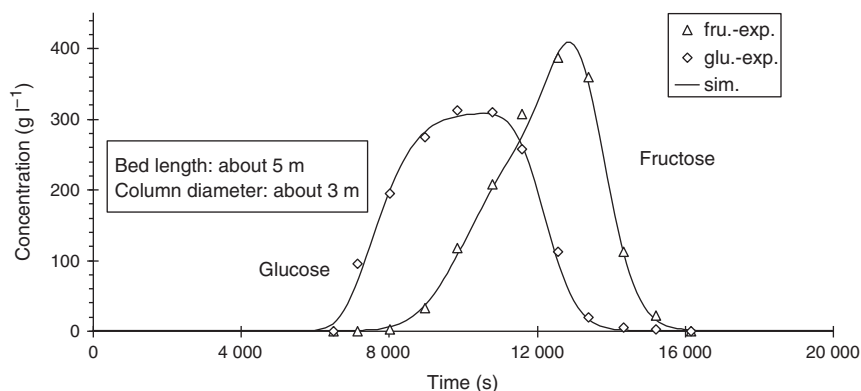
Figure 7.20 Measured and simulated pulse experiment for the glucose–fructose mixture on an industrial plant (see Appendix A.3).

After the appearance of the second edition of this book, numerous other successful applications of the described modeling concepts and parameter estimation strategies have been reported regarding simulating batch chromatographic separations. The provision of a detailed summary was outside the scope of this new edition.

7.8.2 Simulated Moving Bed Chromatography

7.8.2.1 Model Formulation and Parameters

As described in (Section 5.2.4 and Figure 7.21), in SMB chromatography a countercurrent movement of the liquid and solid phases is achieved by shifting in a cascade of connected columns the positions of the inlet and outlet streams in the direction of the fluid by valve switching. The process reaches after a certain number of shifts a cyclic steady state. Assuming identical columns, the spatial profiles are identical after each shifting time, just shifted by one column length. The complex dynamics, cyclic operation, and numerous influence parameters make a purely empirical design of SMB process difficult or even impossible. Since the introduction of this technology, models with different levels of details have been used to obtain the operating parameters (Ruthven and Ching 1989; Storti et al. 1993).

In the case of linear isotherms, there are analytical solutions available (Ruthven and Ching 1989; Storti et al. 1993; Zhong and Guiochon 1996). More complex isotherm equations require the application of numerical methods). The SMB simulation approach takes into account the shifting of the inlet and outlet streams just as in the real plant, and the process reaches a cyclic steady state.
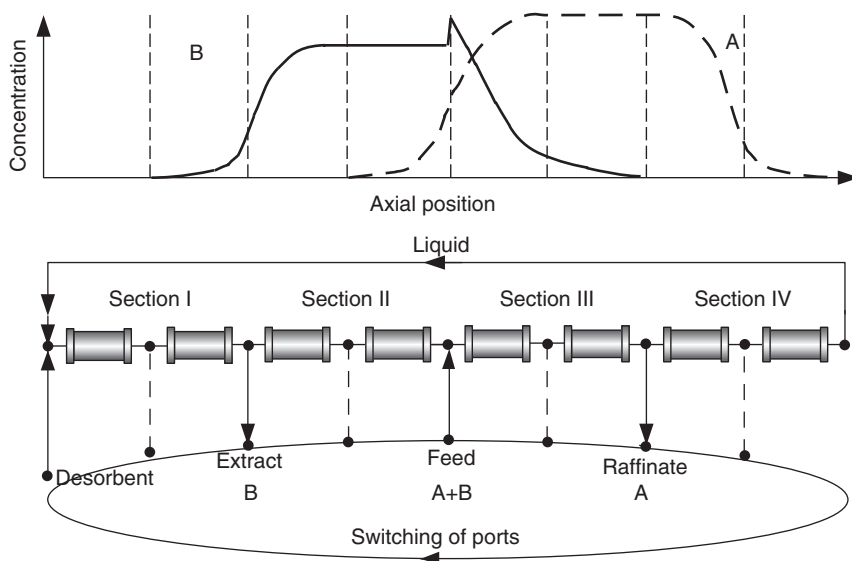
Figure 7.21 Simplified axial concentration profile and flow sheet for an SMB process (standard configuration).
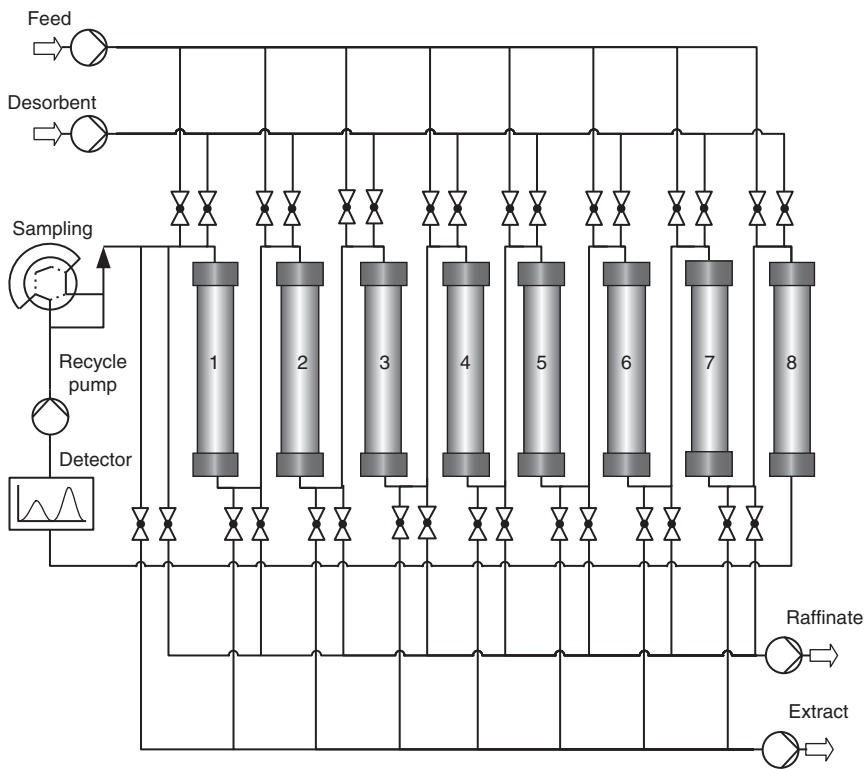
Figure 7.22 Principle setup of an SMB plant including detector systems in the recycle stream (eight-column standard configuration).
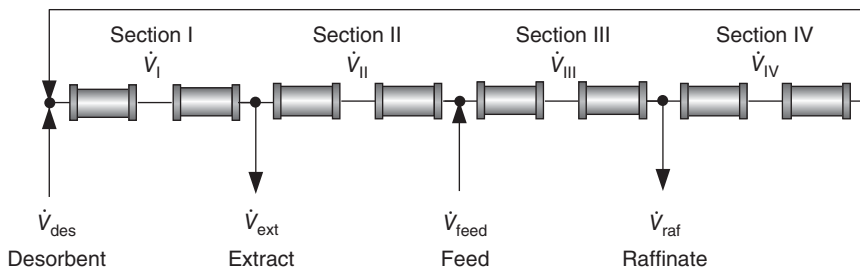
Figure 7.23 Simulation flow sheet of the SMB process ("SMB column model").

An SMB plant consists, for instance, of eight chromatographic columns connected by pipes (Figure 7.22). The piping also includes valves for attaching external streams as well as measurement devices or pumps.

The overall model of an SMB process is developed by linking the models of individual chromatographic columns (Section 6.2). As with the chromatographic batch process, the plant setup of Figure 7.22 is converted into a simulation flow sheet. Figure 7.23 shows the SMB column model.

Mathematically, a SMB model can be set up by connecting the boundary conditions of each column model, including nodes represented by material balances of splitting or mixing models. These so-called node models (Ruthven and Ching 1989) are given for a component i in the sections I–IV by the following:

- Desorbent node:

$$\dot{V}_{des} = \dot{V}_I - \dot{V}_{IV}$$
$$c_{des,i} \cdot \dot{V}_{des} = c_{in,I,i} \cdot \dot{V}_I - c_{out,IV,i} \cdot \dot{V}_{IV} \qquad (7.47)$$

- Extract draw-off node:

$$\dot{V}_{ext} = \dot{V}_I - \dot{V}_{II}$$
$$c_{ext,i} = c_{out,I,i} = c_{in,II,i} \qquad (7.48)$$

- Feed node:

$$\dot{V}_{feed} = \dot{V}_{III} - \dot{V}_{II}$$
$$c_{feed,i} \cdot \dot{V}_{feed} = c_{in,III,i} \cdot \dot{V}_{III} = c_{out,II,i} \cdot \dot{V}_{II} \qquad (7.49)$$

- Raffinate draw-off node:

$$\dot{V}_{raf} = \dot{V}_{III} - \dot{V}_{IV}$$
$$c_{raf,i} = c_{out,III,i} = c_{in,IV,i} \qquad (7.50)$$

Concentrations c_{in} are the inlet boundary conditions (Eqs. (6.101) or (6.102)) of the columns at the beginning of each section, while c_{out} are the outlet concentrations calculated at the end of each section. Intermediate node balances consist of setting equal volume flows and assigning the outlet concentration to the inlet concentration of the subsequent column. Since SMB is a periodic process, the boundary conditions for every individual column are changed after a switching period t_{shift}. If SMB modifications such as Varicol, Modicon, and so on (Chapter 5) are used, the boundary conditions have to be modified accordingly.

Further extensions of the SMB model are necessary to account for the fluid dynamic effects of piping and other peripheral equipment such as measurement devices (Figure 7.22), especially for plants with large recycle lines (Jupke 2004). This is achieved by adding stirred tanks and pipe models (Section 6.3.2) to the simulation flow sheet, resulting in the extended SMB model given in Figure 7.24. If the distribution of the dead volumes in the process is uneven, an asynchronous shifting (Chapter 5) of the inlet and outlet ports is required (Hotier and Nicoud 1995). Sources for the dead volume between the columns are the connecting pipes as well as the switch valves. Dead volume in the recycle stream additionally includes the recycle pump and the measurement systems.

If the number of columns is increased, the process characteristics gradually approach to the characteristics of a hypothetical process, in which the solid and liquid phases are moving continuously in countercurrent directions. This hypothetical process is designated as a true moving bed (TMB) process. It reaches a real steady state that can be described mathematically much easily compared with the approach described above based on exploiting a dynamic model.
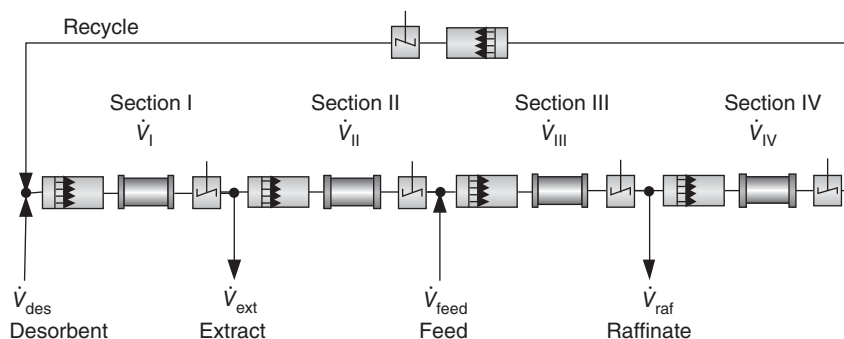
Figure 7.24 Simulation flow sheet for the "extended SMB model."
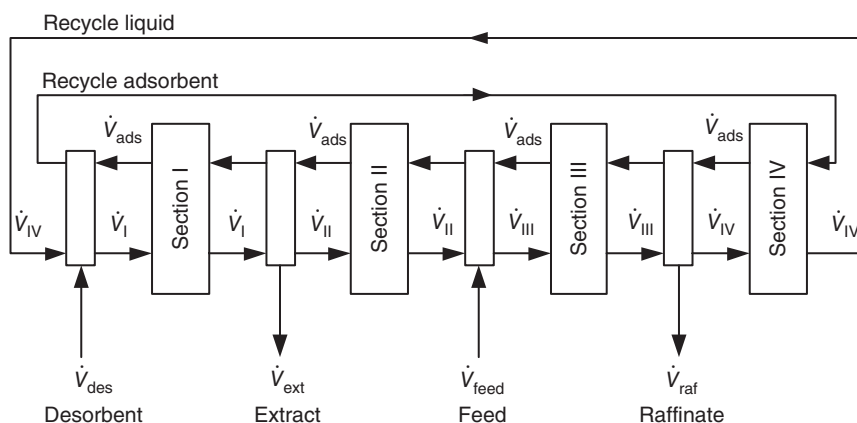
Figure 7.25 Node model for the TMB process.

Because of the strong analogy between simulated and true countercurrent flows, TMB models are frequently used to design SMB processes, more specifically to find suitable operating parameters (inlet and outlet flow rates and shifting times). The simpler TMB process can be elegantly analyzed with the equilibrium theory using the method of characteristics described in in Section 6.2.3. For applications of the equilibrium theory, see Sections 8.4.2 and 8.6.

As an example of how the basic equations of a TMB model can be formulated, the transport dispersion model for batch columns can be modified by considering a flow of the adsorbent in the opposite direction, $\dot{V}_{\text{ads}}$ (Figure 7.25), which results in a convection term in the solid phase mass balance with the velocity u_{ads}.

The dynamic mass balances for component i and section (zone) j in the liquid phase are

$$\frac{\partial c_{j,i}}{\partial t} = -u_{\text{int},j,\text{TMB}} \cdot \frac{\partial c_{j,i}}{\partial x} + D_{\text{ax},j} \cdot \frac{\partial^2 c_{j,i}}{\partial x^2} - \frac{1-\varepsilon}{\varepsilon} \cdot k_{\text{eff},j,i} \cdot \frac{3}{r_{\text{p}}} \cdot (c_{j,i} - c_{\text{p},j,i})$$

$$(7.51)$$

and the corresponding balances for the adsorbent phase are

$$\varepsilon_p \frac{\partial c_{p,j,i}}{\partial t} + (1 - \varepsilon_p) \frac{\partial q_{j,i}}{\partial t} = +u_{ads} \cdot \left(\varepsilon_p \frac{\partial c_{p,j,i}}{\partial x} + (1 - \varepsilon_p) \frac{\partial q_{j,i}}{\partial x} \right)$$
$$+ k_{eff,j,i} \cdot \frac{3}{r_p} \cdot (c_{j,ij} - c_{p,j,i}) \tag{7.52}$$

For process evaluation, just the stationary form of Eqs. (7.51) and (7.52) is needed, in which the accumulation terms are zero. To transfer the results of TMB to SMB, the interstitial velocity in the SMB process must be equal to the relative velocity of fluid and adsorbent in the TMB process:

$$u_{int,SMB} = u_{int,TMB} + u_{ads} \tag{7.53}$$

u_{ads} is positive, and the direction inverse to u_{int} is specified in Eq. (7.52) by a positive sign in front of the convection term.

Liquid phase velocities are related to the volumetric flows in each section, while the adsorbent movement in the case of SMB is equal to the column volume moved per shifting time:

$$u_{int,j,SMB} = \frac{\dot{V}_j}{\varepsilon \cdot A_c} \tag{7.54}$$

$$u_{ads} = \frac{V_{ads}}{A_c \cdot (1 - \varepsilon)} = \frac{V_c}{A_c \cdot t_{shift}} = \frac{L_c}{t_{shift}} \tag{7.55}$$

Below, an illustration is given for the similarity between predictions generated by TMB and SMB models.

Figure 7.26 gives an example of the difference in axial concentration profiles between TMB and SMB models, where the number of columns per SMB section is varied while the overall bed length is kept constant. The operating parameters are taken from an optimized TMB process with 99.9% purity of the product streams. Clearly, the end-cycle SMB profiles approach the TMB profile only for a high number of columns.

Quite similar concentration profiles generated with the two models were reported for less or more columns per section. However, due to high investment costs, SMB plants often exploit fewer columns. Then real SMB plants behavior starts to differ considerably from the TMB process (Chapter 8). Nevertheless, initial process design can be efficiently performed based on true moving bed assumptions (Storti et al. 1993; Charton and Nicoud 1995). This will be outlined further in Chapter 8.

To accurately simulate an SMB process, the model parameters of the individual columns (Section 7.1–7.6), and, if necessary, the dead volumes (Figure 7.24) must be known.

It is advisable to use nearly identical columns (concerning bed length and packing structure), which is easily checked by comparing their outgoing signals from batch experiments with small injected amounts and determining the Henry coefficient. Comparison of the product peaks for the individual columns may also be used as a test for the packing. If strong deviations occur, the packing procedure must be repeated and checked for errors.
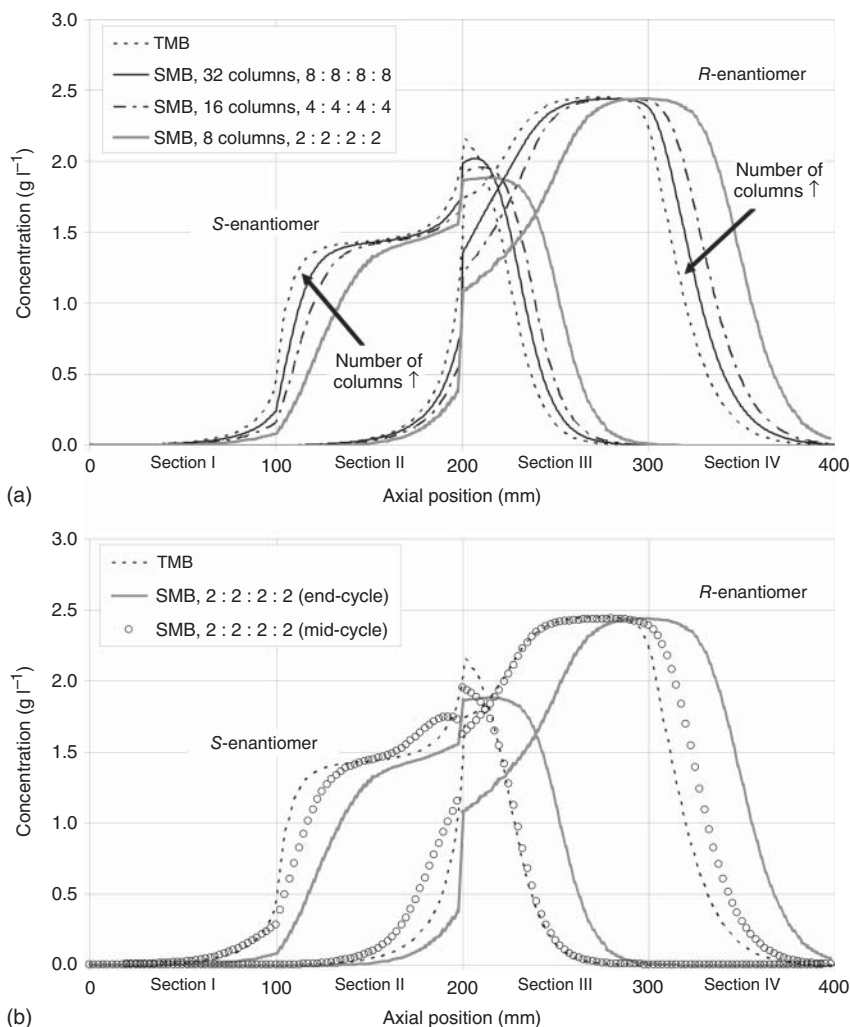
Figure 7.26 Axial concentration profile for (a) TMB and SMB processes with different number of columns per section (end-cycle profiles) and (b) TMB and SMB processes with eight columns and profiles at end-cycle and mid-cycle (separation of EMD53986, Appendix A.1, equal operating parameters).

Model parameters should then be obtained only for one column, as these should be the same for all. Column parameters are determined by batch experiments or are known from previous tests. Finally, the dead volume inside an SMB plant (Figure 7.24) can be determined performing tracer pulse experiments by connecting the respective part of the plant directly to the pump and a detector.

With respect to the operating parameters, it is necessary to specify five independent variables. A useful method is to specify the four internal flow rates ($\dot{V}_{I-IV}$) and the switching time (SMB model) or the corresponding solid flow

(TMB model). Note that the four external flow rates have to fulfill the overall mass balance and only three flow rates are independent.

7.8.2.2 Experimental Validation

Ever since the development and application of mathematical models for the design of SMB processes, beginning in the 1980s, efforts have been made to validate these models by comparing measured and simulated data. SMB and TMB models of different complexity have been used for this task, for example, the ideal and equilibrium dispersion SMB model as well as TMB and SMB transport dispersion models. A common approach is to compare the internal concentration profile with the simulation results. Another way is to use the product concentrations at extract and raffinate and their temporal evolution. Some characteristic points of the internal profiles can be obtained from taking samples (see sample valve in Figure 7.22) and offline analysis. Classical examples include those from applications in the petrochemical and sugar industries (Ruthven and Ching 1989; Ma and Wang 1996). Example applications in enantioseparation were given for example by Heuer et al. (1998) and comprehensively by Rajendran et al. (2009).

As depicted in Figure 7.22, one or more detector scan be placed in the recycle stream. They are positioned in front of the recycle pump. Due to the shifting of external streams, the detector "travels" through all process section during one cycle.

Yun, Zhong, and Guiochon (1997) placed one UV detector in the recycle stream to measure the fronts in sections I and IV for the separation of phenylethanol and phenylpropanol. The use of only one detector allows the measurement of the pure components in each regeneration section, but the concentration of the mixture in the separation section cannot be determined. Jupke et al. used a multi-detector setup for binary separation, which gave the possibility of measuring the concentration profiles of all components in all sections individually (Jupke 2004; Epping 2005; Mannschreck 1992; Mihlbachler et al. 2002b).

The general relation between the data obtained in the recycle stream, which can be used for model validation, and the axial profile, which can be used for process analysis, is given in Figure 7.27. The setup is identical to Figure 7.22. In Figure 7.27a, the simulated temporal profile measured behind column 8 during one complete cycle is shown. The concentration values after each shifting interval are given as symbols. In the ideal case, they are identical to those of the samples taken for offline analysis. As the process is in cyclic steady state, the axial profiles after each switching time are identical; only their position is shifted by one column. Thus, the symbols marked above can be translated into points of the axial profile at the end of one shifting period (Figure 7.27b). Simulated curves are added for comparison. If no asymmetrical distribution of dead volumes is present in the plant, the end-of-shifting-interval profiles are identical to those at the end of a cycle.

The axial position in Figure 7.27b is normalized to the length of each column, and, therefore, column 1 lies between the coordinates 0 and 1. The temporal positions 0, 1, 2, … , 8 correspond to the axial positions 8, 7, … , 0. The feed is injected

(a)

(b)
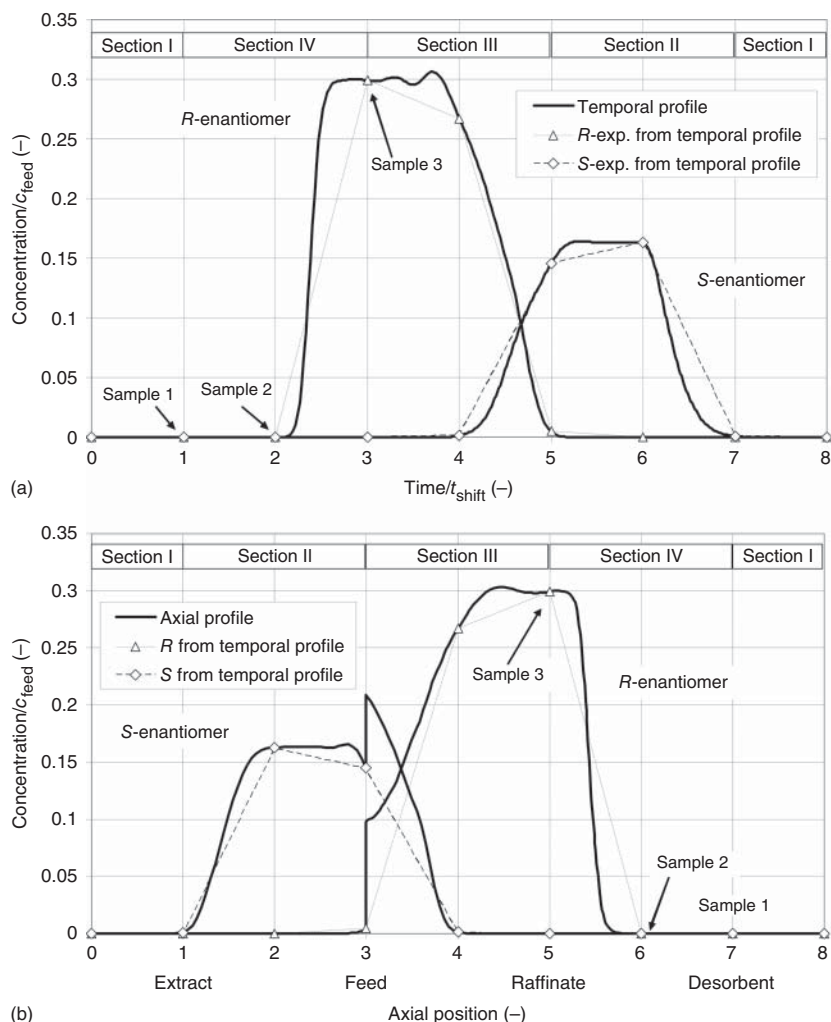
Figure 7.27 Relationship between the temporal profile measured behind the eighth column (a) and the axial profile at the end of cycle just before the feed position is switched in front of the fifth column (b); symbols represent the identical points.

in front of column 5 at the start of the cycle, and the last feed position at the end is in front of column 4 (Figure 7.27).

Importantly, sampling gives only a limited number of points in the axial profile. The complete curve cannot be reconstructed from any temporal measurement, as the concentration fronts inside the columns change from the beginning to the end of the shifting interval. However, increasing the number of experimental samples per interval, of course, allows a comparison of the simulated temporal profile on a broader base without online measurement.

In the following, examples based on our own research are given for the validation of the SMB transport dispersion model, using an online detection system in

the recycle stream. All flow sheet, column, and plant models were implemented in the gPROMS (PS Enterprise, UK) simulation tool and solved with OCFE methods (Section 6.4.2).

A more detailed discussion of the experiments and simulations for various operating points and conditions can be found in Jupke (2004). and Mihlbachler et al. (2002b). Example results for the three systems EMD53986, enantiomers of Tröger's base, and fructose–glucose are discussed. Pulse tests with the solutes proved that all columns for each SMB setup behaved identically within small deviations. Most of the experiments were performed on a commercial plant "Licosep Lab" from Novasep (France).

In all cases relative good agreement between simulation and experiment was found.

Simulations were performed considering the extended SMB configuration (Figure 7.24), which included dead volumes and synchronous as well as asynchronous port switching. The latter accounts for the dead volume in the recycle stream, which is the dominant contribution (Hotier and Nicoud 1995). The temporal concentration profiles are shown, and the partitions of the time axis mark the switching time. The additional time added after the eighth period is the asynchronous switching time.

Figure 7.28 shows the simulated and measured concentration profiles for EMD53986. Good agreement can be observed for this system, which is characterized by its strong coupled and nonlinear adsorption behavior. Only slight deviation in the position of the fronts and the maximum height is observed. Especially, the steepness of the fronts is reproduced very well. The model can also predict the start-up of the SMB plant (Figure 7.29) correctly. Deviations in the first cycle are presumably due to the pressure fluctuations often encountered
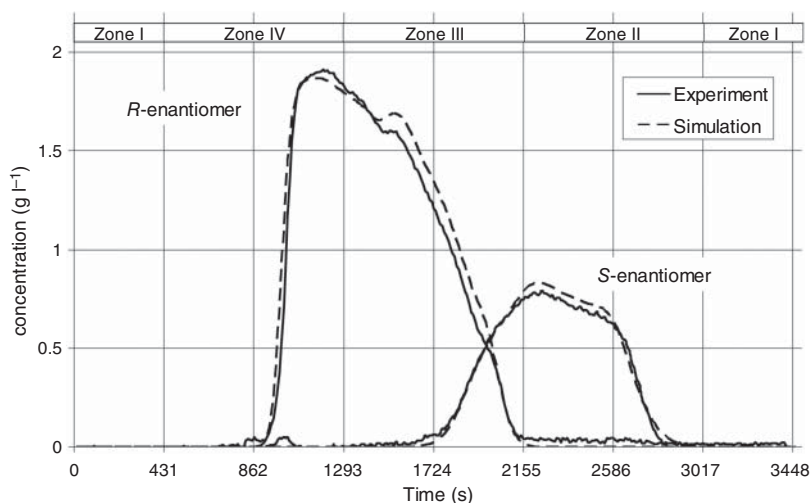
Figure 7.28 Measured and simulated concentration profiles in the SMB for EMD53986 (cycle 8, $c_{feed} = 5\,\mathrm{g\,l^{-1}}$; for additional data see Appendix A.1). Source: Jupke, Epping, and Schmidt-Traub (2002). Reproduced with permission of John Wiley and Sons.
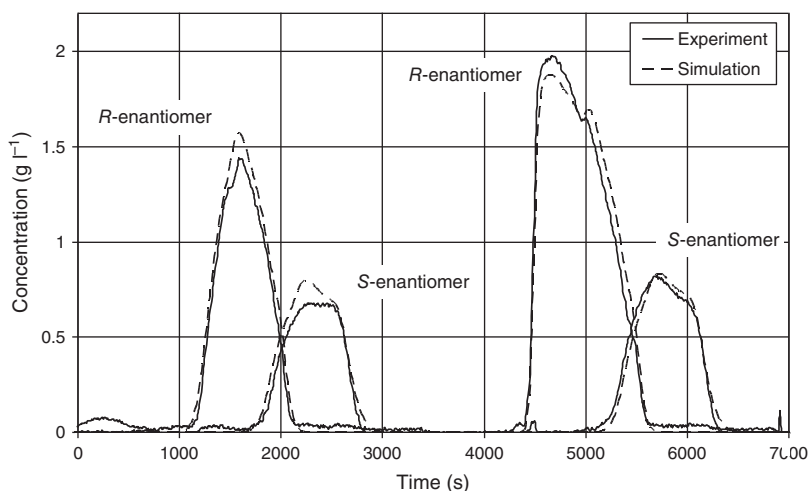
Figure 7.29 Measured and simulated concentration profiles in the SMB for EMD53986 during start-up (one and two cycles; for other data see Figure 7.26).
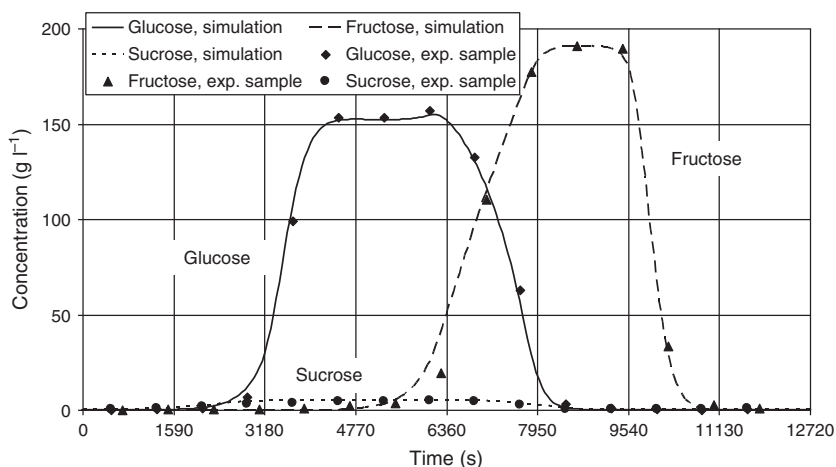
Figure 7.30 Simulated and measured (sampled) concentration profiles in the SMB for fructose–glucose ($c_{feed} = 300 \, g \, l^{-1}$) and sucrose ($c_{feed} = 18 \, g \, l^{-1}$) (eighth cycle; for additional data see Appendix A.3).

directly after start-up. Good agreement between simulation and experiment was observed for other operating conditions, too.

The separation of an industrial feed mixture of fructose–glucose ($c_{feed} = 300 \, g \, l^{-1}$) containing 6% sucrose as an impurity is displayed in Figure 7.30. Once again, good agreement between experiment and simulation is found. The individual concentration profiles of this three-component mixture cannot be determined by two-detection systems. Therefore, additional samples (two per shifting interval) were taken and analyzed by HPLC.

Isotherm data for the third sugar sucrose were determined from pulse experiments and represented by a linear isotherm. Because of the low adsorptivity, this impurity is collected at the raffinate together with the glucose.

The examples for experimental validation of the SMB model are based on the "extended model" (Figure 7.24) that takes into account the fluid dynamic effects of the piping, especially the recycle lines and other peripheral equipment such as measurement devices.

Finally it should be mentioned that regarding the simulation of SMB chromatography, numerous more successful reports were published. This does not only include isocratic process operation but also more advanced concepts, e.g. gradient chromatography (Antos and Seidel-Morgenstern 2001; Wekenborg, Susanto, and Schmidt-Traub 2005).

References

Altenhöner, U., Meurer, M., Strube, J., and Schmidt-Traub, H. (1997). Parameter estimation for the simulation of liquid chromatography. *J. Chromatogr. A* 769: 59–69.

Antos, D. and Seidel-Morgenstern, A. (2001). Application of gradients in the simulated moving bed process. *Chem. Eng. Sci.* 56: 6667–6682.

Arnell, R. and Fornstedt, T. (2006). Validation of the tracer-pulse method for multicomponent liquid chromatography, a classical paradox revisited. *Anal. Chem.* 78: 4615–4623.

Ashley, J.W. and Reilley, C.N. (1965). De-tailing and sharpening of response peaks in gas chromatography. *Anal. Chem.* 37 (6): 626–630.

Baerns, M., Hofmann, H., and Renken, A. (1999). *Chemische Reaktionstechnik in Lehrbuch der Technischen Chemie Band 1*. Stuttgart: Georg Thieme Verlag.

Barns, J.W. (1994). *Statistical Analysis for Engineers and Scientists*. McGraw-Hill.

Blümel, C., Hugo, P., and Seidel-Morgenstern, A. (1999). Quantification of single solute and competitive adsorption isotherms using a closed-loop perturbation method. *J. Chromatogr. A* 865: 51–71.

Charton, F. and Nicoud, R.-M. (1995). Complete design of a simulated moving bed. *J. Chromatogr. A* 702: 97–112.

Chung, S.F. and Wen, C.Y. (1968). Longitudinal dispersion of liquid flowing through fixed and fluidised beds. *AIChE J.* 14 (6): 857–866.

Cornel, J., Tarafder, A., Katsuo, S., and Mazzotti, M. (2010). The direct inverse method: a novel approach to estimate adsorption isotherm parameters. *J. Chromatogr. A* 1217: 1934–1941.

Epping, A. (2005). *Modellierung, Auslegung und Optimierung chromatographischer Batch-Trennung*. Aachen: Shaker-Verlag.

Golshan-Shirazi, S. and Guiochon, G. (1989). Experimental characterization of the elution profiles of high concentration chromatographic bands using the analytical solution of the ideal model. *Anal. Chem.* 61: 462–467.

Guiochon, G., Felinger, A., Shirazi, D.G., and Katti, A.M. (2006). *Fundamentals of Preparative and Nonlinear Chromatography*. Amsterdam Press: Elsevier.

Heuer, C., Küsters, E., Plattner, T., and Seidel-Morgenstern, A. (1998). Design of the simulated moving bed process based on adsorption isotherm measurements using a perturbation method. *J. Chromatogr. A* 827: 175–191.

Hill, T.L. (1960). *An Introduction to Statistical Thermodynamics.* Addison-Wesley, Reading.

Hotier, G. and Nicoud, R.M. (1995). Separation by simulated moving bedchromatography with dead volume correction by desynchronization of periods. *Europäisches Patent EP*688589A1.

James, F., Sepúlveda, M., Charton, F. et al. (1999). Determination of binary competitive equilibrium isotherms from the individual chromatographic band profiles. *Chem. Eng. Sci.* 54: 1677–1696.

Jupke, A. (2004). *Experimentelle Modellvalidierung und modellbasierte Auslegung von Simulated Moving Bed (SMB) Chromatographieverfahren*, Fortschrittbericht VDI: Reihe 3 Nr. 807. Düsseldorf: VDI Verlag GmbH.

Jupke, A., Epping, A., and Schmidt-Traub, H. (2002). Optimal design of batch andSMB chromatographic separation processes. *J. Chromatogr. A* 944: 93–117.

Korns, G.A. (2000). *Mathematical Handbook for Scientists and Engineers.* Dover Publications Inc.

Kubin, M. (1965). Beitrag zur theorie der chromatographie. *Collect. Czech. Chem. Commun.* 30: 1104–1118.

Kucera, E. (1965). Contribution to the theory of chromatography/linear non-equilibrium elution. *J. Chromatogr. A* 19 (2): 237–248.

Lapidus, F.L. (1962). *Digital Computation for Chemical Engineers.* New York: McGraw-Hill.

Levenspiel, O. (1999). *Chemical Reaction Engineering*, 3e. New York: John Wiley & Sons, Inc.

Lin, B., Ma, Z., Golshan-Shirazi, S., and Guiochon, G. (1989). Study of the representation of competitive isotherms and of the intersection between adsorption isotherms. *J. Chromatogr. A* 475 (1): 1–11.

Ludemann-Hombourger, O., Bailly, M., and Nicoud, R.-M. (2000). Design of a simulated moving bed: optimal size of the stationary phase. *Sep. Sci. Technol.* 35 (9): 1285–1305.

Ma, Z., Whitley, R.D., and Wang, N.-H. (1996). Pore and surface diffusion in multicomponent adsorption and liquid chromatography systems. *AlChE J.* 42 (5): 1244–1262.

Mackie, J.S. and Meares, P. (1955). The diffusion of electrolytes in a cation-exchange resin membrane. *Proc. R. Soc. London A* 267: 498–506.

Mannschreck, A. (1992). Chiroptical detection during liquid chromatography. *Chirality* 4: 163–169.

Mihlbachler, K., Kaczmarski, A., Seidel-Morgenstern, A., Guiochon, G. (2002a). Measurement and modeling of the equilibrium behavior of the Troger's base enantiomers on an amylose-based chiral stationary phase. 955: 35–52.

Mihlbachler, K., Jupke, A., Seidel-Morgenstern, A. et al. (2002b). Effect of the homogeneity of the column set on the performance of a simulated moving bed unit, *Part II: Experimental study. J. Chromatogr. A* 944: 3–22.

Nowak, J., Gedicke, K., Antos, D. et al. (2007). Synergistic effects in competitive adsorption of carbohydrates on an ion-exchange resin. *J. Chromatogr. A* 1164: 224–234.

Press, W.H., Flannery, B.P., Teukolsky, S.A., and Vetterling, W.T. (2002). *Numerical Recipes in C++: The Art of Scientific Computing*, 2e. Cambridge: Cambridge University Press.

Qamar, S., Abbasi, J.N., Mehwish, A., and Seidel-Morgenstern, A. (2015). Linear general rate model of chromatography for core–shell particles: analytical solutions and moment analysis. *Chem. Eng. Sci.* 137: 352–363.

Qamar, S. and Seidel-Morgenstern, A. (2016). Extending the potential of moment analysis in chromatography. *TrAC Trends Anal. Chem.* 81: 87–101.

Qamar, S., Bashir, S., Perveen, S., and Seidel-Morgenstern, A. (2019). Relations between kinetic parameters of different column models for linear chromatography applying core-shell particles. *J. Liq. Chromatogr. Related Technol.* 42 (1–2): 16–30.

Rajendran, A., Paredes, G., and Mazzotti, M. (2009). Simulated moving bedchromatography for the separation of enantiomers. *J. Chromatogr. A* 1216: 709–738.

Rastegar, S.O. and Gu, T. (2017). Empirical correlations for axial dispersion coefficient and Peclet number in fixed-bed columns. *J. Chromatogr. A* 1490: 133–137.

Reilley, C.N., Hildebrand, G.P., and Ashley, J.W. Jr., (1962). Gas chromatographic response as a function of sample input profile. *Anal. Chem.* 34: 1198–1213.

Ruthven, D.M. (1984). *Principles of Adsorption and Adsorption Processes*. New York: Wiley.

Ruthven, D.M. and Ching, C.B.(1989) Review article no. 31: counter-current and simulated counter-currentadsorption separation processes. *Chem. Eng. Sci.*, 44 (5): 1011–1038.

Saska, M., Clarke, S.J., Wu, M.D., and Iqbal, K. (1991). Applications of continuous chromatographic separation in the sugar industry: Part I. Glucose/fructose equilibria on Dowex Monosphere 99 Ca resin at high sugar concentrations. *Int. Sugar J.* 93: 1115.

Saska, M., Clarke, S.J., and Iqbal, K. (1992). Continuous separation of sugarcane molasses with a simulated-moving-bed adsorber: absorption equilibria, kinetics and applications. *Sep. Sci. Technol.* 27: 1711–1732.

Seidel-Morgenstern, A. (2004). Experimental determination of single solute and competitive adsorption isotherms. *J. Chromatogr. A* 1037 (1–2): 255–272.

Seidel-Morgenstern, A. (1995). Mathematische Modellierung der präparativenFlüssigchromatographie.Wiesbaden: Deutscher Universitätsverlag.

Seidel-Morgenstern, A. and Nicoud, R.-M. (1996). Adsorption isotherms: experimental determination and application to preparative chromatography. *Isolation Purif.* 2: 165–200.

Storti, G., Mazzotti, M., Morbidelli, M., and Carrà, S. (1993). Robust design ofbinary countercurrent adsorption separation processes. *AlChE J*. 39: 471–492.

Vajda, P., Felinger, A., and Cavazzini, A. (2010). Adsorption equilibria of proline in hydrophilic interaction chromatography. *J. Chromatogr. A* 1217: 5965–5970.

Van Deemter, J.J., Zuiderweg, F.J., and Klinkenberg, A. (1956). Longitudinal diffusion and resistance to mass transfer as causes of nonideality in chromatography. *Chem. Eng. Sci.* 5: 271–289.

Wekenborg, K., Susanto, A., and Schmidt-Traub, H. (2005). Modelling and validated simulation of solvent-gradient simulated moving bed (SG-SMB) processes for protein separation. In: *Computer Aided Chemical Engineering*, vol. 20 (eds. L. Puigjaner and A. Espuña), 313–318. Elsevier.

Wen, C.Y. and Fan, L.T. (1975). *Models for Flow Systems and Chemical Reactors*. New York: Marcel Dekker.

Wilson, E.J. and Geankoplis, C.J. (1966). Liquid mass transfer at very low Reynolds numbers in packed beds. *Ind. Eng. Chem. Fundam.* 5: 9.

Yun, T., Zhong, G., and Guiochon, G. (1997). Simulated moving bed under linearconditions: experimental vs. calculated results. *AlChE J*. 43 (4): 935–945.

Zhong, G. and Guiochon, G. (1996). Analytical solution for the linear ideal model ofsimulated moving bed chromatography. *Chem. Eng. Sci.* 51 (18): 4307–4319.

8

Process Design and Optimization*

Andreas Jupke[1], Andreas Biselli[1], Malte Kaspereit[2], Martin Leipnitz[1], and Henner Schmidt-Traub[3]

[1] *RWTH Aachen University, Fakultät Maschinenwesen, AVT – Aachener Verfahrenstechnik, Lehrstuhl für Fluidverfahrenstechnik, Forckenbeckstraße 51, 52074 Aachen, Germany*
[2] *Friedrich-Alexander-Universität Erlangen-Nürnberg, Lehrstuhl für Thermische Verfahrenstechnik, Egerlandstr. 3, 91058 Erlangen, Germany*
[3] *TU Dortmund, Fakultät für Bio- und Chemieingenieurwesen, Lehrstuhl für Anlagen- und Prozesstechnik, Emil-Figge-Str. 70, 44227 Dortmund, Germany*

The previous chapters deal with the selection of chromatographic systems and process concepts as well as the modeling of chromatographic processes. On this basis, the present chapter focuses on process design and optimization of a chromatographic process. First, performance criteria of chromatographic separation processes will be introduced, which act as indicators of efficiency and quality of preparative chromatographic separations. Beginning with the design and optimization of batch and recycling chromatography, the step to continuous processes will be done. Design and optimization strategies for conventional isocratic simulated moving bed (SMB) chromatography, isocratic SMB chromatography under variable conditions, and gradient SMB chromatography will be presented, covering the most important continuous chromatographic concepts. In the end of this chapter, process concepts specifically for the separation of biomolecules will be presented. All properties and parameters of the chromatographic systems that are used for exemplary calculations are documented in Appendix A.

8.1 Basic Principles and Definitions

8.1.1 Performance, Costs, and Objective Functions

Performance and economic criteria are indicators of efficiency and quality of preparative chromatographic separations. They depend on the operating and design parameters of a plant. Hereby, they are potential variables for any optimization problem and the basis for the formulation of objective functions. The definitions of objective functions are often identical for diverse chromatographic

*The following authors Achim Epping and Arthur Susanto have contributed to the first and/or second edition.

processes (e.g. batch or SMB), but different operating and design parameters must be applied for their calculation.

8.1.1.1 Performance Criteria

In the following, the performance criteria yield, productivity, eluent consumption, and purity will be presented.

The yield Y_i of a process is the ratio between the amount of a product of component i that can be collected in the outlet and the amount that was introduced into the system through the feed stream within a batch cycle. Due to the continuous operation mode in an SMB plant, amounts of introduced and collected component i are calculated within a shifting interval:

$$Y_{i,\text{Batch}} = \frac{m_{\text{out},i}}{\dot{V} \cdot c_{\text{feed},i} \cdot t_{\text{inj}}} \tag{8.1}$$

$$Y_{i,\text{SMB}} = \frac{m_{\text{out},i}}{\dot{V}_{\text{feed}} \cdot c_{\text{feed},i} \cdot t_{\text{shift}}} \tag{8.2}$$

The amount of component i in the outlet stream for a batch chromatographic process can be calculated using Eq. (8.3), whereby $t_{1,i}$ and $t_{2,i}$ are the beginning and the end of the fraction collection for pure component i:

$$m_{\text{out},i} = \dot{V} \cdot \int_{t_{1,i}}^{t_{2,i}} c_{i,\text{out}}(t) \cdot dt \tag{8.3}$$

In comparison with batch chromatography, t_1 and t_2 for an SMB plant are the beginning and the end of a shifting interval. Furthermore, component i can be collected from either the raffinate or the extract stream:

$$m_{\text{out},i} = \dot{V}_{\text{raf/ext}} \cdot \int_{t_1}^{t_2} c_{i,\text{raf/ext}}(t) \cdot dt \tag{8.4}$$

The efficiency of a chromatographic separation can be expressed by comparing the purified amount of product i with the time taken and the resources necessary to produce it. This expression is referred to as productivity and can be applied in terms of:

- cross section-specific productivity ASP_i (production rate over free cross section of the column):

$$\text{ASP}_{i,\text{Batch}} = \frac{\dot{m}_{\text{prod},i}}{A_c \cdot \varepsilon_e} \tag{8.5}$$

$$\text{ASP}_{i,\text{SMB}} = \frac{\dot{m}_{\text{prod},i}}{N_{\text{COL}} \cdot A_c \cdot \varepsilon_e} \tag{8.6}$$

and

- volume-specific productivity VSP_i (production rate over total solid adsorbent volume):

$$\text{VSP}_{i,\text{Batch}} = \frac{\dot{m}_{\text{prod},i}}{V_{\text{solid}}} = \frac{\dot{m}_{\text{prod},i}}{V_c \cdot (1 - \varepsilon_t)} \tag{8.7}$$

$$\text{VSP}_{i,\text{SMB}} = \frac{\dot{m}_{\text{prod},i}}{V_{\text{solid,total}}} = \frac{\dot{m}_{\text{prod},i}}{N_{\text{COL}} \cdot V_c \cdot (1 - \varepsilon_t)} \tag{8.8}$$

In Eq. (8.8), the number of columns N_{COL} in SMB has to be considered.

Using the purified amount of product i within a batch cycle, the average mass flow of purified product i (also called as production rate $\dot{m}_{prod,i}$) in batch chromatography can be expressed as

$$\dot{m}_{prod,i} = \frac{m_{i,out}}{t_{batch\text{-}cycle}} \tag{8.9}$$

For an SMB plant the production rate must be determined within a shifting interval:

$$\dot{m}_{prod,i} = \frac{m_{i,out}}{t_{shift}} \tag{8.10}$$

In cases where the costs of eluent are not negligible and may even represent the highest contribution to the total separation costs, it is advisable to observe the eluent consumption or better the efficiency of eluent usage during the chromatographic separation. This can be characterized by the specific eluent consumption EC_i, which corresponds to the amount of eluent required to purify a certain amount of product i. The EC_i can be calculated for batch processes as follows:

$$EC_{i,Batch} = \frac{\dot{V}}{\dot{m}_{prod,i}} \tag{8.11}$$

Since in SMB plants the eluent is introduced into the system through the desorbent port as well as feed port, both flow rates have to be considered in the calculation:

$$EC_{i,SMB} = \frac{\dot{V}_{feed} + \dot{V}_{des}}{\dot{m}_{prod,i}} \tag{8.12}$$

Notably, eluent consumption is calculated by neglecting the influence of solute concentration since the change in liquid volume during the dissolution of solid components can generally be neglected.

Another performance criterion that is also often used as a boundary condition for a separation problem is the purity of a product i, Pu_i. Product purity in a chromatographic process can be calculated according to Eq. (8.13), where N_{COMP} is the number of components in the solution:

$$Pu_i = \frac{m_{i,out}}{\sum_{i=1}^{N_{COMP}} m_{i,out}} \tag{8.13}$$

8.1.1.2 Economic Criteria

Katti and Jagland (1998) give a complete description of the contribution of different kinds of costs to the total separation costs for batch chromatography. Also, the influence of different physical properties of the separation system and the plant design is discussed. The authors demonstrated that the cost structure of the separation problem changes with the scale of the separation. For smaller production amounts, the contribution of capital, labor, and maintenance costs to total costs is significantly higher than for bigger production rates. On this account, it is very important to consider the total separation costs because only consideration of these will lead to an economic optimal process for both batch and SMB chromatography. Yield, productivity, eluent consumption, and purity are clearly defined performance criteria, while total separation costs and other economic

criteria depend on the individual cost structure and are based on site-related parameters. Therefore, the calculation of total separation costs is complex due to various influencing parameters and cost structures.

This chapter proposes the following costs functions, which can be easily adapted to specific conditions:

Separation Problem Independent Costs (Fixed Costs) These can be considered as fixed costs. They are specific for each company and can be divided into the following:

- *Annual operating costs* ($C_{operating}$): Operating costs, including overhead costs as well as wages and maintenance costs.
- *Annual depreciation* ($C_{depreciation}$): Annual depreciation is the allocation of investment costs over the depreciation years.

Separation Problem Dependent Costs (Variable Costs) These costs are directly correlated to a given separation problem and the desired production rate. These are the annual costs for eluent, adsorbent, and lost feed (also known as crude loss). All of these costs can be calculated by applying previously introduced performance criteria that characterize the efficiency of the separation process (e.g. yield, productivity). Further, requirements for the calculation of separation problem dependent costs are the production rate or the annual produced amount $\dot{m}_{prod,\ annual}$ and prices for eluent f_{el} (€ per l eluent), for adsorbent f_{ads} (€ per kg adsorbent), and for feed f_{feed} (€ per kg feed). Additionally, to calculate the annual adsorbent costs C_{ads}, the lifetime of the adsorbent t_{life} has to be known or estimated:

$$C_{el} = EC_i \cdot \dot{m}_{prod,annual} \cdot f_{el} \tag{8.14}$$

$$C_{ads} = \frac{1}{VSP_i} \cdot \dot{m}_{prod,annual} \cdot \frac{\varrho_{ads} \cdot f_{ads}}{t_{life}} \tag{8.15}$$

$$C_{crudeloss} = \frac{1 - Y_i}{Y_i} \cdot \dot{m}_{prod,annual} \cdot f_{feed} \tag{8.16}$$

The total annual separation costs C_{total} can then be determined by adding up the fixed costs as well as the variable costs:

$$C_{total} = C_{operating} + C_{depreciation} + C_{ads} + C_{el} + C_{crudeloss} \tag{8.17}$$

However, to be able to compare the total annual separation costs for different production scales, the production-specific costs (costs per product amount) should be used instead:

$$C_{spec,total} = \frac{C_{total}}{\dot{m}_{prod,annual}} \tag{8.18}$$

8.1.1.3 Objective Functions

At the beginning of a chromatographic separation process, one should define objective functions. Objective functions specify the aim of an optimization process that is by convention stated as a minimization problem. A general mathematical formulation is, for example,

$$\min f(x^*) \le f(x), \quad \text{for} \|x - x^*\| < \delta \tag{8.19}$$

where x are the degrees of freedom for the given problem.

Performance and economic criteria, defined in Sections 8.1.1.1 and 8.1.1.2, or their combinations are potential objective functions, while the design and operating parameters represent the degrees of freedom for the optimization task. Generally, objective functions have to fulfill certain constraints:

$$g(x) \leq 0 \tag{8.20}$$

Related to preparative chromatography, diverse objective functions appear. For instance, they may focus on the economics of a new plant for a certain product or on maximizing the productivity VSP_i as a function of the injection volume under the constraints of minimal purities and yields. In the latter case, a general formulation of the optimization task may be

$$\min f(x^*) = \frac{1}{VSP_i} \tag{8.21}$$

under the constraints

$$Pu_i \geq Pu_{i,min} \text{ and } Y_i \geq Y_{i,min} \tag{8.22}$$

In order to reduce the complexity of an optimization task, it is recommended to minimize the number of parameters by introducing dimensionless parameters, which will be described in Section 8.1.2.

The solution of an optimization problem depends very much on the complexity of the decision space and the available tools. At first, overall decisions based on experience, for example, the selection of a certain process flow sheet, might be necessary to reduce the number of degrees of freedom. An optimal solution can be approached by trial-and-error or case studies based on experiments and/or simulations. Other options are mathematical procedures for a rigorous determination of an optimal solution of the objective function. Direct mathematical optimizations are essential for advanced process control (Chapter 9), but in the case of process optimization, it is recommended that the design engineer also checks the robustness of the solution. This will usually require parametric studies in order to verify that within the operation plane, the gradients, which surround the evaluated optimum, are not too steep. Goal-oriented case studies based on rigorous simulation and additional shortcut calculations are beneficial to gain a better understanding of the process performance.

Mathematical single-objective as well as multi-objective optimizations are out of the scope of this book; for certain applications in preparative chromatography, the interested reader is referred to citations in the following sections.

8.1.2 Degrees of Freedom

8.1.2.1 Categories of Parameters

Models for a chromatographic column consist of many parameters that have already been classified into three groups in Section 7.1:

(1) *Design parameters*: Design parameters define the appearance of a plant and cannot be changed during line operation, for example:
   - Column geometry (length and diameter);
   - Diameter of adsorbent particle;
   - Maximum pressure drop;
   - Additional degree of freedom of an SMB plant: number of columns in each SMB section.

(2) *Operating parameters*: Alterable parameters during the operation of a plant, for example:
- Flow rates;
- A number of operating parameters in batch chromatography result from the batch operation mode: switching times;
- To characterize the operation of an SMB plant precisely, the following additional parameters are necessary: flow rate in each SMB section and shifting time.

(3) *Model parameters*: Model parameters are system inherent parameters that result from the choice of chromatographic system and the chosen model. They describe, for example, the following phenomena:
- Thermodynamics, like adsorption behavior;
- Fluid dynamics;
- Dispersion effects;
- Mass transfer resistance.

A good process description based on validated models is needed to predict the position of the optimal state accurately. Since model parameters are determined experimentally on the chromatographic system, which is generally predefined before optimization starts, model parameters remain unchanged during the optimization. On this basis, all model-based optimization strategies in the following sections apply only to operating and design parameters.

8.1.2.2 Dimensionless Operating and Design Parameters

The chromatographic process contains many design and operating parameters. Hence, the optimization of all parameters requires a great amount of resources (e.g. fast computer) and complex optimization algorithms. To reduce the complexity of the optimization problem, summarizing the numerous design and operating parameters into a smaller number of dimensionless parameters, thus reducing the number of optimization parameters and the complexity of the optimization problem, is beneficial.

Dimensionless formulation of model equations for a chromatographic column can be found in Chapter 6. Useful dimensionless parameters and the phenomena described by them are provided here:

(1) *Axial dispersion and convection*: Péclet number:

$$Pe_i = \frac{\text{convection}}{\text{dispersion}} = \frac{u_{\text{int}} \cdot L_c}{D_{\text{ax},i}} \tag{8.23}$$

(2) *Mass transfer and convection*: Modified Stanton number:

$$St_{\text{eff},i} = \frac{\text{mass transfer}}{\text{convection}} = k_{\text{eff},i} \cdot \frac{6}{d_p} \cdot \frac{L_c}{u_{\text{int}}} \tag{8.24}$$

(3) *Adsorption*: For linear chromatography, adsorption behavior is determined by the dimensionless Henry coefficient H_i:

$$H_i = \frac{Q_{\text{DL},i}}{C_{\text{p,DL},i}} \tag{8.25}$$

In the case of nonlinear chromatography, however, the feed concentration plays a major role regarding the adsorption behavior. In these cases, the adsorption behavior is determined, for example, by the Langmuir isotherm:

$$Q_{\mathrm{DL},i} = \frac{H_i \cdot C_{\mathrm{p,DL},i}}{1 + (c_{\mathrm{feed},i} \cdot b_i) \cdot C_{\mathrm{p,DL},i}} \tag{8.26}$$

Here, the additional dimensionless number (product of $c_{\mathrm{feed},i} \cdot b_i$) must also be taken into account.

(4) *Process-related boundary conditions*:

- *For batch processes*: Dimensionless injection time $t_{\mathrm{inj}}/t_{0,\mathrm{int}}$. In this chapter, another dimensionless parameter is used to represent the injection time, namely, the loading factor LF_i, which was introduced by Guiochon and Golshan-Shirazi (1989) and is defined as

$$\mathrm{LF}_i = \frac{\text{injected feed amount}}{\text{saturation capacity}} = \frac{c_{i,\mathrm{feed}} \cdot \dot{V} \cdot t_{\mathrm{inj}}}{q_{\mathrm{sat},i} \cdot V_{\mathrm{c}} \cdot (1 - \varepsilon_{\mathrm{t}})} \tag{8.27}$$

The saturation concentration ($q_{\mathrm{sat},i}$) can be easily determined for all isotherm types with saturation concentration, for example, the Langmuir type:

$$q_{\mathrm{sat},i} = \lim_{c_i \to \infty} \frac{H_i \cdot c_i}{1 + b_i \cdot c_i} = \frac{H_i}{b_i} \tag{8.28}$$

It is advisable to use the solid-phase concentration at maximum feed concentration in the separation problem for other isotherm types with no saturation concentration (e.g. linear type):

$$q_{\mathrm{sat},i} = q_i(c_{\mathrm{feed,max}}) \tag{8.29}$$

Usage of the loading factor as degree of freedom is equivalent to the use of dimensionless injection time, as can be seen in Eq. (8.30):

$$\mathrm{LF}_i = \frac{c_{i,\mathrm{feed}}}{q_{\mathrm{sat},i}} \cdot \frac{\varepsilon_{\mathrm{e}}}{1 - \varepsilon_{\mathrm{t}}} \cdot \left(\frac{t_{\mathrm{inj}}}{t_{0,\mathrm{int}}} \right) \tag{8.30}$$

Since the loading factor is a more common parameter in practice, it is preferred in this chapter.

- *For SMB processes*: Dimensionless shifting times $t_{\mathrm{shift}}/t_{0,\mathrm{int},j}$. Similar to batch processes, other dimensionless numbers are used to represent the shifting boundary conditions in SMB processes. The periodic behavior of SMB processes is induced by the stepwise switching of the inlet and outlet ports. To describe this operation as a quasi-stationary process comparable to the true moving bed (TMB) process, the following flow rates are introduced:

$$\text{Net liquid flow rate}: \dot{V}_{j,\mathrm{net}} = \dot{V}_j - \frac{V_{\mathrm{c}}\varepsilon_{\mathrm{t}}}{t_{\mathrm{shift}}} \tag{8.31}$$

$$\text{Simulated solid flow rate}: \dot{V}_{\mathrm{ads}} = \frac{V_{\mathrm{c}}(1 - \varepsilon_{\mathrm{t}})}{t_{\mathrm{shift}}} \tag{8.32}$$

The ratio of these flow rates results in the following dimensionless parameter that is essential for the design of countercurrent chromatographic separation processes (Storti et al. 1993):

$$m_j = \frac{\text{net fluid flow rate in section } j}{\text{simulated solid flow rate}} = \frac{\dot{V}_j - [(V_c \cdot \varepsilon_t)/t_{\text{shift}}]}{[V_c \cdot (1 - \varepsilon_t)]/t_{\text{shift}}} \quad (8.33)$$

Similar to the injection time in batch processes, the use of the dimensionless flow rate ratio m_j as a degree of freedom is equivalent to the use of dimensionless shifting time. Modifying Eq. (8.33) leads to Eq. (8.34):

$$m_j = \frac{\varepsilon_e}{1 - \varepsilon_t} \cdot \left(\frac{t_{\text{shift}}}{t_{0,\text{int},j}} - \frac{\varepsilon_t}{\varepsilon_e} \right) \quad (8.34)$$

After transforming the model equations and boundary conditions into their dimensionless form, quite a number of parameters remain, which have to be taken into account for process optimization.

In the case of high-performance liquid chromatography (HPLC), the complexity of a design or optimization problem can often be reduced without significantly reducing the accuracy of the solution by simplifications as discussed below. However, the validity of these simplifications should be checked for each practical application. The first important simplification is based on the assumption of linear isotherms (Guiochon et al. 2006). In this case, the influences of mass transfer and axial dispersion are added to each other. The Péclet (Pe_i) and modified Stanton ($St_{\text{eff},i}$) numbers are combined into the number of stages N_i, which is the more common parameter in practice (Eq. (8.35)):

$$N_i = \frac{2}{Pe_i} + \frac{2\varepsilon_e}{1 - \varepsilon_e} \left(\frac{\tilde{k}_i'}{1 + \tilde{k}_i'} \right)^2 \frac{1}{St_{\text{eff},i}} = f\left(Pe_i, St_{\text{eff},i} \right) \quad (8.35)$$

Equation (8.35) defines the number of stages for a transport dispersion model. It indicates that, for the assumptions mentioned above, the influence of Pe_i and $St_{\text{eff},i}$ is summarized by the number of stages, which reduces the number of parameters for process optimization. From Eq. (8.35) follows the equation for height of an equivalent theoretical plate (HETP):

$$\text{HETP}_i = \frac{L_c}{N_i} = \frac{2 \cdot D_{ax,i}}{u_{\text{int}}} + \frac{2\varepsilon_e}{1 - \varepsilon_e} \cdot \left(\frac{\tilde{k}_i'}{1 + \tilde{k}_i'} \right)^2 \cdot \frac{d_p}{6 \cdot k_{\text{eff},i}} \cdot u_{\text{int}} \quad (8.36)$$

Please note that Eq. (8.36) is not used to calculate the number of stages during the optimization. Instead of this, HETP is calculated by Eq. (8.37):

$$\text{HETP}_i = A_i + \frac{B_i}{u_{\text{int}}} + C_i \cdot u_{\text{int}} \quad (8.37)$$

The coefficients in Eq. (8.37) (A_i, B_i, and C_i) are determined based on results of experimental investigations (cf. Chapter 7).

For preparative liquid chromatographic processes, the HETP equation can be simplified further by taking a closer look at the axial dispersion coefficient

as discussed in Chapter 7.4.2. $D_{\mathrm{ax},i}$ is generally described as the sum of the contributions of eddy diffusion and molecular diffusion:

$$D_{\mathrm{ax},i} = \lambda \cdot d_{\mathrm{p}} \cdot u_{\mathrm{int}} + \gamma \cdot D_{\mathrm{m},i} \tag{8.38}$$

where $D_{\mathrm{m},i}$ is the molecular diffusion coefficient for component i and λ and γ are the irregularity in the packed column and the obstruction factor for the diffusion in the packed column, respectively. In preparative liquid chromatography, the contribution of molecular diffusion can often be neglected due to high flow rates and relatively small molecular diffusion coefficients in liquids:

$$D_{\mathrm{ax},i} \approx \lambda \cdot d_{\mathrm{p}} \cdot u_{\mathrm{int}} \tag{8.39}$$

Therefore, Pe_i is independent of interstitial velocity:

$$Pe_i = \frac{u_{\mathrm{int}} \cdot L_{\mathrm{c}}}{D_{\mathrm{ax},i}} \approx \frac{L_{\mathrm{c}}}{\lambda \cdot d_{\mathrm{p}}} \neq f(u_{\mathrm{int}}) \tag{8.40}$$

The HETP equation in preparative liquid chromatography can then be simplified to

$$\mathrm{HETP}_i = 2 \cdot \lambda \cdot d_{\mathrm{p}} + \frac{2\varepsilon_e}{1 - \varepsilon_e} \cdot \left(\frac{\tilde{k}_i'}{1 + \tilde{k}_i'} \right)^2 \cdot \frac{1}{k_{\mathrm{eff},i}} \cdot \frac{d_{\mathrm{p}}}{6} \cdot u_{\mathrm{int}} = A_i + C_i \cdot u_{\mathrm{int}} \tag{8.41}$$

In general, the substitution of two degrees of freedom by a single degree of freedom is mathematically incorrect. However, in many cases, the influence of one of these dimensionless parameters (Pe_i or $St_{\mathrm{eff},i}$) on chromatographic processes can be neglected, thus reducing the degrees of freedom into a single dimensionless parameter and justifying the simplification into the number of stages N_i. Cases in which the influence of axial dispersion (Pe_i) or mass transfer resistance ($St_{\mathrm{eff},i}$) can be neglected are as follows:

(1) *Dominant mass transfer resistance (characterized by $St_{\mathrm{eff},i} \ll Pe_i$)*: Compared with Pe_i, which is independent of the interstitial velocity (Eq. (8.40)), $St_{\mathrm{eff},i}$ is inversely proportional to interstitial velocity (Eq. (8.24)). Accordingly, the influence of mass transfer resistance will grow and surpass the influence of axial dispersion at high interstitial velocity, which is usually the case for preparative chromatographic processes. In some extreme cases, where the mass transfer coefficients are small and the chromatographic column is operated at high flow rates, the HETP Eq. (8.41) for the calculation of N_i can even be simplified further to

$$\mathrm{HETP}_i \approx C_i u_{\mathrm{int}}$$

(2) *Dominant axial dispersion (characterized by $Pe_i \ll St_{\mathrm{eff},i}$)*: In chromatographic systems with relatively large effective mass transfer coefficients $k_{\mathrm{eff},i}$ (i.e. low mass transfer resistance), the influence of axial dispersion, especially eddy diffusion, dominates the concentration profile. HETP_i and N_i are then independent of the interstitial velocity:

$$\mathrm{HETP}_i \approx A_i \neq f(u_{\mathrm{int}})$$

Since column efficiency is usually expressed by the number of stages, the flow rate through the column can be increased without changing the column efficiency, thus increasing the production rate of the column. The optimal flow rate for such chromatographic systems is therefore limited by the maximum allowed pressure drop.

In other words, the simplification of using the number of stages for process optimization is best applied if either mass transfer or dispersion dominates the peak broadening. Therefore, the optimization strategies discussed later in this chapter apply a validated transport dispersion model, which can flexibly consider mass transfer and/or dispersion effect. Here, the number of stages is used as an independent variable for the optimization criteria such as productivity or eluent consumption. Other possible approaches would be the use of simplified simulation models such as transport model or equilibrium dispersion model.

Another important simplification, which makes the scale-up of chromatographic plants easier, is to use always the same feed concentration. Since higher feed concentration results in higher productivity, feed concentration should be at the maximum allowed concentration, which depends on the chromatographic system and the solubility of the feed components. However, in SMB processes, feed concentration affects the size of the operating parameter region for a total separation and, therefore, should not be fixed at too high values in order not to hinder the ability to get "robust" operating parameters (Section 8.4).

Thus, the remaining and applied degrees of freedom for the design and optimization methods for batch as well as SMB processes in this chapter are as follows:

- *For batch processes*:
  - The number of stages N_i;
  - The height of a theoretical plate HETP_i (representing the flow rate);
  - The loading factor LF_i (representing the injection conditions).
- *For SMB processes*:
  - The total number of stages $N_{\text{tot},i}$;
  - The dimensionless flow ratios m_j.

8.1.3 Scaling by Dimensionless Parameters

One of the advantages of the presented dimensionless parameters is the use of only a reduced number of optimization parameters, although nearly all design and operating parameters are considered. Furthermore, chromatographic processes with identical dimensionless parameters will have similar behavior. In other words, the values of many performance criteria (e.g. specific productivity, specific eluent consumption) for those processes will be the same, and their dimensionless concentration profiles will be identical. Therefore, no new optimization must be done after upscaling (or downscaling) the chromatographic plant, because the optimal dimensionless parameters from the old plant can be easily adapted to the new plant. This means:

- *For batch processes*:

$$N_{i,\text{new}} \geq N_{i,\text{old}} \tag{8.42}$$

$$\text{LF}_{i,\text{new}} = \text{LF}_{i,\text{old}} \tag{8.43}$$

- *For SMB processes*:

$$N_{\text{tot},i,\text{new}} \geq N_{\text{tot},i,\text{old}} \tag{8.44}$$

$$m_{j,\text{new}} = m_{j,\text{old}} \tag{8.45}$$

Since the adoption of the number of stages from the old chromatographic column into the new column can never be done exactly, greater than or equal to signs are placed in Eqs. (8.42) and (8.44) instead of equal to signs. This should guarantee the separation performance of the new column to be equal to or better than the performance of the old column even if the concentration profiles and the values of performance criteria are not exactly the same. The reason of this difference will be illustrated in the following sections with the aid of numbers of stages for two different chromatographic plants (an old, optimized plant and a new plant):

$$N_{i,\text{old}} = \frac{L_{c,\text{old}}}{\text{HETP}_{i,\text{old}}} \tag{8.46}$$

$$N_{i,\text{new}} = \frac{L_{c,\text{new}}}{\text{HETP}_{i,\text{new}}} \tag{8.47}$$

8.1.3.1 Influence of Different HETP Coefficients for Every Component

By scaling up a chromatographic plant for a specific separation problem, more than one component has to be taken into account. Two different plants will behave similarly only if the numbers of stages *for all components* are equal. If the equality condition is valid for the first component, then

$$N_{1,\text{new}} = N_{1,\text{old}} \Leftrightarrow L_{c,\text{new}} = L_{c,\text{old}} \cdot \frac{\text{HETP}_{1,\text{new}}}{\text{HETP}_{1,\text{old}}} \tag{8.48}$$

Substituting this equation into the new number of stages for component 2 will result in

$$N_{2,\text{new}} = \frac{L_{c,\text{old}}}{(\text{HETP}_{1,\text{old}} \cdot \text{HETP}_{2,\text{new}})/\text{HETP}_{1,\text{new}}} \tag{8.49}$$

The equality condition will therefore only be valid for the second component if

$$N_{2,\text{new}} = N_{2,\text{old}} \Leftrightarrow \frac{\text{HETP}_{1,\text{old}} \cdot \text{HETP}_{2,\text{new}}}{\text{HETP}_{1,\text{new}}} = \text{HETP}_{2,\text{old}} \tag{8.50}$$

or as general expression

$$\frac{\text{HETP}_{i,\text{new}}}{\text{HETP}_{i,\text{old}}} = \frac{A_i + C_i \cdot u_{\text{int,new}}}{A_i + C_i \cdot u_{\text{int,old}}} = \text{constant} \tag{8.51}$$

Therefore, the equality condition for the number of stages is only fulfilled exactly by all components if the ratios between HETP of the old column and that

of the new column are *equal for every component.* Due to the different HETP coefficients for each component, the equality condition can only be exactly fulfilled if:

(1) *Both columns have the same length but different cross-sectional areas*: Due to the identical column length, the interstitial velocity in both columns must be kept constant in order to have the same column efficiency (i.e. same number of stages). Both columns have, however, different flow rates due to different cross-sectional areas:

$$u_{\text{int,new}} = u_{\text{int,old}} \Leftrightarrow \frac{\text{HETP}_{i,\text{new}}}{\text{HETP}_{i,\text{old}}} = 1 = \text{constant} \tag{8.52}$$

(2) *Dominant eddy diffusion*: For chromatographic systems with negligible mass transfer resistance, the eddy diffusion is the dominant effect. Therefore, HETP values are constant and independent of the interstitial velocity:

$$\frac{\text{HETP}_{i,\text{new}}}{\text{HETP}_{i,\text{old}}} \approx 1 = \text{constant} \tag{8.53}$$

(3) *Dominant mass transfer resistance*: In this case the approximated HETP value is directly proportional to the interstitial velocity. Thus, the HETP ratios between old and new columns are identical for all components: they are always equal to the ratio of interstitial velocities:

$$\frac{\text{HETP}_{i,\text{new}}}{\text{HETP}_{i,\text{old}}} \approx \frac{u_{\text{int,new}}}{u_{\text{int,old}}} = \text{constant} \tag{8.54}$$

Whenever those cases apply, the number of stages in the new and old columns for other components will remain the same if the number of stages of one single component is not varied. Therefore, the column can be optimized by considering the loading factor and the number of stages of only one component (i.e. the reference component). Generally, the equality condition for all the number of stages cannot be fulfilled exactly, so a certain deviation has to be accepted. The magnitude of the deviation depends on the magnitude of the contributions to the HETP. The more dominant the influence of mass transfer resistance or eddy diffusion, the smaller the deviation between the concentration profiles. However, if the modified equality condition (Eqs. (8.42) and (8.44)) is applied, the separation performance of the new column can be guaranteed to be equal to or better than that of the old column.

8.1.3.2 Influence of Feed Concentration

Actually, the definition of number of stages and HETP originates from linear chromatography, although it can also be formulated for nonlinear chromatography. In nonlinear chromatography, the number of stages and HETP are affected by the varying gradient of the adsorption isotherm. Therefore, their value depends on the concentration range in the column. Due to the concentration dependency in the nonlinear case, the number of stages loses its original practical meaning as a measure of column efficiency.

For preparative chromatography, where we usually have to deal with high feed concentrations and nonlinear adsorption isotherms, the following approach to the appropriate choice of feed concentration during model-based optimization is recommended:

(1) Determination of HETP coefficients in the linear adsorption region (i.e. low feed concentration) as explained in Chapter 7.
(2) Execution of model-based optimization using the same feed concentration that will be applied later in the preparative column. Generally, a high feed concentration is applied, which is close to the solubility limit of the feed components. Feed concentration is, therefore, not an optimization parameter and should not be varied during optimization. The number of stages, however, is calculated by applying the known HETP coefficients from the linear adsorption region.

Application of concentration-independent HETP coefficients from the linear isotherm region in calculating the number of stages in a nonlinear region is only a formalism. However, since feed concentration is not varied during the optimization, the calculated number of stages can nevertheless be used further as it is a characteristic value for the specific chromatographic separation. Scale-up of the chromatographic column using an identical dimensionless number of stages will continue to produce identical concentration profiles and identical values of many performance criteria (with relatively small deviation), provided the feed concentration is also constant during scale-up.

8.1.3.3 Examples for a Single-Column Batch Chromatography

In the following, the equality of concentration profiles resulting from a simulation using a transport dispersion model with different design and operating parameters but identical number of stages and loading factors will be presented. Model calculations agree with experiments within measurement accuracy.

The first exemplary problem is the separation of a racemic mixture EMD53986 (R:S-enantiomers $= 1 : 1$) on the chiral stationary phase Chiralpak AD from Daicel ($20 \, \mu m$ particle diameter) (Table 8.1).

R-enantiomer is used as the *reference component* in this separation problem. Thus, only the number of stages and loading factor of the R-enantiomer are taken into account. Furthermore, the number of stages is calculated using the experimentally determined HETP coefficients (Eq. (8.37)). All applied model parameters (adsorption isotherms, mass transfer coefficients, etc.) for the simulation of this enantiomeric separation are already experimentally validated. The

Table 8.1 Different design and operating parameters for a single column (EMD53986); $N_R = 25$; $LF_R = 1.25$; $c_{feed,R} = c_{feed,S} = 2.5 \, g \, l^{-1}$.

	$\dot{V}$ (ml min^{-1})	u_{int} (cm s^{-1})	t_{inj} (s)	L_c (cm)	d_c (cm)	$St_{eff,R}$ (−)	Pe_R (−)
EMD-1	23.5	0.2247	208.0	10.8	2.5	21.63	3061.22
EMD-2	54.8	0.5237	206.6	25.0	2.5	21.48	7108.14
EMD-3	109.0	0.2605	207.7	12.5	5.0	21.59	3544.69
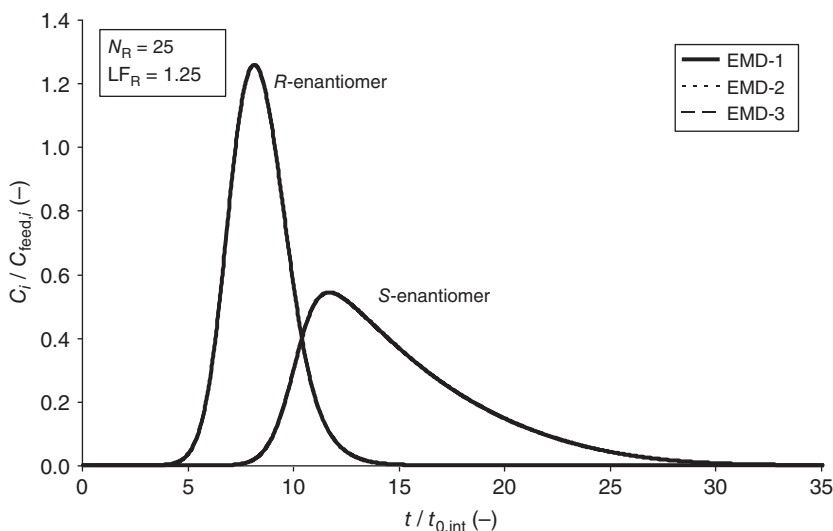
Figure 8.1 Equality of concentration profiles in a chromatographic column (EMD53986).

simulation results are presented in Figure 8.1 in dimensionless form using the ratios $c_i/c_{feed,i}$ and $t/t_{0,int}$ instead of c_i and t, whereby $t_{0,int}$ is the mean residence time under nonadsorbing, nonpenetrating conditions (i.e. the residence time of large tracer molecules, e.g. dextran):

$$t_{0,int} = \frac{L_c}{u_{int}} \tag{8.55}$$

As it can be seen in Table 8.1, Pe_i far exceeds $St_{eff,i}$, clearly indicating that mass transfer resistance has a major role in this separation problem. Therefore, the concentration profiles are completely identical for equal $St_{eff,i}$ values, despite the different Pe_i. This justifies the simplification of the optimization method by using the number of stages instead of Pe_i and $St_{eff,i}$. Furthermore, the number of stages is calculated using the HETP coefficients determined in the linear isotherm region. However, even if the concentration range in the column no longer lies within the linear region of the adsorption isotherms, deviations of the concentration profiles are insignificant as long as the same feed concentration is used (Figure 8.1).

Dimensionless degrees of freedom do not always transfer to other column designs as perfectly as shown in Figure 8.1. In many cases some deviations in the concentration profiles have to be taken into account. These cases will now be demonstrated using a second exemplary separation problem: the chromatographic separation of 1 : 1 mixture of glucose and fructose on ion-exchange resin Amberlite CR1320 Ca from Rohm and Haas (325 μm particle diameter) (Table 8.2).

Compared with the EMD53986 separation, Pe_i are smaller, although they are still much larger than $St_{eff,i}$. This indicates that although mass transfer effects still dominate, axial dispersion now plays a small but significant role. One reason why the axial dispersion coefficient grows is surely the bigger particle diameter

Table 8.2 Different design and operating parameters for a single column (Glu/Fruc); $N_{Glu} = 100$; $LF_{Glu} = 0.5$; $c_{feed,Glu} = c_{feed,Fruc} = 300 \, g \, l^{-1}$.

	$\dot{V}$ (ml min^{-1})	u_{int} (cm s^{-1})	t_{inj} (s)	L_c (cm)	d_c (cm)	$St_{eff,Glu}$ (–)	Pe_{Glu} (–)
FG-1	5.8	0.0490	328.1	56	2.6	14.76	950.15
FG-2	2.4	0.0201	428.0	30	2.6	19.25	505.52
FG-3	13.6	0.0313	367.7	40	5.0	16.54	676.07
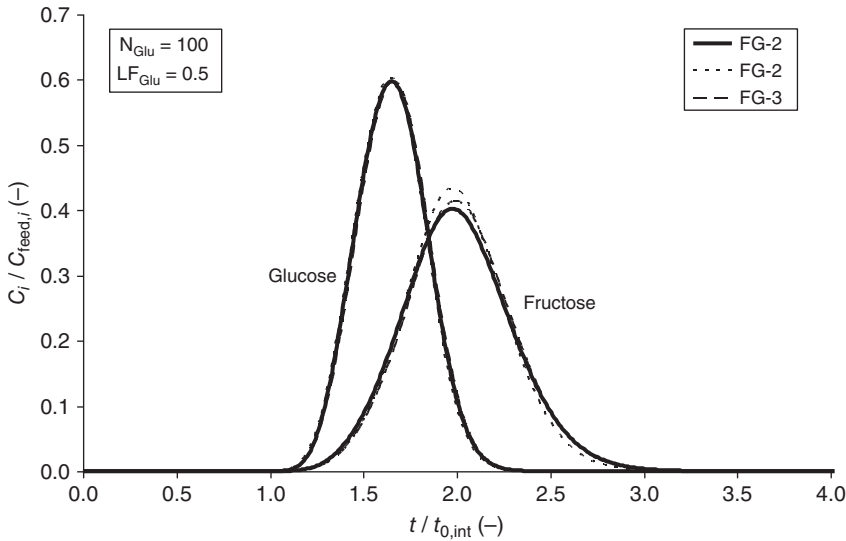
Figure 8.2 Comparison of concentration profiles from different columns (Glu/Fruc).

at 325 µm. A certain deviation during the scale-up has therefore to be taken into account (Figure 8.2).

Since the concentration profiles for this exemplary system are not perfectly identical, scale-up has to be done with caution. Especially, the "greater than or equal to" condition (Eqs. (8.42) or (8.44)) has to be fulfilled for all components. Therefore, in this case, it is not sufficient to look only at the number of stages of one component, but the number of stages of all components has to be taken into account. Table 8.3 and Figure 8.3 depict the resulting operating points and concentration profiles if only the number of stages of glucose is considered during the scale-up. In this example, the column "FG-2" is scaled up by changing its length from 30 to 100 cm.

Table 8.3 indicates that there are fewer stages of fructose in the new column ("FG-4") than in the old column ("FG-2"). This causes a peak broadening of fructose, thus worsening the separation of glucose and fructose (Figure 8.3). This can be avoided by taking fructose as reference component instead of glucose.

In summary, the transport dispersion model together with the simplified degrees of freedom N_i and LF_i is very useful for optimization and scale-up of chromatographic processes.

Table 8.3 Different design and operating parameters with $N_{i,\text{new}}$ less than or equal to $N_{i,\text{old}}$.

	$\dot{V}$ (ml min^{-1})	t_{inj} (s)	L_c (cm)	d_c (cm)	N_{Glu} (–)	N_{Fruc}	LF_{Glu} (–)	LF_{Fruc}
FG-2	2.4	428.0	30	2.6	100.0	48.2	0.5	0.3
FG-4	11.5	293.4	100	2.6	100.0	38.8	0.5	0.3
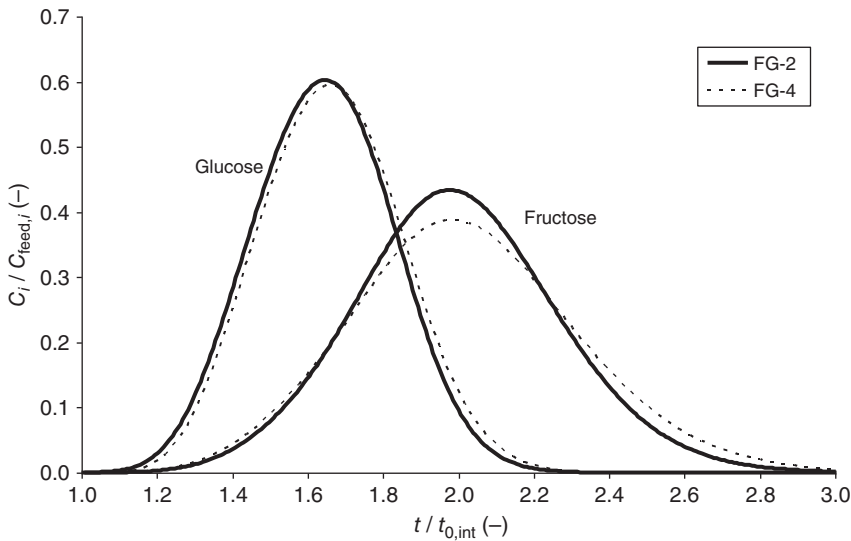
Figure 8.3 Comparison of concentration profiles with $N_{i,\text{new}}$ less than or equal to $N_{i,\text{old}}$.

8.1.3.4 Examples for SMB Processes

An analogous procedure can also be applied for SMB processes (Table 8.4). The following compares the axial concentration profile of several eight-column SMB processes with different operating and design parameters but identical number of stages and dimensionless flow rates in each SMB section m_j (Table 8.5). For this purpose, we use the same separation problem, a racemic mixture EMD53986, and the same feed concentration (i.e. 2.5 g l^{-1}) as before. Once again, R-enantiomer is used as reference component.

Table 8.4 Identical dimensionless parameters for the SMB processes.

SMB-1, SMB -2, and SMB -3	
$N_{\text{tot,R}}$	66.5
m_{I}	34.0
m_{II}	6.9
m_{III}	10.9
m_{IV}	5.7

Table 8.5 Different operating and design parameters for SMB plant.

	SMB-1	SMB-2	SMB-3
N_{COL} (–)	8 (2 per section)	8 (2 per section)	8 (2 per section)
L_c (cm)	4.5	5.2	7.6
d_c (cm)	2.5	2.5	2.5
t_{shift} (s)	153.7	153.5	153.0
$\dot{V}_{des}$ (ml min^{-1})	68.3	79.1	115.9
$\dot{V}_{ext}$ (ml min^{-1})	65.4	75.7	111.0
$\dot{V}_{feed}$ (ml min^{-1})	9.7	11.2	16.4
$\dot{V}_{raf}$ (ml min^{-1})	12.6	14.5	21.3

After the process simulation applying the experimentally validated model, all axial concentration profiles are plotted in a dimensionless diagram using $c_i/c_{feed,i}$ and L/L_c as axes. These profiles are taken at the end of a shifting interval from quasi-steady state. Figure 8.4 illustrates that all concentration profiles are completely identical.

Similar to batch processes, the transfer of number of stages is not always as perfect as in the case of enantiomeric separation of EMD53986. If significant deviations between the concentration profiles are observed, another component has to be taken as reference component so that the total number of stages of every component in the new design is greater than or equal to the number of stages in the old design (Eq. (8.44)).
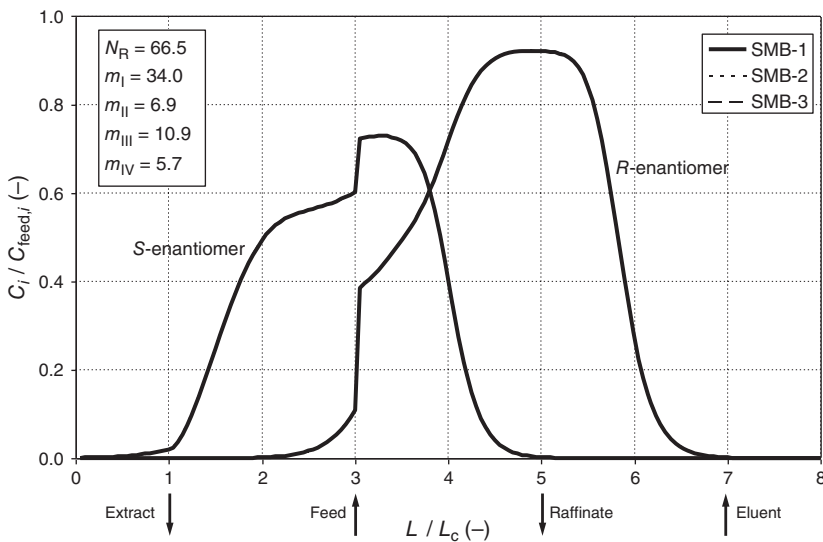
Figure 8.4 Equality of axial concentration profiles in SMB plant (EMD53986).

8.2 Batch Chromatography

8.2.1 Fractionation Mode (Cut Strategy)

The existing approaches for optimization of batch chromatography can be classified into two categories, which differ in their fractionation mode or cut strategy (cf. Figure 8.5).

In cut strategy II, the products are collected consecutively. Each fraction collection starts immediately after the previous fraction. High purity demand can therefore only be satisfied by well-separated peaks, which is realized through reduced feed throughput. Furthermore, purity and yield are coupled and cannot be varied independently. A high purity demand will consequently result in low yield. One limit of this cut strategy is the touching band or baseline separation. In this special case, the concentration profiles do not overlap, and 100% purity and yield are gained.

Cut strategy I allows a waste fraction between the product fractions, which can either be discarded or processed further (e.g. by recycling the waste fraction). Due to the introduction of a waste fraction, the optimization problem gains additional degrees of freedom, which are times for the beginning and the end of waste collection. However, these additional degrees of freedom will not increase the complexity of the optimization, since they are pinpointed automatically by the purity demand, which serves as a boundary condition for the optimization problem.

By use of cut strategy I, the optimization problem can now be formulated with greater flexibility. For example, high purity demand can be satisfied either by reducing feed throughput or by increasing waste fraction, thus reducing the yield of the separation. It is essential in this cut strategy to consider the additional cost due to feed loss or cost for further treatment of the waste fraction. Separation cost optimization with very high feed cost will often result in a very small waste fraction or even "baseline separation," which can be interpreted as the marginal case for cut strategy I if t_{A2} is equal to t_{B1} (cf. Figure 8.5). However, if feed cost is comparable with other costs, then it is more favorable to apply a waste fraction, thus reducing the yield but maximizing feed throughput at constant purity. Strategies to determine suitable cut times for multicomponent mixtures are also discussed by Shan and Seidel-Morgenstern (2004).
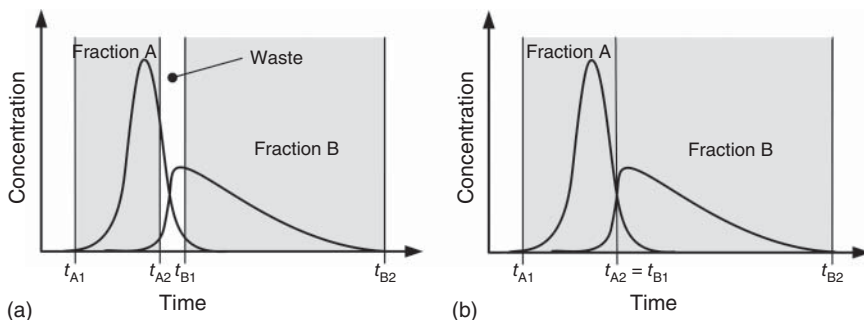
Figure 8.5 Cut strategies for a binary mixture. (a) Cut strategy I and (b) cut strategy II.

Since cut strategy II is only the marginal case of cut strategy I and since the application of cut strategy I provides more flexibility and leads often to a better global optimum, only *cut strategy I* will be used for model-based optimization in this chapter.

8.2.2 Design and Optimization of Batch Chromatographic Columns

The main idea behind the design and optimization strategy for batch chromatographic columns is the equality of concentration profiles with identical values in dimensionless parameters (i.e. number of stages and loading factor). As mentioned previously, column performance under these conditions will also be identical (e.g. volume-specific productivity, specific eluent consumption, and yield at a defined purity). In other words, process performance will only vary if the number of stages and loading factor are varied. Therefore, it does not really matter which design or operating parameters are varied during the optimization as long as this variation does not involve a variation of number of stages and loading factor.

8.2.2.1 Process Performance Depending on Number of Stages and Loading Factor

To improve the basic understanding of column performance in a batch chromatographic separation, the dependency of yield, eluent consumption, and productivity on the applied dimensionless parameters (i.e. number of stages and loading factor) will be investigated. Once again, the batch chromatographic separation of a racemic mixture EMD53986 on chiral stationary phase Chiralpak AD from Daicel (20 µm particle diameter) will be used as an exemplary chromatographic system. All the figures in this chapter result from the dynamic simulation of an experimentally validated column model.

Figure 8.6 illustrates the dependency of yield for 99% purity on the dimensionless parameters, showing that high yields can be realized at very low column loadings (which correspond to loading factors <1). Here, only a small amount of waste fraction is required. As the loading factor increases, the overlapping region in the concentration profile grows rapidly. This causes the amount of waste fraction to increase in order to meet the purity demand, thus reducing the yield. However, the size of the overlapping concentration region and consequently the amount of waste fraction can be reduced by increasing the number of stages, which also increases the peak resolution. Therefore, high yield at relatively higher loading factor can be realized in a column with a large number of stages.

Contrary to yield, the productivity has a maximum in the investigated parameter region (cf. Figure 8.6). An increase of number of stages increases the yield due to better peak resolution. Separation becomes more efficient and a higher loading factor can be applied at constant yield, which, at first, results in a steep rise of production rate and volume-specific productivity. However, a higher number of stages also involve greater column length (i.e. larger column) and/or reduction of interstitial velocity. The decrease of interstitial velocity increases the mean residence time of solutes in the column, thus increasing the batch cycle time. If the interstitial velocity falls below a certain point, the high batch cycle time will
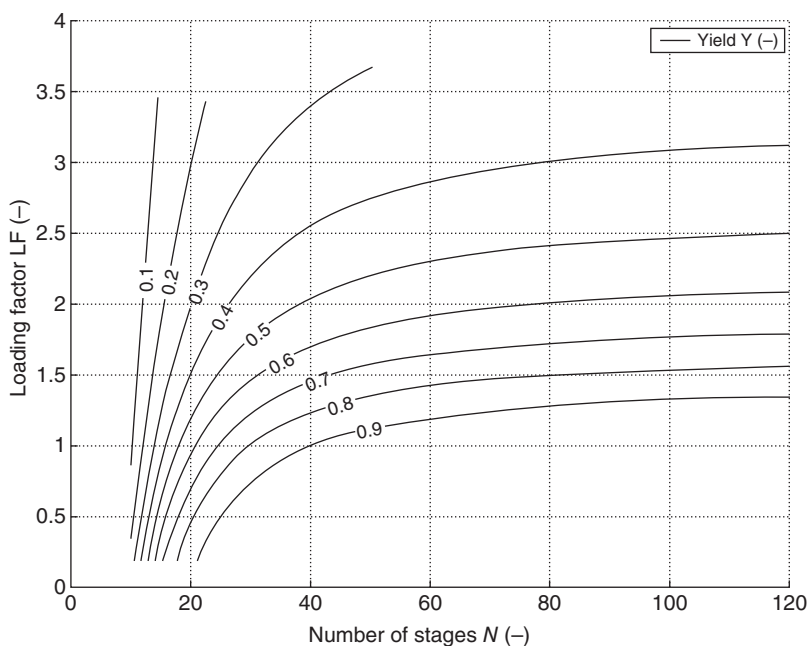
Figure 8.6 Dependency of yield for 99% purity on number of stages and loading factor.

start to reduce production rate in spite of the higher loading factor. Therefore, a further increase in the number of stages will cause a smooth decrease in the volume-specific productivity, which is defined as production rate over required adsorbent volume.

The influence of loading factor on productivity is roughly similar to that of the number of stages. At first, the higher the loading factor, the higher the production rate, and thus productivity increases. However, as seen in Figure 8.7, the yield already drops rapidly at low loading factors (at about 1). Therefore, a further increase of loading factor will cause the production rate and productivity to decrease despite higher feed throughput since a considerable amount is lost in the waste fraction.

Figure 8.8 illustrates the *inverted* values of specific eluent consumption in dependency of dimensionless parameters. Higher values are therefore the more favorable values in Figure 8.8 as they indicate small eluent consumption. The dependency of specific eluent consumption on the loading factor is similar to that of productivity, although the absolute eluent amount does depend not only on the loading factor but also on the number of stages. However, in this chapter, *specific* eluent consumption is used instead of just the amount of consumed eluent in order to compare the efficiency of eluent consumption. Since specific eluent consumption is defined as eluent per product amount (or as flow rate over production rate), a higher loading factor causes, at first, more favorable values, but further increase in loading factor shifts the specific eluent consumption to less favorable values due to decreasing production rate caused by an increasing amount of waste fraction.
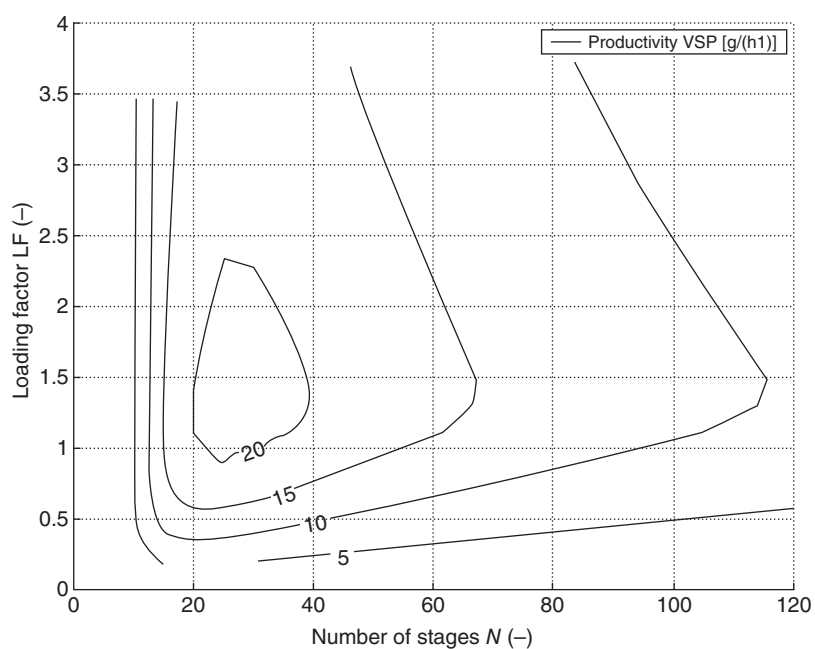
Figure 8.7 Dependency of volume-specific productivity on number of stages and loading factor.
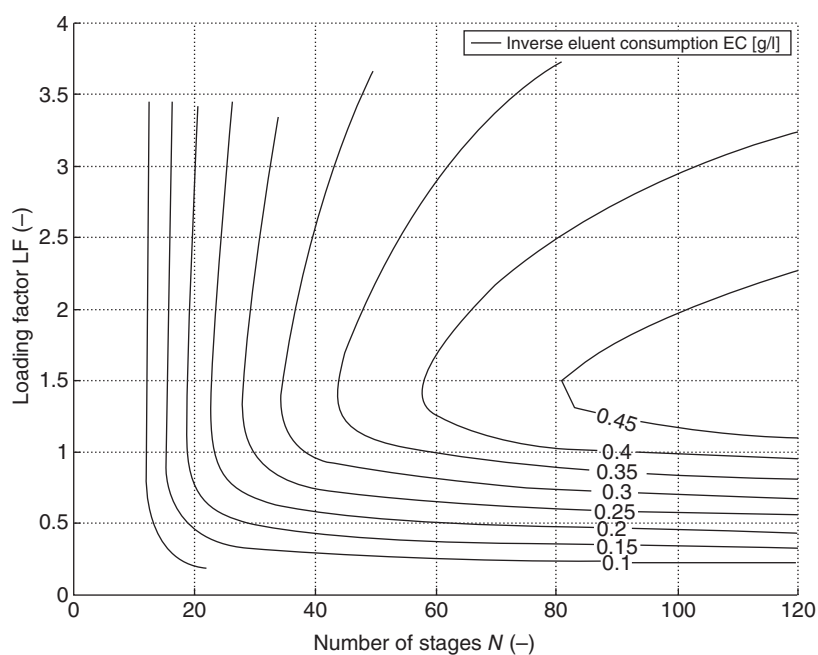
Figure 8.8 Dependency of specific eluent consumption on number of stages and loading factor.

Contrary to productivity, a high number of stages do not result in less favorable values for specific eluent consumption. As mentioned before, a high number of stages occur in columns with relatively low interstitial velocity. A definite increase in the number of stages causes a decrease of flow rate (eluent flow rate) at the same degree, whereas the production rate drops slowly. Further increase of their number will continue to improve the specific eluent consumption, at least in the parameter region investigated in this chapter.

A very important conclusion from the case study in this chapter is that yield, productivity, and eluent consumption represent oppositional optimization goals during the design and optimization of batch chromatographic columns. To demonstrate this, three particular examples within the LF–N diagram for a given column geometry are compared. The positions in N–LF diagram and the values of the objective functions for each case are shown in Figure 8.9 and Table 8.6. Each of these exemplary operating points represents one of the following three extreme cases:

- Maximum productivity;
- High yield;
- Low eluent consumption.

A closer look at the chromatogram at maximum productivity (cf. Figure 8.10) reveals a large overlapping area (i.e. large waste fraction) between the concentration peaks of the pure components. This confirms the fact that maximum productivity can be reached in the region with relatively high loading factor, where
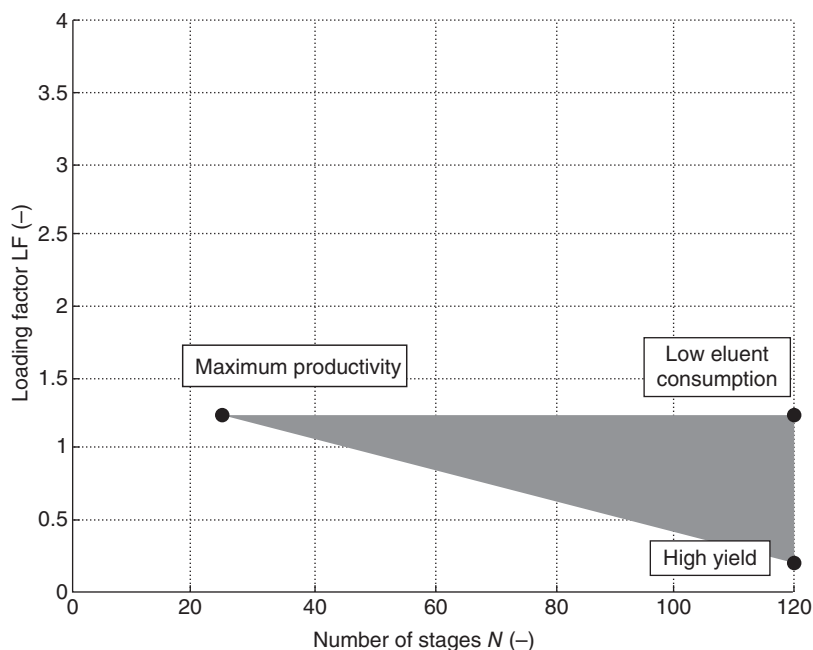
Figure 8.9 Positions of the three exemplary operating points with oppositional optimization goals.

Table 8.6 Values of the objective functions at the exemplary operating points.

	$\dot{V}$ (ml min^{-1})	t_{inj} (s)	N_R (–)	LF_R (–)	VSP g (l^{-1} h^{-1})	EC (l g^{-1})	Y (–)
Maximum productivity	23.5	208.0	25	1.25	23.36	4.07	0.60
Low eluent consumption	4.7	1045.2	120	1.25	9.89	1.92	0.94
High yield	4.7	167.2	120	0.20	1.80	10.53	1.00

Column geometry: $d_c = 2.5$ cm, $L_c = 10.8$ cm.
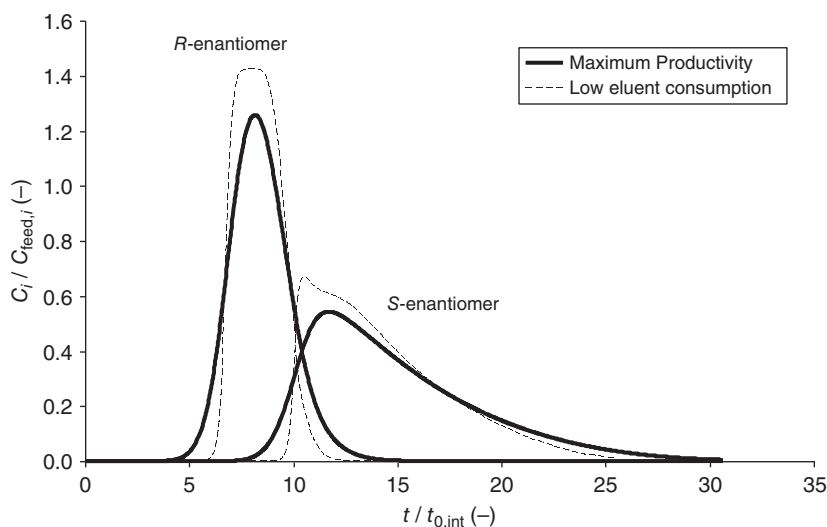
Figure 8.10 Comparison of chromatograms (maximum productivity; low eluent consumption).

the yield already drops significantly below 100% (i.e. 60%). Furthermore, although productivity is at its maximum, there is still an optimization potential for the eluent consumption (Table 8.6).

High numbers of stages for a given column always represent low flow rate. Additionally, by increasing the number of stages, the peak width will become smaller (Figure 8.10), thus reducing the batch cycle time but increasing the production rate. Both phenomena benefit the eluent consumption. Low eluent consumptions can therefore be reached in the region with very high number of stages, although the productivity already decreases significantly below its maximum value (Table 8.6).

As can be seen in Table 8.6 and Figure 8.11, a high yield can be reached by reducing the amount of feed introduced into the column (i.e. low loading factor) and by reducing the flow rate (i.e. high number of stages). However, at very low loading factors, the productivity of the column and the efficiency of eluent usage will deteriorate seriously. Therefore, low loading factors benefit only yield of separation and not utilization of adsorbent and eluent.
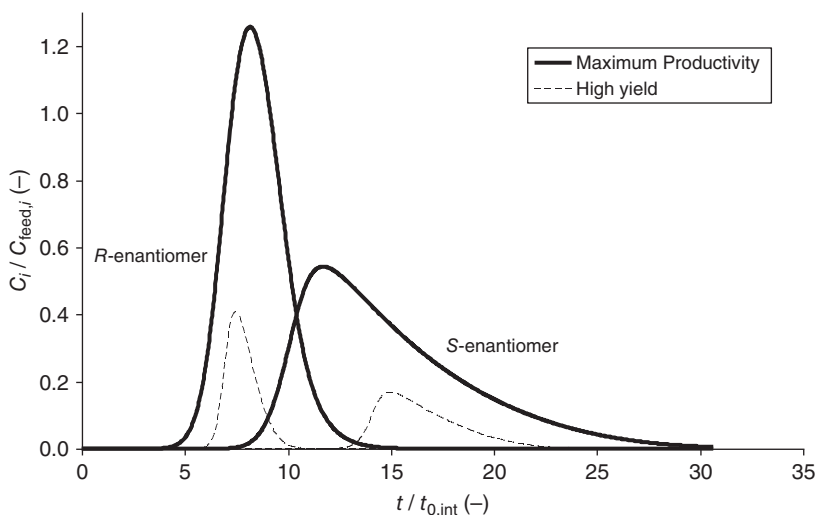
Figure 8.11 Comparison of chromatograms (maximum productivity; high yield).

The only evaluation method that unifies the contributions of these optimization goals is the total separation cost. The position of the optimum after a cost optimization depends heavily on the magnitude of each contribution relative to each other. If the price of adsorbent or fixed costs (maintenance and capital cost) is a dominant factor, then the cost optimum will coincide with the maximum productivity. For separation problems with low solubility of the components and/or very high eluent price, the cost optimum is approximately equal to the minimum of eluent consumption (i.e. very high number of stages). In other words, only the optimization of total separation cost leads to the "real" (economically) optimum of the separation problem.

8.2.2.2 Design and Optimization Strategy

Based on the beforehand presented main idea, a strategy will be developed that is suitable for the individual demand and boundary condition of the separation problem. First, the framework of the exemplarily chosen separation problem and the used model is introduced. Second, a strategy is proposed, which is suitable for the optimization of operating parameters of an existing plant as well as the design of a new column.

- *Applied column model*: Experimentally validated transport dispersion model.
- *Applied cut strategy*: Waste fraction is allowed (cut strategy I; cf. Figure 8.5).
- *Objective function*: To be able to compare total separation costs independently of the production rate, the total separation cost per product amount $C_{\text{spec,total}}$ is used. Since the consideration of fixed costs in the cost structure is usually handled differently and is subject to company policies, it does not make sense to consider the fixed costs in this book. Therefore, the optimization is focused on variable costs only (Section 8.1.1.2):

$$C_{\text{spec,total}} = C_{\text{spec,el}} + C_{\text{spec,ads}} + C_{\text{spec,feedloss}}$$

$$C_{\text{spec,total}} = EC \cdot f_{\text{el}} + \frac{\widetilde{n}_{\text{ads}}}{\text{VSP} \cdot t_{\text{file}}} f_{\text{ads}} + \frac{1 - Y}{Y} \cdot f_{\text{feed}} \tag{8.56}$$

- *Boundary conditions*: Purity, maximum pressure drop Δp_{max}, and desired production rate $\dot{m}_{prod}$. Since purity demand has to be fulfilled, the switch times for the fraction collection (t_{A1}, t_{A2}, t_{B1}, and t_{B2}) can be determined, and they are not subjects of optimization.
- *Number of stages*: The number of stages plays a major role in this optimization strategy and can be easily calculated using the HETP equation (Eq. (8.37)). Therefore, experimental HETP coefficients for every feed component, or at least for the reference component in the separation problem, have to be acquired before running this optimization strategy.

The first step in this design strategy is to assume any initial values for the column geometry (L_c and d_c) (cf. Figure 8.12). At this step of the optimization strategy, only the operating parameters of an existing chromatographic plant are considered as variable for optimization. Using these initial values, a series of dynamic simulations can be started to determine the values of following functions that characterize the column performance at different numbers of stages and loading factors:

- volume-specific productivity VSP
- specific eluent consumption EC
- yield at predefined purity Y
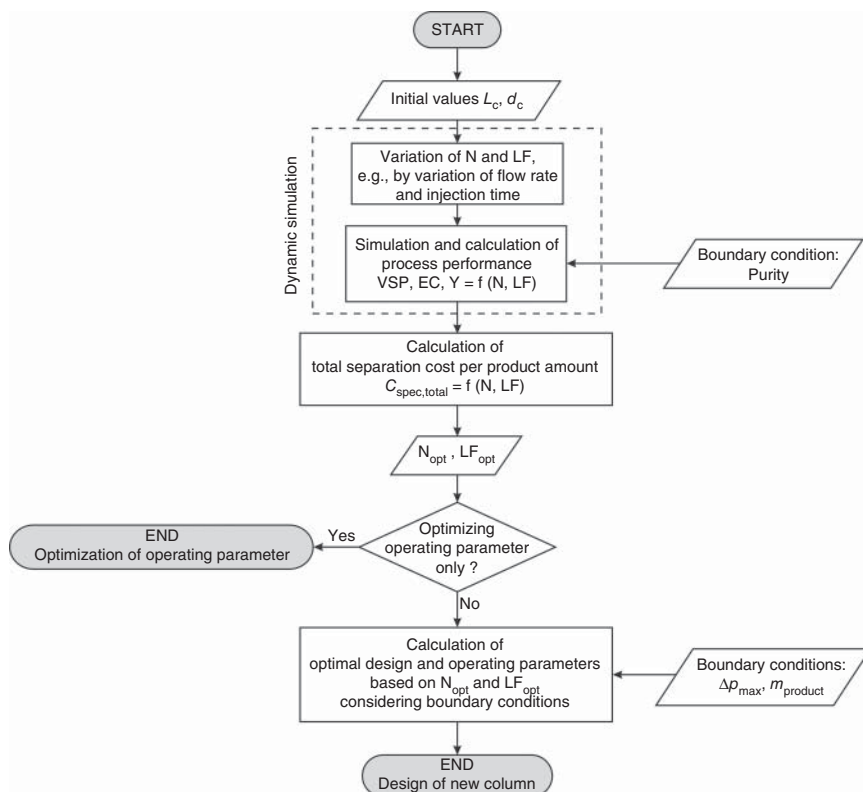
Figure 8.12 Design and optimization strategy for batch chromatographic column.

Provided prices for eluent, adsorbent, and feed loss are known. The total separation cost per product amount $C_{spec,total}$ at each number of stages and loading factor can also be calculated (Eq. (8.56)). As explained in Section 8.1.3.1, it is sufficient in most cases to take the number of stages and loading factor of a reference component into account. The number of stages and loading factor can be easily varied, for example, by varying the injection time t_{inj} and flow rate $\dot{V}$, whereby the maximum pressure drop can be neglected for the time being. However, during optimization of an existing plant, it has to be taken into account that a very small number of stages (i.e. very large flow rates) cannot be realized due to the limiting pressure drop of the plant.

Afterward, with the help of the results from dynamic simulation, the optimal number of stages N_{opt} and loading factor LF_{opt} can be determined where the value of objective function (i.e. total separation cost per product amount) is at its minimum. The applied total separation cost per product amount depends on productivity, eluent consumption, and yield, which in turn depend only on the number of stages and loading factor. Therefore, any process with an identical number of stages and loading factor will also have the same total separation cost per product amount. Please consider that this is only valid for variable costs. Fixed costs should not be expressed as functions of number of stages and loading factor, because they depend only on instrumental effort, not process performance. Therefore, consideration of fixed costs in the total separation cost would require an additional optimization loop to optimize the instrumental effort. However, in practice, fixed costs will hardly be an object of global optimization. In most cases, several options will exist, and the optimization task will be reduced to several case studies.

If only operating parameters of an existing plant are optimized, the determination of the optimal column design with the help of N_{opt} and LF_{opt} is not needed. Optimization procedures can be terminated at this point because the operation of the batch column already reaches its optimum here. However, during the design of a new column, one more step to determine the optimal column geometry, operating parameters, and the boundary conditions is necessary:

(1) N_{opt} and Δp_{max}: Using optimal number of stages N_{opt}, the unknown interstitial velocity $u_{int,opt}$ and column length $L_{c,opt}$ can be correlated as

$$N_{opt} = \frac{L_{c,opt}}{HETP(u_{int,opt})} = \frac{L_{c,opt}}{A + Cu_{int,opt}} \tag{8.57}$$

where A and C are the HETP coefficients of the reference component. At the same time, the maximum limit for pressure drop should not be violated. If the Darcy equation (Eq. (2.33)) is applied, $L_{c,opt}$ and $u_{int,opt}$ can also be correlated as

$$\Delta p_{max} = \psi \cdot \frac{u_{int,opt} \cdot L_{c,opt} \cdot \eta_1}{d_P^2} \tag{8.58}$$

It is very often assumed that $u_{int,opt}$ for a column is always the maximum allowed interstitial velocity, which is limited by the pressure drop for a certain column length. However, it has to be kept in mind that for every performance

criterion numerous optimal combinations of interstitial velocities and column lengths exist, which are represented by one optimal number of stages N_{opt}, provided mass transfer or axial dispersion is dominating (Section 8.1.2.2). Scherpian (2009) investigated this effect in case studies. He points out that in the case of congruent dimensionless concentration profiles, eluent consumption and yield are constant for all combinations of column length and interstitial velocity. Nevertheless, the specific productivity will vary depending on the A-term of the van Deemter equation. Additionally, productivity will decrease if the column length is shortened and is limited by the maximum allowable pressure drop. The latter indicates that N_{opt} cannot be realized if the selected column length is too large, so the corresponding interstitial velocity exceeds the maximum velocity due to the limiting pressure drop. Therefore, the column length should be selected such that the optimal number of stages can be realized at the maximum or less pressure drop. Both unknown variables ($L_{c,opt}$ and $u_{int,opt}$) can therefore be calculated, considering both N_{opt} and Δp_{max}:

$$L_{c,opt} \leq \frac{1}{2} \cdot \left(N_{opt} \cdot A + \sqrt{N_{opt}^2 \cdot A^2 + 4 \cdot N_{opt} \cdot C \cdot \frac{\Delta p_{max} \cdot d_p^2}{\psi \cdot \eta_1}} \right) \tag{8.59}$$

$$u_{int,opt} \leq \frac{\Delta p_{max} \cdot d_p^2}{\psi \cdot \eta_1 \cdot L_{c,opt}} \tag{8.60}$$

If the effect of mass transfer resistance on the HETP equation is very dominant, then Eq. (8.59) can be simplified to

$$L_{c,opt} \leq \sqrt{N_{opt} \cdot C \cdot \frac{\Delta p_{max} \cdot d_p^2}{\psi \cdot \eta_1}} \tag{8.61}$$

(2) *Desired production rate*, $\dot{m}_{product}$: Since values that characterize column performance (i.e. yield, eluent consumption, and productivity) at the optimal point are known, the required column diameter for a desired production rate can be easily determined using the volume-specific productivity at the optimal point (Eq. (8.7)):

$$d_{c,opt} = \sqrt{\frac{\dot{m}_{prod}}{VSP_{opt} (1 - \varepsilon_t)} \frac{4}{\pi L_{c,opt}}} \tag{8.62}$$

The optimal flow rate can then be determined:

$$\dot{V}_{opt} = u_{int,opt} \cdot \varepsilon_e \cdot \frac{\pi}{4} \cdot d_{c,opt}^2 \tag{8.63}$$

(3) *Optimal loading factor*, LF_{opt}: Using the optimal loading factor, the last unknown operating parameter, the injection time, can be determined:

$$t_{inj,opt} = \frac{LF_{opt} \cdot q_{sat} \cdot \pi \cdot d_{c,opt}^2 \cdot L_{c,opt} \cdot (1 - \varepsilon_t)}{4 \cdot c_{feed} \cdot \dot{V}_{opt}} \tag{8.64}$$

8.2.2.3   Other Strategies

In many studies, production rate is generally maximized while tolerating a decrease in yield, thus neglecting the potentially very high costs resulting from feed loss. Felinger and Guiochon (1996) proposed the product of yield and production rate as objective function in order to solve this problem. Other investigations of Felinger and Guiochon (1998) use this objective function in dealing with the optimization and comparison of elution, displacement, and nonisocratic chromatography. This investigation covers a wide range of retention factors, but neglects the fact that the retention factor in real systems generally cannot be varied independently of other material-dependent parameters. Further information on economics of chromatographic separations is given in Guiochon et al. (2006).

Katti and Jagland (1998) have performed a systematic analysis of different parameters that influence the separation cost. They investigate cost contributions of eluent, feed loss, packing materials, equipment, and investment. Each cost contribution is also examined individually, depending on various free optimization parameters. Their work gives good insight into the general correlations and dependencies in a cost optimization.

Epping (2005) and Jupke, Epping, and Schmidt-Traub (2002) optimized batch (and SMB) processes, regarding not only the common process performance (eluent consumption, productivity, etc.) but also the total separation cost, which is the summation of various cost contributions. Based on design data of Dünnebier, Weirich, and Klatt (1998) and specific cost data from Jupke, Epping, and Schmidt-Traub (2002), Chan, Titchener-Hooker, and Sørensen (2008) extended the economic evaluation of standard batch (and SMB chromatography) to single columns with recycling as well as recycling with peak shaving, but their findings are restricted to linear isotherms. They investigated three scenarios for the economic optimization of large-scale plants (2000 kg a^{-1}): maximizing a weighted objective function (recovery·yield) proposed by Felinger and Guiochon (1996), minimizing production cost and maximizing annual net profit. Their comparison of standard batch (and SMB) production affirms the general trend that batch production is favorable for short-term application while multicolumn processes are more economic for long-term production (>5 years).

A novel method to designing chromatographic separation units of varying process concepts, including inter alia batch chromatography, is presented by Siitonen and Sainio (2015). Using the so-called unified design method, boundaries of dimensionless operating parameters for a complete separation of a binary mixture can be predicted, assuming ideal conditions and infinite column efficiency. Cut strategy II has been applied, since a touching band separation was considered. In the case of batch chromatography, the operating parameters such as duration of the feed pulse, beginning and end of product fractions A and B, and the volumetric flow are converted into "m-values" m_1 to m_4. Boundaries of these m-values are defined analog to the triangle theory (Storti et al. 1993) for complete separation and different adsorption isotherms (Siitonen and Sainio 2015). Applying the unified method, the triangle theory can be applied for design of discontinuous processes. Further, operating parameter of different process concepts can be designed if operating parameters of one process concept are known. An

approach similar to the unified design method has been applied for comparison of different multicolumn processes by David, Yun, and Nicoud (2017). Further, the unified design method has been extended to separation of ternary mixtures (Sainio 2017).

8.3 Recycling Chromatography

The principles of closed-loop as well as steady-state recycling chromatography (SSRC) have already been explained in Sections 5.1.3 and 5.1.4. In general, these process schemes may be chosen if for standard batch chromatography the number of plates has to be increased in order to get an efficient separation and the column length is restricted by the maximum allowable pressure drop. At the column outlet, certain volumes of pure products are separated, while the rest of the mixture is recycled to the column inlet. Through this a virtually longer column is achieved and maximum pressure drop is not exceeded.

Additionally to the operating and design parameters known for standard batch chromatography, cut or fraction times have to be determined. For the design of SSRC, these are the cut times for the steady state, while for closed-loop recycling chromatography (CLRC) the cut times of the last cycle (cut times of all cycles in the case of peak shaving) have to be determined. As shown by Scherpian and Schembecker (2009), Kaspereit and Sainio (2011), or von Langermann et al. (2012), the performance of these processes can be theoretically calculated by rigorous process simulation based on the transport dispersion model without decreasing accuracy inadmissibly because of accumulation of inaccuracies. For the design of new processes, it is recommended first to determine the approximate operating map in order to estimate optimal process conditions. These data can be used to improve process design by rigorous process simulation or experiments. For a first approximate design, the following design strategies can be applied. Section 8.3.1 describes shortcut methods for the approximate determination of operating conditions for SSRC, while Section 8.3.2 outlines how for CLRC, for example, satisfying lab results are scaled up to production scale and how the process data can additionally be optimized based on experiments with the production plant.

8.3.1 Design of Steady-State Recycling Chromatography

The major challenge in designing any recycling chromatography process is to determine the cut times required to fulfill the given purity requirements. In most cases this task can be accomplished only using a dynamic process model or by experimental trial and error. However, for steady-state recycling in mixed recycle mode (MR-SSR) (Section 5.1.4), simple shortcut design methods allow estimating a priori and rather accurately the cut times required in steady state – without performing any dynamic simulation. This facilitates a straightforward basic process design and rough performance evaluation and is the basis for a subsequent more detailed design, optimization, and scale-up.

Two such shortcut approaches exist. The first neglects any band broadening effects and applies to systems with Langmuir isotherms (Eq. (2.42)), of which the parameters have to be known. Based on equilibrium theory (Section 6.2.3), Bailly and Tondeur (1982) derived explicit equations for designing MR-SSR processes for the case of complete separation, that is, 100% pure products. This approach was extended by Sainio and Kaspereit (2009) to any combination of purity requirements. In connection with a recent extension of equilibrium theory for Langmuir isotherms by Siitonen and Sainio (2011), these methods predict explicitly, for a given column geometry and injection volume, the cut times and the steady state of the process a priori. Dynamic simulation is not required.

The second methodology, which is explained in more detail below, is an extension of the former to systems with significant dispersion and favorable isotherms in general. Although it covers a broader range of problems, it is even simpler to apply. It requires only a measured and deconvoluted chromatogram. Neither a process model nor isotherm parameters are required.

Figure 8.13a illustrates the approach for a system with bi-Langmuir isotherms (Eq. (2.44)). The required purities are set to $Pu_{A,req} = Pu_{B,req} = 99\%$. Further details of the simulation results are given in the reference. For the injection volume to be investigated, an experimental chromatogram is analyzed to obtain the underlying individual concentrations. If available, also simulated data can be used (as in the figure). Based on the chromatogram, the four cut times required to achieve the purity requirements in steady state can be determined (Kaspereit and Sainio 2011). During operation of an SSR process, these times are being held constant with respect to the start of each injection.

As for the four cut times, the end of fraction product fraction B, t_{B2}, is selected as the end of the chromatogram – for example, based on a low threshold concentration. If the initial slope of the isotherm of the stronger adsorbing component is known, Eq. (8.65) might be used instead:

$$t_{B2} = t_{inj} + t_0 \left(1 + \frac{1 - \varepsilon_t}{\varepsilon_t} \frac{dq_2}{dc_2}\bigg|_{c_1 - c_2 - 0} \right) \tag{8.65}$$

where t_{inj} is the duration of the injection. The start of fraction B, t_{B1}, which defines the end of the recycle fraction R, is found by backward integrating the dispersive rear of the profile, until the determined amounts m_{iB} ($i = 1, 2$) fulfill exactly the purity requirements, $Pu_{B,req}$, on this fraction:

$$t_{B1} = \max \left\{ t < t_{B2} \; : \; Pu_B(t) = \frac{m_{2B}(t)}{m_{1B}(t) + m_{2B}(t)} = Pu_{B,req} \right\} \tag{8.66}$$

It can be shown that for favorable isotherms this rear part of the chromatogram does not change during SSR operation (Sainio and Kaspereit 2009; Kaspereit and Sainio 2011). Thus, from a global material balance and the cycle-invariant amount of the target compound in fraction B, m_{2B}, an expression can be derived for the end time of fraction A, equal to the start of the recycle R:

$$t_{A2} = t_{B1} - t_{inj} + \frac{m_{2B}}{Y_2 \dot{V} c_{2F}} \tag{8.67}$$
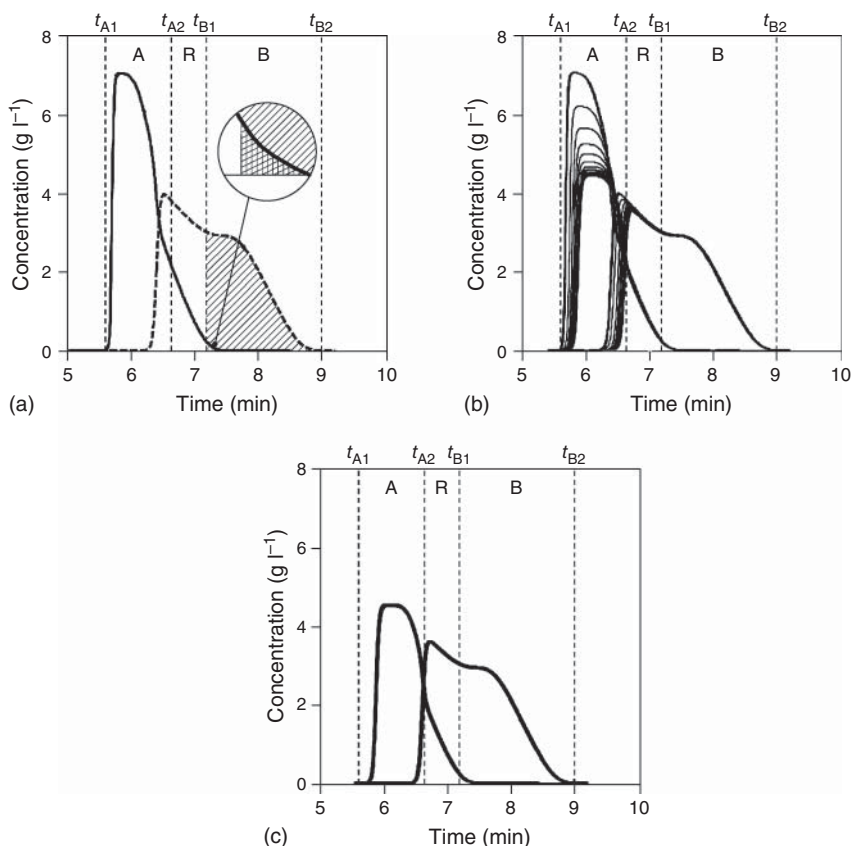
Figure 8.13 Shortcut design of SSRC. (a) Determination of cut times by integrating the rear of an initial batch chromatogram. (b) Transient behavior of the designed SSR process (overlay of 50 cycles, steady-state purities 95.6% and 99.4%, respectively). (c) Improved design and elimination of start-up phase by applying the shortcut method to the last chromatogram of (b) (overlay of 50 cycles, purities 96.0%, and 99.3%). Source: Kaspereit and Sainio (2011). Reproduced with permission of Elsevier.

where c_{2F} is the fresh feed concentration of this compound. Y_2 is its overall yield, which is already fully specified through the two given purity requirements:

$$Y_2 = \frac{\mathrm{Pu_{B,req}}}{100\% - \mathrm{Pu_F}} \frac{\mathrm{Pu_{A,req}} - \mathrm{Pu_{B,req}}}{\mathrm{Pu_{A,req}} + \mathrm{Pu_{B,req}} - 100\%} \tag{8.68}$$

Finally, for the start of fraction A, t_{A1}, some suitable value $t_{A1} \geq t_0$ is chosen. This time can be optimized later.

Figure 8.13b shows an overlay of the elution profiles of 50 SSR cycles performed using the cut times determined in Figure 8.13a, which is the reason why the elution profiles of the first cycle (largest concentrations) are identical to those in (panel a). The process reaches a steady state after about 10 cycles. Note that the second fraction is virtually invariant from cycle to cycle, while the purity for fraction A is fulfilled only after the process, which was started here with a full

injection of fresh feed, reaches steady state. The purity requirement on A can be fulfilled also during start-up if the process is initiated using a lower injection concentration. However, the most elegant option is to eliminate the start-up completely, as shown in Figure 8.13c. As proposed by Bailly and Tondeur (1982), this is achieved when using for the first few injection(s) a prepared mixture that corresponds to the steady-state injections and switching to the fresh feed after these eluted from the column.

This efficient approach was successfully validated experimentally by Kaspereit and Sainio (2011) for two cycloketones with bi-Langmuir isotherms, as well as for an enantioseparations for a pharmaceutically relevant compound with complex quadratic isotherms (von Langermann et al. 2012).

The design method was extended to processes with an additional solvent removal in the recycle (Siitonen, Sainio, and Kaspereit 2011). Furthermore, although it does not directly apply to SSR processes operated in closed-loop mode, it can be used to obtain initial guesses on cut times and performance of such process.

It is recommended to apply the shortcut method in a parametric study in order to optimize also the injection volume and column dimensions. The results should then be used in a detailed design study where all relevant design parameters are optimized against the performance criteria and objective functions discussed in Section 8.1.1. In particular, the mentioned transport dispersion model is a good choice for such studies since it affords a high degree of accuracy when simulating recycling processes (Scherpian 2009; Kaspereit and Sainio 2011). Scale-up of the process can be performed using such model, preferably using dimensionless representations along the lines of Section 8.3.2.

8.3.2   Scale-Up of Closed-Loop Recycling Chromatography

In Section 8.1.2, it is shown that in the case of high efficient chromatography, the number of dimensionless parameters reduces and instead of Stanton and Péclet numbers the number of plates is the dominating parameter. In order to proof these findings for CLRC, Scherpian and Schembecker (2009) measured the elution profiles for three different process setups for which the number of plates, the loading factor, and the recycle number are constant. The characteristic data of these experiments are presented in the reference.

Figure 8.14 presents the measured CLRC elution profiles. For the first cycle, all profiles are in very good agreement and confirm the expected congruency. The deviations of setup B in the second and third cycles are due to dominating plant effects.

Comparable elution profiles for CLRC with peak shaving as depicted in Figure 8.15 are again in good congruence for types A and C. In the case of peak shaving, pure product is extracted from each recycle. The slight deviations of type B are caused by backmixing effects as mentioned above. The characteristic process data are the same as in Figure 8.14.

In Section 8.1.2, it has been confirmed that elution profiles of chromatographic processes are congruent if the parameters of the dimensionless transport dispersion model are identical. Based on these results, Section 8.2 presents an
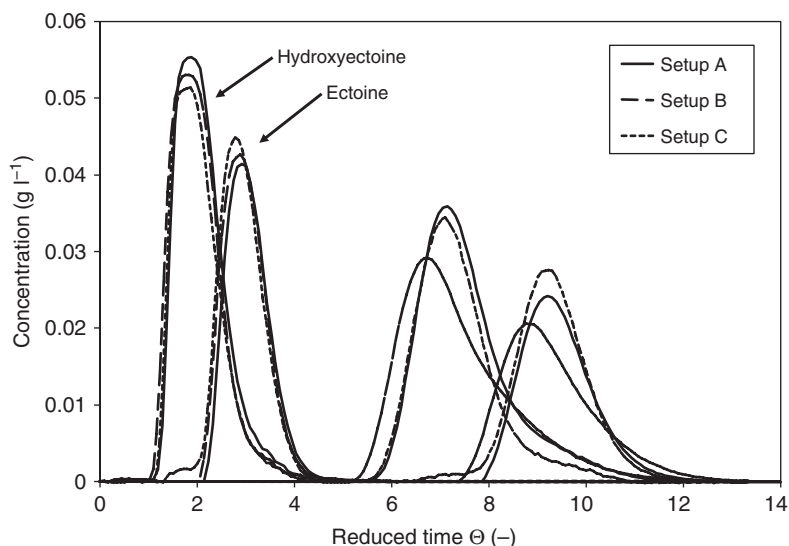
Figure 8.14 CLRC elution profiles of three different experiments for constant loading factors, number of plates, and recycle numbers. Source: Scherpian and Schembecker (2009). Reproduced with permission of Elsevier.
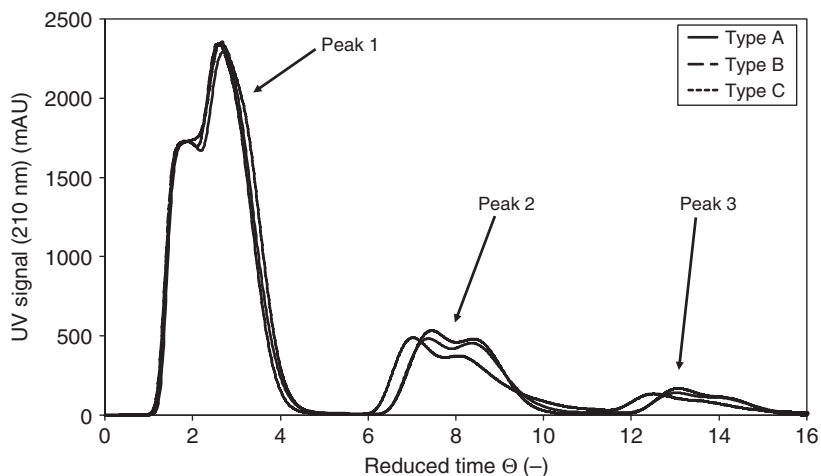
Figure 8.15 CLRC elution profiles with peak shaving for constant loading factors, number of plates, and recycle numbers. Source: Scherpian and Schembecker (2009). Reproduced with permission of Elsevier.

optimization strategy for batch chromatography. A corresponding procedure is applicable for the theoretical optimization of recycle processes, but it is very time consuming. An alternative for practical purposes is a scale-up based on experimentally optimized lab results or a practically satisfying process.

Figure 8.16 depicts a strategy to scale up CLCR processes. The idea is to start with experimental results that shall be transferred into a production-scale
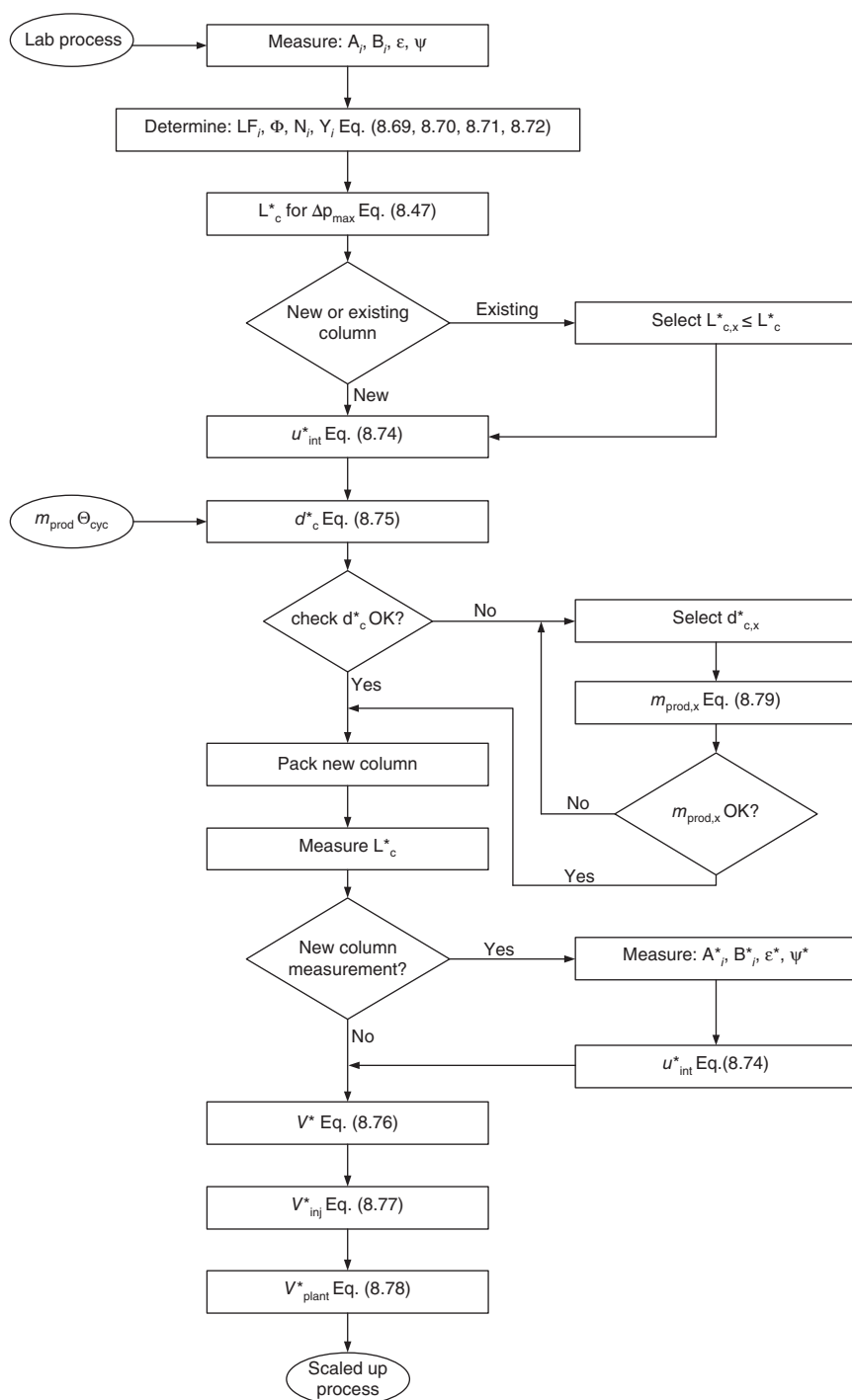
Figure 8.16 Scale-up strategy for closed-loop recycling chromatography.

process. The same procedure can be applied if optimal figures for the dimensionless parameters have been evaluated by theoretical optimization.

Following the left-hand side of Figure 8.16,

- The scale-up strategy starts with a lab process that has been optimized experimentally.
- In order to determine the relevant parameters, the coefficients of the van Deemter plot A_i and C_i are measured. Additionally the void fraction ε and the resistance factor ψ are measured or estimated.
- The dimensionless parameters that have to be equal for the lab- and process-scale plants are defined as follows:

$$\text{Loading factor, LF}_i = \frac{c_{i,\text{feed}} \cdot \dot{V} \cdot t_{\text{inj}}}{q_{\text{sat},i} \cdot V_c \cdot (1 - \varepsilon_t)} \tag{8.69}$$

$$\text{Recycle number, } \Phi = \frac{t_{\text{plant}}}{t_{0,\text{int}}} = \frac{V_{\text{plant}}}{V_{c^\varepsilon}} \tag{8.70}$$

$$\text{Number of plates, } N_i = \frac{L_c}{\text{HETP}_i} \approx \frac{L_c}{A_i + C_i u_{\text{int}}} \tag{8.71}$$

These parameters ensure congruent elution profiles. In order to achieve the same production rate, the yield has to be constant:

$$Y_i = \frac{m_{\text{prod,cyc}}}{c_{\text{feed},i} V_{\text{inj}}} = \frac{\dot{m}_{\text{prod}} \Theta_{\text{cyc}} t_{0,\text{int}}}{c_{\text{feed},i} V_{\text{inj}}} \tag{8.72}$$

where Θ_{cyc} is the reduced time of one injection cycle, that is, the time between two consecutive injections. In the case of CLRC with peak shaving, the dimensionless cutting times of the lab process are also the same for the scaled-up process (Scherpian 2009).

Most parameters are different for each component. As already pointed out in Section 8.1.3, for all components, the number of stages of the new column should be greater than or equal to the old one $N_i^* \geq N_i$, hence the key component $N_i^* = N_i$

- The maximum column length, which can be realized for the given number of stages and the maximum allowable pressure drop, is

$$L_c^* \leq \frac{1}{2} \left(N_i A_i + \sqrt{N_i^2 A_i^2 + 4 N_i C_i \frac{\Delta p_{\text{max}} d_p^2}{\psi \eta}} \right) \tag{8.73}$$

- The first decision is to get a new column of the calculated length or to take an already existing column of a given length.
- The interstitial velocity for the new column length is

$$u_{\text{int}}^* = \left(\frac{L_c^*}{N_i} - A_i \right) \frac{1}{C_i} \tag{8.74}$$

- The column diameter depends on the expected production rate and the cycle time of the process:

$$d_c^* = \sqrt{\frac{4}{\pi} \frac{\dot{m}_{\text{prod},i} \Theta_{\text{cyc}}}{Y_i \text{LF}_i (1 - \varepsilon_t) u_{\text{int}}^*}} \tag{8.75}$$

- After the dimensions are determined, the column is packed with the same solid phase used for the lab process. The real column length is measured and it has to be decided if the parameters of the new packing shall be determined or not.
- Finally, the volumetric flow rate, the injection volume, and volume of the plant are determined:

$$\text{Volumetric flow rate, } V^* = \frac{\pi}{4} d_c^2 u_{int}^* \varepsilon_e \tag{8.76}$$

$$\text{Injection volume, } V_{inj}^* = \frac{\text{LF}_i q_{sat,i} V_c^* (1 - \varepsilon_t)}{c_{feed,i}} \tag{8.77}$$

$$\text{Plant volume, } V_{plant}^* = \Phi V_c^* \varepsilon_e \tag{8.78}$$

The design strategy described so far is a theoretical approach. In practice, additional aspects will influence the scale-up strategy. They are characterized by three decision cycles that are depicted on the right-hand side of Figure 8.16:

- First, a column of a given length $L_{c,x}^*$ may be selected. It has to be equal to or smaller than the maximum allowable column length (Eq. (8.73)).
- Second, the calculated column diameter does not match with standard dimensions or an available column shall be used. In this case a certain diameter $d_{c,x}^*$ is selected, and the resulting production rate is

$$\dot{m}_{prod,i} = \frac{\pi}{4} d_c^2 \frac{Y_i \text{LF}_i (1 - \varepsilon_t) u_{int}}{\Theta_{cyc}} \tag{8.79}$$

- Third, the conditions for scale-up from lab to process plant are constant figures for the dimensionless parameters. However, in practice, it is not certain that the packing of the columns is always identical. Slight variations of the void fraction and HETP may occur. Additionally, differences in the fluid dynamics, especially at the column inlet and outlet, have to be taken into account. The theoretical scale-up strategy ignores these deviations. However, in order to make sure that real numbers of plates of both plants are really the same, it is recommended to determine the van Deemter plot, void fraction, and friction number for the new packing and to correct the interstitial velocity, the flow rate, and the injection volume.

Please note that the scale-up strategy is not influenced by dimensionless number Pe_{plant}. The "plant" that summarizes the effect of all equipment besides the column has two effects: the band broadening of the elution profile and the holdup. Pe_{plant} stands for the band broadening that depends on the axial dispersion as well as backmixing and has to be maximized by the equipment design. The holdup determines the recycle time and is a boundary condition for the chromatographic column. Therefore, the recycle number has to be constant for scale-up.

Batch chromatography is a special case of the CLRC. Therefore, the same scale-up strategy is applicable if the reduced time of one injection and the recycle number are set:

$$\Phi = \frac{t_{plant}}{t_{0,int}} = \frac{V_{plant}}{V_\varepsilon} = 0 \text{ and } \Theta_{cyc} = 1 \tag{8.80}$$

8.4 Conventional Isocratic SMB Chromatography

Continuously operated chromatographic processes, such as SMB, are well established for the purification of hydrocarbons, fine chemicals, and pharmaceuticals. They have the ability to improve the process performance in terms of productivity, eluent consumption, and product concentration, especially for larger production rates. These advantages, however, are achieved with higher process complexity with respect to operation and layout. A purely empirical optimization is rather difficult, and, therefore, the breakthrough for practical applications is linked to the availability of validated SMB models and shortcut methods based on the TMB model as described in Section 7.8.2.

In this section, first some considerations regarding the optimal axial concentration profile in SMB systems are mentioned to increase the process understanding of the interested reader. Afterward, design methods based on TMB models for different types of isotherms are presented. Finally, strategies to estimate operating parameters based on the introduced design methods as well as optimization strategies for operating and design parameters are introduced.

8.4.1 Considerations to Optimal Concentration Profiles in SMB Process

During operation of an SMB plant, the propagation of components to be separated is influenced by the internal fluid flow rates in the different sections as well as the switching time that simulates countercurrent movement of the solid phase. By an appropriate choice of the operating parameters, the movement of the less retained component is focused on the raffinate port, while the more retained component is collected in the extract stream. Figure 8.17 depicts an optimal axial profile of the liquid concentrations at the end of a switching interval after the process has reached a periodic steady state. The adsorption and desorption fronts of both components have to start or stop at given points to achieve complete separation at maximum productivity.
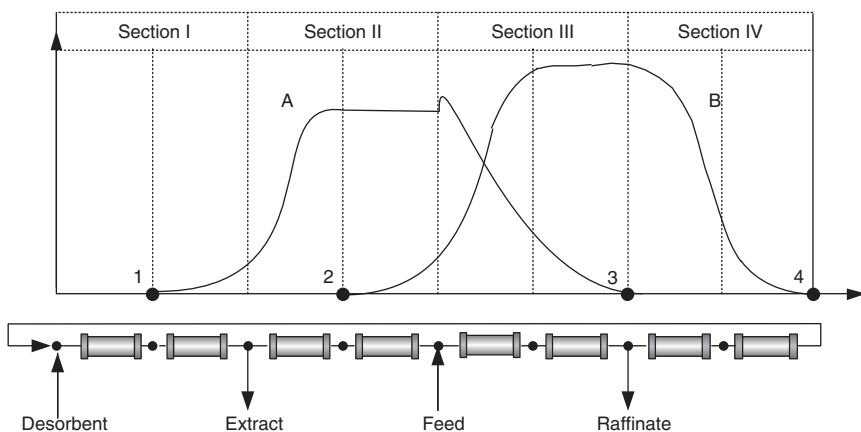
Figure 8.17 Optimal axial concentration profile of an SMB process at the end of a switching interval.

For complete separation the desorption fronts of the two components must not exceed points 1 and 2, respectively, which are located one column downstream the desorbent and extract port. Since the concentration profile displayed in Figure 8.17 demonstrates the situation at the end of a switching interval, all ports will move one column downstream in the next moment. If the desorption front of component B exceeds point 2, the extract stream will be polluted with B after the ports have been switched. The same applies to point 1. If component A is shifted into section IV, the adsorbent will transfer it to the raffinate port and the raffinate will be polluted. For the adsorption fronts, components A and B must not violate points 3 and 4, respectively, at the end of the switching period. Otherwise, component A will pollute the raffinate, and component B will enter section I and pollute the extract.

To achieve 100% purity for both components, it is necessary to fulfill the constraints mentioned before. In addition, it is favorable to push the fronts as far as possible toward points 1–4 to realize the highest throughput as well as the lowest eluent consumption.

If product purities lower than 100% are required, there are generally two possibilities to achieve this with a positive impact on other process parameters:

- A higher feed rate at constant eluent consumption can be realized when the adsorption front of component A exceeds point 3 and/or the desorption front of component B exceeds point 2.
- A lower eluent consumption at constant feed rate can be realized when the adsorption front of component B exceeds point 4 and/or the desorption front of component A oversteps point 1.

In these cases the raffinate will be polluted with the more retained component A and/or the extract will be polluted with the less retained component B. Depending on purity requirements and the objective function, any combination of these two cases can also be chosen.

Whenever dealing with the operation of SMB units, one always has to consider the time needed to reach a periodic steady state. Depending on the chromatographic system, process setup, and column geometry, it might take 15 or more complete cycles to reach steady state.

8.4.2 Process Design Based on TMB Models (Shortcut Methods)

The operating point of an SMB unit is characterized by the flow rates of the liquid phase in the four sections $\dot{V}_j$ as well as the switching time t_{shift}. Another degree of freedom is the concentration of the solute in the feed stream. According to Charton and Nicoud (1995), the feed concentration should be at its maximum to achieve largest productivity. For the following considerations, feed concentrations as well as temperatures are kept constant.

Due to the comparability between TMB and SMB processes (Section 7.8.2), the TMB design approach is quite often used to estimate operating parameters of SMB units. Operating parameters for TMB processes are the liquid flow rates in the four sections $\dot{V}_{j,TMB}$ and the volumetric flow rate of the adsorbent $\dot{V}_{ads}$. To transfer these TMB parameters to SMB operating parameters ($\dot{V}_{j,SMB}$ and t_{shift}),

the interstitial velocity in the SMB process must be equal to the relative velocity of fluid and adsorbent in the TMB process (Section 7.8.2.1). Therefore, the following relationships can be derived:

$$\dot{V}_{ads} = \frac{(1 - \varepsilon) \cdot V_c}{t_{shift}} \tag{8.81}$$

$$\dot{V}_{j,SMB} = \dot{V}_{j,TMB} + \frac{V_c \cdot \varepsilon}{t_{shift}} \tag{8.82}$$

8.4.2.1 Triangle Theory for an Ideal Model with Linear Isotherms

Ruthven and Ching (1989), Hashimoto et al. (1983), and Nicoud (1992) have used analytical solutions of a TMB process under the assumption of the ideal model (neglecting axial dispersion and mass transfer phenomena) and linear isotherms. The fluid phase in each section j of the TMB process moves with the flow rate $\dot{V}_{j,TMB}$ in one direction and the solid phase with $\dot{V}_{ads}$ in the opposite direction. Figure 8.18 depicts the directions of migration of the two components for a TMB separation. Since equilibrium is assumed to be reached immediately in the ideal model, the mass flow $\dot{m}_{i,j}$ of component i depends on these two flow rates and the isotherm:

$$\dot{m}_{i,j} = (\dot{V}_{j,TMB} - \dot{V}_{ads} \cdot \varepsilon_p) \cdot c_{i,j} - \dot{V}_{ads} \cdot (1 - \varepsilon_p) \cdot q_{i,j} \tag{8.83}$$

Storti et al. (1993) introduced the dimensionless flow rate ratio m_j as the ratio between liquid and solid flows in every section:

$$m_j = \frac{\dot{V}_{j,TMB} - \dot{V}_{ads} \cdot \varepsilon_p}{\dot{V}_{ads} \cdot (1 - \varepsilon_p)} \tag{8.84}$$

This was the impulse for the research groups of Morbidelli, Mazzotti, and Storti at the ETH Zurich to develop a method, which is most instructive for the understanding of SMB separations and pioneered the design of SMB processes.
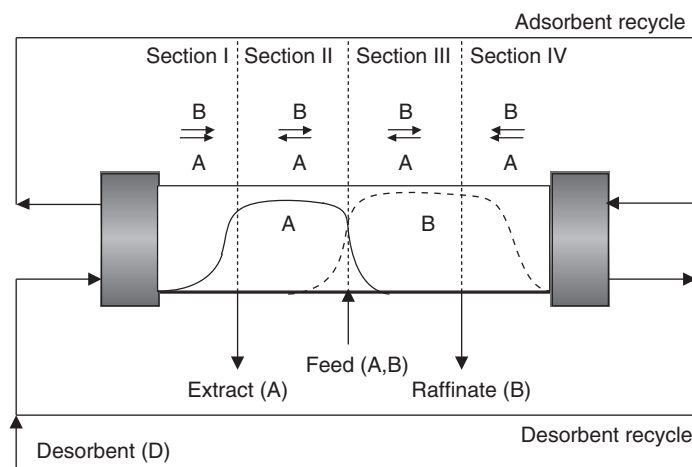
Figure 8.18 Directions of migration of two components in a TMB separation.

The basic idea is to determine an operating area for the dimensionless flow rate ratios m_{II} and m_{III} of sections II and III, for which a complete separation of a two-component mixture is realized in a TMB process. This operating area of different dimensionless flow rate ratios is often illustrated in a m_{II}–m_{III} diagram. As shown in Figure 8.19, the resulting operating area is bordered by the diagonal and has the shape of a triangle for linear isotherms. Therefore, this method is often called "triangle theory." A two-component mixture is separated into pure products for m_{II} and m_{III} operating points within the triangle, while outside the triangle only pure extract, pure raffinate or impure products are achieved. The decisive point is the applicability of the TMB operating plane on the estimation of SMB operating parameters using Eqs. (8.81) and (8.82) due to the comparability of TMB and SMB processes. Nevertheless, especially for SMB systems with a low number of columns, the eligibility of the determined operating point of the TMB model for usage in SMB processes has to be validated by laboratory experiments. The basic principles of this method and the application for different types of isotherms are outlined more detailed in Storti et al. (1993, 1995) and Mazzotti, Storti, and Morbidelli (1994, 1996, 1997).

A complete separation of a two-component feed mixture (A and B) is achieved if the following constraints of the analytical solution of the ideal model for linear isotherms are fulfilled:

$$\text{Section I}: \quad m_I \geq H_B, \quad m_I \geq H_A \tag{8.85}$$

$$\text{Section II}: \quad H_A \geq m_{II} \geq H_B \tag{8.86}$$

$$\text{Section III}: \quad H_A \geq m_{III} \geq H_B \tag{8.87}$$

$$\text{Section IV}: \quad m_{IV} \leq H_B, \quad m_{IV} \leq H_A \text{ and} \tag{8.88}$$

$$H_B \leq m_{II} \leq m_{III} \leq H_A \tag{8.89}$$
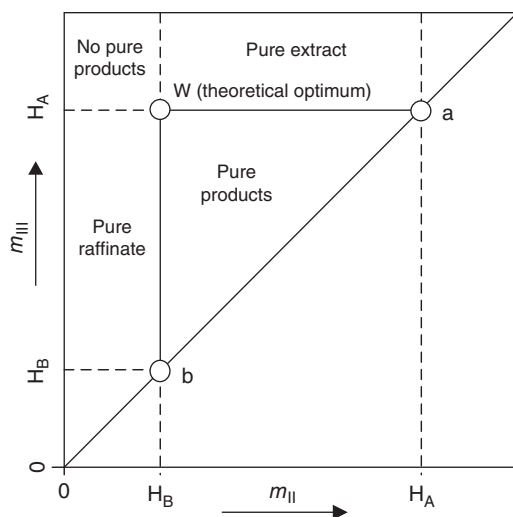
Figure 8.19 Operating plane or triangle diagram for linear isotherms.

As shown in Figure 8.19, the points a and b result from Henry coefficients. The theoretical optimum for process productivity is achieved at point w, where the difference between m_{II} and m_{III} is largest and hence the feed flow rate is at its maximum value for complete separation. Rigorous process simulations as well as experiments prove that SMB operating points for 100% purities are placed within this "triangle," but certain safety margins, especially to the vertex w, have to be considered in practice. The flow rate of fresh desorbent and, therefore, the eluent consumption can be minimized by choosing m_I as low and m_{IV} as high as possible.

8.4.2.2 Triangle Theory for an Ideal Model with Nonlinear Isotherms

Application of the method described so far becomes more complicated when isotherms are no longer linear and, therefore, the migration velocities of the components become strongly influenced by fluid-phase concentrations. One approach for determining the operating parameters is the explicit solution of the ideal TMB process model (Eqs. (7.78) and (7.79)), as proposed by Storti, Mazzotti, and Morbidelli. By introducing the dimensionless time

$$\tau = \frac{t \, \dot{V}_{ads}}{V_c} \tag{8.90}$$

and the dimensionless axial position

$$z = \frac{x}{L_c} \tag{8.91}$$

as well as the flow rate ratios m_j, the balance for the TMB process under the assumption of ideal conditions is

$$\frac{d}{d\tau}[\varepsilon_t \cdot c_{i,j} + (1 - \varepsilon_t) \cdot q_{i,j}] + (1 - \varepsilon_t) \cdot \frac{d}{dz}[m_j \cdot c_{i,j} - q_{i,j}] = 0 \tag{8.92}$$

This partial differential equation can be solved analytically for certain types of isotherms by applying the method of characteristics (Helfferich and Klein 1970; Rhee, Aris, and Amundson 1970). Following this approach, direct solutions are available for isotherms with constant selectivity, such as the multi-Langmuir or the modified competitive multi-Langmuir isotherm (Storti et al. 1993, 1995; Mazzotti, Storti, and Morbidelli 1994, 1996, 1997). For multi-bi-Langmuir isotherms with nonconstant selectivities, a numerical determination is necessary (Gentilini et al. 1998; Migliorini, Mazzotti, and Morbidelli 2000).

In the following, the procedure for determining the operating diagram for a chiral mixture of EMD53986 is explained (Appendix A.1). The adsorption equilibrium of this system can be described by the multi-Langmuir isotherm (Eq. (8.93)):

$$q_i = \frac{H_i \cdot c_i}{1 + \sum b_i \cdot c_i}, \quad i = A, B \tag{8.93}$$

Based on these isotherms, the nulls ω_G and ω_F ($\omega_G > \omega_F > 0$) have to be determined for the following quadratic equation:

$$(1 + a_A \cdot c_{A,F} + a_B \cdot c_{B,F}) \cdot \omega^2$$
$$- [H_A \cdot (1 + a_B \cdot c_{B,F}) + H_B \cdot (1 + a_A \cdot c_{A,F})] \cdot \omega - H_A \cdot H_B = 0 \tag{8.94}$$
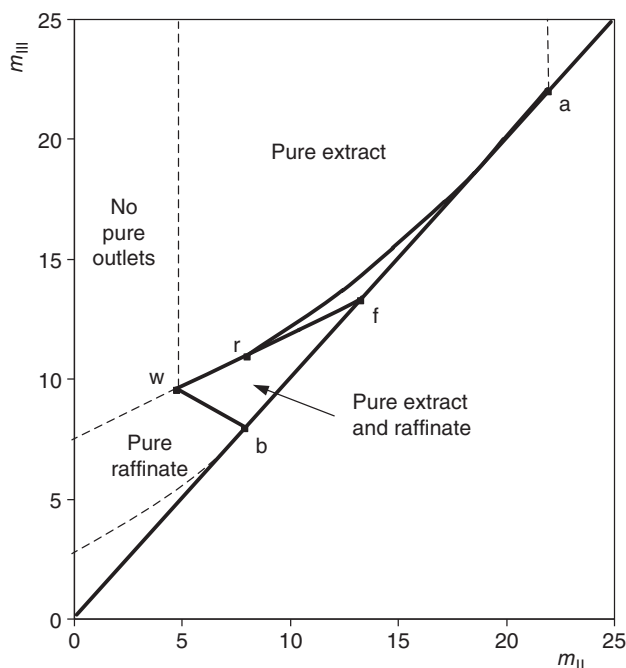
Figure 8.20 Operating plane or triangle diagram for nonlinear isotherms.

With these data, the isotherm parameters for EMD53986 and the feed concentration, which is $2.5 \, \text{g} \, \text{l}^{-1}$ for each component, a graph as shown in Figure 8.20 can be created. The points and lines are defined as follows:

$$\text{Line wf} : \quad [H_A - \omega_G \cdot (1 + b_A \cdot c_{\text{feed,A}})] \cdot m_{II} + b_A \cdot c_{\text{feed,A}} \cdot \omega_G \cdot m_{III}$$
$$= \omega_G \cdot (H_A - \omega_G) \tag{8.95}$$

$$\text{Line wb} : \quad [H_A - H_A \cdot (1 + b_A \cdot c_{\text{feed,A}})] \cdot m_{II} + b_A \cdot c_{\text{feed,A}} \cdot H_B \cdot m_{III}$$
$$= H_B \cdot (H_A - H_B) \tag{8.96}$$

$$\text{Curve ra} : \quad m_{III} = m_{II} + \frac{(\sqrt{H_A} - \sqrt{m_{II}})^2}{b_A \cdot c_{\text{feed,A}}} \tag{8.97}$$

$$\text{Point a} : (H_A, H_A), \quad \text{point b} : (H_B, H_B), \quad \text{point f} : (\omega_G, \omega_G) \tag{8.98}$$

$$\text{Point w} : \quad \left(\frac{H_B \cdot \omega_G}{H_A}, \frac{\omega_G \cdot [\omega_F \cdot (H_A - H_B) + H_B \cdot (H_B - \omega_F)]}{H_B \cdot (H_A - \omega_F)} \right) \tag{8.99}$$

Due to strong nonlinearity of the isotherms as well as competitive adsorption behavior, the triangle is completely different compared to the operating space for linear isotherms.

Since the slope of the isotherms is strongly dependent on the fluid-phase concentration, the feed concentration has a remarkable influence on the shape of the separation region. Figure 8.21 illustrates the influence of the feed concentration on the operating diagram.
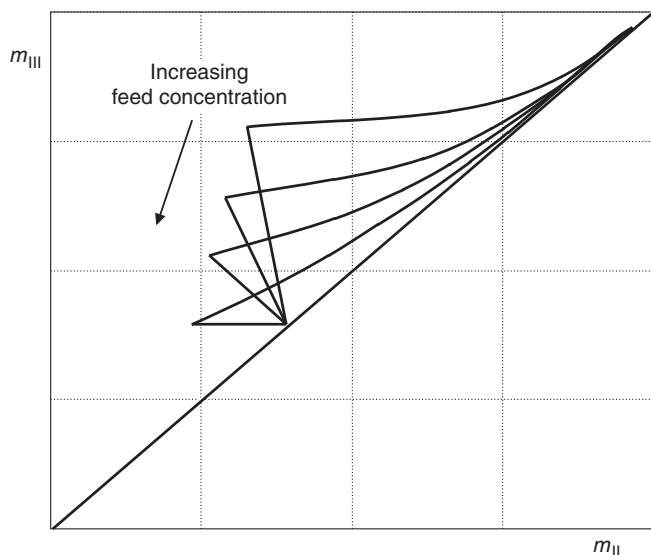
Figure 8.21 Influence of the feed concentration on the operating diagram.

To complete the set of possible operating parameters for a four-section SMB unit, values for the dimensionless flow rate ratios m_I and m_{IV} have to be determined as well. The determination of m_I and m_{IV} is less complicated since only the adsorption of single components is involved.

Because the solid phase is regenerated in section I, the more retained component A has to be desorbed by the fluid flow. This can be guaranteed for all Langmuir-type isotherms by the following condition:

$$m_I \geq m_{I,min} = H_A \tag{8.100}$$

In section IV, the less retained component B has to be adsorbed and carried toward the raffinate port in order to regenerate the liquid phase. For EMD53986 with its multi-Langmuir isotherm, the corresponding constraint on the dimensionless flow rate ratio m_{IV} is

$$\frac{-\varepsilon_P}{1 - \varepsilon_P} < m_{IV} \leq m_{IV,max} = \frac{1}{2}\Big[H_B + m_{III} + b_B c_{feed,B}(m_{III} - m_{II})$$
$$- \sqrt{(H_B + m_{III} + b_B c_{feed,B}(m_{III} - m_{II}))^2 - 4 H_B m_{III}}\Big] \tag{8.101}$$

The maximum m_{IV} is seen to be a function of flow rate ratios m_{II} and m_{III} as well as the feed concentration.

Table 8.7 lists the theoretical optimal values of all flow rate ratios for the separation of EMD53986 at a feed concentration of $2.5\,\mathrm{g\,l^{-1}}$. These values indicate the set of operating parameters, for which the productivity is at its maximum (point w), since the difference between m_{II} and m_{III} is largest. In addition, eluent consumption reaches its minimum since the difference between m_I and m_{IV} is smallest.

Table 8.7 Operating parameters for EMD53986 obtained by the TMB shortcut method.

$m_{I,min}$	19.75
m_{II} (at point w)	5.29
m_{III} (at point w)	10.57
$m_{IV,max}$	6.28

8.4.2.3 Shortcut to Apply the Triangle Theory on a System with Unknown Isotherms Assuming Langmuir Character

The procedure described so far requires a detailed knowledge of the adsorption equilibrium. Naturally, the more accurate the isotherm parameters have been determined, the more reliable are the obtained operating parameters m_j. However, as discussed in Section 7.5, experimental determination of isotherm parameters might consume quite a lot of time and substance.

Therefore, the basic correlations for situations present in the different sections of the SMB process, combined with a simplified shortcut approach, will be presented. Without knowing the adsorption equilibria, an operating point can be generated with a minimum number of experiments. All considerations made in the following are valid only for Langmuir-type isotherms.

The retention time for a concentration c_i^+ of the dispersed desorption front can be described as a function of the isotherm derivative (Section 6.2.3). This implies that the maximum time for desorption or the minimum migration velocity is given by the derivative of the isotherms at lowest concentration ($c_i^+ \to 0$), which is equal to the Henry coefficient:

$$t_{R,i}(c^+) = t_0 \left(1 + \frac{1 - \varepsilon_t}{\varepsilon_t} \cdot \frac{dq_i}{dc_i}\bigg|_{c^+ \to 0} \right) = t_0 \left(\frac{1 - \varepsilon_t}{\varepsilon_t} \cdot H_A \right) \tag{8.102}$$

For an adsorption shock front, the time for the front's breakthrough under Langmuir behavior can be calculated according to Eq. (8.103), where the isotherm's secant at feed concentration is relevant. The smaller the ratio q_i/c_i, the higher the velocity of the shock front:

$$t_{R,i,shock}(c^+) = t_0 \left(1 + \frac{1 - \varepsilon_t}{\varepsilon_t} \cdot \frac{q_i}{c_i}\bigg|_{c^+ = c_{feed}} \right) \tag{8.103}$$

These correlations can be transferred to continuous SMB or TMB chromatography where disperse as well as shock fronts are also present. The dimensionless flow rate ratios m_j can then be described as function of either the initial slope or the secant of the isotherm, depending on the situation in every zone.

Section I: The more retained component A has to desorb while no B is present. The minimum m_I is therefore the initial slope or the Henry coefficient of the isotherm:

$$m_{I,min} = \frac{dq_A}{dc_A}\bigg|_{c_A \to 0; c_B = 0} = H_A \tag{8.104}$$

As described in Section 7.5.8, the Henry coefficient can be determined by single pulse experiments at low concentrations of component A.

Section II: The minimum value for the corresponding flow rate ratio m_{II} is fixed to the maximal possible initial isotherm slope of the less retained component, which has to be desorbed here. The highest initial slope for component B is reached if no A is around. Of course, A is always present in this zone (Figure 8.18). Since it is quite difficult to predict the concentration of A in this section, its presence causes a further decrease of the initial slope, and the worst-case estimation of m_{II} is

$$m_{II,min} = \left. \frac{dq_B}{dc_B} \right|_{c_A=0;c_B\to0} = H_B \tag{8.105}$$

Again, the initial slope of the isotherm has to be determined by a pulse experiment of B.

Section III: The third section of an SMB process is characterized by the adsorption of more retained component A. To achieve complete separation, one has to ensure that the shock front of A does not exceed the raffinate port. The highest possible velocity of that front occurs when q_A/c_A is smallest. This is the case when both components are present at their highest possible concentration. Again, the difficulty to determine the exact concentrations must be pointed out. However, the feed concentrations are a good first guess as well as the worst-case estimation:

$$m_{III,max} = \left. \frac{q_A}{c_A} \right|_{c_A=c_{feed};c_B=c_{feed}} \tag{8.106}$$

Experimentally, this parameter is determined by a breakthrough experiment where both components are fed at feed concentration to the chromatographic column.

Section IV: The eluent is regenerated by complete adsorption of component B. Again, the velocity of a shock front is limiting. In this case, the highest possible velocity is determined by the lowest slope of the tangent to the isotherm of component B. Since no A should be present, the minimum slope is reached when B appears at feed concentration. Therefore, the correlation for this section is as follows:

$$m_{IV,max} = \left. \frac{q_B}{c_B} \right|_{c_A=0;c_B=c_{Feed}} \tag{8.107}$$

This parameter can be extracted from a breakthrough experiment with pure component B. Following this procedure, a first initial guess for the four dimensionless operating parameters can be obtained with a minimum number of experiments. The resulting parameters for EMD53986 are listed in Table 8.8.

A comparison of these results with the set of operating parameters obtained by the first shortcut method for nonlinear isotherms shows that, especially for the separation sections II and III, a point (m_{II}, m_{III}) has been found, which is located within the area of complete separation (Figure 8.20).

Table 8.8 Operating parameters for EMD53986 obtained by the experimental shortcut method.

$m_{I,min}$	19.75
$m_{II,min}$	7.88
$m_{III,max}$	10.15
$m_{IV,max}$	6.53

Again, it must be pointed out that this procedure for determining the operating diagram is based on strong simplifications and represents a worst-case scenario. Nevertheless, this can be done very quickly, leading to quite safe operating parameters. More detailed shortcut methods, which also need rather small experimental effort, have been published by Mallmann et al. (1998) and Migliorini, Mazzotti, and Morbidelli (2000). The advantage of these approaches is a more detailed estimation of the amount of components entering sections II and III. This can be achieved by hodographic analysis of breakthrough experiments.

Besides the description of the TMB process based on the ideal model, other model approaches can be used to follow the same goal of determining reasonable operating parameter for an SMB unit. One possibility is to utilize stage models as introduced in Section 6.2 for the batch column and extend these to the TMB setup (Ruthven and Ching 1989; Pröll and Küsters 1998). In addition to determining operating parameters, TMB stage models have also been used to optimize the design of SMB plant in terms of, for example, column geometry (Charton and Nicoud 1995; Biressi et al. 2000). Heuer et al. (1998) have applied a TMB equilibrium dispersion model for the determination of operating parameters. In this approach, effects such as axial dispersion and mass transfer are lumped together in an apparent dispersion coefficient. Hashimoto et al. (1983) and Hashimoto, Adachi, and Shirai (1993) have used a TMB transport model to assist the layout.

Another design approach for SMB processes is proposed by Kaspereit and Neupert (2016). They state that the equilibrium theory is in practice seldom used due to the needed numerical integration of the nonlinear equation system. In order to overcome this mathematical barrier, they present a shortcut method to determine the boundaries of the operating area of the separation region. Based on the eigenvalues and eigenvectors of the Jacobi matrix of the partial derivatives of the adsorption isotherms, concentration pairs, which occur in standing waves, as well as their corresponding flow velocities can be calculated. For a more detailed presentation of the shortcut approach, the interested reader is referred to the publication of Kaspereit and Neupert (2016).

The advantages of all approaches based on the stationary TMB process are quite simple models and, in some cases, the possibility of direct analytical solutions. Without the need of dynamic simulations, much information with respect to the operation of an SMB unit can be gathered. Nevertheless, these methods described so far can only provide the basis for a more or less proper guess of the operating parameters, since the dynamics due to port switching as well as mass transfer and dispersion are neglected. Further, the quality of the isotherm plays still a major role. Incomplete (e.g. neglecting competitive adsorption behavior)

or wrong parameter determination influences the quality of the operating point significantly. Therefore, safety margins have to be considered. Further optimization can be done afterward by applying a more detailed model as presented below. The necessity of extra operating parameter optimization is shown in Figure 8.25, in which the theoretical and the real optimal operating points of an SMB process, which do not coincide, are shown.

8.4.3 Process Design and Optimization Based on Rigorous SMB Models

Several approaches based on SMB models have been suggested in the past to improve the predictability and optimization of SMB operations. Zhong and Guiochon (1996) have presented an analytical solution for an ideal SMB model and linear isotherms. The results of this ideal model were compared with concentration profiles obtained by an equilibrium dispersion model as well as experimental data. Strube et al. (1997a,b) used a transport dispersion model in a systematic case study to optimize operating parameters. The strategy has been successfully tested on an industrial-scale enantioseparation (Strube et al. 1999). A similar approach has been published by Beste et al. (2000) to optimize the separation of monosaccharides. A more detailed model, a general rate model (GRM), was used by Dünnebier and Klatt (1999), Dünnebier, Fricke, and Klatt (2000), and Dünnebier, Jupke, and Klatt (2000) to optimize SMB operating parameters.

The selected research contributions of the previous paragraph point out a trend in the field of research of "modelling chromatographic separation processes" at that time. Starting with the ideal model (cf. Figure 6.3), complexity of used models was increased by considering additional phenomena like mass transfer and dispersion, leading to better predictability of simulations of separation of different mixtures. After successful application of the most detailed model, the GRM, the focus shifted from raising complexity of the models to usage of more efficient computing algorithms. Selected attainments of different research groups are, without claim of completeness, development of a fast and accurate solver using, inter alia, the weighted essentially non-oscillatory discretization scheme implemented at CADET by the group of von Lieres and Andersson (2010), usage of surrogate models by the group of Seidel-Morgenstern (Li et al. 2014), parameter estimation and optimization of chromatography processes using the adjoint method by the group of Hubbuch (Hahn et al. 2014), and applying optimization algorithms like the non-dominated sorting genetic algorithm (NSGA) by the groups of Hidajat and Ray (Subramani, Hidajat, and Ray 2003a).

Even though a broad variety of optimization strategies for SMB processes are available in literature, a fundamental process understanding of the influence of process parameters on the performance of an SMB process shall be given in this section. In the following, a first approximation of operating parameters is performed by applying the triangle theory described above. Further, systematic strategies for the optimization of operating and design parameters are presented based on axial concentration profiles resulting from simulations using the

transport dispersion model (Sections 7.10.2 and 6.2.5). Notably, the basic strategy of these procedures is not limited to a model-based design, but can also be applied for the experimental optimization of a running separation process.

8.4.3.1 Estimation of Operating Parameter

Knowing the adsorption isotherms, an initial guess of operating parameters can be performed by applying the shortcut methods described in depth in Section 8.4.2. With the triangle theory, values for the four dimensionless operating parameters m_j are obtained. Since simplifying assumptions have been made, a safety margin of at least 10% should always be considered. The four dimensionless parameters m_j have then to be transferred to a "real" SMB process where the number of independent operating parameters is five (four flow rates and one switching time). Thus, for a given plant setup, one of these five parameters has to be fixed first. One possibility is to set the flow rate in section I to the maximum allowable pressure drop Δp_{max}, assuming that this flow rate is predominant in all sections. If Darcy's correlation for the description of the pressure drop is used, the flow rate in section I can be calculated by Eq. (8.108):

$$\dot{V}_I = \frac{\Delta p_{max} \cdot A_c \cdot d_P^2}{\psi \cdot N_c \cdot L_c \cdot \eta_f} \tag{8.108}$$

Here, N_c stands for the total number of columns in the SMB plant. The flow rate in section I is estimated to the safe side applying this procedure. Since the number of columns in section I is smaller than the total number of columns N_c in the SMB plant and the flow rates of sections II to IV are smaller than of section I, the total pressure drop in the real plant will be smaller than estimated. Therefore, exceeding of the allowable pressure drop is prevented in the real SMB plant. As demonstrated later, it is not necessary to fix the flow rate in section I to the maximum allowed pressure drop to achieve optimal process performance. However, for a given flow rate in section I and all dimensionless flow rate ratios m_j, the switching time can be calculated according to Eq. (8.109):

$$t_{shift} = \frac{[m_I \cdot (1 - \varepsilon_t) + \varepsilon_t] \cdot V_c}{\dot{V}_I} \tag{8.109}$$

The missing internal flow rates $\dot{V}_j$ are calculated by Eq. (8.110):

$$\dot{V}_j = \frac{[m_j \cdot (1 - \varepsilon_t) + \varepsilon_t] \cdot V_c}{t_{shift}} \tag{8.110}$$

The flow rates of all external streams such as desorbent, feed, extract, and raffinate are determined by the balances for the port nodes as given by Eqs. (7.74)–(7.77).

Applying this strategy, a first set of operating parameters is generated, and it is possible to either run the SMB separation or make further optimizations using a more detailed model. Since the determination of these operating parameters is based on the TMB model with all its simplifying assumptions (neglecting all nonidealities such as axial dispersion, mass transfer, and port switching), the estimated operating point should always be handled with care.

8.4.3.2   Optimization of Operating Parameters for Linear Isotherms Based on Process Understanding

Figure 8.22 shows the internal axial concentration profiles at the end of a switching interval for a system of linear isotherms and no competitive interaction of the two components. After switching all ports downstream in the direction of the liquid flow, the initial concentration profile is represented by the upper gray line. In this case, the extract will be polluted with component B because the desorption front of B violates point 2.

To improve process performance and achieve a complete separation of the two components, the desorption front of component B has to be pushed in the direction of the feed port. Since the isotherms of both components are linear in this example and the isotherm of one component is not influenced by the presence of the other, the front can be moved in the desired direction by simply increasing the internal flow rate in section II, $\dot{V}_{II}$. This can be realized by decreasing the flow rates of extract and feed by the same amount. The effect of a stepwise decrease of these external flow rates with the associated increase of $\dot{V}_{II}$ is depicted in Figure 8.22.

Only the desorption front of component B is influenced by the increased flow rate in section II – all other fronts are not influenced and remain at their initial position. The decrease in feed flow rate has an impact on the total height of the concentration plateaus, especially in section III. This procedure of shifting the fronts is also applicable for all other sections of the SMB process to optimize the internal concentration profile according to Figure 8.17 and to improve the process performance with respect to purities, productivity, and eluent consumption.
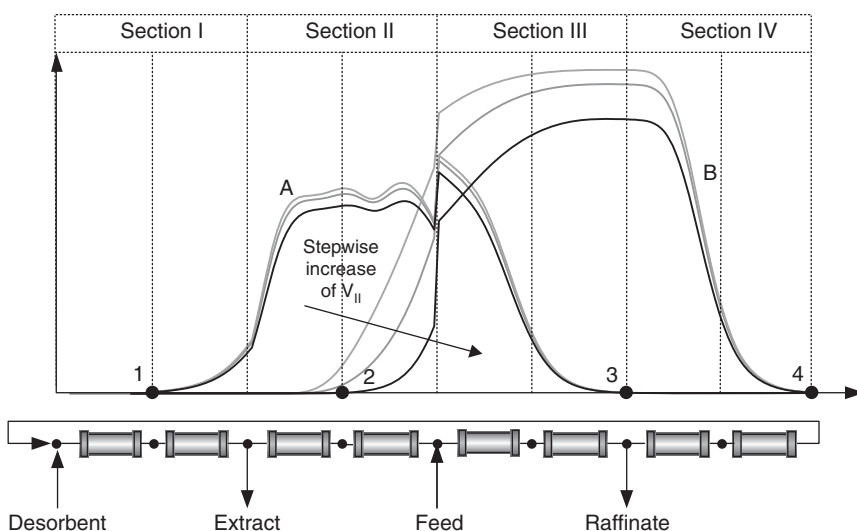
Figure 8.22 Axial concentration profiles for different flow rates in section II (system with linear isotherms).

8.4.3.3 Optimization of Operating Parameters for Nonlinear Isotherms Based on Process Understanding

Process optimization gets more difficult when the isotherms are no longer linear and the equilibrium of one component is strongly influenced by the presence of the other, as is the case for EMD53986. Again, an initial guess based on the TMB model has been made for a given plant setup. The resulting internal concentration profile is plotted in Figure 8.23. Again, the desorption front of component B violates the optimization criterion for point 2, leading to pollution of the extract stream.

Applying the same strategy as introduced for linear isotherms, an internal concentration profile as shown in Figure 8.24 is obtained. Only the flow rate in section II has been increased by decreasing both extract and feed flow rate. The desorption front of component B is again pushed in the correct direction. However, in this case, a change of flow rate in section II does also affect the concentration profiles in other sections of the SMB process. In this example, the adsorption front of component A has moved away from the raffinate port, where the stopping point 3 is located. Even though the two products can now be withdrawn with maximum purity, the whole process is not operated at its optimum with respect to productivity.

To achieve optimal productivity, an optimization strategy has to be applied. The most difficult step is to adjust the flow rate ratios in sections II and III, especially for strongly nonlinear isotherms with competitive interaction. Therefore, the m_{II}–m_{III} plane is divided into segments by parallel lines to the diagonal. Each of these lines represents combinations of m_{II} and m_{III} values of constant feed flow – the so-called isofeed lines (Figure 8.25).
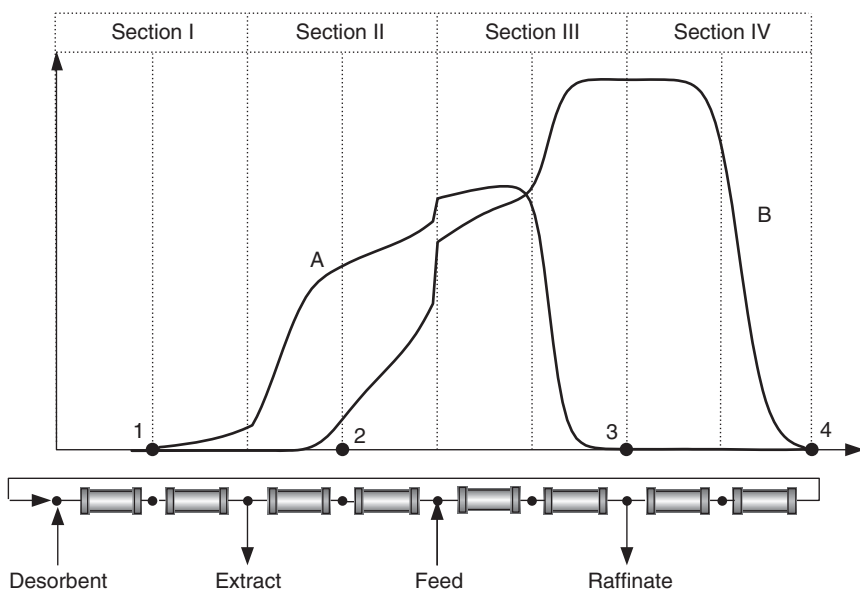
Figure 8.23 Axial concentration profile with pollution of the extract (system with nonlinear isotherms).
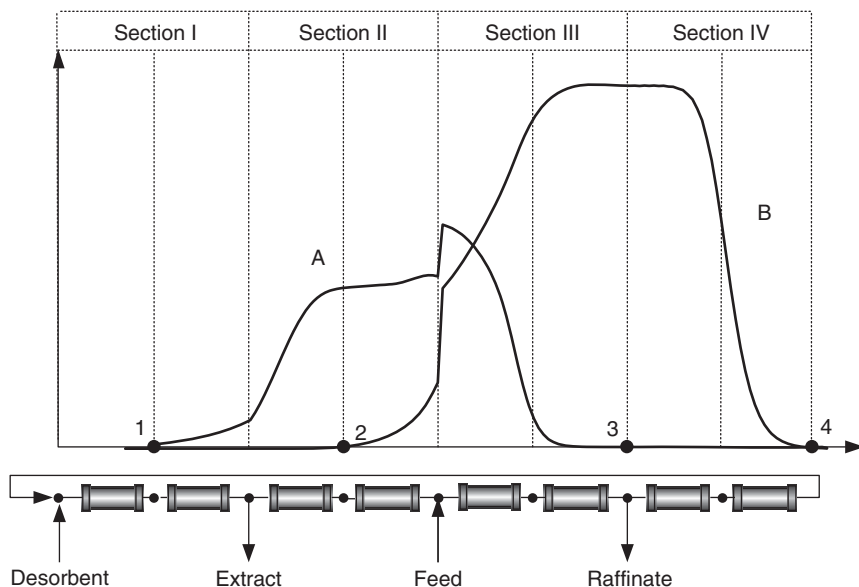
Figure 8.24 Suboptimal axial concentration profile for complete separation (system with nonlinear isotherms).
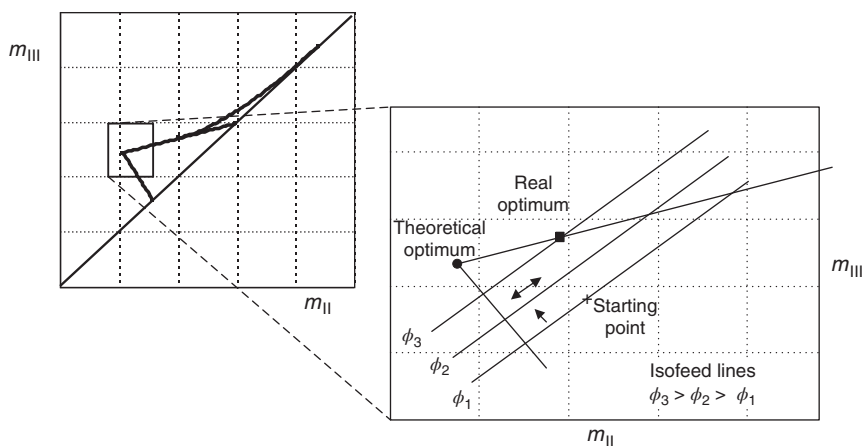
Figure 8.25 Strategy for the optimization of operating parameters . Source: Jupke, Epping, and Schmidt-Traub (2002). Reproduced with permission of Elsevier.

If, for instance, the purity of the extract stream is too low while the adsorption front of component A is still far from stopping at point 3, which is the case in the shown example, the operating point has to be varied along one isofeed line. As a result, m_{II} and m_{III} as well as the flow rates in sections II and III are increased by the same amount. This can be done by decreasing the extract flow rate and increasing the raffinate flow rate while the feed flow rate is held constant. When both the extract and the raffinate purity are higher than required, or the

concentration profile can still be optimized according to Figure 8.17, the total feed flow rate can be increased by jumping to the next isofeed line closer to the vertex of the operating triangle. Otherwise, if both purities are too low, the feed flow rate has to be decreased. When the flow rates in sections II and III have been optimized to achieve the required purities and the highest productivity, sections I and IV have to be checked and optimized separately.

After adjusting the flow rates in all sections, process conditions for complete separation with highest productivity and lowest solvent consumption have been found. The resulting internal concentration profile exhibits all the constraints of an optimal concentration profile (cf. Figure 8.17).

From this optimization with a detailed SMB model, another very important aspect can be observed. Due to the simplifying assumption made to determine the operating diagram (Section 8.4.2), the "real" optimum of the SMB process does not coincide with the predicted theoretical optimum, as can be seen in Figure 8.25.

The mentioned optimizations of operating parameters can be performed for a given plant setup, where the total number of columns, their distribution over the different sections, and their geometry are given. With such information and all operating parameters, the specific process parameters such as productivity $\mathrm{VSP}_{i,\mathrm{SMB}}$ (Eq. (8.8)) and eluent consumption $\mathrm{EC}_{i,\mathrm{SMB}}$ (Eq. (8.12)) can be calculated. However, since these parameters are only valid for one given set of design parameters, a strategy to optimize these will be presented next.

8.4.3.4 Optimization of Design Parameters

Besides the operating parameters, the geometry and configuration of columns of an SMB plant have significant influence on the process performance in terms of various objective functions such as the volume-specific and cross-section-specific productivity ($\mathrm{VSP}_{i,\mathrm{SMB}}$ and $\mathrm{ASP}_{i,\mathrm{SMB}}$) as well as the eluent consumption $\mathrm{EC}_{i,\mathrm{SMB}}$. As introduced in Section 7.1.1, important design parameters for SMB processes are:

- column geometry L_c and A_c;
- total number of columns N_c;
- distribution of columns over different sections j ($N_{\mathrm{c},j}$);
- maximum pressure drop Δp_max;
- particle size d_p.

Few published papers deal with the detailed optimization of design parameters. Charton and Nicoud (1995) and Nicoud (1998) have presented a strategy based on a TMB stage model to optimize the operation as well as the design of SMB processes. The basic influence of the number of stages and the particle diameter on productivity and eluent consumption is illustrated and compared with batch elution chromatography. Based on this work, Biressi et al. (2000) presented a method to optimize operating parameter and investigate the influence of the particle diameter as well as the feed concentration on process performance. Ludemann-Hombourger, Bailly, and Nicoud (2000) have also analyzed the influence of particle diameter on the productivity.

Here, the focus will be on the optimization of column geometry for a fixed column distribution first, while the influence of the total number of columns as well as their distribution will be shown for some examples afterward. A more detailed description of this strategy has been published by Jupke (2004) and Jupke, Epping, and Schmidt-Traub (2002).

The basic idea for the optimization of the process performance is similar to batch chromatography (see Section 8.1.2.2), the summarization of all influencing parameters into dimensionless parameters. Relevant dimensionless parameters for an SMB process are the total number of stages (N_{tot}) in the system and the four dimensionless flow rate ratios m_j. Therefore, a single set of N_{tot} and m_j represents not only one unique SMB configuration but also a series of different SMB configurations with similar behavior. As demonstrated before, nearly identical concentration profiles (Figure 8.4) can be observed for different plant layouts if the dimensionless parameters are kept constant. Since only the dimensionless parameters are used as optimization parameters, violation of the maximum pressure drop can be neglected during optimization. The maximum pressure drop is considered only at the end of the optimization in order to determine the "real" SMB configuration based on optimal values for the dimensionless parameters $N_{tot,opt}$ and $m_{j,opt}$.

Figure 8.26 illustrates the design procedure for a new SMB plant. For an initial column geometry and a fixed column distribution (e.g. 2/2/2/2), the optimal operating parameters, namely, the flow rate ratios m_j, can be obtained following the strategy described in the Section 8.4.3.1. The present dimensionless design parameter N_{tot} as well as the corresponding objective functions can be calculated from these parameters. Since the initial values for the column geometry, especially the column length, do not consequently represent the optimal design parameters, other numbers of stages have to be examined. The number of stages can be varied by changing the column length and/or flow rate in section I (cf. Eq. (8.57)). Therefore, the number of stages is changed by keeping one of the two parameters constant while varying the other compared to the initial conditions. For the new setup, an optimization of operating parameters has to be performed again to fulfill purity requirements. An optimization scheme is deduced from these considerations and shown in Figure 8.26.

The shown optimization scheme (Figure 8.26) is characterized by two optimization loops. The inner loop describes the operating parameter optimization based on the strategies introduced before. When for one setup (e.g. one column length) the optimized operating parameters have been found, a new setup (e.g. another column length) has to be chosen, represented by the outer loop for design parameter optimization. Both loops are stopped after reaching the optimum value for the chosen objective function (e.g. VSP, EC, costs).

Results for the systematic optimization of the VSP for the separation of EMD53986 are summarized in Table 8.9. In this example, starting with a given setup, the flow rate in section I was kept constant, while the column length has been changed to realize different plate numbers. Again, it must be pointed out that the pressure drop is not considered during the optimization.

According to Table 8.9, a maximum VSP is reached for a total number of plates of approximately 65 and the corresponding flow rate ratios m_j. This is more than
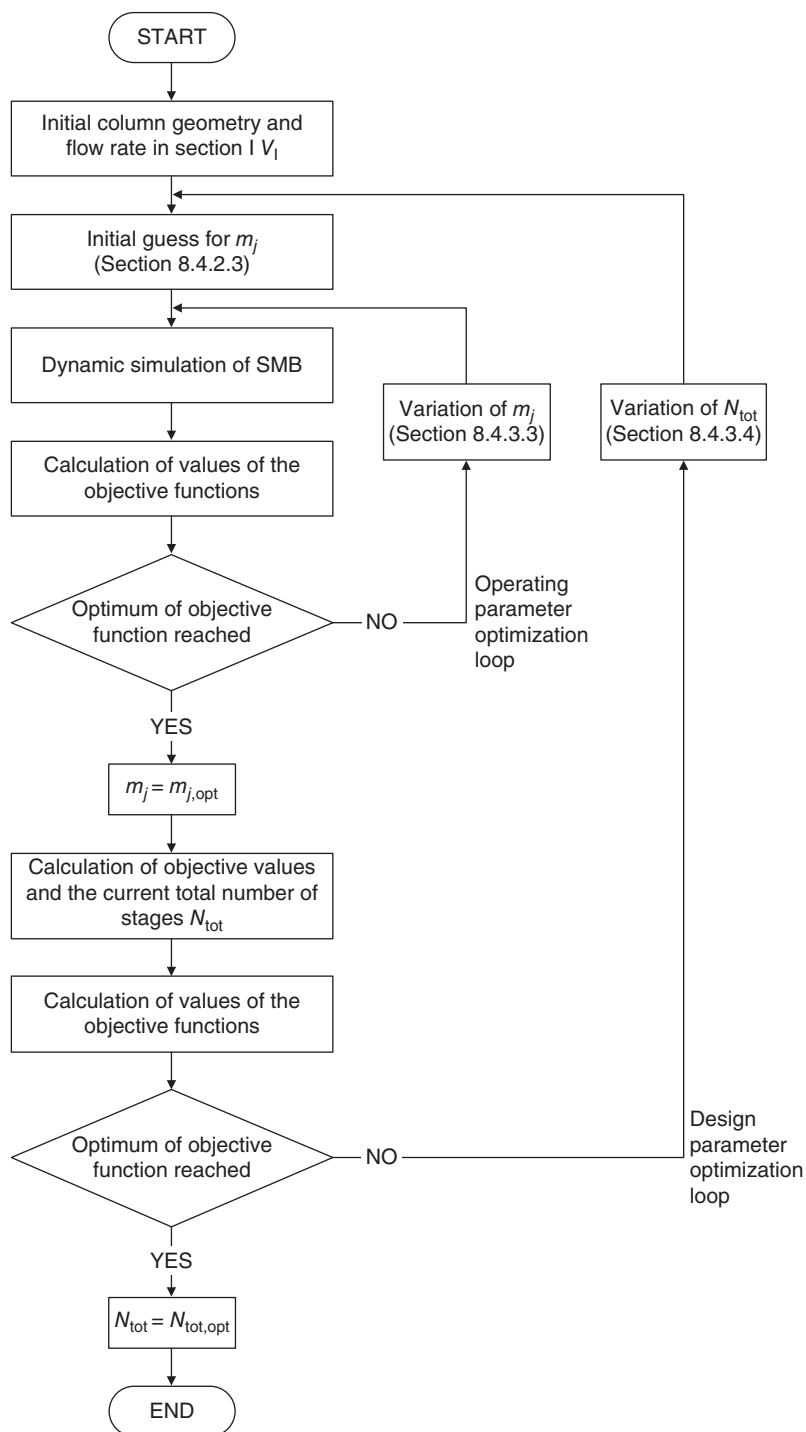
Figure 8.26 Scheme for optimization of design and operating parameter of SMB processes.

Table 8.9 Optimization of plate number for EMD53986.

Constant parameters							
N_c	8 (2/2/2/2)						
d_c (cm)	2.5						
$\dot{V}_I$ (ml min−1)	1.472						
$c_{\text{feed},i}$ (g l^{-1})	2.5						
Parameters varied during optimization							
Step	1	2	3	4	5	6	7
L_c (cm)	20	10	6	5	4.5	4.26	4.0
N_{tot} (−)	231.3	124.6	83.3	71.9	65.6	62.3	57.1
t_{shift} (s)	500.7	275.5	187.7	163.4	151.2	145.1	136.3
m_I (−)	24.30	27.00	31.00	32.50	33.50	33.99	34.00
m_{II} (−)	5.55	5.89	6.30	6.57	6.90	7.15	8.00
m_{III} (−)	10.63	10.71	10.80	10.84	10.95	11.00	11.00
m_{IV} (−)	6.32	6.20	5.90	5.75	5.70	5.70	5.70
VSP (g h−1 l−1)	11.42	19.70	26.98	29.41	30.13	29.85	24.77
EC (l g−1)	1.81	2.12	2.63	2.91	3.15	3.34	4.17

a twofold increase over the productivity at a plate number of 231. However, in addition to the development of productivity, the specific EC has increased. As reported by Jupke, Epping, and Schmidt-Traub (2002), corresponding correlations can be found for different particle diameters. With decreasing particle diameter, an increase in terms of productivity can be observed, while the total number of stages remains nearly constant.

The separation problem has been transferred completely to the dimensionless space, where the best performance in terms of productivity VSP, eluent consumption EC, and so on can be achieved by one set of five parameters (N_{tot}, m_j). The next step is to transfer these parameters to an SMB process by considering a given production rate $\dot{m}_{\text{prod},i}$, purity requirements, and pressure drop limitations.

For the desired production rate, $\dot{m}_{\text{prod},i}$, together with the volume-specific productivity $\text{VSP}_{i,\text{SMB}}$, as it had been introduced before (Eq. (8.8)), the optimal volume of one column $V_{c,\text{opt}}$ can be calculated according to Eq. (8.111):

$$V_{c,\text{opt}} = A_{c,\text{opt}} \cdot L_{c,\text{opt}} = \frac{\dot{m}_{\text{prod},i}}{(1 - \varepsilon_t) \cdot N_c \cdot \text{VSP}_{i,\text{SMB}}} \tag{8.111}$$

This will lead to an infinite number of possible A_c/L_c ratios, and, therefore, the column length has to be chosen according to the following equations.

The first equation represents the total number of stages of one component in the system, which has to be kept constant to enable a proper scaling of the process:

$$N_{\text{tot},i} = \sum_{j=I}^{IV} \left(\frac{N_{c,j} \cdot L_{c,\text{opt}}}{A_i + C_i \cdot u_{\text{int};j}} \right) \tag{8.112}$$

However, in analogy to the procedure in batch chromatography, one has to ensure that for both components the total number of stages of the new process is equal to or greater than for the old one. This can be done, as introduced for the single column before, by choosing the correct reference component.

In addition to the plate number, the dimensionless flow rate ratios should remain constant:

$$m_{j,\text{opt}} = \frac{u_{\text{int},j} \cdot A_{\text{c,opt}} - \left[\left[V_{\text{c,opt}} \cdot \varepsilon_e\right]/t_{\text{shift}}\right]}{\left[V_{\text{c,opt}} \cdot \left[1 - \varepsilon_e\right]\right]/t_{\text{shift}}} \tag{8.113}$$

Additionally, as a final constraint, pressure drop limitations have to be considered, which are described by Eq. (8.114):

$$\Delta p_{\max} = \frac{\psi \cdot \eta_{\text{f}}}{d_{\text{p}}^2} \cdot \sum (u_{\text{int},j} \cdot N_{\text{c},j} \cdot L_{\text{c,opt}}) \tag{8.114}$$

This procedure leads to one $L_{\text{c,opt}}/A_{\text{c,opt}}$ ratio that exactly fulfills the maximum pressure drop condition for the given feed stream. Of course, smaller $L_{\text{c}}/A_{\text{c}}$ ratios are also applicable to reach the same optimal performance of the SMB plant but with a lower pressure drop. Notably, a lower pressure drop will decrease the investment cost of a chromatographic unit. However, the smaller that ratio becomes, and with that the lower the pressure drop is, the shorter the columns will be. Consequently, this might lead to difficulty in ensuring a proper fluid distribution inside the column.

Finally, it is worth mentioning that, in the presented strategy, besides the total number of stages, the operating parameters in terms of the flow rate ratio were also kept constant. Therefore, no further optimizations of the operating parameters have to be done.

Besides the column's geometry, the total number of columns and their distribution over the unit are design parameters that influence the process performance. To compare different process configurations with the initial 2/2/2/2 setup, a complete optimization of the column geometry based on optimization of the number of stages has been performed for different configurations. Productivity was the objective function to be optimized in these considerations. The results for selected configurations (2/3/2/2, 2/2/3/2, 2/3/3/2, and 3/3/3/3) are shown, relative to the data for the initial eight-column setup, in Figure 8.27.

This example indicates that the column configuration can be used to improve the process performance. However, for optimization, it is not sufficient just to change the number of columns for every configuration and optimize the operating parameters, since each of the configurations shows the best result in terms of productivity at different optimal total number of stages.

Process configurations with a reduced number of columns, such as 1/2/2/2, 2/2/2/1, and 1/2/2/1, are not considered. Since the number of columns is reduced in the sections meant to regenerate the solid phase (section I) as well as the fluid phase (section IV), a large increase in eluent consumption will be the result. Nevertheless, these configurations should also be taken into account when fresh eluent is not the major factor in the cost structure.
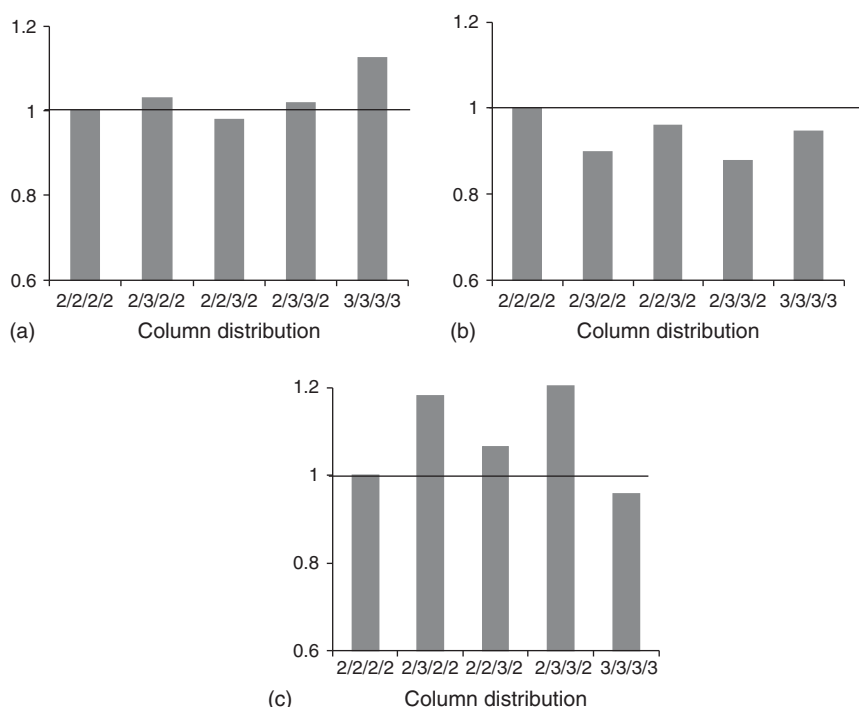
Figure 8.27 Influence of the number of columns and column distribution on the specific productivity and the specific eluent consumption. (a) Productivity, (b) eluent consumption, and (c) number of stages.

8.5 Isocratic SMB Chromatography Under Variable Operating Conditions

The introduced SMB process enhanced the performance of several separation tasks compared with batch processes additionally to enabling a continuous process. However, certain limitations concerning different performance criteria could not be overcome, which is indicated in Figures 8.23 and 8.24. The conventional SMB process is run under constant operating conditions such as the configuration of columns per zone, flow rate per zone, and concentration of feed streams. In order to enhance the process performance of SMB processes even further, different research groups investigated SMB processes under variable operating conditions (Seidel-Morgenstern, Keßler, and Kaspereit 2008a,b; Sá Gomes and Rodrigues 2012; Faria and Rodrigues 2015). The first idea to abandon the constraints of conventional SMB resulted in the Varicol process (Ludemann-Hombourger, Nicoud, and Bailly 2000). The most frequently investigated process concepts were already introduced in Section 5.2.5. These

SMB processes under variable conditions can be categorized in three classes (Faria and Rodrigues 2015):

- Modes with dynamic zone configurations;
- Modes with variable flow rates;
- Modes with variable feed concentrations.

The affiliation of different process concepts to these classes is illustrated in Table 8.10.

In the following, an overview of selected results of recent research is given, comparing the performance of Varicol, PowerFeed, and Modicon, frequently investigated representatives of the beforehand defined classes (Kawajiri and Biegler 2006a; Schramm, Grüner, and Kienle 2003; Toumi, Engell, and Hanisch 2002; Yao et al. 2014; Yu, Wood, and Liu 2015; Zhang, Hidajat, and Ray 2009), to conventional SMB performance. Further, an attempt is made to summarize trends of the performance applying the discussed SMB concepts.

8.5.1 Performance Comparison of Varicol and Conventional SMB

In the first paper describing the Varicol process, Ludemann-Hombourger, Nicoud, and Bailly (2000) investigated Varicol by theoretical case studies and experiments for a chiral separation. Varicol subdivides one switching period into subintervals (generally three or four), whereby the number of columns is altered for each subinterval, so the mean number of columns per zone for the switching period becomes non-integer (cf. Section 5.2.5.1). The case studies are based on stage model calculations and competitive modified multicomponent Langmuir isotherms. The optimal internal flow rates for a given operating pressure are estimated by equilibrium theory and afterward tuned to utilize the no leak condition in zones I and IV completely. The switching times of the subintervals are always the same. A comparison with standard SMB (Table 8.11) shows that Varicol outperforms SMB for five and six columns. Based on these results, it is possible to increase productivity by increasing the feed rate until maximum allowable pressure drop is reached, since Varicol achieves comparable purities for fewer columns. Please keep in mind that these design data are determined by case studies and do not represent a global optimum.

These findings are proven by experimental results as shown in Table 8.12. Varicol, with the same number of stages as SMB, achieves higher purities, slightly

Table 8.10 Classes of SMB process concepts under variable conditions.

Modes with dynamic zone configuration	Modes with variable flow rates	Modes with variable feed concentrations
Varicol	PowerFeed	Modicon
Pseudo-SMB	iSMB	Enriched Extract SMB
	Partial-Feed	
	Partial-Discard	
	Partial-Withdrawal	

Table 8.11 Theoretical case study for SMB and Varicol.

No. of columns	SMB		Varicol		Varicol–SMB
Total	Columns/ zone	Raff./extr. purity (%)	Columns/ zone	Raff./extr. purity (%)	Increase of average purity (%)
5	1/2/1/1	98.55/93.13	1.25/1.25/1.25/1.25	97.89/95.98	1.10
6	1/1/2/2	98.55/95.15	1.75/1.25/1.25/1.75	98.67/97.12	1.07
8	2/2/2/2	98.55/97.95	2.5/1.5/1.5/2.5	98.95/97.81	0.21

Source: Ludemann-Hombourger, Nicoud, and Bailly (2000). Reproduced with permission of Taylor and Francis.

Table 8.12 Experimental case study for five-column SMB and Varicol processes.

	Columns/zone	Extract purity (%)	Raffinate purity (%)	Increase in productivity (%)	Decrease in eluent (%)
SMB	1/2/1/1	91.2	96.3		
Varicol 1	1.25/1.25/1.25/1.25	92.7	96.9	1.8	10.7
Varicol 2	1.0/1.5/1.5/1.0	92.4	97.7	18.5	−0.3

Source: Ludemann-Hombourger, Nicoud, and Bailly (2000). Reproduced with permission of Taylor and Francis.

increases productivity, and at the same time reduces the eluent consumption by more than 10%. According to the second Varicol configuration, it is possible to increase productivity by 18.5% compared with an optimized SMB process, while the eluent consumption of both processes remains similar.

Contrary to the design of conventional SMB processes, no design method like the triangle theory is available for SMB processes under variable conditions. Therefore, model-based approaches, especially for optimizing performance, are needed.

However, design advices can be found in literature. Yao et al. (2014) investigated the influence of the total number of port switches per cycle on the performance of Varicol process. They compared five different schemes for enantioseparation of 1,1′-bi-2-naphthol with the same average configuration but different count of port switches evaluating purity, recovery, eluent consumption, and yield of extract and raffinate (cf. Figure 8.28). The scheme with the lowest number of switches showed highest purity, recovery, and yield and lowest eluent consumption, with exception of eluent consumption regarding extract, in which one scheme with higher number of switches showed a slightly lower consumption.

Even though no optimization of operating parameters has been performed, in order to compare the best possible result of each scheme, a trend of the influence of the number of port switches became apparent. Based on the presented results, the authors concluded that the lowest possible number of port switches per cycle leads to the best performance of Varicol (Yao et al. 2014). In fact, this designing advice has been applied in most publications investigating Varicol processes.
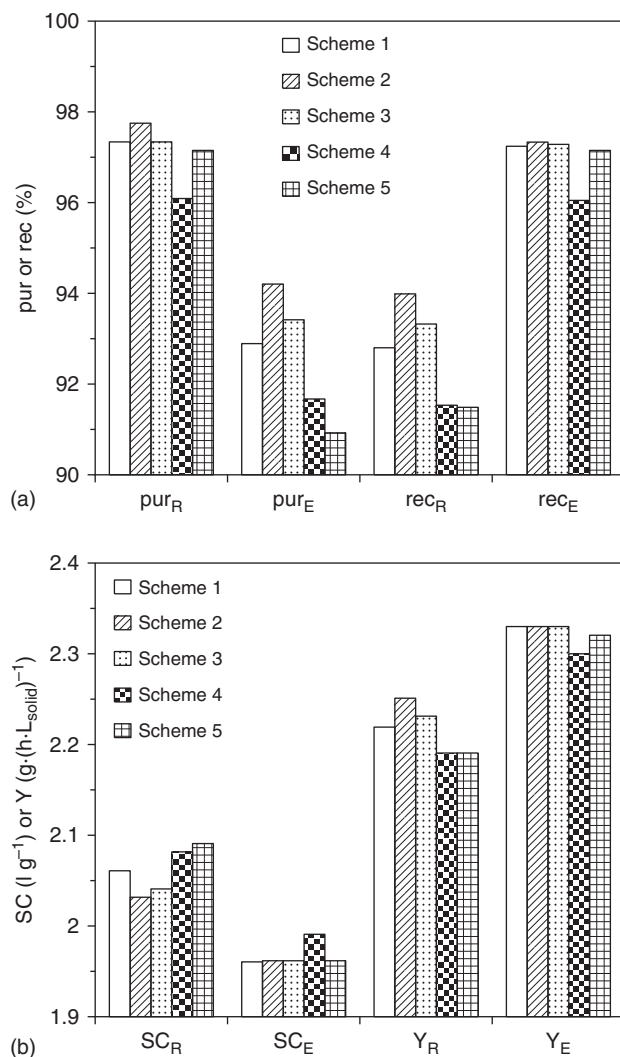
Figure 8.28 Performance evaluation criteria of different switching schemes of Varicol processes for enantioseparation of 1,1′-bi-2-naphthol with same average configuration of <1.5/2/2.25/2.25> but different number of port switches per cycle. Schemes 1 and 3 consist of six port switches, schemes 4 and 5 eight switches, and scheme 2 four switches. Source: Yao et al. (2014). Reproduced with permission of Elsevier.

After this first presentation of the novel process concept, different research groups tried to apply this technology to separate a broad variety of products and challenge their optimization algorithms to find optimal designs and operating points for different objective functions (Toumi, Hanisch, and Engell 2002; Subramani, Hidajat, and Ray 2003a,b; Wongso, Hidajat, and Ray 2004; Yu, Hidajat, and Ray 2005; Zúñiga and Wouwer 2014; Yu, Wood, and Liu 2015).

The well-known group headed by Ray investigated inter alia the enantioseparation of pindolol (Zhang, Hidajat, and Ray 2009). Five-column SMB and Varicol

processes are compared; the latter is divided into four subintervals. The rigorous multiobjective optimizations are based on the equilibrium dispersion model and bi-Langmuir isotherms (Zhang, Hidajat, and Ray 2007).

The authors present Pareto-optimal solutions for different objectives:

- *Simultaneous maximization of raffinate and extract purity for a given capacity (product of feed concentration and feed flow rate) at two different feed concentrations*: The resulting purities for Varicol are higher than for SMB with the same number of columns, although the differences are smaller than those reported by Zhang, Mazzotti, and Morbidelli (2003a,b), who performed comparable investigations for a chiral separation of 1,2,3,4-tetrahydro-1-naphthol. A comparison of low and high feed concentrations confirms that "higher feed concentration and lower feed flow rate is superior to that of lower feed concentration and higher feed flow rate in achieving higher productivity without consuming more desorbent." This confirms the general rule to choose high feed concentrations.
- *Maximization of recovery and minimization of desorbent flow for a 97.1% purity of the raffinate*: As shown in Figure 8.29a, the recovery increases nearly linearly with the eluent consumption. For a given eluent flow rate, the recovery of a Varicol process is approximately 0.5% higher compared with SMB with the same number of columns and the same maximum pressure drop. Hence, Varicol can save operating cost as it achieves higher recovery for the same eluent consumption or, vice versa, saves eluent for the same recovery.
- *Maximization of recovery and minimization of desorbent flow at design stage*: The optimization task is similar to the second case, but here additionally the column design was optimized with the constraints of raffinate and extract purities higher than 99.0% and 95.0%, respectively. Figure 8.29b depicts a five-column Varicol ($L = 12.9$ cm) to outperform a five-column SMB ($L = 14.4$ cm) but performs inferior than a six-column SMB ($L = 10.6$ cm). In this context, it is worth noting that the column length is lowest for a six-column SMB. Compared with the five-column SMB and Varicol, the recovery increases for a six-column SMB by about 1% and 0.4%, respectively. Therefore, Zhang, Hidajat, and Ray (2009) concluded, "better performance can be achieved by increasing the number of columns while having a reduced length."

Zhang, Hidajat, and Ray (2009) also used a laboratory SMB setup to carry out three experimental runs to verify the optimization results corresponding to the points in the Pareto sets of case 2. It was found that for SMB as well as Varicol operation, the recoveries and the extract purities are much lower than the optimization calculations. The authors state that limitations of the pump performance and hence severe fluctuations of the recycling flow rate to be the major cause for such deviations. They point out that their "experimental results indicate the great importance of flow rate control and pump performance in SMB and Varicol operation." Therefore, they also recommended, "operating conditions for SMB and Varicol processes should be selected as a compromise between separation performance and robustness."
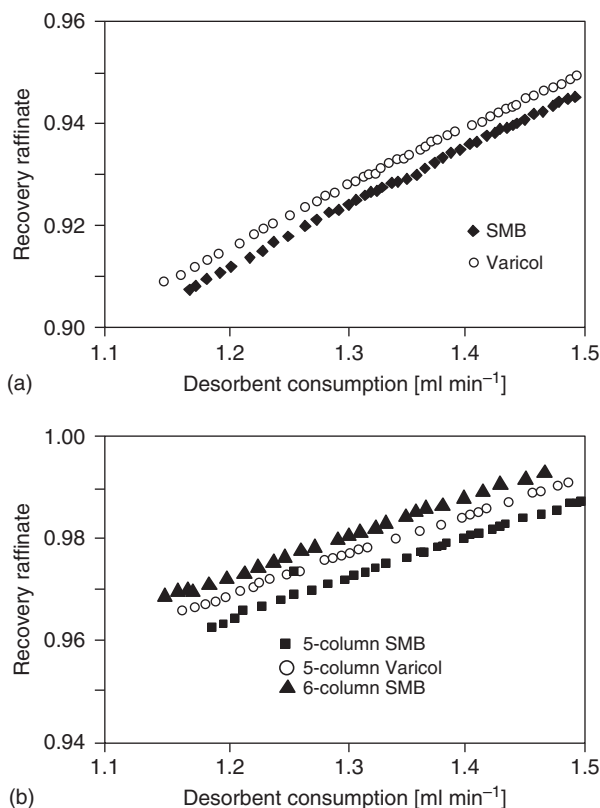
Figure 8.29 Pareto-optimal solutions for recovery and desorbent consumption: (a) given design and (b) optimal design of the chromatographic plant. Source: Zhang, Hidajat, and Ray (2009). Reproduced with permission of Elsevier.

In preparative chromatography, standard SMB processes usually comprise up to eight columns in total. In open literature, the application of nonstandard SMB processes is mainly discussed for four or five columns as these configurations offer interesting opportunities for saving investment cost along with production cost savings. In this context an investigation by Kurup, Hidajat, and Ray (2005) about an industrial Parex process, which typically has a relative large number of columns ($N = 24$), is worth noting. The authors identified several opportunities to optimize the standard SMB process but also point out that Varicol performs much better regarding eluent consumption and product recovery than an equivalent SMB.

8.5.2 Performance Comparison of Varicol, PowerFeed, and Modicon with Conventional SMB

Zhang, Mazzotti, and Morbidelli (2004a) present the first systematic comparison of the optimal separation behaviors of SMB, Varicol, PowerFeed, and Modicon for small number of columns. The nonstandard SMB processes subdivide the

switching period into subintervals (generally three or four) and alter for each subinterval the number of columns, feed flow rate, or feed concentration, respectively (cf. Section 5.2.5). The authors' investigations are based on the following assumptions and constraints: three-, four-, and five-column processes, three subintervals for the nonstandard SMB processes, particle diameter of 30 μm, and eluent consumption not minimized or constrained. The processes are described by a stage model. As objective functions for optimization, extract purity and productivity are chosen, while the raffinate concentration is set to >90%. The maximum pressure drop along the entire process is 70 bar. The optimization variables are feed flow rate, flow rate in section I, flow ratios m_I, m_{II}, and m_{IV}, total feed concentration of the racemic mixture, and unit configuration. A genetic algorithm is applied for the multiobjective optimization.

Figure 8.30 depicts the optimization results for the four- and five-column processes. Varicol, PowerFeed, and Modicon clearly outperform SMB, while the performance of PowerFeed and Modicon is slightly better than that of Varicol for five-column processes. The influence of the number of columns on the extract purity for a given productivity is shown in Table 8.13. These data are extracted from results published by Zhang, Mazzotti, and Morbidelli (2004a). The data should be generalized cautiously, but they show definite tendencies: performance of SMB is clearly lower than the performance of nonstandard SMB processes, which change their operating mode during the switching period. For three-column processes, PowerFeed and Modicon achieve higher extract purities than SMB and Varicol. However, the profitability of all processes decreases as the extract purity is much lower than for higher number of columns. For three-column processes, it has also to be kept in mind that during a switching period, only Varicol is able to operate with a fraction of a column in all four zones, while the column configuration for all other multicolumn processes is 1/1/1/0. Based on theoretical simulations, Modicon is advantageous, but apart from additional hardware, the practical realization is limited as the feed concentration
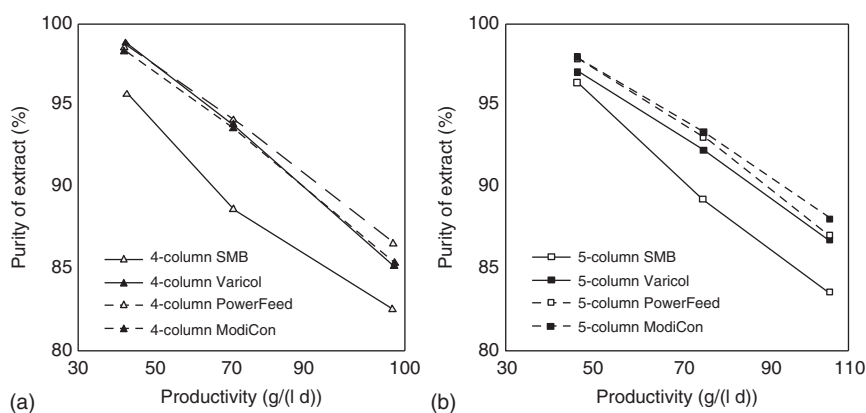
Figure 8.30 Comparison of the optimal separation performances of the (a) four- and (b) five-column SMB, Varicol, PowerFeed, and Modicon processes. Source: Zhang, Mazzotti, and Morbidelli (2004a). Reproduced with permission of Springer Nature.

Table 8.13 Influence of the number of columns on extract purity for a given productivity.

Columns	Productivity	SMB	Varicol	PowerFeed	Modicon
			Extract purity (%)		
3	50	90.4	91.4	94.9	92.7
4	50	94.0	97.4	97.3	97.0
5	50	95.8	96.8	97.7	97.8
3	90	81.3	82.7	86.7	85.8
4	90	86.2	90.1	90.9	90.5
5	90	86.6	89.7	90.3	91.2

Source: Data taken from Zhang, Mazzotti, and Morbidelli (2004a).

is upper bounded by the solubility and, in general, the feed concentration of optimized SMB processes will already be close to this limit.

For the same nonlinear chiral separation as reported by Ludemann-Hombourger, Nicoud, and Bailly (2000), Zhang, Mazzotti, and Morbidelli (2003a,b) compare SMB, PowerFeed, and Varicol, which are simultaneously optimized regarding extract and raffinate purity for all purities >90%. The authors also describe different alternatives for the operation of PowerFeed. In one case only the feed flow rate is changing in the subintervals, and in a second case it is investigated to what extent the process can be improved if flow rates of feed and eluent as well as the flow rate in section II are changed in the subintervals. These data are compared to equivalent Varicol and SMB processes. In all cases, the average feed and eluent flow rates are the same, and constant maximal pressure drop is reached by fixing the flow rate in section I. All processes are optimized for five columns; SMB is additionally designed for six columns.

The multiobjective optimization is based on a stage model and a NSGA. The Pareto-optimal results are shown in Figure 8.31. The Pareto curve illustrates how the two conflicting objective functions influence each other; that is, when one concentration is increased, the other will decrease. All points in this curve are equally good (nondominating) optimal solutions. Points below the Pareto curve represent non-optimal sets of purities, while all points above the Pareto curve do not fulfill the constraints for the optimization, that is, constant productivity and eluent consumption. The discontinuities of the Pareto curves are due to changes of the optimal column configuration. In the case of the five-column SMB, the configuration changes, for instance, from 1/2/1/1 to 1/1/2/1, with increasing raffinate concentration as the fifth column must be located to the port where the highest purity is required. The corresponding configuration of the five-column Varicol is optimized in three steps: from C–C–B–B to C–C–C–B to C–C–C–A with A = 2/1/1/1, B = 1/2/1/1, and C = 1/1/2/1.

The lower continuous curve represents optimal PowerFeed-F separation with feed rate as the only variable, while the upper curve (PowerFeed-F-Q-D) stands for an optimization, in which the flow rates of feed, section II, and eluent are
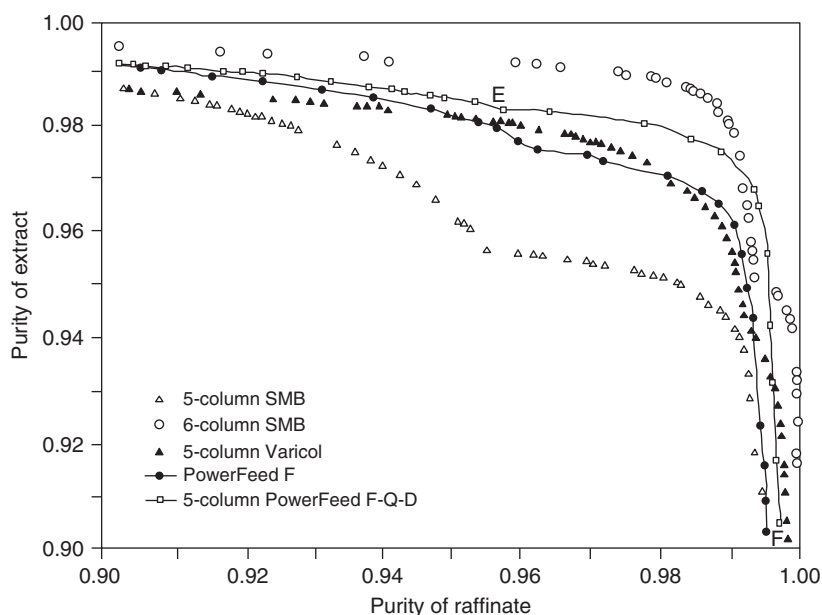
Figure 8.31 Pareto-optimal curves of PowerFeed and Varicol and SMB processes. Source: Zhang, Mazzotti, and Morbidelli (2003a,b). Reproduced with permission of Elsevier.

variable in each subinterval. For PowerFeed-F and Varicol, the results are nearly the same, while the more sophisticated optimization with three variables is slightly better for the sake of a more difficult operation, because three flow rates have to be controlled in each subinterval instead of only one. All in all, the investigations of Zhang, Mazzotti, and Morbidelli (2003a,b) show that for the same productivity, eluent consumption, and stationary phase, standard SMB processes can be substantially improved by Varicol or PowerFeed operation. This is particularly significant for small numbers of columns. For a better performance, it is necessary to run a six-column SMB. In another publication, Zhang, Morbidelli, and Mazzotti (2004b) prove experimentally that PowerFeed outperforms a corresponding SMB process in terms of purity.

The research group of Engell developed alternative optimization methods and applied them to design and especially control of SMB, Varicol, PowerFeed, and Modicon processes. For rigorous modeling, they used the GRM that additionally to other models regards pore diffusion. Process optimization based on the Fortran Feasible Sequential Quadratic Programming (FFSQP) algorithm highlights the advantage of the Varicol process. A general conclusion is that in comparison with SMB, the productivity of Varicol is increased up to 40% for the same number of columns; alternatively, the number of columns can be reduced by 1–2 to achieve the same performance of SMB (Toumi, Engell, and Hanisch 2002; Toumi et al. 2003; Engell and Toumi 2005). For further process optimization, the direct multiple shooting method, where the optimal state trajectory and corresponding operation parameters are determined simultaneously, was used (Toumi et al. 2007; Küpper and Engell 2011).

Another approach is the simultaneous optimization of process setup and operating conditions as performed for various processes by the group around Biegler and specifically for SMB processes by Kawajiri. The partial differential algebraic equations are fully discretized in temporal and spatial domains and the resulting mixed-integer nonlinear programming (MINLP) problem is handled by an interior-point solver IPOPT (Kawajiri and Biegler 2006a,b,c). MINLP was also applied for the optimal synthesis of complete flow sheets based on SMB chromatography, crystallization, and chemical reactions (Kaspereit, Swernath, and Kienle 2012).

Based on experimental experience, different authors indicate that besides an optimized design, robustness has to be kept in mind before starting a commercial production. Rodrigues and his group, who are known for theoretical and experimental research on various SMB processes (Rodrigues et al. 2007; Rodrigues, Araújo, and Mota 2007), investigated this question in a publication on optimal design of multicolumn processes under flow uncertainties (Mota, Araújo, and Rodrigues 2007). They optimized the feed rate, productivity, and the eluent consumption of four-column SMB, Varicol, and PowerFeed processes under uncertainties of the flow rates of $\pm 2.5\%$. Their example system is a linear separation of two nucleotides. The two-objective optimization problem, in which productivity is to be maximized and eluent consumption is to be minimized, was solved as nonlinear programming problem as described by Kawajiri and Biegler (2006a,b). Figure 8.32 shows the nominal and robust Pareto curves for four-column SMB, Varicol, and PowerFeed processes.
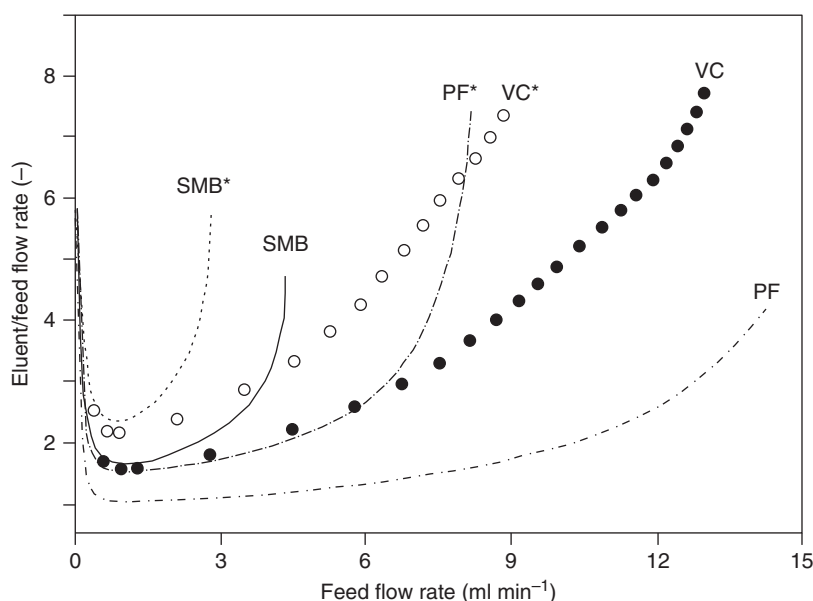
Figure 8.32 Nominal and robust Pareto curves for four-column SMB, Varicol (VC), and PowerFeed (PF) processes; * represents the robust Pareto curves. Source: Mota, Araújo, and Rodrigues (2007). Reproduced with permission of John Wiley and Sons.

Each point in the Pareto curve represents an optimal combination of the objective functions. Sets of operating conditions above the Pareto curve will lead to a lower performance compared with sets of operating parameters on the Pareto curve, since sets with identical productivity and less eluent consumption can be found. Sets of operating parameters located below the Pareto curve will violate the restriction in purity demand. The selection of the operating conditions for a production is a matter of additional economic considerations (Mota, Araújo, and Rodrigues 2007).

Both processes under variable process conditions, Varicol as well as PowerFeed, outperform the conventional SMB process in terms of productivity and eluent consumption. The authors conclude PowerFeed to be the best operating scheme of the investigated comparison since it exhibits the lowest Pareto curve additional to the widest extent of it, which represents the lowest specific eluent consumption. Further, PowerFeed enables higher feed throughput without violating the purity constraints. However, Varicol outperforms PowerFeed at high feed flow rates for robust operating conditions (Mota, Araújo, and Rodrigues 2007).

In Figure 8.32, the performance of all processes degrades significantly for small feed rates. Mota, Araújo, and Rodrigues (2007) point out that this has to be traced back to the process model that includes perfectly mixing cells between the columns. Overall, Figure 8.32 exemplifies that robust performance is gained at the expense of higher eluent consumption and/or lower feed throughput.

For the sake of completeness, it has to be mentioned that further improvements of nonstandard SMB processes by combining Varicol, PowerFeed, and/or Modicon to hybrid processes have also been investigated (e.g. Rodrigues, Araújo, and Mota 2007; Zhang, Mazzotti, and Morbidelli 2004a). The presented results indicate further improvements, but these hybrids also increase the requirements on process control and robustness.

8.5.3 Performance Trends Applying SMB Concepts Under Variable Operating Conditions

The abovementioned investigations do not cover the whole range of SMB processes with variable operating conditions, so it has to be kept in mind that conclusions based on these results and other publications are of limited validity. However, the following trends become apparent:

- For the same number of columns, Varicol, PowerFeed, and Modicon can outperform standard SMB processes concerning product purities, productivity, and eluent consumption.
- Although theoretical optimizations indicate slight advantages of PowerFeed, at the stage of process design, it should be considered equivalent to Varicol. Modicon and FF-SMB behave the same way.
- Modicon is an alternative if the solubility is sufficiently high.
- There are indications that combinations of nonstandard SMB processes (e.g. Varicol and PowerFeed) are superior. However, before taking into account such designs, process operability, and robustness have to be proven.

- The number of columns has an important influence on process performance. For example, it can be expected that SMB with an additional column can outperform the processes under variable conditions.

Additionally, the following advices should be considered before designing separation processes using SMB concepts under variable conditions:

- Appropriate optimization tools are needed before Varicol, PowerFeed, or Modicon can be taken into account for process design, since, in contrast to SMB, no shortcut methods such as "triangle theory" are available for these processes.
- The final decision on process design has to take into account process economics. These are ruled primarily by savings in production costs compared with SMB and additional hardware as well as software for process control and additional pump systems in the case of PowerFeed and Modicon. For Varicol only additional hardware and software for process control are necessary.
- The process conditions for production-scale applications have to guarantee robustness, in particular against flow rate fluctuations.

8.6 Gradient SMB Chromatography

Like in batch chromatography, it may be of interest to apply gradients in continuous chromatographic processes to manipulate the elution strength. Exemplarily, the selectivity of the components in a separation problem may be very large. Then, the process efficiency can be increased by changing the elution strength of the solvent during the separation. Such gradients of the solvent composition can be realized linearly, stepwise, or in other modes. In comparison with batch chromatography, this represents a more complex task in continuous processes. In the following, two kinds of gradients in continuous chromatographic processes, namely, using a step gradient in SMB processes and using a linear gradient in the continuous multicolumn solvent gradient purification (MCSGP) process, will be presented.

8.6.1 Step Gradient

In the case of SMB processes, a step gradient as described in Section 5.2.6 is easily accomplished as no changes of the SMB plant itself are required. The process scheme for gradient SMB chromatography is depicted in Figure 5.25. Ideally, there is a step gradient between sections II and III, while the solvent strength in sections I and II, respectively, III, and IV is constant. In practice, certain disturbances occur because of the column switching.

Ziomek et al. (2005) and Ziomek and Antos (2005) developed a procedure to optimize the productivity and eluent consumption for purity constraints of $Pu_{ext,raff}$ >90% based on a random search routine. They applied a stage model and competitive Langmuir isotherms. The modifier concentration was optimized in a stepwise search. Figure 8.33 compares the operating points for optimal
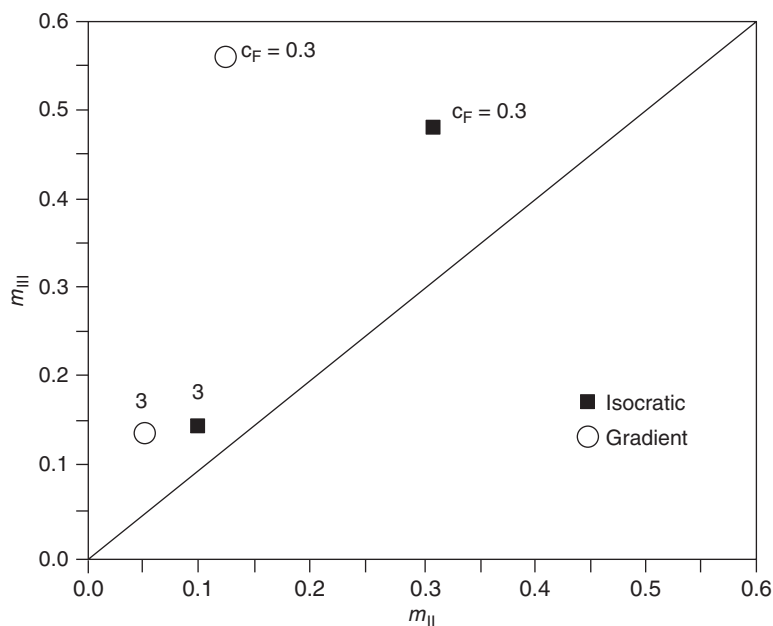
Figure 8.33 Operating points for optimal productivity in the m_{II}–m_{III} plane. Source: Ziomek et al. (2005). Reproduced with permission of Elsevier.

productivity in the m_{II}–m_{III} plane. Parameters are the feed concentration and isocratic as well as gradient operation. The corresponding operating points for minimum eluent consumption are rather close to these operating conditions. The data emphasize the advantage of gradient SMB by increasing productivity and reducing eluent consumption. The authors point out that based on their model calculations, the modifier concentration is crucial for successful separation as its influence on the sensitivity of extract and raffinate purities is approximately 1 order of magnitude higher compared with the flow rate (Ziomek and Antos 2005).

Validated models for rigorous simulations of gradient SMB processes are available. But again, the estimation of favorable process conditions is going to be a problem as the range of process parameters is large and rigorous simulation is too time consuming.

In the following, a shortcut method based on the TMB model is applied for parameter estimation for solvent gradient SMB processes. Knowing these parameters, it is much easier to evaluate the final operation conditions for practical productions by targeted rigorous simulation. The mass balance for the TMB process under the assumption of ideal conditions is given by Eq. (8.92). For isotherms with constant selectivity, such as multi-Langmuir and modified competitive multi-Langmuir isotherms, analytical solutions are available (Section 8.4.2). For isotherms with nonconstant selectivity, such as multi-bi-Langmuir and the ideal adsorbed solution (IAS) theory model, Migliorini, Mazzotti, and Morbidelli (2000) developed numerical methods to calculate the triangle plane of complete separation for two-component systems. They

also simplified this procedure to a shortcut method that makes the applicability for complex isotherms easier without significantly affecting the accuracy of the triangle plane.

Wekenborg, Susanto, and Schmidt-Traub (2004, 2005) and Wekenborg (2009) applied this method to estimate the operating plane for the nonisocratic SMB separation of β-lactoglobulin A and B proteins. The isotherm is described by the steric mass action (SMA) model developed for ion-exchange chromatography by Brooks and Cramer (1992) (Section 2.4.2.4).

The complete operating plane is shown in Figure 8.34. As for isocratic operation shown in Figure 8.21, the operating planes reduce with increasing feed concentration. For comparison, Figure 8.34 also includes the wr line for an isocratic separation. In this case, the constant salt concentration in sections III and IV is equal to the value in sections I and II. Comparing both areas illustrates the advantage of the solvent gradient operation.

For a constant feed concentration of $0.1\,g\,l^{-1}$ and increasing step gradients, Figure 8.35a,b shows how the operating area enlarges and process efficiency increases in comparison to an isocratic separation at 156 mM salt concentration. The comparison of the theoretically optimal values of the different triangle planes represented by the vertex illustrates the significant advantage of nonisocratic chromatography in comparison with isocratic chromatography. For an increasing step gradient, the optimal values of m_{II} are reduced, while the optimal values of m_{III} are increased, which leads to higher productivity and reduced eluent consumption.

Figure 8.36a,b proves the applicability of shortcut calculations based on the ideal equilibrium model for the estimation of process conditions. The results of rigorous process simulation based on the transport dispersion model are in good agreement with the shortcut calculation for isocratic (panel a) and nonisocratic (panel b) SMB processes. Expectedly, safety margins have to be taken into
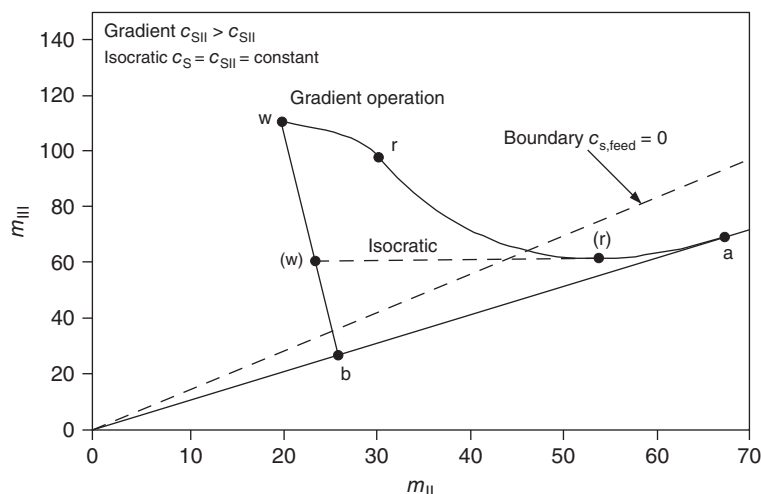
Figure 8.34 Operating map for a solvent gradient TMB process. Source: Reproduced with permission of Wekenborg (2009).
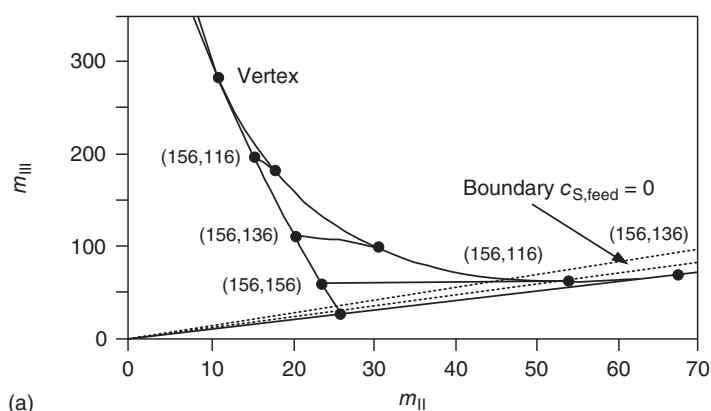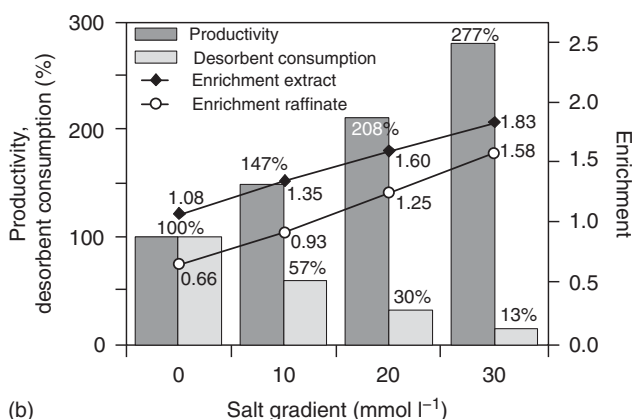
Figure 8.35 Influence of salt concentration on (a) the operating map and (b) productivity and eluent consumption of a solvent gradient process. Source: Reproduced with permission of Wekenborg (2009).
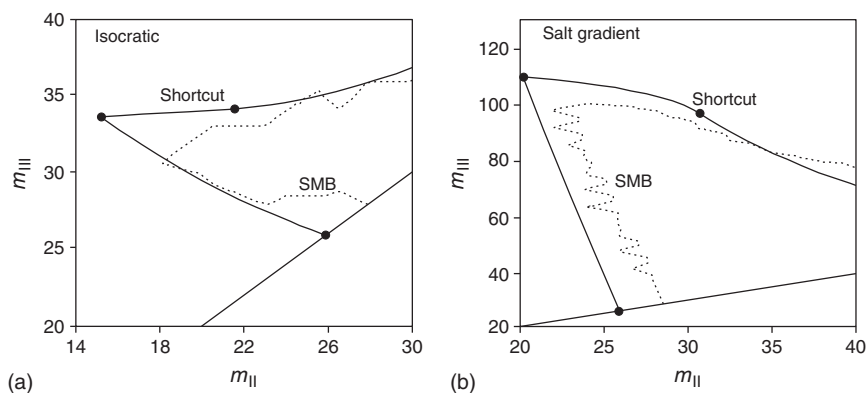
Figure 8.36 Comparison of shortcut calculations and rigorous SMB simulations for (a) an isocratic process and (b) a nonisocratic process. Source: Reproduced with permission of Wekenborg (2009).

account when the process conditions of an SMB process are estimated by shortcut calculation. The scattering of the numerical data results from an increased grid size for the numerical calculations that has been chosen in order to reduce computer time.

The above describes a method how to estimate possible operating points and has proven that a 100% purity chromatographic separation is reached within the triangle plane if a certain safety margin is taken into consideration. However, in practice, such purities are often not economic and not necessary for both components. In such cases, it is the aim to identify operating points beyond the triangle plane. This can be done by case studies based on rigorous simulation; a more direct procedure would be an optimization procedure based on a less time-consuming model.

First steps to investigate protein separations by solvent gradient SMB trace back to the research group of van der Wielen (Jensen et al. 2000) based on an extension of the "triangle method." It was found that compared with isocratic SMB, an up to 50% decrease of eluent consumption and a twofold enrichment of the product can be achieved. Later, the separation of bovine serum albumin (BSA) and myoglobin on Q Sepharose FF was investigated experimentally (Houwing et al. 2002). This system, which is described by linear isotherms and an azeotrope with increasing salt concentration, was adopted by the research group of Rodrigues for further studies on gradient SMB configurations with open loop, closed loop, and closed loop with holding vessel (Li, Xiu, and Rodrigues 2007, 2008). They recommend the following process configurations for binary separation of proteins:

- If closed-loop gradient SMB is favored in order to reduce the solvent consumption, a holdup vessel should be installed between sections IV and I. In this vessel, the desorbent and the solvent recycle are mixed during the switching period to prevent solvent strength fluctuations in section I.
- Open-loop gradient SMB is advantageous if weak adsorbing impurities are present. A sufficiently high salt concentration is necessary in sections III and IV to prevent adsorption of the impurities and to dispose them with the solvent.

A research group in Magdeburg investigated a three-section SMB process for the purification of recombinant proteins by hydrophobic interaction chromatography (HIC) (Keßler et al. 2007; Palani et al. 2011; Gueorguieva et al. 2011). They developed an equivalent TMB scheme for the three-section SMB process as shown in Figure 8.37a. The aim of the open-loop gradient process is to purify the target product recombinant streptokinase from impurities. The product is drawn off at the extract port while the impurities go with the raffinate stream. Since cheap aqueous buffers are used, the fourth section for regeneration of the mobile phase is not required. The step gradient occurs between sections II and III. Due to the HIC mode, the salt concentration in sections I and II is lower than in section III (Figure 8.37b). The process design includes two extra sections for regeneration and equilibration of the solid phase. These sections are operated independently and use different mobile phases. For the estimation of the operating parameters of the corresponding SMB process, Gueorguieva et al. (2011) used the ideal model based on the equilibrium theory to calculate the m_{II}–m_{III} operating plane as shown in Figure 8.38. This operating plane

Figure 8.37 (a) Scheme of a three-section open-loop gradient TMB process and (b) two-step salt gradient for HIC chromatography. Source: Gueorguieva et al. (2011). Reproduced with permission of Elsevier.

Figure 8.38 Separation region based on equilibrium theory and equilibrium stage model. Source: Gueorguieva et al. (2011). Reproduced with permission of Elsevier.

(P1–P2–P3) corresponds to a number of stages $N \to \infty$. The smaller operating plane in Figure 8.38 that results from the equilibrium stage model for $N = 20$ in each section is source for the selection of operating parameters of experiments. It was possible to separate streptokinase with relatively high purities, but due to insufficiencies of the plant, the predicted enrichment was not reached. Depending on purity and yield constraints, the described continuous purification process can be applied for initial capture or intermediate purification of recombinant proteins.

8.6.2 Multicolumn Solvent Gradient Purification Process

The MCSGP process, described in Section 5.2.9.2., is a continuous countercurrent chromatographic process for the separation of biomolecules using a solvent gradient.

The following design procedure for the six-column MCSGP process was presented by Aumann and Morbidelli (2007). Their approach is fully independent of any knowledge about the adsorption isotherms and mass transfer characteristics. In their presented empirical approach, a batch chromatogram of a separation task is sliced into intervals that represent certain steps for the MCSGP process. Therefore, the characteristic data like flow rates and solvent gradients are transferred from the batch process into operating data for the MCSGP process.

In Figure 8.39 an optimized batch chromatogram is shown, which transfer into the MCSGP process is described in the following according to Aumann and Morbidelli (2007).
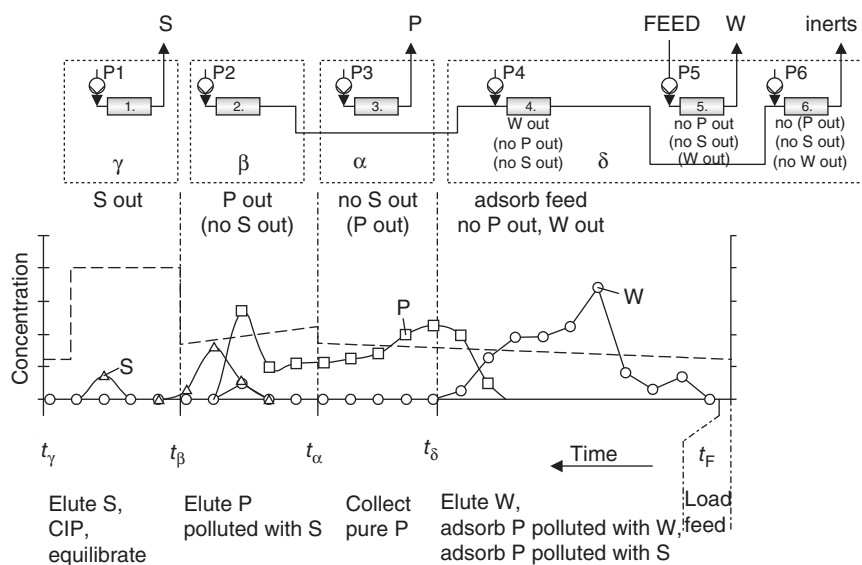
Figure 8.39 Empirical design procedure of the 6-column MCSGP process. Source: Aumann and Morbidelli (2007). Reproduced with permission of John Wiley and Sons.

The first step in transferring an optimized batch chromatogram into the continuous MCSGP process is to slice the chromatogram into four zones, α, β, γ, and δ. The zones have individual tasks. Major tasks have to be fulfilled in order to meet purity and yield constraints, whereas minor tasks do not need to be fulfilled, but improve the process performance. The zone α has the major task to retain all strongly adsorbing impurities (S) and the minor task to elute the product (P). The major task of the zone β is to let out P and the minor task to retain S, whereas in the zone γ, S has to leave the system. The zone δ has three major tasks, namely, to adsorb feed, retain all product, and elute weakly adsorbing impurities (W).

For a rough estimation of the flow rates in the columns in the zones, Aumann and Morbidelli (2007) propose the following procedure: the switch time t^*, in which a full batch cycle is completed, is calculated via Eq. (8.115). Here, Q_4 is set as the flow rate used in the batch run. Parameters of the batch run are indexed by "Batch":

$$Q_4 = Q_{\text{Batch}} \left(\frac{\varepsilon_e V_C}{\varepsilon_{e,\text{Batch}} V_{C,\text{Batch}}} \right) \frac{t_\delta - t_F}{t^*} \tag{8.115}$$

The flow rates in the columns 1, 2, and 3 can now be computed according to

$$Q_3 = Q_{\text{Batch}} \left(\frac{\varepsilon_e V_C}{\varepsilon_{e,\text{Batch}} V_{C,\text{Batch}}} \right) \frac{t_\alpha - t_\delta}{t^*} \tag{8.116}$$

$$Q_2 = Q_{\text{Batch}} \left(\frac{\varepsilon_e V_C}{\varepsilon_{e,\text{Batch}} V_{C,\text{Batch}}} \right) \frac{t_\beta - t_\alpha}{t^*} \tag{8.117}$$

$$Q_1 = Q_{\text{Batch}} \left(\frac{\varepsilon_e V_C}{\varepsilon_{e,\text{Batch}} V_{C,\text{Batch}}} \right) \frac{t_\gamma - t_\beta}{t^*} \tag{8.118}$$

Since columns 5 and 6 are used for loading the feed and regenerating the stationary phase, respectively, the flow rates are set higher. Q_5 is computed in such a way that the overall mass balance is fulfilled and a steady state can be reached:

$$Q_5 = Q_{\text{Batch}} \frac{c_{P,t_\delta} + c_{P,t_\alpha}}{2} \frac{1}{c_{P,\text{feed}}} \tag{8.119}$$

After calculating the flow rates, Aumann and Morbidelli (2007) propose the setting of modifier concentrations according to Table 8.14 in order to transfer the batch chromatogram into the MCSGP process scheme.

The presented procedure is useful for a rough estimation of operating conditions, which do not take nonidealities like internal dead volumes into account. An optimization of the operating parameters is necessary. Possible parameters for tuning are the switch time, the column flow rates, and, in the case of nonlinear adsorption behavior, the feed concentration. Aumann and Morbidelli (2007) performed an experimental optimization via the adjustment of the feed flow rate and the product outlet flow. Optimization is done based on qualitative process understanding. Further, Aumann, Stroehlein, and Morbidelli (2007) performed a parametric study of a six-column MCSGP process using a lumped kinetic model.

Table 8.14 Transfer of the modifier concentrations from the batch chromatogram into the MCSGP process.

Column	c_{mod} at $t = 0$	c_{mod} at $t = t^*$
1	$c_{Batch,mod}$ at t_β	$c_{Batch,mod}$ at t_γ
2	$c_{Batch,mod}$ at t_α	$c_{Batch,mod}$ at t_β
3	$c_{Batch,mod}$ at t_δ	$c_{Batch,mod}$ at t_α
4	$c_{Batch,mod}$ at t_F	$c_{Batch,mod}$ at t_δ
5	$c_{Batch,mod}$ at t_F	$c_{Batch,mod}$ at t_F
6	To be optimized	To be optimized

Source: Aumann and Morbidelli (2007). Reproduced with permission of John Wiley and Sons.

It was shown that a model-based optimization is possible. Krättli, Müller-Späth, and Morbidelli (2013) successfully extended the classical three-fraction process to a *n*-fraction process via integration of one extra column per additional fraction, which is limited only by the column pressure drop. The design procedure is based on the one presented by Aumann and Morbidelli (2007). A detailed process design description can be found in Krättli, Müller-Späth, and Morbidelli (2013).

A semicontinuous version of the MCSGP process using just three columns was proposed by Aumann and Morbidelli (2008). The general design procedure stays the same like for the six-column MCSGP process. It takes advantage of the fact that the batch and interconnected lanes work independently of each other. Therefore, an additional degree of freedom, namely, the possibility to set different switching times for the batch and interconnected lane, is added. The process was successfully modeled with a lumped kinetic model with competitive multicomponent bi-Langmuir isotherm, making a model-based optimization possible. Grossmann et al. (2010) proposed an optimizing model predictive control approach for the three-column MCSGP process using a linear model predictive control. The flow rates and modifier gradients are presented as variables. Krättli et al. (2011) presented a closed-loop control strategy using a PID controller. The ultraviolet (UV) signals at the column outlets are the only (online) input signals. The control strategy does not guarantee any purity or yield constraints, but guarantees the compliance of previously set positions of the UV chromatogram.

Steinebach et al. (2017a) present an empirical design procedure for the MCSGP process with the minimum number of columns: the twin-column MCSGP process. As the previously presented design procedure for the six-column MCSGP process, Steinebach et al. (2017a) propose to start from a batch chromatogram. Figure 8.40 shows a schematic batch chromatogram, which got sliced into different zones according to tasks in the batch chromatogram, namely, elute W, recycle W/P, elute P, and recycle P/S.
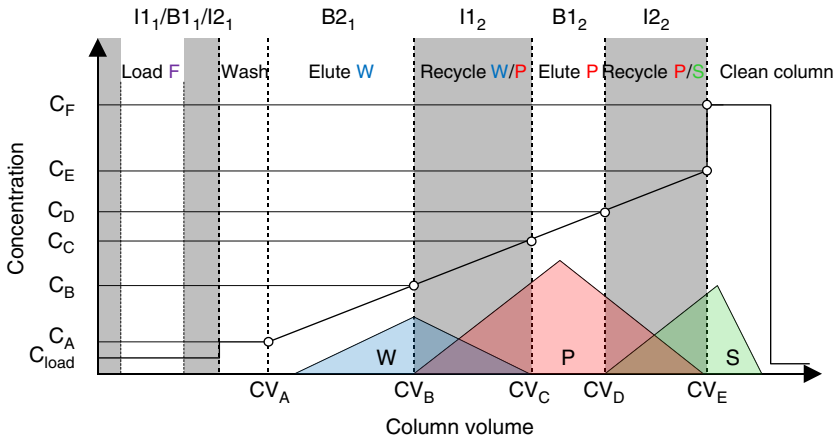
Figure 8.40 Empirical design procedure for the twin-column MCSGP process. Transfer of the time intervals of the batch process into the sections of the MCSGP process. Source: Steinebach et al. (2017a). Reproduced with permission of Elsevier.

Steinebach et al. (2017a) propose the following procedure: first of all, the number of column volumes CV_j (j = A, B, C, D, E), necessary to fulfill each task, has to be determined. Afterward, the slope of the modifier gradient can be computed according to

$$m = \frac{c_E - c_A}{CV_E - CV_A} \tag{8.120}$$

The fraction of product recycled in the process y is computed as follows:

$$y = \frac{\int_{CV_B}^{CV_C} c_P(CV)dCV + \int_{CV_D}^{CV_E} c_P(CV)dCV}{\int_{CV_B}^{CV_E} c_P(CV)dCV} \tag{8.121}$$

The feed volume in one switch can be computed using the recycled product fraction y as follows:

$$V_{\text{feed,MCSGP}} = (1 - y)V_{\text{load,Batch}} \tag{8.122}$$

Modifier gradients can be directly computed using the information from the batch chromatogram:

$$c_j = c_A + m(CV_j - CV_A) \, [j = B, C, D] \tag{8.123}$$

After having determined the modifier gradients, the critical modifier concentration (modifier concentration during feed or wash step) and the maximum flow rate Q_{max}, according to the maximum pressure drop, need to be set. Having all these information, Steinebach et al. (2017a) propose the calculation of all relevant operating parameters for the four steps of the twin-column MCSGP process according to Figure 8.41 and the following:
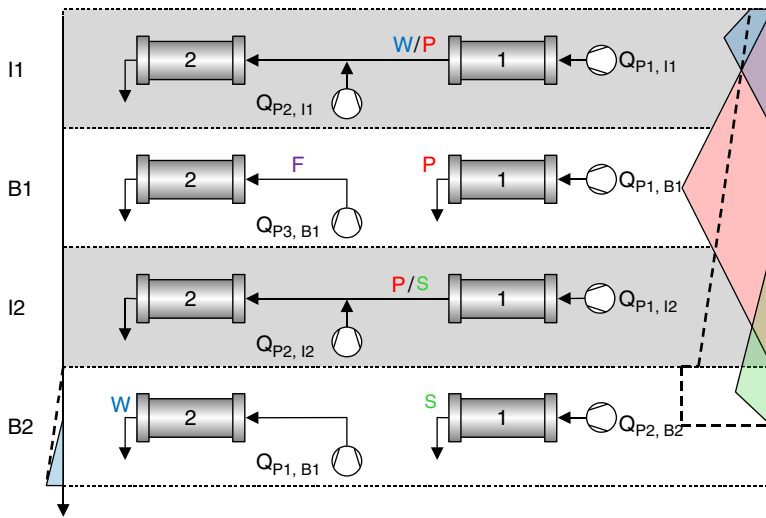
Figure 8.41 Empirical design procedure of the twin-column MCSGP process. Overview of the process steps in combination with gradient development. Source: Steinebach et al. (2017a). Reproduced with permission of Elsevier.

Step	Operation Mode:	Necessary equations	
I1	Interconnected mode	$Q_{P1,I1} \leq Q_{max} \dfrac{c_{crit} - c_{P2}}{c_C - c_{P2}}$	(8.124)
		$Q_{P2,I1} = Q_{max} - Q_{P1,I1}$	(8.125)
		$t_{I1} = \dfrac{(CV_C - CV_B)V_{col}}{Q_{P1,I1}}$	(8.126)
B1	Batch mode	$Q_{P1,B1} = \dfrac{(CV_D - CV_C)V_{col}}{t_{B1}}$	(8.127)
		$Q_{P3,B1} = \dfrac{V_{feed,MCSGP}}{t_{B1}}$	(8.128)
		t_{B1} = Time needed for the step, which takes longer (operated at Q_{max})	(8.129)
I2	Interconnected mode	$Q_{P1,I2} \leq Q_{max} \dfrac{c_{crit} - c_{P2}}{c_E - c_{P2}}$	(8.130)
		$Q_{P2,I2} = Q_{max} - Q_{P1,I2}$	(8.131)
		$t_{I2} = \dfrac{(CV_E - CV_D)V_{col}}{Q_{P1,I2}}$	(8.132)
B2	Batch mode	$Q_{P2,B2}$ = Performance of whole strip/ CIP/ reequilibration procedure as in design batch	(8.133)
		$Q_{P1,B2} = \dfrac{(CV_A - CV_B)V_{col}}{t_{B2}}$	(8.134)
		t_{B2} = Time of the step, which takes longer – usually the strip/ CIP/ reequilibration step	(8.135)

A control concept for the twin-column MCSGP process using two decoupled PID controllers and at-line HPLC was presented by Krättli, Steinbach, and Morbidelli (2013). Later, control strategies for the twin-column MCSGP process based on the PAROC framework were presented by Papathanasiou et al. (2016a,b, 2017). A procedure to identify the operating parameter space for the twin-column MCSGP process based on an equilibrium theory model, where the process runs under stable conditions within the set constraints, was presented by Steinebach et al. (2017b).

8.7 Multicolumn Systems for Bioseparations

The separation of proteins and other biopolymers has some distinctly different features in comparison with the separation of low molecular weight molecules. Biopolymers have a molecular weight ranging from several thousand to several million Daltons. They are charged and characterized by their isoelectric point. Further, they have a dynamic tertiary structure, which can undergo changes known as conformation. These changes can influence or even destroy the bioactivity if a protein denaturates permanently. Biopolymers are present in aqueous buffered eluents under conditions maintaining their bioactivity and preventing denaturation. Due to the molecular sizes of biopolymers, one has to deal with molecules that exhibit approximately 100 times lower diffusion coefficients and consequently much slower mass transfer than small molecules. In order to resolve these species by selective solute–surface interactions in a chromatographic column, the linear velocity of the eluent at optimum conditions has to be 100 times lower as well. However, access of biopolymeric solutes to the functional groups at the pore surface (stationary phase) is mandatory. While liquid chromatography of small molecules is performed using adsorbents with 10 nm average pore diameter, peptides require packings with pores of approximately 30 nm and proteins need materials with pore diameters in excess of 50 nm to enable a suitable mass transfer (Unger et al. 2010).

In the recent past, an increasing number of therapeutic monoclonal antibodies have been discovered and approved for clinical trials (Gjoka, Gantier, and Schofield 2017). At the same time, titers of cell cultures increased and the transfer from batch to continuous bioreactors improved productivity. To prevent that protein A chromatography is becoming a bottleneck in the manufacture of mAbs, novel protein adsorbents have been developed. Nevertheless, additionally more efficient processes are necessary, in particular the transition from batch to continuous chromatography. As described in Section 5.2.9.1, various continuous processes were developed with the aim of increasing productivity and reducing manufacturing cost while retaining high purity and high yield. As shown in Figure 5.29, a sequence of several chromatographic units is necessary to gain biopharmaceutics in high purity. The first step is generally a protein A capture chromatography followed by polishing steps. In the recent past, several multicolumn capture (MCC) processes were proposed (Warikoo et al. 2012; Ng et al. 2014; Gjoka et al. 2015; Angarita et al. 2015; Steinebach et al. 2017a; Girard et al. 2015). The main advantage of these processes is the more efficient use of

the protein A adsorbent, which costs is usually of one magnitude higher than other non-affinity adsorbents.

In the following the design of a twin-column CaptureSMB process (Angarita et al. 2015), representing the MCC process with the lowest number of columns and therefore the process with the lowest amount of adsorbent used, will be presented exemplarily.

8.7.1 Design of Twin-Column CaptureSMB

The twin-column CaptureSMB process (Section 5.2.9.1.2) was presented by Angarita et al. (2015). The process is divided into two phases: a batch phase and an interconnected phase. Angarita et al. (2015) propose the determination of the necessary operating parameters for the process according to Figure 8.42.

Based on the results of three single-column breakthrough curves (BTC), depicted in Figure 8.43, all operating parameters are determined. Two BTC are recorded with one and two columns, respectively, using the chosen interconnected feed flow rate Q_{IC}, which is set according to the maximum allowable pressure drop. The third BTC is recorded using one column and a flow rate Q_L, which is set as 50% of the interconnected feed flow rate Q_{IC}. On the basis of these three BTC, five different elution volumes $EV_{j,k,l}$ ($j \in [Q_{IC}, Q_L]$, k – percentage of breakthrough, l – number of columns) can be determined, which are shown exemplarily in Figure 8.43. EV_y represents the smaller elution volume of $EV_{QIC,60\%,1C}$ and $EV_{QIC,1\%,2C}$.

On this basis, Angarita et al. (2015) propose the determination of all necessary operating parameters as follows: the preload (PL) of the column catching the breakthrough and the final targetload (TL) can be calculated according to

$$PL = \frac{A_{EV_y} \cdot c_{feed}}{V_{col}} \tag{8.136}$$

$$TL = \frac{(SF \cdot EV_{Q_L,1\%,1C} - V_{dead}) \cdot c_{feed}}{V_{col}} - PL \tag{8.137}$$
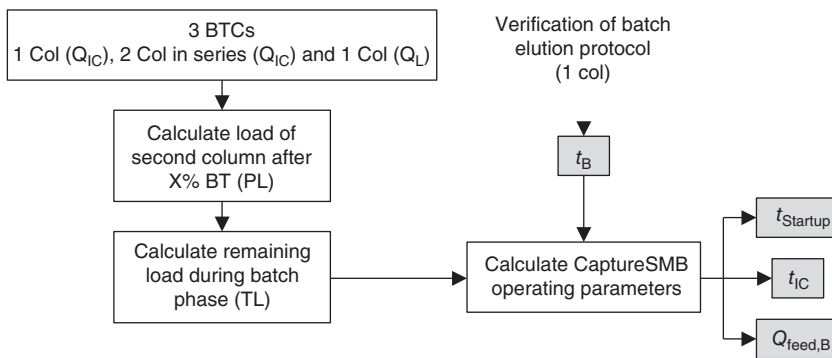
Figure 8.42 Scheme for the determination of operating parameters for the twin-column CaptureSMB process (BT, breakthrough). Source: Angarita et al. (2015). Reproduced with permission of Elsevier.

Figure 8.43 Exemplary breakthrough curves for the determination of the operating parameters of a twin-column CaptureSMB process. Source: Angarita et al. (2015). Reproduced with permission of Elsevier.
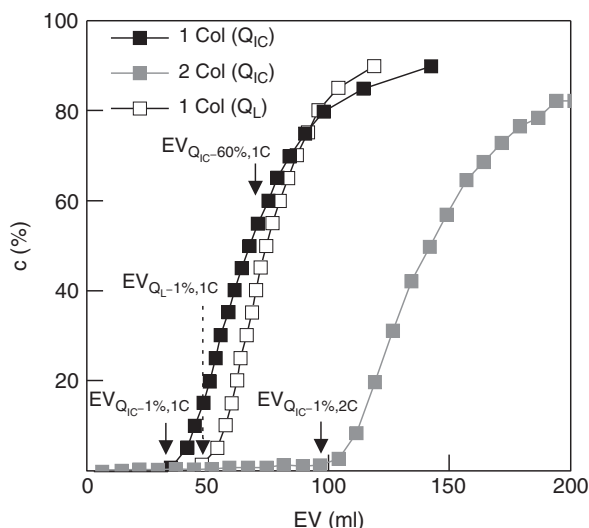
Here A_{EV_y} is the integral of the BTC up to EV_y, c_{feed} is the feed concentration, V_{col} is the column volume, V_{dead} is the dead volume of the column, and *SF* represents a safety factor. Using the EVs, preload, targetload, and the overall batch time t_b, all operating parameters for a CaptureSMB process can be calculated:

The feed flow rate during the batch phase is calculated via:

$$Q_{feed,B} = \frac{TL \cdot V_{col}}{c_{feed} \cdot t_B} \tag{8.138}$$

The feed flow rate in the batch phase, which is applied in the process, is the smaller value of $Q_{feed, B}$ and Q_L in order to avoid product loss. Besides the cleaning in place (CIP) step, all steps of the elution batch protocol are performed using Q_{IC}.

The duration of the interconnected phase and the start-up time are calculated according to

$$t_{IC} = \frac{EV_y - SF \cdot EV_{Q_L,1\%,1C} + \frac{TL \cdot V_{col}}{c_{feed}} - Q_B \cdot t_B}{Q_{IC}} \tag{8.139}$$

$$t_{start-up} = \frac{EV_y - V_{dead}}{Q_{IC}} \tag{8.140}$$

First effort into model-based design and optimization of the twin-column CaptureSMB process was spent by Baur et al. (2016). Based on a lumped kinetic model, an optimization and comparison of a batch process with dual loading flow rate and the twin-column CaptureSMB process was performed identifying a trade-off between the competitive acting objectives "productivity" and "capacity utilization" while setting the constraints of constant purity and yield. Based on the competitive behavior between the two objectives, Pareto fronts were identified. Besides for processes with very low productivity, Baur et al. (2016) proved that the CaptureSMB shows better performance than a corresponding batch process using the same total resin volume.

8.7.2   Modeling of Multicolumn Capture processes

Ng et al. (2012, 2014) developed a general model for MCC processes. It consists of different unit operations, which are linked to each other corresponding to the process schedule. As described in Section 5.2.9.1, these unit operations are:

- column loading;
- washing;
- eluting;
- regeneration;
- equilibration.

Thereof, the most important model for rigorous simulations and optimization of MCC processes is a batch column model, which covers the operations loading, washing, and elution. The model equations as well as the estimation and experimental verification of model parameters are described in the following.

Elements of a batch column model for capture chromatography are similar to model approaches presented in Section 6.2:

- Transport dispersion model (Section 6.2.5.1);
- Initial and boundary conditions (Section 6.2.7);
- Langmuir isotherm for adsorption of the protein product;
- Linear adsorption for the impurities Eq. (2.39);
- Determination of model parameters:
  - Porosity
  - Axial dispersion
  - Pressure drop parameter
  - Isotherm parameters
  - Mass transfer coefficient.

These model parameters have to be determined experimentally and consistent to each other as described in Section 7.2.

Ng et al. (2012) selected a Langmuir isotherm, which considers pH as modifier and is therefore most commonly used for protein A chromatography (Ströhlein et al. 2006). They used a small-scale column ($D = 5$ mm, $L = 50$ mm) to determine the isotherm parameters for human immunoglobulin G (IgG) by breakthrough experiments and to estimate the parameters for the transport dispersion model. Figure 8.44 shows a comparison between experimental and simulated data for breakthrough and elution curves, which are in good agreement.

To validate their model regarding the optimization of productivity for a given minimum yield, Ng et al. (2012) optimized the batch process by determining the decision variables on the load, wash, and elution volumes at predefined column lengths while keeping the column pressure drop below an allowable maximum of 2.5 bar. For regeneration and equilibration, predefined constant column volumes were set. Figure 8.45 illustrates the results of these optimization runs for a column of 5 mm diameter and an optimized length of 85 mm. In the presented as well as a further case, the experimentally obtained results were above the constraints of productivity (98%) and yield (95%).

A multicolumn process model for a MCC process as described by Ng et al. (2014) consists of the following elements:
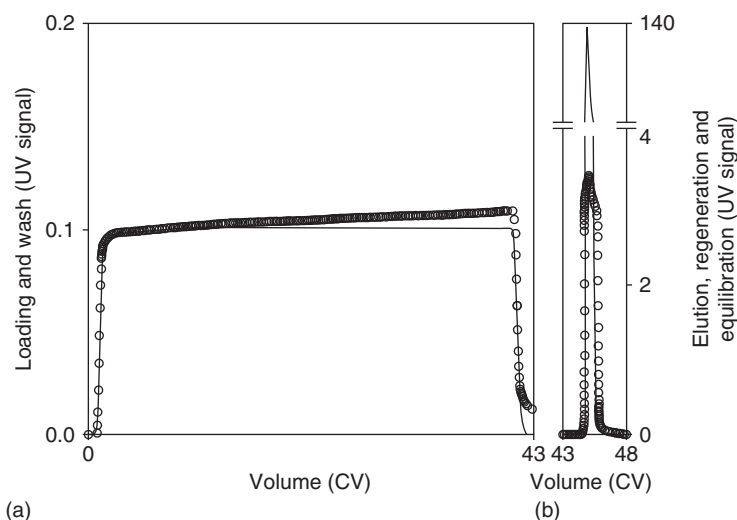
Figure 8.44 Human IgG batch chromatography: comparison of experimental (○) and simulated (—) breakthrough, wash (a), and desorption (b) curves. Source: Ng et al. (2012). Reproduced with permission of Elsevier.
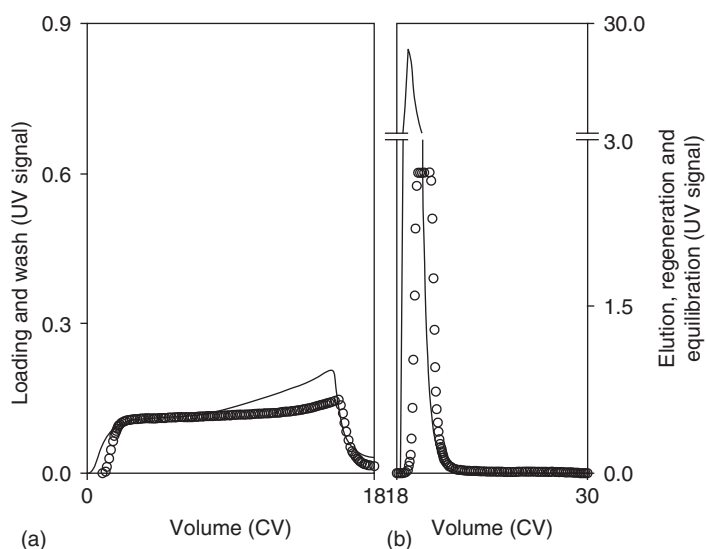
Figure 8.45 Optimized batch run for IgG capture: comparison of experimental (○) and simulated (—) chromatograms for loading and wash (a) as well as elution, regeneration, and equilibration (b). Source: Ng et al. (2012)). Reproduced with permission of Elsevier.

- Transport dispersion models for loading, wash, and elution as described above;
- Black box models determining the regeneration and equilibration by a constant number of buffer volumes (CV) as they are practically independent of the flow rate;
- Node models, which have no holdup and are free of dispersion, for connecting, respectively, separating the columns and switching inlet and outlet streams.
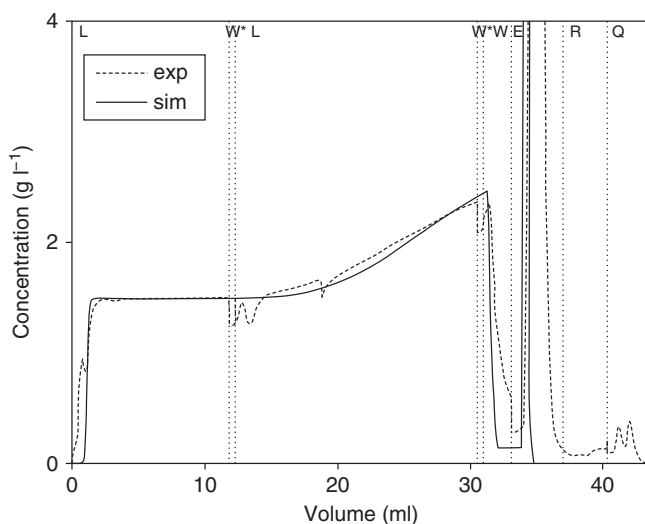
Figure 8.46 Internal chromatogram at cyclic steady state for a three column SMCC run. Source: Ng et al. (2014). Reproduced with permission of Elsevier.

Figure 8.46 depicts a comparison of simulation and experimental results for a complete process cycle of a three-column sequential MCC (SMCC) process as shown in Figure 5.36 of Section 5.2.9.1.3. The different intervals of the chromatogram in Figure 8.46 refer to detection at the outlet of column 3 in Figure 5.36, when the process is at a cyclic steady state.

As Figure 8.46 shows satisfying agreement between simulation and the experimental evaluation, the models were used to optimize the productivity of capture processes with 1, 2, and 3 columns under the constraints of minimum 95% yield and 98% purity and a maximum pressure drop of 2.5 bar. Decision variables were the load, wash, and elution volumes as well as predefined column lengths with constant diameter of 5 mm. In Figure 8.47, the optimal column length for the batch process (one column) is compared with a two-and three-column SMCC process. With increasing number of columns, the optimal column length decreases (1C: 85 mm, 2C: 54 mm, 3C: 32 mm), while the maximum productivity increases. This indicates a more efficient use of the adsorbent in the case of MCC processes. Since the curve shapes are getting steeper and upstream disturbances have to be taken into account, a robust process control system is necessary to run the process close to the optimum (Ng et al. 2014).

Figures 8.44–8.47 illustrate the potential of rigorous simulation to design optimal multicolumn chromatographic processes. Investigations of Ng et al. (2014) and Baur et al. (2016) confirm a good agreement between theoretical optimizations and corresponding experiments. In numerous theoretical and experimental studies, MCC processes are compared with traditional batch capture chromatography (Warikoo et al. 2012; Mahajan, Anupa, and Wolk 2012; Godawat et al. 2012; Ng et al. 2014; Girard et al. 2015; Baur et al. 2016; Gjoka et al. 2015; Angarita et al. 2015; Gjoka, Gantier, and Schofield 2017). Due to the expensive protein A resins and products, experiments are done in lab-scale plant
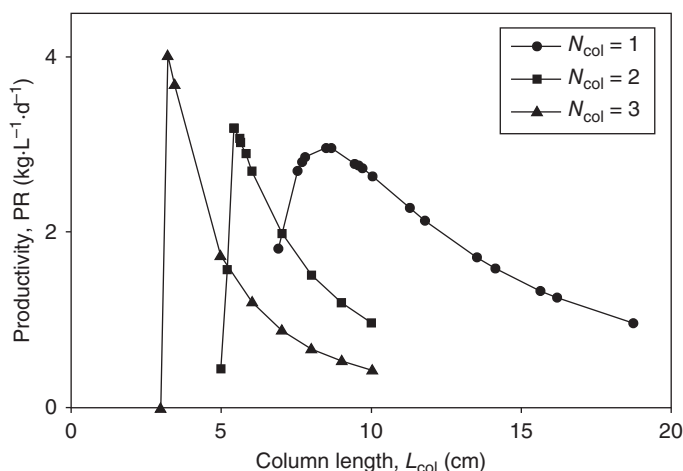
Figure 8.47 Comparison of the optimal productivity capture between batch chromatography ($N_{col} = 1$) and SMCC ($N_{col} = 2$ and 3). Source: Ng et al. (2014). Reproduced with permission of Elsevier.

with columns of 0.5–6 ml. The number of columns ranges mostly from 2 to 4 and in special cases up to 8 or 10 (Steinebach, Müller-Späth, and Morbidelli 2016). In summary, all authors point out that compared with batch chromatography, the productivity of an MCC process is about 40% higher, which results in considerable costs reductions for protein A resin (approximately 40%) and buffer consumption (approximately 40%). Besides the saving of consumables, the residence time is reduced as well, which is, for instance, favorable for the preparation of unstable proteins like blood factors (Girard et al. 2015; Godawat et al. 2012).

The comparison of batch and MCC processes is associated with the basic question if a pharmaceutical process will be operated in batch or continuous mode. As already mentioned in Section 5.2.9, increasing titers and perfusion operation of bioreactors are fulfilling the precondition for continuous downstream processes. The abovementioned investigations confirm that MCC processes can be run continuously for a reasonable period (Warikoo et al. 2012) and the amount of person-hours for process optimization is acceptable (Ng et al. 2012, 2014). In order to realize the potentials of a continuous downstream process including their reduced facility footprints, all other units including the utility infrastructure have to match continuous operation, and finally the overall costs of the commercial plant can reduce the balance.

References

Angarita, M., Müller-Späth, T., Baur, B. et al. (2015). Twin-column CaptureSMB: a novel cyclic process for protein A affinity chromatography. *J. Chromatogr. A* 1389: 85–95.

Aumann, L. and Morbidelli, M. (2007). A continuous multicolumn countercurrent solvent gradient purification (MCSGP) process. *Biotechnol. Bioeng.* 98: 1043–1055.

Aumann, L. and Morbidelli, M. (2008). A semicontinuous 3-column countercurrent solvent gradient purification (MCSGP) process. *Biotechnol. Bioeng.* 99: 728–733.

Aumann, L., Stroehlein, G., and Morbidelli, M. (2007). Parametric study of a 6-column countercurrent solvent gradient purification (MCSGP) unit. *Biotechnol. Bioeng.* 98: 1029–1042.

Bailly, M. and Tondeur, D. (1982). Recycle optimization in non-linear productive chromatography – I. Mixing recycle with fresh feed. *Chem. Eng. Sci.* 37: 1199–1212.

Baur, D., Angarita, M., Müller-Späth, T., and Morbidelli, M. (2016). Optimal model-based design of the twin-column CaptureSMB process improves capacity utilization and productivity in protein affinity capture. *Biotechnol. J.* 11: 135–145.

Beste, Y.A., Lisso, M., Wozny, G., and Arlt, W. (2000). Optimization of simulated moving bed plants with low efficient stationary phases: separation of fructose and glucose. *J. Chromatogr. A* 868: 169–188.

Biressi, G., Ludemann-Hombourger, O., Mazzotti, M. et al. (2000). Design and optimisation of a simulated moving bed unit: role of deviations from equilibrium theory. *J. Chromatogr. A* 976: 3–15.

Brooks, C. and Cramer, S. (1992). Stericmass-action ion exchange: displacement profiles and induced salt gradients. *AlChE J.* 38: 1968–1978.

Chan, S., Titchener-Hooker, N., and Sørensen, E. (2008). Optimal economic design and operation of single- and multi-column chromatographic processes. *Biotechnol. Progr.* 24: 389–401.

Charton, F. and Nicoud, R.-M. (1995). Complete design of a simulated moving bed. *J. Chromatogr. A* 702: 97–112.

David, L., Yun, J., and Nicoud, R.M. (2017). Comparing multi-column chromatographic processes for purifying monosaccharides part I: a simplified approach. *Adsorption* 23: 577–591.

Dünnebier, G. and Klatt, K.-U. (1999). Optimal operation of simulated moving bed chromatographic separation processes. *Comput. Chem. Eng.* 23: 189–192.

Dünnebier, G., Weirich, I., and Klatt, K.-U. (1998). Computationally efficient dynamic modelling and simulation of simulated moving bed chromatographic processes with linear isotherms. *Chem. Eng. Sci.* 53: 2537–2546.

Dünnebier, G., Fricke, J., and Klatt, K.-U. (2000). Optimal design and operation of simulated moving bed chromatographic reactors. *Ind. Eng. Chem. Res.* 39: 2292–2304.

Dünnebier, G., Jupke, A., and Klatt, K.-U. (2000). Optimaler betrieb von smb-Chromatographieprozessen. *Chem. Ing. Tech.* 72 (6): 589–593.

Engell, S. and Toumi, A. (2005). Optimization and control of chromatography. *Comput. Chem. Eng.* 29: 1243–1252.

Epping, A. (2005). *Modellierung, Auslegung und Optimierung chromatographischer Batch-Trennung*. Aachen: Shaker-Verlag.

Faria, R.P.V. and Rodrigues, A.E. (2015). Instrumental aspects of simulated moving bed chromatography. *J. Chromatogr. A* 1421: 82–102.

Felinger, A. and Guiochon, G. (1996). Optimizing preparative separations at high recovery yield. *J. Chromatogr. A* 752: 31–40.

Felinger, A. and Guiochon, G. (1998). Comparing the optimum performance of the different modes of preparative liquid chromatography. *J. Chromatogr. A* 796: 59–74.

Gentilini, A., Migliorini, C., Mazzotti, M., and Morbidelli, M. (1998). Optimal operation of simulated moving-bed units for non-linear chromatographic separations, II. Bi-Langmuir isotherm. *J. Chromatogr. A* 805: 37–44.

Girard, V., Hilbold, N.-J., Ng, K.S.C. et al. (2015). Large-scale monoclonal antibodies purification by continuous chromatography, from process design to scale-up. *J. Biotechnol.* 213: 65–73.

Gjoka, X., Rogler, K., Martino, R.A. et al. (2015). A straightforward methodology for designing continuous monoclonal antibody capture multi-column chromatography processes. *J. Chromatogr. A* 1416: 38–46.

Gjoka, X., Gantier, R., and Schofield, M. (2017). Transfer of a three step mAB chromatography process from batch to continuous: optimizing productivity to minimize consumable requirements. *J. Biotechnol.* 242: 11–18.

Godawat, R., Brower, K., Jain, S. et al. (2012). Periodic counter-current chromatography – design and operational considerations for integrated and continuous purification of proteins. *Biotechnol. J.* 7: 1496–1508.

Grossmann, C., Strohlein, G., Morari, M., and Morbidelli, M. (2010). Optimizing model predictive control of the chromatographic multi-column solvent gradient purification (MCSGP) process. *J. Process Control* 20: 618–629.

Gueorguieva, L., Palani, S., Rinas, U. et al. (2011). Recombinant protein purification using gradient-assisted simulated moving bed hydrophobic interaction chromatography. Part II: Process design and experimental validation. *J. Chromatogr. A* 1218: 6402–6411.

Guiochon, G. and Golshan-Shirazi, S. (1989). Theory of optimizing of the experimental conditions of preparative elution using the ideal model of liquid chromatography. *Anal. Chem.* 61: 1276–1287.

Guiochon, G., Felinger, A., Shirazi, D.G., and Katti, A.M. (2006). *Fundamentals of Preparative and Nonlinear Chromatography*. Amsterdam: Elsevier.

Hahn, T., Sommer, A., Osberghaus, A. et al. (2014). Adjoint-based estimation and optimization for column liquid chromatography models. *Comput. Chem. Eng.* 64: 41–54.

Hashimoto, K., Adachi, S., Noujima, H., and Maruyama, H. (1983). Models for separation of glucose–fructose mixtures using a simulated moving bed adsorber. *J. Chem. Eng. Jpn.* 16 (4): 400–406.

Hashimoto, K., Adachi, S., and Shirai, Y. (1993). Operation and design of simulated moving-bed adsorbers. In: *Preparative and Production Scale Chromatography* (eds. G. Ganetsos and P.E. Barker). New York: Marcel Dekker Inc.

Helfferich, F.G. and Klein, G. (1970). *Multicomponent Chromatography – Theory of Interference (Chapter 13)*. New York: Marcel Dekker Inc.

Heuer, C., Küsters, E., Plattner, T., and Seidel-Morgenstern, A. (1998). Design of the simulated moving bed process based on adsorption isotherm measurements using a perturbation method. *J. Chromatogr. A* 827: 175–191.

Houwing, J., van Hateren, S., Billiet, H., and van der Wielen, L. (2002). Effect of salt gradients on the separation of dilute mixtures of proteins by ion-exchange in simulated moving beds. *J. Chromatogr. A* 952: 85–98.

Jensen, T., Reijns, G., Billiet, H., and van der Wielen, L. (2000). Novel simulated moving-bed method for reduced solvent consumption. *J. Chromatogr. A* 873: 149–162.

Jupke, A. (2004). Experimentelle modellvalidierung und modellbasierte auslegung von simulated moving bed (SMB) chromatographieverfahren. Fortschrittbericht VDI: Reihe 3 Nr. 807. Düsseldorf: VDI Verlag GmbH.

Jupke, A., Epping, A., and Schmidt-Traub, H. (2002). Optimal design of batch and simulated moving bed chromatographic separation processes. *J. Chromatogr. A* 944: 93–117.

Kaspereit, M. and Neupert, B. (2016). Vereinfachte Auslegung der simulierten Gegenstromchromatographie mittels des Hodographenraums. *Chem. Ing. Tech.* 88 (11): 1628–1642.

Kaspereit, M. and Sainio, T. (2011). Simplified design of steady-state recycling chromatography under ideal and nonideal conditions. *Chem. Eng. Sci.* 66: 5428–5438.

Kaspereit, M., Swernath, S., and Kienle, A. (2012). Evaluation of competing process concepts for the production of pure enantiomers. *Org. Process Res. Dev.* 16 (2): 353–363.

Katti, A.M. and Jagland, P. (1998). Development and optimisation of industrial scale chromatography for use in manufacturing. *Anal. Mag.* 26 (7): 38–46.

Kawajiri, Y. and Biegler, L. (2006a). Optimization strategies for simulated moving bed and PowerFeed processes. *AIChE J.* 52: 1343–1350.

Kawajiri, Y. and Biegler, L. (2006b). Nonlinear programming superstructure for optimal operation of simulated moving bed processes. *Ind. Eng. Chem. Res.* 45: 8503–8513.

Kawajiri, Y. and Biegler, L. (2006c). Large scale nonlinear optimization for asymmetric operation and design of simulated moving beds. *J. Chromatogr. A* 1133: 226–240.

Keßler, L.C., Gueorguieva, L., Rinas, U., and Seidel-Morgenstern, A. (2007). Step gradients in 3-zone simulated moving bed chromatography, application to the purification of antibodies and bone morphogenetic protein-2. *J. Chromatogr. A* 1176: 69–78.

Krättli, M., Ströhlein, G., Aumann, L. et al. (2011). Closed loop control of the multi-column solvent gradient purification process. *J. Chromatogr. A* 1218: 9028–9036.

Krättli, M., Steinbach, F., and Morbidelli, M. (2013). Online control of the twin-column countercurrent solvent gradient process for biochromatography. *J. Chromatogr. A* 1293: 51–59.

Krättli, M., Müller-Späth, T., and Morbidelli, M. (2013). Multifraction separation in countercurrent chromatography (MCSGP). *Biotechnol. Bioeng.* 110: 2436–2444.

Küpper, A. and Engell, S. (2011). Optimization of simulated moving bed processes. In: *Constrained Optimization and Optimal Control of Partial Differential Equations* (eds. Leugering, G.; Engell, S.; Griewank, A. et al.), 559–582. Basel: Birkhäuser.

Kurup, A., Hidajat, K., and Ray, A. (2005). Optimal operation of an industrial-scale Parex process for the recovery of *p*-xylene from a mixture of C_8 aromatics. *Ind. Eng. Res.* 44: 5703–5714.

von Langermann, J., Kaspereit, M., Shakeri, M. et al. (2012). Design of an integrated process of chromatography, crystallisation and racemisation for the resolution of 2′,6′-pipecoloxylidide (PPX). *Org. Process Res. Dev.* 16 (2): 343–352.

Li, P., Xiu, G., and Rodrigues, A. (2007). Protein separation and purification by salt gradient ion-exchange. *AlChE J.* 53: 2419–2431.

Li, P., Xiu, G., and Rodrigues, A. (2008). Separation region and strategies for protein separation by salt gradient ion-exchange. *Sep. Sci. Technol.* 43: 11–28.

Li, S., Feng, L., Benner, P., and Seidel-Morgenstern, A. (2014). Using surrogate models for efficient optimization of simulated moving bed chromatography. *Comput. Chem. Eng.* 67: 121–132.

von Lieres, E. and Andersson, J. (2010). A fast and accurate solver for the general rate model of column liquid chromatography. *Comput. Chem. Eng.* 34: 1180–1191.

Ludemann-Hombourger, O., Bailly, M., and Nicoud, R.-M. (2000). Design of a simulated moving bed: optimal size of the stationary phase. *Sep. Sci. Technol.* 35 (9): 1285–1305.

Ludemann-Hombourger, O., Nicoud, R.M., and Bailly, M. (2000). The "VARICOL" process: a new multicolumn continuous chromatographic process. *Sep. Sci. Technol.* 35: 1829–1862.

Mahajan, E., Anupa, G., and Wolk, B. (2012). Improving affinity chromatography resin efficiency using semi-continuous chromatography. *J. Chromatogr. A* 1227: 154–162.

Mallmann, T., Burris, B., Ma, Z., and Wang, N.-H. (1998). Standing wave design for nonlinear SMB systems for fructose purification. *AlChE J.* 44: 2628–2646.

Mazzotti, M., Storti, G., and Morbidelli, M. (1994). Robust design of countercurrent adsorption separation processes: 2. Multicomponent systems. *AlChE J.* 40: 1825–1842.

Mazzotti, M., Storti, G., and Morbidelli, M. (1996). Robust design of countercurrent adsorption separation processes: 3. Nonstoichiometric systems. *AlChE J.* 42: 2784–2796.

Mazzotti, M., Storti, G., and Morbidelli, M. (1997). Robust design of countercurrent adsorption separation processes: 4. Desorbent in the feed. *AlChE J.* 43: 64–72.

Migliorini, C., Mazzotti, M., and Morbidelli, M. (2000). Robust design of countercurrent adsorption separation processes: 5. Nonconstant selectivity. *AlChE J.* 46: 1384–1399.

Mota, J., Araújo, J., and Rodrigues, R. (2007). Optimal design of simulated moving-bed processes under flow rate uncertainty. *AlChE J.* 53: 2630–2642.

Ng, C.K.S., Osuna-Sanchez, H., Valery, E. et al. (2012). Design of high productivity antibody capture by protein A chromatography using an integrated experimental and modelling approach. *J. Chromatogr. A* 899: 116–126.

Ng, C.K.S., Rousset, F., Valery, E. et al. (2014). Design of high productivity sequential multi-column chromatography for antibody capture. *Food Bioprod. Process.* 92: 233–241.

Nicoud, R.M. (1992). The simulated moving bed: a powerful chromatographic process. *Mag. Liq. Gas Chromatogr.* 5: 43–47.

Nicoud, R.M. (1998). Simulated moving bed (SMB): some possible applications for biotechnology. In: *Bioseparation and Bioprocessing*, vol. I (ed. G. Subramanian), pp. 3–39. Weinheim: Wiley-VCH.

Palani, S., Gueorguieva, L., Rinas, U. et al. (2011). Recombinant protein purification using gradient-assisted simulated moving bed hydrophobic interaction chromatography. Part I: Selection of chromatographic system and estimation of adsorption isotherm. *J. Chromatogr. A* 1218: 6396–6401.

Papathanasiou, M., Avraamidou, S., Oberdieck, R. et al. (2016a). Advanced control strategies for the multicolumn countercurrent solvent gradient purification process. *AlChE J.* 62: 2341–2357.

Papathanasiou, M., Sun, M., Oberdieck, R. et al. (2016b). A centralized/decentralized control approach for periodic systems with application to chromatographic separation processes. *IFAC – PapersOnLine* 49: 159–164.

Papathanasiou, M., Steinebach, F., Morbidelli, M. et al. (2017). Intelligent, model-based control towards the intensification of downstream processes. *Comput. Chem. Eng.* 105: 173–184.

Pröll, T. and Küsters, E. (1998). Optimization strategy for simulated moving bed systems. *J. Chromatogr. A* 800: 135–150.

Rhee, H.-K., Aris, R., and Amundson, N.R. (1970). On the theory of multicomponent chromatography. *Philos. Trans. R. Soc. London, Ser. A* 267: 419–455.

Rodrigues, R., Araújo, J., Eusébio, M., and Mota, J. (2007). Experimental assessment of simulated moving bed and Varicol processes using a single-column setup. *J. Chromatogr. A* 1142: 69–80.

Rodrigues, R., Araújo, J., and Mota, J. (2007). Optimal design and experimental validation of synchronous, asynchronous and flow-modulated, simulated moving-bed processes using a single-column setup. *J. Chromatogr. A* 1162: 14–23.

Ruthven, D.M. and Ching, C.B. (1989). Review article no. 31: counter-current and simulated counter-current adsorption separation processes. *Chem. Eng. Sci.* 44 (5): 1011–1038.

Sá Gomes, P. and Rodrigues, A.E. (2012). Simulated moving bed chromatography: from concept to proof-of-concept. *Chem. Eng. Technol.* 35 (1): 17–34.

Sainio, T. (2017). Unified design of chromatographic processes with timed events: separation of ternary mixtures. *Chem. Eng. Sci.* 152: 547–567.

Sainio, T. and Kaspereit, M. (2009). Analysis of steady state recycling chromatography using equilibrium theory. *Sep. Purif. Technol.* 66: 9–18.

Scherpian, P. (2009). *Zur Auswahl und Auslegung chromatographischer Prozesskonzepte mit Recycling*. München: Verlag Dr. Hut.

Scherpian, P. and Schembecker, G. (2009). Scaling-up recycling chromatography. *Chem. Eng. Sci.* 64: 4068–4080.

Schramm, H., Grüner, S., and Kienle, A. (2003). Optimal operation of simulated moving bed processes by means of simple feedback control. *J. Chromatogr. A* 1006: 3–13.

Seidel-Morgenstern, A., Keßler, L., and Kaspereit, M. (2008a). Neue entwicklungen auf dem gebiet der simulierten gegenstromchromatographie. *Chem. Ing. Tech.* 80: 725–740.

Seidel-Morgenstern, A., Keßler, L., and Kaspereit, M. (2008b). New developments in simulated moving bed chromatography. *Chem. Eng. Technol.* 31: 826–837.

Shan, Y. and Seidel-Morgenstern, A. (2004). Analysis of the isolation of a target component using multicomponent isocratic preparative elution chromatography. *J. Chromatogr. A* 1041: 53–62.

Siitonen, J. and Sainio, T. (2011). Explicit equations for the height and position of the first component shock for binary mixtures with competitive Langmuir isotherms under ideal conditions. *J. Chromatogr, A* 1218: 6379–6387.

Siitonen, J. and Sainio, T. (2015). Unified design of chromatographic separation processes. *Chem. Eng. Sci.* 122: 436–451.

Siitonen, J., Sainio, T., and Kaspereit, M. (2011). Theoretical analysis of steady state recycling chromatography with solvent removal. *Sep. Purif. Technol.* 78: 21–32.

Song, I.H., Lee, S.B., Rhee, H.K., and Mazzotti, M. (2006). Identification and predictive control of a simulated moving bed process: purity control. *Chem. Eng. Sci.* 61: 1973–1986.

Steinebach, F., Müller-Späth, T., and Morbidelli, M. (2016). Continuous counter-current chromatography for capture and polishing steps in biopharmaceutical production. *Biotechnol. J.* 11: 1126–1141.

Steinebach, F., Ulmer, N., Decker, L. et al. (2017a). Experimental design of a twin-column countercurrent gradient purification process. *J. Chromatogr. A* 1492: 19–26.

Steinebach, F., Krättli, M., Storti, G., and Morbidelli, M. (2017b). Equilibrium theory based design space for the multicolumn countercurrent solvent gradient purification process. *Ind. Eng. Chem. Res.* 56: 13482–13489.

Storti, G., Mazzotti, M., Morbidelli, M., and Carrà, S. (1993). Robust design of binary countercurrent adsorption separation processes. *AIChE J.* 39: 471–492.

Storti, G., Baciocchi, R., Mazzotti, M., and Morbidelli, M. (1995). Design of optimal conditions of simulated moving bed adsorptive separation units. *Ind. Eng. Res.* 34: 288–301.

Ströhlein, G., Aumann, L., Mazzotti, M., and Morbidelli, M. (2006). A continuous, counter-current multicolumn chromatographic process incorporating modifier gradients for ternary separations. *J. Chromatogr. A* 1126: 338–346.

Strube, J., Altenhöner, U., Meurer, M., and Schmidt-Traub, H. (1997a). Optimierung kontinuierlicher simulated-moving-bed-chromatographie-prozesse durch dynamische simulation. *Chem. Ing. Tech.* 69 (3): 328–331.

Strube, J., Altenhöner, U., Meurer, M. et al. (1997b). Dynamic simulation of simulated moving-bed chromatographic processes for the optimisation of chiral separations. *J. Chromatogr. A* 769: 328–331.

Strube, J., Jupke, A., Epping, A. et al. (1999). Design, optimization and operation of smb chromatography in the production of enantiomerically pure pharmaceuticals. *Chirality* 11: 440–450.

Subramani, H.J., Hidajat, K., and Ray, A.K. (2003a). Optimization of simulated moving bed and Varicol processes for glucose-fructose separation. *Trans. IChemE* 81: 549–567.

Subramani, H., Hidajat, K., and Ray, A. (2003b). Optimization of reactive SMB and Varicol systems. *Comput. Chem. Eng.* 27: 1883–1901.

Toumi, A., Hanisch, F., and Engell, S. (2002). Optimal operation of continuous chromatographic processes: mathematical optimization of the VARICOL process. *Ind. Eng. Chem. Res.* 41: 43287–44337.

Toumi, A., Engell, S., and Hanisch, F. (2002). Asynchron getaktete Gegenstromchromatographie – Prinzip und optimaler Betrieb. *Chem. Ing. Tech.* 74: 1483–1490.

Toumi, A., Engell, S., Ludemann-Hombourger, O. et al. (2003). Optimization of simulated moving bed and VARICOL processes. *J. Chromatogr. A* 1006: 15–31.

Toumi, A., Engell, S., Diehl, M. et al. (2007). Efficient optimization of simulated moving beg processes. *Chem. Eng. Proc.* 46: 1067–1084.

Unger, K., Ditz, R., Machtejevas, E., and Skudas, R. (2010). Liquid chromatography – its development and key role in life sciences applications. *Angew. Chem.* 49: 2300–2312.

Warikoo, V., Godawat, R., Brower, K. et al. (2012). Integrated continuous production of recombinant therapeutic proteins. *Biotechnol. Bioeng.* 109: 3018–3029.

Wekenborg, K. (2009). *Kontinuierliche Trennung von Proteinen durch nicht-isokratische SMB-Chromatographieprozesse*. Aachen: Shaker-Verlag.

Wekenborg, K., Susanto, A., and Schmidt-Traub, H. (2004). Nicht-isokratische SMB-Trennung von Proteinen mittels Ionenaustauschchromatographie. *Chem. Ing. Tech.* 76 (6): 815–819.

Wekenborg, K., Susanto, A., and Schmidt-Traub, H. (2005). Modelling and validated simulation of solvent-gradient simulated moving bed (SG-SMB) processes for protein separation. In: *Computer-Aided Chemical Engineering (ed. Puigjaner, L.)*, vol. 20A, 313–318.

Wongso, F., Hidajat, K., and Ray, A. (2004). Optimal operating mode for enantioseparation of SB-553261 racemate based on simulated moving bed technology. *Biotechnol. Bioeng.* 87: 704–722.

Yao, C., Tang, S., Yao, H.-M. et al. (2014). Study on number of decision variables in design and optimization of Varicol process. *Comput. Chem. Eng.* 68: 114–122.

Yu, W., Hidajat, K., and Ray, A. (2005). Optimization of reactive simulated moving bed and Varicol systems for hydrolysis of methyl acetate. *Chem. Eng. J.* 112: 55–72.

Yu, Y., Wood, K.R., and Liu, Y.A. (2015). Simulation and comparison of operational modes in simulated moving bed chromatography. *Ind. Eng. Chem. Res.* 54: 11576–11591.

Zhang, Z., Mazzotti, M., and Morbidelli, M. (2003a). PowerFeed operation of simulated moving bed units: changing flow-rates during the switching interval. *J. Chromatogr. A* 1006: 87–99.

Zhang, Z., Mazzotti, M., and Morbidelli, M. (2003b). Multiobjective optimization of simulated moving bed and Varicol processes using a genetic algorithm. *J. Chromatogr. A* 989: 95–108.

Zhang, Z., Mazzotti, M., and Morbidelli, M. (2004a). Continuous chromatographic processes with a small number of columns: comparison of simulated moving bed with Varicol, PowerFeed and ModiCon. *Korean J. Chem. Eng.* 21: 454–464.

Zhang, Z., Morbidelli, M., and Mazzotti, M. (2004b). Experimental assessment of PowerFeed chromatography. *AlChE J.* 50: 625–632.

Zhang, Y., Hidajat, K., and Ray, A.K. (2007). Enantio-separation of racemic pindolol on α1-acid glycoprotein chiral stationary phase by SMB and Varicol. *Chem. Eng. Sci.* 62: 1364–1375.

Zhang, Y., Hidajat, K., and Ray, A.K. (2009). Multi-objective optimization of simulated moving bed and Varicol processes for enantio-separation of racemic pindolol. *Sep. Purif. Technol.* 65: 311–321.

Zhong, G. and Guiochon, G. (1996). Analytical solution for the linear ideal model of simulated moving bed chromatography. *Chem. Eng. Sci.* 51 (18): 4307–4319.

Ziomek, G. and Antos, D. (2005). Stochastic optimization of simulated moving bed process; sensitivity analysis for isocratic and gradient operation. *Comput. Chem. Eng.* 29: 1577–1589.

Ziomek, G., Kaspereit, M., Jezowski, J. et al. (2005). Effect of mobile phase composition on the SMB processes efficiency; stochastic optimization of isocratic and gradient operation. *J. Chromatogr. A* 1070: 111–124.

Zúñiga, I.T. and Wouwer, A.V. (2014). Optimization of VARICOL SMB processes using hybrid modelling and nonlinear programming. *Comput. Chem. Eng.* 71: 1–10.

9

Process Control*

Sebastian Engell[1] and Achim Kienle[2,3]

[1] *TU Dortmund, Fakultät Bio- und Chemieingenieurwesen, Lehrstuhl für Systemdynamik und Prozessführung, Emil-Figge-Str. 70, Dortmund 44227, Germany*
[2] *Otto-von-Guericke-Universität Magdeburg, Lehrstuhl für Automatisierungstechnik/Modellbildung, Universitätsplatz 2, Magdeburg 39106, Germany*
[3] *Max-Planck-Institut für Dynamik komplexer technischer Systeme, Process Synthesis and Dynamics Group, Sandtorstrasse 1, Magdeburg 39106, Germany*

As discussed in Chapters 6 and 7, the use of detailed process models in the design and in the choice of the operating parameters of chromatographic separation processes may lead to considerable improvements. However, optimal settings of the operating parameters do not guarantee an optimal operation of the real plant. This is due to imperfect behavior of the column packing and the peripherals, the effect of external disturbances, changes of plant behavior over time, and the inevitable discrepancy between the model and the real system.

Any real process is therefore operated using some sort of feedback control. Feedback control means that some variables (degree of freedom) of the plant are modified during the operation based upon observation of some measurable variables. These measurements may be available quasi-continuously or with a more or less large sampling period (results of a laboratory analysis), and accordingly the operation parameters (termed inputs in feedback control terminology) are modified in either a quasi-continuous fashion or intermittently. In chromatographic separations, feedback control is most often realized by operators, who change the operating parameters until the specifications are met.

Automatic feedback control is the continuous or repetitive modification of some operating parameters based on measurement data. Due to the dynamic nature of the process, the control algorithm is usually also dynamic and has to be designed carefully to avoid instability. We have to distinguish between two types of process control: standard and advanced one. Standard controllers have a static algorithm like PID controller type or cascade mode for the temperature control. Advanced control schemes use a more sophisticated algorithm that could be based on shortcut models or dynamic process models.

9.1 Standard Process Control

Standard feedback laws are proportional (P), integral (I), and differentiating (I) control and combinations thereof, for example, PI control where the controlled input depends on the instantaneous control error and on its integral, guaranteeing steady-state accuracy and a more or less quick response to sudden disturbances.

Different standard PID controllers are used within chromatographic processes. Controllers are used, for instance, to adjust the flow rate, to temper properly the process, and to control the air pressure, the sterilization temperature, the pressure before the column, and the level of the tank. In the latter case, simpler schemes like a two-point controller can be adopted, which mainly close/open the tank bottom valve based on two-level switches placed at the top and bottom positions within the vessel.

Fine-tuning schemes exist to assist the process and control engineers in optimizing the PID parameters. Rules like the one proposed by Ziegler and Nichols (1942) (see also Aström and Hägglund, 1995) can be used. They are based on some measurements of the dynamic system response. The Ziegler–Nichols rules allow furthermore the calculation of the PID parameter for different target criteria (classic rule, integral rule, some overshoot, no overshoot, etc.). Additionally, the majority of decentralized automation system vendors provide some sort of automatic fine-tuning software. Clear recommendations cannot be given, as the authors have not collected reliable positive experience with such tools so far.

If the process dictates tighter process requirements, for instance, following a precise gradient, then more sophisticated process control schemes are required. Such schemes integrate in addition to classical PID controller static and dynamic calculation and logic blocks. Feedforward controllers integrates the dynamic trajectory of the manipulated variable to follow the target set point. Dynamic elements might be added to filter noise from measured variables or to add delays or ramp values to avoid abrupt changes in valve positions or pump flow rates. Advanced controllers employ dynamic process models in one way or the other and may implicitly or explicitly perform an optimization of the operating parameters to maximize throughput or yield or to minimize the solvent consumption while ensuring the specified product purities and recoveries.

9.2 Advanced Process Control

Chromatographic separations usually are operated manually, that is, the main operating parameters are determined or optimized as discussed in Chapter 7 and implemented at the separation unit, and from the observation of the resulting performance, small iterative changes are made in order to meet the specifications and to gradually improve the process efficiency, for example, by increasing the throughput or by decreasing the solvent consumption. Advanced process control aims at performing this adaptation automatically, hence more reliably, faster, and with a better reproducibility. Advanced control schemes always rely on the

use of a process model, but the required precision of the models differs among the different proposed schemes. Due to the feedback nature of advanced control, the controller reacts, for example, to the observed purities – model inaccuracies can be compensated to some extent. Despite intense academic research and successful demonstrations at real plants, advanced control however has not yet been implemented in industry on a large scale.

9.2.1 Online Optimization of Batch Chromatography

Online optimization of batch chromatography is based on the same basic considerations as described for process design in Section 8.2 for the choice of the operating parameters, but this optimization is performed during the operation of the process. The operational degrees of freedom, for example, injection time and cutting times, are adapted automatically to increase the productivity while maintaining the desired product purities and recoveries. The process models used are dynamic in nature, but as the operating parameters can only be varied for the next injection, the optimization problem that results is static in nature. The model predicts the resulting purities, recoveries, and productivity as a function of the operational degrees of freedom and a nonlinear optimization problem is solved to compute the optimal operating parameters.

The crucial issue here is the handling of the inevitable discrepancies between the behavior of the plant and the predictions by the model. For example, if a mismatch of the predicted purities is observed, this can be used to modify the target values such that the resulting true purity is as specified (bias correction). While this approach assures the meeting of the specifications, it is not sufficient to obtain optimality of the operating parameters in the case of model errors. For optimality, either the process model has to be adapted by online parameter estimation, or a suitable modified scheme has to be used as described below in this section.

It is possible to estimate key separation parameters, in particular the parameters of the isotherms, from batch chromatograms using nonlinear optimization techniques. However, usually only a small number of parameters can be estimated simultaneously, and the estimation has to be initialized carefully, for example, by first performing an estimation based on shortcut models. Gao and Engell (2005b) demonstrated that it is even possible to estimate black box models of the isotherms from batch experiments so that no assumptions on the mathematical form of the isotherms have to be made. Parameter adaptation however leads to a small mismatch between the plant model and the real process only if the model is structurally correct, that is, able to predict the observations for suitably chosen parameters, which is not always the case. Especially for high purity requirements, small deviations of the chromatograms, for example, due to the presence of components that are not considered in the model, can lead to significant errors in the predicted purities and therefore to the need of measurement-based adaptation of the operating policy.

In the iterative online optimization scheme proposed by Gao and Engell (2005a), the gradients of the cost function and of the constraints (e.g. purity requirements) are modified based on the available measurements in a fashion

that ensures convergence to the true optimum for the real plant despite the error between the behavior of the real plant and the prediction of the model that is used in the optimization. This also reduces the necessary effort for modeling and model parameter estimation because coarse models are sufficient to perform the iterative online optimization. For the estimation of the true gradients of the constraints and of the performance criterion with respect to the operating parameters, the observed outcomes of the recent iterations are used, but in some cases, additional experiments have to be performed to improve the estimation that temporarily reduce the performance but are necessary to reach true optimum. The number of iterations (injections) needed to approach the optimum is typically around 10. The online optimization algorithm is depicted graphically in Figure 9.1.

Simulation results of the algorithm for an enantiomer separation with bi-Langmuir isotherms are shown in Figure 9.2. The discrepancies between the chromatograms that are predicted by the optimization model and that are assumed for the real plant are shown in Figure 9.3.

The first iterations $u^{(-2)} - u^{(0)}$ are needed to collect the information that is required to estimate the empirical gradients. Thereafter, the iterative improvement starts. It can be seen that despite a significant error in the chromatograms, the iterative optimization converges to the true optimum and establishes the desired purities and recoveries of the components. In related work, this approach has been applied to continuous annular electrochromatography (Behrens and Engell 2011).
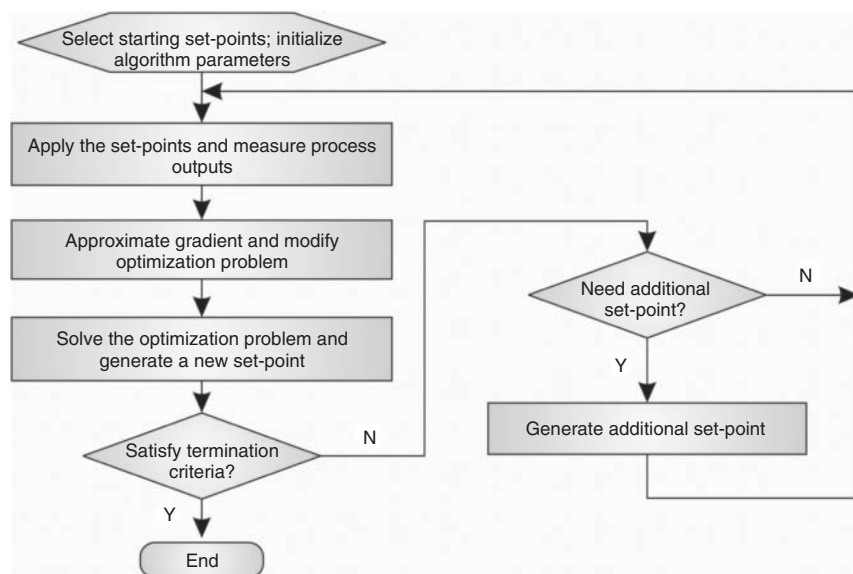
Figure 9.1 Flowchart of the iterative online optimization algorithm for batch chromatography proposed in Gao and Engell (2005a). Source: Gao and Engell (2005a). Reproduced with permission of Elsevier.

Set-point trajectory
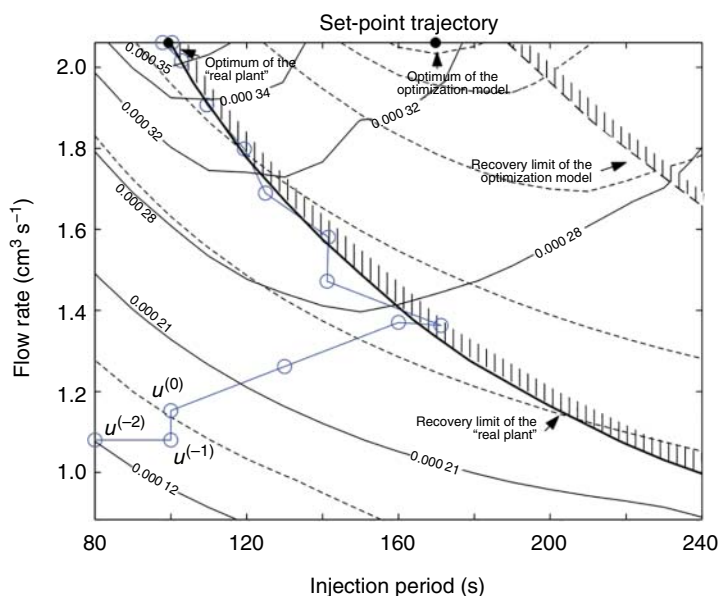
Figure 9.2 Iterative optimization of the operating parameters of a batch separation with plant–model mismatch.
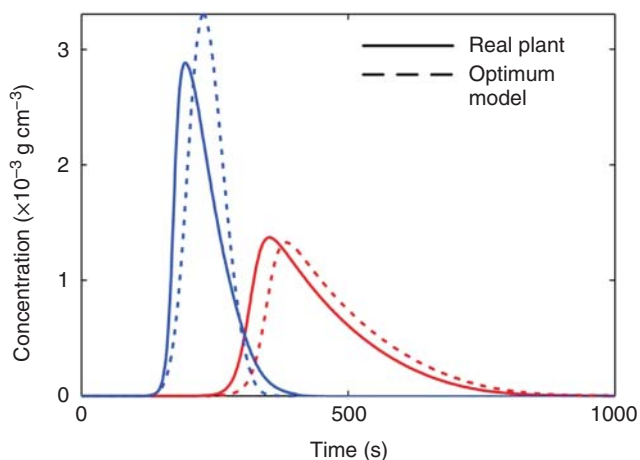
Figure 9.3 Discrepancy between real and predicted chromatograms for the iterative optimization shown in Figure 9.2.

9.2.2 Advanced Control of SMB Chromatography

In this section, we are concerned with the higher control level of guaranteeing the desired product purities and recoveries and optimizing the performance/performance optimization/of the plant.

As discussed in several chapters of this volume, the use of detailed process models in the design and in the choice of the operating parameters of

chromatographic separation processes may lead to considerable performance improvements. However, optimal settings of the operating parameters for simulation models do not guarantee an optimal operation of the real plant. This is due, for example, to nonidealities of the flows and of the column packings, unmodeled peripherals, the presence of additional substances in the mixture, inaccuracies in the actuators (pumps and valves), and changes of the plant behavior over time. As an optimal operating point always is at the constraint of at least one performance criterion, the specifications are most likely not met at the real plant if the operation parameters that were obtained from offline optimization are applied.

In principle, there are three possible remedies for this problem. First, the plant can be operated with a safety margin – the most common but not the most economic approach. Second, some critical specifications can be controlled online, by feeding back the measured values to a controller, especially the product purities as the most critical parameters. This feedback can also be realized manually, which requires the continuous presence of skilled operators. The most advanced approach is to establish the optimality of the operation continuously and automatically based on more or less sophisticated plant models and the available measurements.

If the variation of the flow rates with the aim to reach the desired product purity is done manually, the modification of the operating parameters is based on either heuristic rules or relying on the expertise of the operators. Antia (2003) proposed the following practical scheme:

- Start with low feed concentrations in order to achieve linear separation conditions.
- Increase $\dot{V}_{\mathrm{I}}$ to a large value and decrease $\dot{V}_{\mathrm{IV}}$ to a low value so that the design criteria for the sections I and IV are satisfied by a large margin. Then, the attention is focused on the appropriate choice of the flow rates in the central sections II and III.
- Increase the concentration of the feed in steps. Determine which outlet is polluted and correct the flow rates according to predefined rules. This can be repeated until the feed concentrations reach their upper limits.
- Once the flow rates in the central sections are chosen appropriately, increase $\dot{V}_{\mathrm{IV}}$ and decrease $\dot{V}_{\mathrm{I}}$. This ensures that a minimal flow of eluent is used and thus near-optimal process performance is reached.

For more details on the background of these rules, we refer to Section 8.4.

In practice, simulated moving bed (SMB) processes are controlled using similar manual schemes (Küsters, Gerber, and Antia 1995; Juza 1999; Miller et al. 2003). Antia (2003) suggested to include these heuristic rules into a fuzzy controller in order to achieve full automatic control of SMB processes.

9.2.2.1 Purity Control for SMB Processes

For automatic purity control of SMB processes, it is assumed that the plant is operated near a fixed, well-designed or optimized, operating point. The degrees of freedom available for online control are the (external or internal) flow rates and the switching time; these can be adapted to meet the purity specifications.

Automatic control of purities is difficult due to the long time delays and the complex dynamics that are described by nonlinear distributed parameter models and switching of the inputs, leading to mixed discrete and continuous dynamics, small operating windows, and a pronouncedly nonlinear response of the purities to input variations. Because of the complex nonlinear dynamics of SMB processes, their automatic control has attracted the interest of many academic research groups, and many different control schemes have been proposed; however, few of them have been tested in experimental work for real plants with limited sensor information.

Automatic purity control was reported for the separation of aromatic hydrocarbons where online Raman spectroscopy can be used to measure the concentrations of the compounds at the outlet of the chromatographic columns (Marteau et al. 1994). This approach, as well as the geometrical nonlinear control concept described by Kloppenburg and Gilles (1999), is based on a model that describes the corresponding true moving bed (TMB) process, so the cyclic port switching is neglected.

Natarajan and Lee (2000) investigated the application of a repetitive model predictive control (RMPC) technique to SMB processes. RMPC is a model-based control technique that results from incorporating the basic concept of repetitive control into the model predictive control (MPC) framework (Qin and Badgwell 2003). The switching period of the process is assumed to be constant. This is limiting, since the switching time can also be manipulated to control the process. In this approach, a rigorous model discretized process model is linearized along the optimal trajectory.

Schramm et al. (2001) and Schramm, Grüner, and Kienle (2003) presented a model-based control approach for the direct control of the product purities of SMB processes. Based on wave theory, relationships between the front movements and the flow rates of the equivalent TMB process were derived. Using these relationships, a simple control concept with two PI controllers was proposed.

Cox, Khattabi, and Dapremont (2003) reported a successful control and monitoring system for the separation of an enantiomer mixture based on the concentration profiles in the recycle loop.

Klatt et al. (2000) and Klatt, Hanisch, and Dünnebier (2002) proposed a two-layer control architecture where on the upper level the optimal operating regime is calculated at a low sampling rate by dynamic optimization based on a rigorous nonlinear process model. The low-level control task is to keep the process at the optimal operating point, which is realized by stabilizing the concentration fronts. This leads to a multivariable control problem, which for linear isotherms can be approximately decoupled by using the m-parameters or the β-factors as manipulated variables instead of flow rates and the switching time. For the stabilization of the concentration fronts, in the case of linear isotherms, linear SISO IMC controllers were used. The dynamic models for the stabilization of the concentration fronts are obtained by identifying black box models using simulation data of the rigorous process model for small changes of the inputs around the optimal operating point. The scheme was validated experimentally. It turned out that the localization of the concentration fronts based on measured chromatograms is difficult even when two independent sensors are available per

outlet stream and in the recycle (ultraviolet [UV] detectors and polarimeters) due to backmixing effects and that stabilizing the front positions does not suffice to guarantee the product purities due to plant–model mismatch such that an additional control layer for purity control is needed (Hanisch 2002). In the case of nonlinear isotherms, dynamic neural network models were used in a nonlinear MPC scheme (Wang et al. 2003).

The same idea of bilevel optimization is pursued in Kim, Lee, and Lee (2010a) and demonstrated experimentally using an RMPC scheme on the lower (purity control) level (Kim et al. 2010b).

Song et al. (2006) proposed a multivariable purity control scheme using the *m*-parameters as manipulated variables and an MPC scheme based on linear models that are identified from nonlinear simulations. The approach proposed by Schramm, Grüner, and Kienle (2003) for purity control has been modified by several authors (Kleinert and Lunze 2008; Fütterer 2008). It gives rise to relatively simple decentralized controllers for the front positions, but an additional purity control layer is needed to cope with plant–model mismatch and sensor errors. Vilas and Van de Wouwer (2011) augmented it by an MPC controller based on a POD (proper orthogonal decomposition) model of the plant for parameter tuning of the local PI controllers to cope with the process nonlinearity.

Automatic control concepts have not only been developed for the SMB process but also for the multicolumn countercurrent solvent gradient purification (MCSGP) process. Krättli, Steinebach, and Morbidelli (2013) developed a purity control concept for MCSGP process that uses two independent PID controllers to directly control impurities in the product stream. Papathanasiou et al. (2016) propose an advanced control strategy for the MCSGP process using an mp-MPC controller with an approximate model that tracks the integral of the concentrations at the outlet stream.

9.2.2.2 Direct Optimizing Control of SMB Processes

Due to the nonlinear behavior of SMB processes in particular if the adsorption isotherms are nonlinear, simple purity control schemes only work in a narrow range around a fixed operating point and can only react slowly to disturbances or changes of the set points. More sophisticated schemes make use of nonlinear or adapted models and are relatively complex. As only two purities are to be controlled, purity control defines only 2 of the at least 4 degrees of freedom that can be used online. A new idea that was proposed independently by the research groups at TU Dortmund and ETH Zürich in 2003/2004 (Erdem et al. 2004; Toumi and Engell 2004; Engell and Toumi 2005) is to perform a direct model-based optimization of the operating regime online using the purity requirements not as set points for the controller but as constraints in the optimization of the operating point. This principle can be generalized to other processing units (Engell 2007).

Both approaches are based on the same principle: a sequence of future operating parameters is computed employing a model of the SMB process such that a performance criterion is optimized over the so-called prediction or look-ahead horizon, respecting constraints, for example, on the product purities and the maximum column pressure. The two approaches differ in the type of models used and the degrees of freedom that are considered in the optimization. In the work

of the ETH group, linear prediction models are used, and only the flow rates but not the switching time are used as manipulated variables. Changes of the manipulated variables are realized at shorter intervals than the switching time. In the Dortmund approach, a discretized nonlinear general rate model (GRM) (Gu 1995) is employed, and a rigorous nonlinear online optimization of all degrees of freedom is performed, including the switching time. Changes of the controlled variables are only implemented after a switching of the ports has occurred. In the implementation, a sequential approach was employed where the process is simulated over the prediction horizon and the degrees of freedom are optimized based on the simulation results using a sequential quadratic programming (SQP) solver.

Both groups have validated their approaches successfully at laboratory-scale SMB plants. The Dortmund approach, due to its general nature, can be applied without conceptual changes also to reactive separations. Below we briefly report on the application to the isomerization of glucose to fructose. For further details, see Toumi and Engell (2004) and Engell and Toumi (2005).

Process Description   The reactive SMB process considered here is the isomerization of glucose to fructose. The plant consists of six reactive chromatographic fixed beds that are interconnected to form a closed-loop arrangement. As shown in Figure 9.4, a pure glucose solution is injected to the system at the feed line. At the extract line, a mixture of glucose and fructose, called high-fructose corn syrup (HFCS), is withdrawn. Water is used as solvent and is fed continuously to the system at the desorbent line. In this special SMB process, no attempt is made to achieve a complete separation of glucose and fructose since the most common type of fructose syrup, usually called high-fructose syrup, is mainly produced either as HFCS42 (42% fructose) or as HFCS55 (55% fructose). For some purposes, syrup with more than 55% fructose, called higher-fructose syrup, is desirable. In any case, the objective is to transform a feed containing pure glucose to a stream where the glucose is partially converted to fructose.
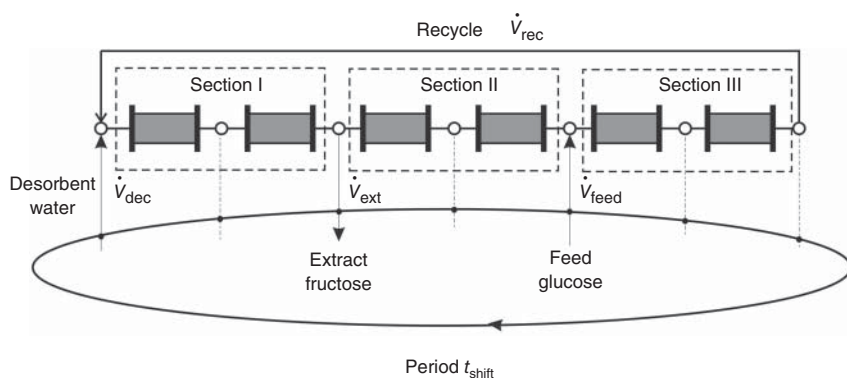
Figure 9.4 Three-section reactive SMB process for glucose isomerization.
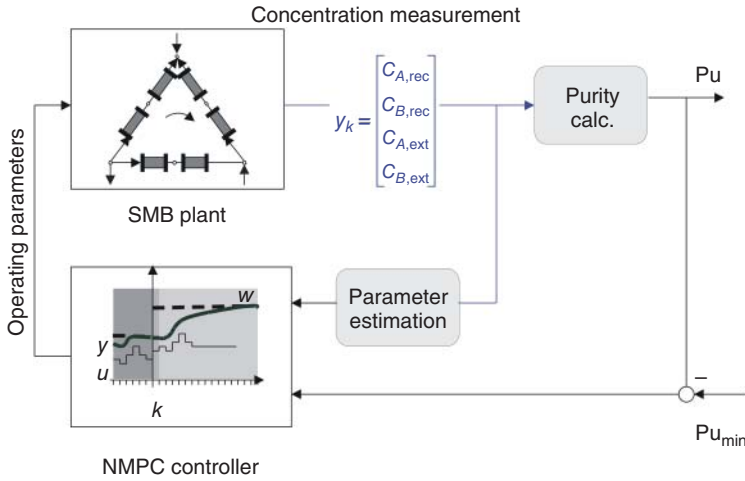
Figure 9.5 Online optimizing control structure.

Formulation of the Online Optimizing Controller A schematic representation of the optimizing controller is shown in Figure 9.5. As discussed above, the task of the controller is to optimize the performance of the process over a certain horizon in the future, the prediction horizon. The specifications of the product purities, the limitations of the equipment, and the dynamic process model (a full hybrid model of the process including the switching of the ports and a GRM of all columns) appear as constraints. The control algorithm solves the following nonlinear optimization problem online (Eq. (9.1)):

$$\min_{[\beta_k, \beta_{k+1}, \dots, \beta_{k+Hr}]} \Gamma = \sum_{i=k}^{k+H_\mathrm{p}} (\mathrm{Cost}(i) + \Delta\beta_i^\mathrm{T} \mathbf{R}_i \Delta\beta_i)$$

$$\text{subject to } 0 = \mathbf{f}(\dot{\mathbf{x}}_i, \mathbf{x}_i, \boldsymbol{\beta}_i, \mathbf{p}_i)$$

$$\frac{1}{H_\mathrm{r}} \sum_{j=k}^{k+H_\mathrm{r}} \mathrm{Pu}_{\mathrm{ext},j} + \Delta\mathrm{Pu}_{\mathrm{ext},i} \geq \mathrm{Pu}_{\mathrm{ext,min},i}$$

$$\frac{1}{H_\mathrm{p}} \sum_{j=k}^{k+H_\mathrm{p}} \mathrm{Pu}_{\mathrm{ext},j} + \Delta\mathrm{Pu}_{\mathrm{ext},i} \geq \mathrm{Pu}_{\mathrm{ext,min},i}$$

$$\dot{V}_\mathrm{I}^i \leq \dot{V}_{\max}$$

$$g(\boldsymbol{\beta}_i) \geq 0$$

$$i = k, (k+1), \dots, (k + H_\mathrm{p}) \tag{9.1}$$

The natural degrees of freedom of the process are the flow rates of desorbent $\dot{V}_{\mathrm{des}}$, $\dot{V}_{\mathrm{feed}}$, and recycle $\dot{V}_{\mathrm{IV}}$, and the switching period t_{shift}. However, this results in an ill-conditioned optimization problem. The numerical tractability is improved by introducing the so-called β-factors via a nonlinear transformation of the natural degrees of freedom (Eq. (9.2)):

$$\dot{V}_{\text{solid}} = \frac{1-\varepsilon}{V_s t_{\text{shift}}}, \quad \beta_1 = \frac{1}{H_A}\left(\frac{\dot{V}_I}{\dot{V}_{\text{solid}}} - \frac{1-\varepsilon}{\varepsilon}\right)$$

$$\beta_2 = \frac{1}{H_B}\left(\frac{\dot{V}_{II}}{\dot{V}_{\text{solid}}} - \frac{1-\varepsilon}{\varepsilon}\right), \quad \beta_3 = \frac{1}{H_A}\left(\frac{\dot{V}_{III}}{\dot{V}_{\text{solid}}} - \frac{1-\varepsilon}{\varepsilon}\right) \tag{9.2}$$

Here, $\dot{V}_{\text{solid}}$ is the apparent solid flow rate, and H_A and H_B describe the slopes of the adsorption isotherm, which are calculated in the nonlinear case by linearization of the adsorption isotherm for the feed concentration $c_{\text{feed},i}$. The prediction horizon is discretized in cycles, where a cycle is a switching time t_{shift} multiplied by the total number of columns. Equation (9.1) constitutes a dynamic optimization problem with the transient behavior of the process as a constraint. It describes the continuous dynamics of the columns based on the GRM as well as the discrete switching from period to period.

For the solution of the partial differential equation (PDE) models of the columns, a Galerkin method on finite elements is used for the liquid phase and orthogonal collocation for the solid phase. The switching of the node equations is considered explicitly, that is, a full hybrid plant model is used. The objective function Γ is the sum of the costs incurred for each cycle (e.g. the desorbent consumption) and a regularizing term that is added in order to smooth the input sequence in order to avoid high fluctuations of the inputs from cycle to cycle. The first equality constraint represents the plant model evaluated over the finite prediction horizon H_p. Since the maximal attainable pressure drop by the pumps must not be exceeded, constraints are imposed on the flow rates in section I. Further inequality constraints $g(\beta)$ are added in order to avoid negative flow rates during the optimization.

The objective to meet the product specifications is reflected by the purity constraint over the control horizon H_r that is corrected by a bias term $\delta\,\text{Pu}_{\text{ext}}$ resulting from the difference between the last simulated and the last measured process output to compensate unmodeled effects (Eq. (9.3)):

$$\Delta\text{Pu}_{\text{ext},i} = \text{Pu}_{\text{ext},(i-1),\text{meas}} - \text{Pu}_{\text{ext},(i-1)} \tag{9.3}$$

The second purity constraint over the whole prediction horizon acts as a terminal (stability) constraint forcing the process to converge toward the optimal cyclic steady state. The goal of feedback control in a standard control approach (i.e. to fulfill the extract purity) is introduced as a constraint here.

The concentration profiles in the recycle line are measured and collected during a cycle. Since this measurement point is fixed in the closed-loop arrangement, the sampled signal includes information from all three sections. During the start-up phase, an online estimation of the actual model parameters is started in every cycle. The quadratic cost functional (Eq. (9.4)) is minimized with respect to the parameter p. The model parameters are equal for all columns:

$$J_{\text{est}}(p) = \sum_{i=1}^{n_{\text{sp}}}\left(\int_0^{N_{\text{col}}} c_{i,\text{meas}}(t) - c_{i,Re}(t))^2 \mathrm{d}t\right) \tag{9.4}$$

For the prediction of the evolution of the process, the actual state (i.e. the concentration profiles over the columns) is needed. It is computed by simulation of

the process model using the measurements in the recycle line as input functions. As the model is adapted online, this is sufficiently accurate.

Experimental Study For experimental investigations, a LicoSEP 12–50 plant (Novasep, France) was used. An analysis based on the Fisher information matrix showed that the process model is highly sensitive to the values of the Henry coefficients, the mass transfer resistances, and the reaction rate. These parameters are therefore re-estimated online at every cycle. Figure 9.6 shows the evaluation of these parameters. In order to change the model parameters during process operation, the water temperature was reduced by 10 °C at the end of the sixth cycle. At the end of the experiment, all system parameters have converged toward stationary values as shown in Figure 9.6. The mathematical model thus describes the behavior of the simulated moving bed reactor (SMBR) process sufficiently well.

The desired purity for the experiment reported below was set to 55.0% and the controller was started at the 60th period. Figure 9.7 shows the evaluation of the product purity as well as of the controlled variables. In the open-loop mode where the operating point was calculated based on the initial model, the product purity was violated at periods 48 and 54. After one cycle, the controller drove the purity above 55.0% and kept it there. The controller first reduces the desorbent consumption. This action seems to be in contradiction to the intuitive idea that more desorbent injection should enhance the separation. In the presence of a reaction, this is not true, as shown by this experiment. The controlled variables converge toward a steady state, but they still change from period to period, due to the nonideality of the plant.
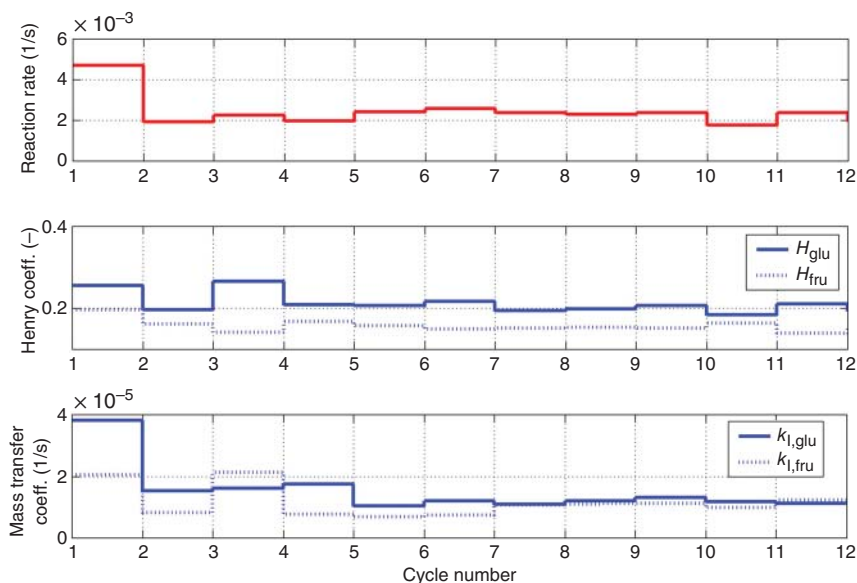
Figure 9.6 Evaluation of the estimated parameters. Source: Toumi and Engell (2004). Reproduced with permission of Elsevier.
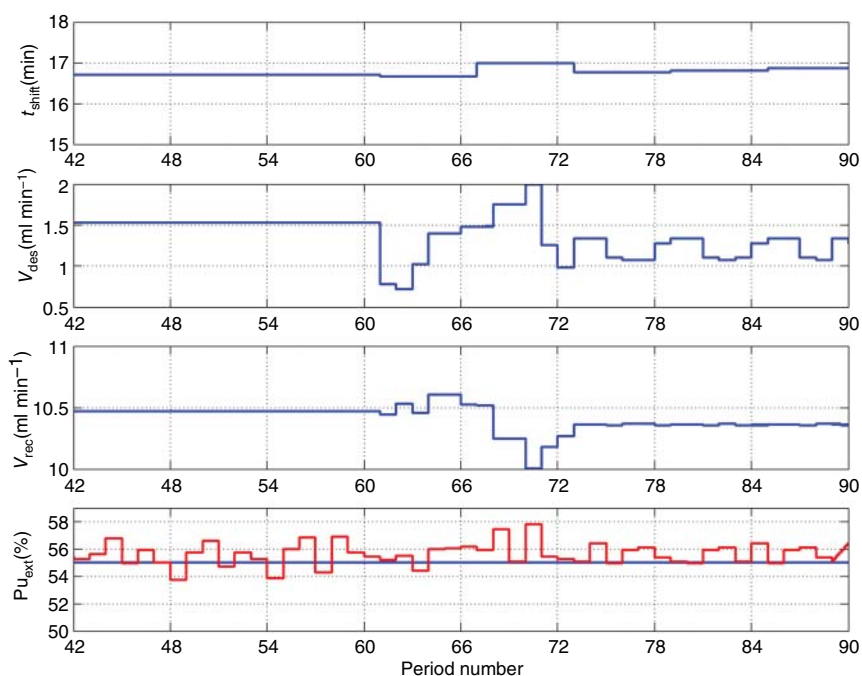
Figure 9.7 Experimental control result for glucose isomerization. Source: Toumi and Engell (2004). Reproduced with permission of Elsevier.

In the same spirit, Alamir, Ibrahim, and Corriou (2006) proposed an online optimizing controller that switches between different performance criteria.

The optimizing control scheme based on a rigorous nonlinear process model has been successfully applied also to the racemization of Troeger's base in a Hashimoto SMB process (Küpper and Engell 2007, 2009). For this process, simulation studies revealed that the optimal operation of the process with respect to the solvent consumption is a nonconventional one where the impurities in the extract stream result from an impure recycle stream. At this operation point it was observed that a parameter error of 5/10% in the Henry parameters leads to large discrepancies in the chromatograms that cannot be compensated by the usual bias correction scheme, whereas if the operation is constrained to the conventional operation mode, it can be controlled also in the presence of plant–model mismatch without problems (Küpper and Engell 2008), however at the expense of a significantly higher solvent consumption. The robustness of advanced control schemes continues to be a topic of ongoing research.

9.2.3 Advanced Parameter and State Estimation for SMB Processes

For monitoring and advanced control of SMB processes, the estimation of important column parameters and of the concentration profiles along the columns is needed. This problem is characterized by a large number of unknown variables (typically several hundred states, the discretized concentration profiles along

the columns, and some other parameters) and very scarce and time-varying measurement information. It has been demonstrated recently (Küpper et al. 2009, 2010) that the concentration profiles and the isotherms can be reconstructed from this measurement information using a moving horizon estimation scheme (Rao and Rawlings 2000). The estimation scheme works well also in the start-up phase of an SMB plant so that a coarse model can be improved online for use in the optimization of the operating conditions in the cyclic steady state. This work also showed that changes of the porosity and of the isotherms cannot be distinguished in practice. In this approach, uniform parameters of all columns are assumed. For monitoring of an SMB plant, information on the parameters of individual columns is desirable. A switched estimation scheme for state and parameter estimation for individual columns in an SMB plant that uses concentration measurements in the product streams, and one stream has been proposed in Küpper and Engell (2006). Figure 9.8 shows a simulation where one Henry parameter of one column was changed and the change was correctly identified by the switched estimation scheme. In Lemoine-Nava and Engell (2014), a similar scheme is suggested that only needs concentration measurement in the two product streams.
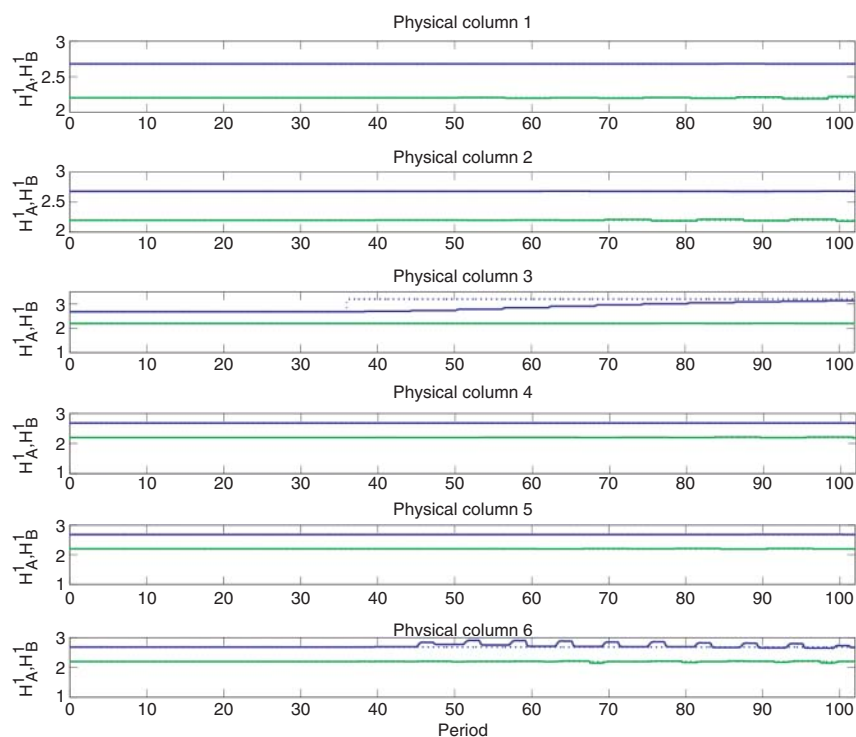
Figure 9.8 Reaction of the switched online parameter and state estimation scheme to a change in one Henry parameter of column 3. Source: Küpper and Engell (2006). Reproduced with permission of Elsevier.
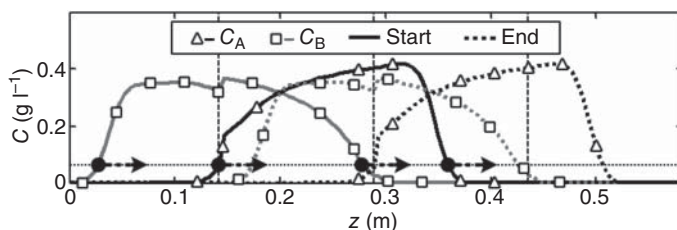
Figure 9.9 Moving concentration fronts in a four zone SMB plant. Solid lines represent the concentration at the beginning of the cycle. Dashed lines represent the concentration profiles at the end of the cycle. Source: Suvarov et al. (2016). Reproduced with permission of IFAC.

9.2.4 Adaptive Cycle-to-Cycle Control

The dynamics of SMB chromatographic processes is characterized by moving concentration fronts as illustrated in Figure 9.9. Based on the work of Fütterer (2010), these moving concentration fronts have been used to develop a simple cycle-to-cycle control strategy (Suvarov 2016; Suvarov et al. 2016). The control strategy consists of a parameter estimator and a controller. The parameter estimator determines recursively optimal operating conditions for total separation from retention time measurements using a simple footpoint model of the wave dynamics. It automatically accounts for dead volumes and degradation of the solid phase. Detailed knowledge of the adsorption isotherm is not required. The parameter estimator can therefore also be used for open-loop (re)adjustment of optimal operating conditions for total separation. Details are given in Suvarov et al. (2019) and Suvarov et al. (2016). The control law uses the estimated parameters for feedforward action and employs standard PI controllers for feedback to adjust the outlet purities to the given set points. In contrast to the more advanced concepts presented in Section 9.2.2.2, only suboptimal operation can be achieved for reduced product purities.

The cycle-to-cycle concept has been validated experimentally for the separation of bicalutamide enantiomers in methanol using Chiralpak ID as the stationary phase. First, focus was on the open-loop validation of the parameter estimator as illustrated in Figure 9.10a. Since the nonlinear adsorption isotherm was not available, the plant was started up with unsuitable operating parameters, which were calculated from the Henry coefficients and which were leading to a product purity in the raffinate of about 70%. In parallel the estimator determines the correct operating parameters leading theoretically to 100% purity according to the triangle theory (phase 1 in Figure 9.10a). Afterward, controllers for total regeneration in zones 1 and 4 as described in Suvarov (2016) and Suvarov et al. (2016) are activated (phase 2 in Figure 9.10a). To avoid breakthrough under nonideal conditions, safety margins are applied for m_1 and m_4. Finally, the estimated operating parameters for zones 2 and 3 are applied in two steps (phases 3 and 4 in Figure 9.10a) to the plant, yielding in fact a separation with high purity of both product streams. Finally, the switching time is reduced in phases 5 and 6 of Figure 9.10a to increase the throughput. The feed concentration for this experiment was high with $5\,\mathrm{g\,l^{-1}}$ for each component. Further experiments
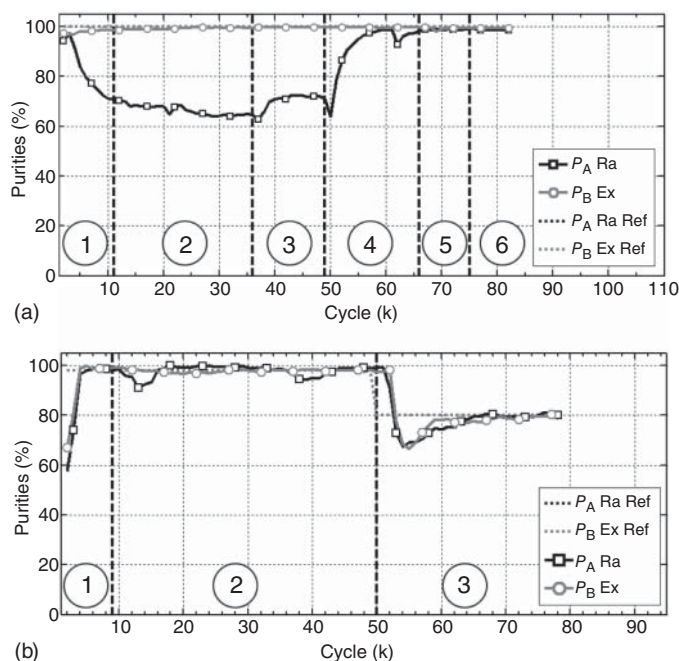
Figure 9.10 Experimental validation: (a) parameter estimator and (b) closed-loop control. $P_A \cdot$Ra – raffinate purity of component A, $P_B \cdot$Ex – extract purity of component B. Source: Suvarov (2016) and Suvarov et al. (2016). Reproduced with permission of Elsevier.

demonstrating close to optimal operation for total separation are reported in Suvarov et al. (2019).

The closed-loop behavior with feedback control as described above is illustrated in Figure 9.10b. The plant is started up with optimal operating conditions for total separation as determined by the parameter estimator (phase 1 in Figure 9.10b). Afterward, in phase 2 of Figure 9.10b, all four control loops are activated, and the reference value for both product purities is reduced to 80%. Within 10 cycles the new reference values are met by the controller with only small overshoot. The experiment in Figure 9.10b is for a relatively low feed concentration of $0.5\,\mathrm{g\,l^{-1}}$. In general, the sensitivity of the controlled variables to changes in purity requirements increases with increasing feed concentration. This is mainly due to an increased coupling between the control loops for high feed concentrations. Therefore, to further improve the performance for high feed concentrations, some decoupling or a centralized control algorithm can be applied.

At ETH the research teams of Morari, Morbidelli, and Mazzotti have modified their control scheme (see Section 9.2.2.2) also to a cycle-to-cycle control scheme where the control is based on averaged online high-performance liquid chromatography (HPLC) purity measurements that are available once per cycle (Grossmann et al. 2008, 2010a) and combined it with the previous scheme to a multirate controller that also uses UV measurements that are available at a much faster sampling rate (Grossmann et al. 2010b). Here, a simple model of the SMB

process is used, so the only needed model parameters are the Henry coefficients and the bed porosity. Despite the use of a quite simple model, processes with nonlinear isotherms can be controlled well over a significant range of operating conditions. Recently, the control scheme has also been applied to the multicolumn solvent gradient purification process (MCSGP process) (Grossmann et al. 2010c).

9.2.5 Control of Coupled Simulated Moving Bed Processes for the Production of Pure Enantiomers

Enantiomers play an important role in the pharmaceutical industry. They are stereoisomers with similar properties in an achiral environment but may have different physiological effects, which in turn motivates the production of pure enantiomers from racemic mixtures. For this purposes chiral SMB chromatographic processes can be applied (Lorenz and Seidel-Morgenstern 2014). The performance of these processes can be further improved by combination with crystallization and/or racemization processes (Kaspereit, Swernath, and Kienle 2012; Lorenz and Seidel-Morgenstern 2014) as illustrated in Figure 9.11.

Coupling with crystallization implies that the product purity requirements of the SMB plant can be relaxed, which can be used to increase the productivity (Lorenz, Sheehan, and Seidel-Morgenstern 2001). Coupling with racemization can be used to increase the yield of the desired enantiomer (Kaspereit, Swernath, and Kienle 2012). Ideally, in such a system, a racemic feed, i.e. a 50 : 50 mixture of both enantiomers, can be converted to 100% of the desired enantiomer, which is very attractive if the feed is valuable like in many pharmaceutical production processes.

Besides economic aspects, dynamics and operability are very important for a practical implementation of such process schemes. A characteristic feature of both continuous processes depicted in Figure 9.11 is the recycle of the undesired product fraction to the SMB plant. This recycle may lead to unfavorable dynamics as illustrated in Figure 9.12 for an SMB process with subsequent crystallization for different step changes of the feed concentration. Depending on the size of the disturbance, either crystallization of the undesired enantiomer or even instability in terms of oscillatory behavior is observed. To overcome this problem, feedback control can be applied. It was shown (Swernath, Kaspereit, and Kienle 2013) that a direct control of the SMB plant is not required for this setting. Instead, the additional degrees of freedom introduced by the crystallizer can be used for stabilizing and controlling the overall process. The solvent removal unit between the SMB unit and the crystallizer can be used for this purpose. The mass fraction of the undesired enantiomer in the mother liquor is used as the controlled variable, whereas the solvent removal rate is used as the manipulated variable. For the control algorithm, standard PI controllers were used. Results are illustrated in Figure 9.13 for the largest disturbance in Figure 9.12 of a +17.5% increase in feed concentration. It can be seen that closed-loop control is able to stabilize the process and to avoid the crystallization of undesired enantiomers.

A second important finding is that the pump configuration of the SMB plant, which is shown in Figure 9.11 for the extract recycle, has to be adapted for a
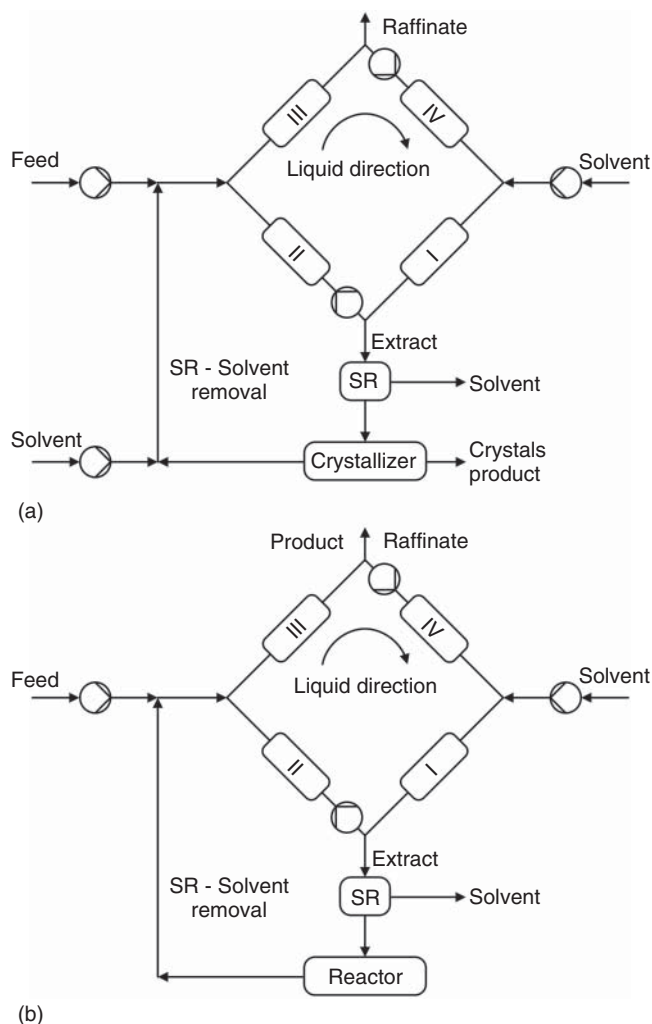
Figure 9.11 Simulated moving bed processes coupled with (a) crystallization and (b) racemization. Source: Swernath, Kaspereit, and Kienle (2013). Reproduced with permission of John Wiley and Sons. Source: Swernath, Kaspereit, and Kienle (2014). Reproduced with permission of John Wiley and Sons.

configuration with raffinate recycles, i.e. when the undesired enantiomer has a higher affinity to the solid phase. The pump configuration has to be modified in such a way that at least one flow rate in the recycle is fixed to avoid a high sensitivity of the flow rates to disturbances (Swernath, Kaspereit, and Kienle 2013).

A similar approach as outlined above for SMB + crystallization is possible for SMB + racemization if the desired product purity is not too high (Swernath, Kaspereit, and Kienle 2014). For SMB + racemization according to Figure 9.11b, the raffinate purity was selected as the controlled variable, and the solvent removal in front of the reactor was taken as the manipulated variable. However,
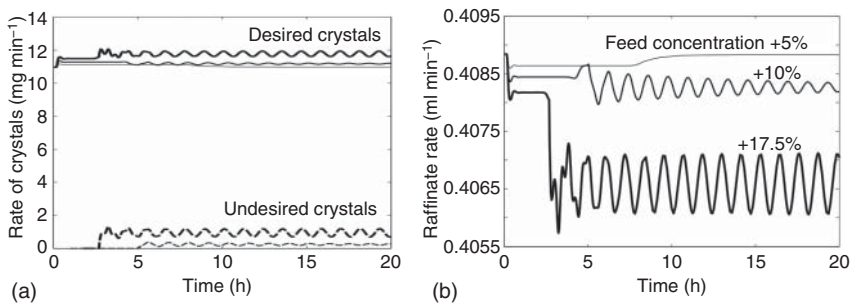
Figure 9.12 Dynamic responses to different step disturbances of the overall feed concentration for the process in Figure 9.11a. Source: Swernath, Kaspereit, and Kienle (2013). Reproduced with permission of John Wiley and Sons.
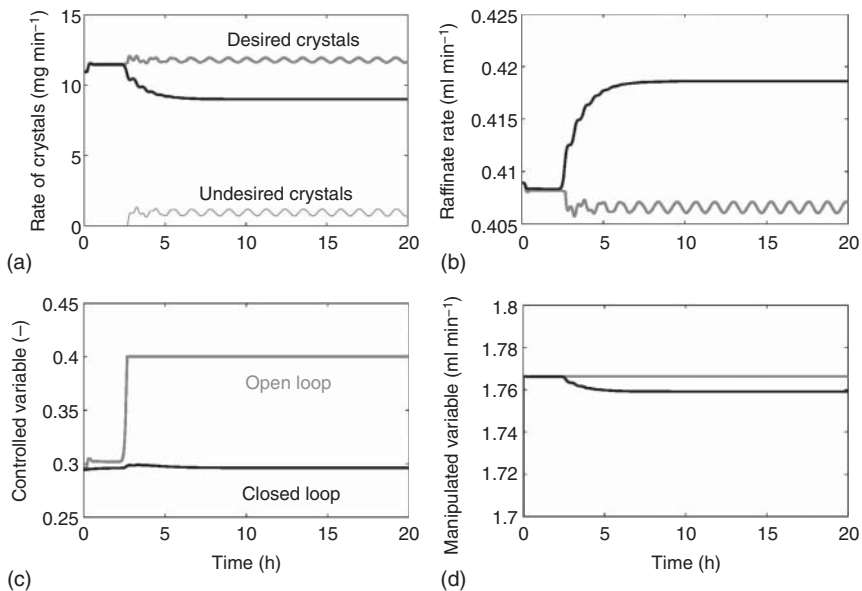
Figure 9.13 Open-loop (grey line) compared with closed-loop (black line) dynamics for the +17.5% disturbance of the overall feed concentration in Figure 9.12. Source: Swernath, Kaspereit, and Kienle (2013). Reproduced with permission of John Wiley and Sons.

this simple concept may fail for a high product purity of 99% in the case study presented in Swernath, Kaspereit, and Kienle (2014). For high product purities, more complex concepts are required, which also manipulate the operational variables of the SMB plant to achieve the overall specifications.

References

Alamir, M., Ibrahim, F., and Corriou, J.P. (2006). A flexible nonlinear model predictive control scheme for quality/performance handling in nonlinear SMB chromatography. *J. Process Control* 16: 333–344.

Antia, F. (2003). A simple approach to design and control of simulated moving bed chromatographs. *Chromatogr. Sci. Ser.* 88: 173–202.

Aström, K.J., and Hägglund, T. (1995). Automatic tuning of PID controllers. In: *The Control Handbook* (ed. William S. Levine), Chapter 52. IEEE/CRC Press.

Behrens, M. and Engell, S. (2011). Iterative set-point optimization of continuous annular electro-chromatography. In: *Proceedings of the 18th IFAC World Congress, Milano*, vol. 18, Part 1, pp. 3665–3671.

Cox, G., Khattabi, S., and Dapremont, O. (2003). Real-time monitoring and control of a small-scale SMB unit from a polarimeter-derived internal profile. In: *16th International Symposium on Preparative Chromatography, San Francisco, USA (29 June 2003 to 2 July 2003)*, pp. 41–42.

Engell, S. (2007). Feedback control for optimal process operation. *J. Process Control* 17: 203–219.

Engell, S. and Toumi, A. (2005). Optimisation and control of chromatography. *Comput. Chem. Eng.* 29: 1243–1252.

Erdem, G., Abel, S., Morari, M. et al. (2004). Automatic control of simulated moving beds. *Ind. Eng. Chem. Res.* 43: 405–421.

Fütterer, M. (2008). An adaptive control concept for simulated moving bed plants in case of complete separation. *Chem. Eng. Technol.* 31: 1438–1444.

Fütterer, M. (2010). On design and control of simulated moving bed processes. PhD. thesis. Otto-von-Guericke-Universität Magdeburg.

Gao, W. and Engell, S. (2005a). Iterative set-point optimization of batch chromatography. *Comput. Chem. Eng.* 29: 1401–1410.

Gao, W. and Engell, S. (2005b). Estimation of general nonlinear adsorption isotherms from chromatograms. *Comput. Chem. Eng.* 29: 2242–2255.

Grossmann, C., Erdem, G., Morari, M. et al. (2008). 'Cycle to cycle' optimizing control of simulated moving beds. *AICHE J.* 54: 194–208.

Grossmann, C., Langel, C., Morbidelli, M. et al. (2010a). Experimental implementation of automatic 'cycle to cycle' control to a nonlinear chiral SMB separation. *J. Chromatogr. A* 2117: 2013–2021.

Grossmann, C., Langel, C., Mazzotti, M. et al. (2010b). Multi-rate optimizing control of simulated moving beds. *J. Process Control* 20: 490–505.

Grossmann, C., Strohlein, G., Morari, M., and Morbidelli, M. (2010c). Optimizing model predictive control of the chromatographic multi-column solvent gradient purification (MCSGP) process. *J. Process Control* 20: 618–629.

Gu, T. (1995). *Mathematical Modelling and Scale Up of Liquid Chromatography*. New York, NY: Springer.

Hanisch, F. (2002). Prozessführung präparativer Chromatographieverfahren. Dr.-Ing. Dissertation. Universität Dortmund, Department of Biochemical and Chemical Engineering, Shaker-Verlag, Aachen (in Germany).

Juza, M. (1999). Development of a high-performance liquid chromatographic simulated moving bed separation form an industrial perspective. *J. Chromatogr. A* 865: 35–49.

Kaspereit, M., Swernath, S., and Kienle, A. (2012). Evaluation of competing process concepts for the production of pure enantiomers. *Org. Process. Res. Dev.* 16: 353–363.

Kim, K., Lee, K.S., and Lee, J.H. (2010a). Bilevel optimizing control structure for a simulated moving bed process based on a reduced-order model using the cubic spline collocation method. *Ind. Eng. Chem. Res.* 49: 3689–3699.

Kim, K., Kim, J.I., Kim, H. et al. (2010b). Experimental verification of bilevel optimizing control for SMB technology. *Ind. Eng. Chem. Res.* 49: 8593–8600.

Klatt, K.-U., Hanisch, F., Dünnebier, G., and Engell, S. (2000). Model-based optimization and control of chromatographic processes. *Comput. Chem. Eng.* 24: 1119–1126.

Klatt, K.-U., Hanisch, F., and Dünnebier, G. (2002). Model-based control of a simulated moving bed chromatographic process for the separation of fructose and glucose. *J. Process Control* 12: 203–219.

Kleinert, T. and Lunze, J. (2008). Decentralised control of chromatographic simulated moving bed processes based on wave front reconstruction. *J. Process Control* 18: 780–796.

Kloppenburg, E. and Gilles, E.D. (1999). Automatic control of the simulated moving bed process for C8 aromatics separation using asymptotically exact input/output linearization. *J. Process Control* 9: 41–50.

Krättli, M., Steinebach, F., and Morbidelli, M. (2013). Online control of the twin-column countercurrent solvent gradient process for biochromatography. *J. Chromatogr. A* 1293: 51–59.

Küpper, A. and Engell, S. (2006). Parameter and state estimation in chromatographic SMB processes with individual columns and nonlinear adsorption isotherms. In: *Proceedings of the IFAC Symposium ADCHEM, Gramado*, 611–616.

Küpper, A. and Engell, S. (2007). Optimizing control of the Hashimoto SMB process: experimental application. In: *Proceedings of the 8th International Symposium on Dynamics and Control of Process Systems (DYCOPS), Cancun*, –.

Küpper, A. and Engell, S. (2008). Engineering of online optimizing control – A case study: reactive SMB chromatography. In: *Proceedings of the 17th IFAC World Congress, Seoul*, 964–969, International Federation of Automatic Control.

Küpper, A. and Engell, S. (2009). Optimierungsbasierte Regelung des Hashimoto-SMB-Prozesses. *at-Automatisierungstechnik* 57: 360–370.

Küpper, A., Diehl, M., Schiöder, J. et al. (2009). Efficient moving horizon state and parameter estimation for SMB processes. *J. Process Control* 19: 785–802.

Küpper, A., Wirsching, L., Diehl, M. et al. (2010). Online identification of adsorption isotherms in SMB processes via efficient moving horizon state estimation. *Comput. Chem. Eng.* 34: 1969–1983.

Küsters, E., Gerber, G., and Antia, F. (1995). Enantioseparation of a chiral epoxide by simulated moving bed processes. *AICHE J.* 42: 154–160.

Lemoine-Nava, R. and Engell, S. (2014). Individual column state and parameter estimation in the simulated moving bed process: an optimization-based method. In: *Proceedings of the 18th IFAC World Congress, Cape Town*, 9376–9381, International Federation of Automatic Control.

Lorenz, H. and Seidel-Morgenstern, A. (2014). Processes to separate enantiomers. *Angew. Chem. Int. Ed.* 53: 1218–1250.

Lorenz, H., Sheehan, P., and Seidel-Morgenstern, A. (2001). Coupling simulated moving bed chromatography and fractional crystallization for efficient enantioseparation. *J. Chromatogr. A* 908: 201–214.

Marteau, P., Hotier, G., Zanier-Szydlowski, N. et al. (1994). Advanced control of C_8 aromatics separation process with real-time multiport on-line Raman spectroscopy. *Process Qual.* 6: 133–140.

Miller, L., Grill, C., Yan, T. et al. (2003). Batch and simulated moving bed chromatographic resolution of a pharmaceutical racemate. *J. Chromatogr. A* 1006: 267–280.

Natarajan, S. and Lee, J.H. (2000). Repetitive model predictive control applied to a simulated moving bed chromatography system. *Comput. Chem. Eng.* 24: 1127–1133.

Papathanasiou, M.M., Mantalaris, A., Steinebach, F. et al. (2016). Advanced control strategies for the multicolumn countercurrent solvent gradient purifiction process. *AICHE J.* 62: 2341–2357.

Qin, S. and Badgwell, T. (2003). A survey of industrial model predictive control technology. *Control. Eng. Pract.* 11: 733–764.

Rao, C. and Rawlings, J. (2000). Nonlinear moving horizon state estimation. In: *Progress in Systems and Control Theory*, vol. 26 (eds. F. Allgöwer and A. Zheng), 45–69. Basel/Switzerland: Birkhäuser-Verlag.

Schramm, H., Grüner, S., Kienle, A., and Gilles, E.D. (2001). Control of moving bed chromatographic processes. In: *Proceedings of the European Control Conference*, 2528–2533.

Schramm, H., Grüner, S., and Kienle, A. (2003). Optimal operation of simulated moving bed processes by means of simple feedback control. *J. Chromatogr. A* 1006: 3–13.

Song, I.H., Lee, S.B., Rhee, H.K., and Mazzotti, M. (2006). Identification and predictive control of a simulated moving bed process: purity control. *Chem. Eng. Sci.* 61: 1973–1986.

Suvarov, P. (2016). Robust control methods for simulated moving bed chromatographic processes. PhD Thesis. Otto-von-Guericke-Universität Magdeburg & University of Mons (Cotutelle).

Suvarov, P., Vande Wouwer, A., Lee, J.-W. et al. (2016). Control of incomplete separation in simulated moving bed chromatographic processes. In Proceedings of the 11th IFAC Symposium on Dynamics and Control of Process Systems, including Biosystems, Trondheim, June 6-8. *IFAC-PapersOnLine* 49 (7): 153–158.

Suvarov, P., Lee, J.-W., Vande Wouwer, A. et al. (2019). Online estimation of optimal operating conditions for simulated moving bed chromatographic processes. *J. Chromatogr.* https://doi.org/10.1016/j.chroma.2019.05.042.

Swernath, S., Kaspereit, M., and Kienle, A. (2013). Dynamics and control of coupled continuous chromatography and crystallization processes for the production of pure enantiomers. *Chem. Eng. Technol.* 36: 1417–1429.

Swernath, S., Kaspereit, M., and Kienle, A. (2014). Coupled continuous chromatography and racemization processes for the production of pure enantiomers. *Chem. Eng. Technol.* 37: 643–651.

Toumi, A. and Engell, S. (2004). Optimization-based control of a reactive simulated moving bed process for glucose isomerisation. *Chem. Eng. Sci.* 59: 3777–3792.

Vilas, C. and Van de Wouwer, A. (2011). Combination of multi-model predictive control and the wave theory for the control of simulated moving bed plants. *Chem. Eng. Sci.* 66: 632–641.

Wang, C., Klatt, K., Dünnebier, G. et al. (2003). Neural network based identification of SMB chromatographic processes. *Control. Eng. Pract.* 11: 949–959.

Ziegler, J.G. and Nichols, N.B. (1942). Optimum settings for automatic controllers. *Trans. ASME* 64: 759–768.

10

Chromatography Equipment: Engineering and Operation*

Henner Schmidt-Traub[1] and Arthur Susanto[2]

[1]TU Dortmund, Fakultät für Bio- und Chemieingenieurwesen, Lehrstuhl für Anlagen- und Prozesstechnik, Emil-Figge-Str. 70, 44227 Dortmund,, Germany
[2]Bayer AG, Product Supply Pharmaceuticals, PH8 DSP Process Specialist, 42117 Wuppertal, Germany

The previous chapters describe how to select a chromatographic system for a given task, followed by modeling and simulation to find out optimal process conditions and design parameters. The final task is to realize a plant, which meet the process requirements including the design and operating parameters for the chromatographic separation. During the first step an optimal process configuration, which takes into account additional equipment like tanks for buffer, cleaning and regeneration as well as filters has to be evaluated. The conceptual process design assesses different process scenarios; this involves time schedules for batch and continuous operations, resulting mass balances as well as sizes of auxiliary equipment, and an overall cost estimation. When the process scenario is fixed, block flow diagrams and piping and instrumentation diagrams (PIDs) have to be developed, which adds valves, pipes, and fittings as well as control instruments. Finally, the 3D plant layout is worked out for the existing building. So far, a classical work flow as in chemical industries; but in addition to this, bioburden contamination and cross-contamination need to be avoided in pharmaceutical production plants. Furthermore, the quality of chromatographic separations depends on conformance with important construction details and manufacturing guidelines. For example, dead legs have to be reduced or avoided, improper pipe construction may lead to undesirable cross-contamination, pipe length is affecting residence times and insufficient frit design worsens the flow distribution in a column. Other objectives are operability of the plant and the compliance with resin regeneration, cleaning and storage procedures.

10.1 Challenges for Conceptual Process Design

Chromatographic processes are typically developed in the laboratory with milligram quantities of product, and this is the case for the majority of drug

---

*The following authors Abdelaziz Toumi, Jules Dingenen, Joel Genolet, Olivier Ludemann-Hombourger, Andre Kiesewetter, Martin Krahe, Michele Morelli, Andreas Stein, and Eric Valery have contributed to the first and/or second edition.

substances. Purely chemically synthesized products could start at a larger scale. However, for regulated applications a current good manufacturing practice (cGMP) at pilot-scale will be needed to produce many tens of kilograms or even tons per batch before commercial launch. Production facilities for pharmaceutical applications are often designed before the drug achieves full commercial approval, so this will occur in parallel to the second and third phases of clinical investigations. This is mainly due to the fact that qualification and validation processes, especially those involving the automation systems, require substantial time to complete.

The starting point for process design is often a small-scale example or a laboratory recipe of the worst-case scenario. All available information has to be collected and used as basis for the first step of process design, which defines the different process sequences and specifies all boundary conditions, like binding capacity of the resin, filtrate throughput of a given membrane, and reactor concentration (titer) in biotechnological applications. Next, a first attempt is made to size the equipment (reactors, product vessels, chromatography columns, solvent/buffer vessels).

The scale-up of manufacturing processes can be divided into a number of stages (Aldington and Bonnerjea 2007). In some organizations, this is formalized in a kind of manufacturability reviews that correspond to the project moving from one department to the next, for example, from research to process development, from process development to pilot plant, and from pilot plant to large-scale manufacturing. The desired outcomes of the final large-scale manufacturing have to be kept firmly in mind even for the early research phase. This is the reason why many manufacturers and associated equipment suppliers tend to standardize a manufacturing platform to cope with the whole cycle from early development until large-scale manufacturing, that is, lab- and pilot-scale plants represent already the different process steps of the intended large-scale production plant. It might be also that no one size fits all existing solutions and one has to distinguish between two different platforms like an early clinical platform and a large-scale platform. Both platforms do not necessarily have the same objectives. While in early clinical phase, the major objective is time, costs become more relevant for a large-scale facility. The main challenge here is how to cope with the different objectives and assure at the same time scalable and compatible processes when you move from one platform to the next.

For the large-scale manufacturing, production costs have to be minimized. The use of large volumes of buffer at a slow flow rate to wash a chromatography column or the use of chemicals that cannot be routed to the wastewater treatment plant has to be avoided. Thus, process optimization is essential and often goes hand-in-hand with process scale-up.

Multipurpose flexibility is another major requirement for process engineering. Nowadays, plants are not built just for one single product; they have to cope rather with a certain variety of products. Some of the major multipurpose considerations are straightforward, for example the use of chromatographic resins that are chemically and physically robust and easy to clean to prevent product cross-contamination. There are other issues that are less obvious and have to be considered early in the research activities, like the use of full traceable cell lines

and the use of endotoxin-free components supplied with certificates of analysis (Aldington and Bonnerjea 2007).

10.1.1 Main Cost Factors for a Chromatographic System

Economics is a driving force in general chromatography separations to minimize waste and input materials and to maximize output. For many years, it could be debated as to whether upstream or downstream operations were rate-limiting steps within a bioprocess. Now, with fermentation titers or product concentrations rising inexorably, purification is likely to remain rate limiting, for a given facility layout.

In pharmaceutical or biotechnological separations chromatography steps make about half of the purification costs, that is approximately 30% of the total manufacturing cost. This increases with the further concentration of the product. In other sectors, this factor is not so accentuated but still the operation cost of chromatography steps are relatively high compared to other separation processes.

Chromatography costs are dependent on following major aspects:

- *Hardware cost*: The cost of the equipment depends upon its installed cost amortized over its lifetime, which will generally range from 3 to 10 years. Hardware costs are determined by the design of the chromatography system. They depend on the material type used for the construction (e.g. stainless steel type), the instrumentation, and the valve design (e.g. sanitary valve design).
- *Stationary phase cost*: With the increase of titers in fermentation processes and the increasing complexity of purification task, suppliers of the stationary phase always work to increase the performances of their phases.

  Protein A or other immunoaffinity sorbents used in capture steps within the purification process of biologics are typically the most expensive; but have also seen the most improvement with time. To decrease costs, the lifetime of media has to be increased while keeping the adsorption characteristics.

  The lifetime of a stationary phase in small molecule purification strongly depends on the type of crude material that has to be purified. In general, the current spherical phases (bare silica, C8, C18, cyano, diol, amino, etc.) based on purified metal-free silica have a very good mechanical as well as a long-term chemical stability if they are used under the appropriate conditions. For example, on production scale, a cyano-modified silica stationary phase could be kept in the same column for about four years allowing to purify multi-ton quantities of product.

  Chiral stationary phases, chemically grafted on a silica matrix, can also be used for quite a long period. The same holds true for the very versatile physically coated cellulose and amylose phases if they are treated with care.
- *Mobile phase cost*: Solvent, salts, and water (especially highly purified water [HPW] and water for injection [WFI] typically in bioprocesses) could have a big impact on the purification costs. Similarly, in small molecule purification, solvent cost is a very important cost factor and requires an intensive investigation regarding solvent recovery and reuse.

  It is also important not only to consider the consumption of buffer solutions during the chromatographic process steps, but also to consider the cost of

cleaning and storage solutions. At the end of product elution chromatographic columns need to be regenerated/stripped (e.g. with high salt concentration for ion-exchange resin) to remove bound impurities on the column and to put the resin once again into the same condition as at the beginning of the process. Both the chromatographic column and equipment need to be sanitized (e.g. with caustic solution) to prevent the accumulation of microbial contamination. In multi-purpose plants or when the idle time between purification batches is relatively long, the column and equipment must be stored in a storage solution. Often the storage solution for columns and equipment are different, because columns are usually stored in bacteriostatic solutions whereas the equipment is stored in bacteriostatic solutions, which preferably also have chemical passivation effect to prevent corrosion.

Furthermore, some specific organic solvents, for example, acetonitrile, can strongly influence the cost of a chromatography process: In large-scale preparative reversed phase (RP) chromatography, an alcohol is preferentially used as the organic modifier in the mobile phase, although in some cases the use of acetonitrile is required to obtain the desired solubility or selectivity. Trends are going toward the usage of semi continuous process steps like the simulated moving bed (SMB) technology as well as recycling technology.

- *Single-use material cost*: Typically, in a bioprocess, many single-use materials (i.e. disposables, Section 10.7) are used to minimize the risk of microbial contamination and cross-contamination, thus also reducing time and material for cleaning/sanitization of the chromatographic system. These single-use materials include, e.g. C-flex-hose, sanitary connectors (Lynx-connector, Steam-thru-connector, etc.), 0.2 μm filters. Some commercial chromatography systems even use single-use materials for all product contacting surfaces. The application of single-use materials represents a cost reduction regarding cleaning procedure (time and material), but it also increases input material cost significantly, thus it has to be evaluated carefully.

10.1.2 Conceptual Process Design

During the conceptual design phase, it is common to create many possible process design scenarios, evaluate them, and finally compare them using an objective function. In many cases, cost of goods (COGs) is used as an objective function considering all cost types. However, it is also often desirable to use an objective function, which unites both quantitative factors (e.g. costs) as well as qualitative factors (e.g. risk of contamination, risk of handling error, etc.). In such cases, a weighting coefficient (based on criticality/priority) for each evaluated factor must be agreed upon with all stakeholders, e.g. production team, engineering team and quality unit. The design of a chromatography system has to consider, but not limited to, following criteria:

- costs
- space and layout requirements;
- required auxiliary equipment like recycling units or process analytical technology (PAT) instrumentation;

- packing and unpacking units for chromatography columns;
- the level of automation integration required;
- the amount of single-use materials used in the equipment;
- the risk of microbial contamination and cross-contamination;
- batch versus continuous process.

Conceptual design of chromatography equipment is not a stand-alone exercise and often needs to consider the whole plant design, as dependencies between the different process steps and bottlenecks in utilities system might affect the size of the equipment. Due to the necessity to consider the whole plant design combined with a great number of possible process scenarios, the conceptual design can become very complex and tedious. Therefore, to enable the evaluation of all process scenarios with sensible effort, the complexity of mathematical process models for each unit operation should be kept low. Considering total mass balance or component balance with rough estimation of separation factor is generally sufficient, thus avoiding the necessity for additional calculation of complex thermodynamic phase equilibrium.

Discrete event simulation software (e.g. SuperPro & SchedulePro from Intelligen Inc., Inosim) can be used for this purpose. Although the model complexity in that software is generally limited to short-cut models, such software packages are versatile and powerful tools. They enable the calculation and analysis of complex production schedules (e.g. bottleneck identification) with event-triggered alternative branches, for example: the execution of additional cleaning procedures prior to production start when clean equipment hold time is exceeded. They also allow to analyze the impact of the probabilistic occurrence of an event, like the impact of the maintenance (regularly planned event) or the breakdown (irregular event) of a process unit on plant capacity.

10.1.2.1 A Case Study: Large-Scale Biotechnology Project

The objective of a large-scale biotech project was to extend (double) the production capacity at an existing manufacturing site of Merck Serono in Vevey, Switzerland. The plant was initially dedicated to the parallel production of two different molecules, a monoclonal antibody (mAb) and a fusion protein. Additional mAbs and related molecules from the Merck Serono pipeline were expected to be manufactured in the same facility. The limited space available for the construction of the new facility made the design very challenging and the project highly complex. A computerized process model built in SuperPro Designer has been developed in a very early stage of the basic design phase of the project to support all design activities and facilitate scenario analysis and evaluation (Toumi et al. 2010).

Three chromatography steps were used: a Protein A binding step, a flow-through step, and a hydrophobic interaction step (Figure 10.1). Such processes utilize a large number of buffer and cleaning solutions (usually 20–30) that must be prepared on time and be ready for delivery when required by the main process. The preparation and storage of such buffers involve a large number of tanks (Figure 10.2). Most of the tanks are used for the preparation and storage of multiple solutions and require cleaning and validation of cleanliness after
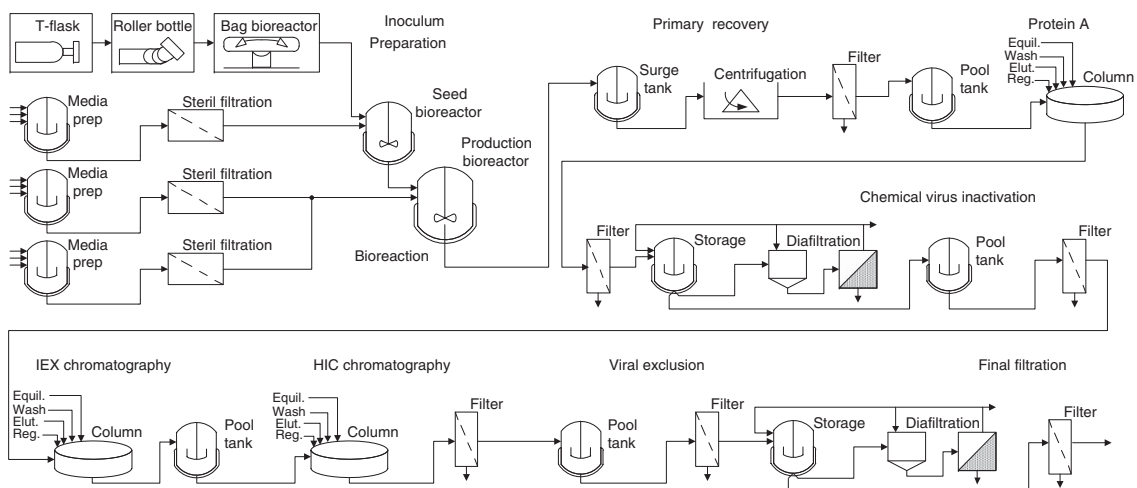
Figure 10.1 Principle of monoclonal antibody production. Source: Reproduced from Toumi et al. (2010).

Figure 10.2 Buffer tanks and plant space requirement in a typical biotech facility.

each use. For every chromatographic step, a list of operational steps was defined according to Table 10.1 and was introduced into a mathematical model.

The results of process scheduling and cycle time analysis are typically visualized with Gantt charts that display equipment occupancy as a function of time. These types of charts enable engineers to resolve scheduling conflicts and reduce the cycle time of a process.

The models were mainly used to size shared resources (e.g. chromatography columns, utilities, and media/buffer preparation tanks) and evaluate various capacity scenarios. The impact of different shift patterns on equipment demand for buffer preparation was also evaluated. Using such tools makes it easier to quantify the trade-off between labor cost and capital investment. The model was able to generate different options based on different work organizations. For example, two options were explored:

(1) buffers are prepared 24 hours a day/7 days a week;
(2) buffers prepared only during the day shifts.

Option 2 involves lower labor cost but higher capital investment. However, it also provides flexibility for future changes in increased plant operation and capacity challenges. More specifically, if product titers increase in the future and there is a need for reduced purification cycle times, the plant may switch to a three-shift operation for buffer preparation and accommodate the increased demands of the purification trains.

The tools also were used to analyze the impact of buffer expiration times, shift patterns, equipment sizes, and number of equipment items. Approximately, 35 different scenarios were evaluated during the project and most of the scenarios included major model updates. As the project evolved, the team's understanding of the processes, the facility, the underlying links, and constraints improved and the knowledge gain was used to improve the models. Figure 10.3 shows the evolution of the models up to scenario no. 15.

It can be summarized that when applied early, simulation tools can support plant design and technology transfer and can facilitate the communication

Table 10.1 Modeling of a chromatographic step (Toumi et al. 2010).

	Chromatographic sequences				Capture					
Step	Description	No.	Buffer	Column volume	Total volume per cycle (l)	Cycle (S, start; E, end)	Number of cycles required	Flow rate (l min⁻¹)	Linear flow rate (cm h⁻¹)	Processing time (min)
1	Rinse I	W1	HPW	2.0	420	S	1	50.9	270	8.3
2	Equilibrium			0.0	0	S	1	0.2	1	0.0
3	Regeneration I			0.0	0	S	1	0.2	1	0.0
4	Equilibration	E1	PPAEB	5.0	1050	S–E	2	71.6	380	14.7
5	Load	Pr	Product	N/A	8098	S–E	2	71.6	380	113.0
6	Wash I	E1	PPAEB	5.0	1050	S–E	2	71.6	380	14.7
7	Wash II	E1	PPAEB	5.0	1050	S–E	2	71.6	380	14.7
8	Wash III			00	0	S–E	2	0.2	1	0.0
9	Elution	E7	PPAEB	4.0	840	S–E	2	50.9	270	16.5
10	Regeneration	E6	Acetic acid	2.0	420	S–E	2	50.9	270	8.3
11	Regeneration 1	E11	0.1 M NaOH	2.0	420	E	1	12.3	65	34.3
12	Regeneration 2	E6	Acetic acid	2.0	420	E	1	12.3	65	34.3
13	Regeneration 3	W1	HPW	1.0	210	E	1	33.0	175	6.4
14	Storage	E10	PPAEB	2.0	420	E	1	33.0	175	12.7

PPAEB, POROS protein A equilibrium buffer; HPW, highly purified water.
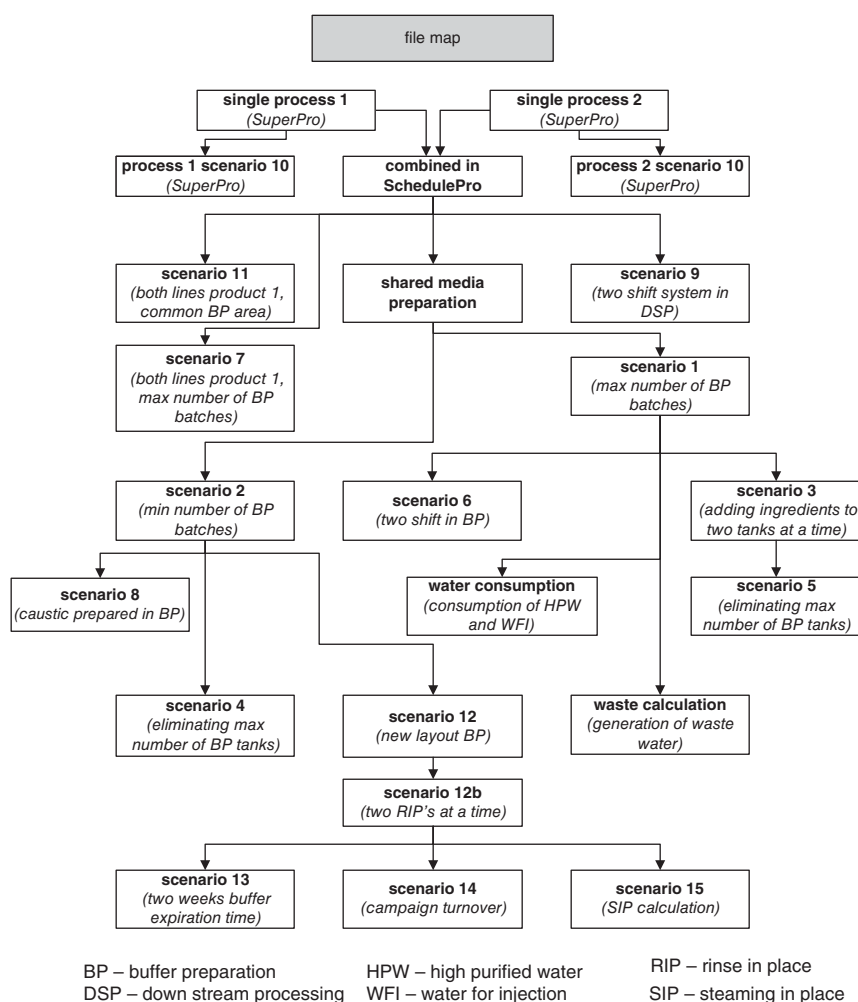
Figure 10.3 Different scenarios of a large-scale biotech project. Source: Reproduced from Toumi et al. (2010).

between the engineering and operations teams. It is an important engineering tool to have the ability to design the proper size of the chromatographic steps (column diameter and piping skid size). The insight that modeling provided for the design of the support areas, such as buffer preparation and holding, utilities, and equipment cleaning requirements, was of particular importance.

10.2 Engineering Challenges

After it was decided to move on with the most promising process scenario, it is time to put more details into the process concept. Generally, the engineering challenges start with specifying the right requirements for the equipment design and

performance. Those requirements are summarized in so-called user requirement specification (URS) and have to be chosen wisely. An unwisely chosen requirement, especially in the early engineering phase, will cause a lot of troubles in the later phase, which will, e.g. make the specification of acceptance criteria during equipment qualification very difficult, or even make the construction of the equipment impossible. A correction of unwisely chosen requirement in the later project phase can take a lot of labor and consume a great deal of budget.

The specification of proper requirements for the equipment design and performance can be supported by creating risk assessments, in which the perspectives of production team, engineering team and quality unit are put together. During risk assessments, all possible failure modes are discussed and evaluated together by:

- assessing the impact severity on product quality (or safety);
- identifying the possible causes;
- determining the risk mitigation measures for each possible cause;
- assessing the effect of risk mitigation measures (e.g. how often can this failure occur, how soon can it be detected, etc.);
- adding new mitigation measures if current measures are not enough.

In pharmaceutical industries, risk assessments are considered to be a central basis document which defines the necessity of every single process feature or measure in the production plant. They are life-cycle documents, which need to be updated regularly even later during running production, so the rationale of every process change can be understood and implemented properly. Risk assessments are divided into two different documents: quality risk assessment (considers all failure modes, which could have impact on product quality including also microbial and cross-contamination risk) and safety risk assessment (considers safety hazards for operators, environment and equipment).

Knowing and understanding the possible failure risks will contribute greatly to the process understanding. In addition, this knowledge will support us to determine the proper equipment design suitable for a specific purification task. Following topics (and more) should be discussed during the quality and safety risk assessments:

- *Measuring devices*: What are the critical process parameters? What kind of device do we need to measure them? What is the necessary measurement range and accuracy?
- *Safety measures*: What is the design pressure and temperature of each component? Where are the weak spots? What are the preventive and corrective actions?
- *Control loops*: Which process parameter needs to be set during process? Which device can measure this parameter? Which component can be controlled and has impact on this parameter?
- *Alarms and interlocks*: How big is the operating range? How severe is the impact on product quality or safety? What kind of action should be taken in case of range violation? How is the failsafe state of the equipment? Is it necessary to define different failsafe states depending on the events?

- *Sanitary design* (more about this in Section 10.2.1): Are the tubing gradients designed correctly and venting positions sufficiently available so the equipment is completely drainable? Where are the dead legs? Can dead legs be minimized or avoided by sanitary design? If not, can the flow path of the cleaning solution be directed through them? Can we use single-use articles (e.g. single-use connectors)?
- *Material type*: Is the type of stainless steel compatible with the mobile phase (e.g. high salt buffers, corrosive mobile phase)? Is it also suitable for the applied cleaning solutions (for internal as well as for external surfaces)? Is the type of elastomer compatible in case of steam sanitization? Does it have the necessary certificates (e.g. United States Pharmacopoeia (USP) Class VI, animal derivative ingredients (ADI) free free)? Are there any filling liquids in the equipment components, which could leak into the product space?
- *Utilities*: What Utilities are required for the operation (e.g. cooling/heating medium, instrument air, etc.)? What are their specifications (e.g. temperature and pressure range)?
- *Cleaning solution*: What kind of and how many cleaning solutions do you need? Are they compatible with the construction material? Is the supply line for cleaning solution connected permanently to the chromatographic equipment? What are the technical measures to avoid contamination with product? Would you prefer temporary supply line (i.e. by hoses)?
- *Maintenance*: Are the components easily accessible? What should be done during maintenance? Do you have to disassemble the instrument for calibration?
- *Ergonomic*: Which part of the equipment has to be disassembled regularly? How heavy is it? Is there any instrument, which is not connected to the distributed control system (DCS), i.e. manual reading necessary? Is it easily accessible?

10.2.1 Challenges Regarding Sanitary Design

The impact and severity of contamination from the environment and cross-contamination should be discussed in quality risk assessment. Depending on the results of that discussion it must be decided, what kind of countermeasure is necessary and must be implemented to the equipment design. The following bullet points are meant as guidance and examples from biopharmaceutical manufacturing:

- *Closed or functionally-closed process design*: Although it is possible to design the chromatography equipment with fully hard-piped connections to all peripheral equipment (e.g. feed and eluate tank, buffer supply, utilities), in most cases (especially in biopharmaceutical manufacturing) it is desirable to apply single-use materials (Section 10.7) in several sections of the chromatographic equipment, usually single-use connectors, hoses, and filters. This creates the necessity to replace those single-use materials frequently thus opening the product-contact area at the end of the chromatographic process. A process sequence must be added to drain the chromatographic equipment and then after the replacement to clean the equipment as well as the part of

the newly installed single-use connectors, which are not gamma-sterilized by the manufacturer. The realization of the closed or functionally closed process can also be a challenge for the process control. The process must be continuously monitored to avoid contact with the environment and only to allow it prior to cleaning procedures or if the equipment pressure is greater than the environment. This continuous monitoring must also be applied for the operation of bubble traps, in which venting should be allowed only when the pump is also running. Furthermore, in accidental breach events due to triggered pressure safety valve or rupture disc all inlet and outlet valves should be closed and all pumps should be stopped (so-called hold position). The chromatographic equipment should remain in hold position until the root-cause for the breach is found.

- *Drainability and steam sanitization*: Make sure to design the tubing with sufficient gradient in the direction of drain outlet or steam trap, which is located in the lowest position of the equipment. Furthermore, a sufficient number of venting positions should be designed at several high positions to improve the drainability. If the chromatographic equipment needs to be steam sanitized, the drainable design will also support proper flow of steam condensate to the direction of steam trap and prevent condensate accumulation in the tubing section, thus also preventing the formation of cold spots.

- *Pressure safety valve or rupture disc*: Chromatography equipment are a pressure equipment. Thus it is necessary to place pressure safety valves or rupture discs as a safety precaution in strategic places (e.g. generally between the pump(s) and column inlet) to protect the equipment against accidental high pressure. However, it is also critical to be able to detect it when a pressure safety valve is triggered or a rupture disc bursts, because this represents a breach into the supposedly closed process space and thus a product contamination risk. The position sensor in the safety valve or wire sensor at the rupture disc generally detects such an event. However, be aware that those sensors are not 100% foolproof. The position sensor cannot detect a relatively small movement of the valve and the wire sensor cannot detect a hairline rupture. If necessary, the risk of undetected breach can be mitigated by placing the end of the vent line from pressure safety valves/rupture discs not directly over the drain, but somewhere on the floor but outside of walking space, so that spills can be detected by operators as an evidence of system breach.

- *Dead legs*: Dead legs represent dead zones in tubing with no sufficient liquid exchange during rinse. Thus, they are a source of microbial- or cross-contamination or even unnecessary product dilution due to residual liquid within them. Possible dead legs can be identified by measuring the ratio between length to diameter L/D of the tubing branch outside of the flow path (see Figure 10.4). According to American Society of Mechnical Engineers (ASME) BPE 2016 L/D-ratio should be kept lower than 6.0. However, depending on the risk of contamination, it is generally desirable to have L/D-ratio lower than 2.0. Dead legs can be avoided or reduced by:
  - Placing T-branches in vertical tubings rather than horizontal.
  - Low/zero deadleg T-valve or multi-port valve design. Hereby, the valve body and branches are shaped from one metal block, thus eliminating the necessity to leave some spaces for welding the tubings together.

Figure 10.4 Definition of *L/D* ratio according to ASME BPE.
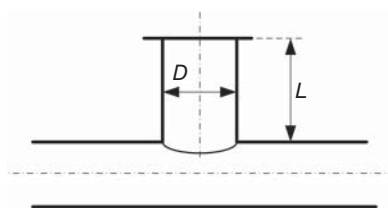
– Using instrument-tee. Installing pressure gauges can be tricky, because pressure gauges need sufficient measurement area to be precise, which is difficult to realize if the tubing size is relatively small (e.g. <$1\frac{1}{2}$ in.). An instrument tee represents a local expansion of the tubing diameter (see Figure 10.5a).

– Using inline diaphragm seal. A circular inline diaphragm seal (Figure 10.5b) can also be used for pressure gauges instead of instrument-tees. Since the inline diaphragm is placed at the circumference of the tubing, a local expansion of the tubing diameter is not necessary, thus eliminating the dead flow zone.

In case dead legs cannot be avoided, make sure to direct the cleaning solution flow path through them and introduce priming sequences in your process to flush the dead zone with the same buffer used in the next process step.

● *Separation of process space from supply line for cleaning solution*: In the pharmaceutical and biotechnology industry, it is often desirable to reduce the risk of cross-contamination further by placing an air gap between the supply line for cleaning solution and the product-contact area in the equipment tubing. This can be done by using double block and bleed valve configurations

(a)

(b)
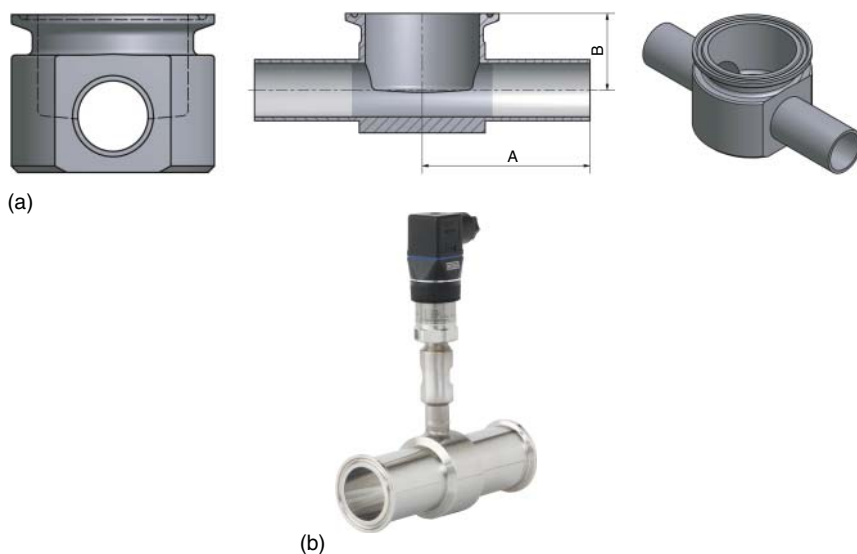
Figure 10.5 (a) Instrument tee. Source: Reproduced with permission of Dockweiler AG. (b) Inline diaphragm seal with sterile connection and pressure transmitter. Source: Reproduced with permission of WIKA Alexander Wiegand SE & Co. KG.
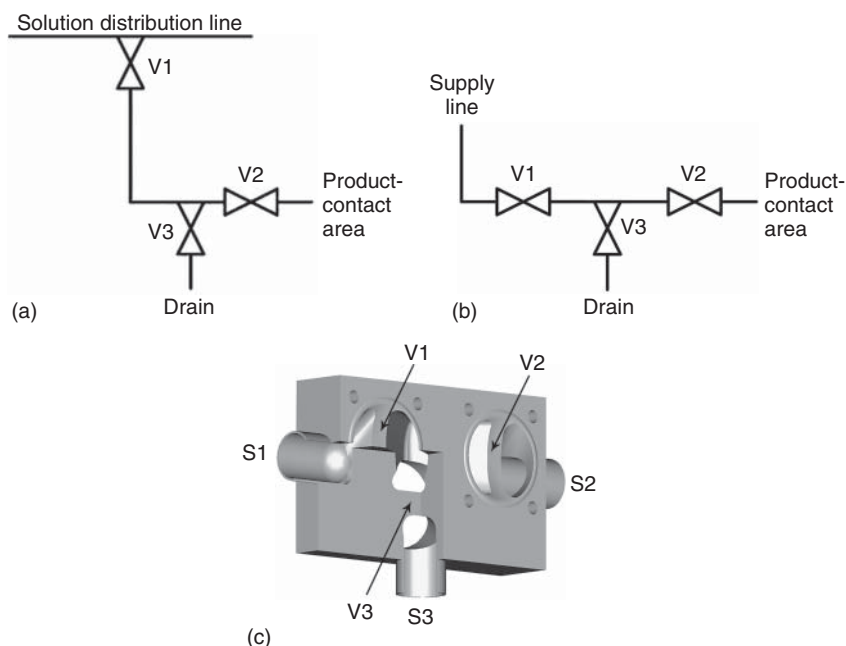
Figure 10.6 Double block and bleed concept: (a) separation from distribution line, (b) separation from simple supply line, and (c) as multiport valve with one valve body and minimum dead leg. Source: Reproduced with permission of GEMÜ GmbH & Co. KG).

(see Figure 10.6). A bleed valve is closed in the supply mode, but opened in the idle mode to drain the tubing content between both block valves. Thus, in case of defective valves the leaking solution shall not contaminate the product-contact area but will be discarded through the bleed line. The "double-block-and-bleed" concept can be realized by simply using three separate valves, or by uniting those three valves into one multi-port valve.

- *Design of buffer and cleaning solution inlets*: Buffer and cleaning solution inlets (aka buffer header) are generally designed as straight tubings with many inlet branches leading to the pump and product-contact area. Thus, buffer headers should be designed with minimal dead legs to avoid cross-contamination of the buffer solutions. This can be critical when the inlets of two buffer solutions with different chemical properties (e.g. pH, conductivity) are placed closely beside each other. In case of cross-contamination a residual amount of a buffer solution is carried over in the next flush step (in worst case undetected), which creates the necessity to prime the flush flow path thoroughly between each step thus increasing the buffer demand. Furthermore, the location of the solution inlets should be considered carefully. In downstream direction, the correct inlet sequence should be from the least sensitive to the most sensitive solution, which means: cleaning solutions at the beginning, followed by process buffers, and feed inlet as last inlet. It can be recommended to separate the mentioned three sections of the buffer header with an isolation valve to further mitigate the cross-contamination issue (see Figure 10.7).
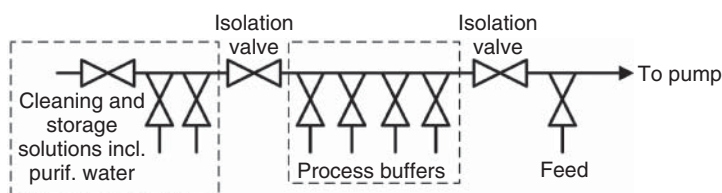
Figure 10.7 Inlet sequence at the buffer header including isolation valves.

10.2.2 Challenges During Acceptance Tests and Qualifications

It is also very important not only to think about the chromatographic process itself during routine production but also to think about how to test the fabricated chromatographic equipment whether it meets the specified requirements or not, because this can be a problem during acceptance tests (Factory resp. Site Acceptance Test, FAT/SAT) or during equipment qualification. This issue could be challenging and its solution will require thinking ahead during the detailed engineering phase. Generally, the solution of this issue can be summarized as to create the specification carefully by thinking ahead and not only to copy the process from product development and not only to think what is best for the process. The following bullet points are meant to be suggestions and examples:

- *Identify specifications, which might exceed the technical limitation*: Simply said, avoid making specifications, which might get us into troubles later. This might sound easy, but it requires strategic planning and good understanding of the process. Good examples are specifications regarding flow rate, temperature, pressure or other measurement range. Be very careful when they are specified far beyond the necessary process requirement, so-called "nice-to-have" specifications. It would also be wise not to consider them individually but in combination; e.g. what is the flow rate range under operating condition at a certain temperature and at a certain pressure.
  Another example is the specification of maximum allowable tubing dead legs. It is recommended not to specify L/D ratio too tightly but to allow a suitable range due to geometrical limitation or due to space requirements for welding activity.
  Sometimes a technical specification can be eliminated by creating a workaround. For example, in a biopharmaceutical process there might be a requirement that pH of the mobile phase (i.e. buffer solutions) must be within a tight operating range. The simplest solution is, of course, to have an on-line pH measurement in the equipment design. However, designing a robust on-line pH measurement could be challenging and will increase the operational and maintenance effort, thus on-line pH measurement is usually omitted. In that case, suitable sampling positions can be added in the equipment design to enable the operator to take sample and measure the pH using benchtop pH meter. It is, however, also worthwhile to think about deleting the requirement that the chromatographic equipment should be responsible for checking the compliance of pH operating range. This task can be taken over by operator during buffer solution release, thus guaranteeing that all solutions

entering the chromatographic equipment are within the specified operating limits. On the other hand, it might be necessary to consider additional flush sequences to mitigate the risk of having residual acid or caustic inside the equipment. Such technical measures will guarantee that the pH of all solutions entering the chromatographic column complies with the specified limits even without an on-line pH measurement.

- *Consider sufficient number of spool pieces/removable components*: Usually a sanitary design will require the fully drainability of the chromatographic equipment. If the chromatographic equipment is designed only with a few tubing flanges/clamps, it would be very challenging to proof that there is no significant liquid drop left after draining the equipment. Thus, make sure to put flanges/clamps on "risky" spots (e.g. low points, tubing section with only shallow tubing gradient), so the tubing can be easily dismantled during acceptance tests or qualifications to check for significant liquid drop after draining. Furthermore, a sufficient number of removable components will make the equipment maintenance easier, since some components might require "off-line" check (e.g. pressure relieve valve) or calibration (e.g. conductivity sensor).
- *Consider sufficient number of sampling positions*: Another example is the proof of successful cleaning. Hereby, sampling positions have to be defined and planed in the chromatography equipment to check for remaining contamination within one section of the equipment. Make sure to plan sampling positions not only for the routine production, but also additional positions for cleaning validation. If only one sampling position at the end of the flow path through the equipment is designed, then it might be challenging to pinpoint the source of contamination in case a contamination is identified in the collected cleaning sample. In case a particular sampling position is not needed anymore for the routine production, it can be designed as a spool piece (e.g. a removable tubing section) which can be easily replaced by a sampling valve (e.g. a zero deadleg T-valve) during cleaning validation.

10.3 Commercial Chromatography Columns

When discussing columns, several items should be addressed: the column technology, the column design, the packing material, and the packing procedure. Particular emphasis is put on the column because this is a most critical part of the equipment. However, the column is just one critical aspect of chromatography purification. A good column associated with a poorly designed pumping and auxiliary unit is often worth nothing.

The design of the commercial columns has to be optimized for the chromatographic technique to be used. For instance, the pressure and protocols to pack successfully and robustly middle- or low-pressure media are quite different. In the end, the operating condition of the column determines the design of the chromatographic system, for example, if it is a high-or low-pressure system. Here important differences due to size of the solute molecules, thermodynamics,

and the mass transfer resistance have to be realized. For liquid chromatography, the challenges for separating fine chemicals and other low-weight molecules or biopolymers with molecular weights (MWs) ranging from several thousand to several million Daltons are quite different. Stationary phases and appropriate chromatographic systems for these different separation tasks are explained in Chapters 3 and 4. One dominating factor for column design is the diffusivity that is by a factor of 100 or smaller for proteins than for small molecules. Consequently, biopolymers need much more time to diffuse into and out of the pores and the linear velocity of the eluent in the column has to be about 100 times lower in order to achieve a sufficient separation (Unger et al. 2010). Comparing high performance liquid chromatography (HPLC) chromatography with low-pressure liquid chromatography (LPLC) can be summarized by considering kinetics of diffusions of molecules on the stationary phase. On HPLC, particle size is smaller and diffusion is elevated, therefore, elevated mobile phase flow rates are applied while the separation is still very efficient (HP means high performance) but generates pressure (explaining that many consider that HP means high pressure). Column length is fine-tuned in both chromatographic regimes regarding pressure constraints and kinetic effects, 10 and 20 cm bed length columns can be found at industrial scale for HPLC and LPLC applications.

In the following discussion, it is considered that a preparative column is a column with an internal diameter exceeding 50 mm. This is obviously an arbitrary limit but it is more or less the maximum diameter of commercially available prepacked columns.

Equipment used for preparative and large size biochromatography is very different compared to the equipment used for fine chemicals and pharmaceutically active small molecules. Biological separations are mostly using high concentration of salts and there are some specific aspects of the equipment for such separations. Today companies like General Electric, Pall, Novasep, and Merck Millipore have developed different technologies. These columns are often used at high flow rates (200–1000 cm h^{-1}) in order to maximize productivity and or minimize purifications costs.

The purpose of this chapter is to discuss equipment for preparative chromatography in general and to outline additionally aspects that are typical for the separation of fine chemicals and low-molecular-weight products as well as the separation of biopolymers like proteins.

10.3.1 General Design

What is the main purpose of a chromatography column? This question can be answered in several ways:

- contain the media;
- provide uniform plug flow;
- minimize band broadening;
- withstand pressure;
- compatible materials (solvent/chemical);
- scalable performance;

- facilitate packing/unpacking;
- meet regulatory compliance needs;
- allow cleaning in place (CIP).

Today we can find different established column designs. Concurrent technologies exist to lower and upper the piston like hydraulic pumps, manual moving, or an electrical motor. The different designs have different drawbacks and advantages, but have to obey the following criteria:

- *Reproducibility*: complex standard working procedure may impact reproducibility and operators may also require specific training;
- *Operator interaction and safety*: column manipulation, contact with media, and GMP;
- *Plant constraint*: size-floor space, compatibility with solvent/chemicals, pressure vessels, ex-proof for explosive solvents.

Chromatography columns have three basic components:

- *Top flow cell assembly*: distributes flow evenly across the bed;
- *Column tube unit*: houses the media;
- *Bottom flow cell assembly*: retains media, collects effluent flows.

10.3.1.1 Manually Moved Piston

Generally used on columns packed with low-pressure media, this technology could be applied on columns up to 600 mm. One of the advantages of this system is the reduction of column cost because the use of automated technology is limited. This kind of system is often used in the biotechnology field for column packed with low-pressure bed, which does not require high pressure for packing.

10.3.1.2 Electrically or Hydraulically Moved Piston

In terms of column technology, there is a consensus today that the best (and probably only) feasible approach at any size is dynamic axial compression (DAC; Section 10.5.5). The piston can be driven by a hydraulic jacket, or pushed by a liquid, by a spring, or by an electrical motor. Radial compression is an alternative but it does not seem to be available at (very) large column diameter sizes. It also requires the use of prepacked cartridges, thus reducing the operator's freedom compared to DAC. Under appropriate conditions, the DAC technology ensures bed stability and reproducible performance. DAC can be scaled-up to very large size with remarkable reproducibility in performance. This has been verified with columns up to 1600 mm internal diameter.

When fragile and/or soft packing media are used, special care must be taken to ensure that the compression energy is compatible with the mechanical properties of the particles. In addition, the shrinking–swelling phenomena observed with some organic materials under certain mobile phase conditions should not result in over-compressed beds. To address this issue, columns with an "intelligent" piston are available. With such columns, a given bed compression can be programmed and the hydraulic system is able to adjust the piston position so that a constant compression is maintained.

In terms of column technology, another special situation is encountered in supercritical fluid chromatography (SFC). Here, rather elevated pressures must be used in order to attain the supercritical state. The fluid pressure in the column varies a lot, depending on whether the column is in use or not. The effective pressure exerted by the piston on the bed is the difference between the compression pressure and the fluid pressure under the piston. The compression pressure should then be adjusted depending on the internal pressure of the column, since too high a piston pressure may crush the stationary phase, whereas a too low pressure may prevent the piston from effectively compressing the bed. It seems that only DAC columns are suitable for large-scale SFC. These columns are, for example, equipped with "smart" compression units that maintain adequate bed compression without allowing the packing material to be overpressurized when the mobile phase pressure is released. Alternatively, it is also possible to use for SFC a specifically designed DAC column equipped with high-pressure valves in the two lines of the hydraulic oil circuit, which are closed during normal use of the column. After the process is finished and the gas pressure has been released from the column, the valves in the oil circuit can be opened and the oil pump activated to compensate for an eventually created void volume during the process. Thereafter, both valves are closed again and the column is ready for further use.

10.3.2 High- and Low-Pressure Columns

Stainless steel, glass, and plastic materials (cross-linked organic polymers) are employed as tube materials. Usually stainless steel is used for high-pressure columns. The stainless steel tubes have a mirror finish inside with a surface roughness smaller than 1 μm. The column material should be mechanically stable toward high flow rates and high pressure and chemically resistant toward aggressive eluents. Table 10.2 gives for certain columns dimensions an overview of typical flow rates and maximum allowable pressure drops. If stainless steel is used for biopharmaceuticals' separations, it is recommended that only high quality stainless steel be used to avoid any problems related due to corrosion of the metal from the use of salts in biotechnology processing. Usually stainless steel 316L (stainless steel with low ferrite ratio) is used and the inside of the column has a mirror finished (electro-polishing) with a surface roughness of approximately 0.6 μm. In any case, the construction materials for biopharmaceutical separations have to conform to relevant regulations (Section 10.4.2).

For biopharmaceutical separation, we can also find glass or plastic material (cross-linked polymers like acrylic). Table 10.3 gives typical dimensions and operating pressures of glass and large-scale acrylic columns for low-pressure bioseparations or intermediate purifications that are characterized by a height to diameter ratio < 1, therefore, these columns are sometimes called "pancake" columns.

Construction materials for columns can be chosen according to several attributes; Table 10.4 shows an example of selecting criteria for the most common materials.

Table 10.2 Typical dimensions and operation conditions for stainless steel columns.

Type of column	Column dimensions $L_c \times d_c$ (mm)	Flow rate range (ml min^{-1})	Max. pressure drop (bar)
Preparative	100×20	20–40	300
	300×50	100–200	200
Large scale	300×100	500–1 000	150
	200×300	8 000–12 000	100
	100×600	32 000–48 000	70
	100×1000	80 000–130 000	50

Table 10.3 Typical dimensions and operating conditions for acrylic and glass columns (Chromaflow, BGP™).

Material	Diameter (mm)	Height (mm)	Max. operating pressure (bar)
Acryl	400, 600, …, 2000	100–300	3
Glass	100	50–95	8
Glass	140	50–95	6
Glass	200	50–95	6
Glass	296	50–95	4
Glass	446	50–100	2.5

Source: GE Health Care (2011). Reproduced with permission of John Wiley and Sons.

Table 10.4 Construction materials and selecting attribute for chromatography columns.

Material	Visibility	Solvent/salt resistance	Pressure resistance	A-specific binding
Acrylic	Transparent	High salt	High pressure	Some binding
Glassyx	Transparent	Solvent and salt resistant	Pressure/size limits	Some binding
TPX, poly-methylpentene	Transparent	Solvent and salt resistant	High pressure	Low protein binding
Stainless steel	Not transparent	Solvent resistant, salt resistant, limited low pH	High pressure	Low protein binding

10.3.2.1 Chemical Compatibility

Table 10.5 illustrates the chemical resistance of a series of columns materials across a range of organic solvents and chemical solutions. This list is not exhaustive; the column supplier should provide any detailed information regarding the column's compatibility to a particular solution.

Table 10.5 Construction materials and selecting attribute for chromatography columns.

Solvent	Acrylic	Glass	TPX	Stainless steel 904L (1.4509)	Stainless steel 316L (1.4404)	20% class filled polypropylene	Polypropylene	EPDM	Santoprene™	PTFE	PVC
1,2-Dichloroethane	−	+		+	+	+	+	L	−	+	+
Acetic acid 89%	−	+	−	+	+	+	+	+	+	+	−
Acetic acid 25%	+	+	+	+	+	+	+	+	+	+	−
Acetone 2%	+	+	+	+	+	+	+	+	+	+	−
Acetone 5%	+	+	+	+	+	+	+	+	+	+	−
Acetone 10%	+	+	+	+	+	+	+	+	+	+	−
Acetone 100%	−	+	L	+	+	+	+	+	−	+	−
Acetonitrile	−	+	L	+	+	+	+	+	L	+	−
Acrylonitrile	−	+	−	+	+	+	+	−	+	+	−
Ammonia aqueous <25%	+	+	+	+	+	+	+	+	+	+	+
Ammonium sulfate (10–40%)	+	+	+	+	+	+	+	+	+	+	+
Amyl alcohol (1-pentanol)	−	+	L	+	+	+	+	+	L	+	+
Aniline	−	+	−	+	+	+	+	+	+	+	−
Beer	+	+	+	+	+	+	+	+	L	+	+
Benzaldehyde	−	+	+	+	+	+	+	+	+	+	−
Benzene	−	+	−	+	+	+	+	−	−	+	−
Benzoic acid	−	+	+	+	+	+	+	−	+	+	+
Benzyl alcohol 1%	+	+	+	+	+	+	+	+	N/A	+	L

L, low; N/A, not available.
Source: Courtesy of Merck-Millipore.
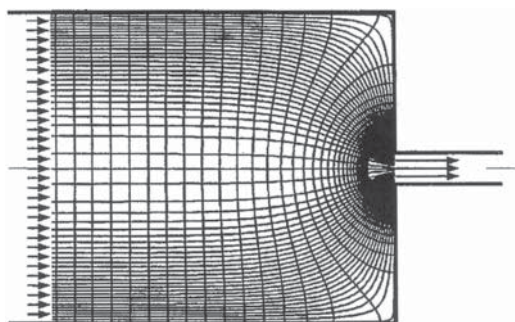
Figure 10.8 Isobars and streamlines for a cylindrical column outlet.

10.3.2.2 Frit Design

Band broadening and thus the quality of chromatographic separations depends on axial dispersion within the column. Apart from the fluid flow through the packing, axial dispersion is mainly influenced by the inlet and outlet of the column where the liquid should enter or leave, respectively, the column as a plug flow. Quite obviously, the bigger the column diameter the more severe the problems of equal distribution and collection are, for example, with a flow coming from a 2 mm tube diameter into a column with a diameter of more than 1000 mm and collecting the effluent again in a 2 mm tube (Figure 10.8). To optimize the fluid flow in a chromatographic column, several attempts have been made with regard to the fluid distributor and collector systems and the shape of the column tube itself.

The easiest means of fluid distribution at the column inlet is by using a high-pressure drop of the packed bed, which forces the fluid inside the inlet frit into the radial dimension (Figure 10.9).

The layer design of the frits and the quality of the radial flow characteristics of the frit are of great importance to obtain a good distribution. Distribution by using the column pressure drop has nevertheless a severe drawback: every HPLC plant should be designed to show the lowest possible system pressure drop (i.e., to allow the maximum linear velocity with a given maximum pressure drop). Therefore, efficient pressure-less distribution systems had to be designed. One approach is the integration of distribution plates into the column inlet. Nowadays, their design is optimized by computational fluid dynamics (CFD), as shown by Boysen et al. (2002). The most advanced approach uses distribution channels with engineered fractal geometries as an alternative to random-free turbulence (Kearney 1999, 2000).

The homogeneity of flow distribution for LPLC columns depends on the flow cell design; the objective is to have the fluid reaching the top of the resin at the same time. Geometric modeling of flow cells has shown that concaved flow cell design provides constant velocity along the flow cell radius (Figure 10.10).

Standard and engineered columns feature removable frit plates for easy replacement, in order to cleaning purpose or product change. Frit plates are available within a range of material and frit pore sizes from 2 to 75 μm. The materials used could be plastic (polymeric) or metal.
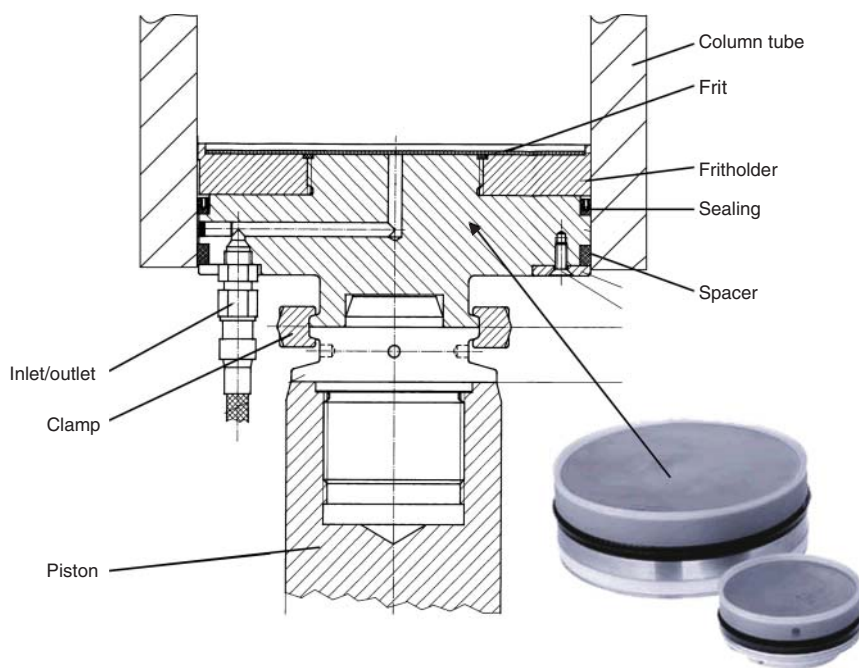
Figure 10.9 Cross section of a column inlet with frit system.

Stainless steel bed supports are used extensively in standard and engineered chromatography columns. In contrast with hydrophobic polyethylene sinters, they are easily "wetted." The multilayer woven mesh construction offers high porosity and mechanical strength, it may in many cases be cleaned of media particles mechanically or by ultrasonic means. However, all stainless steel products are susceptible to corrosion when in prolonged contact with chloride-containing solutions and especially at low pH.

In general, properly passivated mesh of Deutsches Institut für Normung (DIN) grade 1.4404 (approximately equivalent to type 316L) is suitable for prolonged immersion in 2 M sodium chloride solution at neutral pH and at ambient temperature (approximately 20 °C).

Typical cleaning procedures are:

- NaOH 0.5–2 M soaking solution contact time 24 hours;
- ultrasonic bath (refer to http://www.southern-metal.com);
- passivation (refer to http://www.poligrat.de).

In biochromatography, flow distribution of commercial packed beds is challenging as diameters are often in the order of 1.0–2.0 m while bed heights are around 0.2 m leading to rather low H/D ratios. Johnson, Natarajan, and Antoniou (2014) investigated two headers of commercial size (1.4 m) by experiments and CFD simulation. A "flat" header has four inlets and utilizes anti-jets at the inlet while the "ribbed" design has a single central entrance with radial oriented
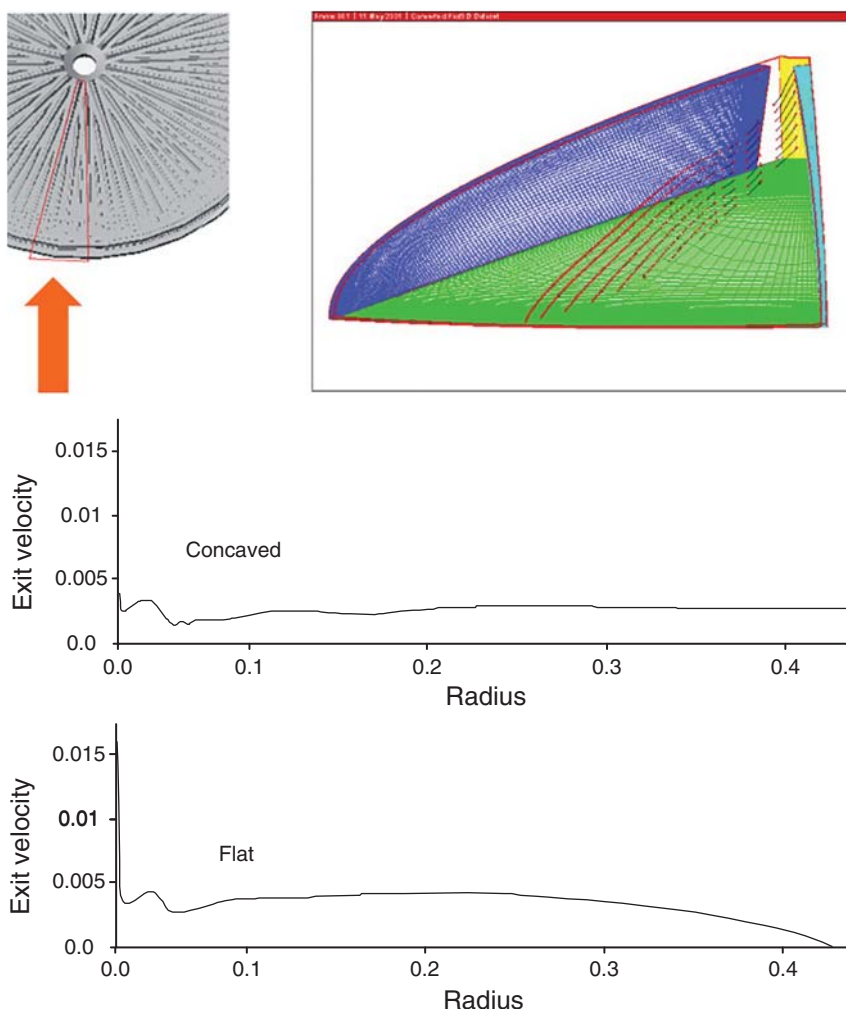
Figure 10.10 Flow cell geometry design and impact on exit velocity.

channels. Experimental and simulated dye traces are in very good agreement. A comparison of both headers result in a lower quality of the "flat" design because of a more uneven flow distribution represented by a higher *A*-term of the van Deemter equation (2.24) (Section 2.2.3). Figure 10.11 illustrates the effect of these differences by tracer transition profiles at the column outlet(s). The "ribbed" design converges closer to the ideal plug flow profile and achieves 99% saturation at the outlet after 1.32 column volume (CV) while the "flat" design needs 1.5 CV.

Differences of viscosity between the mobile phase and the sample may also influence the flow distribution. As Shalliker, Broyles, and Guiochon (1999) point out, nothing except sample dilution will prevent viscous fingering from
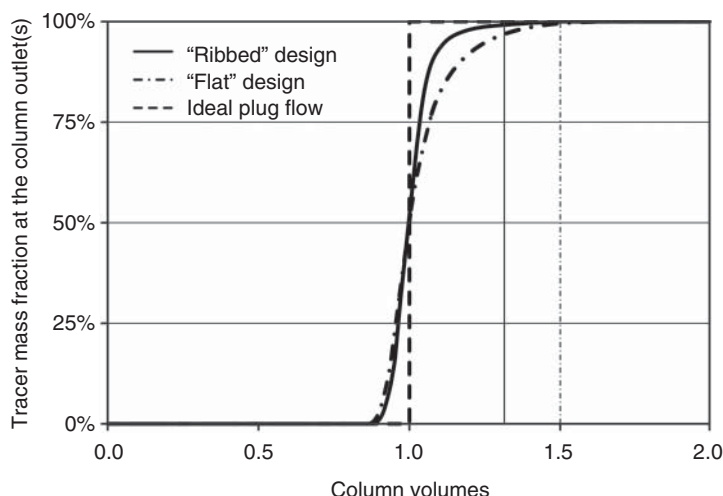
Figure 10.11 Tracer transition profiles at the column outlet(s) obtained with a "ribbed" and a "flat" design. Source: Johnson, Natarajan, and Antoniou (2014). Reproduced with permission of John Wiley and Sons.

occurring if the viscosities are sufficient different. Due to their experiments, even an appropriate frit design was not able to prevent fingering.

10.3.2.3 Special Aspects of Bioseparation

Biomolecular separation requires different techniques than the separation of small synthetic molecules. Biological molecules are sensible to heat and solvents, which can destabilize the three-dimensional structure of proteins resulting in loss of the molecule's function (Carta and Jungbauer 2010).

Protein Binding Most materials used in the manufacturing of chromatographic columns exhibit some degree of nonspecific protein binding. In the purification of biological products, it is of paramount importance for regulatory compliance that equipment suppliers provide experimental investigation data to such binding and show that the levels involved are very low and the bound protein can be efficiently removed by a cleaning-in-place (CIP) wash with a sodium hydroxide solution.

Table 10.6 gives some basic information on protein binding for common column construction materials.

Sanitary Design and Sanitization Sanitary design is necessary to ensure hygienic performance and thorough cleaning; standard column attributes to minimize bacterial contamination are listed below:

- Fully flushed flow path and adjuster seal for CIP;
- Minimum dead space for seal arrangements;
- Reduced risk of corrosion;
- Leachable free tube material;
- Minimize unswept areas in flow path.

Table 10.6 Protein binding for construction materials.

Material	Protein (mg cm^{-2})
Borosilicate glass	0.030
Polypropylene	0.027
TPX (polymethylpentene)	0.009
Acetal	0.030
Stainless steel	0.001
Acrylic (Perspex)	0.012
Santoprene	0.023
EPDM	0.032
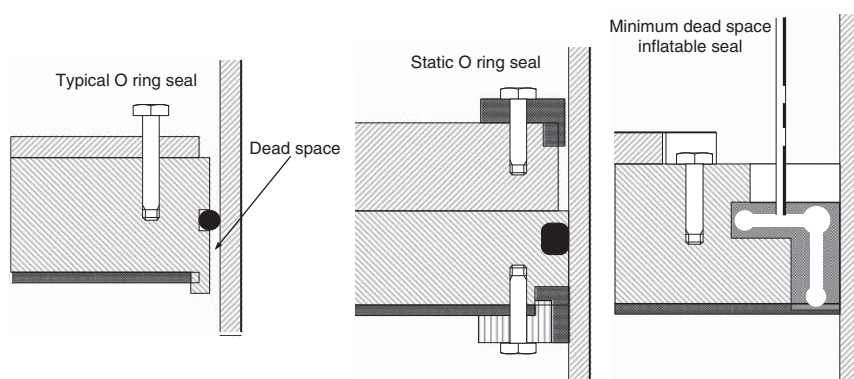
Figure 10.12 Hygienic criteria for pharmaceutical applications.

Figure 10.12 depicts design principles for equipment seals with minimum dead space.

For proof of cleanability column suppliers need to provide data of how the equipment performs under bacterial challenge. An example of bacterial challenge is expressed in the next paragraph.

The chromatography column can be challenged with *Escherichia coli* to test cleanability under standard operating conditions. Sodium hydroxide (1 M solution) can be used as a sanitizing agent and loaded with a minimum concentration of 105 cfu ml^{-1}. The column should be left to incubate overnight at room temperature and washed with two column volumes of 1 M NaOH recirculated for one hour. After neutralization, the column should be sampled for residual microbial contamination. Sample should be taken from the critical points as shown in Figure 10.13.

A result of no viable target organisms found in the process liquid flow path and no viable cells detected on the clean sides indicates that the column design provides an effective flow path for chromatography with no unswept areas and that the cleanability is maintained.
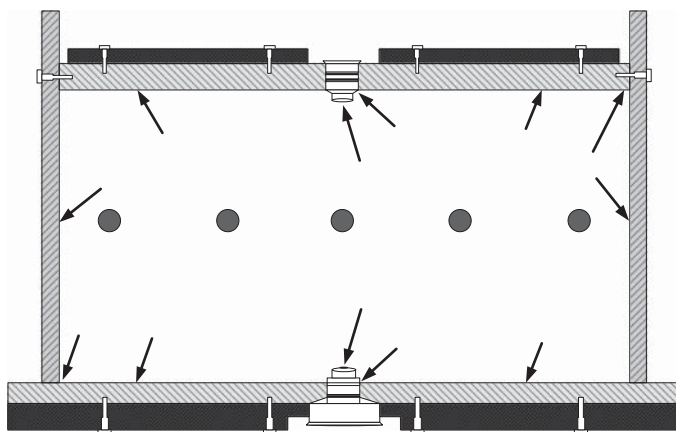
Figure 10.13 Sampling for cleanability test.

10.4 Commercial Chromatographic Systems

The market can be divided into different main segments:

- Analytical and preparative equipment;
- High-pressure/high-performance systems;
- Low-pressure systems.

Analytical systems do equip almost all laboratories. Many different kinds of particle sizes are used: from 20 to 2 μm (from HPLC to ultrahigh-performance liquid chromatography [UPLC]), using liquid or supercritical fluid mobile phases. An intermediate market is to be considered using 10 mm i.d. columns for small-scale purifications. The term preparative chromatography is dedicated to purification units using column diameters from 50 up to 1600 mm i.d.

10.4.1 General Design Aspects: High-Pressure and Low-Pressure Systems

The chromatographic column is responsible for performing the purification, and the chromatography system is responsible for optimizing the separation.

A preparative system has to:

- minimize loss in efficiency of the chromatographic separation;
- allow the use of one or many mobile phases, with the ability to utilize isocratic conditions, step gradients, or sloped gradients;
- carry out the injection of feed mixture;
- monitor and control chromatography separation;
- collect the different fractions;
- protect the column against misuses.

The system when connected to the column has to avoid any kind of mixing before or after the column. Therefore, the system needs to be designed to minimize the dispersion within its different elements. For a targeted flow rate, the

different elements have to be minimized to find a good compromise between internal volume and induced pressure drop.

A chromatographic system is always a combination of compromises between chromatographic and technical constraints.

For HPLC systems, the stationary phases often use small particles from 10 to 50 μm; the number of plates generated by the chromatographic column can reach up to 50 000 plates per meter. The constraint of avoiding any kind of dispersion is then a major priority. An important action to minimize the dispersion from the moment the feed is introduced to the moment where the fractions are collected is to reduce volumes and to design smooth connections between the different parts of the plant. Small piping diameters are also a requirement because the operating pressure introduced by the column can go up to 50 bar or even higher. HPLC systems are mainly used for the separation of fine chemicals and small pharmaceutical molecules.

LPLC systems are generally used for the purification of biomolecules like proteins. In contrast to HPLC, these systems are mainly operated with step gradients and use stationary phases with large particle size (50–200 μm). Their column technologies are not designed to resist to high pressure. The volumes of the different equipment are larger than on HPLC systems, and the corresponding pressures are of course significantly lower (<5 bar). Furthermore, the operating conditions have to be compatible with biological molecules, as particularly proteins are sensible to heat and solvents that can destabilize their three-dimensional structure, resulting in loss of the molecule's properties (Carta and Jungbauer 2010).

In order to satisfy these requirements, chromatographic systems need to have the following basic components:

- Inlets for buffers, mobile phase, product, and sample addition;
- Pumps and/or switching valves (for gradient mixing);
- Specific protection devices like filters and bubble trap to avoid loss of efficiency due to potential introduction of particles or air;
- Sensors (pre- and post-column);
- Valves to control flow direction and collect fractions;
- Automation system to control all electronic and pneumatic devices and run properly recipes;
- Data collection and reporting.

Different preparative chromatographic equipment should be considered for the following applications:

- To carry out batch or continuous purifications;
- To carry out different kinds of chromatographic separations: from chiral purifications to the binding of mAbs on Protein A resins.

Different layouts will be presented in this chapter, considering:

- Batch HPLC equipment;
- Batch LPLC equipment;
- Continuous HPLC equipment;
- Continuous LPLC equipment.

10.4.2 Material

The construction material of the piping could be made of stainless steel or plastic according the application and the size of the equipment. Stainless steel is available in different grades that are resistant against high salt concentration. High surface finish is required for effective cleaning. Plastic is available in different materials that may have limited resistance to pressure than stainless steel.

In the case of biochromatography, all materials used in the manufacture of columns for biopharmaceuticals' separations, which come into contact with the process stream, should be selected so as to either conform to relevant sections of the FDA Code of Federal Regulations, Volume 21, parts 170–199, or have passed USP Class VI tests for *in vivo* toxicity.

Stainless steel can be supplied with a batch-specific material certificate that details the exact composition of the alloy. Plastics and rubber components cannot be so easily defined. For this reason, certification of particular polymers is rarely provided on a batch-by-batch basis but by "generic" assurance that relates to a particular grade of material from a particular supplier.

Two types of conformance criteria are used, and a specific material may conform to one or both of these. The first is that material suppliers provide written confirmation that specific materials conform to the relevant section(s) of the FDA Code of Federal Regulations, Volume 21, parts 170–199.

The second is that representative samples of the material are independently tested according to a method described in USP 23. In the Biological Test for Plastics Class VI (70 °C), the test sample is extracted at 70 °C in a range of solutions, and both these extracts and the test material itself are checked for direct biological reactivity, leading to a pass/fail result.

10.4.3 Batch Low-Pressure Liquid Chromatographic (LPLC) Systems

Figure 10.14 shows a typical PID for a batch LPLC system.

10.4.3.1 Inlets

The system inlets' number may vary according to user requirements; three to five inlets are common in preparative chromatography where the process is in general simple and repetitive. Development or pilot systems can be featured with a larger number of inlets to allow more flexibility in the development or optimization of the chromatographic separation.

In the case of bioseparations, it is mandatory to be able to process effectively cleaning chemicals, that is, CIP. CIP is executed with the use of chemicals with the purpose of minimizing bioburden. In most applications sterility as in fermentation is not claimed. In large manufacturing installation, the chromatography system can be connected directly by stainless steel piping to the tanks containing product that needs to be purified and the buffers necessary for the chromatography process. These tanks as well as the transfer lines need to tolerate steam cleaning in place (SIP), and the chromatography systems connected to it should be designed to allow this sterilization process. An additional possibility needs to be foreseen to protect the column and any other sensitive material during this
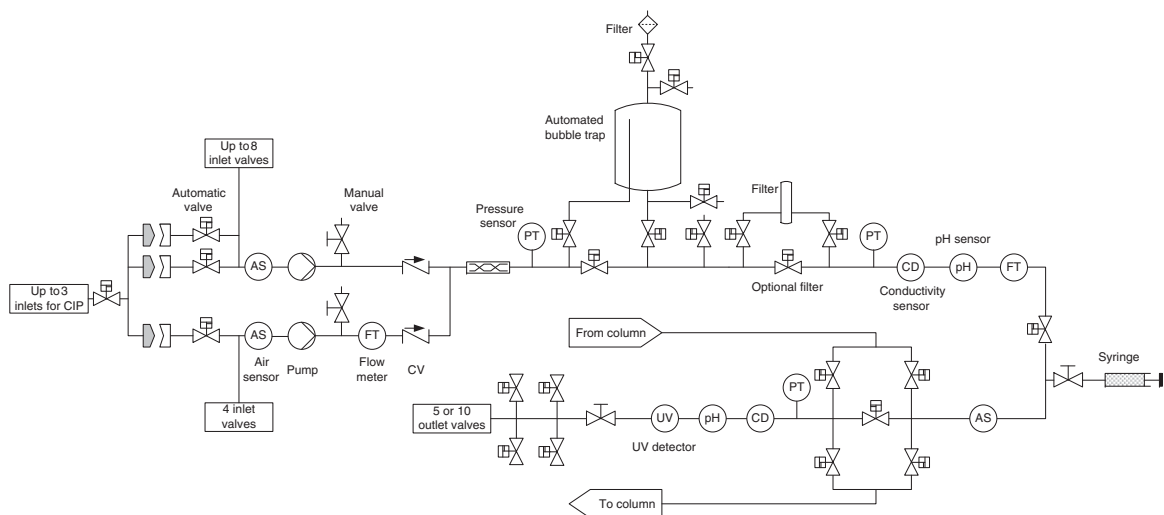
Figure 10.14 P&ID of a valve gradient-based LPLC system. Source: Reproduced with permission of HiperSep Bio, Novasep.

process step. This can be performed using valves equipped with a steam trap or even a switching valve embedded into the system design.

10.4.3.2 Valves to Control Flow Direction

Valves are integral components in piping systems; they are the primary method of controlling the flow, pressure, and direction of the fluid. Valves may be required to operate continuously, for example, control valves, or they may be operated intermittently, for example, isolation valves, or they may be installed to operate rarely if ever, for example, safety valves. A valve can be an extremely simple, low-cost item, or it may be an extremely complicated, expensive item. In piping design, the valves probably require more engineering effort than any other piping component.

The properties of the fluid to be controlled have a major impact on the design and materials of construction of the valve. The piping industry, over the years, had developed a wide range of valve designs and materials to handle virtually all fluids. The selection of the valve should take into account fluid viscosity, temperature, density, and flow rate. The valve must be suitable to withstand resulting corrosion and erosion, and if necessary, the valve may have to be designed for no internal hold up of fluids. Figure 10.15 illustrates how impurities because of dead volumes influence the quality of a chromatographic separation.
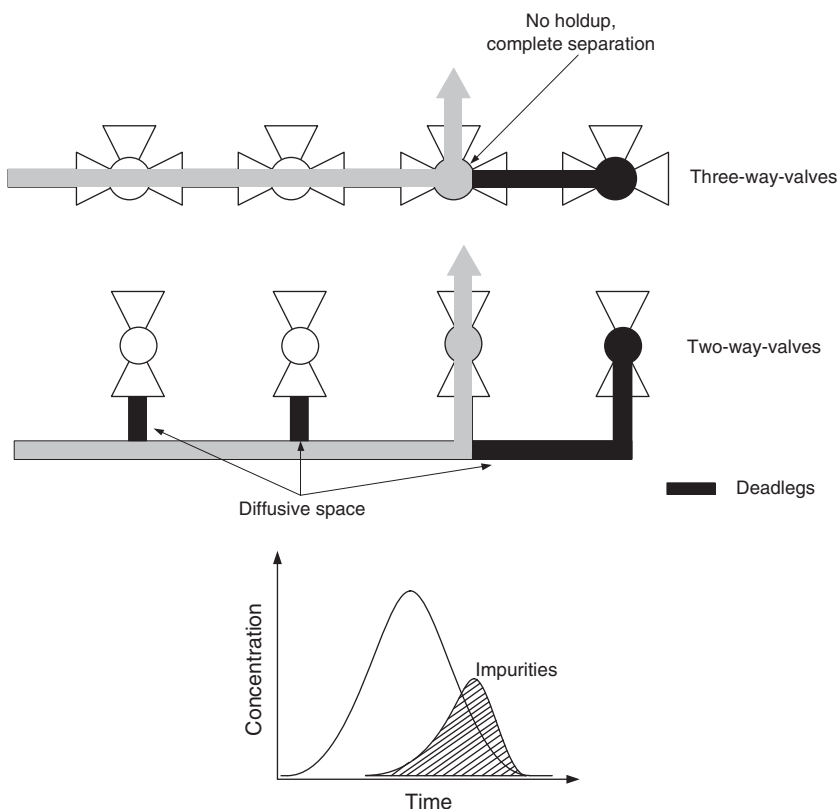
Figure 10.15 Influence of holdup volume and diffusive space in a chromatogram.

In addition to the low or no dead volume feature, valves should also be fully drainable and of fast actuation especially if they are used for the gradient formation. In the past, there were Gemü, Saunders, and ITT; nowadays new vendors offer designs that feature improved chromatographic performance, that is, NOVA-SEPTIC, Furon, Robolux (Burkert), and Swagelok.

10.4.3.3 Pumps

Pumps are major components of all chromatography systems, as they have to induce the driving force for the elution and separation process. In any case, process pumps should be able to maintain their set-point flow rate in a smooth manner. Positive displacement pumps, such as diaphragm pumps, are often used in preparative and large-scale chromatography systems.

Some key requirements for pumps used in chromatography systems are as follows:

- The set-point flow rate should be maintained irrespective of any backpressure.
- The pulsation should be minimized to avoid disturbance of the chromatographic bed. Thus, the usage of multihead pumps is favorable.
- The handling of any biological solution should be gentle, so as not to shear or denature any biological product.

None of the pumps currently on today's market can meet all those requirements, except smooth flow diaphragm pumps. The major disadvantages of peristaltic pumps are the likelihood of breakage of the flexible tubing, pressure limits with no more than 30 psi, potential contamination of product/matrices with leachables, and the difficulty of making truly sanitary and strong connections between flexible tubing and steel piping. Table 10.7 describes some features and limitations of different pump types.

10.4.3.4 Pump- and Valve-Based and Gradient Formation

In the case of large retention factors of the last eluting component, which happens very often in bioseparations, chromatographic processes require the means to change the composition of the mobile phase in order to control the elution rate from the column. The rate at which the mobile phase composition

Table 10.7 Examples of available pumps, features, and limitations.

Pump type	Features	Limitations
Diaphragm pump	Precise flow control	Only true positive displacement pump
		For low flow applications
		Must manage pulsation
Lobe pump	Low pulsations	High flow applications
Peristaltic pump	No shearing	Unreliable, tube breakage
		Not suitable for process chromatography

changes concurs precisely with the elution time for each peak for a given process (Section 5.1.2).

Two factors affect the viability of the elution profile:

- Accuracy;
- Reproducibility.

Each characteristic is important; however, the most critical factor for process-scale pharmaceutical purification applications is reproducibility. Processes that are required to be validated must yield consistent results between operations. For a chromatography process to be reliable, the gradient profile must be reproduced consistently during each operation. Several approaches are used to control the formation of a gradient profile. As the most important principle, valve- or pump-based mixing systems can be identified.

For many applications, the system forms the gradient mix by cycling the valve at the ratio required by the process (Figure 10.16a). Simply cycling the valve will result in the proper gradient mix being formed if the mix frequency is properly tuned prior to use. In order to provide steady flow, gradient valves need to have the same inlet pressure; this means that a regulation valve at the tanks outlet should control inlet pressure.

Pump-based gradient (Figure 10.16b) works very well for bench-scale equipment, and it can be very accurate in a limited flow interval. Unfortunately, the individual reciprocating pumps may show inaccurate functioning at very low flow rates (Figure 10.17). In addition, these pumps require extensive calibration procedure and expensive maintenance. Compared with pump-based gradients, valve systems are in general cheaper and can achieve 1–2% accuracy in a broad operating interval.

Figure 10.17 depicts an example for the acceptance range for the mixing of two solvents A and B. The diagram makes clear that in the low range of flow rate from 0 to $200\,l\,h^{-1}$, valve-based gradients can be mixed effectively within the ratio of 10–90%, while pump-based mixing assures acceptable accuracies only between
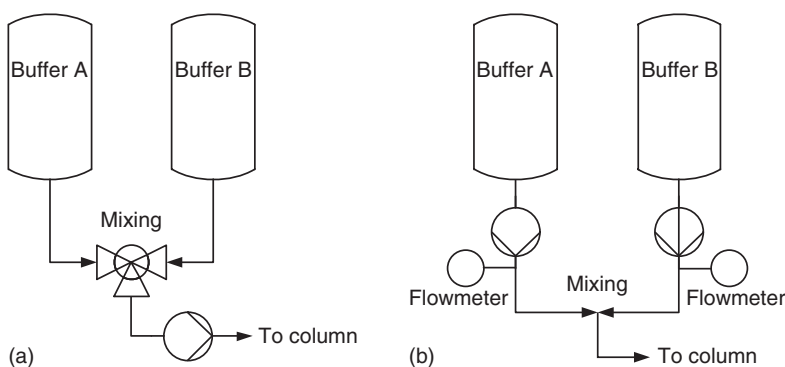
Figure 10.16 Valve-based and pump-based mixing.
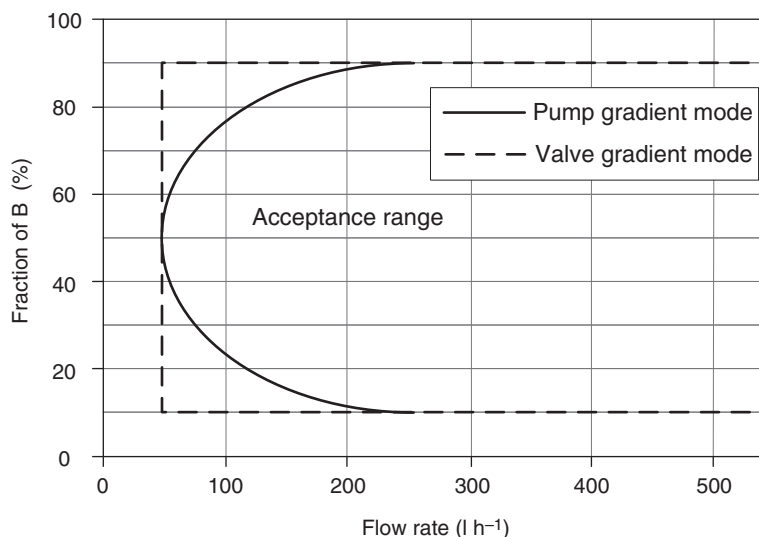
Figure 10.17 Acceptance range for the mixing of two solvents.

40% and 60%. For higher flow rates, both methods offer effective gradient mixing. These differences between valve and pump mixing are valid independently from the flow rate or pump capacity.

Some applications require gradients to be formed to a prescribed set-point value. The most common parameter used to identify the set-point value is the ionic strength or conductivity of the buffer solution. Another possibility for alcohol or acetonitrile–water mixtures is the use of a near-infrared sensor.

A very reliable but more expensive gradient mixing unit is based on the use of regulation valves combined with mass flow meters.

10.4.4 Batch High-Pressure Liquid Chromatography

10.4.4.1 General Layout
By design HPLC separations use small stationary phase particles to increase the column efficiency and improve the resolution between peaks, enhancing product purity and recovery yield. At a given linear eluent velocity, small particles cause higher pressures than large particles. Therefore, HPLC systems are operated at high pressures in order to increase the eluent flow rate, hence the productivity of the separation. HPLC systems represent different constraints compared with LPLC systems. These are in a large majority of the cases:

- To scale up the high efficiencies obtained at small scale, the preparative HPLC systems have to be designed in order to minimize all the dead volumes.
- The mobile phases use organic solvents. It is rare to use only pure water most of the time in reversed phase chromatography; water is combined with acetonitrile or with an alcohol.

10.4.4.2 Inlets and Outlets

Mobile Phases   Figure 10.18 shows a P&ID of a typical gradient mode HPLC system that allows a binary analog gradient working from 5% to 95% in the dynamic range of the system flow rate, with an absolute accuracy of ±0.5% or better. The different gradient modes have already been described on LPLC systems.

Feed Injection   The number of plates of the HPLC column may be very high (e.g. 10 000 plates), often resulting in narrow peaks. The ideal injection is obtained when a perfect step of feed concentration "as thin as possible" is performed: in HPLC separations, the injected volume is generally small (<1%) compared with the volume of the column.

   The injection of the feed mixture can be performed through many different ways; three of them are described as follows:

- The feed injection is performed as a "step gradient," through the main eluent pump (called "low-pressure injection"). The advantage of this method is the simplicity and the speed: a valve is switched to the feed line without changes in the flow of the main pump. The injected volume is regulated by the opening time of the feed valve. The main drawback of this method is that for small-injected volumes and in strongly nonlinear conditions, the reproducibility of the chromatograms may be poor. Additionally, the "pulse" of feed is sent through the main pump and may be potentially diluted, eventually leading to a loss of efficiency. However, this method is appropriate for gradient chromatography as well as for isocratic elution chromatography. Another possibility is the use of the combination of a three-way valve combined with of a mass flow meter to improve the reproducibility of injection for smaller volumes.
- An additional pump (called high-pressure injection) performs the feed injection. The advantage of this method is that the feed pump is designed and sized in order to inject with a high reproducibility a large range of volumes, avoiding loss of efficiency. One drawback of this method is the use of an additional pump, often with a reduced flow compared with the main pump, leading to an increase of the cycle time and of the equipment cost.
- The feed injection is performed by an injection loop. Advantage of this method is that the loop can be filled during the elution of the column, so the accuracy of the injection can be combined with a single flow rate purification method. This method is the only way to perform the injection in a one-column steady-state recycling system. It is also the most suitable injection method in SFC. The main drawback of this method is that the geometry of the loop has to be carefully designed to avoid dilution or tailing in the case of partially filled loops.

10.4.4.3 Pumps
The flow rate of the eluent and the sample is delivered to the column by a metering pump. The demand on HPLC pumps is very high, because they must guarantee a reproducible flow rate even against high backpressure generated by the column. To prevent mechanical stress to the fixed bed in the column, the solvent flow should have low pulsations. In the start-up period of pumping, the adjusted flow

Figure 10.18 P&ID of an HPLC system. Source: Reproduced with permission of HiperSep, Novasep.

rate should be reached gently (avoiding too high flow rate) so as to prevent damage to the packed bed. The pumps have to be feedback controlled by flow meters (in general mass flow meters).

Based on the system size:

- The main pump (eluent pump) is a two- or three-headed membrane (PTFE) pump, able to operate at up to 100 bar, equipped with membrane failure indicators.
- The high-pressure injection pump is a one- to three-headed membrane (PTFE) pump, able to operate at 100 bar, equipped with membrane failure indicators.

Piston pumps with more than one pump head (in most cases two or three) or a pressure regulator downstream of the pump are not so frequently used in industrial units.

The working range of the pump, concerning the maximum pressure difference and flow rate, must be adjusted to the column. An inadequate system causes lower productivities of the separation and thus wastes time and money. Table 10.8 gives typical flow rates and tube diameters for different column geometries.

Piston pumps are used for analytical and small preparative HPLC systems (below $1000\,ml\,min^{-1}$). The major operating problem of piston pumps is dissolved in air, and the formation of bubbles in the eluent. Bubbles in the pump heads cause pulsations of volume flow and pressure. Bubble formation and cavitation problems are promoted at the inlet check valve because the minimum pressure in the system is reached here. In analytical units, degassing can be done online by a membrane degasser, by pearling helium offline through the eluent, or by using an ultrasonic bath. In preparative units, where water and an organic solvent are mixed, a bubble trap is used to solve this problem. Important to mention is also that degassing in the detector can also create very annoying noise problems, which eventually can be solved by creating a small back pressure in the collection line.

Table 10.8 Typical flow rates and tube diameters for different column geometries.

Column ID (mm)	4	25	50	100	200	450	600	1000
$\dot{V}_{min}$ (ml min^{-1})	0.5	20	80	300	1200	6000	10×10^3	30×10^3
$\dot{V}_{max}$ (ml min^{-1})	2	80	300	1200	5000	25×10^3	45×10^3	120×10^3
Tubing OD (mm & in.)	1.56	1.56–3.12	3.12	3–6	6–8	8	16	25
(in.)	1/16	1/16–1/8	1/8	1/8–1/4	1/4–3/8	3/8	5/8	1
Tubing ID (mm)	0.25	0.75–1.6	1.6	1.6–4.0	4.0–5.0	5.0	13.0	21.0
Sample loop volume (ml)	0.01–0.2	1–2	2–5	10–20	Feed introduction via feed pump			
Max. unit dead volume (ml)	0.5	3–5	5–10					

Cavitation is a general operation problem, which can be solved by using tubing with a higher internal diameter or by increasing the pressure at the suction side of the pump. The easiest way to increase the pressure is to lift the eluent reservoir to a higher level than the pump inlet. If this is not sufficient, the pressure in the solvent reservoir must be increased. For this reason, the solvent reservoir should be airtight and isolated from the environment. Isolation of the eluent has the positive side effect that the composition and water content can be held constant during operation. Especially in the case of normal phase chromatography, it is important to control the water content in the range of a few ppm, because of the hygroscopic character of the adsorbent.

10.4.4.4 Valves and Pipes

As presented on the P&ID (Figure 10.18), different valves can be used:

- For the solvent module, two-way ball valves are used in combinations with two-way analog control valves to adjust the composition of the gradient.
- On the flow path, two pneumatic three-way ball valves used to bypass the filter. Pneumatic four-way (or an arrangement of three-way) ball valves are used to bypass the chromatographic column and to revert the elution direction into the chromatographic column.
- On the collection module, two-way ball valves are used, mainly being normally closed (to perform the collection) and one being normally opened (typically defined as the waste).

Volumes and diameters of the pipes are preassigned: large pipe diameters are used on the entrance (suction side) of the pumps, and thin pipes are used on the chromatographic flow path (pressure side). In principle, internal pipe diameters are designed to ensure a turbulent flow with fluid speeds around $2\,\mathrm{m\,s^{-1}}$. On industrial systems, all pipes have to be connected to the mass in order to prevent the buildup of electrostatic charges, which is especially a danger in case of nonconducting solvents and high fluid velocities.

In large systems, pipes connect the different parts of the chromatographic plant. The tubes are made of stainless steel, Teflon, or polyetheretherketone (PEEK). However, care has to be taken when pure tetrahydrofuran is used together with PEEK tubing at higher pressures, because after prolonged usage, the tube wall can become permeable for this type of solvent. Selection of the right material depends on the mobile phase used for the separation. The choice of the internal diameter of these tubes should be a compromise between small dead volume and low backpressure. Small diameters result in high pressure drops in the system and higher diameters lead to higher dead volume, causing backmixing and, thereby, peak distortion. More important than the absolute tube length is the smooth connection of tubes via connectors, reducers, and ferrules to different system parts. Abrupt changes of cross sections induce turbulence and vortices, which increase axial dispersion and consequently band broadening. Another aspect of pipe design is cross-contamination. All pipe connections must avoid dead spots that cannot be sufficiently cleaned before a product change.
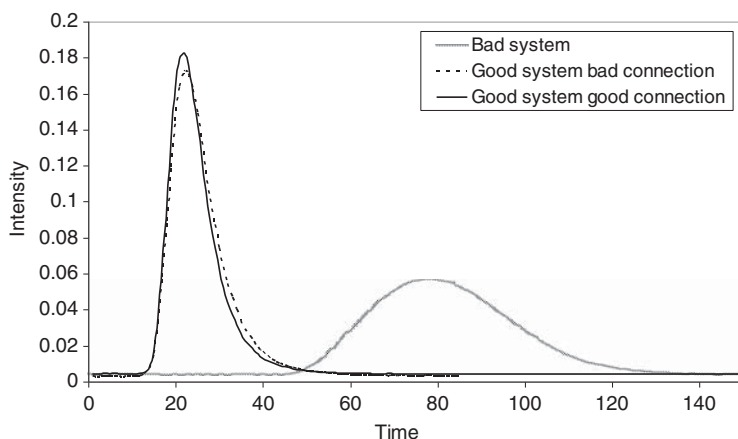
Figure 10.19 Influence of system design on dead time and peak distortion.

Figure 10.19 shows the influence of dead volume, connection design on the peak distortion, and dead time on the analytical HPLC unit. Three runs were performed with the same flow rate and sample size (injection time: two seconds). The straight black line describes the elution profile of a tracer in an optimal system with small dead volume and optimal connections. In the next example one of the tube connections was insufficient because, within the connector, the tube endings did not touch and a small dead volume is formed. The dashed line shows the new elution profile. A poor connection results in higher backmixing and, thus, peak distortion. This effect should be kept in mind for systems with many connections and small tube diameters where bad connections can have a larger impact.

The third experiment, represented by the gray line, shows the elution profile of the same tracer in the same unit, but in this case one tube with a small internal diameter was replaced by a bigger one. Dead volume and peak distortion are dramatically increased. This increase in dead volume results in a loss of baseline separation. For preparative separations, the higher backmixing in the unit leads to decreased productivity and economy of the process.

10.4.5 Continuous Systems: Simulated Moving Bed

10.4.5.1 General Layout

Principles and interests of continuous chromatography are presented in Chapter 5.

The SMB process was patented in 1961 by Universal Oil Products (UOP) (Broughton and Gerhold 1961). The technical realization of this process is presented in Figure 10.20a. It suits well the petroleum industry applications like the PAREX process where 24 columns were used in a system with a small pressure drop. A recycling pump characterizes this design and in particular a rotary valve that periodically switches the lines so that a simulated countercurrent flow of the solid and liquid phase is achieved.
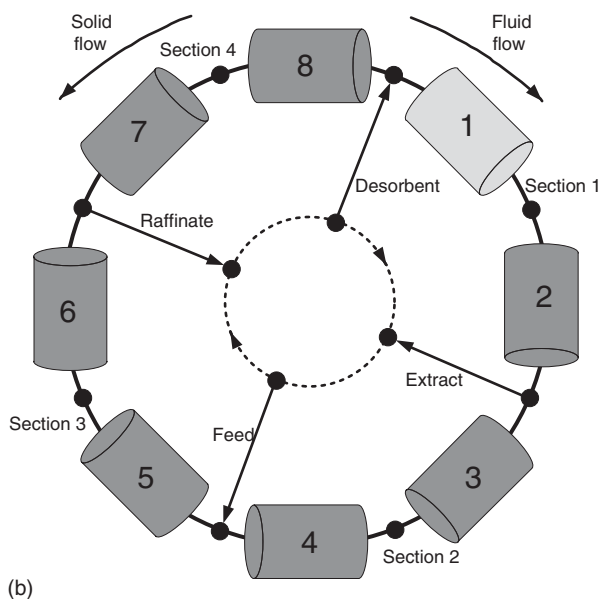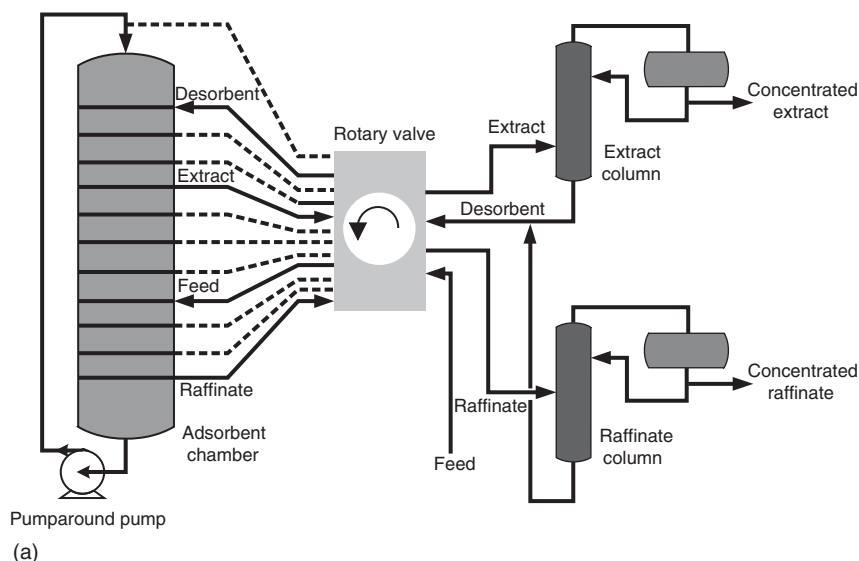
Figure 10.20 (a) UOP PAREX process with rotary valve and (b) SMB process with valves between the columns and port switching.

The alternative design of SMB processes uses valves between all columns instead of one rotary valve as shown in Figures 10.20b and 7.24. Here the countercurrent flow is realized by switching the ports in the direction of the liquid flow. This design has the advantage that for process optimization the ports can be switched individually as the Varicol process (Section 5.2.5.1), for instance, applies it. Figures 10.21 and 10.22 show corresponding commercial plants for SMB separations.

Figure 10.21 AZURA Lab SMB System. Source: Reproduced with permission of KNAUER wissenschaftliche Geräte GmbH.
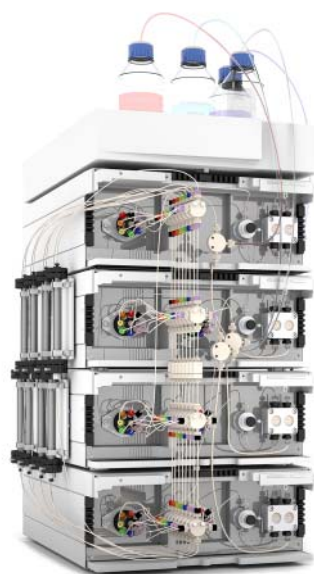
This section presents industrial solutions developed for preparative continuous chromatography of pharmaceuticals and fine chemicals. The technical choices will be presented for HPLC applications.

10.4.5.2 A Key Choice: The Recycling Strategy

As shown in Figure 5.17, fixed pumps can be placed in different ways between two cells or columns.

Figure 10.22 Varicol multicolumn (1 m i.d.) continuous process. Source: Reproduced with permission of NOVASEP.

In configurations shown in Figure 5.17b as well as Figure 5.17c,d, the fluid loop is broken at the eluent line. Therefore, the highest pressure is located at the entrance of the column connected to the pressure side of the pump and the lowest pressure at the outlet of the column connected to the suction side and the process outlet. In these cases, the pump operates at constant flow rate. When the eluent line is switched from one column to the next, the points of high and low pressures are switched by one column as well. In configuration shown in Figure 5.17a, the pressure all along the system is more or less constant, irrespective of the position of the eluent, extract, feed, and raffinate lines. However, the pump has to change its flow rate if it enters a different zone of the SMB process.

In HPLC applications, the pressure drop along the columns of the system is around 30 bar, and the order of magnitude of the switching time is the minute. Therefore, industrial applications promoted over the years are configured with a fixed recycling pump and control of the flow rates as this leads to a smoother operation and lower stress on the stationary phase, hence increasing its lifetime.

10.4.5.3 Pumps, Inlets, and Outlets
Considering the recycling strategy with a fixed pump, five flow rates have to be controlled:

- *Eluent and feed inlets*: constant flow rates that can be achieved with two-or three-headed HPLC membrane pumps.
- *Extract and raffinate outlets*: constant flow rates that can be controlled using pumps or by analog control valves.
- *Recycle stream*: high-pressure liquid pumps, mainly three-headed HPLC membrane pumps, are used, or high-pressure centrifuge pumps in large industrial systems. If because of the line switching the recycling pump is located in a different zone of the process, the flow rate has to be controlled accordingly.

It has to be noticed that as two inlets and two outlets are applied to a closed loop, even if the sum of the inlet flow rates are equal to the sum of the outlet flow rates, a small difference will strongly increase or decrease the internal pressure of the process. Thus, the outlet flow rates have to be regulated based on the internal pressure of the liquid loop.

10.4.5.4 Valves and Piping
Considering Figure 7.24 (Section 7.8.2.1), it appears that two inlets and two outlets have to be installed between the columns of the system. Thus, four valves are necessary between all the columns.

The use of many valves instead of one large rotary valve offers many advantages: for maintenance, small valves are easier and much cheaper to replace. However, the main advantage is that all ports can be shifted independently from each other. SMB plants are very often designed with a suction line of the recycling pump, which is much longer than the other lines between the columns. In the case of asynchronous shifting, it is necessary to compensate the unequal distribution of the dead volume. In the case of the Varicol process, an asynchronous

multicolumn continuous system derived from SMB (Section 5.2.5.1) individual switching of the inlet and outlet lines is obligatory.

The internal diameters of the pipes are designed in the same manner as for batch HPLC systems.

10.4.6 Auxiliary Systems

Auxiliary systems surround the chromatography columns and their attached equipment. They are particularly required to pack the columns (Section 10.5) to maintain or qualify the system and to test the integrity of filters.

10.4.6.1 Slurry Preparation Tank
Slurry preparation tanks are used for several operations:

- Pool new resins being delivered in 1–25 l bottles;
- Resuspend already used resins in buffer;
- Exchange storage solution of resins with packing buffer (sedimentation/decantation);
- Wash used resins and remove fines (particle sedimentation/decantation);
- Pack and unpack columns.

If a stainless steel tank is used, it must be able to suspend the resins (and fines) but avoid high shear stress, which would damage the resin. Axial mixers introduced from the top are appropriate. For decantation, a height adjustable dip tube is required. High flow rates at the entrance of the dip tube must be avoided. To control the suspension/sedimentation, a viewing glass and a separate lamp are required. The bottom of the tank is often discussed; dished bottom or conical bottoms are used. Dished bottoms are preferred to provide homogeneous conditions; conical bottoms have better sedimentation/decantation characteristics and are suitable to recover all resin materials. In both cases, a bottom valve, sealing with the vessel wall, shall be used. Slurry preparation tanks need to be cleaned, but a steam sanitization for bioburden reduction is typically not required.

An alternative to stainless steel tanks are open cylindrical storage tanks. Plastic tanks or single-use liner can be used as well. Closed single-use bags with a top-mounted paddle mixer and a valve closing with the wall can also be taken into consideration.

Slurry tanks should be carefully designed to allow a homogeneous mixing with minimal impact on the resin. To avoid particles' degradation that could reduce resin lifetime, shearing should be very low. Therefore, it is recommended to use a tank size that is four times of the packed bed volume (BV), to use the following ratios for tank design $D/T \sim 0.35$ and $C/D \sim 0.9$, and to locate the mixer centrally and to select mixers with a rotor tip velocity that does not exceed $3.3\,\mathrm{m\,s^{-1}}$ (Figure 10.23).

Chromatography resins for manufacturing scale are delivered in standard containers of 10, 20, or 25 l. Transferring sedimented resin from shipping containers (drums or jerry cans) to the mixing tank can be performed with specific equipment like drum rollers.
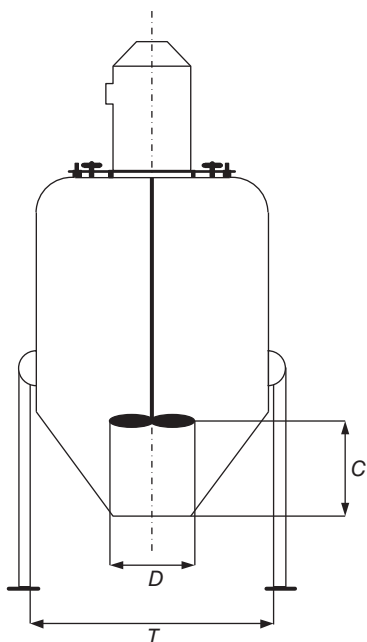
Figure 10.23 Slurry tank and stirrers for low shear stress.

10.4.6.2 Slurry Pumps and Packing Stations

A pump is necessary to pack, unpack, and provide buffer from the slurry preparation tank to the column. The ideal pump provides constant pressure and flow rate at low shear stress. Because of shear stress reasons, rotating parts have to be avoided: therefore diaphragm pumps are preferred. To dampen the pulsing characteristic of a diaphragm pump, typically two or three "pistons" are used.

Suppliers typically provide movable skids integrating the pump and a valve arrangement. To avoid turbulence and shear stress, true bore valves such as ball and butterfly valves shall be used.

10.4.6.3 Cranes and Transport Units

For maintenance, the columns and/or top plates must be lifted. For this purpose hydraulic/pneumatic lifting pistons integrated in the column or other methods are applied. If several columns are in use, a crane suitable for clean rooms can be used.

To move heavy columns electrically operated, "MasterMover" can be used. Important is to check in advance the appropriate combination of the wheels (diameter and width) with the floor resistance (maximal peak pressure on floor). For fragile floors transport systems with an air cushion (hoover system, for example, from DELU-GmbH/Germany) can be used, but such systems require smooth floors without any cracks or gaps and a compressed air supply on the transport way.

10.4.6.4 Filter Integrity Test

In chromatography skids, liquid absolute filter, depth filter, and/or gas filter might be integrated. Absolute liquid and gas filter are typically integrity tested before

and/or after use offline. An *in situ* integrity testing, requiring additional connection points for the compressed air and water, is seldom designed for chromatography skids.

Hydrophobic gas filter can be tested with the water intrusion test (WIT). Hydrophilic liquid filter is usually tested with water; the often used test method is the pressure decay test (PDT), a variation of the forward flow test (FFT).

10.4.7 Detectors

For process control systems, the accurate detection of the target components is mandatory. The detectors have to be selected and combined carefully in order to get signals as accurate as possible. The assembly of the different detectors is always very similar. The product stream flows continuously through the detector cell, where a physical or chemical property is measured online. The detected value is transformed into an electric signal and transferred to a PC or integrator to record the chromatogram.

The signal should be linear to the concentration of the target component over a wide range – as indicated in Figure 10.24 – because this simplifies the calibration of the detector and the signal represents the real shape of the peaks. The pure eluent signal is recorded as the baseline of the chromatogram. Fluctuations of the baseline are called the noise of the detection system. To qualitatively identify peaks, the signal-to-noise ratio (Figure 10.25) of the chromatogram should be higher than 3, and for quantitative analysis this ratio should be at least 10 (Meyer 1999). The detection limit is defined as amount of a certain substance that gives a signal two times higher than the noise. A detector's dynamic range is the solute concentration range over which the detector will provide a concentration-dependent response. The minimum is bordered by the detection limit, and the maximum is given at the saturation concentration where the detector output fails to increase with an increase in concentration. The dynamic range is usually quoted in orders of magnitude (Scott 1986).
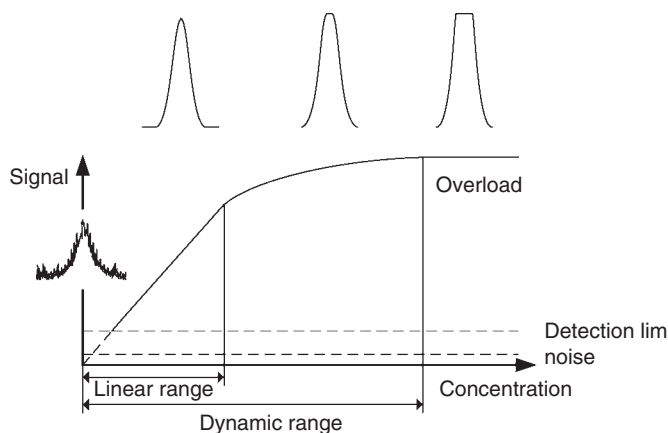
Figure 10.24 Detection regimes of HPLC detectors. Source: Reproduced with permission of Meyer 1999.

S/N = 10

S/N = 3

LOQ   LOD
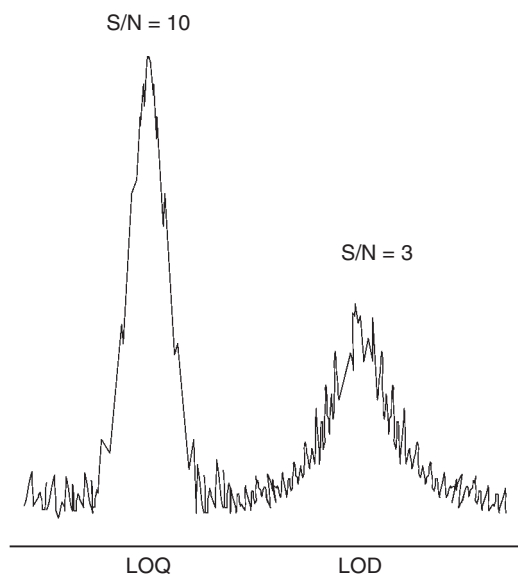
An ideal detector for preparative chromatography has the following properties:

- Good stability and reproducibility, even in the production environment;
- High reliability and ease of use in routine operation;
- Sufficient sensitivity (need not to be too sensitive, as no trace detection is the goal in preparative chromatography, but the sensitivity should be high enough to keep the flow cell volume, which contributes to the axial dispersion, small);
- Short reaction time, independent of flow rate;
- High linear and dynamic range.

Table 10.9 lists the different detectors and their operation principles that are used in (analytical as well as some of them in preparative) chromatography. The optimal detection system only detects the target components and all impurities but is not affected by the solvent. Detectors can be divided into two groups: (i) those that detect any change in composition of the solvent and can, therefore, obviously only be used under isocratic conditions and (ii) analyte-specific detectors – which can be subdivided into detectors with a similar sensibility to all analytes and those that can detect certain components selectively. All the detection principles listed in Table 10.9 may be applied in preparative chromatography, but some of the detectors have limitations with regard to their applicable flow rate range.

If the maximum allowable flow rate of the detector is too low compared with the flow rate of the chosen column diameter, the total solvent stream has to be split into a detector stream and the eluent stream. The easiest splitting principle is the integration of a T connector with a certain diameter for the two different streams. Integration of a connector into the eluent stream increases the system pressure drop and the backmixing of the system. This is a severe drawback of all passive splitting systems. In addition, care has to be taken that the time delay between detection and fractionation is carefully determined and taken into account for

Table 10.9 Chromatographic detection systems and their detection principles.

Detection principle	Detection sensitivity (g)	Stability (sensitive to)	Dynamic range	Full flow or split flow (max flow rate in ml min^{-1})	Detection sensibility
Solvent sensitive					
Refractive index	10^{-6}	Temperature shift, solvent composition	10^4	Full (100)	All analytes
Density	10^{-6}	Solvent composition	10^3	Full	All analytes
Conductivity	10^{-9}		10^6	Full	All ionic analytes
Analyte sensitive					
Light scattering ELSD	10^{-7}	Volatile analytes	10^3	Split (4.0)	All analytes
Electrochemical	10^{-12}	Temperature shift, flow rate, and mobile phase purity	10^8	Split	All analytes
UV/Vis (DAD)	10^{-9}	UV adsorption of solvents	10^5	Full (10 000)	Compound selective (DAD)
Fluorescence	10^{-12}	Fluorescent substances in eluent	10^3	Split	Compound selective
Mass spectrometer	10^{-10}	Inorganic salt in eluent	Wide	Split (0.1)	Compound selective
Polarimetry	10^{-9}	Temperature shift	10^3	Full (5000)	Compound selective (chirals)
Element selective (nitrogen, sulfur)	10^{-8}		10^2	Split (0.4)	Compound selective

exact fractionation. The pressure drop problem is solved by active split principles. These are motor valves where, in short intervals, a portion of the eluent stream is captured and injected via an injection pump into the detector. The need for a second pump is one of the drawbacks of active splitting systems. In addition, the valve seal has to be carefully maintained and changed at regular intervals.

For further information, see, for instance, Snyder, Kirkland, and Dolan (2010).

10.5 Packing Methods

10.5.1 Column and Packing Methodology Selection

The column design and the packing procedure need to be chosen in function of the characteristics of the media that need to be packed. The objective when
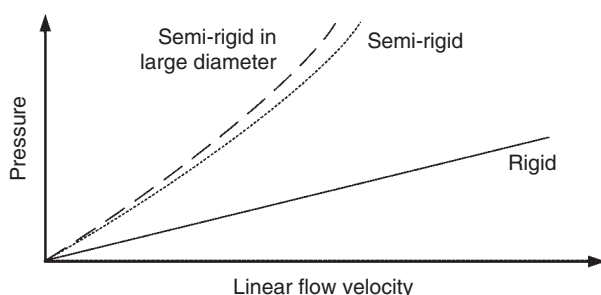
Figure 10.26 Pressure/flow curve according to chromatography media rigidity.

packing a column is to obtain a homogeneous bed with a specific compression rate (or consolidation in the case of rigid matrix as these are not compressible). The packing technology should be robust enough to reproduce consistently the same compression (consolidation) factor as this defines the amount of media for a given bed height required for the chromatographic separation. Semirigid media, for example, cross-linked agarose should be packed, taking into consideration the pressure drop generated and the bed stability (Figure 10.26).

In the case of capital investment in a multipurpose facility, the option that offers a broader panel of packing methodologies should be considered.

10.5.2 Slurry Preparation

The preparation of the slurry is a critical step to ensure a good packing. The critical parameters to be considered are as follows:

- *The quantity to be prepared*: Depending on the packing method selected, an extra quantity has to be provided to take into account the dead volume of the packing system (hoses, packing skid) to avoid introducing air into the column. The other important parameter to consider is the compression factor.
- *Compression factor*: Most of the resins are flexible and have to be compressed during packing; the ratio is provided by the supplier and has to be considered when calculating the volume of resin to prepare. Settled chromatography resin volume = packed bed volume × compression factor.

Table 10.10 gives some general remarks on the amount of packing material per liter of column volume.

- *Media exchange*: The resin is delivered in a storage solution (e.g. 20% ethanol) that has to be replaced by the packing buffer. Several techniques can be used to change the media:

Table 10.10 Amount of packing material per liter of bed volume.

Type of adsorbents	Adsorbent amount per liter bed volume
Silica, normal, and reversed phase	Approximately 0.4–0.6 kg l^{-1}
Polymeric adsorbents	Approximately 0.3–0.4 kg l^{-1}

- The exchange can be performed directly in the original container by removing the supernatant and replacing it by an equivalent volume of packing buffer. This operation has to be repeated several times (with a homogenization in between), until the resin is completely suspended in the desired buffer. All slurry containers can be then pooled in the slurry tank.
- The second solution consists of pooling all the slurry contents needed from the different containers in the slurry tank with the storage solution. After the resin has settled, the supernatant is removed and replaced by the packing buffer. That operation has to be repeated several times (with a homogenization in between), until the resin is completely in desired buffer solution.
- Dilution ratio (= slurry concentration): Slurry concentration refers to the ratio of settled bed volume to total slurry volume. To ensure a good packing performance, a defined appropriate dilution ratio between the slurry and the mobile phase has to be adjusted during the resin preparation. The information is usually provided by the supplier and may range from 30% to 50% (v/v) depending on the packing technique or even up to 70% if hardware or construction restrictions exist.

The process of decanting the resin and removing the supernatant should also be taken into consideration especially for used resin. Chromatography media that have gone through the cleaning process of the active pharmaceutical ingredient (API) purification cycle and potentially through several packs can be partially modified in their particles' size distribution due to chemical and mechanical stress. This small debris generated is called "fines," which could partially block the frit and affect the chromatographic performances. A "defining" performed as described above for the buffer replacement is recommended prior to the use of the resin for purification processes. The only difference is the time required for settling that should be set according to the sedimentation speed of the resin; "fines" should not settle and will be removed siphoning the liquid on the top of the not fully sedimented slurry.

The cloudiness of the supernatant (i.e. the concentration of fines) can be monitored measuring its ultraviolet (UV) absorbance after a referenced settling time. An absorbance value can be set as an acceptance criterion and crosschecked with a calibration curve to validate the resin status.

Table 10.11 gives some general suggestions for solvent buffers in preparative chromatography. Nevertheless, other solvents might be used that are the eluent of the initial step or at least chemically close to that eluent to avoid other solvents and the resulting tedious conditioning steps.

For any column packing, it is critical to know exactly the quantity of resin to be introduced in the column (corresponding to the final bed height). Table 10.12 lists the ratio of total slurry volume to packed bed volume for the different packing technologies. Slurry volumes might have to be adjusted to the given column geometry.

Once the slurry is ready at the right dilution ratio and homogenous, the resin quantity must be determined following procedure (i) or (ii):

(i) Remove a 1 l sample in a graduated cylinder and allow the resin to settle overnight for percent slurry determination or

Table 10.11 Suggestions for slurry solvents.

Normal phase	Methanol (vacuum), toluene–isopropanol (DAC), isopropanol (circle suspension flow – packing (CSF))
Reversed phase	Acetone, ethanol, isopropanol (CSF packing)
Polymeric adsorbents	Ethanol, isopropanol
Chiral stationary phases	Ethanol–isopropanol–n-heptane–isopropanol mixtures
Biopharmaceutical purification	2 M NaCl or process buffer

Table 10.12 Slurry volumes.

Packing technology	Volume slurry/volume packed bed
Dynamic axial compression	3 : 1
Vacuum packing	2 : 1
Circle suspension flow packing	9 : 1

(ii) Dispense the approximate amount of resin into the column. Resuspend the resin to homogeneity and let settle overnight. Measure the settled bed height.

For transparent columns that do not have packing valves, it is easiest to let the resin settle overnight in the column. For all others, calculate the amount of settled resin using the total volume and percent slurry from the 1 l graduated cylinder. If necessary, remove or add resin to achieve the desired packed bed height. Do not rely on the calibration marks on large containers, as they are generally inaccurate.

Homogenize and wet the adsorbent intensively. For small slurry volumes and stable adsorbents, this might be done by ultrasonification for five minutes. For larger slurry volumes, this might be carried out in a mixing device, or the suspension has to be stirred for at least 15 minutes with a paddle stirrer. Never use a magnetic stirrer in any slurry preparation, and make sure that with a paddle stirrer no sediment is built up underneath the stirrer, as this might damage the adsorbent particles.

During ultrasonification, the adsorbent tends to form a sediment on the ground of the container, which has to be carefully rehomogenized. After this final homogenization the slurry should be immediately transferred to the prepared column, and the packing procedure started.

10.5.3 Column Preparation

(1) Clean the frits carefully and inspect them for obvious damage.
(2) Mount, clean, and examine the column for proper sealing according to the manufacturer's operation manual.
(3) Prior to packing, check and adjust the vertical orientation of the column using a spirit level. Move the piston to its maximum bed length position.

(4) Flush the empty column with the slurry solvent prior to use to ensure that the column, column frits, and plumbing are clean and wetted. Empty the column before introducing the slurry suspension.

10.5.4 Flow Packing

The principle of flow packing is to introduce the resin slurry into the column and then to quickly apply a flow to pack the column. To be able to perform a good flow packing, the column tube should be large enough to receive all the slurry. The way to process flow packing may differ slightly because of different equipment. The main steps are as follows:

- Circulate buffer through the system (buffer vessel → pumping module → buffer vessel) in order to remove air.
- Adjust the position of the piston at the maximum height.
- *Wet the bottom frit*: With the packing module introduce buffer in upflow through the process valve (bottom), keeping the process top valve open.
- Introduce the slurry slowly down the inside of the column, rinse any resin particles from the inner wall of the column into the slurry, and add fresh solvent to fill up the column. Insert the top adapter in the top position. Prevent air entrapment. Let the resin settle just a few (2–5) centimeters, and lower the top frit (process top valve open) into the buffer (Figures 10.28a and 10.29a). Make sure that the column tube and entire length of the inlet tubing is full of liquid and free of air.
- An alternative to flow packing is circle suspension flow packing (Figure 10.27). Here the slurry suspension is introduced by lateral openings in the upper
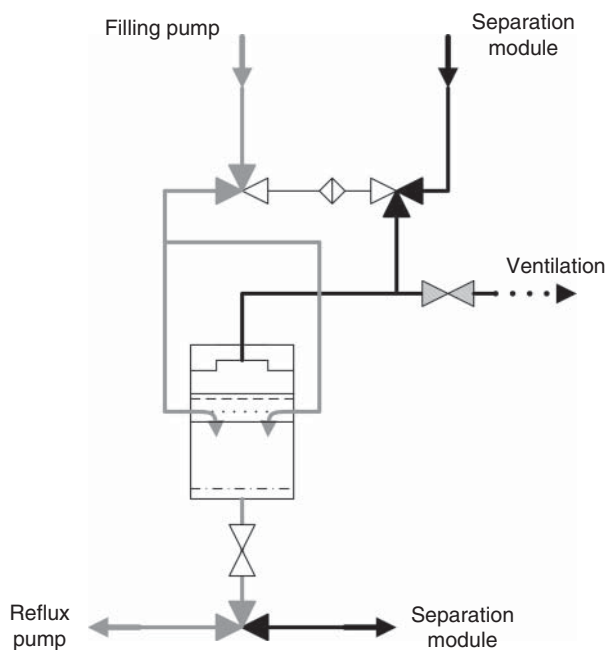
Figure 10.27 Circle suspension flow packing.

part of the otherwise closed column. The slurry suspension is pumped from a stirred tank into the column, which is filled with slurry solvent by means of a slurry pump, and the column bed is built up over the outlet frit. The slurry solvent is recovered in the slurry suspension tank and circulated for a certain time. After introducing all adsorbents, continue following the normal flow packing modes.

- Another good alternative is to start with the piston completely lowered and introducing the resin through the bottom packing valves. The piston is pressure free and is raised by the introduction of the resin. As the complete amount of resin has to be transferred, additional buffer has to be introduced in the slurry tank just before the end of the transfer to avoid introducing air in the system. Let the resin settle just a few centimeters, and lower the top frit (process top valve open) into the buffer, taking care to remove all the air.

- Place the end of the suction tube of the pump in a large container of packing solvent and the outlet tube to waste. Simultaneously open the column outlet (bottom process valve) turn on the pump, and pack the column at a starting flow rate of approximately $1/3$ of the final packing velocity (the packing flow rate has to be bigger than the process flow rate). Ramp up the speed until the packing flow rate is reached. This prevents hydraulic shock to the forming bed and therefore prevents uneven packing of the column. This operation should be performed with the chromatography skid. Some resins require starting with the packing flow rate, not ramping up the speed gradually. After flow has been started, the resin bed starts to form at the bottom, and the mobile phase begins to clear from the top (Figure 10.28b).

- Once the resin bed height is stable, stop the pump and quickly close the bottom process valve (Figures 10.28c and 10.29b).

- Open the process top valve, and lower the top frit until the resin bed; then close the valve.

- Open the column outlet again and restart the pump to compress the bed further.

- Once the resin bed height is stable, stop the pump and, leaving the bottom valve open, lower the top frit to the desired (final) packed bed height (Figures 10.28d and 10.29c).

(a)   (b)   (c)   (d)
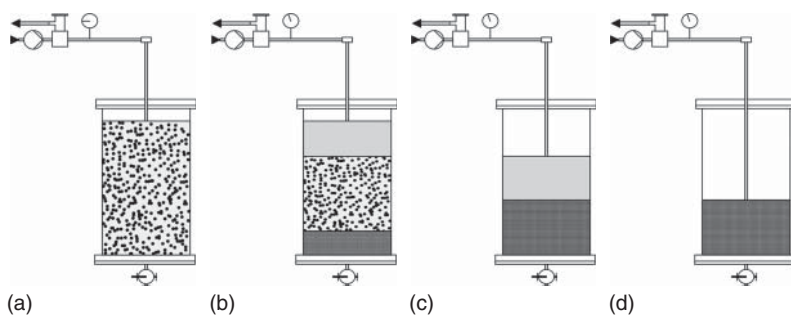
Figure 10.28 The principle of flow packing.

(a)   (b)   (c)
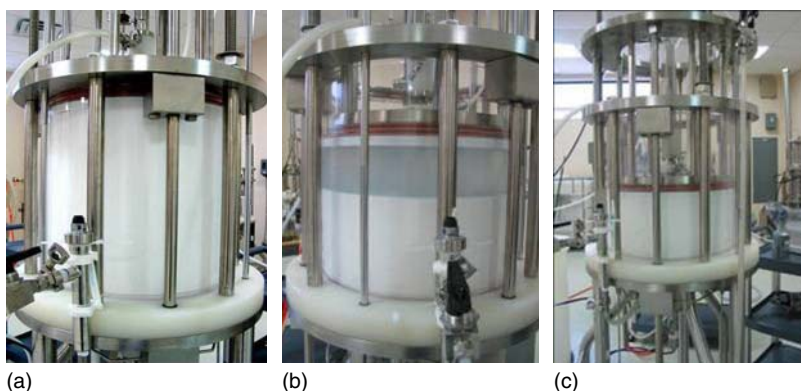
Figure 10.29 Flow packing of chromatography resins (46 cm i.d. Eastern Rivers column).

(a)   (b)   (c)
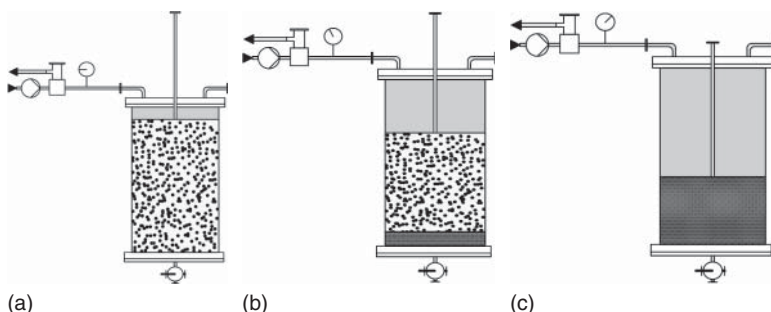
Figure 10.30 The principle of DAC packing.

10.5.5 Dynamic Axial Compression (DAC) Packing

The principle of the DAC packing is to transfer the slurry into the column and then pack using a hydraulic piston. To be able to perform a good DAC packing, the column volume should be sufficient to receive all the slurry, or an extension tube should be attached to the column body (Figure 10.30):

- Transfer the slurry into the column as already described for flow packing (Figures 10.27 and 10.28a).
- After the slurry has been transferred into the column, the piston is slowly lowered with the top valve open to remove air. When the expelled liquid is free of air bubbles, the top valve is closed (Figures 10.30a and 10.31a).
- Open the process bottom valve (column outlet), and lower quickly the piston (Figures 10.30b and 10.31b) until the final bed height (Figures 10.30c and 10.31c). Block then the piston, or keep it in "down" position with the required pressure.

10.5.6 Stall Packing

The principle of the stall packing method is to fix the final bed height of the column in advance, before introducing the media:
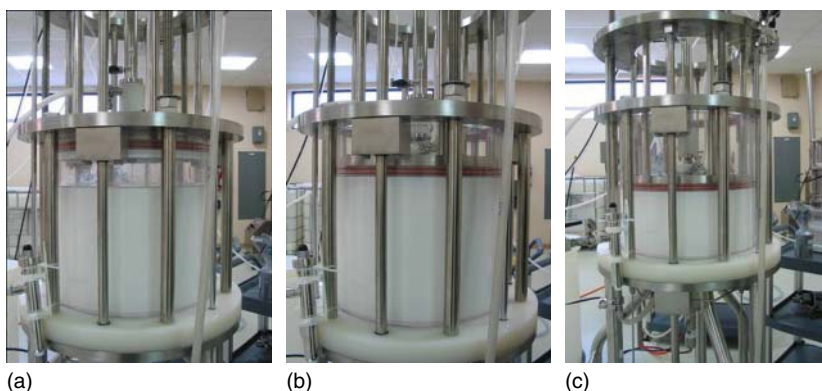
Figure 10.31 DAC packing of chromatography resins (using a 46 cm i.d. Eastern Rivers column).

- Circulate buffer through the system (buffer vessel → pumping module → buffer vessel) to remove air.
- *Wet the bottom frit*: Using the packing module, introduce buffer upflow through the process valve (bottom), keeping the process top valve open, until the column is filled up to the height of several centimeters.
- The column may or may not be filled with packing buffer before introducing the resin slurry. It is usually advantageous to have the column filled with buffer, as this will result in more homogenous slurry distribution. As shown in Figure 10.32, the bottom valve will be used for packing (introduction of the slurry) and is therefore switched to the "Pack" position. Alternatively, the top valve may be used for packing.
- Introduce the resin into the column by the bottom packing valve with the requested flow rate (top process valve open) controlling the pressure (Figure 10.32a); after the column is filled with slurry (Figure 10.32b), slurry is continued to be introduced into the column, with the bed starting to build up from the top (Figure 10.32c).
- Once the packing pressure is reached, decrease the flow rate in order to keep the packing pressure.
- Once no more resin can be introduced into the column, the pump must be stopped, and the column valves set to process mode ("RUN" position) (Figure 10.32d). Finally, flow is started and the packed bed conditioned with buffer in downflow mode (Figure 10.32e).

10.5.7 Combined Method (Stall + DAC)

The principle of this method is to fix first the piston height around 5 cm above the final bed height, pack against the piston (stall), and finally fix the final bed with the DAC:

- Circulate buffer through the system (buffer vessel → pumping module → buffer vessel) to remove air.
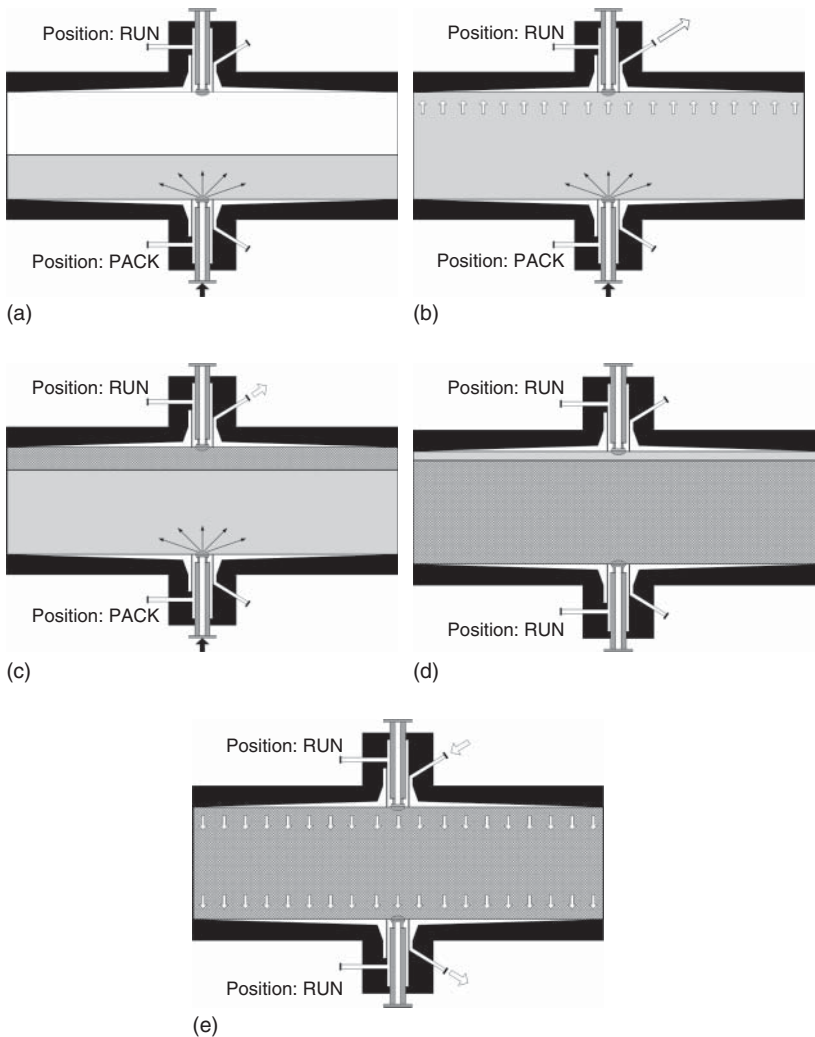
Figure 10.32 The principle of stall packing.

- Adjust the position of the piston around 5 cm higher than the final bed height. Fill the column with buffer: packing buffer is sent upflow into the column in order to remove air. Excess of buffer is sent back to buffer vessel. This operation is performed through the process valves of the column.
- Pump packing buffer with the packing skid through the slurry valves to remove all the air.
- Column filling with slurry: Open the bottom piston process valve, and inject the slurry upflow. This direction is preferred if the hardware allows it otherwise; slurry can be introduced through the top valve in downflow (Figure 10.33a). Buffer is sent back to the buffer tank. The flow of slurry is kept
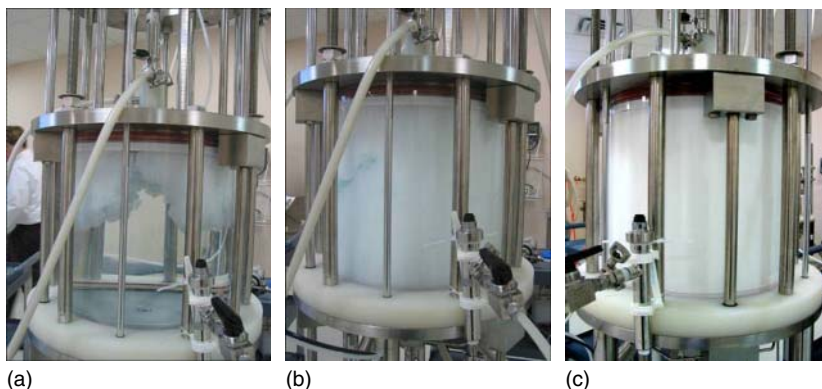
Figure 10.33 Stall packing phase of the combined method (a 46 cm i.d. Eastern Rivers column).

at the desired flow rate until the packing pressure is reached. Thereafter, the flow rate is reduced to avoid that the maximum packing pressure is exceeded.

- Once slurry introduction is almost finished (Figure 10.33b) and the slurry vessel is almost empty, the buffer is sent back to the slurry tank instead of the buffer tank. It is very important not to introduce air in the system at that step!
- Keep that operation running for a few minutes in order to introduce all the resin in the column and stabilize the bed (Figure 10.33c).
- Inject buffer upflow through the packing valves in order to flush them. Buffer is sent back to the buffer tank.
- Bed height adjustment: Close the packing valves but keep the process top valve open. Then move down the piston until the final bed height is reached.
- Close the top process valve and block the piston.

10.5.8 Vacuum Packing

An alternative to using pressure for column packing is the use of vacuum as shown in Figure 10.34:

- Transfer the slurry to the column, equipped with the packing reservoir. After introducing the slurry, apply the vacuum by connecting the column inlet line with the vacuum source through a safety bottle. The vacuum should be approximately 100 mbar. Check the quality of the vacuum before introducing the slurry by closing the top of the packing reservoir.
- Maintain the vacuum constant over the suction time (5–45 minutes, depending on the particle size and the adsorbent quality). Immediately after the top of the column bed falls to dryness, disconnect the vacuum line.
- Remove the packing reservoir, close the column with the top flange, and connect the outlet line to a solvent container. Compress the column with the hydraulic pump to the appropriate compression, and secure the piston from moving back by means of the safety stop. The compression varies from 10 bar for polymeric materials up to 80 bar for very rigid silica adsorbents.
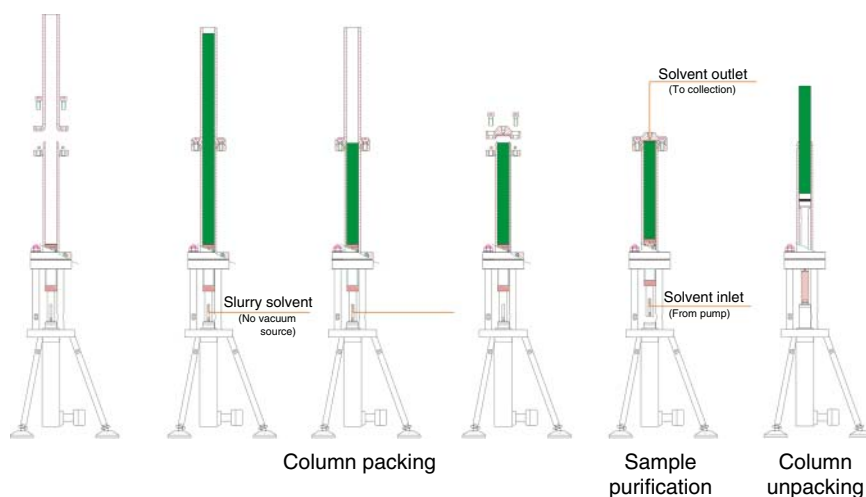
Figure 10.34 Vacuum packing.

- Place the column in the system; do not connect it to any subsequent unit yet to avoid damaging it by particles that may come out of the column.
- Start your preparative system with a mobile phase of known viscosity, for example, methanol–water (80 : 20%) for RP systems or isopropanol for normal phase systems. Use a linear flow rate at least as high as the flow rate later used in operation of the column. The pressure drop should be slightly higher than the operational pressure drop to be used. Let the system run for a short time.
- Stop the pump, recompress the column to the compression pressure, and read-just the safety stop.
- Repeat steps 5 and 6 up to three to four times. During the last repetition, there should be no further movement of the safety stop when compressed.

10.5.9 Vibration Packing

Chromatography media for LPLC applications characterized by particles with rigid and irregular shape, like irregular silica or controlled pore glass (CPG), require a different packing approach. If a force is exerted on such a bed, the incompressible particles form stable bridges that hinder the particles to settle uniformly and to a form stable packing.

At laboratory scale stable beds can be achieved easily just by filling the column and tap packing the column tube with a hard object. This will allow the particles to settle in a uniform bed. However, at large scale the most common packing methods suitable for soft or semirigid resins cannot be used for rigid and irregular matrixes as they may cause nonuniform compression, bed deformation, channeling, void formation, and crushing.

Vibration packing is the method developed specifically for this type of matrixes. A vibration device applied externally at the column tube generates the
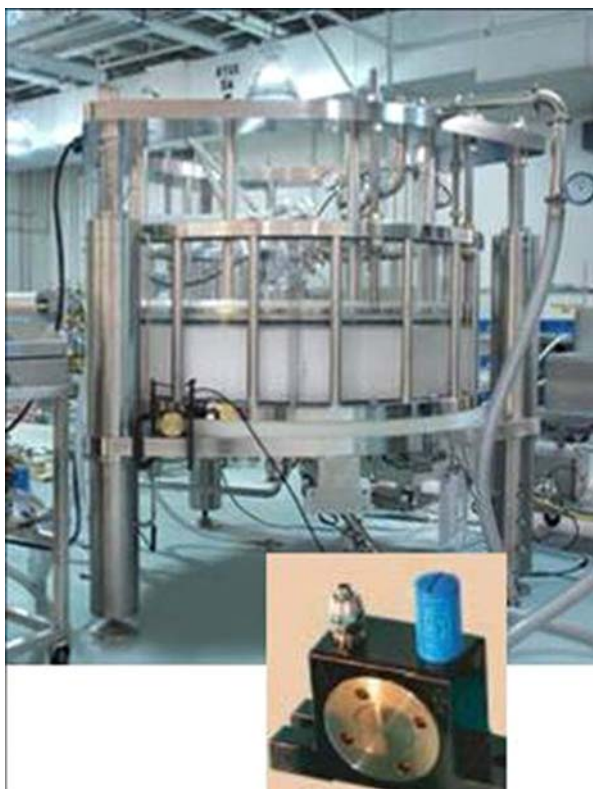
Figure 10.35 Vibration packing of rigid matrices in a process column. The vibration device is clamped externally on the column flange.

right amount of energy to break the bridges (similar to the tap packing at lab scale), allowing particles to settle properly and occupy the minimum bed volume in the column. Alternating vibration sequences and downflow through the bed is also applied to consolidate rigid particles and obtain homogeneous and stable beds without damaging the particles (Figure 10.35).

10.5.10 Column Equilibration

Once the packing is finished, it is recommended to stabilize the bed. Monitoring the pressure/flow curve during the following steps allows to confirm the good packing:

- Connect the column to the chromatography skid (or other type of pumping module).
- Rinse the column with 10 BV of packing buffer downflow.
- Rinse the column with 10 BV of packing buffer upflow (caution: for some resins, reverse flow could damage the bed; in that case, skip that step).
- The column is ready for testing.

Table 10.13 Test systems for normal phase and reversed phase columns.

Normal phase silica	Reversed phase silica
Mixture of 1 ml dimethyl phthalate, 1 ml diethyl phthalate, and 1 ml dibutyl phthalate	
Filled up with *n*-heptane–dioxane (90 : 10) to 100 ml	Filled up with MeOH–H$_2$O (80 : 20) to 100 ml
Addition of 50 µl toluene	Addition of 10 mg uracil
Mobile phase: *n*-heptane–dioxane (90 : 10)	Mobile phase: MeOH–H$_2$O (80 : 20)
Injection amount: 0.1 µl ml^{-1} V_c (40 µl for a 50 mm × 200 mm column)	

If dimethyl phthalate is substituted for dipropyl phthalate, the dioxane-based eluent (usage avoided in industry) can be replaced by a mixture of *n*-heptane–ethyl acetate in the same 90 : 10 volume ratio.

10.5.11 Column Testing and Storage

10.5.11.1 Test Systems

For analytical scale columns, a simple test mixture consisting of a t_0 marker and different phthalic acid esters can be used to check the performance and some basic selectivities of packed columns. The advantage of phthalic acid esters as test substances is their liquid nature and good miscibility with different mobile phases. In addition, they can be used in normal phase as well as reversed phase systems. Table 10.13 gives the compositions of test mixtures for normal and reversed phase columns.

Figure 10.36 shows a typical chromatogram of the test mixture described in Table 10.13 on a $d_c = 50$ mm column packed with LiChrospher Si 60, 12 µm.

The diethyl phthalate peak (third peak of the test mixture in normal phase systems as well as reversed phase ones) can be used to calculate the number of theoretical plates (N) per meter of bed height according to Section 2.2.3.

Production-scale columns can be easily tested using a small quantity of reference standards of the products to be separated using the standard elution conditions. Also a good strategy (especially for very challenging separations) is to provide the supplier of the used stationary phase with these standards to evaluate
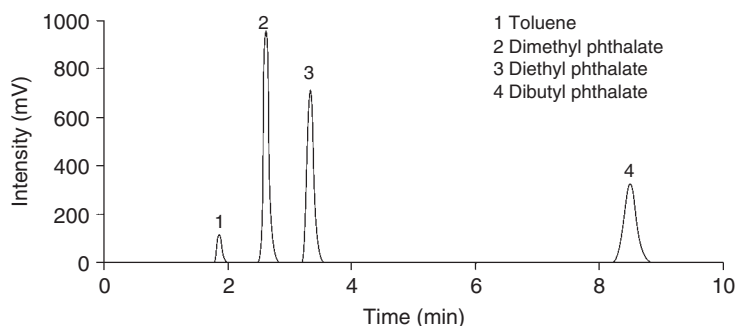
Figure 10.36 Test chromatogram of a t_0 marker and three phthalic acid esters.

a new batch of their product prior to shipment to always assure a product fulfilling the requested purification task.

For LPLC production with large-scale packing, the efficiency is usually checked by introducing a simple marker that is detected after elution with an appropriate detector. Most common markers are:

- 1 M NaCl detected by conductivity;
- acetone (around 2%) detected by UV (280 nm).

The volume of the marker to be introduced on the column is usually 2.5% of the bed volume. The chromatogram is then analyzed, and the acceptance criteria are typically based on:

- peak profile (a unique peak without shoulders);
- height equivalent to the theoretical plate (HETP);
- asymmetry of the peak.

The values expected for HETP or asymmetry may vary depending on the resin and the equipment used. Nevertheless, it is important to reduce the dead volume between the inlet port of the tracer and the column itself to avoid dilution of the tracer.

10.5.11.2 Hydrodynamic Properties and Column Efficiency

For complete characterization of the column performance, the efficiency has to be tested over the whole operation range of linear velocities. The injection of a test mixture at different flow rates can be easily automated with modern HPLC equipment and yields the pressure drop versus flow curve of the adsorbent as well as its HETP curve. By using marker substances with different molecular weights, the influence of the mass transfer resistance (C term: Section 2.2.3) can be investigated. Figure 10.37 shows the HETP curve for two similar adsorbents, which exhibit large differences at high flow rates.

Two test compounds with molecular weights of 110 and 11 000, respectively, were used to obtain the data. The minimum plate height at the lowest velocity
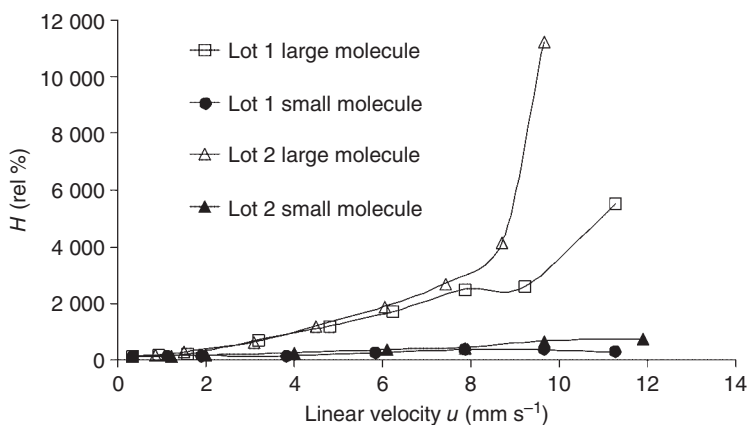
Figure 10.37 Plate height–linear velocity curve of two different adsorbents obtained with a low-molecular-weight (MW = 110) marker and a high-molecular-weight (MW = 11 000) marker.

Table 10.14 Recommended solvents for storage and flushing.

Adsorbent type	Flushing solvent	Storage solvent
Normal phase	Methanol or other polar solvent	Heptane + 10% polar compound (isopropanol, ethyl acetate)
Reversed phase	Methanol or acetonitrile, tetrahydrofuran (THF), or dichloromethane for oily samples	>50% organic in water
Ion exchange (silica based)	Methanol	>50% organic in water
Biopharmaceutical purification	2 M NaCl and 1 M NaOH For more sensitive ligands: elution buffer and/or alcohol in water	<0.1 M NaOH For more sensitive ligands: equilibration buffer

was set to 100%, and the percentage increase in plate height is plotted against the linear velocity. For both adsorbents, the plate height for the large molecule clearly shows a steeper increase than for the small molecule. At a linear velocity of approximately $8\,\text{mm}\,\text{s}^{-1}$, the plate height for the large molecule increases dramatically for one of the adsorbents. This gives a hint of some obstacles within the pore system of that adsorbent, which are of course more severe for larger molecules. Even if the preparative process is not operated at such high linear velocities, the adsorbent properties should be carefully examined beforehand to avoid any unnecessary extra contribution to the axial dispersion.

10.5.11.3 Column and Adsorbent Storage

If packed columns or adsorbents removed from columns are to be stored for a period of time, the adsorbent should be carefully washed and then equilibrated with a storage solvent. Compounds strongly adsorbed to the adsorbent and, especially, any source of microbial growth have to be carefully removed before the adsorbent is stored. In addition, any buffer substances or other additives, which might precipitate during storage, have to be washed out. For flushing and storage different solvents are recommend (Table 10.14).

10.6 Process Troubleshooting

The chromatographic equipment is quite complex, and many technical failures may happen when operating a preparative device. Most of the time, a technical problem is directly visible or even detected by the system if this one is automated.

However, several technical problems are not trivial to identify. It is impossible to give an exhaustive list of the problems that may occur, but the attempt of this section is to give advice to troubleshoot the most frequent problems observed on a preparative chromatographic process (for additional information and discussion on troubleshooting, see monthly columns of Dolan et al. in LCGC Chromatographyonline.com or Dolan and Snyder 1989).

This section is divided into three parts: The first one will describe the main technical failures that occur in the process and give the way to diagnose the failure and the way to troubleshoot it. In a second part, we will examine the loss of performances that can be observed on a system and list the most probable root causes and the way to avoid or correct it. In the third part, we will deal with the stability of the column and the way to monitor it.

10.6.1 Technical Failures

Table 10.15 describes technical failures that may happen in chromatographic systems.

Table 10.15 Possible technical failures in a chromatography system.

Equipment part	Problem	Diagnosis	Corrective action
Gradient valve	Leakage	Wrong gradient composition–variation retention	Check tightness and repair/replace valve
Injection pump	Wrong flow rate	Wrong injected volume–modification peak shape and height	Check flow rate
	Pressure fluctuation		Clean/replace check valve Check membrane integrity Check volume hydraulic oil
Eluent pump	Wrong flow rate	When flow rate is controlled by a flow meter, an increase of the pump frequency is observed	Check frequency compared to expected value
	Pressure fluctuation		Clean/replace check valve Check membrane integrity Check volume hydraulic oil
Column	Pressure increase Loss of efficiency Variation retention Loss of purity/yield	See next section for diagnosis and corrective action	
Detector	No signal	Check UV light intensity	Change UV light
	Smaller signal Noise increase	Check solvent degassing (noise)	Check bubble trap/degas solvent
Collecting valve	Leakage of one valve	Loss of purity/yield	Check tightness and repair/replace valve

10.6.2 Loss of Performance

During the operation of a chromatographic process, a loss of performance may occur. It is important to track the process drifts that may announce a more serious issue. Sometimes, the problem can be quickly corrected in order to prevent the loss of the purified products.

The most common issues encountered when operating a chromatographic device are:

- an increase in the pressure measured after the eluent pump;
- a progressive loss of peak resolution (due to loss of efficiency);
- a variation of the elution profile (change of retention);
- a loss of purity/yield of the purified products without any significant change in the preparative chromatogram.

The most common root causes for these problems are examined to define the way to troubleshoot it.

The lifetime of a chromatographic column strongly depends on the application and on basic precautions to protect it. Some applications require to repack the column with fresh packing material after each injection (e.g. purification of specific natural substances), whereas several large-scale HPLC equipment are used continuously during few years without any significant loss of performances (e.g. chiral separations).

10.6.2.1 Pressure Increase

Most of the time, the pressure is measured after the eluent pump. On well-designed HPLC equipment, the operating pressure is mainly due to the pressure drop in the column.

A pressure increase can also be observed when inline filtration is implemented. Appropriate positioning of the pressure sensors is required to measure the pressure drop on the filters. When the pressure drop is too large, the filters need to be replaced or cleaned. If the frequency is too high, prefiltration of the crude can be implemented or should be revised.

When the pressure increase is linked to the column, several root causes are possible:

- *Insolubles in the crude or in the eluent*: A chromatographic column contains a bed of particles, which constitutes an excellent filter media. Most of the micron-sized particles pumped through the column will be systematically retained on an HPLC system packed with 10–20 μm particles. It is therefore strongly recommended to filter the inlet streams of the process. Prefiltration and online filtration of the crude solution are strongly recommended. It is also recommended to filter the eluent used for the separation. Even if the insoluble content is low, the solvent volume pumped through the column is large and could rapidly lead to an accumulation of these particles in the column and to a pressure increase. Most of the time, this kind of problem is difficult to detect; the pressure increase starts slowly, but the evolution of the pressure in a contaminated column is exponential. A column backflush can potentially remove the particles accumulated on the inlet frit.

- *Strongly retained compounds – gelation at the inlet of the column*: An increase in the column pressure drop can also be linked to the retention of strongly retained compounds. When the injected crude mixture contains impurities with a strong affinity to the stationary phase, a progressive accumulation of these compounds happens at the inlet of the column. This could lead to a gelation or precipitation of these accumulated products.

  This will progressively limit the flow and increase the pressure in the column. In order to avoid it, several solutions exist:

  – *Washing*: Column wash with the appropriate eluent in order to desorb the strongly retained impurities. This can be performed between the injections or at an appropriate periodic interval.

  – *Online-precolumn*: This is a good way to preserve the stationary phase of the column. This pre-column can be washed and/or repacked, keeping the integrity of the column. However, the type of the pre-column can also affect the efficiency and therefore reduce the achieved resolution.

  – *Pretreatment of the crude*: An alternative to the preceding solution is to pre-purify the crude solution on another column filled with a similar material or a simple filtration aid as diatomaceous earth or activated carbon to remove strongly retained impurities. If eventually chromatographic conditions for this pretreatment should be developed to remove the critical impurities, most of the time, a two-step approach is more favorable than a single step. This could also help to work under isocratic conditions and to get favorable process conditions to recycle solvent.

- *Apolar solvents and polar impurities*: When a very apolar solvent is used as the eluent, a column can completely be blocked within a very short period of time by the introduction of small traces of a viscous polar substance (e.g. glycerol, dipropylene glycol), which are not soluble in the used solvent system. This might happen if, for instance, the solvent supplier has insufficiently cleaned the filling equipment used to fill the drums. Therefore, a thorough analysis of the incoming solvent batch is necessary.

- *Fines in the stationary phase*: According to Darcy's law (Section 2.2.5) describing the pressure drop through a bed of monodispersed particles, the pressure is inversely proportional to the square of the particle size.

  The situation changes dramatically when the stationary phase is polydispersed and contains small particles. These fines will fill the empty space between the beads and will therefore significantly increase the pressure drop through the particle bed. The smallest particles will also migrate through the bed and get accumulated on the outlet frit, which will be rapidly clogged.

  Most of the modern stationary phases offer a good control of the particle size dispersity, but fines can appear under stressed conditions: frictions of particles, inappropriate packing conditions, too high hydraulic pressure on a DAC column, repetitive packing/unpacking of the same stationary phase, and so on. Irregular stationary phases are generally more sensitive to mechanical attrition than spherical material.

  The following advice should be followed to avoid an unexpected increase of the pressure drop during operation:

o *Visual check of the stationary phase before packing*: A small sample can be used for a quick lab test. A sedimentation trial can be performed in the lab with less than a gram of stationary phase. The solvent should be selected so that the particles can sediment in a few minutes. Methanol is often an appropriate candidate for this test.

The stationary phase should sediment, and the turbidity of the supernatant clearly shows if fines are present in the sample. A reference trial can be made with a new batch of stationary phase to evaluate the aging of a reused batch.

When the supernatant is turbid, fines are present that will potentially lead to a too high pressure drop on the column. It is advised either to change the stationary phase or to regenerate it. A mechanical sedimentation process can be applied to remove fines (repetition of 5–10 successive sedimentations and removal of the supernatant to eliminate fines).

o *Check of the packing procedure*: The packing procedure could potentially create a mechanical stress to the stationary phase and break the silica beads, leading to fines in the column. This mechanical stress could be linked to the slurry preparation (inappropriate mixing device, transfer pump), to the hydraulic pressure, and so on. Most of the packing suppliers assist their customers with detailed protocols for an efficient column packing.

o *Check of the hydraulic system*: A too low hydraulic pressure compared with the column operating pressure could potentially damage the stationary phase. The hydraulic pressure should always stay higher than the operating pressure to ensure the best stability of the stationary phase. When the hydraulic pressure gets closer to the operating pressure, the piston could have small displacements and stress the particles.

o *Check pressure pulsation of the elution module*: Depending on pumps' technologies, pulsations of a single or multiple head pump could be quite important, and some industrial systems are equipped with a pulse dampener to smooth the flow variations. A lack of dampening could lead to a mechanical stress on the phase particles (small displacement of piston, mechanical stress on fragile packings). It has to be emphasized that with multiple head pumps, pulse dampener is not necessary on HPLC units with traditional preparative packings.

o *Check the hydraulic pressure*: Each packing has its own mechanical resistance. For example, a 100 Å silica material resists to a mechanical pressure of more than 100 bar, whereas wide pore silica (for example, 3000 Å) has a more limited mechanical resistance and could potentially break with a hydraulic pressure of 30–40 bar. The hydraulic pressure of a DAC column must be selected according to the stationary phase specifications.

A column backflush could temporarily reduce the pressure drop by removing the fines accumulated in the outlet frit. However, a backflush will not solve the problem, and the pressure will rapidly increase again. The only way to come back to an acceptable pressure is to unpack the column and to change the stationary phase or to remove the fines.

• *Cleaning of the frits*: The column frits are often reused when repacking a large-scale column. However, small particles (fines or insoluble particles)

are probably present in the frit. De-packing the column also generates fines that would stay trapped in the frits. This would potentially lead to an increased pressure drop on the column after repacking. It is therefore strongly advised to systematically clean the frits or replace the frits when repacking a chromatographic column.

Two main ways can be used to clean the frits:

o *Chemical cleaning*: Concentrated caustic sodium hydroxide is often used to dissolve silica.

o *Mechanical cleaning*: Mechanical cleaning used to clean the frit. A high-pressure water system is often the most efficient way to clean blocked frits. This can be combined with a chemical cleaning to get rid of all residues in the frits (Section 10.3.2.2).

10.6.2.2 Loss of Column Efficiency

The column efficiency characterizes the dispersion of the product in the chromatographic column. A loss of efficiency will directly affect the peak resolution and therefore the achieved purity and/or yield for the purified product(s).

Several physical causes could disturb the elution stream through the column, leading to a loss of efficiency:

- *Clogged frits*: Accumulated insoluble particles from the crude or fines from the stationary phase can progressively block the frits and disturb the flow distribution in the column. This phenomenon is often associated with an increased pressure drop on the column, as explained in Section 10.6.2.1. A lack of efficiency can also be observed on a newly packed column when the frits are not appropriately cleaned before used.

- *Fine particles in the stationary phase*: Fines will progressively migrate through the bed and block the outlet frit, leading to a disturbance of the flow within the column. The column efficiency can be good right after the packing but could progressively become worse, and the pressure drop could increase due to the migration of the fines. A column backflush could improve the situation, but for a very limited duration. The only way to come back to a stable and efficiency column is to unpack it and to remove fines.

- *Heterogeneous packing*: Inappropriate conditions (e.g. slurry concentration, slurry solvent, speed) could lead to a heterogeneous packing with unordered particles, leading to preferential paths through the bed. This will disturb the flow and will strongly affect the column efficiency. A backflush could sometimes help, but most of the time, the column needs to be repacked.

- *Temperature*: This criterion is often underestimated in the operation of a preparative chromatographic process. Temperature has a direct impact on the adsorption isotherms and modifies the retention of the separated compounds. A significant loss of efficiency can be observed with a radial heterogeneity of the temperature, which will modify the retention of the products. This heterogeneity is linked to a difference between the temperature of the eluent and the temperature of the column body. This is particularly important to consider on small-scale preparative devices (5–10 cm i.d. columns); the wall effect is less significant for larger columns.

A favorable effect on the column efficiency can be achieved when the column body is slightly warmer than the eluent (1–2 °C) (Dapremont et al. 1998) to correct the bed heterogeneity near the column wall.

- *Viscous fingering effect*: This phenomenon is observed when the viscosity of the injected sample is significantly larger than the eluent viscosity. A hydrodynamic instability appears within the column, leading to a fingering elution of the viscous solution in the bed. This disturbance of the flow will strongly affect the obtained efficiency. A reduction of the injected concentration is efficient to correct this effect, which can appear during a process scale-up (Section 10.3.2.2).

10.6.2.3 Variation of Elution Profile

This section mainly focuses on the parameters that could lead to an evolution of the elution profile during a purification campaign. Several root causes are listed, which could affect the elution profile and modify the retention or disturb the peak shape.

- *Variation of temperature*: As described in the preceding section, temperature has a major impact on the retention and could potentially affect the column efficiency.
  This should be taken into account to ensure the reproducibility of the chromatographic process, and a temperature control with an online heat exchanger is preferred to get a reproducible process.
  A variation of the elution profile could potentially occur when the temperature is not controlled and when a fresh solvent is loaded in the eluent tank used to feed the system. The stored solvent could potentially be cooler or warmer, leading to a disturbance of the elution profile.
- *Solvent composition of the eluent*: Most of the chromatographic separations use a binary solvent mixture for the separation and sometimes a buffer solution. A wrong solvent preparation could lead to a wrong composition and therefore modify the retention of the products. A technical failure of the gradient module could also disturb retention.
- *Solvent contamination*: Contamination of the solvent used for the eluent preparation could disturb the separation. This could, for example, happen with a recycled solvent: this is particularly critical when the crude contains volatile impurities, which could be evaporated together with the solvent and progressively concentrated in the recycled eluent.
- *Solvent grade*: A modification of the solvent grade could potentially affect the obtained separation. For example, the variation of the water content of the organic solvent used under normal phase conditions could modify the activity of silica. Therefore, it is suggested to keep the same solvent grade between the development and the production stage.
- *Solvent composition to dissolve crude*: The crude product needs to be dissolved before injection. The solvent composition used to dissolve the crude should theoretically be identical to the eluent composition used after injection. Sometimes, another solvent composition is used to get a better solubility of the

crude. This solvent could potentially have higher eluent strength and could therefore disturb the retention of the products.

- *Remaining impurities/solvent in the crude*: The crude could potentially contain remaining traces of solvent or impurities from the preceding process step, which could disturb the chromatographic separation. A variation of the solvent content in the crude could lead to a variability of the elution profile, which could be strongly disturbed.
- *Loss of capacity of the stationary phase*: Impurities could be strongly retained on the stationary phase, leading to a progressive loss of loading capacity. This will progressively lead to a loss of retention and of resolution. Regeneration of the stationary phase with a strong desorbent could potentially help to recover the initial properties.
- *Pumping module problems*: A pumping issue could potentially disturb the obtained elution profile. Stability of the obtained flow rate should be controlled if an online flow meter is available.
- *Valve leakage*: A leak of one valve, for example, in the gradient module, could disturb the elution profile.

10.6.2.4 Loss of Purity/Yield

The last (and probably most difficult) situation described is when a loss of purity and/or yield occurs without any modification of the preparative chromatogram.

- *Modification of the feed impurity profile*: The impurity content may change, leading to a more difficult separation. The injected crude mixture may also contain new impurities, which might be coeluted under the applied preparative conditions. An liquid chromatography mass spectrometry (LC-MS) analysis using an analytical method based on the preparative conditions (same stationary phase, same eluent, but small injection amount) could be used to identify new coeluted impurities.
- *Valve leakage*: A leak of one valve of the collecting module could potentially lead to a cross-contamination between the collected fractions. This could be checked by changing the collecting ports.
- *Design of the collector*: An inappropriate design of the collecting module can lead to a cross-contamination between the collected fractions due to the dead volumes of the common pipe. Changing the order of the collecting port could potentially reduce the impact of the cross-contamination.

10.6.3 Column Stability

Any resin, once packed, has a "shelf life" for a determined process. The number of cycles a packed chromatography column can be used has to be validated in order to guarantee specified yields and product quality.

Nevertheless, some unexpected events may occur during the process, influencing the resin integrity or the stability of the chromatographic bed:

- Introduction of air into the column;
- Overpressure inside the column;
- Use of an inadequate solution;

- Use of a correct sanitizing solution but during a too long period;
- Defect of the inflatable gasket of the column;
- Movement of the piston that is not stabilized or fixed correctly.

Only referring to the validated number of cycles is of course not enough to guarantee a reproducible performance of the column. Additional measures can be foreseen in order to identify quickly any problem:

- Regular HETP and asymmetry test (for example, after each production batch or any other period);
- Comparison of each elution peak with a reference chromatogram;
- Calculation of the column performance by integrating the chromatogram profile.

Different symptoms allow to suspect a problem with the resin integrity or the bed stability:

- decrease of the yield from batch to batch;
- increase of impurity rate from batch to batch;
- several peaks or shoulders during elution (comparison to reference peak);
- increase of the back pressure of the column;
- tailing or fronting increasing from batch to batch;
- shifting of the retention time.

Note that these symptoms can also have other causes, like defaults on the batch loaded, and are not necessarily linked to the column itself.

10.7 Disposable Technology for Bioseparations

Compared to fine chemicals, processes for the production of biopharmaceuticals have to fulfill more strict regulations of the surveillance authorities in order to meet extensive requirements concerning purity, quality, and stability of the product.

Pharmaceutical companies are continually striving to improve and optimize the process of manufacturing biotherapeutics in order to increase productivity, reduce capital investments, reduce operational downtime, and minimize risk of process failure due to cross-contamination. A lot of money, time, and resources are spent on equipment cleaning and sanitization.

Especially in a multipurpose manufacturing plant, in which cross-contamination during product changeover is a critical issue, the use of disposables in greater extent should be considered. Nowadays, disposables are used even in a single-product manufacturing plant to save resources for equipment sanitization and to allow a flexible and modular equipment setup.

Several common applications of disposables within chromatography equipment are as follows:

- *Single-use bags for the numerous chromatographic buffers*: Especially in the chromatographic purification of biologics, a great number of buffer types

are needed. Generally, the chromatographic resin needs to be equilibrated before loading the product and then flushed with wash buffer to eliminate the impurities and finally flushed with elution buffer to collect the purified product. Some resins, for example, immobilized metal ion affinity resins, require more than one equilibration buffer, because the resins need to be prepared and charged with metal ions prior to product run. Furthermore, after product run the resin also needs to be regenerated to replace lost ions (for ion-exchange resin) or strip off the metal ion (for immobilized metal ion affinity resin) and then sanitized and stored in a bacteriostatic storage solution. One should also not forget the necessity to regularly check for irregularities in the packed bed by using tracer compounds. Due to many buffer types used in chromatographic processes, the application of single-use bags can be recommended to prevent buffer cross-contamination and to save a lot of production area. Single-use bags are available in different sizes. Large bags are usually placed inside stainless steel bins, which can be stacked to save spaces. Connection between bags and buffer header of the chromatographic equipment can be established by welding connection hoses and by sterile connectors.

- *Single-use sterile connectors*: Sterile connectors are usually used to establish a sterile flow path between the chromatographic equipment and other flexible exchangeable units, e.g. feed or eluate tanks, buffer bags, and filters. They can also simplify the equipment design significantly if used in a single-use transfer line, because any hard-piped transfer line must be designed to be suitable for CIP procedures. It is common that a sterile connector (e.g. Lynx connector) has two separated sides. The gamma-sterilized side contains a hose, which can be welded to another sterile hose, so that a connection can be established without compromising the sterile space. The other side of the connector, which is not gamma-sterilized, is connected manually to the equipment. After the equipment has been cleaned, the flow path between both previously separated sides can be opened.
- *Single-use filters*: It is common to install a single-use guard 0.2 μm filter in front of the column to protect the resin from any incidental particle, e.g. unsolved buffer component or defective gasket material.
- *Single-use flow path*: Especially in a multipurpose plant, the necessity to avoid cross-contamination and to reduce product turnover time induces a trend to use disposables for those parts of the equipment (including pipes, valves, and pumps), which are wetted by process fluids (Figure 10.38). The costs of these disposable facilities have to be balanced by direct savings of costs for buffer, cleaning and sanitizing solutions, and labor costs, but overall profitability is also influenced by additional factors like decreasing time to clinic and time to market.
- *Single-use membrane capsule*: When comparing column and membrane chromatography, the differences in mass transfer have to be kept in mind. As illustrated in Figure 2.11, mass transfer resistance of porous adsorbents is depending on convective transport, film diffusion at the surface of the solid phase, and pore diffusion within the beads, while the resistance of membranes occurs mainly by convection and minimal surface diffusion.

Figure 10.38 Disposable multicolumn purification unit (Cadence™ BioSMB Process System, by permission of Pall Corporation).

Compared to packed columns the pressure drop of membrane adsorbers is small and therefore allows extremely high flow rates. On the other hand, the capacity and selectivity of membranes is restricted. This causes the trend that in bioprocesses membrane adsorbers are predominantly used for polishing steps, while capture separation is mainly done by multicolumn chromatography (Section 5.2.9) (Fraud et al. 2010; Brod, Vester, and Kauling 2012; Gottschalk 2008; Bisschops 2012). One of the most frequently applied single-use membrane capsule in biotechnology is anion exchanger, which are used as polishing step in flow-through mode to remove residual host cell DNA.

Brod, Vester, and Kauling (2012) are discussing the application of disposables in biopharmaceutical processes and point out the following:

– Disposables are provided for all unit operations, but they are limited in size depending on the kind of operation. Therefore, pilot scale is offering more opportunities to take full advantage of disposables than production processes.

- In practice, pharmaceutical processes are often of hybrid designs, i.e. a combination of disposables and standard equipment.
- Construction materials for classical equipment are glass and stainless steel, while disposables are made of polymers. This is one reason for size limitations, but besides this, the compatibility of polymers to pharmaceutical products has also to be taken into account.
- For the same process, disposables can be applied repeatedly for a certain process step (single-batch usage). Single-use equipment is a subset of disposables.
- To benefit from the application of disposables, economic decisions have to include plant design, utilities, and manpower.
- Usage of disposables does not exempt the manufacturer from quality assurance, i.e. he has to control disposables delivered by a subcontractor.

10.7.1 Prepacked Columns

Prepacked columns are applied at different stages of process development. The first step is dedicated to scouting for resins, which are appropriate for a given task; it is followed by the refinement of process development by testing and selecting the best resin out of the scouted candidates. Nearly all resin vendors offer prepacked columns of 1–2 ml volume for scouting. The trend goes to microscale columns with further reduced volumes of 50–600 μl, which are predominantly appropriate for screening of numerous resins under different conditions in lab robots (Tingley 2017).

During the next step of process design, the resins are tested under varying process conditions in 0.5–1.2 cm diameter columns (approximately 3–10 ml volume) in order to identify the most appropriate process conditions. These columns have to be carefully packed and should closely simulate the performance of larger production-scale columns. In the course of process optimization and troubleshooting, prepacked columns for pilot- and large-scale application are the scale-up version of the small bench-scale devices. Large-scale columns (packing volumes between 10 and 30 l of resin) are designed for easy installation and for use in any clinical or commercial manufacturing setting. They are packed, tested, and released with specifications for HETP, asymmetry, and pressure drop; all materials wetted by the fluid flow are made from USP Class VI compliant raw materials and must not use animal-derived components in their processing. Columns are first packed under GMP conditions at the vendor manufacturing site, and after quality control (QC) release, each column is tested for specific criteria such as HETP and asymmetry. These columns are manufactured from suppliers presanitized in a similar manner as bulk media so the column is immediately usable for all applications. They are ideal in any application where reproducible column packing is a critical success parameter and where reduced process time and frequent batch changes are of paramount importance.

Nevertheless, some limitations exist for the implementation of prepacked columns. The limited range of diameters and bed heights may restrict the scouting options. This may require multiple cycles on the prepacked column, resulting in greater buffer and time consumption than a traditional column

setup. These are typically offset by the fact that customers do not need to pack and validate the column packing.

Clinical batches are considered to be an ideal application for disposable columns since the batch sizes required at this stage of development are particularly suited to the volumes of resins provided in prepacked columns. Because prepacked columns can be reused and stored between campaigns, they require shelf life data to confirm stability and no leachability from the storage buffers. Additionally, the customers will need to validate and determine what their policies are regarding columns that fail qualification tests such as HETP and asymmetry after they have been used and stored in between campaigns.

Another important aspect is the GMP requirement of quality checking the resin prior to any clinical or manufacturing batch. Resin needs to be analyzed by QC; hence, a sample of the resin stemming from the same lot as the disposable column should be supplied by the manufacturer and be available for testing.

10.7.2 Membrane Chromatography

Membrane chromatographic systems are currently available in two different device formats. Membranes are pleated or wrapped into cartridges (Figure 10.39);

Figure 10.39 Examples of disposable membrane devices. Mustang® Q XT Ion Exchange Chromatography Capsules, by permission of Pall Corporation

alternatively, they are flat sheets stacked into disposable capsules. Both formats allow high flow rates, good adsorption capacities, and good resolving capabilities in an easy-to-use disposable format with the second providing superior scalability from small to product scales. The good resolution provided by membranes allows immediate inclusion into an existing process chain for applications such as DNA viral clearance and removal of endotoxins. An alternative device format consists of up to 80 membranes stacked together in stainless steel housings. This format is designed to withstand higher pressure and is reusable with the drawback of operation downtime due to stacks installation, regeneration cleaning, and validation paperwork.

On the membrane surfaces different active groups are located ranging from quaternary ammonium groups for anion exchange over strong acidic groups for cation exchange to hydrophobic and affinity ligand, e.g. Protein A. A special chemistry has been introduced by the Canadian company Natrix (now Merck Millipore) with a hydrogel polymerized into the large pores of a nonwoven backbone. The larger pore diameter compared to beads is the main advantage of membrane adsorbers especially for the purification of large biomolecules, e.g. plasmid DNA and viruses.

In comparison with membranes, the binding of biomolecules to resins is restricted because in many instances biomolecules are too large to diffuse into the pore structure. Therefore, binding is limited to those active chemistry groups that are on the outer surface of the beads. The more open structure and immediate availability of all active chemistry groups on the surface of a membrane allows greater binding capacities of even very large particles such as plasmids, DNA, and viruses.

The advantages of membranes for the biopharmaceutical manufacturer are savings in cost and volumes of WFI, buffers, and chemicals since single-use membranes do not require cleaning to regenerate the packed columns between cycles/campaigns and the validation and testing of the cleaning process every time. Additional advantages of membranes are time saving since membranes do not require dedicated resources to pack/unpack resins and qualify column chromatography. This greatly reduces operating time for single-use membranes. Finally, due to the high throughput of membranes, large-diameter stainless steel columns weighing several tons can be replaced by a capsule of few liters, which means reduced plant space utilization and increased manufacturing process flexibility.

Due to these early advantages, chromatography membranes were launched in the early 1990s. Unfortunately due to their limited capacity versus chromatography media as well as their lack of capacity at high salt, they did not achieve significant market penetration versus traditional chromatography media (<10%).

Moreover, the reduced salt tolerance of these membranes compared to typical anion exchanger (AIEX) and cation exchanger (CIEX) agarose resins requires at a minimum twofold dilution doubling the volume to be processed. This puts an even greater burden at a critical bottleneck for drug manufacturers since additional buffer tanks are required in the limited floor space of the plant negating the advantage of membrane technology. As discussed earlier, a major component of

inflexibility in plant design is efficient utilization of floor space. Membrane technology substituted column footprint but at the expense of increasing the buffer tank footprint required to operate them.

Other major limitations are related to scaling issues due to distorted or poor inlet flow distribution, nonidentical membrane pore size distribution, and uneven membrane thickness (Zhou and Tressel 2006). Orr et al. (2013) are reviewing technological merits and disadvantages associated with membrane chromatography for bioseparations and provide detailed data about practical applications of membranes for the purification of large biomolecules. They conclude: "low binding capacity continues to be a major limitation but the emergence of membrane adsorbers with an improved binding capacity has significantly widened research scopes and industrial application of membrane chromatography."

To sum up, membranes are an interesting alternative format for column chromatography, especially for disposable applications; however, the pros and cons have to be balanced carefully. Flow-through chromatography is one area where membranes are successfully applied. In this case membranes can process several kilograms of mAb per liter of membrane as compared with only <0.1 kg of mAb per liter of traditional resins.

References

Aldington, S. and Bonnerjea, J. (2007). Scale-up of monoclonal antibody purification processes. *J. Chromatogr. B*, 848: 64–78.

Bisschops, M., (2012) BioSMB^{TM} technology: continuous countercurrent chromatography enabling a fully disposable process, *Biopharmaceutical Production Technology*, 1st Ed. by Subramanian, G., (769–791), Wiley-VCH Verlag GmbH & Co KGaA.

Boysen, H., Wozny, G., Laiblin, T., and Arlt, W. (2002). CDF simulation of preparative chromatography columns considering adsorption isotherms. *Chem. Ing. Tech.* 74: 294–298.

Brod, H., Vester, A., and Kauling, J. (2012). Möglichkeiten und Grenzen von Disposable-Tehnologien in biopharmazeutischen Verfahren. *Chem. Ing. Tech.* 84: 633–645.

Broughton, D.B. and Gerhold, C.G. (1961). Continuous sorption process employing fixed bed of sorbent and moving inlets and outlets. US Patent No. 2,985,589.

Carta, G. and Jungbauer, A. (2010). *Protein Chromatography: Process Development and Scale-Up*. Weinheim: Wiley-VCH Verlag GmbH.

Dapremont, O., Cox, G., Martin, M. et al. (1998). Effect of radial gradient of temperature on the performance of large-diameter high-performance chromatography columns, I. Analytical conditions. *J. Chromatogr. A* 796: 81–99.

Dolan, J.W. and Snyder, J.J. (1989). *Troubleshooting LC Systems: A Comprehensive Approach to Troubleshooting LC Equipment and Separations*. Totowa, NJ: Humana Press Totowa.

Fraud, N., Gottschalk, U., Lim, J., and Sinclair, A. (2010). Technical and economic benefits of membrane chromatography during polishing steps. *BioPharm Int.* 23: 46–52.

Gottschalk, U. (2008). Bioseparation in antibody manufacturing: the good, the bad and the ugly. *Biotechnol. Prog.* 24: 496–503.

GE Health Care (2011). Ion exchange chromatography & chromatofocusing, principles and methods, http://www.gelifesciences.com/aptrix/upp00919.nsf/content/LD_273053445-R350 (viewed Oct. 2011).

Johnson, C., Natarajan, V., and Antoniou, C. (2014). Evaluating two Process scale chromatography column header designs using CFD. *Biotechnol. Prog.* 30: 837–844.

Kearney, M. (1999). Control of fluid dynamics with engineered fractals – adsorption process applications. *Chem. Eng. Commun.* 173: 43–52.

Kearney, M. (2000). Engineered fractals enhance process applications. *Chem. Eng. Prog.* 96 (12): 61–68.

Meyer, V.R. (1999). *Fallstricke und Fehlerquellen der HPLC in Bildern*. Heidelberg: Wiley VCH.

Orr, V., Zhong, L., Moo-Young, M., and Chou, C.P. (2013). Recent advances in bioprocessing application of membrane chromatography. *Biotechnol. Adv.* 31: 450–465.

Scott, R.P.W. (1986). *Liquid Chromatography Detectors*. Amsterdam: Elsevier Science Publishers.

Shalliker, R.A., Broyles, B.S., and Guiochon, G. (1999). Visualization of viscous fingering in high-performance chromatographic columns: influence of the header design. *J. Chromatogr. A* 865: 73–82.

Snyder, L.R., Kirkland, J.J., and Dolan, J.W. (2010). *Introduction to Modern Liquid Chromatography*, 3e. Hoboken, NJ: Wiley.

Tingley, S.K., (2017). Disposable prepacked-bed chromatography for downstream purification: form, fit, function, and industry adoption, *Process Scale Purification of Antibodies*, 2. by Gottschalk, U. (269-302), Wiley.

Toumi, A., Jürgens, C., Jungo, C. et al. (2010). Design and optimization of a large scale biopharmaceutical facility using process simulation and scheduling tools. *Pharm. Eng.* 30: 1–9.

Unger, K., Ditz, R., Machtejevas, E., and Skudas, R. (2010). Liquid chromatography – its development and key role in life science applications. *Angew. Chem. Int. Ed.* 49: 2300–2312.

Zhou, J.X. and Tressel, T. (2006). Basic concepts in Q membrane chromatography for large-scale antibody production. *Biotechnol. Prog.* 22: 341–349.

Appendix A

Data of Test Systems

A.1 EMD53986

EMD53986   [5-(1,2,3,4-*tetra*-hydroquinolin-6-yl)-6-methyl-3,6-dihydro-1,3,4-thiadia-zin-2-one] (Figure A.1) is a chiral precursor for a pharmaceutical reagent. After chemical synthesis, it is present as a racemic mixture of the *R*- and *S*-enantiomers. The target component for the separation is the *R*-enantiomer.

Given below are the separation conditions (Table A.1) and typical model parameters (Table A.2 and Table A.3) used in this book (Jupke 2004; Epping 2005):

Eluent: ethanol (gradient grade), LiChrosolv®, 99–100%, Merck (Darmstadt)
Adsorbent: Chiralpak AD, Daicel (Japan)
(Amylose-tris[3,5-dimethylphenylcarbamet]-phase)
Temperature: 25 °C

HETP correlation:

$$R - \text{enantiomer} : \text{HETP}_R = 5.03 \times 10^{-3} + 1.9\, u_{\text{int}} \tag{A.1}$$

$$S - \text{enantiomer} : \text{HETP}_S = 1.26 \times 10^{-2} + 1.63\, u_{\text{int}} \tag{A.2}$$

Isotherms for 25 °C (Section 7.5.5):

$$R - \text{entiomer} : q_R = 2.054\, c_R + \frac{5.847\, c_R}{1 + 0.129\, c_R + 0.472\, c_S}$$

$$S - \text{entiomer} : q_S = 2.054\, c_S + \frac{19.902\, c_S}{1 + 0.129\, c_R + 0.472\, c_S} \tag{A.3}$$

Alternatively, the isotherm can also be expressed by a multi-Langmuir equation:

$$R - \text{enantiomer} : q_R = \frac{7.859\, c_R}{1 + 0.295\,43\, c_R + 0.082\,93\, c_S}$$

$$S - \text{enantiomer} : q_S = \frac{19.75\, c_S}{1 + 0.295\,43\, c_R + 0.082\,93\, c_S} \tag{A.4}$$

Pressure drop correlations:

$$\Delta p = 1233.4\, \frac{u_{\text{int}}\, h_l\, L_c}{d_p^2} \tag{A.5}$$
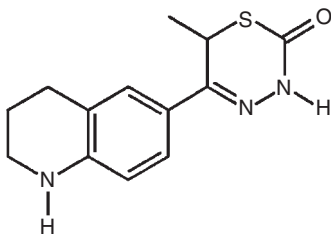
Figure A.1 Chemical structure of EMD53986.

Table A.1 Typical design and model parameters for EMD53986.

Design parameter	Value
Particle diameter	20 μm
Column diameter (d_c)	2.5 cm
Column length (L_c)	11.5 cm
Division (for SMB)	2/2/2/2

Model parameter	Value
Void fraction (ε)	0.355
Total porosity (ε_t)	0.72
Dispersion coefficient (D_{ax})	Eq. (7.15) (Section 7.4.2)
Viscosity (η_l)	0.0119 g cm^{-1} s^{-1}
Density (ϱ_l)	0.799 g cm^{-3}
Effective transfer coefficient (k_{eff}) R-enantiomer	1.50×10^{-4} cm s^{-1}
Effective transfer coefficient (k_{eff}) S-enantiomer	2.00×10^{-5} cm s^{-1}

Table A.2 Parameters for model validation batch column (EMD53986).

Typical plant parameters (batch experiments)	Value
Pipe volume (V_{pipe})	12.3 cm^3
Dispersion coefficient pipe ($D_{ax,pipe}$)	~3000 cm^2 s^{-1}
Pipe diameter (d_{pipe})	0.05 cm
Tank volume (V_{tank})	3.1 cm^3

A.2 Tröger's Base

Tröger's base (Figure A.2) was the first example of a chromatographic separation of an enantiomeric mixture. Since then it has been the subject of several publications.

Given below are the separation conditions and typical model parameters used in this book (Table A.4 and Table A.5) (Jupke 2004; Mihlbachler et al. 2001, 2002):

Table A.3 Parameters for model validation SMB (EMD53986).

SMB experiments (Figure 7.30)	Unit	Value
Shifting time (t_{shift})	s	431
Asynchronous shift time	s	40.4
Feed flow rate	ml min^{-1}	5.54
Desorbent flow rate	ml min^{-1}	57.5
Extract flow rate	ml min^{-1}	47.97
Raffinate flow rate	ml min^{-1}	15.06
Recycle flow rate	ml min^{-1}	72.0
m_I	—	30.14
m_{II}	—	8.34
m_{III}	—	10.86
m_{IV}	—	4.02

Figure A.2 Chemical structure of Tröger's base.
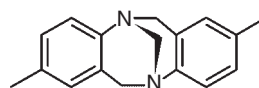
Eluent: isopropanol (HPLC grade), Fisher Scientific (Pittsburgh, USA)
Adsorbent: Chiralpak AD, Daicel (Japan)
Amylose-tris[3,5-dimethylphenylcarbamet]-phase
Solute: Tröger's base, Aldrich (Milwaukee, USA)
Temperature: 25 °C

Isotherms from breakthrough experiments (Section 7.5.8):

$$R-\text{enantiomer}: q_R = \frac{54\, c_R(0.035 + 0.0046\, c_S)}{1 + 0.035\, c_R + 0.062\, c_S + 0.0046\, c_R\, c_S + 0.0052\, c_S^2}$$

$$S-\text{enantiomer}: q_S = \frac{54\, c_S\, (0.062 + 0.0046\, c_R + 2{\cdot}0.0052\, c_S)}{1 + 0.035\, c_R + 0.062\, c_S + 0.0046\, c_R\, c_S + 0.0052\, c_S^2}$$

$$\text{(A.6)}$$

Isotherms from perturbation experiments (Section 7.5.8) are

$$R-\text{enantiomer}: q_R = \frac{0.0311\, c_R(54 + 0.732\, c_S)}{1 + 0.0311\, c_R} + \frac{0.732{\cdot}0.0365\, c_R\, c_S}{1 - 0.0365\, c_R}$$

$$S-\text{enantiomer}: q_S = \frac{27\, c_S(0.1269 + 2.0.0153\, c_S)}{1 + 0.1269\, c_S + 0.0153\, c_s^2}$$

$$\text{(A.7)}$$

Table A.4 Typical design and model parameters for Tröger's base.

Design parameter	Value
Particle diameter	20 μm
Column diameter (d_c)	1 cm
Column length (L_c)	10 cm
Division (for SMB)	2/2/2/2

Model parameter	Value
Void fraction (ε)	0.355
Total porosity (ε_t)	0.648
Dispersion coefficient (D_{ax})	Eq. (7.15) (Section 7.4.2)
Viscosity (η_l)	$0.012\,\mathrm{g\,cm^{-1}\,s^{-1}}$
Density (ϱ_l)	$0.785\,\mathrm{g\,cm^{-3}}$
Effective transfer coefficient (k_{eff}) R-enantiomer	$5 \times 10^{-4}\,\mathrm{cm\,s^{-1}}$
Effective transfer coefficient (k_{eff}) S-enantiomer	$4.5 \times 10^{-5}\,\mathrm{cm\,s^{-1}}$

Table A.5 Parameters for model validation SMB (Tröger's base).

SMB experiments (Figure 7.32)	Unit	Value
Shifting time (t_{shift})	s	962
Feed flow rate	$\mathrm{ml\,min^{-1}}$	0.30
Desorbent flow rate	$\mathrm{ml\,min^{-1}}$	0.46
Extract flow rate	$\mathrm{ml\,min^{-1}}$	0.33
Raffinate flow rate	$\mathrm{ml\,min^{-1}}$	0.43
Recycle flow rate	$\mathrm{ml\,min^{-1}}$	1.05
m_I	—	4.24
m_{II}	—	2.50
m_{III}	—	3.43
m_{IV}	—	1.70

A.3 Glucose and Fructose

Glucose (Figure A.3) and fructose (Figure A.4) are monosaccharides. Separation of their isomeric mixture is of industrial importance to produce sugar syrups or for further synthesis of sorbitol, gluconic acid, and vitamin C. Due to higher sweetness, fructose is often used as an alternative sweetener for sucrose.

Figure A.3 Chemical structure of glucose.
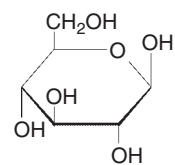
Figure A.4 Chemical structure of fructose.
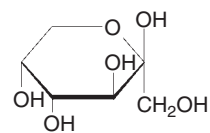
Table A.6 Typical design and model parameters for fructose–glucose.

Design parameter	Value
Particle diameter	325 μm
Column diameter (d_c)	2.6 cm
Column length (L_c)	~56.5 cm[a]
Division (for SMB)	2/2/2/2

Model parameter	Value
Void fraction (ε)	~0.36
Total porosity (ε_t)	~0.36
Dispersion coefficient (D_{ax})	Eq. (7.15) (Section 7.4.2)
Viscosity (η_l)	$4.7 \times 10^{-3} \, \mathrm{g \, cm^{-1} \, s^{-1}}$
Density (ϱ_l)	$0.983 \, \mathrm{g \, cm^{-3}}$
Effective transfer coefficient (k_{eff}) glucose	$7 \times 10^{-4} \, \mathrm{cm \, s^{-1}}$, $5.7 \times 10^{-5} \, \mathrm{cm \, s^{-1}}$
Effective transfer coefficient (k_{eff}) fructose	$6.5 \times 10^{-5} \, \mathrm{cm \, s^{-1}}$, $8.9 \times 10^{-5} \, \mathrm{cm \, s^{-1}}$
Equilibrium constant (K_{eq})	1.079
Reaction rate constant (k_{reac})	$1.427 \times 10^{-3} \, \mathrm{s^{-1}}$

a) Due to slightly different adsorbent amounts and packing compressions for different experiments.

Separation conditions and typical model parameter used in this book are given below (Table A.6 and Table A.7) (Jupke 2004):

Eluent: deionized and microfiltered water
Adsorbent: ion-exchange resin Amberlite CR 1320 Ca (Rohm u. Haas, Frankfurt)
Solute: glucose, fructose (pure, Merck, Darmstadt)
Temperature: 60 °C

Table A.7 Parameters for model validation SMB (fructose–glucose).

SMB experiment	Unit	Value
Shifting time (t_{shift})	s	1590
Asynchronous shift time	s	171.8
Feed flow rate	ml min^{-1}	0.56
Desorbent flow rate	ml min^{-1}	4.24
Extract flow rate	ml min^{-1}	3.35
Raffinate flow rate	ml min^{-1}	1.45
Recycle flow rate	ml min^{-1}	10.0
m_{I}	—	0.82
m_{II}	—	0.36
m_{III}	—	0.43
m_{IV}	—	0.23

For chromatographic reactors additionally:

Catalyst: immobilized glucose invertase Sweetzyme IT (Novozymes, Mainz)

HETP correlations for 60 °C:

$$\text{Glucose} : \text{HETP}_{\text{glu}} = 0.1188 + 8.997 \, u_{\text{int}} \tag{A.8}$$

$$\text{Fructose} : \text{HETP}_{\text{fru}} = 0.1163 + 25.155 \, u_{\text{int}} \tag{A.9}$$

Isotherms for 60 °C: (Section 7.5.5):

$$q_{\text{glu}} = 0.27 \, c_{\text{glu}} + 0.000\,122 \, c_{\text{glu}}^2 + 0.103 \, c_{\text{glu}} \, c_{\text{fru}}$$

$$q_{\text{fru}} = 0.47 \, c_{\text{fru}} + 0.000\,119 \, c_{\text{fru}}^2 + 0.248 \, c_{\text{glu}} \, c_{\text{fru}} \tag{A.10}$$

A.4 β-Phenethyl Acetate

β-Phenethyl acetate (Figure A.5) is used for the production of scents and perfumes.

Separation conditions and model parameter used in this book are given below (Table A.8):

Eluent: 1,4-dioxan
Adsorbent and catalyst: ion-exchange resin Amberlite 15 (Rohm u. Haas)
Solute: acetic acid and β-phenethyl alcohol
Temperature: 85 °C

Isotherms for 85 °C:

$$q_{\text{alcohol}} = \frac{0.884 \, c_{\text{alcohol}}}{1 + 24.16 \, c_{\text{alcohol}}} \tag{A.11}$$

$$q_{\text{acid}} = 0.687 \, c_{\text{acid}} \tag{A.12}$$

Figure A.5 Chemical structure of β-phenethyl acetate.
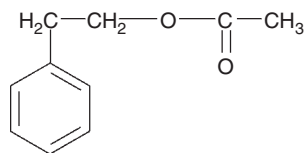
Table A.8 Typical design and model parameters for β-phenethyl acetate.

Design parameter	Value
Particle diameter	590 μm
Column diameter (d_c)	1 cm
Column length (L_c)	30 cm

Model parameter	Value
Total porosity (ε_t)	0.36
Dispersion coefficient (D_{ax})	Eq. (7.15) (Section 7.4.2)
Viscosity (η_l)	$5.8 \times 10^{-3}\ \mathrm{g\,cm^{-1}s^{-1}}$
Density (ϱ_l)	$1.03\ \mathrm{g\,cm^{-3}}$
Effective transfer coefficient (k_{eff}) alcohol	$4.39 \times 10^{-4}\ \mathrm{cm\,s^{-1}}$
Effective transfer coefficient (k_{eff}) acid	$4.82 \times 10^{-4}\ \mathrm{cm\,s^{-1}}$
Effective transfer coefficient (k_{eff}) ester	$4.17 \times 10^{-4}\ \mathrm{cm\,s^{-1}}$
Effective transfer coefficient (k_{eff}) water	$1.11 \times 10^{-3}\ \mathrm{cm\,s^{-1}}$
Equilibrium constant (K_{eq})	3.18
Reaction rate constant (k_{reac})	$0.165\,326\ \mathrm{cm^3\,s^{-1}\,g^{-1}}$

$$q_{ester} = 0.479\, c_{ester} \tag{A.13}$$

$$q_{water} = \frac{11.126\, c_{water}}{1 + 568.54\, c_{water}} \tag{A.14}$$

References

Epping, A. (2005). *Modellierung, Auslegung und Optimierung chromatographischer Batch-Trennung*. Aachen: Shaker.

Jupke, A. (2004). *Experimentelle Modellvalidierung und modellbasierte Auslegung von Simulated Moving Bed (SMB) Chromatographieverfahren, Fortschrittbericht VDI: Reihe* 3 *Nr*. 807. Düsseldorf: VDI Verlag GmbH.

Mihlbachler, K., Fricke, J., Yun, T. et al. (2001). Effect of the homogeneity of the column set on the performance of a simulated moving bed unit: I. Theory. *J. Chromatogr. A* 908: 49–70.

Mihlbachler, K., Jupke, A., Seidel-Morgenstern, A. et al. (2002). Effect of the homogeneity of the column set on the performance of a simulated moving bed unit: II. Experimental study. *J. Chromatogr. A* 944: 3–22.

Index